Proceedings of the

14th International Conference on Condensed Matter Nuclear Science

and the

14th International Conference on Cold Fusion (ICCF-14)

10-15 August 2008
Washington DC

Volume 2

General Editors:

David J. Nagel and Michael E. Melich

Theory Editors:

Rodney W. Johnson and Scott R. Chubb

Copy Editor:

Jed Rothwell

ISBN: 978-0-578-06694-3

Printing was done by the
Marriott Library of the University of Utah

Copies of these proceedings can be purchased on a DVD for $20 from:

New Energy Foundation, Inc.
P.O. Box 2816
Concord, NH 03302-2816

http://www.infinite-energy.com
Phone: 603-485-4700

Table of Contents

VOLUME 1

Materials *425*

Theory Papers *475*

Introduction to Cavitation Experiments

The Preface described four methods for loading isotopes of hydrogen into materials. They are electrochemical loading from a liquid, gas loading, plasma loading and beam loading. Over the years, there has been a steady stream of results reporting cavitation loading of solids in LENR experiments. So, how does cavitation loading work? Does it fit into one of the four classes of loading?

Cavitation is the process where pressure within water or another liquid is quickly reduced, so that the liquid rapidly vaporizes and forms bubbles even at ordinary temperatures. The bubbles then collapse, which results in a self-collision in the center of the bubble. That generates both high temperatures and high pressures. If the bubble is in the liquid and away from any solids, the collapse is symmetric in all three dimensions. The radius of a cavitation bubble varies from about 4 micrometers to 40 nanometers during its lifetime of about 100 nanoseconds. It collapses at a speed of about Mach 4 and produces a million-fold increase in density over the initial vapor density. Light generated at the center of a collapsed cavitation bubble is called sonoluminescence. The collapse of cavitation bubbles also induces chemical reactions.

For LENR cavitation experiments, a thin solid foil is placed into heavy water. An ultrasound transducer produces intense sound in the water, leading to formation of transient bubbles. If the bubbles are on the surface of the metal foil, the collapse is cylindrically symmetrical around an axis normal to the foil surface. As a cavitation bubble on a solid surface collapses, a jet of material impacts the surface. This phenomenon is responsible for cavitation erosion of the surfaces of materials, such as the propellers of ships, and also for acoustic emissions. However, in LENR experiments, the collapse of cavitation bubbles on the surface of a solid effectively injects nuclei of the vapor into the foil. These include protons in the case of light water and deuterons in the case of heavy water. The chemical state of the vapor, that is, molecules, atoms or ions, is an important consideration for understanding the advantages of cavitation loading and its energetic efficiency.

Returning to the questions about the types of loading due to cavitation bubble collapse, we have a mixed situation. The collapsing bubble contains gas (the vapor) for most of its motion, and then a plasma of increasing temperature, when it is near fully collapsed. And, the jet of material is like a beam impacting the surface of the foil. So, cavitation loading spans at least two of the major classes of loading, plasma and beam, both of which involve higher energies per particle than electrochemical or ordinary gas loading. But, however complex is cavitation loading, it is effective.

The use of cavitation to load materials with H or D in LENR experiments is sometimes called sonofusion. That is a correct term only if fusion is the sole resulting nuclear reaction. This terminology also has one other disadvantage. In the past several years, another line of experiments involving insonification, cavitation and fusion has arisen, and received a lot of attention. It is best called “bubble fusion”. Such fusion is not LENR because no solid lattice is involved. In the case of bubble fusion, sound is used to produce cavitation in a liquid with a

nearby source of neutrons. The hot plasma produced by the cavitation bubble collapse in heavy water is postulated to cause hot fusion. The experimental measurement of such plasmas is challenging because of their small size and very transient lifetimes. And, there is a wide range of opinions on the reality as well as the characteristics of bubble fusion. However, the field of bubble fusion is of no concern to LENR.

There were two papers on cavitation induced effects presented at ICCF-14. The first was by Stringham, who has worked on sonofusion for many years and presented some remarkable results at earlier conferences in this series. This time, his paper was a useful review of the basics of sonofusion, and a summary of some results. Some of his excess heat data is at Stringham's web site: http://sonofusionjets.com. There he shows excess power data to almost 40 W.

The second paper on bubble cavitation was qualitatively different from most experimental papers at the conference. There was no lattice involved in these experiments. In this paper, Kornilova and her associates reported the production of x-rays, as well as light, from cavitation bubbles produced when light oil was forced through an orifice at pressures up to 80 to 90 atmospheres. First, very soft x-rays (1-2 keV) were measured, a remarkable result given the very short ranges of such radiation in condensed matter. Then, fine copper powder was placed on the exterior of the experiment, and x-rays peaking at 3 keV and extending to 5 keV were recorded. These unusual results challenge explanations.

In general, the work on cavitation fusion has produced enticing results, but has not been adequately replicated in other laboratories. Such work is on the very long list of LENR and related experiments that should be done.

Bubble Driven Fusion

Roger Stringham
First Gate Energies

Abstract

Experimentally, heat and ^{4}He are sonofusion (SF) fusion products. SF boosts a naturally occurring phenomenon with cavitation-induced bubbles and their collapse to high energy densities. One unique fusion path to heat and ^{4}He is shown. What has been increasingly evident is that high-density experiments of ICF and astrophysical relations of fermions and bosons show a plausible path to SF products. SF focuses around implantation of nanometer jet volumes and picosecond time scales. Several high-density systems like those of WDS, MF, z-pinch systems, and ICF have influence over this model path.

Acronym list

BCS Bardeen, Cooper, Schrieffer; superconductivity theory
BDS Black dwarf star; an old and cool WDS
BEC Bose Einstein Condensate; follows Bose Einstein statistics
DOE Department of Energy
EM Electromagnetic
HDZP High density z-pinch using a deuterium frozen fiber and high current
ICF Inertial confined fusion; an approach to fusion via hot fusion
MF Muon fusion; a muon replaces an electron in D_2 and has a pseudo density of a WDS
MS Mass spectrum; helium measurement by DOE's Brian Olive
Qa Acoustic power input to piezo reactor in watts
Qi Total power input in watts
Qo The calorimetric measured heat out of reactor in watts
Qx Heat measured above that expected heat in watts
Rf The final transient cavitation bubble radius
Rmax Maximum transient cavitation bubble radius
SEM Scanning Electron Microscope
SF Sonofusion; fusion source from collapsing cavitation bubbles
SL Sonoluminescence; acoustic light emission from bubble collapse
TCB Transient cavitation bubble; a bubble with at least 3 watts of power/cm^2
WDS White dwarf star; a collapsed star no longer generating heat

Introduction

The experimental part of this paper draws from many years of compelling results pointing to fusion events in target foils produced by TCBs in D_2O. TCBs produce high-density plasma jets, which coincide with SL during the TCBs collapse process [1], where EM fields compress the jet's contents. SL is used to monitor SF experiments. Jets implant the target foil forming

deuteron clusters. The transient deuteron clusters, with temperature and density consideration, are deuteron coherent BECs where the De Broglie wave exceeds the DD cluster spacing. The femtosecond endothermic recombination of the implanted free electrons with the surface deuterons of the cluster cools and compresses its contents. The implosion of the recombination shockwave creates enough contact time for DD fusion event(s) to occur. The expected gamma radiation is not found, as this expected product is replaced by heat. (The mechanism for the gamma is slower than the direct conversion fusion energy to heat. The single wave function involves all of the BEC cluster deuteron bosons.) The conversion of fusion energy to a lattice heat pulse is shown in the many SEM photos of target foil surface ejecta sites. In piezo systems that resonated at 20 and 40 KHz, ejecta were expelled into the circulating D_2O, where the fusion ^4He and heat were circulated and measured. The measurements of ^4He products, at 550 ppm were measured in a Department of Energy laboratory [2]. 1.6 MHz produce much smaller but more numerous jets with similar energy densities. Heat measurements showed Qx that increased with Qa. Qi was varied from 4 to 50 watts where Qx was 0 to 40 watts [3,4].

The fermion isotopes of hydrogen have a possibility to pair in crossover high-density environments forming a fermion boson, a behavior similar to Cooper pairing. Clusters and their recombination shockwave that will promote the fusion of pairs of hydrogen isotopes may behave in a mode parallel to DD fusion and heat.

The Transient Cavitation Bubble, TCB

A quick view of cavitation follows [1]. A sinusoidal wavelength defines the time for a generation of bubbles that cycle through a birth, growth, collapse, and jet formation modes as the D_2O prepares for its next bubble generation [5]. An oscillator drives a 1.6 MHz resonance system that produces millions of bubbles with an initial radius of around 0.4 microns. As the bubble expands in the low-pressure isothermal growth phase, it picks up D_2O mass from the bubble's interface. Crossing over into the positive pressure zone of the acoustic wave, the partially evacuated bubble reaches its Rmax of about 4 microns; then begins its rapid collapse. The bubble surface accelerates towards its center at Mach 4 velocity or greater [6]. In 0.1 microsecond the bubble's somewhat leaky adiabatic Rf of about 0.04 microns is reached. The 1 million-fold energy density increase is enough to dissociate some of the D_2O. Here two events occur: a burst of photons is emitted as SL and the plasma contents of the bubble are transferred to a jet where EM compression pressures squeeze the jet's contents [7]. See Figure 1-1. The jet — a high-density deuteron plasma — is confined by EM pressures [8]. The first step in producing heat and ^4He in SF is the TCB and jet system. Photos of cavitation jets will be found in reference [9].

Other Fusion Systems

Other fusion systems exist. The first is Muon Fusion (MF), where a heavy muon replaces an electron in the D_2 molecule, shrinking its orbit to 1/207 of its normal orbit size. [10] In MF the two deuterium atoms of D_2 fuse at 100 K. The density or separation of the two deuterons is about the same as in a BDS environment. The gravitational forces present in a BDS would compress these boson deuterons to fusion densities in less than a picosecond. The BDS's high-density environment lacks internal radiation pressure, has no fuel for fusion, and is equivalent

to the density of muon fusion systems. The second is the high density z-pinch (HDZP), a vacuum system that feeds a shaped high current pulse into a 50 micron frozen D_2 fiber. The magnetic pressures around the fiber are very similar to the EM pressures of the SF jet. The magnetic pressure squeezes the fiber's deuterons to the fusion point [11]. The third is the backlighting experiments performed by MIT and the University of Rochester where transient EM fields were measured in ICF systems using the plastic CR39 to establish deflection patterns of synchronized mono energetic protons. These fields were measured at 60 Tesla and 10^9 V/m. at densities of 300 gm/cc [12]. The fourth is the astrophysics of the BEC and the BCS systems. Information gathered from these systems gives substance to the formulation of a SF path to the fusion products heat and ^{4}He. From experiments, it is shown that DD fusion occurs via the cavitation bubble. So the objective is fitting the SF experimental work to extrapolated hot fusion systems into a coherent path.

Experimental Set-up

The objective is experimentally boosting the naturally occurring cavitation phenomenon to a controlled bubble system. Important parameters are controlled, creating the transient high-density, environment. A complex system is used to gather the data, but is not necessary for the devices operation. The cavitation device is energized by an ultrasound piezo, producing micron size bubbles in circulating D_2O. A pump circulates the D_2O through the SF device to a heat exchanger, a flow-meter, a bubbler and back to the pump [7].

The piezo device responds to its feedback oscillator that tracks the small changes of its resonance frequency due to the influence of small changes in temperature and pressure. This keeps the device well tuned to its resonant frequency. The adiabatic bubble collapse compresses and dissociates D_2O into its ions. For the 1.6 MHz system the measurement of SL photons were emitted and counted via a photomultiplier and counter system as they pass through the reactor window. SL is used as a tool for evaluating and maintaining control of the SF parameters; temperature, pressure, and acoustic input. The measurements were made in a light proof box where the air circulation keeps the box and the SF device at constant temperature. The photon background count was 200 photons/sec. The box contains the main components of the SF apparatus. The maximum photon count was near 2,000,000/sec. [3].

SF is a collection of billions of one cycle acoustic events that include the bubble's collapse, the transfer of the bubble's contents into a jet, the target foil Boson cluster and the fusion heat pulse. The jet is very small and contains high velocity sheath electrons. The 1.6 MHz jet has a volume $2x10^{-23}m^3$, 10 nm in diameter and 100 nm in length, with a lifetime of a picosecond. It is in the jet where the high densities are reached via z-pinch SF EM pressures producing very high-densities, 10^{27}D/cc, of very compressible bosons in the jet and cluster. The jet sheath electrons produce the EM compression pressures perpendicular to their Mach 20 velocity vector. The jet, located close to a 100 micron thick target foil, implants electrons and then deuterons into the foil lattice to form a cluster. See figure 1 - 1, 2. What is increasingly evident is that high-density experiments of ICF and the astrophysical relations of deuterons and electrons, bosons and fermions, add a great deal of reality to the picture of this transient jet and cluster [13].

The Path and Experimental Evidence

A connection between experimental evidence and transient high densities is shown. During the target implantation, electrons and deuterons, are momentarily separated as deuteron clusters and free electrons moving back to the cluster reacting with outer deuterons squeezing the cluster. The transient deuteron clusters are stabilized for a picosecond by their high-density (close packed structure), the de Broglie wave in the cluster producing a coherent BEC. See figure 1 - 3, 4.

In the closely packed cluster deuterons the shockwave initiates the ^{4}He fusion event. See figure 1 – 4, 5. The favored path produces heat and not gamma radiation [14]. The fusion heat pulse destroys the very high-density cluster and as the spherical heat pulse passes into the target foil lattice, it reaches the foil surface producing an ejecta site. See figure 1 – 6. The nm size ejecta sites are easily photographed using SEM analysis. In piezo systems that resonate at 20 KHz, the heat pulse's vaporous ejecta were expelled into the circulating D_2O, where the fusion products, ^{4}He and heat, are circulated and measured. This explains why little of the ^{4}He fusion product is found in exposed target foils.

The SEM photos show an uncountable number of ejecta sites. Several SEM photos of Pd foils have been analyzed by counting one square μ^2 areas of exposed target surfaces to find the distribution of the diameter sizes of ejecta sites. The plots of site diameters versus their number show a skewed distribution. Assuming that the depth of the ejecta site is the same as its diameter, the volume of the spherical heat pulse and ejecta relate to ejecta energy. A clear maximum for ejecta site diameter distribution was found to be near 100 nm. This falls off rapidly as the ejecta site diameter increases for multiple fusion events. Using these ejecta volumes and site diameters a conversion to about 20 +/- 10 Mev is the expected value for a single DD fusion event. The exposed target foils show surface distribution of ejecta sites in the form of permanent surface patterns of standing waves.

Gases from 20-KHz experiments were collected from directly over the SF reactor's circulating D_2O. This gas was expanded into 50 cc evacuated stainless steel cylinders for MS measurement, which was performed by Brian Oliver in a DOE laboratory specializing in helium MS analysis of the gas samples. The data from sample cylinder #3 measurement for ^{4}He, using three different small aliquots of gas from the sample cylinder, shows the average number of ^{4}He atoms that were in the sample cylinder to be 7463×10^{14} ^{4}He atoms of with a sigma of +/- 1. Only 50% of the gas in the experiment was collected in the sample cylinder. The remaining helium was equally distributed throughout the circulation volume. So the total ^{4}He was 1.5×10^{18} atoms. The calculated ^{4}He in the gas sample was 552 ppm, which is 100 times that found in atmospheric air. This experiment produced 80 watts with respect to helium production over a 19 hr. period. 64 watts of excess heat was measured by calorimetry. (B. Oliver's data is on DVD shown at ICCF-14 Wash. DC, 2008.)

The determination of excess heat was done using the D_2O flow-through calorimetric measurements of the 1.6 MHz piezo driven, low mass, 20 g device [15]. Measured the temperature of the D_2O flow into and out of the device, DT, and its flow rate in cc/s were measured, these two were multiplied together to give calories/s. This result is multiplied by

4.184 Joules/calorie to give Qo. Now, Qo was the sum of Qa and Qx. The efficiency of Qi was measured at 0.33 [2] so Qa = .33 Qi. Some of Qi powered a transformer and the 1.6 MHz oscillator. That is the basic calorimetry.

The experimental data for the 1.6 MHz device data is plotted in the web site www.sonofusionjets.com. [4] The series of runs is listed in the table shows increasing values of Qi, SL, and Qx. Qx reaching a maximum of 40 watts, with a Qa of 16.5 watts, and a Qi of 50 watts. A one second was the residence time for D_2O in the reactor volume and a flow rate of 1cc/sec. The external pressure was one atmosphere of argon. The SF device used a joule heater replacing Qa in the calibration mode. One must be careful to guard against radio-frequency interference during thermocouple measurements and heat lost via device's surface convection.

Summary

The robust 1.6 MHz SF device can be ganged together to make high energy-density systems of any size. SF can serve in the work place as space heating where about 0.3 of the grid power is used today. With future improvements it will be a self-supporting unit using thermoelectric devices to convert heat directly to electricity [2]. SF applied to space travel has the advantage of a high power/mass ratio. SF is a million times more mass efficient than hydrocarbon fuels or a $O_2 + H_2$ mix. This paper is about transient densities with parameter control of temperature, pressure, and acoustic input.

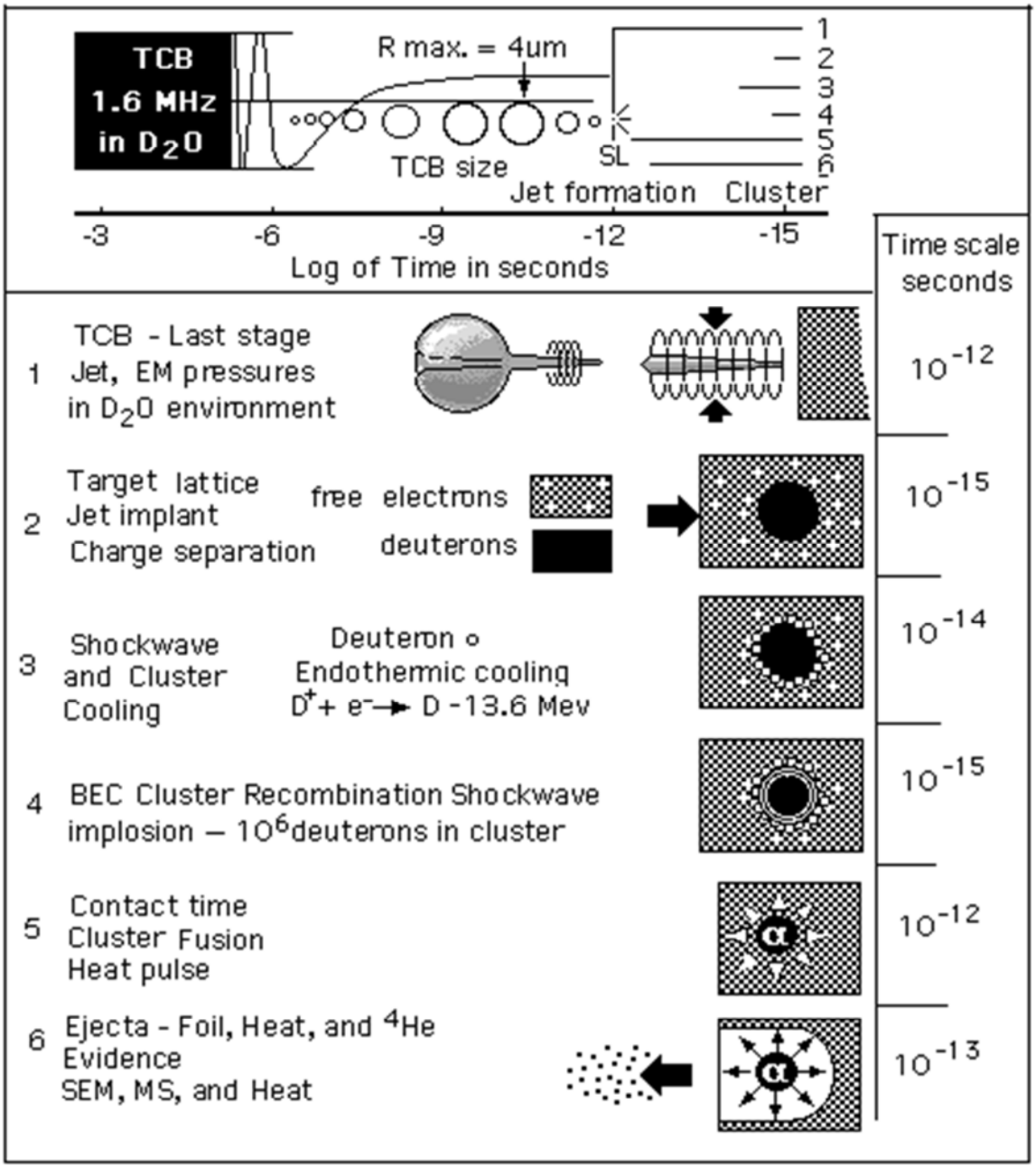

Figure 1. Six steps to SF.

Acknowledgements

Thanks to Julie Wallace for editing.

References

1. M. P. Brenner, S. Hilgenfeldt, D. Lohse, Rev. Mod. Phys., vol 74, No 2, 425-484, (2002).
2. B. Oliver, Report, DOE lab. at Rockwell International, CA 91309, 642/NAO2 (1994).
3. R. Stringham, ICCF11 Proc., J. Biberian Ed. Marseilles, France, 238, 31, (Oct.-5 Nov.'04)
4. Web site, www.sonofusionjets.com - one page, (2006)
5. R. Stringham, IEEE US Symp. Proc.; Sendai, Japan; 98CH36102; Vol. 2, 1107, (1998).
6. K. R. Weninger, P. G. Evans, and S. J. Putterman, Phys. Rev. E., 61(2), 3, 2000.
7. R. Stringham, ICCF-10 Proceedings, Poster, P. Haglestein, S. Chubb ed. Boston, USA, LANL-CANR web library, (2003).
8. R. Stringham, ICCF 9 Proceedings, Ed Zing Z. Li, Beijing, China, p 323, May 19-24, (2002)
9. Y. Tomita, A. Shima; Acoustica, 71,161, (1990). and M. P. Felix, A. T. Ellis, Appl. Phys. Lett., 19, 484, (1971), and W. Lautterborn, H. Bolle, J. Fluid Mech., 72, 391 (1975).
10. W. Alvarez, et al, Catalysis Nuclear Reactions by μ Mesons, Phys. Rev.; 105 1127, (1957).
11. M. A. Liberman, J. S. De Groot, A. Toor, R. B. Spielman; Physics of High-Density Z-Pinch Plasmas; Springer-Verlag NY, QC718.5.P45P48, 1998, pages 37 and 238-241
12. R. D. Petrasso, et al, Science, 319: 1223-1225, (29 Feb. 2008)
13. R. Stringham, ACS book to be published, (2008-9).
14. S. Chubb, T Chubb, P. Hagelstein, Y. Kim and others who have presented theories on why gammas are not present, most recently at the Proceedings of ICCF 12, A. Takahashi ed. Yokohama, Japan, Nov. – Dec. 2, 2005
15. R. Stringham, ICCF-10 Proceedings, P. Haglestein, S. Chubb ed. Boston, (Aug 2003)

Investigation of Radiation Effects at Bubble Cavitation in Running Liquid

Alla A. Kornilova[1], Vladimir I. Vysotskii[2], Nickolai N. Sysoev[1] and Andrey V. Desyatov[3]
[1] *Moscow State University, 119899, Moscow, Russia*
[2] *Kiev National Shevchenko University, Kiev, Ukraine*
[3] *Federal State Unitary Enterprise "Keldysh Research Center", Moscow, Russia*

Abstract

In this work a new method of generating hard radiation with a cavitation chamber is presented. This mechanism is connected with the sequential events of cavitation and shock-wave processes inside the chamber with liquid, and in the volume of the chamber wall when there is perfect acoustic contact between them. The result of the tandem action is the passing of the cavitation energy from the cavitation area across a stream of running liquid to atoms situated on the external surface of the chamber. Shock excitation of these atoms leads to the generation of X-rays outside of the cavitation chamber.

1. Introduction

The cavitation phenomenon is one of the most promising perspective physical mechanisms for the realization of low energy nuclear interaction. It is very important to understand the nature and mechanisms of radiation processes that are connected with the cavitation. In our earlier works [1,2] the anomalous optical phenomena accompanying cavitation processes from directed motion of running liquids through thin dielectric channels to large-size working chamber were investigated.

A schematic of the experiment is shown in Fig. 1. The cylindrical cavitation chamber is 15 cm long, with a diameter of 8 cm, and is made of Plexiglas. Inside the chamber the special diaphragm with an orifice hole is situated. It is 1 mm in diameter, 2 cm in length. To observe the optical effects two opposite lateral faces of the cylinder have been vertically cut. Within these faces the thickness of the wall is increased from 2 to 3 cm.

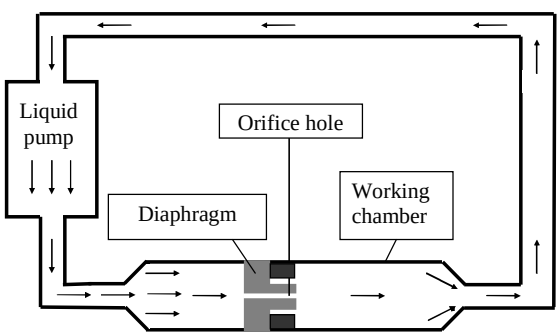

Figure 1. Schematic and overall view of the experimental setup

Experiments on stimulation of cavitation in pumped liquid (spindle oil) were performed with a step-by-step increase of pressure. At low pressure (P≤20 atm) the color of moving oil in the working chamber is tawny (Fig. 2a). At P≈25...30 atm the process of formation of cavitation bubbles in the volume behind the orifice starts. At such pressure the processes of initial turbulence and the generation of large size fluctuations of machine oil density take place. These fluctuations are visible. At P≈35...40 atm the averaged size of any fluctuation becomes small. The space behind the orifice hole is similar to a fog without any transparency and has the color like milk instead of the initial tawny color (Fig. 2b). At P≈60 atm a rapid increase of transparency of the turbulent oil takes place. As a result the chamber with cavitations at the downstream of the orifice hole becomes completely transparent (Fig. 2c). As the liquid pressure increases up to 80-90 atmospheres, in the central part of the chamber the directed bright light beam is shaped (Fig. 2d).

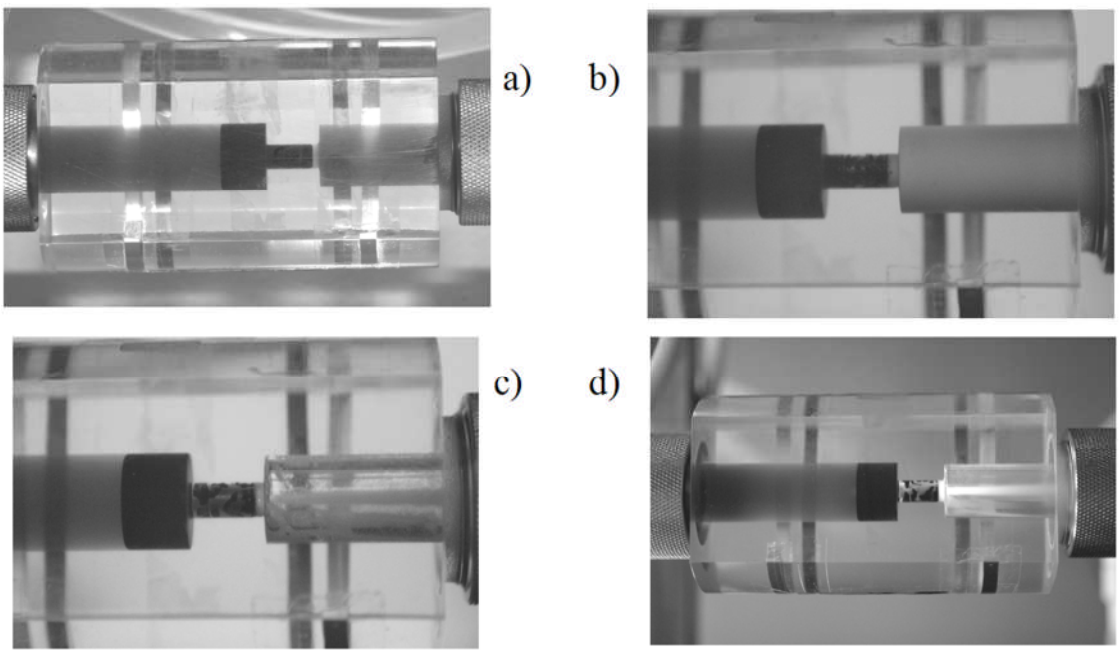

Figure 2. General view of the working chamber: a) at low pressure (P<20 atm) of moving oil; b) at the beginning of the cavitation process (P=25...40 atm); c) at separation of the liquid stream from the chamber walls at the condition of intensive cavitation (P>60 atm). d) Bright luminescence of the directed liquid stream with cavitation bubbles (P≥80...90 atm).

It is obvious that this bright luminescence of the directed liquid stream is connected with the cavitation process, but it differs greatly from usual low intensity sonoluminescence (which is equilibrium thermal optical radiation from the heated portion of the machine oil in the volume of the cavitation area). In previous papers [1,2] several possible mechanisms of this bright luminescence were proposed, but a definitive conclusion has not been reached. In the present work the results of investigation of X-Ray radiation processes connected with cavitation phenomena in running liquids are presented. It will be shown that formation of bright visual luminescence is also connected with these processes.

2. Investigation of characteristic X-ray generation from the cavitation phenomena

After a detailed examination we have found that at critical regime of bubble cavitation, the process of stationary generation of X-radiation with energy of 1 to 2 keV (or more) takes place. This radiation is detected outside the cavitation chamber at about 3 mm from the external surface.

To detect the radiation, an X-Ray and gamma detector XR-100T-CdTe with CdTe monocrystal was used. Cylindrical collimator of the detector had a length about $L \approx 6$ cm and an internal cross-section $S_0 \approx 0.5$ cm^2. The solid angle of detection was $\Omega \approx 0.02$ sr. The entrance cross-section of the collimator was closed by a very thin Be foil.

The results of X-Ray detection are presented on Fig. 3. Registration of such soft X-ray radiation with energy of about 1...2 keV (which is connected with the cavitation phenomena inside the chamber) outside of the thick-walled cavitation chamber is, at first sight, very strange because of the very low absorption mean free path (less than 10-20 microns) in the oil and Plexiglas.

We have studied this paradox using different methods.

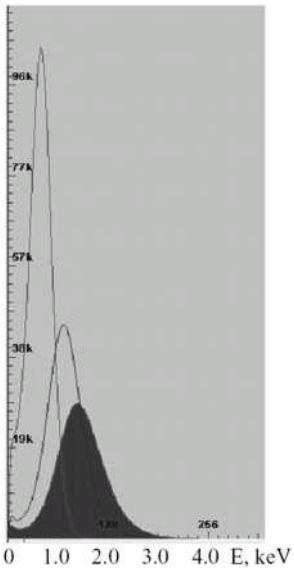

Figure 3. The change (shift) of the X-Ray spectrum that was detected near the surface of the cavitation chamber at stage-by-stage increases of oil pressure (left to right - 20, 40 and 65 atm).

2.1. Controlled stimulation of generation of additional X-radiation

Finely-dispersed copper powder was placed on an external surface of the chamber (on its flat surface). Acoustical contact of this powder was ensured by using a special acoustic gel. It was shown that the presence of copper powder during cavitation leads to generation of additional hard radiation with the energy in a maximum nearby 3...3.5 KeV (Fig. 4a). When thin copper

foil (thickness 0.1 mm) was situated in front of detector window there is a natural screening of softer part of the spectrum (Fig. 4b).

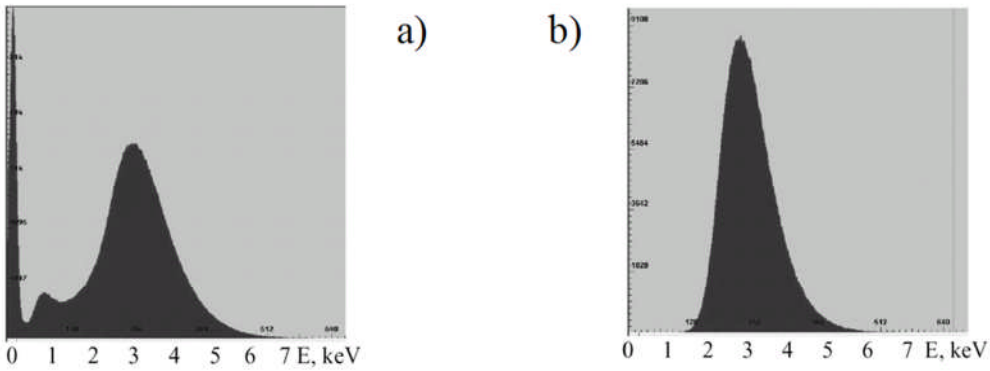

Figure 4. Spectrum of X-Ray radiation outside of the chamber during cavitation in the presence of: a) copper powder, mechanically and acoustically connected with its external surface; b) the same powder and additional thin copper absorber which has not been mechanically connected with the chamber.

2.2. Investigation of space distribution of X-radiation sources

We have studied the dependency of intensity of the hard part of X-radiation J(x) on the distance between the detector window and the surface of the chamber that was covered by copper powder. A schematic of the experiment and resulting dependency J(x) are presented in Fig. 5.

From Fig. 5 it follows that maximal intensity of X-radiation correspondents to $x_{opt} \approx 3.5...4$ cm.

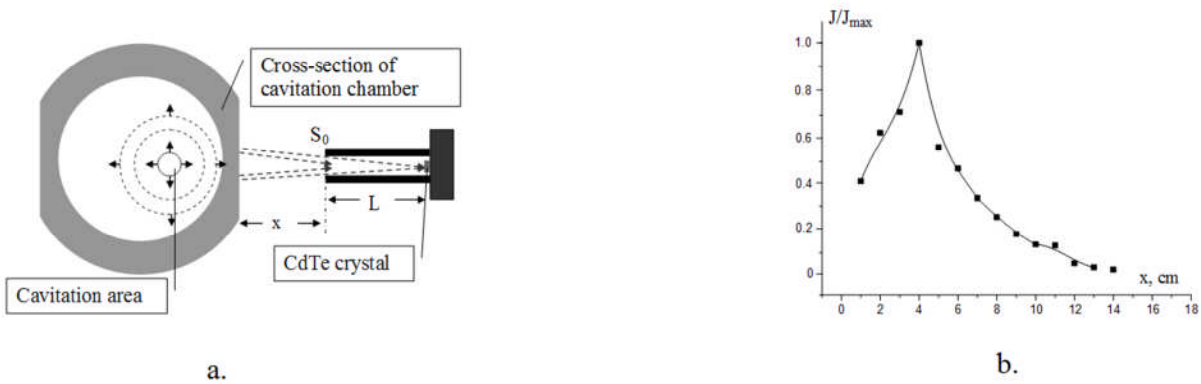

Fig. 5. Schematic of experiment. a) and the dependency of the X-ray registration intensity J(x) on the distance between the detector and the surface of cavitation chamber b).

Let us consider the same effect from another point of view. This dependency J(x) is described by the obvious expression $J(x) = J(0)\{1 + x/L\}^2 e^{-x/\bar{l}}$ ($\bar{l}$ - absorption path of X-quanta in air).

From this formula it follows that maximal intensity of registered X-rays will be at the distance $x_{opt} = 2\overline{l} - L > 0$. From the last equation we have $\overline{l} = \left(x_{opt} + L\right)/2 \approx 4cm$. In air such value of $\overline{l}$ corresponds to the energy of X-radiation E_X≈3...3.5 keV that was earlier independently determined by the detector!

So the sources of X-radiation really really are situated on the chamber surface.

2.3. Investigation of acoustic impulses generated by cavitation bubbles in the running liquid

To measure the acoustic impulses on the surface, a piezoelectric converter with a diameter of 20 mm and an oscilloscope were used. This converter was attached to a flat surface of the chamber. Figure 6 shows a time sample of acoustic converter signal with the duration of 100 microsecond at P = 37 atm and T= 37^{o}C, and the spectrum of this sample. The averaged amplitudes of acoustic impulses of pressure on the surface are δx≈200-300 A.

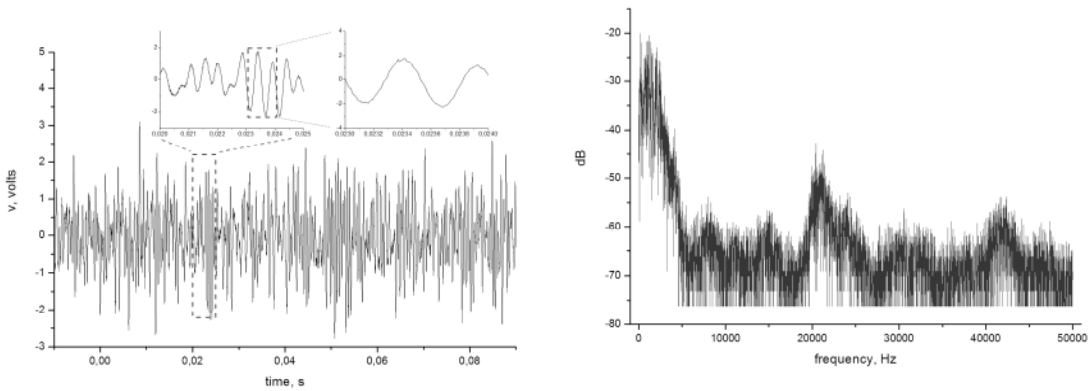

Figure 6. Time sample of the acoustic impulses on the surface of the cavitation chamber a) and Fure-spectrum of the sample b)

2. Combined both cavitation and shock wave mechanism of the generation of characteristic X-ray radiation outside the strongly absorbing cavitation chamber

The typical evolution of any bubble cavitation process in unbounded liquid is described by a strict succession of the physical processes: a) formation of micro-nucleus of a gas bubble in the compressed liquid; b) the beginning of growth of a gas bubble in the tensioned liquid; c) growth phase of a gas bubble (growth speed of the bubble is less than the speed of sound); d) the phase of unstable balance at the maximum size of the bubble; e) the phase of bubble collapsing (the speed of squeezing is more than the speed of sound); f) the collapse ends with an explosion and the formation of a divergent shock wave with supersonic speed.

The same process takes place in the liquid stream moving through the thin channel in the volume of the cavitation chamber (Fig. 7). Interaction of divergent shock wave with internal surface of thick wall of cavitation chamber leads to the formation of a sound wave inside wall that transforms to the shock wave at this wall. Subsequent reflection of this shock wave from

the external surface of thick wall leads to surface atoms excitation and external X-Ray generation.

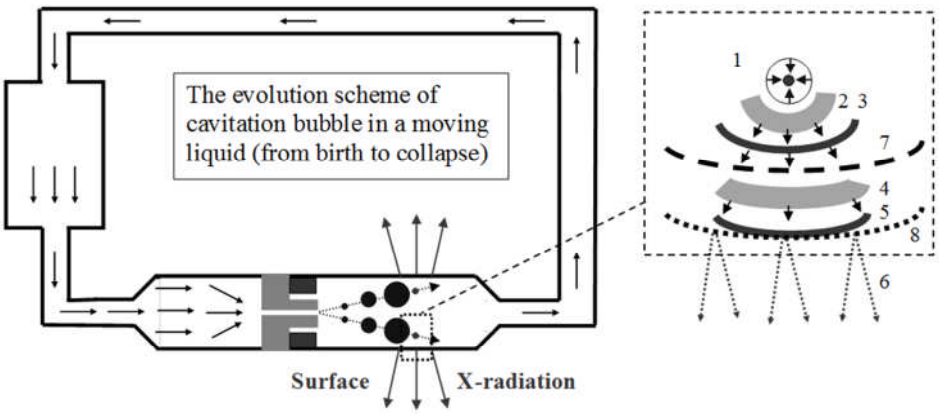

Figure 7. Schematic of transformation of the energy of bubble cavitation collapse to the outside X-ray radiation: 1) - cavitation collapse; 2) acoustic impulse; 3) shock wave in liquid; 4) formation of elastic wave in the wall of the cavitation chamber; 5) shock wave in the wall of the cavitation chamber; 6) excitation of surface atoms of the cavitation chamber during the reflection of shock wave; 7) and 8) internal and external surfaces of the cavitation chamber wall.

The process of atom excitation from the action of a shock wave is the result of atom pulse acceleration during the reflection of shock wave from the border between chamber wall and air. This effect may be calculated by the theory of abrupt acceleration. The probability of atom excitation (e.g. $1s_0 \rightarrow 2p_0$) at abrupt acceleration from v=0 to the velocity of shock wave $v=v_{sw}$ is the following:

$$W_{100,210} = \left| \int_V \Psi^*_{100}(\vec{r}) \Psi_{210}(\vec{r}) e^{imvz/\hbar} dV \right|^2 = \frac{9}{32} \frac{\left(v_{sw}/v_{100}\right)^2}{\left\{9/4 + \left(v_{sw}/v_{100}\right)^2\right\}^6} \approx 2.2 * 10^{-3} \left(\frac{v_{sw}}{v_{100}}\right)^2,$$

$$\vec{r}' = \vec{r} + i\vec{e}_z vt,\ v_{100} = Ze^2/\hbar \approx 2.3 * 10^8 Z \ \ cm/s$$

At intermediate pressure (P=25...60 atm) the liquid jet touches the internal surface of the chamber wall. It leads to the passing of the energy from the cavitation area across the running liquid and chamber wall to atoms situated on the external surface of the chamber and to the external X-Ray radiation.

At high pressure (P≥80...90 atm) the liquid jet does not touch the internal surface of chamber wall and the cavitational shock waves leads (through the reflection from the jet-vacuum border) to the excitation of liquid jet surface atoms and to the subsequent generation of optical and X-ray radiation in the jet. This generation was observed in our earlier experiments (see Fig. 2d).

References

1. A. I. Koldamasov, Hyun Ik Yang, Denis B.McConnell, A.A.Kornilova, V.I.Vysotskii, A. V. Desyatov //12th CMNS Proceedings, Japan, p. 97-107.
2. A. A. Kornilova, V. I. Vysotskii, A. I. Koldamasov, Hyun Ik Yang, Denis B. McConnell, A. V. Desyatov //Surface, № 3 (2007) p. 55-60.

Introduction to Materials

The outcome of a LENR experiment depends on several major things, the scientist conducting the experiment, the procedures employed, the equipment for the experiment and the materials within the experiment. All of these things are important. The skill, experience, intuitions and hard work of the experimenter are clearly critical. The protocols used during an experiment, such as the time history of applied voltages, also largely determine the results. The performance, stability and precision of the apparatus greatly influence the outcome. And, materials are absolutely central to any LENR experiment. What happens to the matter and energy put into the system depends on the contents of the experimental system. Adequately characterized materials constitute one of the most critical and most vexing aspects of LENR. It is not agreed if the LENR effects arise only on surface or at boundaries or if they are a bulk property or even what is the appropriate scale of consideration – nuclear, atomic or both.

Whether the LENR experiment is electrochemical, gaseous, plasma or a beam in terms of loading hydrogen isotopes into lattices, the elemental and molecular materials within the central cell can vary widely, and are both difficult to know and control. Knowledge and manipulation of low levels of impurities are particularly difficult.

Beam experiments are conducted in vacuum systems that can be pumped to very low pressures and heated to drive off many impurities. They, along with gas permeation experiments with one side of the Pd or other foil in a vacuum, are generally the cleanest LENR experiments. The incident beams are carefully controlled in direction and energy. Hence, even though they carry much kinetic energy, they usually do not make the experiment “dirty”. Spectroscopic and other tools can be used to perform qualitative and quantitative analysis of impurities *in situ* before, during and after runs.

Plasma experiments are also conducted in vacuum vessels. They are first pumped down, and then filled with low pressures of the gases, which will be ionized to form the plasma. In LENR experiments, the plasmas are commonly a glow discharge but sometimes an arc discharge. Many of the analytical tools applicable to vacuum systems can be used for analysis of plasma loading experiments. Others, like optical spectroscopy, are very useful for monitoring plasmas. However, the ions and photons in and from plasmas go off in most directions. Their impact with nearby solids, including the materials to be loaded with H or D, leads to sputtering and contamination of the experiment.

Gas loading experiments are usually conducted in a strong vessel that can be pressurized and heated. Such vessels can be purged, cleaned and filled with high purity gases prior to experimental runs. The thermal energies in such experiments are relatively low compared to beam and plasma experiments. Here again, many *in situ* diagnostics can be brought to bear. However, some incisive analytical methods require vacuum conditions for their operation, so they are excluded from use in gas experiments when the gas is present.

Electrochemical LENR experiments can be relatively clean if great care is taken to start with clean equipment and high purity chemicals are used. Both light and heavy water with high purity are available. And, the salts that dissolve to form the electrolyte can also be obtained

with few impurities. However, the container that forms the cell and any other materials in contact with the electrolyte can provide contamination. The range of diagnostics that can be used within electrochemical cells during their operation is more restricted than in the other types of loading. There is no agreement on what purity is required. For example, the original experiments suggested that materials that were too pure did not produce FPE heat. Subsequent work has found that stress induced by loading hydrogen causes the metal to crack and that low levels of alloying elements can prevent cracking.

The “joker” in all of these types of loading approaches is the solid material(s) put into the heart of the experiments, the materials in or on which the LENR occur. They vary greatly in their composition, that is, the elements present and their spatial distributions, both of which can change with time. And, the structural arrangements of the atoms on nano-, micro- and macro-scales before, during and after an experiment also vary widely. The interactions of the experimental protocols with the composition and structure of the cathodes, other electrodes and probes within experiments are both central to the outcome and poorly known in most cases.

Impurities from any source might either promote or degrade production of excess power. They could be deleterious to the point of poisoning an experiment. Or, they might be beneficial to the extent of enabling power production. These very fundamental possibilities are little explored and essentially not understood at this time.

That features of key materials in LENR experiments are not known adequately should not be surprising. After all, nuclear reactions take place on size scales of femtometers, the metric for nuclear dimensions. This scale is 100,000 times smaller than the scale of atoms. Nanometers are the scale at which proper conditions for the occurrence of LENR probably take place. But, the tools of nanotechnology for determining the type and locations of atoms and molecules are yet to be widely brought to bear on LENR experiments. Part of the reason is lack of funding. But, even if atomic force microscopes and other atomic-scale probes were available for analyses before, during and after runs, there is the problem of their small fields of view. It is likely that LENR do not occur uniformly over the surface of a cathode in, say, an electrochemical experiment. Repeated scanning of a small patch, typically 100 micrometers square or smaller, with an AFM could miss the locations of LENR, either by bad luck or because the probe destroys the critical conditions. The situation could be like the old story of looking for lost keys at night only under the street lights. In short, the composition and structure of cathode materials on the nano-meter scale is probably critical to production of LENR, but very difficult to access experimentally in a meaningful way.

Three papers on materials were given at ICCF-14. They are the result of collaborations between scientists from three laboratories, ENEA in Italy and the Naval Research Laboratory and SRI International in the US. The collaboration of these three laboratories, which reported their current results in an on-going program, represents the most thorough approach to the study of materials in this field.

The first paper on materials was an invited presentation by Violante *et al*, which involved correlations between impurities, metallurgy of Pd foils, loading (D/Pd) and production of excess heat. It was found that contaminants control the crystal orientation during annealing of

the foils, and the effects of subsequent chemical etching. The power spectral density (PSD) is a measure of the magnitudes of roughness on the surfaces of the foils. It was measured after etching. Samples that produced excess power had peaks in the PSD in the range of 10^6 to 10^7 m^{-1}. That is, surface roughness in the range of 0.1 to 1 micrometer favored production of excess heat. Further, it was reported that the surface crystallite orientation of <100> also favored power production. The <100> face in Pd is the most open crystallographically, which might help with loading and the occurrence of LENR.

The second materials paper by Sarto *et al* provided details of the characterization of Pd foil surfaces. The data were obtained by use of an Atomic Force Microscope (AFM). This is one of the very few instances when that central tool of nano-science and –technology has been use for materials in LENR experiments. The data obtained by 2-dimensional square scans of the foil surfaces, generally 24 micrometers on a side, was used to compute PSD. The foils were then used in electrochemical calorimetric experiments to test their ability to produce excess heat. The results were stated in the last paragraph above.

The third paper on materials from the tri-laboratory collaboration by Castagna *et al*, gave details of the metallurgical treatment of the Pd foils and the measurements of their surface texture, that is, the orientation of surface grains. Correlations between the ability to produce excess heat and several materials parameters were obtained. They include mean grain size, grain orientation, grain boundaries, hardness, and deuterium loading. This is the work that showed <100> crystallite orientations favored production of power.

Miley and his colleagues presented a materials paper on the evidence for the formation of clusters of deuterons at dislocations within Pd cathodes in heavy-water electrochemical experiments. Such nanometer-scale features are thought to be the locations at which LENR occur. Hence, their increase is desirable. These authors discuss ways in which the density of deuteron clusters can be increased, which they call a “Roadmap to Power Cells”.

Swartz and Verner provided a paper on the spiral cathode (called a Phusor™) used in their electrochemical experiments. The paper makes the case that the spiral structure is a metamaterial. Such a material gets its electromagnetic properties from the structure (shape) of the material, rather than from its chemical composition. The authors report that their cathode shape is the best among many designs and variations for reproducible behavior with good power gains, and that such is the case for several Group VII metals. The electric fields associated with the spiral cathode were computed. The authors focus on the intra-electrode flux of deuterons, which is due to the electrical field distributions that cause asymmetric deuteron entry into the cathode. The authors believe that such deuteron fluxes are necessary to produce LENR.

The papers on materials presented at ICCF-14 illustrate the complexity of the study of materials for LENR experiments. There are many options for acquisition of the base materials, processing prior to experiments and conduct of the experiments. Numerous experimental tools are available for the characterization of the materials at any step in the overall process, and after experiments. Sophisticated and expensive equipments, which generally require skilled scientists for their operation and interpretation of the data obtained, are needed. The work is

slow and requires great attention to details. Hence, the study of materials for LENR experiments is costly. Few research efforts in LENR have the funds to carry out these desirable characterizations of materials.

Material Science on Pd-D System to Study the Occurrence of Excess Power

V. Violante[1], F. Sarto[1], E. Castagna[1], M. Sansovini[1], S. Lecci[1], D. L. Knies[2], K. S. Grabowski[2], and G. K. Hubler[2]

[1] *ENEA Frascati Research Center, Frascati (Rome) 00044 Italy*

[2] *Naval Research Laboratory, Washington DC 20375 USA*

Abstract

A recent joint work [1] identified the crucial role of material science in improving control of the Pd-D system to enhance the production of excess power during electrochemical loading of palladium foils with deuterium. Very high reproducibility, close to 100%, in loading Pd up to D/Pd ~1 (atomic fraction) was achieved. High loading about the threshold value of 0.9 is considered necessary to achieve the effect. This work demonstrated it is necessary but not sufficient. As a consequence, the focus of our research moved to the material properties of cathodes, especially surface characteristics, and an effort to correlate these properties with cathode performance during electrolysis. This paper describes the material properties examined that appear to produce excess heat.

Introduction

Recent evidence indicates that the Pd material plays a fundamental role in the occurrence of excess heat production during electrochemical loading of palladium cathodes with deuterium. This evidence has created a mounting interest in aspects of research related to material science.

A broad effort was carried out in the past to identify the mechanisms controlling hydrogen isotope dissolution into the palladium lattice during the loading process. The study helped define a proper metallurgical treatment to obtain the most suitable metallurgy to facilitate hydrogen absorption into the palladium cathode [2]. This work generated almost 100% reproducibility in achieving a deuterium concentration larger than 0.9 (atomic fraction) that is considered to be the threshold value for observing the effect.

This experimental work also demonstrated that the concentration threshold is a necessary condition for excess heat production, but not necessarily a sufficient one. Such evidence led to a systematic effort to improve knowledge about the status of the material that is required to have the effect.

Let us start from the most significant experimental evidence obtained from a statistical analysis of the data. Three different behaviors were observed with Pd cathodes loaded above the threshold D/Pd = 0.9:

(1) High power gain during the excess.
(2) Low power gain during the excess.
(3) No excess.

McKubre identified two types of excess power production:

> Type A: excess power begins after several days of electrolysis and, in general, depends on the current density.
>
> Type B: excess begins very soon and does not always depend on the current density.

The research described in this work is largely oriented to studying the main differences in materials that produce these two different types of excess power.

Lot-1 and Lot-2

Two different lots of palladium, obtained from the same producer, exhibited remarkably different behavior during the experiments, even though both lots underwent the same metallurgical procedures.

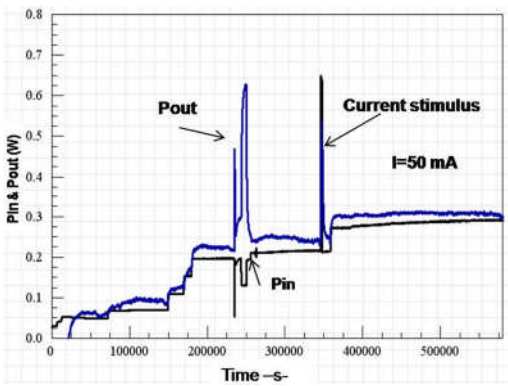

Figure 1. Experiment L17, evolution of input and output power: excess 500%

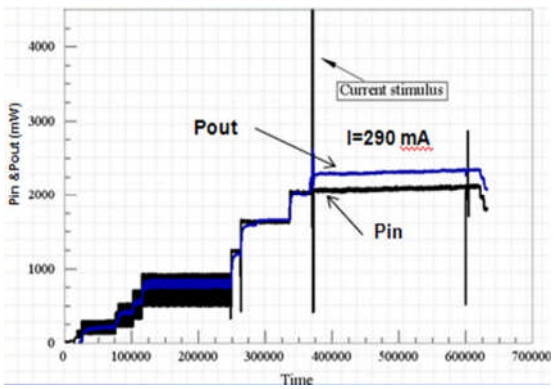

Figure 2. Evolution of input and output power in experiment L39

These two materials served as references in the investigation to identify material that produces the Fleishmann-Pons (FP) effect. The two lots are designated Lot-1 and Lot-2. Lot-1 gave Type B excess power with, in some cases, power gains well above 100%. Figure 1 shows the evolution of the input and output power in experiment L17, performed with a sample from Lot-1. During the main burst that continued long enough to allow the calorimeter to reach a fairly steady state condition, the power gain was up to 500%. The reduction of the input power during the burst occurred because the excess power increased the electrolyte temperature, causing a reduction of impedance of the electrolyte, so that the galvanostat reduced the voltage to maintain the current at the set point value. This lot successful produced excess heat in 75% of tests at SRI and up to 60% at ENEA.

Different behavior was produced by samples from Lot-2. As mentioned above, this lot was obtained from the same producer and had identical characteristics and purity (both 99.95%). Lot-2 gave Type A behavior with excess power of less than 20%. Loading up to the threshold

level required higher current compared to samples from Lot-1, and the reproducibility of excess power production was lower (less than 20%). Figure 2 shows evolution of the input and output power in the experiment L39, performed with Lot-2 material.

Such an experimental difference, based on a significant number of experiments (more than 40), led to a comparative analysis of both raw as-received samples and samples following metallurgical treatments. The first test was a qualitative check for the spectrum of contaminants in the two lots. Fig. 3 shows such a spectra, obtained with SIMS analysis (with sputter erosion). It is evident that some species that are completely absent in Lot-1 are contained as contaminants in Lot-2, for instance Zr. Contaminants may act on grain size, crystal orientation and grain boundaries, so that a different metallurgy may be expected for samples obtained from the two different raw materials, based on differences in the spectra of contaminants.

Scanning electron microscopy (SEM) performed on samples obtained from Lot-1 and Lot-2 after the same treatment steps are confirming this effect. Fig. 4 and Fig. 5 show the metallurgy of samples obtained from Lot-1 and Lot-2, respectively. The main difference is the grain size, being larger for the sample from Lot-1. This difference may be ascribed to the different spectrum of contaminants, with Lot-1 containing fewer grain boundary pinning constituents.

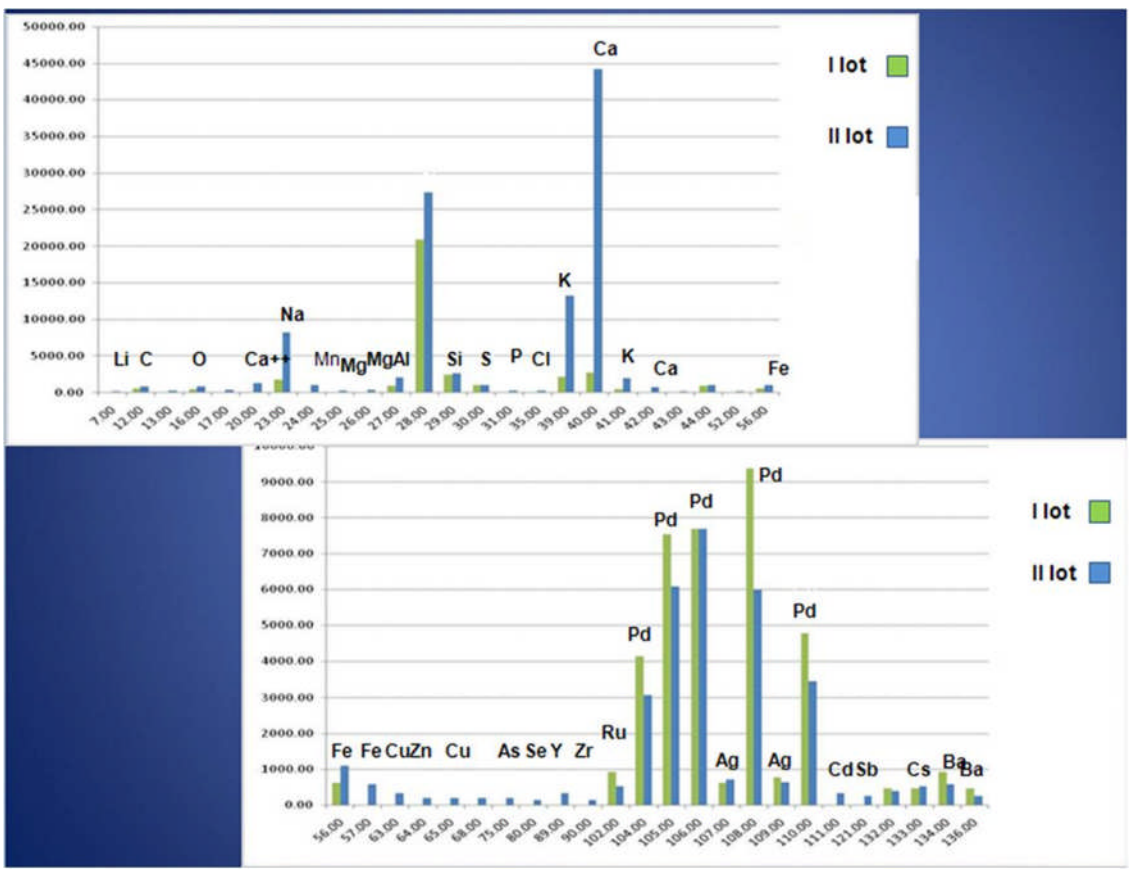

Figure 3. Spectra of impurities for Lot-1 and Lot-2, qualitative analysis (SIMS with erosion)

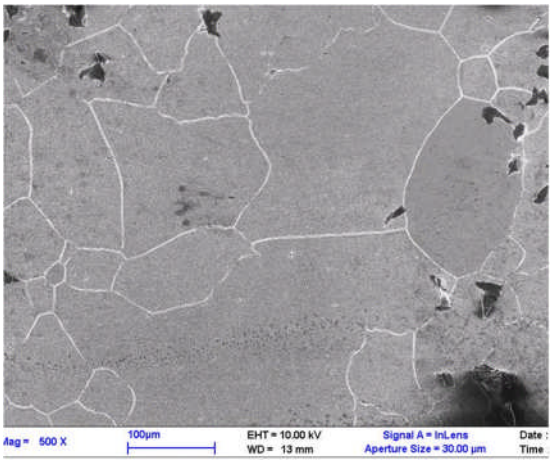

Figure 4. SEM microscopy of a sample from Lot-1

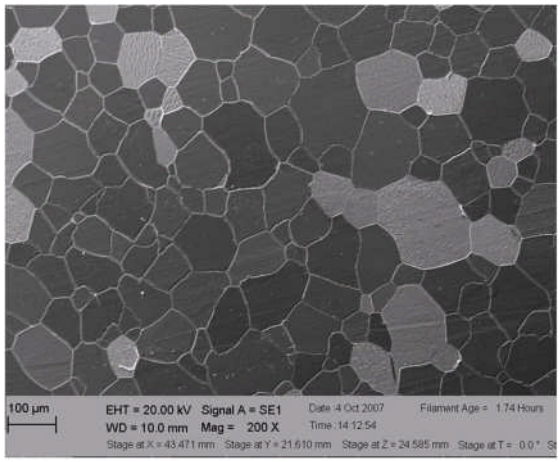

Figure 5. SEM microscopy of a sample from Lot-2

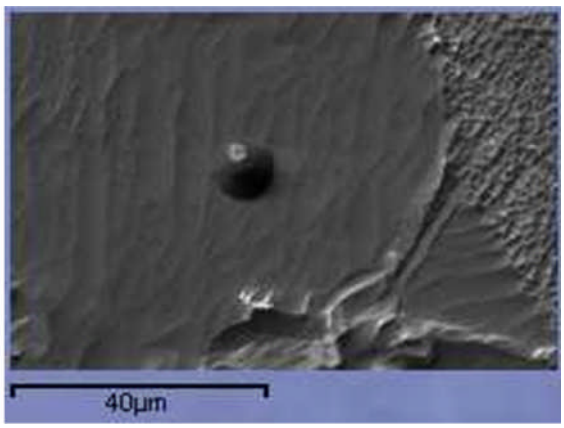

Figure 6. Effect of an iron particle on etching

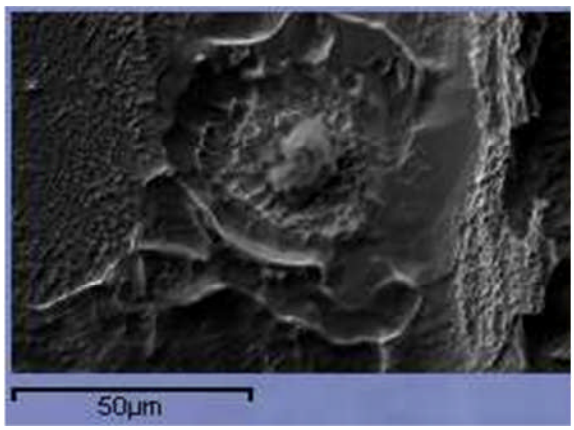

Figure 7. Effect of a dust particle on etching

Crystal orientation after metallurgical treatment was studied by means of X-ray diffraction. The results for Lot-1 indicated these samples to have a well-aligned <100> surface normal, as shown by very sharp X-ray spectra with little or no <110> present. Lot-2 samples had a mix of <100> and <110> surface normals, with the spectra not as sharp as for Lot-1. A third lot of material with a different spectrum of contaminants underwent the same metallurgical and thermal procedure, yet revealed instead mostly <110> and very little <100> surface normal orientation. Cathodes fabricated from this third lot produced no excess power.

A statistical analysis of the collected experimental data revealed that Type B excess power was correlated with <100>-crystal orientation with a correlation factor very close to 0.8 [3]. The different experimental behaviours observed indicate that crystal orientation may be considered a second condition required to produce excess power.

It is very well known from the literature that contaminants modify the effect of chemical etching on surface morphology [4]; Fig 6 and Fig.7 show the effect of etching a Pd sample with either an iron or dust particle, respectively. Also, crystal orientation has an effect on the surface

morphology, and surface morphology as well as crystal orientation has a non-negligible role on electrode kinetics [5]. Observations of different Pd surface activity were identified by Rolison using SEM of etched Pd foils [6].

Material Status and Excess Heat Production

The resulting question is: how do these differences in the status of the material relate to excess power production? The first answer is that the excess power is correlated to the loading dynamics, and the loading dynamics depend on the material status. The evidence is highlighted by the following analysis. Figure 8 shows the ratio between the maximum loading value and the current required for such a loading, an indicator of ease of loading. Cathodes showing good loading at low current, in general, have produced excess power. Furthermore, the easier the loading, the higher the probability is that Type B (red bar) excess power will occur. The correlation factor between the occurrence of the Type B excess heat and easy loading is g=0.813. See ref [3] for additional statistical data.

Preliminary statistics from this report show that:

(1) Contaminants control the crystal orientation during annealing.
(2) Crystal orientation and specific contaminants modify the effect of chemical etching, leading to a different surface status.
(3) The surface morphology modifies the operating conditions in the electrochemical process.

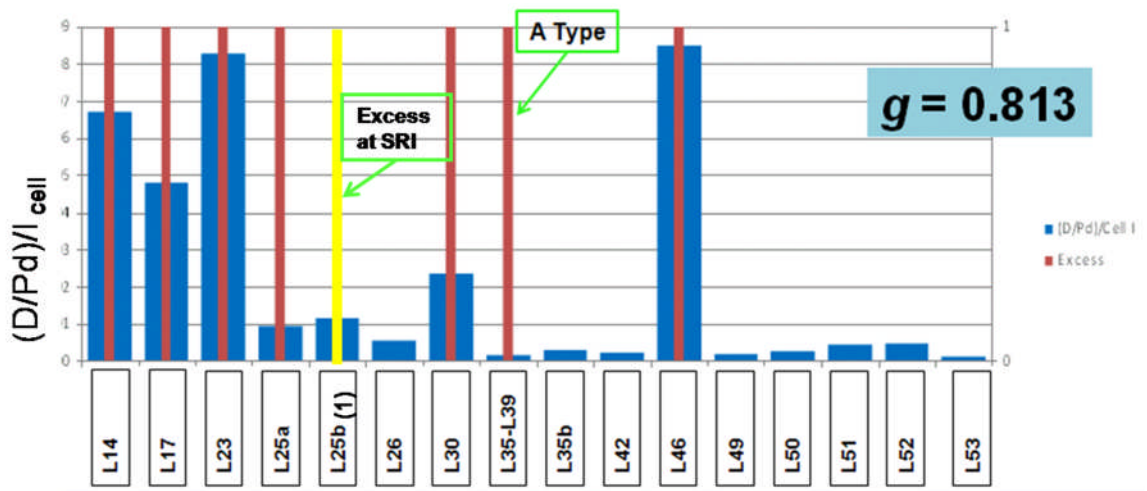

Figure 8. Ratio between the maximum loading value and the current required for such a loading.

We conclude that the status of the surface is a third condition needed to produce excess heat. The Power Spectral Density function (PSD), defined as the squared modulus of the surface roughness Fourier transform, was chosen as a figure of merit representing the status of the surface [7]. The PSD function, after surface etching, was found for samples giving excess power, as in Fig. 9, to have peaks in the wave vector interval $10^6 – 10^7 m^{-1}$. The statistics also revealed that the amplitude of the excess power correlates with the amplitude of the PSD peaks.

On the basis of the results described here, work was carried out to produce material characterized by:

(1) Spectrum of contaminants quite close to the Lot-1 spectrum.
(2) <100> crystal orientation.
(3) Proper metallurgy for easy loading.
(4) PSD characterized by the presence of peaks in the wave vector range $10^6 – 10^7$ m^{-1}.

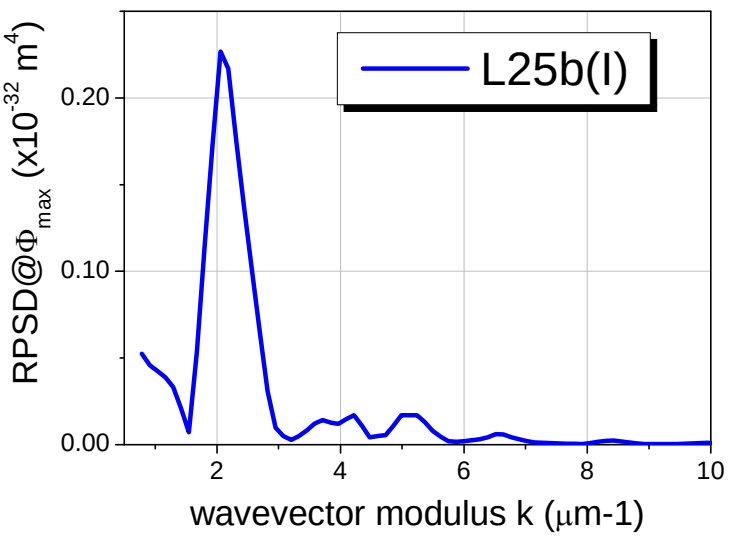

Figure 9. Power Spectral Density (PSD) function of sample L25 producing excess power

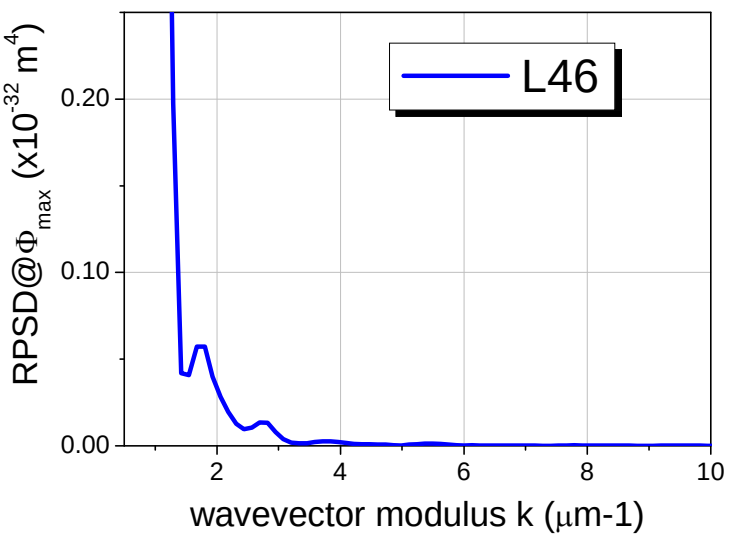

Figure 10. PSD of sample L46, peaks in the identified region are revealed

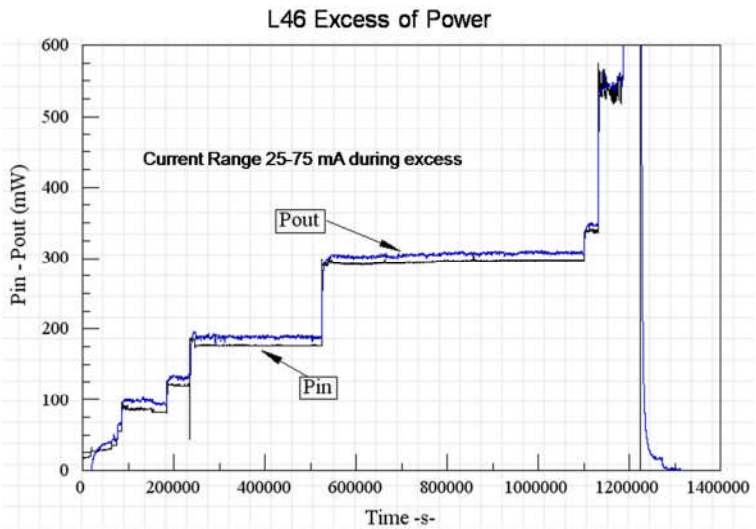

Figure 11. Evolution of the input and output power during experiment L-46: Excess up to 12% was observed and the amplitude results to be proportional to the PSD peaks amplitude

These characteristics were achieved with sample L46, and this sample underwent a calorimetric test with heavy water. Figure 10 shows the PSD of sample L46. We observe that the amplitude of the peaks is lower than given by sample L25, which produced excess power up to 250%. As shown in Fig. 8 the loading of sample L46 was satisfactory. The calorimetric result for this sample is shown in Fig. 11. We observed excess power up to 12% that disappeared completely when the input power exceeded 300 mW.

This result is not extraordinary in terms of power gain, but has a non-negligible value since it represents the first reproduced excess power based on a “designed” material. Furthermore, it provides additional evidence that proper surface morphology, combined with appropriate metallurgy for loading, and with <100> crystal orientation is a third condition for producing excess power. Obviously statistics confirming the result is required, and an enhanced surface analysis study should investigate a wider region of the wave vector range.

Conclusions

Characteristics have been identified that cause different cathode behavior. The probability of excess heat is enhanced when three conditions are met:

(1) Loading is easy at a relatively low current density due to proper metallurgy.
(2) <100> Crystal orientation.
(3) Identified surface morphology by PSD.

A sample demonstrating the three conditions was made, and production of excess heat was observed. Work is in progress to identify other correlations and, on the basis of the material characteristics, the mechanisms producing the effect.

Patent

The work is the object of a Joint Patent by ENEA, NRL, SRI and Energetics Technology.

References

1. V. Violante, et al. "*Calorimetric results of ENEA cooperative experiments*" Proc. XIII Int. Conference on Cold Fusion, Sochi (Ru) June 2007 (in press).
2. De Ninno, A. La Barbera, V. Violante "*Consequences of lattice expansive strain Gradients on hydrogen loading in palladium*" Phys. Rev. B. (1997) **56**, 5, 2417-2420.
3. E. Castagna et al., "*Metallurgical characterization of Pd electrodes employed in calorimetric experiments under electrochemical deuterium loading*" Proc. ICCF14, Washington D.C. 10-15/August/08.
4. M.A. Gosàlvez and R.M. Nieminen, New J. Phys. (2003) **5**, 100
5. M.T. Spitler, Electrochimica Acta (2007) **52**, 2294–2301
6. D. R. Rolison and P.P. Trzaskoma, J. Electroanal. Chem. (1990) **287**, 375
7. F. Sarto et al., "*Electrode surface morphology characterization by atomic force microscopy*," these proceedings

Electrode Surface Morphology Characterization by Atomic Force Microscopy

F. Sarto[1], E. Castagna[1], M. Sansovini[1], S. Lecci[1], V. Violante[1], D. L. Knies[2], K. S. Grabowski[2], and G. K. Hubler[2]

[1] *ENEA Frascati Research Center, Frascati (Rome) 00044 Italy*

[2] *Naval Research Laboratory, Washington DC 20375 USA*

Abstract

The introduction of hydrogen into a metal during electrolysis of water involves primarily the metallic surface. The effect of surface morphology on electrochemical reaction kinetics is well described in the literature [1] therefore it seems to be reasonable to assume that the surface morphology of the cathodes could play a role in the electrochemical metal-hydride formation. Actually, a wide variety of surface features and profiles have been observed in the Pd cathodes typically employed in excess heat production experiments. These features are noted in both the as-prepared samples and the electrolyzed ones. In order to establish a correlation between the occurrence of a particular surface morphology and calorimetric results, it is necessary to identify a useful metric with which to describe and compare the different surface morphologies. In this work an approach based on Atomic Force Microscopy (AFM) has been investigated. The method is oriented toward the identification of parameters suitable for a pre-screening of the materials.

Introduction

In recent years we have begun a research project focused on the study of the material science aspects of cold fusion. In particular, the preliminary results have pointed out a strong correlation existing between the metallurgical and surface properties of the Pd cathodes used in electrochemical experiments, and the occurrence of excess heat production [2]. We investigated cathode features including both bulk features (crystallography, deuterium loading, electrochemical behavior, hardness) and surface characteristics.

In this paper, we concentrate on the study of the surface morphology of the Pd electrodes, leaving the other aspects of material science to other papers [3],[4]. In particular, we limit our analysis to the length scale of a few micrometers, which characterizes the surface morphology "inside" each crystal grain. Grain boundary features fall outside this range, and they have been considered elsewhere [3],[4].

The experimental analysis has been carried out by Atomic Force Microscopy (AFM). This technique [5] is able to collect tri-dimensional surface morphology maps, with spatial resolution up to a fraction of a nanometer. The digitized images have been elaborated to extract numerical parameters and parametric functions, which could make the comparison between the various samples easier and more objective. The numerical procedure, based on the computation

of Fourier transforms, aims to define a surface status function that can describe and compare the surface morphology of different samples, and also to outline correlations between the surface morphology and the excess heat production.

Experimental

The Pd samples investigated in this work were obtained from different commercial lots of pure Pd, having nominal purity above 99.95%. They have been processed by mechanical, thermal and chemical treatments described elsewhere [2], in order to reduce foil thickness to about 50 μm, and to improve metallurgical properties and surface morphology. Most of the samples were mapped by AFM before being electrolyzed, to avoid measurement problems caused by dirt on the surface. Actually, surface morphology changes have to be expected during the electrochemical process and, obviously, this modified morphology plays a role in the excess heat mechanism. By measuring the samples before electrolysis instead of after it, we are mainly interested in establishing a correlation between the initial cathode characteristics and the occurrence of excess heat, with the aim of developing instructions for "good" cathode manufacturing.

For each sample, several images have been taken at different points on the surface, excluding zones close to grain boundaries. The AFM instrument (Assing Corp., "Perception" model) is installed at the ENEA laboratory at the Frascati research centre. The instrument is equipped with a pyramidal silicon nitride probe (Veeco, MLCTAU) and is operated in contact mode. Comparison between samples has been performed by using images that were acquired on the same length scale (typically 24×24 μm^2) and with the same number of pixels (typically 257×257), to avoid experimental and/or numerical artifacts that could affect different samples to varying extents.

Image analysis

The AFM directly measures the 3-D surface height profile of the sample surface. This is different from images acquired by other microscopic techniques, such as scanning electron microscopy or optical microscopy, in which the contrast is not directly related to the changes in height profile, and 3-D profile reconstruction requires stereoscopic methods. The height profiles of non-engineered surfaces, as those of the samples investigated in our study, are generally characterized by random fluctuations superimposed on periodic or quasi-periodic patterns. These surface features are hard to recognize in direct space, but can be effectively revealed in reciprocal space of the spatial frequencies *(kx, ky)*, by computing the Power Spectral Density (PSD) of the height profile. The PSD function provides a decomposition of the surface profile into its spatial wavelength components. Mathematically, the PSD (that we indicate in the following as $PSD_{2D}(kx, ky)$) is defined as the squared modulus of the Fourier transform of the 2-dimensional surface height profile (than we indicate as $h(x,y)$). Assuming the surface profile to be the result of the linear superposition of an infinite ensemble of sinusoidal profiles, each with a different periodicity along the *x* and *y* axis directions, the PSD indicates the weight of each sinusoidal component having a precise periodicity, as a function of the spatial frequencies, which correspond to the inverse of each period length. As an example, a surface characterized by an infinite sinusoidal profile has a PSD spectrum consisting of just one

fundamental peak; on the other hand, a random surface has a PSD spectrum extending over a broad range of spatial frequencies.

Commercial software for image processing is commonly suited for computing the 1-dimensional PSD of isotropic and stationary random surfaces. In that case, the surface profile fluctuations measured along any straight path of the surface are assumed to be independent of both the path direction and origin, so that the 2-dimensional PSD reduces to a 1-dimensional function ($PSD_{1D}(|k|)$), which depends only on the modulus of the frequency vector 5.

In the case of anisotropic and textured surfaces, the computation of the 1-dimensional isotropic PSD may wash out the information about embedded patterns and periodicities, if the computational path is not carefully chosen, and it also cannot outline the height profile anisotropy. This is indeed the case for the samples studied in our work, which are characterized by a strongly anisotropic texture, related to the crystalline structure of the grain. To solve this problem, we have developed software to compute, from the 2-dimensional PSD, a set of 1-dimensional PSD functions, which can give insight also in the anisotropy of the surface, extracting the more relevant patterns. These additional functions are defined below, starting from a representation of the 2-D PSD in polar coordinates ($PSD_{2D}(|k|, \phi)$, where $(|k|, \phi)$ are the polar coordinates of the reciprocal 2-D *k*-space) instead of Cartesian coordinates ($PSD_{2D}(kx, ky)$):

- The Radial Power Spectral Density ($RPSD(|k|)$), is the average of the polar 2-D PSD ($PSD_{2D}(|k|, \phi)$) over all polar angles (ϕ);
- The Angular Power Spectral Density ($APSD(\phi)$), is the average of the 2-D $PSD_{2D}(|k|, \phi)$ over all *k* moduli, along the direction of each *k* polar angle ϕ.
- The Maximum Radial Power Spectral Density ($R@\phi_{max}(|k|)$) is obtained by taking the values of the 2-D polar Power Spectral Density along the *k* vector direction identified by the polar angle ϕ_{max}, which is the abscissa for the maximum of the $APSD(\phi)$ curve.

In Fig. 1 the 2-D k vector space is represented in polar coordinates, and the domains involved in the computation of the Radial (Fig. 1a), Angular (Fig. 1b) and Maximum (Fig. 1c) PSD functions are indicated.

The numerical procedure developed to compute the above functions consists of the following steps:

1. The AFM 2-D digital image is converted to a matrix N×N.
2. The $PSD_{2D}(kx, ky)$ matrix is calculated from the 2-D fast Fourier transform (FFT) of the digitized image.
3. The polar PSD matrix ($PSD_{2D}(|k|,\phi)$) is obtained from the $PSD_{2D}(kx, ky)$ matrix, by data interpolation.
4. The Radial, Angular and Maximum Power Spectral Density functions are computed according to the above definitions.

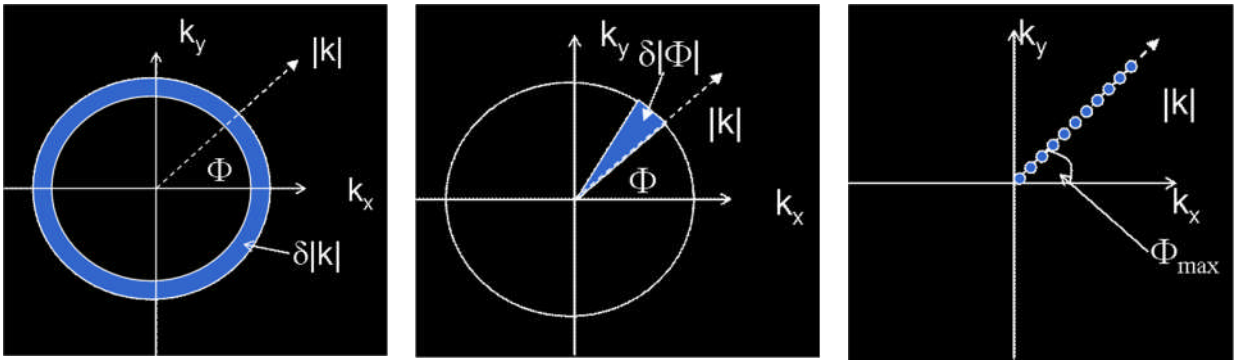

Figure 1. Polar representation of the 2-D reciprocal space in which the 2-D PSD is defined; the light blue areas indicate the domains on which the PSD_{2D} is averaged to compute the Radial Power Spectral Density (Fig. 1a), the Angular Power Spectral Density (Fig. 1b) and the Maximum Power Spectral Density (Fig. 1c).

The analysis has been repeated for different images taken on different sample points (within the same crystal grain), showing similar results within the same crystal grain.

Because of the finite sampling rate and limited scale length of the digital AFM images, the computed PSD functions are band-limited over the space of wave-vectors *k*. In particular, the low frequency cutoff is determined by the scan length, while the high frequency limit is determined by the sampling rate and by the tip geometry. In the present work, the typical wave-vector range is 0.2 – 30 μm^{-1}.

Results and Discussion

The Power Spectral Density spectra of samples giving excess heat have been computed to look for common features. A preliminary screening of the data has outlined a particular "multi-peaked" structure in the Maximum Power Spectral Density function of the samples that gave excess heat (see Fig. 2 right), while this feature was not observed in the samples that did not give excess heat (see Fig. 3 right).

The peak intensities of the analyzed features scale with the peak wave number, which ranges from 1 to 4 μm^{-1}. The similarity in the $R@\phi_{max}(|k|)$ spectrum is indicative of the presence of a pseudo-periodic texture embedded in the surface morphology, with a period in the range of some tenths of microns. Furthermore, as can be seen in Table I, the maximum PSD peak intensity shows a good correlation with the excess heat percentage and reproducibility (when applicable), but it is much lower in the spectra of samples which did not produce excess heat. A similar correlation does not appear to be evident in the specific surface area values, which are shown in Table II and which are scattered less than 10% around the same mean value.

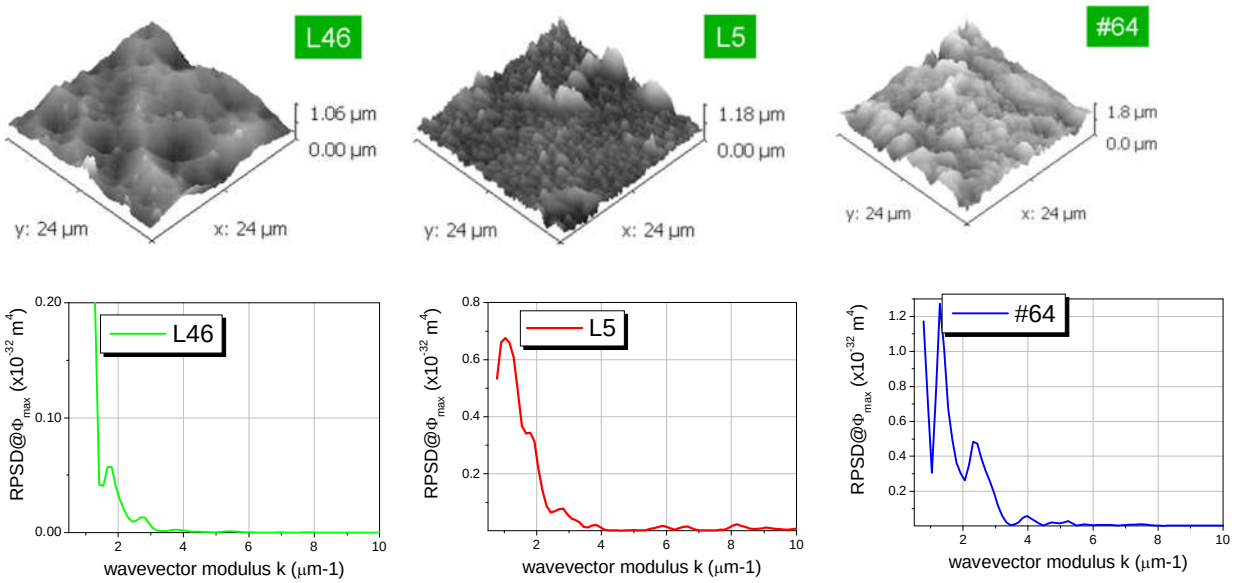

Figure 2. Top: 3-D AFM images of samples L46, L5 and #64, which gave excess heat during electrochemical deuterium loading; Bottom: Maximum Power Spectral Density curves computed from the AFM images shown on the top

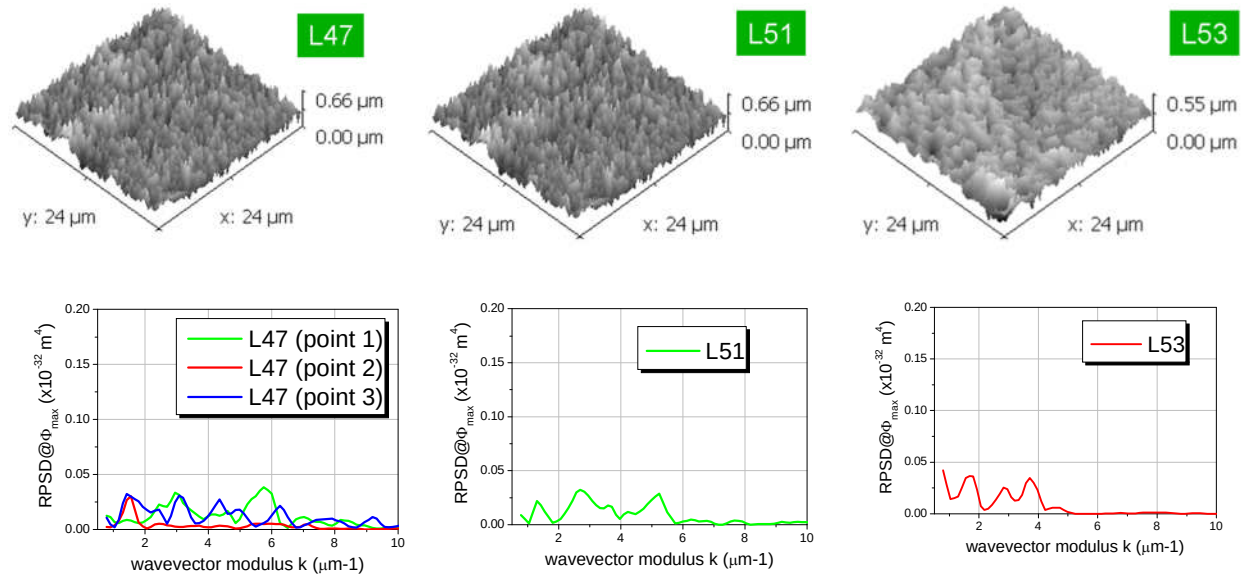

Figure 3. Top: 3-D AFM images of samples L47, L51 and L53, which did not give excess heat during electrochemical deuterium loading; Bottom: Maximum Power Spectral Density curves computed from the AFM images shown on the top; in case of sample L47 the curves obtained by the analysis of three different sample points are also shown.

Table I. Summary of max PSD intensity in the range 1 to 4 μm^{-1} and excess heat data. The second column indicates the excess to input power ratio, the third column indicates the ratio between the number of samples giving excess heat and the total number of experimented samples of the same lot.

Sample	Excess heat %	Reproducibility	Max PSD intensity ($x10^{-32}$ m4)
#64	>1000	2/2	9.5
L5	25-60	2/4	0.7
L46	12	1/1	0.06

Table II. Effective surface area of the studied samples, computed from the AFM images by the free GNU GPL software Gwyddion.

Sample	L46	L5	#64	L47	L51	L53
Surface area (μm^2)	588	653	684	631	640	602

These results suggest that the surface morphology of the Pd cathodes itself plays a role in the excess heat production mechanism. We are not yet able to identify this role, but it cannot be simply reduced to the effect of the change in the specific surface. In this respect, the identified PSD function can be considered as a valid way to estimate the surface morphology.

However, a potential problem with the scale of this method should be noted. The analysis is limited to a small areas of the sample, which may not be representative of the entire specimen. To overcome this problem, a more extended and systematic mapping of the sample surface on different length scales should be done, aimed at eventually discovering scaling behaviors. This may show a relationship, for examples, between the local in-grain morphology and long scale crystal grain distribution. Anyway, even the small-scale investigation has proven to be a worthwhile method, and it has shown the occurrence of a particular PSD spectrum, which we have tentatively identified as a favorable condition for excess heat production, is just one of many other conditions, which involve metallurgical and electrochemical properties of the palladium cathodes 4.

Conclusions

A method of characterizing the surface morphology of Pd cathodes, based on the spatial power spectrum, has been presented. A preliminary screening of the data showed some common features in the spectra of samples giving excess heat, which are not observed in samples not giving heat. The observed features indicate the presence of pseudo-periodic patterns in the surface morphology, whose period is in the range of some tenths of microns. The surface morphology requirement for excess heat is only a necessary condition, not sufficient: other criteria must also be satisfied.

References

1. M.T. Spitler, Electrochimica Acta 52 (2007) 2294–2301.

2. V. Violante, F. Sarto, E.Castagna, C. Sibilia, M.Bertolotti, R. Li Voti, G.Leahu, M. McKubre, F. Tanzella, K.Grabowski, G.Hubler, D. Knies, T. Zilov, and I. Dardik, "Calorimetric Results of ENEA Cooperative Experiments", Proceedings of the *13th International Conference on Condensed Matter Nuclear Science (ICCF13)*, Dagomys, Sochi, Russia June 25 - July 1, 2007
3. V. Violante RdA, E. Castagna, S. Lecci, M. Sansovini, F. Sarto, D.L. Knies, K.S. Grabowski, G.K. Hubler, "Material science on Pd-D system to study the occurrence of excess of power", in these proceedings
4. E. Castagna, S. Lecci, M. Sansovini, A. Rufoloni, F. Sarto, V. Violante RdA, D.L. Knies, K.S. Grabowski, G.K. Hubler, M. McKubre and F. Tanzella, "Metallurgical characterization of Pd electrodes employed in calorimetric experiments under electrochemical deuterium loading", in these proceedings
5. See, for example "Introduction to Atomic Force Microscopy: Theory, Practice, Applications", by Paul West, Pacific Nanotechnology, freely available online: http://www.afmuniversity.org/
6. Duparré. J. Ferre-Borrull, S. Gliech, G. Notni, J. Steinert, J.M. Bennett, Appl. Opt. **41** (2002) pp.154-171

Metallurgical Characterization of Pd Electrodes Employed in Calorimetric Experiments Under Electrochemical Deuterium Loading

E. Castagna[1], M. Sansovini[1], S. Lecci[1], A. Rufoloni[1], F. Sarto[1], V. Violante[1], D. L. Knies[2], K. S. Grabowski[2], and G. K. Hubler[2], M. McKubre[3] and F. Tanzella[3]

[1] *ENEA Frascati Research Center*
Frascati (Rome) 00044 Italy
[2] *Naval Research Laboratory*
Washington, DC 20375 USA
[3] *SRI International*
Menlo Park CA USA

Abstract

A systematic approach has been followed in the production and characterization of Pd foils to be used in excess heat production experiments [1][2][3]. Starting with a metal foil as supplied, palladium samples have been fabricated and characterized in a step by step process, and then subjected to electrolysis deuterium loading. The characterized metallurgical properties include the main grain size, the grain boundary, the material Vickers hardness, and the crystal grain orientation. Electrochemical properties that are recorded include the D/Pd loading ratio and the D/Pd low current loading ratio. A suitable correlation parameter has been defined and correlations have been found between excess heat production and individual properties; i.e. the mean grain size, grain boundary, material hardness, crystal grain orientation, deuterium loading and low-current deuterium loading level.

Introduction

A great deal of experimental evidence indicates that the reproducibility of excess heat production is strongly controlled by the cathode's material properties. To achieve deeper understanding of the phenomenon, a systematic characterization of the metallurgical properties and loading behaviour of Pd cathodes used in excess heat experiments at different laboratories (ENEA, SRI, Energetics Technology), has been performed. A central role in the improvement of the study is the development of a tool for experimental data organization and storage; i.e. a database including all the information collected for each sample. The data is rigorously organized and easily retrieved and compared.

Data analysis aimed to look for correlations with excess heat production. A statistical approach has been followed, as the role played by each material-related issue is not known yet, and an exhaustive theoretical explanation has not been devised.

Experimental

Starting with the metal foil from the supplier, palladium samples have been produced and characterized in a step by step process before being subjected to an electrolysis deuterium loading experiment.

Cathode Manufacturing

Cold rolling and annealing create an optimized metallurgical structure of the material, which increases deuterium loading. The raw starting material was palladium foil 1 mm thick able to reach a loading ratio of about 0.75 - 0.8 hydrogen/palladium atomic ratio.

The initial treatment was done in two steps:

(1) Cold rolling of the raw material produces Pd foils 50 microm thick.
(2) Annealing at temperatures ranging from 800 to 900°C for about 1 hr.

The resulting foils are rectangular, about 20 mm long and 10 mm wide, with a thickness of about 50 μm. These strips are cut into 40 mm long pieces, to make cathodes with appropriate dimensions. Then the samples are chemically etched using nitric acid and aqua regia. This is done to clean impurities from the surface which can contaminate it during the cold rolling and annealing, and also to activate the surface, making it easier for hydrogen to diffuse into the metal lattice. From a metallurgical point of view such treatment reveals material surface morphology, allowing the SEM observation of the grain dimension distribution in the sample. Surface chemical etching is also one of the suitable methods to obtain the required surface roughness.

Cathode Characterization

Because the origin and preparation of the cathode is crucial to the outcome of the experiment, each step in the process should be recorded for each sample. We do this with a protocol for the sample designation. For example, the cathode designated *L54(189-227)RAEF* indicates the following: *L54* is the rolling run; *(189-227)* indicates the sample position inside the original rolled stripe; *R* stands for “rolling performed”; *A* for “annealing performed”; *E* for “etching performed”; and *F* is the deuterium loading specification (i.e. in which electrochemical cell the sample was placed).

Metallurgical properties that have been characterized include the most common grain size found in the sample, the grain boundary, Vickers hardness, and the crystal grain orientation. Because the samples in this study are polycrystalline, the chemical behaviour of the surface is not homogeneous, and strictly dependent on the grain crystallographic orientation.

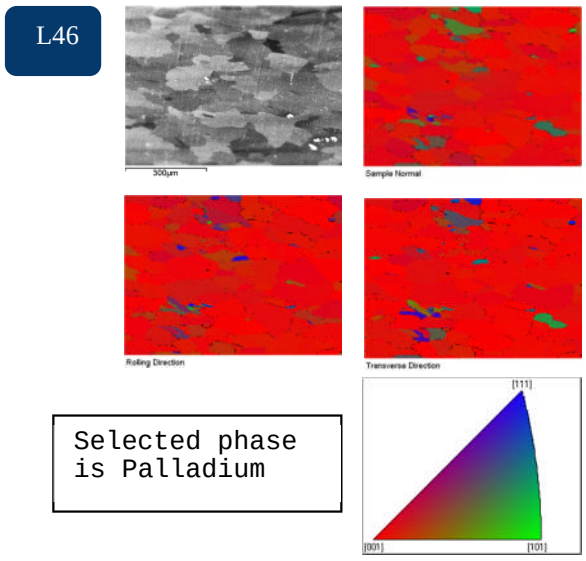

Figure 2.1. Grain orientation distribution as revealed by EBDS on L46 Pd sample

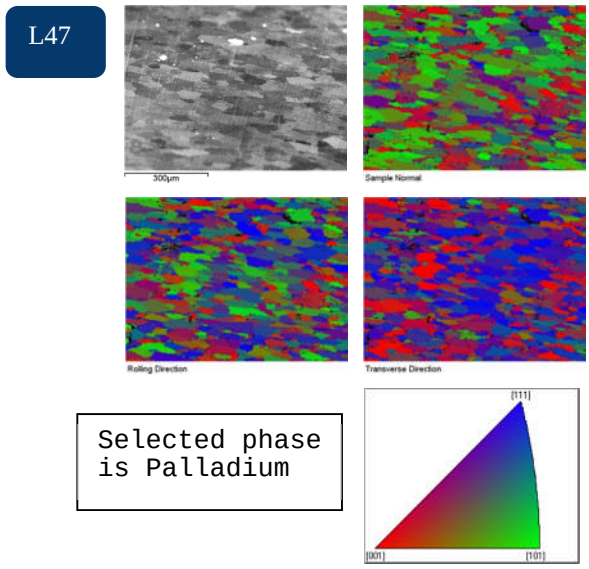

Figure 2.2. Grain orientation distribution as revealed by EBDS on L47 Pd sample

Excess heat experiments

After the Pd samples are fabricated and characterized from a metallurgical point of view, they are used as cathodes in electrochemical cells, which are placed inside a calorimeter. The metal lattice is loaded with deuterium to see if excess heat production occurs.

All the samples used in this study gave a D/Pd loading ratio with values ranging from 0.9 up to about 1.

The calorimetric study allowed us to understand that not only loading but also intrinsic properties of the material controlled the reproducibility of excess power. This evidence prompted us to establish a database of material properties.

Database

The custom- developed database includes all relevant characterization parameters. A typical record is shown in Fig. 3.1. It includes the sample name and its manufacturing specifications, and also the results of materials measurements, together with SEM and AFM images.

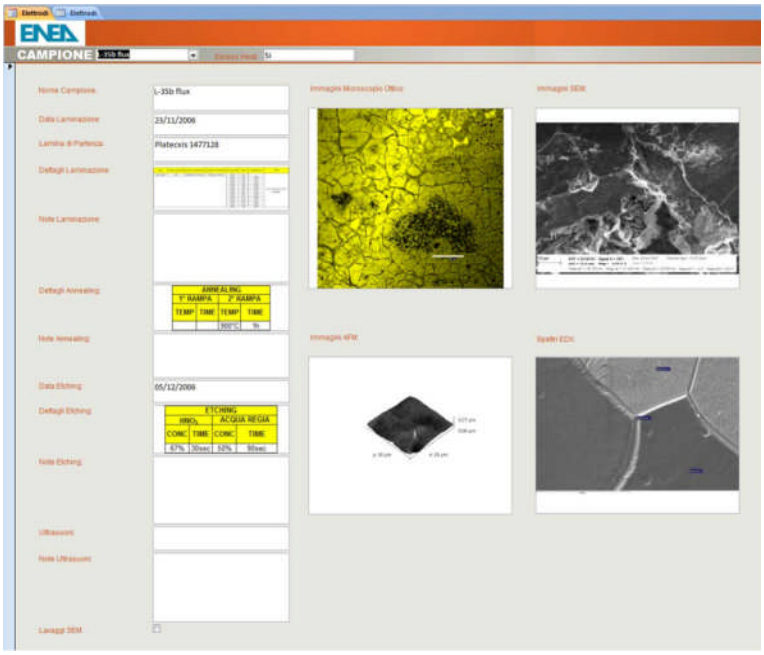

Figure 3.1. A typical database record

Analysis

After systematically characterizing the cathodes, and collecting and organizing the data, a statistical analysis was performed to look for correlations with excess heat. To quantify the correlation a *"degree of correlation" (g)* between a selected property (*f)* and the excess heat occurrence (*h)* has been defined as:

$$g = \frac{\langle f \times h \rangle}{\sqrt{\langle f \rangle^2 \langle h \rangle^2}}$$

Where g=1 then there is full correlation between the selected property and the excess heat production; where g=0 there is no correlation.

Results and Discussion

Figures 4.1 through 4.6 show the histograms of each of the material properties investigated in this work, together with the indication of excess heat production (shown in the graphs with the thinner bars).

It can be seen from these figures that some properties are well correlated with the excess heat production. This is particularly evident in Fig. 4.2, showing that most of the samples giving excess heat have well defined grain boundaries, while samples in which grain boundaries are not clearly identifiable by microscope inspection, in most cases did not produce excess heat.

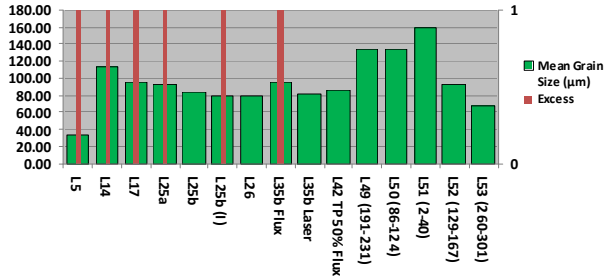

Figure 4.1. Mean grain size correlation with excess heat occurrence

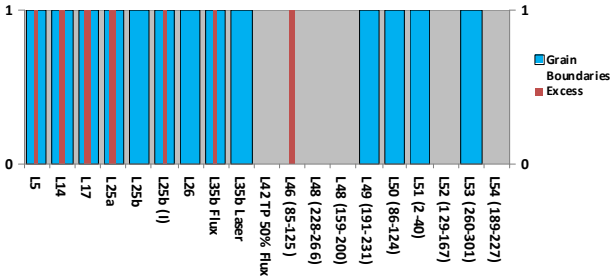

Figure 4.2. Grain boundary correlation with excess heat (1=correlation evident, 0=not evident)

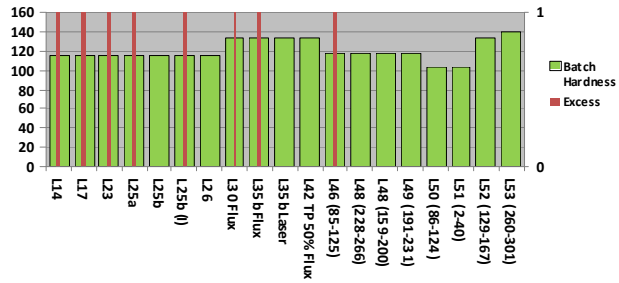

Figure 4.3. Vickers hardness (units areMPa) of batch correlation with excess heat

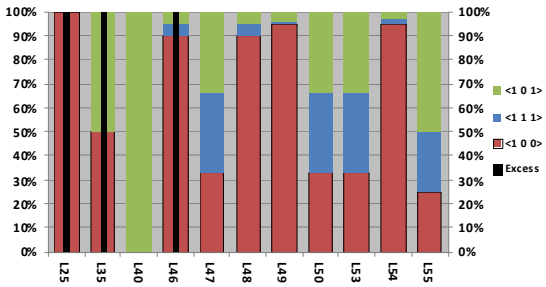

Figure 4.4. Grain crystal orientation correlation with excess heat

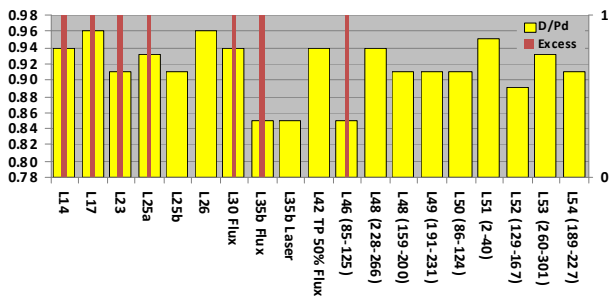

Figure 4.5. D/Pd loading ratio correlation with excess heat

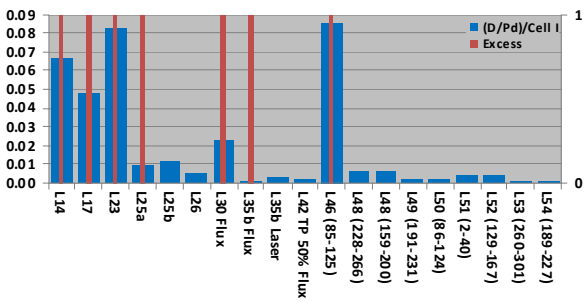

Figure 4.6. Low current D/Pd loading correlation with excess heat (units are mA^{-1})

Figure 4.1 shows the mean grain equivalent radius (units are microns), as it has been measured from the SEM images, by counting the number of grains present in a fixed area.

Figure 4.3 shows that excess heat occurred with more statistical probability with samples which have a Vickers hardness of 120 MPa. The Vickers hardness is measured on the

palladium lot as received. Different hardness values indicate different elastic properties and different impurity content in the original material.

In Fig.4.4 the results of crystal grain orientation are reported. The ordinate axis indicates the percentage of the sample volume which is oriented along a particular crystallographic direction. Three sets of data have been reported, one for each of the main lattice planes: <100>, <101>, <111>. Although the results are not statistically significant because the ensemble of samples on which crystallographic data have been available is limited, the graph shows that only samples having more than 50% <100> orientation gave excess heat, suggesting that <100> orientation is a necessary condition for excess heat to occur.

The last two figures (Fig. 4.5 and 4.6) show data on deuterium loading. In Fig. 4.5 the ordinate axis indicates the values of the D/Pd atomic ratio determined with four point probe resistivity measurements and the Baranowskii – McKubre curve. This is measured during electrolysis. The results confirms what has already been described in literature, that a D/Pd ratio higher than 0.85 is a necessary condition to obtain excess heat. It should be noted, however, that all the samples considered have a D/Pd ratio higher than 0.85; the correlation parameter *g* value would be much higher if samples below the loading threshold had been considered.

Fig. 4.6 gives insight into a more unexplored result. The histogram shows the ratio between D/Pd atomic ratio (also referred as the “maximum loading”) and the electric current that was flowing through the cell when that loading was obtained. McKubre identified two types of excess power production: Type A, excess begins after several days of electrolysis and depends on the current density; and Type B, excess begins soon and does not always depend the current density. [4] The figure shows that when excess heat is produced, a high level of deuterium loading was generally obtained at low electric current (see samples L14, L17, L23, L46); exceptions are samples L25a and L30Flux, which both gave excess heat of type B, while all other samples gave excess heat of type A.

Table 4.1. Correlation factor g value for measured properties of the Pd samples

	Hardness	Mean Grain size	Grain boundary	Grain Crystal Orientation			D_2 Loading	Low Current D_2 Loading
				<100>	<101>	<111>		
Correlation Factor (*g*)	***0.65***	***0.64***	***0.63***	***0.62***	***0.23***	***0.46***	***0.60***	***0.81***

Conclusions

Starting with metal from commercial suppliers, Pd cathodes have been produced and characterized systematically, by performing measures on their metallurgical and electrochemical properties.

The experimental data have been filed and stored in a database.

Suitable correlation parameters have been defined and correlations have been found between heat excess production and individual properties; i.e. the mean grain size, grain boundary, material hardness, crystal grain orientation, deuterium loading and low current deuterium loading level.

Multiple-regression data analysis could also be advantageously applied to our data, because the number of samples in the database is increasing.

References

1. V. Violante, F. Sarto, E.Castagna, C. Sibilia, M.Bertolotti, R. Li Voti, G.Leahou, M. McKubre, F. Tanzella,G. Hubler, D. Knies, T. Zilov and I. Dardik, *Calorimetric Results of ENEA Cooperative Experiments*, in the 13th International Conference on Condensed Matter Nuclear Science, Sochi, 2007
2. F. Sarto, E. Castagna, M. Sansovini, S. Lecci, V. Violante RdA, D.L. Knies, K.S. Grabowski, G.K. Hubler, "*Electrode Surface Morphology Characterization by Atomic Force Microscopy*"
3. G.K. Hubler, *Anomalous effects in hydrogen-charged palladium - a review*, *Surface & Coatings Technology* (2007), doi: 10.1016/j.surfcoat.2006.03.062
4. V. Violante, F. Sarto, E. Castagna, M. Sansovini, S. Lecci, D.L. Knies, K.S. Grabowski, G.K. Hubler, *"Material Science on Pd-D System to Study the Occurrence of Excess of Power*", in these proceedings

Condensed Matter "Cluster" Reactions in LENRs

George H. Miley[1], Heinz Hora[2] and Xiaoling Yang[1]
[1]*Dept. of Nuclear, Plasma and Radiological Engineering University of Illinois, Urbana, Il*
[2]*Dept. of Theoretical Physics, University of New. South Wales, Sydney, Australia*

Abstract

In this paper we first point out evidence for condensed matter cluster formation based on thin-film electrolysis. Next, measurements of superconductivity in condensed matter deuterium "clusters" in dislocation sites loaded-deloaded palladium thin films are briefly reviewed, followed by a discussion of techniques under study to increase the number of such sites per unit volume of the electrodes. Estimates for resulting "cluster reaction" rates – flow enhanced Pycnonuclear fusion are given. If successful, this approach offers a "Roadmap" for future power unit based on thin films and clusters.

Introduction

There is mounting evidence for localized reaction sites in many cold fusion and low energy nuclear reaction (LENR) experiments. Hot spots and damage spots on electrodes have been widely reported (e.g, by Srinivasan, Mizuno, Dash, Boss, …). Also, there have been detection patterns noted in our various types of experiments (Bead x-ray film, transmutation product pattern, MeV charged particles tracking pattern in CR-39 detectors, and observation of soft X-ray beamlets in pulsed plasma bombardment experiments). These observations indicate that localized reaction sites frequently occur and can dominate the reaction mechanism. More insight into the possible character of these sites comes from our earlier studies of the formation of superconducting "clusters" of hydrogen isotopes in dislocation loops formed in thin film palladium electrodes. That work is reviewed next, followed by a discussion of implications for creating highly reactive electrodes based on a high density of these condensed matter "clusters" in the host electrode material.

Condensed Matter Cluster Characteristics and Electrode Fabrication

The squid magnetic measurements described in Ref. 1 show "clusters" have characteristics of a type- II superconductor (See Figure 1). Cluster regions can have hydrogen densities approaching 10^{24}/cc (See Figure 2). Dislocation loop cluster type electrodes are fabricated by cyclic loading-deloading, hence being named "Dislocation Loops by Repetitive Loading-Deloading (DLRLD)"electrodes. These DLRLD electrodes are based on studies where high loadings in dislocation loops in treated Pd have exhibited properties associated with a superconducting phase termed a "cluster." However, the low fractional volume of the clusters (which is where the fusion producing reaction would occur) limits total reactions to low levels. Thus, a second type of cluster forming electrode that employs a manufactured nano-porous structure is under study.

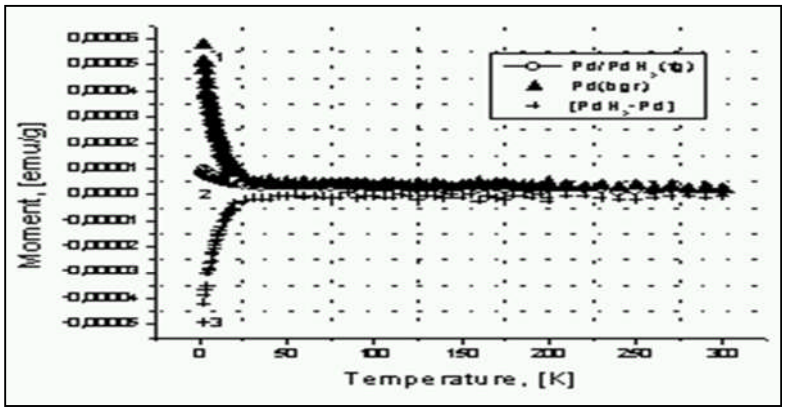

Figure 1. The magnetic moment of H_2- cycled PdHx(fg) samples in the temperature range of $2 \leq T < 50$ K is significantly lower than M(T) for the original Pd(bgr) single crystals.

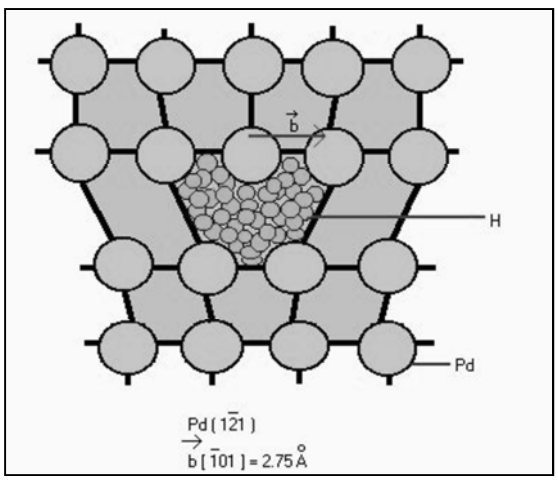

Figure 2. Squid magnetic measurements show clusters have characteristics of a type- II superconductor. Cluster regions can have hydrogen densities approaching 10^{24} 10^{24}/cc.

Fabrication

Cold worked Pd foil is used for Pd/PdO production. Prior to oxidation, the Pd substrate is annealed in a vacuum. It was then briefly treated in an oxygen-butane torch to produce a stable oxide layer, about 40-nm thick. Samples were electrochemically cycled to create a hydrogen filled dislocation structure in the Pd/PdO. The samples serve as the cathode, and a Pt anode is employed along with a high purity electrolyte. Electrochemical "cycling" involves periodically switching the cathode-anodic polarizations (loading – deloading) of the sample. After achieving a cathode loading up to x = H/Pd = 0.7, the voltage polarity is switched to the anodic regime to extract hydrogen from the volume of the lattice. To remove all weakly bound residual hydrogen atoms, the loading–deloading cycles are repeated 5-10 times. The samples are then annealed in a vacuum at 300°C for several hours.

Loading Measurements

A high-vacuum thermal desorption technique is used to estimate residual hydrogen concentration in the PdHx and Pd/PdO:Hx samples (Fig. 3). The samples were heated in a high vacuum (10^{-8} Torr) chamber with a quadruple mass-spectrometer. The hydrogen desorption peak area and the temperature of its maximum were found by analyzing the desorption species and comparing their yields to background data from the Pd(bgr) or Pd/PdO)bgr).

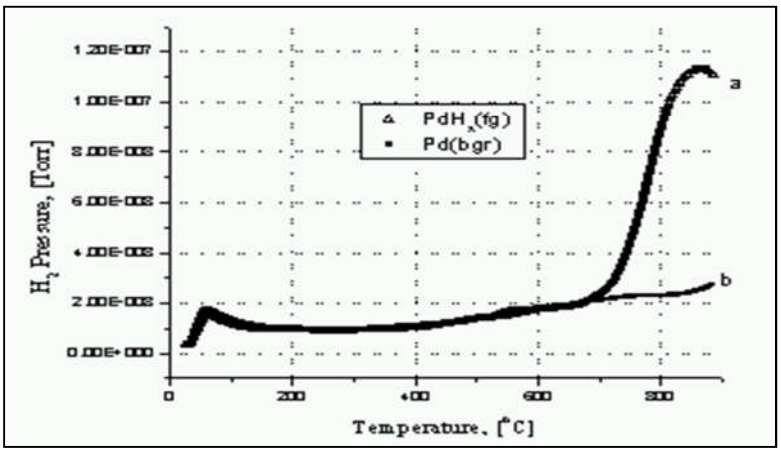

Figure 3. Thermal desorption analysis (TDA) performed with annealed Pd(bgr) samples in the temperature range of 20-900°C

Analysis of Cluster Loading

To obtain an average loading ratio x = H/Pd, special calibration measurements are done with a known mass (0.3 mg) of TiH_2 powder (decomposition temperature ~ 400°C.) A Comparison of the hydrogen pressure from this powder, with that of the PdHx samples gives the residual hydrogen content in the cycled Pd. The typical effective loading ratio is found to be $x \sim (4.5 \pm 0.5) \times 10^{-4}$, much lower than for any known stable phase of Pd hydride. Since this sample underwent annealing at a temperature of 570 K (decomposing the residual α-phase in the lattice), all remaining hydrogen detected is attributed to loading in dislocations, not in the regular lattice.

Cluster Parameters

Extrapolation of results of SANS measurements gives a radius R_H and binding energy of the residual hydrogen distribution with respect to dislocation cores. The Garlic-Gibson kinetics model is used for the kinetics of the second-order thermal activation processes observed in the thermal desorption analysis (TDA) measurements. Then, the activation energy of desorption (effective binding energy of hydrogen atoms within the lattice) is found to be ~ 1.6 ± 0.2 eV, well above the H-trapping activation energy of ~ 0.7 eV normally attributed to bulk hydrogen. This indicates that the hydrogen is solely bound inside the deepest core sites (at a radius R_H = 2.75 A, close to the Burgers vector or minimal radius of H capture in Pd). This suggests that all residual hydrogen is localized inside the dislocation loops (in the direction of Pd [121])

determined by Burgers vector b [101] = 2.75 A. Then, the dislocation density N_d, the effective loading ratio inside the loops is determined by the simple formula: $x_{eff} = \sqrt{2}\langle x\rangle/N_d\langle x\rangle/b^2$., giving $N_d \sim (1.0\text{-}2.0) \times 10^{11}$ cm^{-2} and $\langle x\rangle \sim (4\text{-}6) \times 10^{-4}$ Thus x^{eff} would be in the range of $1.0<x_{eff}<3.0$, suggesting superstoichiometric hydride formation in the deep dislocation cores.

Summary – clusters lead to localized SC

These results show that an anomalous diamagnetic response in these electrodes occurs below 30 K which is attributed to superconductivity in Pd hydride phase ("clusters") inside the deep dislocation cores. This interpretation is also consistent with the temperature and field dependencies of corresponding magnetization curves. Both their shape and field behavior have the characteristics of a non-linear, irreversible magnetization function of a type- II superconductor.

New Nano-Structure Film (NSF) Electrodes/Targets

Recently, a new type of electrode, the NSF electrode, was developed to create cluster formation in nano-porous structures manufactured on a Pd or Ni thin film electrode. The concept is to mimic the dislocation loops, but achieve a larger volumetric concentration or "packing fraction" than in the DLRLD electrode. This method used follows one originally developed by R.N. Rhonda of the International Nickel Plating Company. Palladium is deposited on a nickel substrate using an electroless deposition technique. An ammonium hydroxide solution dissolves palladium chloride tetrammine amine. Disodium EDTA keeps the palladium metal in the solution and the nickel substrate is etched and placed in the plating solution. Aqueous hydrazine is then added, destabilizing the palladium. Hydrazine is introduced using an infusion pump and the solution is placed inside an ultrasonic mixer. The destabilized palladium then plates the nickel substrate.

Auger spectroscopy performed on the electrodes confirms that the plating technique successfully deposited palladium completely and thinly. Roughly 0.05 g of palladium is deposited on each 25 cm^2 electrode at a thickness of roughly 50 nm. Auger scans are shown in Figure 4. The structures provided are thought to provide the conditions needed for cluster formation. Some preliminary electrolytic studies have been encouraging, but much more needs to be studied to understand the true promise of this new electrode design.

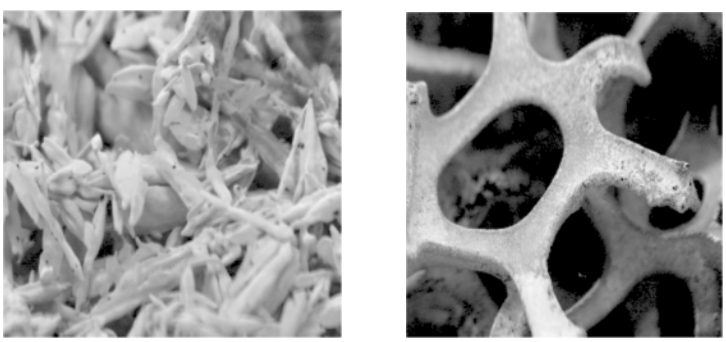

Figure 4. Auger Scan of Ni Microfelt (left) and Ni Foam (right) electrodes -White color indicates Pd-

Reaction Rate Estimates

An estimate of Cluster fusion rates in such dislocation loops at high D density follow from the well known Pycnonuclear reaction theory used for calculation of high density state fusion in astrophysics [6]. In the present case, however, the normal theory must be modified to include the effect of flow of hydrogen (deuterium) ions into the cluster site. This flow is unique to the present case of electrolytic ally driven reactions and it drastically changes the reaction rate. Initial results applying this modified Pycnonuclear theory confirms the rate strongly depends on cluster loading (i.e. on the condensation state and the dislocation geometry) and on the deuterium flux across the loop boundary flux. Results confirm that use of deuteron fluxes consistent with the thin film foil studies using CR-39 tracking foils predict rate of the same order of magnitude as indicated the experimental data. Further details about this theory will be presented in a forthcoming paper.

Implications – A Roadmap to Power Cells

If high volumetric densities of cluster sites can be created via the methods outlined earlier, a high reaction rate per cc should result given a competitive power cell. We term the electrode designed to achieve a “massive cluster electrode” (MCE) for controlled cluster reactions. Some insight to the way we hope to achieve this is illustrated in Figures 5 and 6.

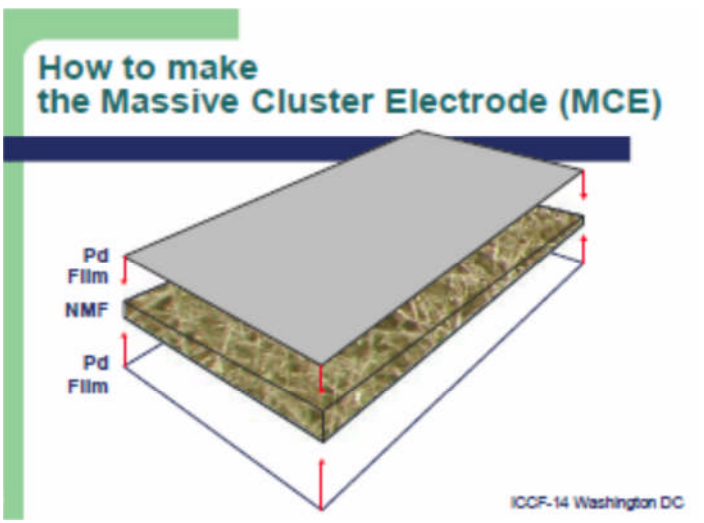

Figure 5. Illustration of construction of MCE.

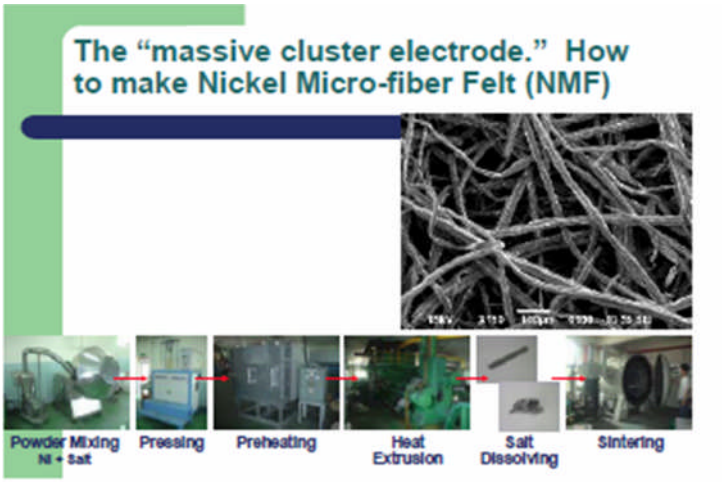

Figure 6. Construction steps for making Micro-fiber Felt (NMF) for the MCE.

The approach starts with creation of a micro-fiber felt sandwich structure as shown in Fig. 5. The MNF is a unique material that is manufactured in a multistep process outlined in Fig. 6. Palladium is then sputtered onto the MNF prior to encapsulating it into the sandwich electrode configuration. Many local defects occur at interfaces in this configuration, giving a high volumetric density of potential cluster sites. This work is currently in progress, and preliminary results to data are encouraging.

In addition to applications to LENR power systems as discussed here, a version of the Massive Cluster Electrode has a very important application in hot fusion. As suggested by the author in Ref. 5, such a structure could be used in the core of an inertial confinement fusion (ICF) target. In that application the objective is to use a laser or ion beam to compress a target, thereby compressing the clusters since the cluster deuterium density is in order of magnitude higher than cryogenic deuterium. The compressed cluster density would also exceed that possible in present cryogenic ICF targets. Since the reaction goes as the square of the density, a very large reaction rate would occur in the cluster region. In addition to power production, such conditions are of strong interest to basic understanding of fusion phenomena and astrophysics [6]. For power production the techniques would need to be extended to develop deuterium-tritium (D-T) clusters to take advantage of the high D-T fusion cross sections. Also, to reduce radiation losses development of a low-Z host material such as lithium or beryllium would be desirable.

Conclusion

This paper makes a strong case that condensed matter deuterium cluster formed in dislocation loops are one way to achieve nuclear reactive sites in LENR electrodes. The problem to date has been that the volumetric density of such cites, which is highly reactive, have a low density of sites per unit volume. Possible methods to achieve a high volumetric density of sites (i.e. achieve a massive cluster electrode (MCE) that are under study are briefly outlined. This is thought to offer an orderly "roadmap' for moving on to competitive power cells.

References

1. Andrei Lipson, Brent J. Heuser, Carlos Castano, George Miley, Boris Lyakhov, and Alexander Mitin, "Transport and magnetic anomalies below 70 K in a hydrogen-cycled Pd foil with a thermally grown oxide" *Physical Review B* 72, 212507, 2005.
2. A. Lipson, C. Castano, G. Miley, A. Mitin, and B. Lyakhov, "Emergence of a High Temperature Superconductivity in Hydrogen Cycled Pd compounds as an Evidence of Super-stochiometric H/D Sites", *Proc. ICCF-11*, Marseilles, France, Oct 31 – Nov 5, (2004).
3. G. H. Miley, A. Lipson, H. Hora and P. J. Shrestha, "Cluster Reactions in LENRs", *Proceedings of 8th International Workshop on Anomalies in H/D Loaded Metals*, Catania, Sicily, October 12-18, (2007).
4. G. H. Miley, et al. "Progress in thin-film electrode research at the University of Illinois." *The 9th International Conference on Condensed Matter Nuclear Science*. 2002. Tsinghua Univ., Beijing, China: Tsinghua Univ. Press. (2003).
5. G. H. Miley, "Novel High Performance Cluster Type ICF Target, DOE Innovative Concepts (ICC) Workshop, Reno NV 2008.
6. S.L. Shapiro and S. A. Teukolsky, "Polynuclear Reactions." Black Holes, White Dwarfs, and Neutron Stars. New York: John Wiley & Sons. 72-81, (1983).

The Phusor®-type LANR Cathode is a Metamaterial Creating Deuteron Flux for Excess Power Gain

Mitchell Swartz and Gayle Verner
JET Energy, Inc. Wellesley, MA 02481(USA)

Dr. Mitchell Swartz does not wish to have his papers uploaded to LENR-CANR.org. A copy of this paper can be found here:

http://www.iscmns.org/iccf14/ProcICCF14b.pdf

This page intentionally left blank

This page intentionally left blank

This page intentionally left blank

This page intentionally left blank

This page intentionally left blank

This page intentionally left blank

This page intentionally left blank

This page intentionally left blank

This page intentionally left blank

This page intentionally left blank

This page intentionally left blank

This page intentionally left blank

This page intentionally left blank

This page intentionally left blank

This page intentionally left blank

This page intentionally left blank

Introduction to the Theory Papers

Persistent resistance to accepting the Fleischmann–Pons Effect (FPE) as an attribute of a nuclear process is due to the need to accept two "miracles": suppression of the Coulomb barrier and lack of high-energy emissions. Both observations contradict textbook nuclear physics and experience with hot fusion. The first problem is how deuterons (or other nuclei) get together to undergo nuclear reactions despite the electrostatic repulsion between them. If one assumes a two-particle scattering model and collision energies commensurate with the temperatures in the experiments, calculations of the tunneling rate through the barrier yield values too low by some tens of orders of magnitude to account for the observed output powers. The second problem is the lack of observed high-energy gammas, alphas, neutrons, protons, or other prompt nuclear signatures. (There are experiments in which low-level energetic emissions from metal deuterides or hydrides *have* been reported, often without measured excess heat. These lend credence to the proposition that nuclear effects are taking place, but the levels are not commensurate with the power observed in excess-heat experiments.) In the hot-fusion regime, the dominant channels for deuterium fusion are $d + d \rightarrow p + t + 4$ MeV and $d + d \rightarrow n + {}^3He + 3.3$ MeV; the expected energetic reaction products are typically not seen in cold-fusion experiments. Correlation of ${}^4He$ production with heat production suggests $d + d \rightarrow \alpha + 24$ MeV (or $d + d + X \rightarrow \alpha + X + 24$ MeV, with X to be determined), but again energetic outputs such as 24 MeV gammas are conspicuously absent. We thus need an explanation for how energy born in multi-MeV nuclear events gets transferred to the lattice as heat.

Over half of the papers in this section—fourteen of the twenty-three—address in some way the suppression of the Coulomb barrier. We will say something about each of them below. Six of the fourteen *also* address the lack of high-energy emissions. Three papers can be classed under the heading of "transmutation," which is used here to refer to transformations of isotopes other than those of hydrogen and helium. Nine other papers attempt to lay a foundation for anyone trying to develop models and theories of the FPE. These are discussed first.

Table 1 has been constructed to provide a characterization of the various papers in this section. The numbers of the papers in the table, and at the end of this introduction, are referred to in the remainder of this introduction. The table answers the following questions:

1. What is the form of the reaction considered? ("*Which LENR?*")
2. Does the paper deal with the Coulomb barrier? ("*Coulomb barrier*")
3. Does the paper deal with the presence or absence of energetic particles? ("*Hi-energy particles*")
4. What is the conceptual foundation of the theory? ("*Concept*")
5. Has the concept been reduced to equations? ("*Equations?*")
6. Have numerical results been provided? ("*Numerical Results?*")
7. Have the results been applied? ("*Use of Results?*")

Table 1. Characterization of the Theory Papers in This Section

	Authors	Which LENR?	Coulomb barrier	Hi-energy particles	Concept	Equations?	Numerical Results?	Use of Results?	Comments
1	Adamenko, Vysotskii	Transmutation	N/A	N/A	Magnetic monopoles	Yes	Approx. bounds	No	
2	Alexandrov	e+p → n+ν	Neutrons	No	Band theory, effective mass	Yes	Yes	Applied to semicond.	
3	Bass, Swartz	D fusion	No	No	Control theory	Computer simul.	Yes	Future work	
4	Breed	4d → α + …	Yes	Yes	Band theory, effective mass, resonance	Yes	No	N/A	
5	S. Chubb	d+d → ^{4}He+heat	Yes	Yes	Nonlocal quantum effects, resonance	Yes	Yes	No	"Real barrier is conceptual"
6	T. Chubb	Various	Yes	Yes	"Ion band states"	No	No	N/A	
7	Cook	Transmutation	No	N/A	Nuclear lattice model	Yes	Yes	Compare with exp't	
8	Dufour et al.	Pd+D, D+D	Yes	Indirectly	New force	No	No	N/A	
9	Fou	d+d fusion	Yes	No	Neutron exchange, electrostatic fields	No	No	N/A	
10	Frisone	D plasma oscillations	Yes	N/A	Gamow and Preparata theory	Yes	Yes	No	
11	Godes	e+p → n+ν	Neutrons	No	Various	No	No	N/A	
12	Hagelstein, Chaudhary	d+d → ^{4}He+24 MeV	Yes	Yes	Coupling 2-level systems to phonons	Yes	Qualitative	N/A	
13	Hagelstein, Melich, Johnson	Various	Yes	Yes	Various	N/A	N/A	N/A	Survey of experiments
14	Hagelstein et al.	Various	No	No	Existing theory	Yes	No	N/A	Gen. framework
15	Kim	d+d → ^{4}He+heat	Yes	Yes	Bose-Einstein condensate	Yes	Yes	Yes	
16	Kozima	Not stated	No	No	Cellular automata, recursion equations	No	No	N/A	Complexity theory
17	Kozima, Date	Transmutation	Neutrons	No	"Neutron drops"	No	No	N/A	
18	Li et al.	d+p+e → ^{3}He+e+ν+$\bar{\nu}$	Neutrons	Indirectly	Resonance, tunneling	Yes	Yes	No	
19	Sinha, Meulenberg	D fusion	Yes	No	Screening via local e^- pairs	Yes	Yes	No	
20	Swartz	D fusion	No	No	Relations between operating params.	Yes	Approx.	Yes	
21	Swartz, Forsley	D fusion	No	No	Relations involving operating params.	Computer calculations	Qualitative	Yes	
22	Takahashi	4d → ^{8}Be* → 2α	Yes	No	"Tetrahedrally symmetric clusters"	Yes	Yes	No	

Foundations: Experimental Evidence, Models of the Physical System, Theoretical Concepts

Explanations or even simple models of the PdD system that account for the FPE heat require simultaneously addressing the problems at nuclear scales, femtometers (fermis), and both atomic and chemical scales, nanometers, in a solid or a liquid where transport of hydrogen isotopes is occurring. We have few integrated theories for any physical science problem of this wide scale and complexity. Instead we develop small model systems to help us explain certain observations and use them to guide our experimental exploration. This is not a problem new to science. Herbert Frohlich in his 1961 review of The Theory of Superconductivity provides us some guidance on what has succeeded in these situations.

> By 1933, when it was clear that the basic physics required for the development of a theory of superconductivity was well understood, many physicists had tried in vain to propose such a theory. A general feeling of frustration arose such that the first thing one did when acquainted with another attempt was to try to find where it was wrong. This feeling found its expression in Pauli's remark, "Theories of superconductivity are wrong", and by Felix Bloch's theorem, "Theories of superconductivity can be disproved". It was astonishing to see how my first paper in 1950—soon followed by Bardeen's first paper—led to a complete reversal of opinion. Schafroth (1951) followed Pauli's suggestion to work further on this theory and he was the first to show that perturbation theory could not be applied. Yet neither he, nor most others, doubted the correctness of the basic assumption that electron-phonon interaction should be principally responsible for superconductivity. This, so far as I have seen, was principally due to the fact that no 'new' interaction between electrons had to be invented but that the theory was completely based on the empirically successful free electron model. …
>
> Yet it appears that all this did not affect some of those physicists who had previously formed an opinion in a different direction. A striking example can be found in the article by W. L. Ginsburg published in 1953…
>
> In contrast to this dangerous dogmatic approach, the development of the theory of superconductivity is an excellent example of the intuitive approach. My idea was foremost that one should consider the small energy involved in the superconductive transition as the first problem to be answered. Electron-phonon interaction provided this possibility from a purely dimensional point of view. When the early attempts did not succeed in solving the problem, then it was required, I thought, to find a new approach to the many-body problem involved. However, intuition won again: Bardeen, Cooper and Schrieffer (1957) proposed their state vector which virtually solved the problem of the gap.

What is to be explained?

Peter **Hagelstein**, Michael **Melich**, and Rodney **Johnson** (13) give a survey of experimental results that have an important feature in common. They show effects, likely nuclear, not explained by existing treatments of nuclear physics, and occurring in condensed-matter systems at relatively low temperatures. These are presented as sources of questions that need to be addressed by possible new theoretical statements or models.

How compelling is the experimental evidence?

The paper by Rodney **Johnson** and Michael **Melich** ("Weight of Evidence for the Fleischmann-Pons Effect") addresses this question and can be found in the section on "Challenges and Summary" The introductory comments on this paper are to be found in that section.

Where shall we start?

The paper by Peter **Hagelstein** *et al.* (14) presents a general framework for formulating problems in CMNS in terms of generally accepted basic principles. The framework is broad enough to encompass problems of nuclear physics and condensed-matter physics on an equal footing, together with interactions between them. The starting point is a representation of a system as a set of electrons and nucleons, interacting via electromagnetism and the strong nuclear force, supplemented if necessary by weak-interaction terms and neutrinos. A set of reductions and approximations is described that allows a problem to be made computationally tractable while retaining necessary detail: empirical potentials may be used for interactions between nucleons; most lattice nuclei may be treated as single entities by writing in terms of center-of-mass coordinates and integrating out the relative coordinates of constituent nucleons; the Born-Oppenheimer approximation may be used; and in problems involving phonons, the center-of-mass coordinates may be re-expressed in terms of phonon-mode amplitudes. The coupling between phonons and internal nuclear coordinates is discussed as an example. This approach reflects Frohlich's notion that progress depends on our dependence on "intuition" or in the jargon, induction as opposed to deduction from axiomatic approaches. John Bardeen, when faced with the 1987 high-temperature superconductivity results, turned immediately to tabulating the experimental data and trying to understand what it was telling us. Bardeen's method of "wallowing in the data" puts the foundation under intuition and lets the experiments guide in the selection of models, as advocated in this paper.

Are there other kinds of mathematical relationships that could be useful in CMNS?

Hideo **Kozima** (16) hints at intriguing connections between cold-fusion processes and two topics related to complexity theory: (1) cellular automata and (2) recursion relations of the form $x_{n+1} = \lambda f(x_n)$. The connection with cellular automata is that the occupation numbers at time $t + 1$ for D (or H) at a lattice site depend on the values at time t at the site and its neighbors. The working out of the exact dependence has been left for future work. For the recurrence relations, the author describes the population model that led to the *logistic equation*, $x_{n+1} = bx_n(1 - x_n)$. Radically different types of behavior, chaotic and non-chaotic, can be obtained by varying b

Such results are applicable to a wide variety of nonlinear dynamical systems. Precise details of the connection with cold-fusion phenomena are left for future work.

Can the methods of Control Theory modeling assist in the design of CMNS experiments?

Mitchell **Swartz** (20) considers phenomenological relations involving various performance parameters of CMNS systems, such as excess heat production and production of helium or tritium. He argues that these relations (referred to as Optimal Operating-Point [OOP] Manifolds) are best presented as functions of electrical input power and that these relations describe many (or most) CMNS systems, provided one distinguishes three regions: surface, subsurface, and deep bulk (the last also including Y. Arata's zirconium / Pd black systems). The author relates OOP manifolds to an equation (eq. 1 in the paper) then relates deuteron fluxes to drift rates (due to applied field) and thermal diffusion rates. On the basis of the equation, he recommends use of low currents, high voltages, and pure D_2O without additives such as LiD.

Robert **Bass** & Mitchell **Swartz** (3) confront Bass's work on system identification ("Empirical System Identification") described in his ICCF-1 paper, with Swartz's work on OOP Manifolds, mentioned just above. Models of various sizes were estimated, and the system output values calculated from them were compared with measured values. On the basis of the results, the authors hold out the possibility of designing a feedback controller for lattice-assisted nuclear reaction (LANR) systems that would yield a substantial improvement in output power.

Mitchell **Swartz** & Lawrence **Forsley** (21) examine results reported by Irving Dardik and others at Energetics Technologies, in which LANR systems were driven by a complex waveform consisting of a sinusoid modulated by another sinusoid, which was modulated in its turn by yet another sinusoid. The authors propose as an explanation for the reported substantial energy gains that the waveform had the effect of driving the system, for at least part of its duty cycle, through its optimal operating point (OOP, mentioned above).

Does CMNS compel us to take a quantum-theoretic view of CMNS?

The paper by **Scott Chubb** (5) is a largely philosophical work that takes as its thesis that the real barrier to progress in Condensed-Matter Nuclear Science (CMNS) is not the physical Coulomb barrier but the conceptual barrier presented by quantum mechanics. We are introduced to the epistemological perplexities of quantum theory and the challenges to our notions of causality presented by Wheeler and Feynman's absorber theory. Towards its end, the paper makes contact with the "Ion Band Theory," which has been developed in many previous publications by the author and Talbot Chubb. Deuterium ions in the lattice are treated as occupying nonlocal states similar to the states occupied by conduction electrons in conventional solid-state theory. Resonant conditions are important, and boundary effects come into play.

Explanation of fusion (with or without high-energy emissions)

Several of the papers involve the notion of *screening*—accumulation of negative charge (electrons) at locations between two nuclei so that the resulting attractive forces partially offset the repulsion between the positive charges of the nuclei. A few circumvent the Coulomb barrier by introducing neutrons into the interaction, neutrons not being subject to electrostatic repulsive forces. Both these ideas are highly intuitive—they are easy to picture in the mind's eye. Many of the papers, however, invoke notions more remote from everyday experience. We find mention of cooperative effects, nonlocality, quasiparticles, resonance, and condensates. The discussion becomes ineluctably quantum-theoretic.

The Ion Band Theory (mentioned above in connection with Scott Chubb's paper) is also the subject of the paper by **Talbot Chubb** (6), who discusses a two- (rather than three-) dimensional version of the theory suitable for treating interfaces, such as that between a ZrO_2 crystal face and a Pd nanocrystal.

The paper by Ben **Breed** (4) studies "heavy electrons," electron pseudo-particle states with high *effective mass*, a well established concept in solid-state physics. Breed points out that while the states are nonlocal in the sense of extending over many lattice cells, they can nevertheless concentrate charge near the lattice sites, or at points midway between, and thus provide a mechanism for screening to suppress the Coulomb barrier. To explain the lack of high-energy emissions, he invokes resonant modes that can bring *four* deuterons close together. Though such multi-particle interactions are virtually impossible in particle-beam experiments, we are told that they are not uncommon in a solid-state environment. Not all four deuterons are required to participate in fusion. However, the additional particles expand the possibilities of sharing energy and momentum while respecting conservation laws.

Four-deuteron interactions are also considered in the paper by Akito **Takahashi** (22) though details differ greatly. Takahashi posits the formation of a "tetrahedral symmetric condensate," involving a cluster of four deuterons with the symmetry of a tetrahedron, an example of what he calls "Platonic symmetry." (The tetrahedron and the octahedron, also mentioned, are regular polyhedra, instances of the classical Platonic solids.) Applying a one-dimensional Langevin equation to the internuclear distance, the author concludes that, once formed, such a cluster, while preserving its symmetry, will with near certainty undergo catastrophic collapse to very small dimensions, fusing to an excited ^{8}Be* state. Takahashi expects this to yield two 24 MeV alpha particles, though details await further work. The energy is predicted to be expressed as kinetic energy of the alphas rather than as gamma radiation.

The paper by Jacques **Dufour** *et al.* (8) concerns a hypothesized new force, derived from a Yukawa-like potential with a greater range than the usual nuclear scale: picometers rather than femtometers. The authors explore some consequences of the existence of the potential, including possible bound states between Pd and D or D and D at a picometer scale, and possible promotion of fusion reactions. They propose an experimental program to test the existence of and to study the potential.

Cheng-ming **Fou** (9) considers a pair of deuterons contained in a void of atomic dimensions in an otherwise homogeneous solid. He proposes mechanisms, namely neutron exchange and

electrostatic fields, that could generate attractive forces between the deuterons, partially offsetting the Coulomb barrier. The author makes the point that knowing what the fields are in the metal environment is an important consideration, and through a simple model calculation, he attempts to find a tractable way of estimating them.

Fulvio **Frisone** (10) studies plasma oscillations of palladium *d*-shell electrons, Pd ions, and deuterons in D-loaded Pd, in an extension of work by Giuliano Preparata. He finds negative charge condensation near D^+ ions, providing a screening potential. However, calculated fusion rates are said to be insufficient to explain substantial heat production in Fleischmann–Pons experiments. The author contemplates further work, exploring the contributions of deformations, micro-cracks, and impurities.

Yeong E. **Kim** (15) proposes that mobile deuterons in a micro- or nano-scale grain of Pd can form a Bose-Einstein condensate. He cites work of Dirac and Bogolyubov to assert that for large occupation number of the ground state, the bosons act independently and largely ignore the Coulomb barrier. He presents selection rules, which suggest that, in contrast to free space, $d + d \rightarrow \alpha$ should dominate, not $d + d \rightarrow p + t$ or $d + d \rightarrow n + {}^3He$. The resulting 24 MeV is said to be taken up by the condensate and shared by the remaining deuterons.

K. P. **Sinha** and A. **Meulenberg** (19) propose a mechanism for screening involving: presence of d-d pairs in linear defects in the Pd lattice; interactions of optical-mode phonons with ions and electrons; consequent formation of local electron pairs; then formation of D^- and D^+ ions and hence resonant D^+-D^- pairs. The local electron pairs have been discussed elsewhere by one of the authors in connection with high-temperature superconductors.

The paper by Dimiter **Alexandrov** (2) is one of three in this section that deal in some way with neutrons as participants in nuclear reactions in solids. The focus of this paper is "heavy electrons." The author considers disordered nitride semiconductors such as $In_xGa_{1-x}N$ and performs band-structure calculations that lead to values (some quite large) for the effective electron mass. He considers conditions under which the enhanced mass can permit an inverse beta-decay reaction: $e + p \rightarrow n + \nu$, as also proposed under other conditions by A. Widom and L. Larson (ref. [3] of the paper). The resulting neutrons can induce various unspecified nuclear reactions. Application of this work to metallic hydrides, such as PdD, is not yet clear and is left to future work.

Robert **Godes** (11) proposes a mechanism to explain FPE devices built by his company, and perhaps other systems. Direct D+D fusion is avoided by an indirect path involving cold neutrons. An assumed Hamiltonian leads to neutron production through inverse beta-decay. Hydrogen isotopes build up to ${}^4H$ by neutron capture, followed by ${}^4H \rightarrow {}^4He + e + \bar{\nu}$.

Xing Z. **Li** *et al.* (18) present a three-parameter empirical formula for cross sections of several processes involving D, T, or ${}^3He$. It shows better fits to data than a much used five-parameter formula. They argue that the form of the formula supports a "selective resonant tunneling" model for the processes and, on the basis of channel-width matching, that the absorption process at low energy must be narrow, long-lived, and therefore a weak-interaction process. They conclude that selective resonant tunneling explains the occurrence of excess heat without high-energy neutron or gamma emission. As a candidate reaction they mention "K-

capture of an electron by a deuteron, followed by decay of a triton." This is written as $p + d + e^- \rightarrow T + \nu$ followed by $T \rightarrow {}^3He + e^- + \bar{\nu}$, though "K-capture of an electron by a deuteron" would seem to hint at the transitory existence of a dineutron, ^2n, during the first reaction.

This brings us to the paper by Peter **Hagelstein** and Irfan **Chaudhary** (12). Though screening is addressed, the main thrust of the paper is how a large quantum of energy, on the order of 24 MeV, can get distributed to the lattice as a very large number of quanta of vibrational modes, each on the order of a small fraction of an eV. The authors have studied models of a two-level system with a large transition energy (such as D_2 and ^{4}He separated by 24 MeV) coupled to a low-energy harmonic oscillator, representing phonon modes. (These are reminiscent of multi-spin spin-boson models that occur in other contexts.) Because the coupling is weak due to the Gamow factor associated with the Coulomb barrier, they are led to consider (1) a loss term to suppress destructive interferences and (2) a second two-level system strongly coupled to the oscillator. Candidates for the second two-level system are discussed. This work is one part of a very ambitious program to model the FPE in detail from established basic principles. It takes place within a general framework described in the paper by Hagelstein *et al.* (14) already discussed above.

Transmutation

In previous work, V. **Adamenko** and V. I. **Vysotskii** (1) reported observations that suggested transmutations such as $^{27}Al + {}^{12}C \rightarrow {}^{39}K$ in high-current electron-beam experiments. They hypothesized that such reactions were promoted by magnetic monopoles. In this paper, they make inferences about the properties of the monopoles and discuss possible mechanisms for their creation.

The paper by Norman D. **Cook** (7) considers a lattice model of nuclear structure, an alternative to the usual shell, liquid-drop, cluster, and other models. The lattice model has previously been applied to explaining the asymmetric fission of uranium. It is applied here to observations of palladium cathodes by T. Mizuno suggesting transmutations of the form Pd + D → (fission products) for various isotopes of Pd.

The "water tree" in the title of the paper by Hideo **Kozima** and Hiroshi **Date** (17) is a micron-scale defect, filled with electrolyte, which forms in polyethylene subjected to intense electric fields and has been implicated in failures of polyethylene-insulated power lines. The authors propose an explanation for observations by T. Kumazawa *et al.* that suggest various transmutations associated with the formation of water trees. The explanation is based on the authors' "neutron-drop model," developed in earlier work, which hypothesized the existence of a "dense neutron liquid at boundary / surface regions of . . . crystals" that contains "neutron drops," denoted ${}^{A}_{Z}\Delta$, having Z protons, Z electrons, and $(A - Z)$ neutrons. The transmutations in question could be attributed to absorption by a nucleus of a neutron, with or without subsequent beta-decay, or to absorption of a ${}^{4}_{2}\Delta$ or an ${}^{8}_{4}\Delta$.

Finally, it should be noted that not all theoretical concepts for LENR were represented at ICCF-14. Hence this section, whilc relatively comprehensive, is necessarily incomplete.

Theory Papers

1. V. Adamenko & V.I. Vysotskii, *The possible mechanism of creation of light magnetic monopoles in strong magnetic field of a laboratory system*
2. D. Alexandrov, *Heavy Electrons in Nano-Structure Clusters of Disordered Solids*
3. R. W. Bass & M. Swartz, *Empirical System Identification (ESID) and Optimal Control of Lattice-Assisted Nuclear Reactors*
4. B.R. Breed, *Can Established Physical Principles Explain Solid-State Fusion?*
5. S.R. Chubb, *Resonant Electromagnetic-Dynamics Explains the Fleischmann-Pons Effect*
6. T.A. Chubb, *Interface Model of Cold Fusion*
7. N. Cook, *Toward an Explanation of Transmutation Products on Palladium Cathodes*
8. J. Dufour et al., *An Experimental Device to Test the YPCP ("Yukawa Pico Chemistry and Physics") Model: Implications for the CF-LENR Field*
9. C. Fou, *Investigation of Deuteron-Deuteron Cold Fusion in a Cavity*
10. F. Frisone, *"The Coulomb Barrier not Static in QED," A correction to the Theory by Preparata on the Phenomenon of Cold Fusion and Theoretical hypothesis*
11. R. Godes, *Quantum Fusion Hypothesis*
12. P.L. Hagelstein & I. Chaudhary, *Excitation transfer and energy exchange processes for modeling the Fleischmann-Pons excess heat effect*
13. P.L. Hagelstein, M.E. Melich, & R. Johnson, *Input To Theory From Experiment In The Fleischmann-Pons Effect*
14. P.L. Hagelstein et al., *A Theoretical Formulation for Problems in Condensed Matter Nuclear Science*
15. Y.E. Kim, *Theory of Low-Energy Deuterium Fusion in Micro/Nano-Scale Metal Grains and Particles*
16. H. Kozima, *Complexity in the Cold Fusion Phenomenon*
17. H. Kozima and H. Date, *Nuclear Transmutations in Polyethylene (XLPE) Films and Water Tree Generation in Them*
18. X.Z. Li et al., *Exploring a Self-Sustaining Heater without Strong Nuclear Radiation*
19. K.P. Sinha & A. Meulenberg, *A model for enhanced fusion reaction in a solid matrix of metal deuterides*
20. M. Swartz, *Optimal Operating Point Manifolds in Active, Loaded Palladium Linked to Three Distinct Physical Regions*
21. M. R. Swartz & L. P. G. Forsley, *Analysis of "Superwave-as-Transitory-OOP-Peak" Hypothesis*
22. Takahashi, *Dynamic Mechanism of TSC Condensation Motion*

The Possible Mechanism of Creation of Light Magnetic Monopoles in Strong Magnetic Field of a Laboratory System

V. Adamenko[1] and V. I. Vysotskii[1,2]
[1] *Electrodynamics Laboratory "Proton-21", Kiev, Ukraine*
[2] *Kiev Shevchenko National University, Faculty of Radiophysics, Kiev, Ukraine*

Abstract

In this work the reasons and mechanism of the creation of unknown magneto-charged particles, which were observed in experiments on supercompression of condensed target in Kiev Electrodynamics Laboratory “Proton-21”, are discussed. It is shown that these particles are most probably the hypothetical light magnetic monopoles that were introduced by George Lochak as magneto-excited neutrinos. The parameters of these particles (including mass of monopole and both size and binding energy of monopole-antimonopole pair) and the method of their creation are discussed and calculated.

Introduction

In our previous work [1,2] we have presented the results of observation and investigation of interaction of unknown magneto-charged particles (hypothetical magnetic monopoles) with surface of MDS (Al-SiO_2-Si) structure. We have observed the traces of ordered thermo-mechanical impact on the surfaces (Fig. 1). The length of trace was L ≈ 2 mm. These results were observed during experiments in Kiev Electrodynamics Laboratory “Proton-21” on achieving the superdense state of matter by using the high-current electron driver [3]. In the experimental setup an impulse electron flux with a total energy about 100...200 J and duration $\tau \approx 50$ ns was used as a coherent driver in every cycle of supercompression. The energy of each electron in different experiments is about 300...400 kV, the total current - 50...70 kA .

It was shown that the source of a great specific energy release, $dQ_{tot}/dl \approx -10^6$ GeV/cm, spent on the formation of these traces, may be the processes of nuclear synthesis reactions $Al^{27}+C^{12} = K^{39}$, $Al^{27}+C^{13} = K^{40}$, which are running with the participation of MDS-structure surface nuclei and are stimulated by the action of magnetic monopoles [1,2].

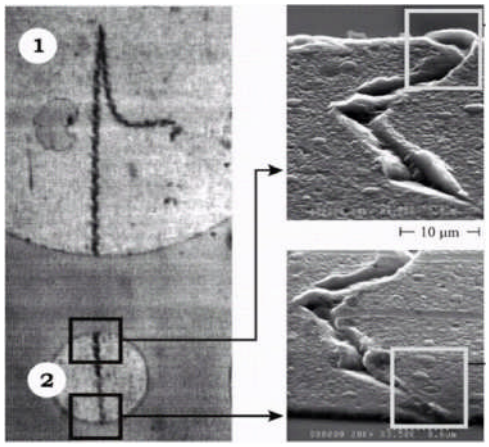

Figure 1. The general view and details of MDS-structure with the tracks

In the present work the parameters of these monopoles and the mechanisms of their creation in Earth laboratory are discussed and calculated.

1. Parameters of magneto-charged particle

In our previous work [1,2] it was shown that the process of formation of periodic tracks is connected with a magnetic interaction of magneto-charged particle with both magnetic field of anode current and multilayer MDS structure, which is the combination of diamagnetics (Si, SiO and melted ionized Al) and paramagnetic (solid Al) layers. In view of the form of a macrotrack (involving the great number of strictly periodic oscillations [1,2]), we may conclude that the controlling magnetic field is approximately the same along the entire trajectory. This corresponds to the fact that formation duration of mentioned track part is significantly less than the total duration $\tau \approx 50$ ns of the current pulse. If this duration was comparable with τ, then the period of oscillations at the beginning and at the end of the track would be essentially different.

This result allows us to assume that the duration of the formation of this part of the track with the length $L \approx 2$ mm is $\Delta t \leq 5$ ns, and the mean longitudinal velocity of motion of the hypothetical magneto-charged particle $\langle v_g \rangle$ is greater than $L/\Delta t \approx 4.10^7$ cm/s.

The maximal longitudinal velocity (in view of periodical stopping and periodical stimulation of fusion reactions along the trace [1,2]) is $v_g \geq 10^8$ cm/s.

During detailed SIMS-researches it was shown that the area of unknown particle "point of reflection" (Fig. 2) is the foreign small-size (about 10 microns) object made of Fe^{56}, Fe^{57} and Co^{59} isotopes and situated on the MDS structure.

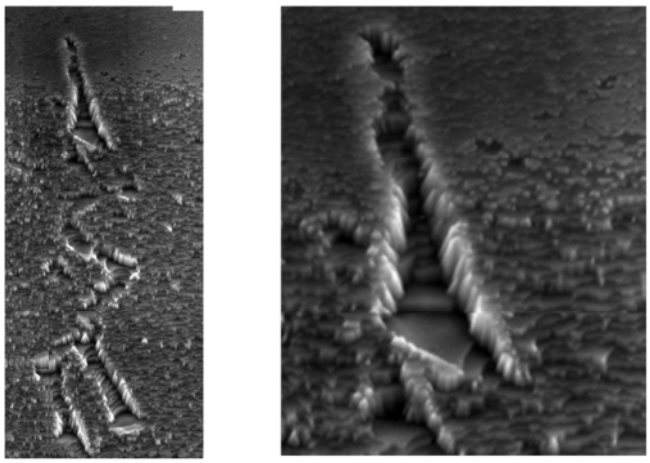

Figure 2. General view and the details of unknown particle reflection area on MDS surface.

This object is made of iron-cobalt alloy and it is probably multi-domain magnetic material with the typical internal magnetic field $H_0 \approx 6...8$ kOe . The typical size of domain wall is about $\Delta r \approx 2$ microns. The same size has the area of magnetic field $H_{out}(r) \approx H_0 \exp(-r/\Delta r)$, outside the magnetic material. If the magnetic charge of the particle equals $g = (137...68)e$ than the magnitude of magnetic potential barrier in the area of «point of reflection» equals (see Fig. 3)

$$V_M \approx \int_0^\infty gH_{out}(r)dr = gH_0\Delta r \approx 50...30\ keV \qquad (1)$$

From these results the upper estimation of unknown magneto-charged particle mass can be made:

$$M_g < \frac{2V_M}{v_g^2} \approx 10^{-23}\ gram \qquad (2)$$

The upper limit of magnetic monopole mass is less than $M_g=10^{-23}$ gram, that is by 10^{16} times less than previous well known cosmological estimations (10^{-7} gram) based on the grand unified theory!

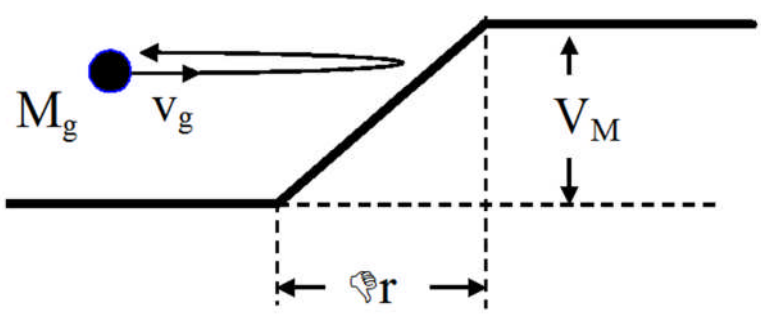

Figure 3. The scheme of reflection of magnetic charge from magnetic domain

So with a high probability the unknown particle is a light magnetic monopole that was introduced by George Lochak [4], and that is the magneto-excited neutrino.

There are two possible ways for generation (creation) of such particles during the experiments in “Proton-21” Lab:

1. These monopoles were created during nuclear processes of protonization and neutronization in collapse zone with the presence of very strong squeezed nonuniform magnetic field in the experimental setup of "Proton21" Lab. Fundamental nuclear transformation in this setup during the formation (shock implosion) and explosion of this zone is described in [3, 5-7]. A specific mechanism of the generation of magnetic charge can be related with the topological features of the collapse zone.
2. Generation of these monopoles took place during the break of stable monopole-antimonopole pair of cosmological origin in very strong squeezed magnetic field.

Let us consider the parameters of such processes.

Parameters of such pair can be calculated with the use of conservation law for its total energy

$$M(r)c^2 \equiv \sqrt{p^2c^2 + 4M_g^2c^4} - \frac{g^2}{r} \geq 0 \tag{3}$$

and uncertainty relation

$$\overline{p^2}\ \overline{r^2} \geq \hbar^2/4 \tag{4}$$

In this case the minimal meansquare size of monopole-antimonopole pair and maximal meansquare impulse of relative motion are following

$$r_{\min} \equiv \sqrt{\overline{r_{\min}^2}} \geq g^2/2M_gc^2, \tag{5}$$

$$p_{\max} \equiv \sqrt{\overline{p_{\max}^2}} \geq \hbar/2r_{\min} = M_gc^2\hbar/g^2 \tag{6}$$

From (5) it follows that $r_{min} \geq 10^{-12}$ cm (if monopole mass M_g equals proton mass $m_p = 1.6.10^{-24}$ g) and $r_{min} \geq 10^{-9}$ cm if monopole mass equals electron mass.

The potential energy of monopole-antimonopole pair with the size of r_{min} is

$$|V_0(r_{\min})| \approx \frac{g^2}{r_{\min}} \geq 2M_gc^2 \tag{7}$$

The maximal kinetic energy for relativistic and nonrelativistic motion of monopole and antimonopole inside the pair is described by the equations

$$T_{\max}^{nonrel} \approx p_{\max}^2/2\mu_g \geq \hbar^2/4M_gr_{\min}^2 = M_gc^2(\hbar c/g^2)^2, \tag{8}$$

$$T_{\max}^{rel} \approx p_{\max}c \approx \hbar c/2r_{\min} \approx M_gc^2(\hbar c/g^2) \tag{9}$$

Here $\mu_g = M_g / 2$ is the reduced mass of monopole. From last two equations it follows that the motion of monopole (antimonopole) inside the pair is nonrelativistic:
$T_{\max}^{nonrel}, T_{\max}^{rel} << M_g c^2$.

From formulas (7-9) it also follows that the ratio of kinetic and potential energies in each pair is very small both in nonrelativistic and relativistic cases

$$T_{\max}^{nonrelat} / |V_0(r_{\min})| \approx (\hbar c / g^2)^2 / 2 << 1, \quad (10)$$

$$T_{\max}^{relat} / |V_0(r_{\min})| \approx (\hbar c / g^2) / 2 << 1 \quad (11)$$

This result proves that monopole-antimonopole pair is very stable neutral system.

The total mass of such system in stable bound state

$$M(r_{\min}) \equiv \sqrt{(p_{\max}^2 / c^2) + 4M_g^2} - \frac{g^2}{r_{\min} c^2} \geq \sqrt{(\hbar^2 / 4r_{\min}^2 c^2) + 4M_g^2} - \frac{g^2}{r_{\min} c^2} \approx$$
$$M_g \left(\frac{\hbar c}{2g^2} \right)^2 \leq \frac{M_g}{(137)^2} \quad (12)$$

is very small.

In fact such pair is an invisible electro- and magneto- uncharged and extremely light object. It is possible that such objects have existed (unnoticed) in the universe from the moment of the Big Bang.

2. Break of monopole-antimonopol pair in a strong magnetic field

In Fig. 4 the structure of the potential hole of monopole-antimonopole bounded pair in the cases of presence and absence of external locally homogeneous magnetic field H_0 is presented.

Under the external magnetic field action the essential deformation of potential hole takes place. It leads to the possibility of tunneling of one monopole and to the spontaneous brake of the monopole-antimonopole pair. The probability P_H and the life-time τ_H of such tunneling effect is similar to the probability of nuclear alpha-decay

$$P_H \equiv 1/\tau_H \approx (v_{\max} / r_{\min}) e^{-2W}; \quad v_{\max} \approx p_{\max} / M_g;$$
$$W = -\frac{1}{\hbar} \int_{r_1}^{r_2} \sqrt{2\mu_g |V_0(r) + V_H(r) - E_{\min}|} dr, \; E_{\min} \equiv V_0(r_1) + V_H(r_1), \quad (13)$$

$$V_o = -g^2 / r, V_H = -gH_0 r,$$

r_1 and r_2 are the classical turning points for the potential energy $V(r) = V_0(r) + V_H(r)$

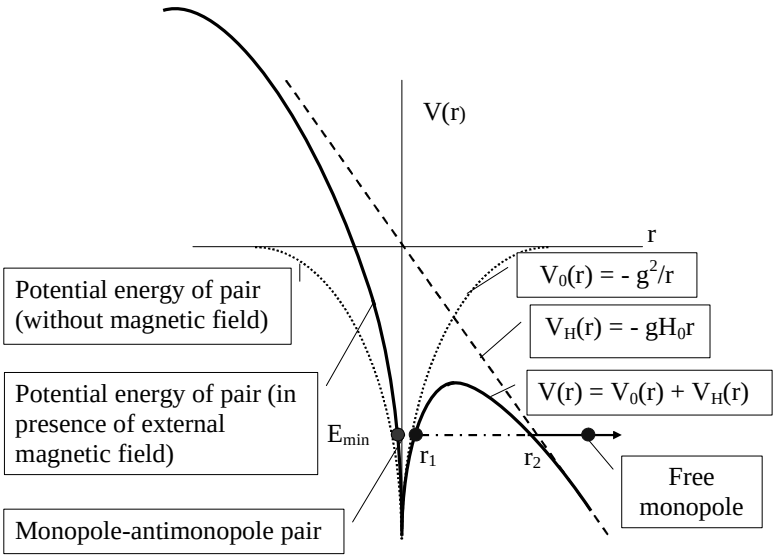

Figure 4. The structure of the potential hole of bounded monopole-antimonopole pair in the cases of presence and absence of external magnetic field.

The resulting expression for the probability of such tunneling effect is the following

$$P_H \equiv 1/\tau_H \approx 10^{12}\left(\frac{M_g}{m_p}\right)^2 e^{-2W}\,(\sec^{-1}),\ 2W \approx 2.10^{19}\left(\frac{M_g}{m_p}\right)^2 \frac{1}{H_0(Oe)} \qquad (14)$$

Here m_p - proton mass.

For light Lochak's monopole with $M_g=m_p$ and $H_0 \approx 10^{15}$ Oe we have $\tau_H \approx 10^{230}$ years.

For light monopole with $M_g=m_e$ and $H_0 \approx 10^{10}$ Oe, $\tau_H \approx 0.1$ s.

For very light "Lochak's" monopole with $M_g c^2 \approx 1$ keV at $H_0 \approx 10^7$ Oe, $\tau_H \approx 10^{-7}$ s. Formation of such (and much more strong) magnetic field takes place in "Proton21" Lab experimental setup during fast pinch-effect of hard-current electron beam [3].

References

1. Adamenko S.V., Vysotskii V.I.// 12th CMNS Proceedings, Japan, p. 356-366.
2. Adamenko S.V., Vysotskii V.I.// Surface, #3 (2006), p. 84-92.
3. Controlled Nucleosynthesis. Breakthroughs in Experiment and Theory, (Editors: S.V.Adamenko, F.Selleri, A.van der Merwe), Series: Fundamental theories in Physics, v.156, Springer, 2007, 773 p.
4. Lochak G. Z.Naturforsch., v.62b (2007) p.231-246.
5. Adamenko S.V., Vysotskii V.I. Foundations of Physics Letters, v. 17, No. 3 (2004), p. 203-233.
6. Adamenko S.V., Vysotskii V.I. Foundations of Physics, v. 34, No. 11 (2004), p. 1801-1831.
7. Adamenko S.V., Vysotskii V.I. Foundations of Phys. Letters, v.19, No. 1 (2006), p. 21-36.

Heavy Electrons in Nano-Structure Clusters of Disordered Solids

Dimiter Alexandrov
Lakehead University, Thunder Bay, Ontario, Canada

Abstract

The existence of heavy electrons is found theoretically in nano-structure clusters of disordered solids. The basis of the investigation is the electron band structures of disordered semiconductors previously determined by the author. The existence of electron energy pockets is found for the electrons in the conduction bands of these semiconductors that are nano-confining potential valleys of dimensions in the range of the primitive cell. The electron wave function of the confined electron is determined in when the electron interacts with local electrical field that is external for the energy pocket, and the average velocity of the electron is found. An expression for electron mass of an electron localized in pocket is derived. It is found that this electron mass is greater than the electron mass at rest and the confined electrons are designated heavy electrons. The possibility of interactions of protons with heavy electrons is discussed.

Introduction

The problem about the electron effective mass in solids is important with regard to both electron and optical properties of solids. The usual methods of determining the electron effective masses are connected with preliminary calculations of corresponding electron band structures and further computations of electron mass values. These approaches assume there are no external radiations (laser, etc.) that interact with the electrons in solids leading to electron mass renormalizations according to a determined rule [1, 2]. Generally it can be considered that all effective mass calculations about the charges (electrons and holes) in solids are based on the corresponding electron band structures ignoring the rule given in [1, 2]. However, recently some authors [3, 4] have considered the impact of interaction of external electro-magnetic field with electrons in solids on the electron effective mass, and they have found that increase of this mass can be expected. Although the authors of [3] in comparison with the authors of [4] give different estimation of the impact of an external electro-magnetic field interacting with electrons on the electron mass both works [3] and [4] can be considered as contributions in the theory of the effective mass of heavy electrons. Both works assume the existence of heavy electrons in nano-layers on the electrode surface.

The author's research progress [5-8] in determining the electron band structures of disordered semiconductors is the basis of this paper. Previously calculated electron band structures of disordered nitride semiconductor compound alloys are used and the existence of energy pockets for electrons in conduction bands is found. These energy pockets are found to be potential energy valleys in the conduction bands having dimensions in the range of the primitive cell. Interaction of external electrical field with electron located in energy pocket is investigated and

the corresponding electron wave function of the confined electron in a free electron approximation is determined. Formula for effective mass of a confined electron in pocket is derived and conclusions are drawn about the existence of heavy electrons. The interaction of the heavy electrons with protons is discussed.

Electron band structures of disordered solids and electron energy pockets

Disordered solids having common formula $A_xB_{1-x}C$ ($0 \leq x \leq 1$, A and B have equal valences) are called multinary crystals. A multinary crystal is considered to be a periodical crystal having a large primitive super-cell, containing a finite number of quasi-elementary cells. It is found [5] that the electron energy in a primitive super-cell of the multinary crystal can be presented in the following way:

$$E(\mathbf{r}) = \sum_{\mathbf{q}} \delta(\mathbf{r} - \mathbf{R_q})\, E(\mathbf{q}) \qquad (1)$$

Where $\mathbf{r}$ is the radius-vector of the electron, $E(\mathbf{q})$ is electron energy in the quasi-elementary cell $\mathbf{q}$ and $\delta(\mathbf{r} - \mathbf{R_q})$ is a delta-function. The electron band structure of the multinary crystal can be determined on the basis of local interactions within the primitive super-cell, which determine the corresponding sub-bands. As a matter of fact the electron band structure of the multinary crystal determined in this way contains the same sub-bands as those determined for the primitive super-cell of the same multinary crystal without consideration of the localizations of the interactions. However the sub-bands determined by (1) are localized in the corresponding quasi-elementary cells. Linear combination of atomic orbitals (LCAO) method is used by the author for electron band structure calculations for disordered solids in case of nitride semiconductors.

After detailed investigation, the author found [5-8] that the properties of a disordered semiconductor can be determined if it is taken only a part of the calculated LCAO electron band structure corresponding to configuration of quasi-elementary cells giving the deepest energy pocket for the electrons in the conduction band, deepest energy pocket for the holes in the valence band, and that these energy pockets are at the shortest distance. To satisfy these three conditions, a configuration of five different types of wurtzite quasi-elementary cells taken in the following order must be used for $In_xGa_{1-x}N$ (Fig. 1):

(1) Pure GaN quasi-elementary cell containing two atoms of Ga and two atoms of N surrounded by second neighboring Ga cations
(2) Mixed In-GaN quasi-elementary cell containing half atoms of In, one and half atoms of Ga and two atoms of N, having second neighboring cations In and Ga
(3) Mixed In-GaN quasi-elementary cell containing one atom In, one atom Ga and two atoms of N, having second neighboring cations In and Ga
(4) Mixed In-GaN quasi-elementary cell containing half atoms of Ga, one and half atoms of In and two atoms of N, having second neighboring cations In and Ga
(5) Pure InN quasi-elementary cell containing two atoms of In and two atoms of N, having second neighboring cations In. Each type of quasi-elementary cell forms sector υ of the corresponding electron band structure ($\upsilon = 1, 2, 3, 4, 5$)

The same method can be used for calculation of energy band structures of other disordered semiconductors – nitrides, arsenides, etc. The author has made LCAO electron band structure calculations [5 – 8] for $In_xGa_{1-x}N$ (Fig. 1), for $In_xAl_{1-x}N$, for $Ga_xAl_{1-x}N$, for InO_yN_{1-y} and for non-stoichiometric InN:In .The energy levels Γ^{υ}_{c1} are the bottom of the conduction band, and the energy levels Γ^{υ}_{v15} are the top of the valence band. All energies are determined by taking the energy of the vacuum as being equal to zero. (The values shown in Fig. 1 correspond to a ratio of 1:1 between the surrounding atoms of different sorts.) The energy difference $E^{\upsilon}_{g} = (\Gamma^{\upsilon}_{c1} - \Gamma^{\upsilon}_{v15})$ gives the energy band gap of sector υ. The energy level Γ^{4}_{c1} for $In_xGa_{1-x}N$ (Fig. 1) is below the neighboring levels Γ^{3}_{c1} and Γ^{5}_{c1}, which means that an electron occupying this level is confined in local potential valley Γ^{4}_{c1} of the conduction band of $In_xGa_{1-x}N$. In addition the dimensions of this valley are equal to the dimensions of the quasi-elementary cell of $In_xGa_{1-x}N$ containing half atoms of Ga, one and half atoms of In and two atoms of N, having second neighboring cations In and Ga, and these dimensions are in the range of the primitive cell – i.e. one can consider that Γ^{4}_{c1} forms an electron energy pocket. The same consideration can be done for the level Γ^{3}_{v15} in regard to holes in the valence band of $In_xGa_{1-x}N$, however in this paper it is assumed that the valence band is fully occupied in term of electrons, i.e. there are no holes, and there are no inter-band electron transitions.

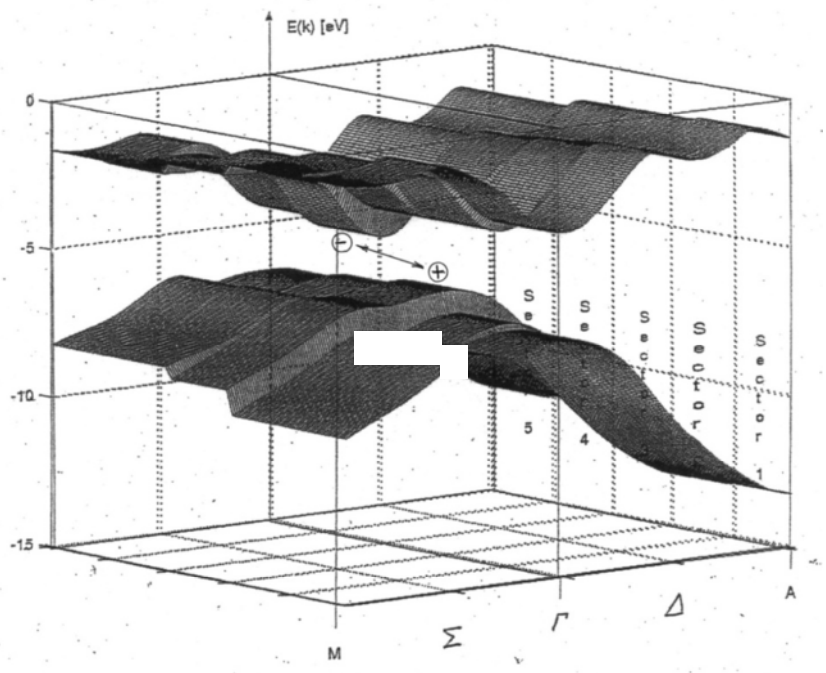

Figure 1. Electron band structure of $In_xGa_{1-x}N$. The electron energy pocket is designated.

Effective mass of confined electron in pocket

If an electron occupies the state Γ^{4}_{c1} in $In_xGa_{1-x}N$ it will be confined in the pocket and its further participation in a charge transfer along the solid will require its removing from the level Γ^{4}_{c1}. One considers this removing to be done by electrical filed in order the results to be

applicable in case of interaction of other charged particles such as protons and deuterium nuclei with confined electrons. An applied electrical field can remove the confined electron by quantum tunneling trough potential barrier [9]. In this case one can write:

$$\Psi_{out}(x_\mu) = D^{1/2} \ \Psi_{in}(x_\mu) \tag{2}$$

Where $\Psi_{in}(x_\mu)$ is the wave function of the confined electron, $\Psi_{out}(x_\mu)$ is the wave function of the electron after the barrier, and D is transmission coefficient. The applied electrical field has strength ξ_μ acting in direction x_μ. According to [9] one can write (k is electron wave vector):

$$\Psi_{in}(x_\mu) = A \exp(i\, k_\mu\, x_\mu) \tag{3}$$

$$\Psi_{out}(x_\mu) = C \exp(i\, k_\mu\, x_\mu) \tag{4}$$

The process of quantum tunneling of an electron confined in pocket Γ^4_{c1} in $In_xGa_{1-x}N$ is schematically described in Fig. 2. In fact the line Γ^{υ}_{c1} is the bottom of the conduction band at point Γ in the electron band structure in Fig. 1, and Γ^{υ}_{v15} is the top of valence band at point Γ of the same electron band structure. The shifts of the lines Γ^{υ}_{c1} and Γ^{υ}_{v15} in Fig. 2 are due to influence of the electrical filed ξ_μ having designated direction on this figure as well.

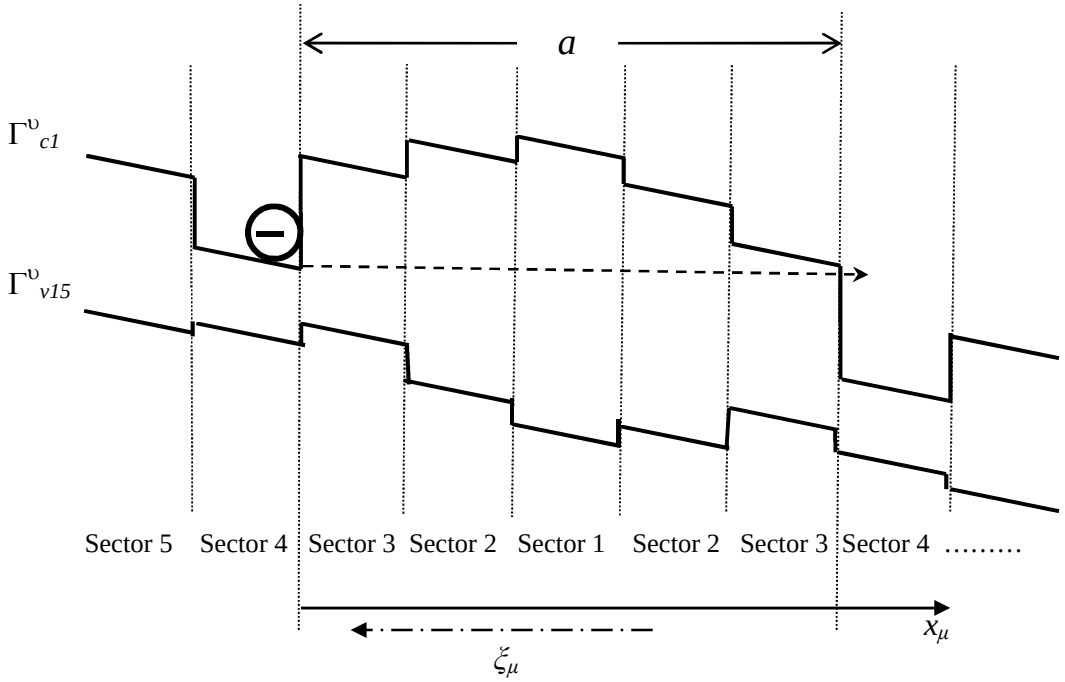

Figure 2. Electron band structure of $In_xGa_{1-x}N$ in external electrical field (not in scale). The tunneling from level Γ^4_{c1} is shown.

According to both [9] and Fig. 2 the transmission coefficient of quantum tunneling trough a potential barrier of with a is

$$D = \exp\{-(2/\hbar)\int_0^a [2m(U(x)-E)]^{1/2} dx\} \quad (5)$$

Where E is the electron energy, $U(x)$ is the potential function of the barrier, m is electron mass on level Γ^4_{c1}, and $x = x_\mu$. Also $m = m^* m_0$ where m^* is electron zone mass and m_0 is the electron mass in rest. The author assumes that the bottom of the conduction band in a pocket has the same behavior as the bottom of the same band of pure semiconductor built by the same chemical elements as these presented in the corresponding sector. In this way the author assumes that $m^* \neq 1$. Using Fig. 2 one can write for $U(x)$ ($x = x_\mu$):

$$U(x) = U_0 - q\xi_\mu x_\mu \quad (6)$$

Where q is electron charge and U_0 is average height of the potential barrier for $\xi_\mu = 0$.

It can be considered a free electron having mass m moving after the barrier. According to [10] the average value of the velocity $\overline{v_{\mu\ out}}$ of this electron in direction x_μ is:

$$\overline{v_{\mu\ out}} = (\hbar / 2\, m\, i)\int \{\Psi^*_{out}(x_\mu)\, \partial\, \Psi_{out}(x_\mu) / \partial\, x_\mu - \Psi_{out}(x_\mu)\, \partial\, \Psi^*_{out}(x_\mu) / \partial\, x_\mu\} d\, x_\mu \quad (7)$$

Considering (2) and (5) one can write

$$\overline{v_{\mu\ out}} = (\hbar / 2\, m\, D^{-1}\, i)\int \{\Psi^*_{in}(x_\mu)\, \partial\, \Psi_{in}(x_\mu) / \partial\, x_\mu - \Psi_{in}(x_\mu)\, \partial\, \Psi^*_{in}(x_\mu) / \partial\, x_\mu\}\, d\, x_\mu \quad (8)$$

or

$$\overline{v_{\mu\ out}} = (\hbar / 2\, m_{eff}\, i)\int \{\Psi^*_{in}(x_\mu)\, \partial\, \Psi_{in}(x_\mu) / \partial\, x_\mu - \Psi_{in}(x_\mu)\, \partial\, \Psi^*_{in}(x_\mu) / \partial\, x_\mu\}\, d\, x_\mu \quad (9)$$

Where m_{eff} is defined to be effective mass of the electron confined in an energy pocket and

$$m_{eff} = m\, D^{-1} = m^* m_0 \exp\{(2/\hbar)\sqrt{2m^* m_0}\int_0^a [U_0 - q\xi_\mu x - E]^{1/2} dx\} \quad (10)$$

Where the condition $U_0 - q\,\xi_\mu\, x - E \geq 0$ must be obeyed. The meaning of (10) is that one can treat a confined electron as a free electron having electron effective mass m_{eff}. The expressions (7) – (10) can be used in case of interactions of a confined electron with local fields of strength ξ_μ – for example with charged particles (other electrons, protons, deuterium nuclei, etc.). The author considers that these expressions can be used for description of currents using confined charges in disordered solids however corresponding corrections accounting other phenomena must be made as well.

The expression in the exponent of (10) is positive and therefore $m_{eff} \geq m^* m_0$. It is the reason that the author to consider that the confined electrons are heavy. The formula (10) provides that if $E \rightarrow U_0$ or/and $a \rightarrow 0$ then $m_{eff} \rightarrow m^* m_0$. This expression includes parameters a, U_0, E and m^*, i.e. m_{eff} depends on the properties of the electron band structure and for ξ_μ = const. (or weak ξ_μ) further change of m_{eff} is possible only by change of m^*. As it was mentioned above the electron effective mass m_{eff} can be used in case of interaction of heavy electron with other charged particles including protons and deuterium nuclei. In this way it is useful the effective Bohr radius [9] to be determined

$$a_{B\,eff} = \hbar^2 / m_{eff}\, q^2 \qquad (11)$$

Using the author's previous results [5 – 8] for LCAO electron band structure calculations and expressions (10) and (11), the parameters m_{eff} and $a_{B\,eff}$ for heavy electrons in $In_xGa_{1-x}N$, in $In_xAl_{1-x}N$, in InO_yN_{1-y} and in non-stoichiometric InN:In are found for: *i)* weak local electrical fields $\xi_\mu << (U_0 - E) / (q\, a)$; and *ii)* strong local electrical fields $\xi_\mu = (U_0 - E) / (q\, a)$. It is accepted that $m^* = 0.18$ for all nitride semiconductor materials. It is assumed that a corresponds to shortest possible distance between two nearest electron energy pockets. This situation is shown in Fig. 2 and it can be achieved technologically in nano-layers. The results are summarized in Table 1. It is important to be noted that the impact of the heavy electrons on the electrical properties can be expected to be significant in nano-structures having low concentrations of light electrons. Also this impact is higher in wide energy band gap disordered materials because the influence of the defects on the conductivity is small. Existence of heavy electrons in non-metal nano-layers – for example in nano-structures of metallic hydrides on metal surfaces – can be expected as well.

Table 1. Effective masses and effective Bohr radii of heavy electrons in several disordered solids

	m_{eff}, in m_0 units		$a_{B\,eff}$, Å	
	weak field	strong field	weak field	strong field
$In_xGa_{1-x}N$	851.02	50.89	$0.62*10^{-3}$	0.0104
$In_xAl_{1-x}N$	3.41	1.28	0.1553	0.4134
InO_yN_{1-y}	11.96	2.96	0.0442	0.1788
InN:In	286.41	24.61	0.0018	0.0215

Discussion about possible interactions of protons with heavy electrons

It can be seen in Table 1 that the effective mass of the heavy electrons can reach high values in some materials. However it depends on the local field. Therefore the necessary and sufficient condition that the heavy electrons to behave as heavy negative particles in interactions with other charged particles is that the field of every interaction must be weak.

In the light of the above if this condition is fulfilled, a heavy electron e_h^- can participate in process [3, 11]:

$$e_h^- + p^+ \rightarrow n + \nu_l \quad (12)$$

Where p^+, n and ν_l designate proton, neutron and neutrino respectively. In order for this process to take place the following threshold condition about the effective mass of heavy electron e_h^- must be fulfilled [3]:

$$\beta = m_{eff} / m_0 > 2.531 \quad (13)$$

The effective masses from Table 1 even for strong field interactions (except for $In_xAl_{1-x}N$) fulfill the condition (13).

It must be noted that certain particles must reach the region where the heavy electron is localized for the interaction to occur; i.e., the probability of the interaction of heavy electron–particle is higher in nano-layers or in nano-structure clusters that are close to the surface.

Conclusion

This paper can be considered the author's first contribution in the field of interaction of charged particles with electrons localized in solids. Although the existence of heavy electrons in nano-structures is shown theoretically the author considers that the conditions about weak interaction in solids must be found in order further study of heavy electron-particle interactions to be performed. Finding of these conditions will be subject of a future work. Future work will also consider the role of heavy electrons in metallic hydride nano-layers.

References

1. L. D. Landau, E. M. Lifshitz, *The Classical Theory of Fields*, Pergamon Press, Oxford (1975)
2. V. B. Berestetskii, E. M. Lifshitz, L. P. Pitaevskii, *Quantum Electrodynamics*, Butterworth Heinmann, Oxford (1997)
3. A. Widom, L. Larsen, *Eur. Phys. Journal C,* **46**, 107 (2006)
4. P. L. Hagelstein, I. U. Chaudhary, *Electron mass shift in nonthermal systems* (D. Nagel, private communication)
5. D. Alexandrov, *Journal of Crystal Growth*, **246**, 325 (2002)
6. D. Alexandrov, S. Butcher, M. Wintrebert-Fouquet, *Journal of Vacuum Science and Technology*, **A22(3)**, 954 (2004)
7. D. Alexandrov, S. Butcher, T. Tansley, *Physica Status Solidi*, **203,** 25 (2006)
8. D. Alexandrov, S. Butcher, T. Tansley, *Journal of Crystal Growth*, **288**, 261 (2006)
9. A. S. Davydov, *Quantum Mechanics*, Pergamon Press, Oxford (1965)
10. K. F. Brennan, *The Physics of Semiconductors*, Cambridge University Press, Cambridge (1999)
11. R. E. Marshak, Riazuddin, C. P. Ryan, *Theory of Weak Interaction of Elementary Particles*, Interscience, New York (1969)

Empirical System Identification (ESID) and Optimal Control of Lattice-Assisted Nuclear Reactors

Robert W. Bass[1] and Mitchell Swartz[2]
[1] *Innoventek Inc.*
[2] *JET Energy, Inc.*

Dr. Mitchell Swartz does not wish to have his papers uploaded to LENR-CANR.org. A copy of this paper can be found here:

http://www.iscmns.org/iccf14/ProcICCF14b.pdf

This page intentionally left blank

This page intentionally left blank

This page intentionally left blank

This page intentionally left blank

This page intentionally left blank

Can Established Physical Principles Explain Solid-State Fusion?

Ben R. Breed
Cone Corporation
Dripping Springs, Texas 78620

ABSTRACT

This report examines, in the light of new evidence, whether low energy nuclear fusion can possibly conform to fundamental laws of physics. The new evidence examined here may explain two cited deficiencies, the lack of a sufficient deuteron coupling mechanism and the lack of certain nuclear by-products. The concept that heavy electrons (fermions, pseudo-particles) are able to screen deuterons may have been dismissed too early. In this paper we show that heavy electrons may cause a high degree of localization, a central effect that is needed in the screening process. Many heavy electron (heavy fermion) materials exist, and in many of these, an increase in electron localization on lattice sites has already been seen directly. The lack of nuclear by-products may in fact be explained by a physically reasonable interaction between four deuterons in which only easily absorbed alpha particles and low energy gammas are produced.

1. INTRODUCTION

The many positive reports of success in recent low energy nuclear reaction (LENR) processes lead one to wonder if there isn't a possible, perhaps unexplored, set of physical or chemical electrolysis principles by which they may be explained. In this paper a set of possibilities is put forward in hopes that experiments will be performed to answer this question. These possibilities consist of the application of heavy pseudo-particles to provide the detailed localization and inertia needed for effective Coulomb screening, and multiple deuteron interactions in which only easily absorbed alpha particles and gammas are produced [1].

The critical view of research in the LENR area is based mainly on the lack of an established screening mechanism, and the lack of observed nuclear by-products, making it hard to reconcile the purported observations with well established physical principles. This situation has continued to the present time in spite of the publication of numerous reports of positive experimental results, with correlated improvements in reproducibility.

Two prominent expositions are those of Leggett and Baym [2] and Koonin and Nauenberg [3]. Each of these is mainly concerned with the lack of a strong coupling method rather than the lack of fusion by-products. A possible method out of this difficulty is addressed in Section 2. In Section 2.1 it is argued that high effective-mass in some cases allows a localization of the pseudo-particles on lattice sites. An operative question is on how fine a spatial scale these heavy mass effects occur. Section 3 discusses the crystalline geometries. Section 4 uses the

results of the previous sections to propose a possible fusion mechanism. The other question, about possible explanations for the absence of fusion by-products, will be addressed in Section 5.

2. POSSIBLE SOLID-STATE MECHANISM TO PROVIDE STRONG COUPLING

It is common knowledge that muon induced fusion has been produced in the hydrogen molecule. The muon, a particle similar to the electron but having a mass 207 times larger, when substituted for an electron in a hydrogen molecule, causes hydrogen isotopic nuclei to come closer to each other (by about 200 times). This is well understood by modern physical principles. The result is a much increased rate at which the nuclei fuse. This increased rate is so much larger than for the normal hydrogen molecule, that the method has been extensively investigated for use in fusion energy production. The muon exists for too short a time to produce enough fusions for a practical application.

Koonin and Nauenberg [3] give details showing that putative electrons with an extra mass can increase the rate of fusion of the nuclei in molecular hydrogen. An electron with five times as much mass could generate fusions at the level reported by Steven Jones, et al. [4], and a mass ten times heavier might generate fusions at a rate in line with the original Pons and Fleishman [5] reports.

Is it possible that deuteron fusion may be enhanced by use of heavy electron materials? If so the enhancement would need to be caused by a more effective negative electron screening of the deuterons' positive charges. The critical question in this regard is whether the action of these pseudo-particles is at all similar to that of heavy electrons on the fine spatial scales required. There are many indications that it is. For many solid state phenomena, such as the de Haas-van Alphen effect (DHVA) [6], experiments show them performing like individual but heavier electrons. Luttinger, in discussing the DHVA effect in a system of interacting pseudo-particles states that his result "… is exactly what one computes on a single-particle basis, except that the true single-particle excitation energies must be used,…[6] " Other phenomena that have been explained using a single-particle description of heavy fermions include electronic heat capacity, Pauli spin susceptibility, Landau diamagnetic susceptibility, and electrical resistance and mobility. It is possible that only experiment will tell the smallest (finest) spatial extent of these effects.

Heavy mass also implies the existence of an inertial effect, and this means that its negative charge could resist being pushed or accelerated out of locations such as between two or more deuterons. This is important since it implies that the heavy-electron has a smaller wavelength in any given energy state than single electrons in a simple tight binding model.

Palladium, platinum, nickel, and cobalt, as tabulated by Kittel [7], are materials with a very high electron effective-mass. Today's interest in heavy fermion materials, on the other hand, arises largely from the fact that many high-temperature superconductors (copper oxides) belong to this class. It may be of interest in this regard that hydrogen doped palladium is a superconductor, with an increasing critical temperature with hydrogen loading. Along with

having superconducting phases these materials often exhibit ferromagnetic and anti-ferromagnetic phases [8, 9]. Heavy fermion properties continue in the so-called normal phase that occurs above the superconducting critical temperatures.

Heavy-electron materials include, but are not limited to palladium, platinum, nickel, cobalt, niobium, tantalum, vanadium, titanium, tungsten, yttrium, and zirconium atoms. Heavy-electron materials may be other than the transition metals. These include $CeCu_2Si_2$, UBe_{13}, UPt_3, URu_2Si_2, UPd_2Al_3, UNi_2Al_3, $CeCu_2Ge_2$, $CeRh_2Si_2$, $CePd_2Si_2$, $CeIn_3$, and many others. To our knowledge, prior to this report this type of material has never been considered for low temperature fusion when embedded with deuterons. An additional fusion possibility occurs when one of the high temperature superconducting materials is substituted for one of the transition metals. These materials include the doped lanthanide copper oxides, the yttrium-barium-copper oxides, those with the generic composition $RBa_2Cu_3O_{7-x}$ in which R stands for yttrium or one of the lanthanide rare earths, and many others in this copper oxide family.

The suggestion is made here for the first time that low temperature fusion might be expected to occur in any of these heavy electron systems if they contain absorbed deuterons. A more reproducible effect may occur. An interesting experiment should be performed by embedding deuterons in these materials and investigating possible fusions at low temperatures. At these temperatures the fermion heavy mass effect is well demonstrated for many of them.

Koonin and Nauenberg point out that effective-mass "should not be associated with any physical excitation in a solid material, as only the bare electron is relevant at the short length scales that are important here." The Energy Research Panel Advisory Board investigating early fusion reports stated that "…this phenomenon is described as… involving strong correlation near the Fermi surface. As such, heavy fermions extend over many lattice sites. …. only short-wavelength 'bare' electron excitations are relevant for screening…" [10].This statement is correct for the classical effective-mass concept. It omits consideration of many materials with very heavy effective masses caused by other strong interactions. Could it be that these authors have inadvertently given away a major advantage of the solid state medium by not expanding the scope of what they mean by effective-mass? Heavy electrons correspond to pseudo-particle peaks in an energy spectrum, and in addition they may be broadly spread in wavelength. This spreading is particularly significant if the pseudo-particle resides on or near the Brillouin zone boundary. Based on elementary Fourier analysis the pseudo-particle spatial distribution is concentrated in smaller regions when the wave number distributions have these broadened properties.

It is because pseudo-particle phenomena are coherent (highly correlated) over macroscopic volumes that the concept of pseudo-particle mass in these heavy fermion materials may be important. Here, 'spatial bandwidth' refers to the width of the band of wave numbers near the peak energy of the pseudo-particle [12]. A Fourier expansion in terms of these wave numbers can produce a periodic but apparent unit-cell-localized result as is easily demonstrated**.** Also Fourier expansion in terms of a band of wave numbers concentrated around one-half this wave-number**,** $\pi/(2a)$ with a equal to the square-lattice spacing, may produce unit cell localized results that occur on every second unit cell, etc.

The higher the mass of a particle (or pseudo-particle) the greater is our ability to localize it, and vice versa [13]. In the following paragraphs this relationship will be used to point to the fact that high effective-mass pseudo-particles can imply high localization of electrons (and charge stiffness) on the atomic lattice sites. This in turn will be used to argue that the effect of the heavy-electrons in a palladium lattice doped with deuterons may be to provide a much more effective screening effect between deuterons.

2.1. HIGH PSEUDO-PARTICLE MASS AND LOCALIZABILITY

Pseudo-particles may acquire the effect of an additional mass through mutual interactions in a many-body system [7, 14, 15]. Consider a many–body system with a Hamiltonian

$$H = H_0 + H_1, \tag{1}$$

where H_0 and H_1 are the free particle and interaction Hamiltonians respectively. If the free particle Green's function G_0 (based on H_0) is known, the many-body Green's function may in principle be found by solving the Dyson equation

$$G = G_0 + G_0 \Sigma G, \tag{2}$$

in which $\Sigma = \Sigma_1 + \Sigma_2 + \Sigma_3 + ...$ is known as the "irreducible self-energy part" or "the mass operator" [14, 16]. It is the expression for the contributions to the mass of a quasi-particle generated in the system due to inter-particle and lattice interactions. The expression for Σ is a sum of progressively larger (but weaker) stages of the interaction. After "mass renormalization" the Green's function is commonly expressed in the frequency-wave number (k, ω) domain as

$$G(k,\omega) = [\omega - e_k - \Sigma(k,\omega)]^{-1}, \tag{3}$$

in which Σ is in general a complex number. e_k is the peak energy in a band at wavenumber k. The corresponding spectral function is

$$A(k, -i\omega) \equiv -\frac{1}{\pi}\,\mathrm{Im}(G(k,\omega)) \tag{4}$$

$$= -\frac{1}{\pi}\left[\frac{\lambda}{(\omega - e_k - \Sigma_r)^2 + \lambda^2}\right],$$

where $\Sigma_r = \mathrm{Re}(\Sigma(k,\omega))$, and $\lambda = \mathrm{Im}(\Sigma(k,\omega))$ are the real and imaginary parts of Σ.

The spectrum is a Lorentzian density if λ, the imaginary part of Σ controlling the lifetime of the pseudo-particle, is independent of energy. If e_k and k are to be good (stable) quantum numbers the imaginary part must be small and the particle lifetime long. The real part of Σ is the contribution to the pseudo-particle's effective-mass in addition to that that an electron has

in, for example, a single electron tight binding approximation [7, 14]. Since the target crystal lattices are mostly cubic, the spectrum may be treated as being isotropic.

An extremum of the spectral function occurs where $E_k \equiv \omega(k) = e_k + \Sigma_r$. For a particular direction in wavenumber space the point at which the extremum occurs will be denoted $k = k_0$. For an isotropic environment the effective-mass [14, 17] evaluated for the pseudo-particle representing the spectral peak, has the definition

$$\frac{1}{m^*} = \left.\frac{\partial^2 E_k}{\partial k^2}\right|_{\substack{\omega=\omega(k_0) \\ k=k_0, e_k=e_{k_0}}} . \tag{5}$$

When the expression for the energy is expanded about this peak it becomes

$$E_k = E_{k_0} + \frac{1}{2}\left(k - k_0\right)^2 / m^* + ..., \tag{6}$$

and if this expression is substituted in the spectral function there results

$$A(k, -i\omega)\,|_{k \approx k_0} = -\frac{\lambda}{\pi}\left|\left[\left(\frac{\left(k-k_0\right)^2}{2m^*}\right) + ... + i\lambda\right]\right|^{-2} , \tag{7}$$

which, for small λ, is the transfer function of a linear system having a peak whose wave number mean-squared bandwidth is proportional to m^*, and this in turn corresponds to an impulse response that is highly peaked spatially with appropriate periodicity and with a mean-squared spatial width at lattice sites proportional to $1/m^*$ [16]. The Fourier transform of a narrow spectral band extends periodically and is seen to have a spatial resolution inversely proportional to the band's wave-number bandwidth. Thus a narrow spectral (energy) bandwidth implies a broad correlation in space, but not necessarily a long wavelength if its wave number contributions are near a zone boundary.

Thus far the objective of this section has been to show that a spectral line corresponding to heavy-electrons or pseudo-particles, though defined over long ranges, is spatially periodic and is locally concentrated within any one or two spatial periods, if its k_0 is near (or a significant way toward) the zone boundary, and if it has a large enough wave-number spread. Alternatively, if k_0 is located half way to the boundary the localization, while still concentrated, may occur at alternate unit cells, etc. Unless the pseudo-particle represents a moving charge density wave, the charge will be concentrated on atomic lattice sites. This implies concentration near the positive hydrogen nuclei. This is particularly true if the heavy-electronic system conforms to a model similar to the Hubbard model, for which (two) electrons being confined on a site, in a lattice with more than one electron per site, is a basic part of the model.

The Hubbard model [18, 19], along with the Kondo model, is commonly used to explain heavy-fermion systems. A characteristic is a configuration of atoms with near-half filled 4d or 5d-shells forming a narrow band interacting with atomic sites. The narrowness of the d-band, along with the interactions, implies a high degree of correlation among the electrons. To explain certain behavior, the Hubbard model contrasts this implied delocalized band motion with the effect of a tight-binding model in which excess d-electrons (or holes) are allowed to spend a proportionately large amount of time in the vicinity of the lattice sites. The Hubbard Hamiltonian may be written in the following form

$$H = -t\sum_{i,i',\sigma} c^{+}_{i,\sigma} c_{i',\sigma} + U\sum_{i} n_{i_\uparrow} n_{i_\downarrow} . \qquad (8)$$

Here the sum over σ means a sum over up and down spins, $c^{+}_{i,\sigma}$ is a creation operator for an electron with spin σ at lattice site i, and $c_{i',\sigma}$ is the corresponding annihilation operator at site i'. If an electron is created at i and another is annihilated at i', one says that the electron has hopped from one site to the other. It is generally found that a physically verifiable model may be achieved even when these hopping transitions are restricted to adjacent lattice sites. This is called hybridization between states on neighboring sites. The second sum is over number operators: $n_{i_\uparrow}$, for example, is the number of electrons with up-spin at site i, etc. As usual, $n_{i_\uparrow} \equiv c^{+}_{i_\uparrow} c_{i_\uparrow}$, and $n_{i_\downarrow} \equiv c^{+}_{i_\downarrow} c_{i_\downarrow}$. Each of the terms in the second sum corresponds to two electrons interacting at the same site. t and U are coefficients that determine the relative contributions of the two terms. From the point of view of wanting charges concentrated at lattice sites for the purpose of screening hydrogen nuclei a large value of U is desirable, but hopping may also be allowed in order to transfer the charges between the transition metal atoms and the hydrogen nuclei and so-forth.

In this section it has been recalled that palladium, and the other metals that have been involved in LENR are members of the class of heavy-electron metals, and it has been demonstrated that this implies, in some metals, a high degree of localizability of the electrons on atomic lattice sites. Thus it is possible to question the claim that there is no conceivable strong coupling between the metal lattice, the electrons, and the embedded hydrogen nuclei. It is possible to argue to the contrary. But the electrons need to screen the positive charges, and the screening effect must be large enough, and must be accompanied by localization of electronic charge at lattice sites. That such a screening effect is large enough has not been proved here. But it has been shown that there that it is reasonable to look for a large effect that localizes charge at lattice sites with attributes of heavy mass. This indicates that a high level of screening by this mechanism may indeed be available.

It has been argued that the heavy nature of pseudo-particles in certain materials can enhance localization of electronic charge on lattice sites. It is appropriate at this point to recall that charge concentration on lattice sites has recently been directly observed on surfaces of high temperature superconductor classes of materials [8, 10].

3. GEOMETRIC STRUCTURES

Before estimating the feasibility of multiple nuclei interactions, it is appropriate to review the crystal geometries that are involved [20, 21]. Henceforth, when the term deuteron is used it will represent any of the three hydrogen isotopic nuclei. Fig. 1 shows an arrangement of palladium atoms and deuterons in a planar configuration that occurs when the 4-d transition metals are highly doped with absorbed deuterons. Palladium is used here as an example of metals that have been used in claims of successful low temperature fusion experiments. It may be of interest to point out the similarity of these planar configurations to the arrangements of copper and oxygen atoms in planes occurring in the copper oxide high temperature superconductors [22]. In the copper-oxygen configuration, there is a plane where the copper atoms occupy the locations of the palladium shown here and the oxygen atoms occupy the locations of the deuterons. The statement of the similarity may imply that the configuration is common to a complete class of heavy electron (high effective-mass) materials. Subsequent figures show how these planar arrangements appear in three types of crystalline unit cells.

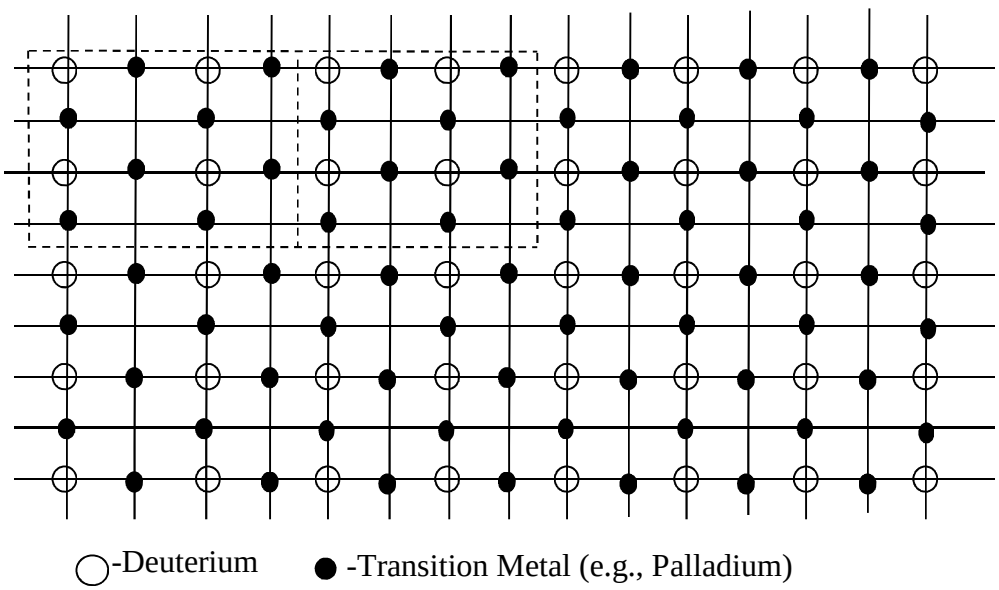

Figure 1. Two-Dimensional Arrangement of Transition Metal and Deuterium in a Disposition Similar to That in the Active Planes of Typical High-Temperature Superconductors.

Fig. 2A shows an atomic arrangement of deuterons in a body centered cubic (bcc) lattice, where the deuterons, with a slight effort, may be seen to be residing on planes. These are planes on which convergence of the deuterons (shown in Fig. 4) may be induced. Fig. 2B shows an atomic arrangement of deuterons in a face centered cubic (fcc) lattice, where the deuterons also reside on planes on which convergence of the deuterons may be induced.

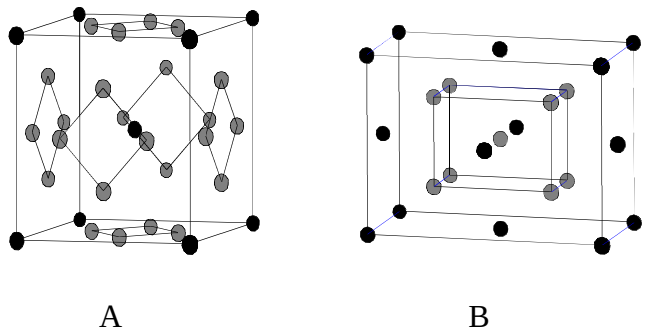

Figure 2. Atomic Arrangements of Hydrogen in a bcc Lattice, Left, and an fcc Lattice, Right. These are Arrangements with Tetrahedral Symmetry.

Fig. 3A shows an octahedron enveloping a deuteron indicating an arrangement in which deuterons have this octahedral coordination. Fig. 3B shows a planar square sub-lattice in the case where deuterons have octahedral coordination. Fig. 3C shows a tetrahedron with a deuteron on each vertex, the center of which may be the locus of convergence of the deuterons.

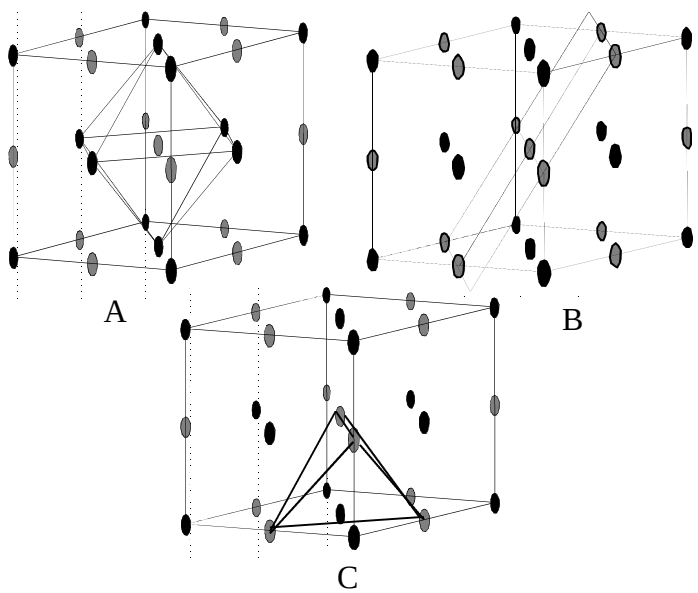

Figure 3. In Lower Concentrations, Hydrogen is in Sites with Octahedral Symmetry in an fcc Lattice. An Octahedron Enveloping a Hydrogen Nucleus is Seen on the Left. A Plane Square Sub-Lattice Containing the Octahedral Hydrogen Nuclei is Indicated on the Right. A Tetrahedron with a Hydrogen Nucleus on Each Vertex is Shown Below.

This last sort of convergence to the center of a tetrahedron is similar to that proposed by A. Takahashi [1, 23] in his electron quasi-particle expansion theory (EQPET). His theory involves the convergence of deuterons (along with certain electrons) toward the centers of the tetrahedrons with convergence being due to “transient Bose-type condensation (TBC) of

deuteron cluster at PdD_x lattice focal points" [23]. This is not required in the mechanism proposed in this report.

4. A MODEL FOR LATTICE, ELECTRON AND DEUTERON INTERACTION

In order to motivate the investigation of whether nuclear reactions could possibly be explained using basic principles, a general concept illustrated in Fig. 4, is introduced. The figure shows a two-dimensional lattice excitation, or motion, with deuterons converging toward one another as a part of general lattice vibration modes, with the arrows being reversed after a 180 degree phase change. The figure is an adaptation of Fig.1 in which lattice motions of the deuterons have been generally indicated. At a time corresponding to a half period later the deuterons have reversed directions. This motion is a part of high wavenumber lattice excitations that are an integral part of an ambient (optical and longitudinal) phonon spectrum. The corresponding wave numbers in the plane are substantially near a Brillouin zone boundary ($k = \left[\frac{\pi}{2a}, \frac{\pi}{a}\right]$ with a equal to the spacing of the square lattice.) Motions of the lattice host atoms (solid circles) are not indicated since they may assume different forms for different lattice normal modes. This particular mode for the vibration of the deuterons is not the only dynamic mode that may be important to the process described here, but it is one which may produce results that are consistent with recent measurements of surface charge ordering [8, 9].

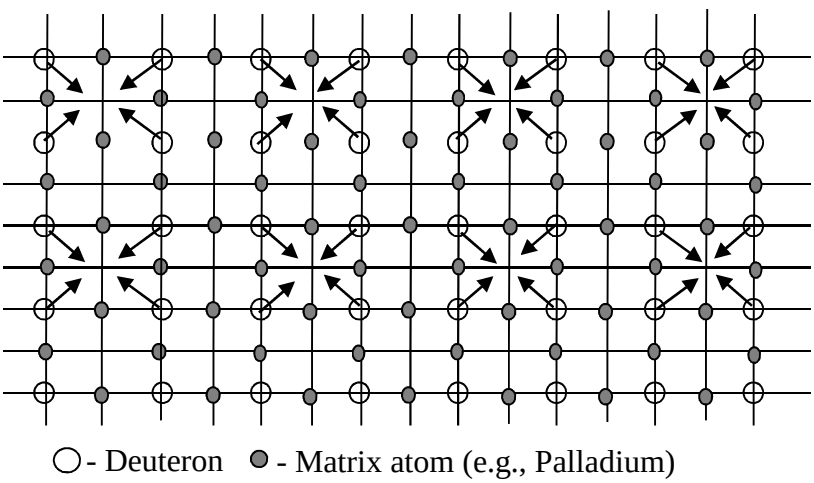

Figure 4. Two-Dimensional Lattice Excitation, with Hydrogen Nuclei Converging as a Part of General Lattice Vibration Modes That are Enhanced by Heavy Electron Screening.

The concept is as follows. The system is chosen to consist of a transition metal in the heavy-electron class in which deuterons are embedded. The extent of loading of the deuterons is stoichometric (Pd_xD, x=2 or less.) An electron model such as the Hubbard model applies. This implies that electronic charge is localized to a large extent on the positive ions, i.e., the metal ions and the deuterons. This charge localization is a result of the heavy-mass-pseudo-particle many-body phenomenon. Because negative charge screens the positive charges of the

deuterons, their interaction is affected and enhanced by this concentrated cloud of negative charge. The Born-Oppenheimer approximation applies only insofar as the positive ions have much greater mass than the electrons, meaning that their displacements are slow variables in the many-body system. The electronic structure however is strongly affected (slaved) by their motions. The closer any number of deuterons is grouped, the greater is the mean positive charge in their vicinity and, in response, the localized negative charge is greater.

The electronic response is not without inertial effects because of its heavy mass, and this offers the possibility of a resonance of sorts with the motion of the deuterons. A set of deuteron motions tending to a common point, as in Fig. 4, induces a screening effect such that the lattice vibration force constants for these motions are greatly reduced. The amount of reduction is greatest on the two-dimensional Brillouin zone-boundaries of the lattice planes containing these vibrating deuteron modes. This is because these are the wavelengths at which the greatest spatial convergence occurs. Being on or near the Brillouin zone boundary, these modes possess phase velocities in the two-dimensional Brillouin zone that are near zero. Considering the use being made here of comparisons to the copper oxides, the two-dimensional, instead of three-dimensional, nature of these lattice excitations, along with their wavenumber dependence, conforms to experimental observations on the "importance of the momentum anisotropy in determining the complex properties of the cuprates….[9]."

The variation of lattice force constants with wavenumber, due to the screening effect, along with their dependence on the wave amplitude, is an indicator of non-linear interactions. A model that fits this type of non-linear wave phenomena, describing the normal modes (phonons), with need for only minor alteration, has already been worked out. It is presented in [24] as one possible derivation of the non-linear Schrödinger equation (NSE). An outline is presented here.

Assume the wave equation $L(\partial_t, \Delta)u = 0$ applies, where L is an operator with constant coefficients. For small amplitudes any non-linear terms may be neglected in which case the solution has a form $u = \varepsilon\psi e^{i(k\cdot x-\omega t)}$, where k and ω are related by the dispersion relation $L(-i\omega, k)u = 0$. ε represents a small number. The non-linearity is introduced by requiring a specific, but alternate, dispersion relation and introducing this dispersion relation in place of the linear one in the form,

$$\omega(i\partial_t, -i\Delta)\psi e^{i(k\cdot x-\omega t)} = 0. \tag{9}$$

For the new dispersion relation the function ψ is constrained to be modulated in space and time in a specified fashion. Without belaboring the point, after expanding the desired dispersion relation about the linear one, the function ψ is found to first-order to be required to satisfy the (NSE)

$$i\frac{\partial\psi}{\partial\tau} + \frac{1}{m_a}\nabla^2\psi + \left[\frac{1}{2}qx^2 + \gamma\left|\psi\right|^2\right]\psi = 0, \tag{10}$$

where the mass at the lattice sites m_a has been replaced by half m_e and q is the vibration force constant for this mode. The parameter γ is proportional to the first order term in the expansion of the non-linear dispersion relation in terms of its dependence on the wave amplitude-squared. This is precisely what is useful in the present context. The parameter γ must be made a function of wavenumber matching the physics expected near the two-dimensional Brillouin zone boundaries as discussed above. Especially it must correspond to a lowering of the mode energy $\hbar\omega$, per phonon, on this boundary (a reciprocal effect of the electron screening). This corresponds to an increase in the occupancy of these deuteron many-body oscillator states.

The conceptual model is based on a coupling between the Hubbard model for the electronic motion and the non-linear Schrödinger -type equation describing the lattice interaction. The coupling is evidenced in the two parameters: U of the Hubbard model and γ of the NSE. An examination of the possibility of resonance phenomena being induced by this type of coupling is planned. It is anticipated that mode locking and mode competition phenomena will exist, and these may lead to highly correlated, large amplitude, deuteron motions.

An effect known as a Peierls instability occurs on a zone boundary when the d-band is not filled and the Fermi level E_f falls within the band as described in [25]. A periodic spatial distortion may happen to induce a lower energy state than that that occurs for the undistorted lattice. The distortions produced by the motions indicated in Fig. 4 are of just this sort. They have a periodicity twice that of the lattice, inducing a spatially periodic lattice distortion. This opens an additional possibility of a time-periodic Peierls instability at the frequency of these vibration modes.

5. MULTIPLE DEUTERON NUCLEAR REACTIONS WITH NO UNACCOUNTED BY-PRODUCTS ARE A POSSIBILITY

Typical experiments in nuclear physics involve a high energy projectile (perhaps a deuteron) directed onto a stationary target (possibly also a deuteron). Also by pointing two high energy beams at one another, particles may be made to interact. In either scenario, the interaction between more than two particles is improbable. The probability of having more than two in the same small volume at the same instant is just too small (unless of course they are already in a common nucleus). In a metallic, crystalline environment the situation is different. Many-body interactions are common and varied.

What is missing in the many-body environment is the high energy provided by particle accelerators, but to compensate for this, electrons are present and they may participate in a role similar to that of a catalyst (by screening positive charge). No such catalyst is present in the normal nuclear physics experiment. These are reasons that it is safe to say that when multiple free deuterons are brought together in the presence of electrons, the detailed physics involved is not completely understood. There is room for new physics but physics that is still based on familiar concepts.

The following discussion of fusion products, being expected but not observed, is based on a fundamental supposition. The reason that proton, neutron, and gamma ray by-products are

expected in D-D reactions is that when energy is released and converted to kinetic energy there must be something for the helium isotope to react against in order to conserve momentum. There is no feasible physical mechanism for it to react directly against the lattice mass itself, often cited as a difficulty for a description of low temperature fusion. But when four deuterons are brought together, whether all of them are involved in the final reaction product or not, there are many alternative methods of sharing energy and conserving momentum. The reaction is expected to involve production of a range of lower energy gammas. The reactions that produce higher atomic masses are improbable compared to those producing one or two helium nuclei. A helium nucleus (alpha particle) is one of the most stable (magic number) nuclei in existence. In the event two helium nuclei are produced they may conserve momentum by reacting one against the other, rather than ejecting smaller sized particles. In the event a single helium nucleus is produced it may react against and share energy with the remaining deuterons.

This is an appropriate juncture to address an important point made by Leggett and Baym [2] to the effect that as two deuterons approach one another the local electron configuration should approach that of a helium atom. This concept is also found in Baym [26]. They argue that helium doesn't have a binding affinity to the metal and as a consequence the deuterons are energetically less likely to converge. If the convergence is that of four deuterons then the same argument says that the electron configuration approaches that of a beryllium atom instead, for which a binding affinity to the host metal is probably more likely.

In this report the possibility of an explanation for the lack of fusion by-products, insofar as multiple deuterons are involved, is similar to that in Takahashi's EQPET theory [23]. In this paper the source of screening would be the heavy-electron character of the materials involved, along with a non-linear enhancement of the screening effect in a layered structure of deuterons distributed in parallel planes. Enhancement would be due to heavy-electron interaction with very short wavelength phonons that are on or near the edge of the planar Brillouin zone. The planes are formed from deuterons on tetrahedral and octahedral sites. Similarly, thicker planes are formed by deuterons on octahedral sites.

It should also be emphasized that although four deuterons may be involved not all of them need to be changed in the nuclear reaction. The dominant expected output is a helium nucleus, and for this the need for other deuterons nearby for momentum conservation may itself be viewed as a type of catalytic phenomenon.

Alpha particles are well known to be easily absorbed in air and much more so in water. A 1 Mev alpha particle is absorbed in less than one centimeter of air. A good explanation why nuclear products haven't been found in abundance in earlier experiments might be that they were absorbed in the electrolysis medium prior to detection. The expectations were for neutrons, protons and gammas. The lack of neutrons or protons observed could actually be a strong confirmation of the arguments herein in the sense that it implies that if any nuclear process occurs it must necessarily involve the production of alphas since others have been eliminated. When alpha particles are absorbed they become helium atoms. If helium atoms are produced where they didn't exist before, there has to have been a nuclear reaction of some sort.

Miles, Bush, Ostrom and Lagowski [26] performed an electrolysis experiment in which the amount of helium produced was measured along with the amount of excess heat. They were able to closely correlate the helium and heat production under the assumption that deuterons fused to form alpha particles with the well known amounts of energy release. This is a strong confirmation of alpha particle production in a multiple deuteron process.

6. LACK OF EXPERIMENTAL REPRODUCIBILITY AND POSSIBLE REMEDIES

The fusion mechanism proposed in this paper would be difficult to initiate. In establishing motivation for the fusion mechanism, various analogies have been drawn between crystal planes of deuterons in the transition metal hydrides and the copper-oxide planes in high temperature superconductors. The transition metal hydrides have a much greater symmetry than the copper-oxides in that there are three or more sets of parallel planes of deuterons in their lattices. There is a need to break this greater symmetry if the desired vibration mode is to be established. Interactions in layered sets of a single one of these planes are what are desirable.

The difficulty in establishing these conditions may well be a source of the difficulty in reproducing these effects. Factors expected to influence the establishment of proper symmetry conditions are crystal shape, orientation, and electrical and thermal fluxes. A promising method for reducing the symmetry is the application of an intense magnetic field perpendicular to one of the planes. As an example, the de Hass-van Alphen effect couples with the electron charge distribution at the requisite length scale, and this in turn couples to the interaction of the electrons and the lattice**.** This effect offers an opportunity to initiate the low temperature fusion process. The remedy for lack of reproducibility is a proper understanding of the physics and the development of any method for setting the two-dimensional process in motion. More details are spelled out in a provisional patent based on this paper.

7. DISCUSSION

This report has not attempted to calculate possible fusion rates. Such calculations are available. The most quoted calculations are those presented in Koonin and Nauenberg [3], where they state "A mass enhancement of $m^* \approx 5m_e$ would be required to bring the cold fusion rates into the range claimed by ref. 7……An enhancement of $m^* \approx 10m_e$ is required by the results of ref.6". References 6 and 7 are to the papers by Fleischmann, Pons, and Hawkins [5], and Jones, et al. [4] respectively. The symbol m^* used here is not the same as the symbol used elsewhere in this report. Here it denotes the mass of a putative electron that is 5 or 10 times the physical electron's mass (similar to the way the muon weighs 207 times as much as the physical electron).

The fact, as quoted by Kittel [7], that palladium has a high effective-mass, $27m_e$ platinum has an effective mass $m^* \approx 13m_e$, nickel, $28m_e$, and many of the transition metals are members of this class may be more than a coincidence.

It is being argued that, while heavy electrons are long range phenomena, their effect is periodic and a significant localization effect may occur within a unit-cell. In this sense a process may have a periodic local effect even if it is itself a long range phenomenon. This is true if the pseudo-particle is long lived, and has sufficient bandwidth in wave-number space substantially near a Brillouin boundary. All that is required is this large spatial bandwidth, e.g. the width of the wave number spectrum around a pseudo-particle peak. That charge concentrations actually occur in heavy electron materials has been demonstrated in many experiments recently by direct observation [8, 9]. These recent measurements are, in particular, indicative of pseudo-particles (resonances) near approximately one-half of the way to the zone boundary.

There have been authors who advocate effective-mass as a contributor two low temperature fusion. Parmenter and Lamb [29] made calculations based on an electron screening approach using a modified Thomas, Fermi, Mott (TFM) equation. Their effective-mass varied with wavenumber, but in a way opposite to that described above. T. Tajima, et al. [30], have found a very large screening effect in their candidate process. An interesting result with regard to screening is that of Hora, et al.[31], who note that the fusion rate changes by five orders of magnitude if the screening factor changes by only a few percent. They also note that D-D and D-T fusion reactions are “rather exceptional as the cross sections are up to several barns and the nuclei react at distances 50 or more times the nuclear diameters.” The implication for multiple deuteron interactions of an expanded strong nuclear range is apparent, especially if the deuterons are well screened.

A notable lack in this report has been any specification of electron configurations expected near the confluence of deuterons on a common site. An investigation of electronic states that are compatible with the 4d and 5d atomic electron configurations and that are most effective for bonding and screening is planned. The complexity involved in the hydrides is expected to be as large if not larger than for the copper-oxides. It is possible that when the transition metal hydride is doped or otherwise has an excess of electrons, more than one for each metal and deuteron site, bonding of the types described by Sachdev [32] based on Anderson’s resonating valence bond idea [33] occurs between the deuterons.

8. CONCLUSIONS

In summary, two major reasons that have been used for rejecting the possibility of low temperature fusions have been addressed in this report. A significant counter-possibility has been produced for each of them. It has been postulated that low temperature fusion may not be barred by any basic principles of physics as has been suggested. Based on this paper, if LENR is barred at all, it is likely due to inadequate strength of the heavy-fermion screening effect that has been discussed here.

APPENDIX: EFFECTIVE-MASS AND THE WIGNER LATTICE

The term ‘effective-mass’ is somewhat ambiguous. It has been used since the quantum theory of metals was first described. If one uses the term effective to mean that effective-mass acts as the mass of an electron different from that of the natural electron, then it appears that one

should include what has recently been described as heavy electrons or heavy fermions in the terminology. In this appendix effective-mass refers to the effect of a heavier mass whatever its cause. The historical effective-mass appears to be a correlated motion effect of a single electron moving in a periodic field, whereas the appearance of heavier electronic effective-mass may be due to correlations with other electrons and the lattice.

One example of electron-electron interactions is found in a Wigner lattice, which is discussed next. This is significant since it has been observed that effective-mass in systems conforming to two-dimensional Wigner lattices can range above 150 electron masses [34].

A description of a Wigner crystal may be found in Philips [35]. As the Wigner-Seitz radius r_s is expanded above one atomic unit an electron gas tends to form an ordered array A Wigner lattice (or crystal) is the name given to a pseudo-equilibrium state involving electrons or holes in which the electrons or holes find that their lowest energy state in a body-centered-cubic (or similar) configuration where the renormalized forces are balanced against each other. Such a state may be stable when situated against a positive lattice background. The configuration is commonly employed in explanations of the Mott transition. It is a good indicator of the tension existing between the delocalized band states and the localized atomic states, in a model such as the Anderson or Hubbard models. The Wigner crystal has been implicated in recent charge-order investigations [34]. In the description below it is used to illustrate the fact that the vibrations induced in the Wigner array of confined electrons produce their greatest charge concentrations on the spatial scale that is conducive to the screening effect described in the main body of this report.

In the model, as a charge moves away from its stable position it influences charges nearby and thus produces a correlation. The precise form of the screened potential between two electrons or holes embedded in a Wigner crystal in metal lattice is not known. Here, with negligible loss of generality, it is assumed to have the Coulomb form. Only nearest neighbor interactions on a cubic lattice will be considered for simplicity. The Hamiltonian operator may be expressed in the form

$$\sum_n \left[-\frac{\hbar^2}{2m}\nabla_n^2 + V(r_n) + \frac{\frac{1}{2}e^2}{4\pi\varepsilon_0}\sum_{[n]}\frac{1}{\left|r_n - r_{[n]}\right|} \right] \tag{A.1}$$

$$\cong \sum_n \left[-\frac{\hbar^2}{2m}\nabla_n^2 + V(r_n - R_n) - \frac{1}{2}K\sum_{[n]}\left|r_n - r_{[n]}\right|^2 \right]$$

where the first sum is over electrons that are each assigned to positively charged lattice locations, r_n, $n = 1,...,N$, and the second sum is over the nearest neighbors to this location. $V(r_n - R_n)$ is the positive potential about the nth lattice site. The summation over [n] is the summation over the nearest neighbors that are interacting with the n^{th} electron. The factor of $\frac{1}{2}$ is to prevent potentials from being counted twice. Otherwise the notation is standard. The total wave function is a sum over permutations of the solutions of the joint Schroedinger equation

with odd permutations weighted by -1. No more than one electron is in any spin-orbit state, thus satisfying the exclusion principle.

In the second expression for the Hamiltonian the inter-electron Coulomb potentials have been expanded about the electron equilibrium positions $|r_n - r_{n-1}| = a$ where a is the nearest neighbor distance in the cubic lattice. The last term in the Hamiltonian has combined the inter-electron coupling into an effective constant $K/2$. The actual coupling constant in a real crystal is the result of a complex renormalization process involving electron screening. The inter-electron interaction will be treated as dominating the electronic correlation. The result is that for small deviations from equilibrium the appropriate Hamiltonian is given by

$$H = H_0 + H_1, \tag{A.2}$$

where $H_1 = \sum_n V(r_n - R_n)$ is treated as a perturbation.

This form of the equation would result from any inter-electron coupling as long as the first term in the potential's expansion in the displacement from equilibrium is quadratic. R_n is the location to which the nth electron is attracted. In this case, H_0 is the Hamiltonian of a lattice of electrons with harmonic nearest neighbor interactions. What is significant here is that this result tells us that, for the simple case of a one-dimensional lattice, the dispersion relation induced in the oscillators has the form

$$\omega_l = (K/m)^{1/2} \sin(k_l a/2) = (K \sin^2(k_l a/2)/m)^{1/2}. \tag{A.3}$$

It is important to note that this form implies that the largest effective electronic coupling constant occurs where $k_l = \pi/a$, e.g., on the Brillouin zone boundary. In two dimensions the loci for the largest coupling parameters are the wave number domain lines $\pm k_{l,x} \pm k_{l,y} = \pi/a$. If the electrons are acting with an increased mass, the effective mass may be substituted in this expression, and it will act to decrease the energy in each mode. The increase in effective inter-electron coupling in this simple model occurs at locations where it is beneficial for the low temperature fusion mechanism discussed in the main body. It is also at these wave numbers that the deuterons are most strongly interacting and it is to be expected that the screening by the electrons will act in concert. The electrons act to screen the deuterons and vice versa. As mentioned above, it has been observed that effective-mass in systems conforming to two-dimensional Wigner lattices can range above 150 electron masses [34].

Locking of the Wigner lattice on atomic lattice sites for this model is provided by the perturbing term in the full Hamiltonian. As the Wigner lattice vibrates, its individual components are induced to remain near the lattice sites. But because the positive potentials at the sites are finite, and in the case where there are excess electrons or holes, motion between sites will occur. At greater energies the electron states merge into the band states and a Hubbard-like model ensues. Quantum mechanically this is described in terms of transition probabilities or, equivalently, by means of a hopping effect. It may also be described as hybridization between band states and atomic states.

ACKNOWLEDGMENT

The author is grateful to Dr. D.R. Word, Dr. P.S. Lowell, Dr. F. Meserole and Prof. J.J. Lagowski, University of Texas, Austin, for helpful comments, suggestions and help in initiating experiments. He is grateful to Dr. Edmund Storms for comments, experimental advice and hospitality. He appreciates Dr. H.R. Byerly's reading of the manuscript and providing useful advice. He appreciates stimulating correspondence with Prof. A. Takahashi whose EPQET theory appears similar and complementary in many aspects.

REFERENCES

1. A. Takahashi, A Theoretical Summary of Condensed Matter Nuclear Effects, Osaka University, Osaka, Japan, www.lenr-canr.org/acrobat/TakahashiAatheoretic.pdf
2. A.J. Leggett and G. Baym, Nature **340**, 45-46 (1989), and Phys. Rev. Lett. **63**, 191-194 (1989)
3. S.E. Koonin and M. Nauenberg, Nature **339**, pp. 690-691 (1989)
4. S.E. Jones, E.P. Palmer, J.B. Czirr, D.L. Decker, G.L. Jensen, J.M. Thorne, S.F. Taylor, and J. Rafelski , Nature **338**, 737-741 (1989)
5. M. Fleischmann, S. Pons, and M. Hawkins , J. Elecroanalyt. Chem. **261**,301-08 (1989)
6. J.M. Luttiinger, Physical Review, 121, pp. 1251-1258 (1961)
7. Charles Kittel, Introduction To Solid State Physics, (John Wiley, New York, p. 259, 1961)
8. M. Franz, Science **305,** pp. 1410-1411 (2004)
9. K.M. Shen, et al., Science **307**, p.901-904 (2005)
10. A Report of the Energy Research Advisory Board to the United States Department of Energy, Washington, D.C., November 1989, Chapter III, p.17.
11. Bernhard Keimer, Science **292**, p.1498-1499 (2005)
12. T.E. Posch and B.R. Breed, Space Wave Number Signal Processing, Chapter 21, Time-Frequency Signal Analysis, Edited by Boualem Boashash, (Longman-Cheshire, Melbourne, and John Wiley, New York 1995)
13. Gerhard Herzberg, Atomic Spectra and Atomic Structure, (Dover Publications, New York. 1945)
14. A.A. Abrikosov, L.P. Gorkov, and I.E. Dzyaloshinsk, Methods of Quantum Field Theory In Statistical Physics, (Dover Publications, Inc., New York 1975)
15. L. P. Kadanoff, and G. Baym, Quantum Statistical Mechanics, (W. A. Benjamin Inc., New York 1962)
16. G. Rickayzen, Green's Functions and Condensed Matter, (Academic Press, New York 1980)
17. J.C. Slater, Symmetry And Energy Bands In Crystals, (Dover Publications, New York 1972)
18. Arianna Montorsi, Ed., The Hubbard Model, A Reprint Volume, (World Scientific, Singapore, 1992)
19. Mario Rasetti, Ed., The Hubbard Model, Recent Results, World Scientific, Singapore, 1991)

20. C. Elsasser, K.M. Ho, C.T. Chan, and M. Fahnle, Phys. Rev. B, **44**, 13, pp. 10377-80, and C. Elsasser, M. Fahnle, L. Schimele, C. T. Chan, and K.M. Ho, Phys. Rev. B, **50**, 8, pp. 5155-5159.
21. H. Wipf, Diffusion of Hydrogen in Metals, in H. Wipf, Ed., Hydrogen in Metals III, (Springer-Verlag, Berlin, New York 1997)
22. A. Montorsi, M. Rasetti, and A.I. Soloman, Chapter 4.3, Fig. 3, in reference 16 above.
23. A. Takahashi, Mechanism Of Deuteron Cluster Fusion By EQPET Model, presented at Tenth International Conference on Cold Fusion, Cambridge, Mass. (2003)
24. C. Sulem and P.-L. Sulem, The Nonlinear Schrödinger Equation, (Springer-Verlag, Berlin, New York 1999)
25. R. E. Peierls, Quantum Theory of Solids, (Oxford University Press, Oxford, pp.108-112 1955)
26. G. Baym, Lectures on Quantum Theory, (W.A. Benjamin, New York, pp 477-478 1969)
27. M.H. Miles, B.F. Bush, G.S. Ostrom, J.J. Lagowski, Conference Proceedings Vol. 33, The Science of Cold Fusion, Bologna (1991)
28. J.R. Huizenga, Cold Fusion, The Scientific Fiasco of the Century, (Oxford University Press, Oxford, pp. 36-37. 1993)
29. R.H. Parmenter and W.E. Lamb,10, Proc. Natl. Acad. Sci. USA, **86**, 8614-8617 (1989), and **87**, 8652-8654 (1990)
30. T. Tajima, H. Iyetomi, and S. Ichimaru, (J. Fusion Energy **9**, 437 1990)
31. H. Hora, J.C. Kelley, J.U. Patel, M.A. Prelas, G.H. Miley and J.W. Tompkins, Phys. Letters **A175**, 138-143 (1993)
32. Subir Sachdev, Reviews of Modern Physics **75**, 913-932 (2003), and arXiv:cond-mat/0211005
33. P. W. Anderson, Science **235**, 1196 (1987)
34. Y.H. Kim and P.H. Ho, Wigner Lattice Order, Collective Modes, and Superconductivity in $LA_{1.985}SR_{0.015}\,CUO_{4+}\,\delta$ System r (2001), arXiv:cond-mat/0112134 v2
35. P. Philips, Advanced Solid State Physics, (Westview Press, Cambridge, MA 2003)

Resonant Electromagnetic-Dynamics Explains the Fleischmann-Pons Effect

Scott R. Chubb
Infinite Energy Magazine, 5023 N. 38th St., Arlington, VA 22207

Abstract

Science requires measurements. Interpreting measurements involves recognizing patterns. How this happens is intimately related to the instruments that are used and how the measurements are performed. One can "interpret" the process in many different ways. Historically, however, in modern physics, quantum mechanics has been used in situations involving "smaller" scale effects. In this form of interpreting science, when "measurements" take place, what is measured involves details about the measurements. A form of communication is involved: What is "seen" depends intimately on how one "looks at it." Abstractly, this can be viewed in a somewhat radical way: Nature is telling us something, but how we "interpret it" involves how we understand what Nature "is telling us". Just as in normal forms of communication, this kind of communication involves being willing to accept information that is sent to us from somewhere else. In other words, a signal is sent. If it is received, communication takes place. If it is not, it does not take place. This paper deals with a radical idea about a radical subject. The radical subject is what used to be called "cold fusion". The radical idea is that basic ideas about quantum mechanics, and the "implicit" form of communication that is present in quantum mechanics can explain this subject.

I Introduction

I argue that the real barrier for understanding how Cold Fusion reactions can take place, in the Fleischmann-Pons effect (FPE), is not overcoming the "Coulomb Barrier" but involves understanding quantum mechanics (QM). Specifically, QM does not require that the "picture" used in conventional fusion apply. A more logical "picture" includes electromagnetism in a time-dependent fashion and the idea that many particles can be involved. Then seemingly impossible "aspects of the "conventional picture" become "not so impossible," but, in fact, "quite reasonable." A key source of confusion is that as opposed to a situation in which potentially reacting deuterons (d's) are required to have such high velocity that they can be treated as if changes in their electromagnetic interaction (EMI) are important only very near the location of the reaction, where the conventional tunneling picture applies (involving a static Coulomb potential), in a situation involving many charged particles, the effects of EMI can result in time-dependent changes that can become important far from the reaction. In fact, in what appears to be the most relevant, conventional fusion reaction (in which helium-4, in the form of alpha particles is released), evidence exists that the conventional "Coulomb Barrier" actually must be modified significantly[1-3] in order to incorporate time-dependent features of the EMI that are necessary to impose the requirement that far from the reaction, the incident d's

must have positive Bose Exchange symmetry and have net, vanishing spin. In this paper, I discuss a particular mechanism involving resonant electromagnetic dynamics. The associated picture is consistent with the conditions that are present in the experiments, the known laws of physics, and the underlying ideas suggested by Giuliano Preparata [13]. Predictions, based upon this alternative picture, imply that particular size crystals, involving Palladium (Pd) and particular, externally applied electromagnetic fields can be used to trigger excess heat in the FPE.

In the next section, I provide an overview of some of the commonly believed ideas about the "Coulomb Barrier" that have resulted in considerable confusion about the FPE. In addition, I explain how conventional QM deals with forms of interaction in general terms and how these can result in a counter-intuitive picture in which "collisions" can be very different than in the conventional "Coulomb Barrier" situation because they do not have to take place "at a point." Instead, collisions can take place over a finite distance through an effect that is referred to as resonance or "near resonance," in which in a particular region of space, effectively, momentum is conserved in a non-local fashion. In conventional solid-state physics, the associated effects are quite well known, but a rigorous treatment of their origin has not been adequately presented. In dealing with the cold fusion problem, I have suggested such a treatment[4, 5].

In the final section, I discuss two different pictures that involve "nearly resonant" forms of collisions in an approximately ordered solid. The first of these is based on an approximate model that was introduced to "overcome" perceived deficiencies involving how the "Coulomb Barrier" frequently has been viewed in the fusion process. But this model uses a language (time-dependent perturbation theory involving bound, ion band states) that is very different from the conventional scattering/tunneling language that is associated with the more conventional picture associated with the "Coulomb Barrier." In the second picture, a generalization of the first picture is presented, using a language that is consistent with more general aspects of QM, based on "nearly-resonant" collisions that can take place involving the lowest energy excitations of an ordered solid, which can include the possibility that all of the particles in the solid can be allowed to move all-at-once rigidly. Here, for illustrative purposes, a semi-classical limit is used to demonstrate how the associated "nearly-resonant" collisions can lead to nuclear-scale forms of overlap. More quantitative arguments that are based on the more general theory are presented elsewhere [1-5]. From these more general arguments, both the earlier picture and its generalization (in the second model) can be shown to involve forms of "nearly resonant" collisions. In the second model, external electromagnetic fields can induce adiabatic changes in the associated scattering. In the initial picture, the energy of the interaction is assumed to result from a uniform shift in the zero of energy. In the second model, these forms of motion occur as a result of a uniform shift in the zero of momentum, and the reaction involves a different final state in which changes at the boundary of the ordered region of the solid occur through a transition in which the momentum from the change in mass (from the $d+d \rightarrow {}^4He$ reaction) is transferred to the center of mass of the lattice as a whole. In this situation, the change in the final state involves coupling through "nearly resonant" collisions in which momentum is either transferred to potentially interacting helium-4 nuclei (in larger crystals) or directly to the lattice (in smaller nm-scale crystals).

II "The Barrier is not "the Coulomb Barrier"-- It is Quantum Mechanics

The idea that Nature is telling us something by sending us signals and requires us to receive them involves a process of interpreting what Nature is telling us. To "understand" what Nature is telling us requires us to "think" about the signal and what it represents. In conventional fusion, this process is relatively simple because an obvious model exists: conventional fusion occurs on the Sun, and it involves hot plasmas, where high velocity hydrogen nuclei (protons, or proton-neutron pairs—d's) can collide in a process that we also seem to think we understand. But our understanding of this is approximate. It is based on a theory that was created well-before details about later information involving experiments that could be explained by a more refined understanding of QM were known. For this reason, it is appropriate to re-examine some of the more common assumptions about the "Coulomb Barrier," and their relevance in our "understanding" of the FPE. With this in mind, I asked three other people who have been paying close attention to issues related to the FPE about their opinions about the importance of "Overcoming Coulomb Barrier." Their opinions and my opinion are expressed in the following:

1. Nuclear Physicists Say: You can't overcome it[6].
2. Nuclear Physicists Say: You can't overcome it. They seem to be wrong. But there is no accepted theory that can account for it[7].
3. Nuclear Physicists don't understand it. Solid State Physicists do. "Accepted theory" involving Nuclear Physics is wrong. Ground state quantum mechanics explains it[8]
4. Time dependent quantum mechanics says it can be overcome using "conventionally accepted" theory and this will eventually "be accepted"[9].

In fact, no one knows how relevant any of these statements actually is. With the exception of statement 4 (which is my opinion), what I suggested in each of these opinions is not based on an objective scientific analysis. I believe, however, there is value in including these statements because in each case, I suggest the particular opinion has resulted from biases and perceptions about the "Coulomb Barrier" that actually are not relevant to the FPE but reflect a more basic source of confusion: Interpreting and understanding what Nature is telling us through QM.

In conventional physics and chemistry, the kind of radical effect that Fleischmann and Pons observed was not at all expected, and, even after many years, statement 1 reflects the predominant opinion of most scientists. The person who made this statement actually is very concerned about and interested in the outcome of the "debate" that has taken place, and I suspect that although he made this statement, as additional facts are revealed, he may change his mind. Statement 2 reflects the opinion of an individual who has initiated a useful, scientific dialogue and debate about the subject. He also has recognized that the lack of scientific discourse about the subject has precluded realistic intellectual investment of time, much less, real investment, through significant funding. Statement 3 was made by a scientist who collaborated with me in developing the initial ideas associated with our ion band state model of the FPE. His opinion reflects a more open-minded perspective, associated with invoking ideas about quantum mechanics and solid-state physics. With time, I have sharpened the associated arguments that are the basis of his opinion. Some of these ideas are the basis of statement 4. Each view captures an important perspective. Obvious differences in opinion are implicit in

these different statements that reflect biases about a seemingly transparent assumption: that opinions about the "Coulomb Barrier" have relevance in understanding the FPE (and why because of these opinions—in statements 1 and 2—it does not seem possible that the FPE can result from nuclear reactions). An important point, associated with statements 3 and 4, involves the potential role of QM and the idea that through QM it is possible to go beyond the limitations of the assumptions, associated with statements 1 and 2. In fact, statements 3 and 4 are based on a model involving QM that actually makes sense in the context of what is known[4] about palladium-deuteride (PdD). But the fact that QM might even be involved (in the PdD situation but also, even in the conventional "Coulomb Barrier" tunneling problem) does not seem to have been widely understood or appreciated. In particular, preconceived ideas about the "Coulomb Barrier", although seemingly quite relevant and "obvious" (as expressed in statements 1 and 2), are actually quite inappropriate and quite wrong in situations in which many particles, potentially interacting electromagnetically, can be involved. In this alternative situation, the relevant dynamical situation can become (and probably is required to be) considerably more complicated. The real situation, even in conventional fusion, does involve QM, but in a very limited way, and this fact, apparently, also, has not been widely appreciated.

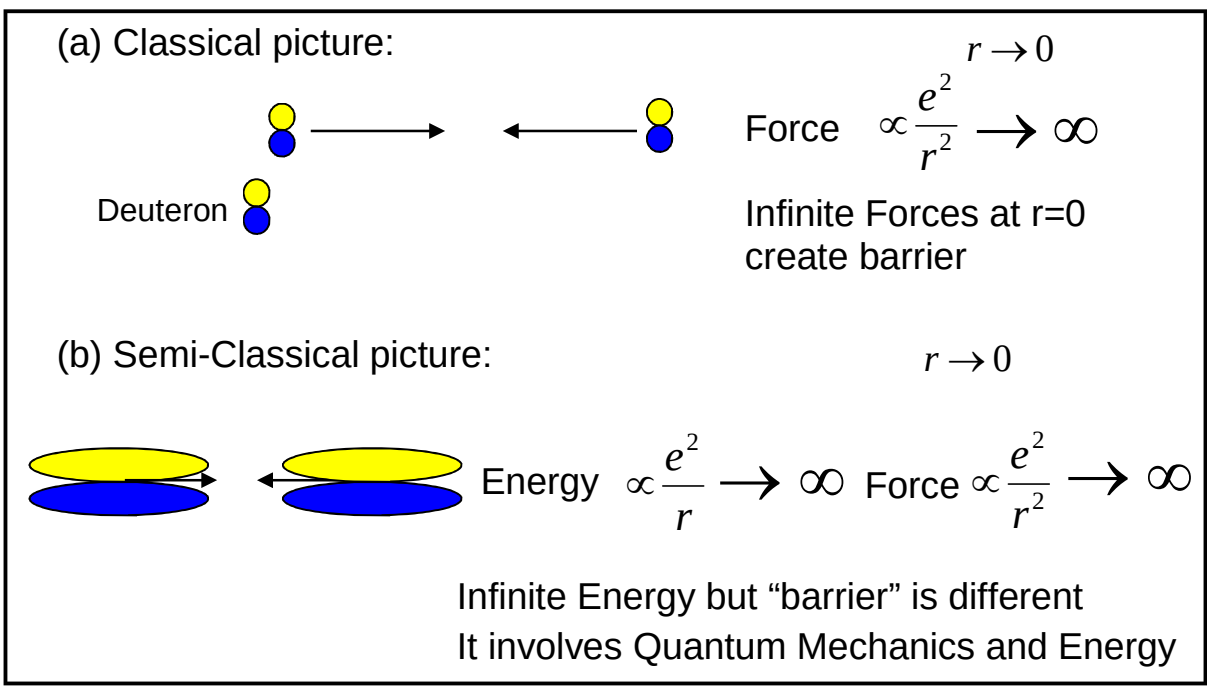

Fig.1: Schematic representations of two commonly-viewed pictures of the "Coulomb Barrier;" in (a), a "classical" point-particle picture is shown. The "perceived barrier" occurs because point particles cannot collide when infinite forces occur. This creates a "Conceptual Barrier." But it is not the "Coulomb Barrier" that is believed to be relevant in QM. The "Coulomb Barrier," which is believed to be relevant to most physicists is shown pictorially in (b). It is based on conventional "Gamow Theory," where because of QM, d's are shown as pancakes, symbolically, representing waves, not point-particles.

Fig. 1 shows a schematic representation of two "perceived" pictures of the "Coulomb Barrier." In the first of these, each d (which is shown as a proton-neutron pair, in which each proton appears as a point-particle lighter circle and each neutron appears as a point-particle darker circle) is a point-particle that cannot collide with a second d because of the infinite forces that occur classically as a result of Coulomb repulsion. Although this picture "seems to" explain why fusion cannot occur, this isn't true: *it over-simplifies the situation.* A more "*realistic*

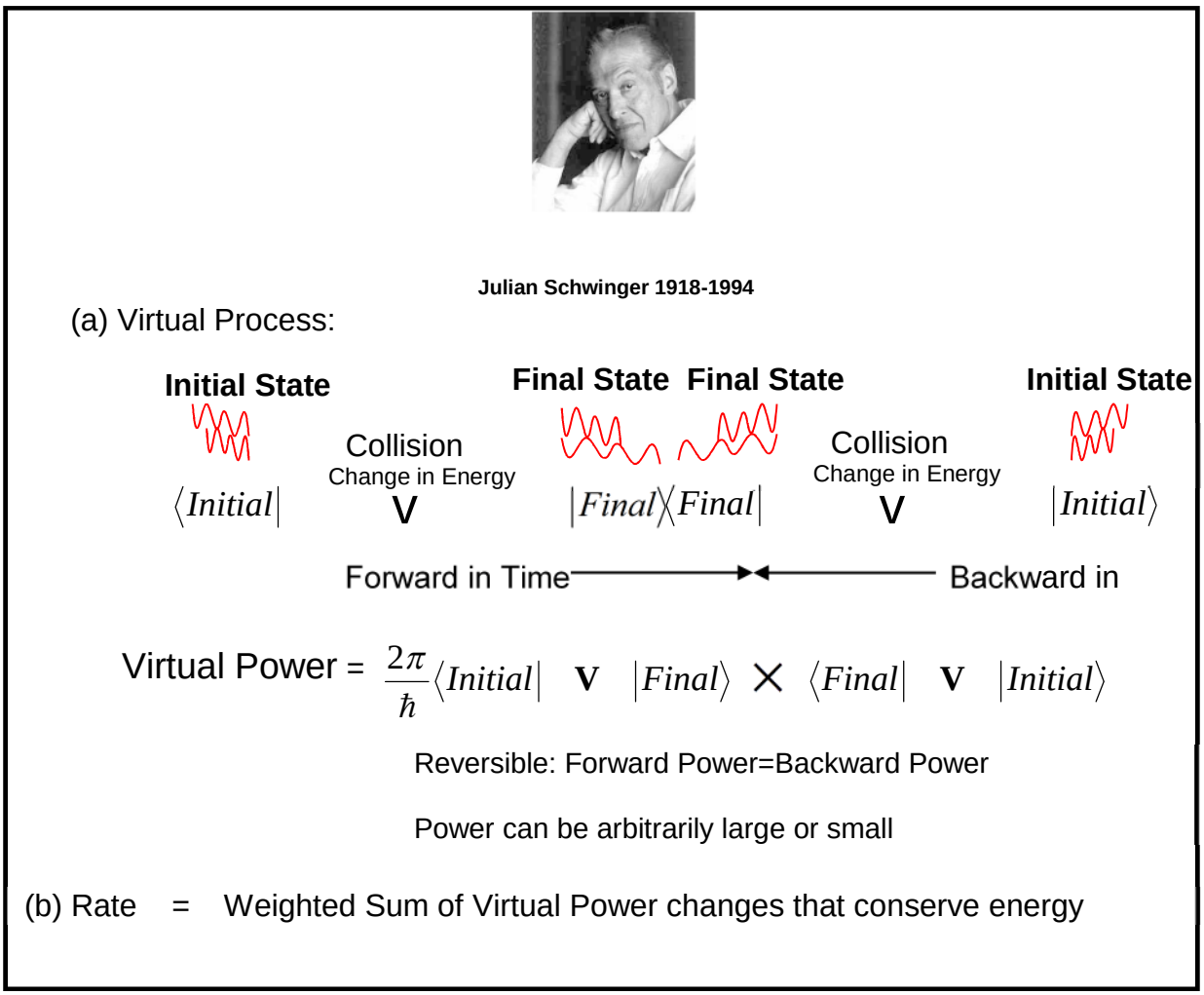

Fig.2: Shows a pictorial representation of the how collisions occur in QM, following an analysis that Julian Schwinger developed (which he presented during ICCF1[10]). The meanings of the various symbols and their significance are discussed in the text.

picture" is shown in (b). Here, "point-particle" d's are replaced by pancakes, which are used to mimic "wave-like" structures that QM requires; these structures can "collide" (their wave functions can have overlap). This can take place, despite the fact that the classical expressions for the energy and force become infinite. The picture in Fig.1b is more realistic. But the associated mathematics is approximate since it requires the d's to have high velocity.

Fig.2 shows a pictorial representation of how collisions occur in QM (and in quantum field theory), based on an analysis that Julian Schwinger developed[10]. Here, in any possible QM process, an initial state (referred to as an initial state, many-body wave function), which can be thought of as a wave, or many waves, and, which is represented schematically as a wavy line, initializes a collision process, that results in the occupation of a final state (associated with a final state many-body wave function), which is also shown as a second, wavy line. (In fact, each of these waves can involve any number of particles—many waves—conceivably.) In particular, collisions involve changes in energy. In principle, they can take place through any possible form of "Virtual Process." Each "Virtual Process" is initiated through a change in the potential energy V, resulting from a collision and leads to a scattering event in the forward direction in time (initial state to final state) and a second scattering event involving the same change V that occurs in the reverse direction in time (final state to initial state). Forward reactions very often are balanced in this equation by backward reactions. When a balance takes place, no reaction occurs (as represented in Fig.2a) by the statement forward power=backward power (which implicitly is used in conventional thermodynamics). A net change in power (referred to as a

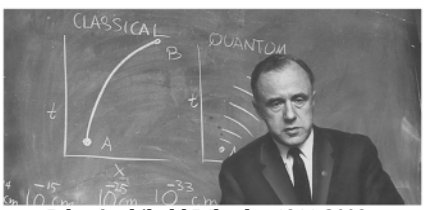

John Archibald Wheeler 1911-2008

In Virtual Processes:

1. Future events can affect (or resonate with) past events.
2. Particles that are far apart can interfere with each other.
3. Sum over final states means creative physics is possible.

Fig.3: Shows a picture of John Wheeler and summarizes some of the novel aspects associated with QM that he and Richard Feynman used throughout their careers that have not been appreciated in "discussions" about the role of QM in cold fusion and low energy nuclear reactions.

"Virtual Power change" in Fig.2a) can occur that is defined by the product of the matrix element of the forward process, $\langle Initial|\boldsymbol{V}|Final\rangle$, with the matrix element of the backward process, $\langle Final|\boldsymbol{V}|Initial\rangle$, provided energy is conserved. During ICCF1, Schwinger explicitly cited this relationship[10], implicitly using a well-known equation (referred to as the

Lippmann-Schwinger equation) that has not been widely-appreciated in the analysis of cold fusion theory:

$$\text{Rate of reaction} = \frac{2\pi}{\hbar}\langle Initial|V\delta(H - E_{Initial})V|Initial\rangle$$
$$= \frac{2\pi}{\hbar}(\sum_f \langle Initial|V|Final\rangle\langle Final|V|Initial\rangle\delta(E_{Initial} - E_{Final})), \quad (1)$$

where $E_{Initial}$ and E_{Final}, respectively, are the energies of the initial and final states, and the summation includes all final states.

In fact, the terminology "collision" is a generalization of the classical concept. In Eq.1, a more appropriate idea implicitly is presented. In the expression, any number of particles, over any length and time scale can be involved in each virtual process. As stated in words in the figure, collisions in QM involve a rate that is formed as a weighted sum of the possible Virtual Power changes that can be created through virtual processes. The possible power (the Virtual Power) resulting from any virtual process can be arbitrarily large or small, and each process, in principle, is reversible. When the sum over final states conserves energy (which is implied through the notation involving the delta function in Eq.1), the process can take place. Time reversibility is broken because it is never possible to determine the change in potential, the initial state and the final state precisely. The associated relationship (Eq. 1), in principle, is exact. It provides a prescription for modeling new and novel effects that is considerably richer than is possible in Gamow theory. In particular, Gamow theory, in the fusion process, assumes a single final state is involved with a collision (consisting of three nucleons, moving away from a third nucleon) at high velocity, except in regions in the immediate vicinity of the collision, and that the essential dynamical changes in the potential energy (V, in Eq. 1) involve the strong force exclusively. This picture ignores many possible final states and implicitly fails for this reason. This occurs because Gamow theory does not include many of the possible "signals" that QM allows. The more complete picture (outlined in Fig.2 and Eq.1), explains how many creative possible forms of interaction ("communication") can occur from "signals" involving the final state (the receiver) and the transmitter (the initial state). Discussions about this involving how light interacts with electrons, between John Wheeler and Richard Feynman, helped Feynman to win a Nobel Prize. He won this prize by explaining how, through a subject that is referred to as Quantum Electrodynamics (QED), electrons must be treated using QM when they interact with light. The three ideas that I "attribute" in Fig.3 to John Wheeler (which were well-known by him and others when he worked with Feynman) are related to the fact that by construction, in QM, in isolation (i.e., without measurements involving collisions and related effects), time has no preferential direction, and implicitly, "time reversal invariance" takes place, which means it is impossible to distinguish between situations in which how electrons and light interact evolves forward in time from situations in which their interaction evolves backward in time.

(a) A Pictorial Representation of Virtual Collision Matrix Elements, $\langle Initial|\mathbf{V}|Final\rangle$

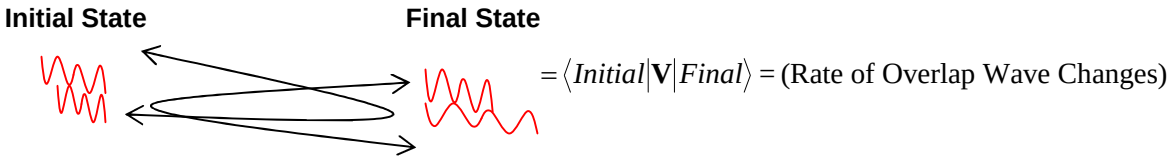

(b) Relationship of $\langle Initial|\mathbf{V}|Final\rangle$ to Density $\langle Initial|\rho(r)|Final\rangle$ and Current $\langle Initial|\vec{j}(r)|Final\rangle$

=0 When energy is conserved

$$\langle Initial|\mathbf{V}|Final\rangle = i\hbar\int d^3r\,\frac{\partial\langle Initial|\rho(r)|Final\rangle}{\partial t} + \int_{\text{Boundary of V}} dA\;\hat{n}\bullet\langle Initial|\vec{j}(r)|Final\rangle$$

(c) How $\langle Initial|\mathbf{V}|Final\rangle$ relates to Currents Outside ($\vec{j}$) and Inside ($\vec{j}_{inside}$) Collision Region

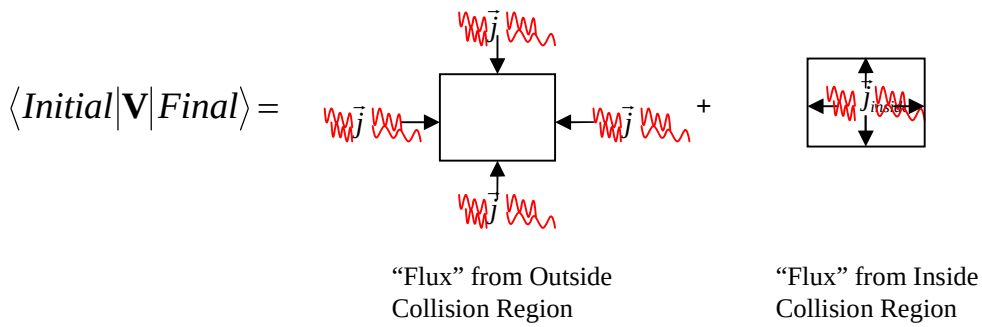

(d) Picture of How Resonance Affects Relationship between $\langle Initial|\mathbf{V}|Final\rangle$ and $\vec{j}$

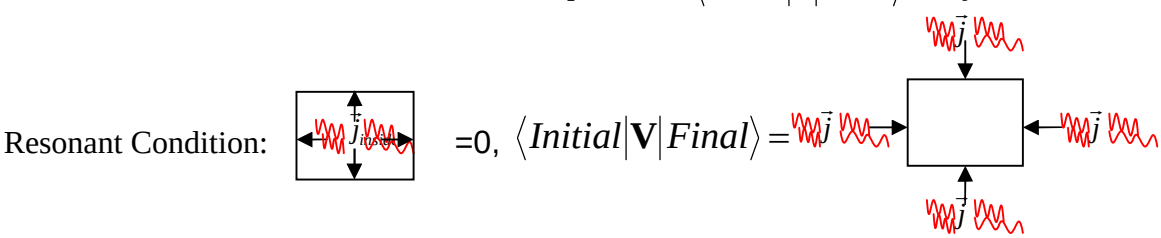

Fig.4: Shows a pictorial representation of each virtual collision matrix element $\langle Initial|\mathbf{V}|Final\rangle$ (in (a)), how (in (b)) $\langle Initial|\mathbf{V}|Final\rangle$ is related to the current and density matrix elements, $\langle Initial|\vec{j}|Final\rangle$ and $\langle Initial|\rho|Final\rangle$ through a surface region integration representation (when energy is conserved) involving flux contributions at the boundaries of the collision region from currents located outside ($\langle Initial|\vec{j}|Final\rangle$) and inside ($\langle Initial|\vec{j}_{inside}|Final\rangle$) and a pictorial representation (in (c)) of this fact. Resonance occurs (in (d)) when the flux contribution from inside the region vanishes.

At a very early stage in the evolution of QED, John Wheeler suggested rather extraordinary ideas (associated with the words in Fig. 3), including this concept of "time reversal invariance" and other "counter-intuitive" features of QM, in which: 1. "Particles" that are located far apart can "interfere" with each other (i.e., the wave-like characteristics of different particles that are far apart can affect each other in measurements); 2. Since it is never possible to identify a particular final state with certainty, assumptions about the behavior of the final state can be used to postulate new and novel physical effects; and (possibly the most novel idea) 3. How light propagates in the future can "affect" (or resonate with) how it has propagated in the past. This kind of logic is a starting point for believing the "real barrier" to our understanding of cold fusion probably is not only understanding "the Coulomb Barrier," but it involves using a more complete picture of what is possible in QM.

III Resonant and Near-Resonant Interactions

A problem, involving the possibility that light being transmitted and received in the future, in the absence of collisions, could alter how it was transmitted and received in the past was suggested by Wheeler to his (at the time) young, graduate student, Richard Feynman. This idea required that Feynman think in basic terms about how light might interact with matter at its most fundamental level. Intuitively, one might view this problem in a paradoxical way: That what happens in the future could affect the past. In fact, as opposed to viewing this problem in this particular way, an alternative way of looking at it involves an important assumption, associated with how quantum mechanics works: In the absence of collisions, it is impossible to "know" anything at a fundamental level, and (possibly more significantly) that how natural forms of harmony (or resonance) might exist in which it is simply impossible to distinguish between the past and future, or even in situations in which "seemingly natural" boundaries are present that can prevent unexpected collisions from taking place. In suggesting this seemingly odd and bizarre idea, Wheeler asked Feynman to address a fascinating question that might be impossible to answer: If a tree falls in a forest and there quite literally is no one around to hear it, does the tree make a sound. Possibly equally remarkable is the conclusion, based on what is known about the existing theory of electromagnetism, that he suggested, is that a sound actually might not be created. In doing this, John Wheeler and Richard Feynman "re-invented" the kinds of ideas associated with how QM works, and the forms of harmony and resonance that I just mentioned, which are not widely appreciated, associated with "time reversal invariance" and causality that (I think) have direct bearing on questions related to cold fusion.

In particular, Wheeler and Feynman made use of ideas related to what we know and can never know about electrodynamics, and the fact that precise solutions of the associated equations are allowed to become non-local both in time and space. By invoking this, they postulated the somewhat "spooky" idea that for radiation to ever be transmitted, it is necessary to have both a "well-defined" receiver and transmitter. Wheeler suggested that if this does not take place, no signal is ever transmitted. Implicitly, in order to account for how the associated signal is transmitted, Feynman invoked a form of the effect that I have referred to as resonance or harmony. When this kind of effect is approximate, a condition that I will refer to as "near

resonance" can take place, in which "collisions" can take place, but their magnitude and duration can be vanishing-ly small. In both situations, as opposed to a "conventional effect" (in which how light and electrons interact only involves how light is emitted in the future), Feynman and Wheeler thought about a very different effect, involving conditions in which how light is emitted involves a situation in which how it interacts with electrons in the future can affect how it has interacted with electrons in the past. They suggested how this occurs "appears" to involve a situation in which what happens in the future "in anticipation" of what will take place can affect what has taken place in the past. This idea is entirely non-classical, in the "real universe," and it also "appears" to violate causality. (But, as stated above, because in QM, by construction, in the absence of collisions, time has no preferential direction, such a violation does not take place.)

In Fig. 4(a), I show a pictorial representation of the overlap between initial and final states using wavy lines, and its rate of change with respect to time (in the interaction picture[11]), using a wavy line that begins and ends with arrows. Each virtual collision matrix element, $\langle Initial|\mathbf{V}|Final\rangle$ (in Fig.4a) that is used to define the virtual power (Eq. 1), can be related (as shown in Fig.4b) to the (Schroedinger picture[11]) "off-diagonal" many-particle current (associated with all, neutral or charged particles) and density (associated with the same particles) matrix elements[11], $\langle Initial|\vec{j}|Final\rangle$ and $\langle Initial|\rho|Final\rangle$, through an integral representation that reduces to a simpler (surface region integration) representation, when energy is conserved, involving flux contributions at the boundaries of the collision region from currents located outside ($\langle Initial|\vec{j}|Final\rangle$) and inside ($\langle Initial|\vec{j}_{inside}|Final\rangle$). The condition associated with future and past forms of scattering being in harmony with each other (as in Fig.3) occurs when particle number and energy are conserved, throughout space. This implicit assumption is illustrated through the arrow, from the first term in the integral equation, shown in Fig.4b, to the symbols and words, associated with the wording, "=0 When energy is conserved." In Fig.4c, a pictorial representation is presented that shows how this can take place.

The resonant condition (shown in Fig.4d) occurs when the contribution from inside the region vanishes. Then, $\langle Initial|\mathbf{V}|Final\rangle$ depends only on contributions $\langle Initial|\vec{j}|Final\rangle$ that occur at the boundaries of the region. Effectively, when this occurs, the "collision" process can become non-local, and through near resonant conditions that "almost mimic" resonance, non-local forms of collisions can occur that can result in gradual increases in momentum. In particular, as opposed to a situation in which particles "collide" in the interior of the collision region, in perfectly resonant situations all of the particles that are external to it pass through it, as if the region is transparent. In near resonant situations, all of the particles either pass through it, or some of them may remain near the boundary or be reflected, in such a way that momentum is transferred non-locally. In both situations, the changes in potential only occur either at the boundaries of the region or in regions external to it.

IV How Resonant Electromagnetic-Dynamics Explains the Fleischmann-Pons Effect

Implicitly, in an approximately ordered solid, a form of "Galilean relativity" exists, associated with the fact that in the limit in which there are no collisions, it is impossible to tell whether or not the "ordered regions" in the solid are in motion or at rest. This can have especially interesting consequences when collisions are weak because their contributions in Eq. 1 can be stifled as a result of periodic order. The associated effect is a specific example of the more general phenomenon, discussed in the last section: near-resonance and nearly resonant collisions. This occurs when contributions from many virtual collision matrix elements (many values of $\langle Initial|\mathbf{V}|Final\rangle$ in Eq. 1) become very small in a particular region of space. In particular, perfect resonance occurs when energy is conserved and the contribution to the "flux" (as in Fig. 4b) from the many-particle current matrix elements, $\langle Initial|\vec{j}(r)|Final\rangle$, over the boundary of the region, from the interior portion of the integral (as in Fig.4d) vanishes. Since energy is conserved in Eq. 1, in this kind of situation, the total contribution from collisions in the interior vanish (so in this region $\langle Initial|\mathbf{V}|Final\rangle = 0$), and with respect to $\langle Initial|$ and $|Final\rangle$, the total Hamiltonian (*H* in Eq. 1) can be viewed as being a self-adjoint (Hermitean) operator in this region.

Formally, as a consequence, perfect resonance can be used to justify the approximate boundary conditions associated with the single-particle, energy band theory, developed by Bloch, which is the basis of heat and charge transport in solids, with the understanding that the theory actually can be applied even in situations in which the crystal lattice that is used has finite extent, provided the energies of the various states that are used are all very close to each other in value. As I have pointed out elsewhere[1-5] the associated conditions are guaranteed to apply to the full many-body Hamiltonian when the initial and final states involve many particles, provided the energies of the states involve the ground state, and the lowest-lying excitations, which, by construction, are all required to be related to each other through rigid Galilean transformations, in which all of the "particles" are allowed to move at once, rigidly, without the separation between any particle and the remaining particles being altered. As a consequence, as opposed to justifying conventional band theory, using stationary, bound, eigenstates of an approximate single-particle Hamiltonian, the theory can be viewed as a near-resonance limit, involving the full Hamiltonian, as it applies to a periodically ordered, finite lattice that is allowed to move rigidly within the interior of a solid, and the associated eigenstates are wave function "resonant states" that preserve periodic order. Because, in fact, it is never possible to determine the boundary of a solid[4,5], formally, the associated picture can be viewed as a definition. This alternative perspective justifies, formally, the implications of the initial ion band state model model[12], in which an approximate "Fermi Golden" rule fusion rate calculation and the possibility of overcoming the "Coulomb Barrier" was inferred from approximate eigenstates, derived from a two-body d-d wave function, that possesses Bloch symmetry (similar to the comparable symmetry that occurs when non-interacting d's occupy ion band states[12] in both its dependence on its center-of-mass and relative d-d separation variables). In this model, the Fermi Golden rule is used to evaluate the fusion reaction rate, using initial and final states, that only change in regions (which are located at the

interior boundaries of the ordered lattice) where nuclear overlap takes place, based on the assumption that in both the initial and final states, the same wave function applies in regions where overlap does not take place but as the separation variable either vanishes or its magnitude approaches the magnitude of a Bravais Lattice vector, overlap becomes possible by allowing the change in momentum to become infinite. When the d-concentration is sufficiently small, this assumed, asymptotic, energy-minimizing solution satisfies a resonant condition, while the Fermi Golden Rule rate expression occurs through nearly-resonant forms of collisions, associated with small (infinitesimal) perturbations, in the zero of energy of the electromagnetic potential, defined by Eq. 1, in regions where nuclear overlap can occur, both in interior and external regions of the lattice. This initial calculation of fusion rate is justified only when the energy per unit cell is on the order of the smallest (optical) phonon energies (~20 meV) which means the lattice must have 23.8 MeV/0.02 eV~10^9 unit cells. However, a considerably smaller lattice size is possible in the presence of very weak externally applied forces. In this case an alternative model, associated with near resonance can take place, in which the zero of momentum adiabatically changes, without exciting the system. This can occur provided the effective change in virtual power associated with the process is sufficiently small. In particular, as a function of time, when an external field $\vec{E}$ is applied, nearly resonant fluctuations in the center of mass momentum can take place that can increase in magnitude, with time. When the complete many-body expression is included (through Eq. 1, based on a generalization of multiple scattering theory[1-4]), as the available momentum builds up, virtual collisions can couple resonantly between the lowest lying excitations of the solid when the product of the force ($e\vec{E}$) on each d, associated with "a collision," with the time *t* that is involved (which, in one dimension, for example defines a particular momentum $p(t) = e\vec{E}t$) obeys a matching condition (in which, for example, again, in one-dimension, the associated deBroglie wavelength $\lambda_{deBroglie} = \frac{h}{p(t)} = \frac{N}{n}a$; *h*=Planck's constant, n = integer$\leq$N, 2N=number of lattice sites). In the many-body generalization[4,5], whenever this condition occurs once, it can occur 2N times. In the simplest (one-dimensional) limit, N=n, $2N\lambda_{deBroglie} = a$, and as p(t) increases in time, $\lambda_{deBroglie}$ can approach nuclear dimension. The apparent "simplicity" of this picture involves relating the microscopic physics to the semi-classical limit involving how light interacts with matter. Here, the underlying idea that coherent oscillations of charge that Giuliano Preparata [13] suggested could be important, in the long-wave limit, in the associated interaction is absolutely correct. His observation about this is truly important.

Ackowledgements

I would like to acknowledge valuable discussions with Mitchell Swartz, David Nagel, Talbot Chubb, and Ileana Rosario.

References

[1] Chubb, S.R., in Proc. 8th Int. Workshop on Anomalies in Hydrogen / Deuterium Loaded Metals, 38 (2008). http://www.iscmns.org/catania07/ChubbSrolesofapproxi.pdf
[2] Chubb, S.R., in Low-Energy Nuclear Reactions Sourcebook (J. Marwan, and S.B. Krivit, eds., American Chemical Society, Washington, DC, 2008) pp. 99-123.)
[3]Chubb, S.R., Proc. ICCF13, (2007), in press.
[4]Chubb, S.R., Proc. ICCF10, 735 (2006). http://www.lenr-canr.org/acrobat/ChubbSRnutsandbol.pdf
[5] Chubb, S.R., submitted to Proc. Roy. Soc., 2005. http://arxiv.org/pdf/cond-mat/0512363
[6] Robert L. Park, (2008) private communication.
[7] David J. Nagel, (2008) private communication.
[8] Talbot Chubb, , (2008) private communication.
[9] Chubb, S.R., claim, based on material presented here and in refs. 1-5.
[10] Schwinger, J., Proc. ICCF1, pp. 130-136 (1990).
[11] $\langle Initial|\mathbf{V}|Final\rangle = i\hbar\frac{\partial\langle Initial(t)\,|\,Final(t)\rangle}{\partial t}$ when $\langle Initial(t)|$ and $|Final(t)\rangle$ evolve in time, in the interaction picture representation, when they (as well as the density operator $\rho(r) \equiv \sum_{r_i}\delta(r-r_i)$ and total current operator $j(r)$) evolve in time, in the Schroedinger picture representation, $\langle Initial|\mathbf{V}|Final\rangle$ (which is the same when all quantities are expressed in a common representation) can be expressed using the expression that is shown in Fig.4b.
[12] Chubb, T.A. and S.R. Chubb, J. Condensed Matter Nucl. , Sci. 2, 1–9 (2008). http://www.cfescience.com/yahoo_site_admin/assets/docs/pdfCoulBar.80171500.pdf
[13] Preparata, G., QED Coherence in Matter (World Scientific, Singapore, 1995).

Interface Model of Cold Fusion

Talbot A. Chubb
Cold Fusion Energy Research Co., 5023 N. 38th St., Arlington VA 22207, USA,
www.coldfusionenergyscience.com

Abstract

The interface theory of cold fusion is a variant of Ion Band State (IBS) Theory.[1] It models Bloch symmetry deuterons in a 2-dimensional metal lattice instead of the 3-dimensional metal lattice first used. Both IBS variants recognize that the required lattice symmetry has limited extent, with the reactive deuterons being bound inside a closed volume like a box. The reactive deuterons are confined within classical turning point boundaries, while within the box their density distributions are modulated by a lattice array potential. Strictly speaking, the IBS fusion theory is a many-body theory. Nuclear dd fusion is one of several LENR processes. Some LENR processes do not require many-body ions and support room temperature nuclear reactions using light ions in single-particle Bloch geometry. For example, the decay of metastable single-body Bloch-function ^{8}Be seems to be the source of MeV alphas in Oriani's light/heavy water electrolysis, and in several co-deposition electrolysis CR39 studies, as described in *ICCF14 Abstracts*.[2] The Oriani MeV alphas are side products of both light water and heavy water electrolysis, using either Pd or Ni cathodes, as shown in highly repeatable tests. Bloch ^{8}Be is likely the nuclearly reactive component in the final step of the Iwamura *et al.* transmutation studies.[3] Despite differences, all LENR systems seem to share some essential physics.

The essential feature that seems to be shared by all LENR processes is a need to produce coherently partitioned light "atoms", where coherent partitioning means the type of partitioning that occurs when a low density Bose condensate becomes partitioned in an optical lattice.[4] As applied to LENR, a coherently partitioned atom means a coherently partitioned ion neutralized by coherently partitioned electron(s). Superfluid behavior marks the presence of coherently partitioned atoms in Bose condensates in lattices. To behave as a superfluid, Bose condensate atoms must occupy a lattice that consists of a communicating network of shallow potential wells that are separated by potential barriers low enough to allow tunneling. Also, the number of Bose atoms in the lattice must be smaller than the number of potential wells, or must be a non-integer times the number of potential wells. The atoms must be indistinguishable in the Pauli sense, i.e., when 2 "indistinguishable" particles collide and move apart, neither of the receding particles can be identified as one of the incident particles. Indistinguishable particle interactions must be modeled using 2-particle wave functions that express coordinate exchange symmetry.

The challenge to LENR experimenters is to create a nuclear reactive environment. In practice, this means to create conditions involving a metal solid that causes coherent partitioning of a feedstock atom. This means that the configuration of the atom must become

describable by a wave function with many equivalent centers. One must create "many-centers" nuclei neutralized by many-centers electrons. A particle is best thought of as a "quantum-of-mass". A quantum of electron mass, if localized, is called an electron; if delocalized in a Bloch configuration it can be called a quasiparticle electron. If 2 quasiparticles interact, their interaction cannot be modeled using an expansion of wave functions around a single center-of-mass. When the interaction is nuclear, the nuclear physics cannot be calculated using a sum over wave-function spherical harmonics about a center-of-mass. This means that quasiparticle-quasiparticle nuclear interactions cannot be modeled using the standard center-of-mass expansions of classical nuclear physics. This incompatibility is a major factor in the nuclear physics community's failure to understand cold fusion. It is also the reason that dd cold fusion reactions do not result in emission of energetic particles or γ-rays.

Providing a nuclearly active environment for reactive deuterons means the same as providing an environment that catalyzes a geometric change in a "D-atom" from a single-center geometry to a many-centers geometry. One strategy is to place deuterons inside a solid which has a very stable and regular lattice symmetry. The first geometry that seems to have catalyzed cold fusion is a 3-dimensional fcc Pd metal lattice with each of its octahedral sites occupied by an interstitial deuteron. In Fleischman-Pons cold fusion, overpotential electrolysis of a D_2O electrolyte deposits deuterons onto a Pd metal cathode to create this environment. Further added deuterons then occupy a communicating network of unit cells containing 2 shallow tetrahedral sites and the periphery of one octahedral site. This paper describes a second strategy. It argues that an interface between an ionic crystal and sputtered Pd metal can provide a 2-dimensional many-centers geometry using equilibrium chemistry. The ZrO_2,nanoPd catalyst developed at Tohoku U. seems to be of this type.[6]

This paper applies IBS theory to many-body interface deuterons located between a ZrO_2 crystal face and a Pd nanocrystal. Photomicrographs of ZrO_2,nanoPd catalyst show fragmented Pd nanocrystals embedded in larger ZrO_2 crystals. At some of the contact surfaces the Pd metal is assumed to have formed an epitaxy fit onto the ZrO_2 substrate.[7] Epitaxy makes an unusually stable, low energy first layer of Pd on the ionic crystal surface. Above the epitaxy Pd layer are transition layers containing interstitial deuterons and vacancies, and above the transition layers is fcc cubic Pd metal. The interface + transition layer constitutes an energy minimizing configuration, and incidentally provides a major reservoir for non-reactive absorbed deuterium.

The stability of the epitaxy Pd layer on a ZrO_2 crystal face is caused by the large negative Gibbs free energy of ZrO_2, and the relative malleability of nanoPd. The stability of the interface is not damaged by its hosting an extremely thin layer or sheet of D^+ quasiparticles (D^+_{Bloch} ions) between the metal oxide and the epitaxial metal layer. The D^+ quasiparticle sheet is extremely thin and resides harmlessly between the epitaxy Pd layer and the ZrO_2 crystal. Normal diffusing deuterons become D^+_{Bloch} ions when they encounter this strictly ordered environment. When a D^+_{Bloch} ion transitions to quasiparticle geometry, it becomes neutralized by an electron quasiparticle, which forces the epitaxy layer to move away from the ZrO_2, but only by about a 0.001 fraction of a metal layer. The resulting layering is: 1) ZrO_2 crystal, 2)

D^{+}_{Bloch} "atom" sublayer, 3) epitaxy Pd layer, 4) transitional Pd layers with interstitial D atoms, 5) fcc Pd nanocrystal.

IBS theory as applied to ZrO_2 + nanoPd interfaces preserves 2-dimensional periodic symmetry. The modeling uses stationary state quantum mechanics and many-body physics. The physics could be called “semi-classical” quantum orbital physics. In atom physics, the word "orbital" does not imply electrons in planetary orbits around a nucleus. Instead, it implies a set of negatively-charged electron wave functions pulled as densely as possible on top of a positively charged nucleus. It is a mistake to think of an atom as being mostly empty space. Instead, it is jam packed with electron charge-density matter. An atom appears as empty space only to a high energy impacting nucleus or γ-ray. Electron density is limited by Pauli exclusion. Atom structure is determined by system energy minimization.

Atom quantum mechanics teaches us about *s*, *p*, *d*, ….wave function states. Each wave function describes an electron density distribution. The distribution is a matter field, i.e., has a value at every point is space. The electrons in H, He, Li, and Be are all in *s*-states. Each *s*-electron has spherical symmetry. The boron atom adds a non-spherical *p*-electron. The *p*-electron is coherently partitioned between two equal volume potential wells. Half the *p*-electron’s density is in one potential well, half is in the other, with zero electron density centered on the boron nucleus where the 2 potential wells touch. One must sum over both potential wells to recover the electron. In other words, boron's *p*-electron displays coherent partitioning behavior.

Figure 1. Density distribution of p-electron orbital in boron. Calculation by D. T. Cromer.

In IBS fusion Bloch deuterons, like *p*-electrons, are coherently partitioned. The IBS Bloch deuterons must be coherently partitioned into 1000 or more potential wells to avoid a Coulomb barrier. Energy minimization calculations show that a deuteron many-body wave function with more than 1000 potential wells will have no Coulomb barrier. Instead, the wave function expresses coordinate exchange symmetry and wave function overlap.

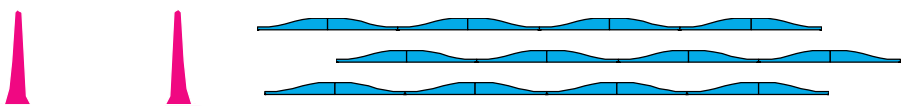

Figure 2. D_2 Molecule. D^{+}_{Bloch} Quasiparticle(s) inside an Interface

The reason that energetic particles and γ-rays do not occur in cold fusion is that they cannot exist as coherently partitioned entities at lattice spacing. Their deBroglie wavelengths are too small. Therefore they cannot be part of the initial and final state wave functions, as required for reaction. The dd-fusion transitions are restricted to transitions that preserve spin and nuclear angular momentum. Unlike hot fusion, the likely dd-fusion initial configuration is a spin-zero pair or pairing, which then undergoes a 0^+ to 0^+ density-distribution changing transition.

Quasiparticle ^{4}He can exist in either (pn,pn) or (pp,nn) nuclear geometry. The initial spin-zero D^+_{Bloch} pairing has (pn,pn) geometry, which is the same as (d,d) geometry. The first transition collapses the wave function from potential well dimensions to nucleus dimensions, creating a metastable excited $^4He^{++}_{Bloch}$ nucleus. A minimal transfer of energy occurs during this step. Transfer of the remaining 23.8 MeV to the metal lattice requires a cascade of transitions between sequential metastable states, with rates determined by the Fermi Golden Rule.

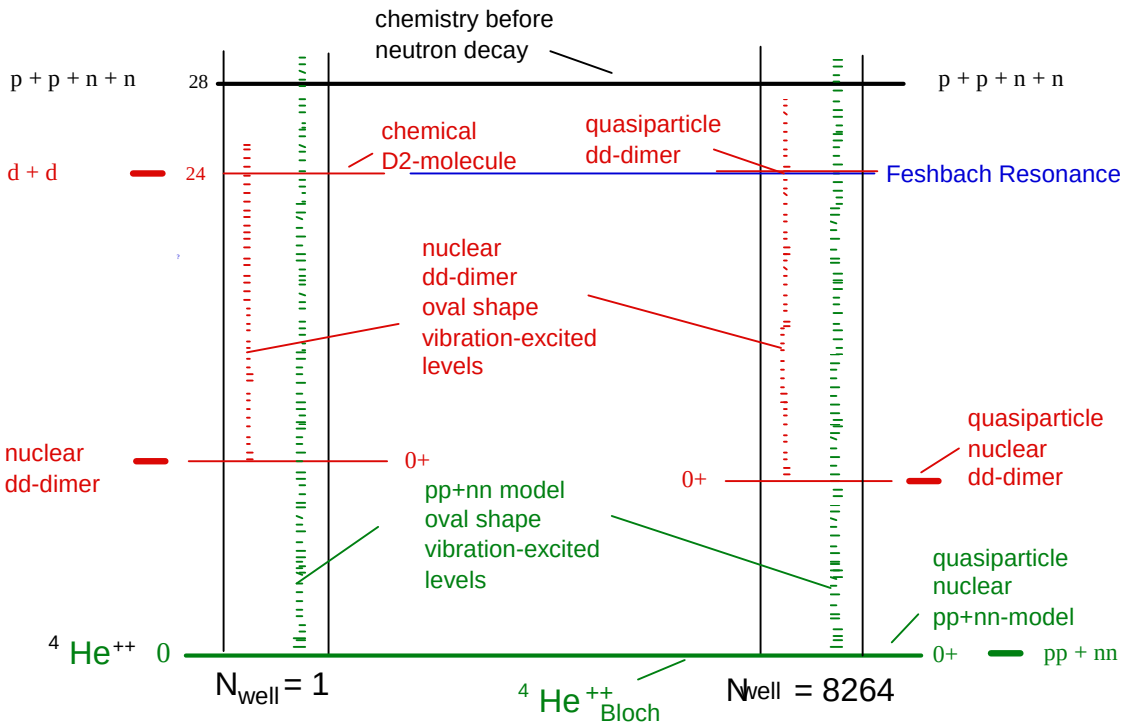

Figure 3. Energy level diagram for d+d and pp+nn ^{4}He in single-center and Bloch geometry.

When a diffusing deuteron transitions to Bloch geometry configuration within a ZrO_2 + nanoPd interface, energy minimization requires an accompanying Bloch electron. If N_{well} = 1000, Pauli exclusion requires the Pd epitaxy metal layer to jump back by 0.001 metal layer thickness. The jump is a momentum shock that pushes ZrO_2 and nanoPd crystallite apart,

sometimes stimulating an irreversible energy transfer from an initial state Bloch deuteron many-body system to a hosting metal lattice. Even a small energy transfer makes the fusion reaction irreversible.

The partitioned electrostatic force between two quasiparticle deuterons decreases with N_{well}. Therefore work done to bring deuterons into contact decreases with N_{well}. [In each well $F_{12}=e^2/r_{12}{}^2N_{well}{}^2$. Summing over potential wells gives $F_{12}=e^2/r_{12}{}^2N_{well}$.] Therefore, a coherently partitioned $^4He_{Bloch}$ product is more stable at higher N_{well}. This lowering of nucleus ground state energy makes the flakelike nuclear product seek larger N_{well}.[2,3]

The wave function boundary within which a D^+ many-body system resides is subject to quantum fluctuations. Boundary fluctuations which change bound volume also change N_{well}. Fluctuations in N_{well} cause the energy of (pn,pn) $^4He^{++}{}_{Bloch}$ to fluctuate, which can "scan" the energy of a nuclear configuration wave function state across the energy of the dd pairing initial state. This phenomenon creates a transient Li-Feshbach energy-match resonance. Scanning across a Feshbach resonance causes geometric change accompanied by a small transfer of momentum + energy to the hosting lattice. A small energy transfer makes the reaction irreversible.

As shown in the energy level chart, quasiparticle ^4He exists in both (pn,pn) and (pp,nn) nuclear geometries. The initial spin-zero $D^+{}_{Bloch}$ pairing has (pn,pn) geometry. The first transition collapses the wave function from potential well dimensions to nucleus dimensions, creating a metastable excited $^4He^{++}{}_{Bloch}$* nucleus. Transfer of 23.8 MeV to metal lattice requires a cascade of transitions between metastable states, with rates determined by the Fermi Golden Rule.

The interface model suggests that the following transitions are supported by 2-dimensional symmetry LENR. The asterisk designates a metastable excited nuclear state. Unbalanced charges reflect electron quasiparticle configuration changes.

1) $D^+{}_{Bloch} + D^+{}_{Bloch} \rightarrow {}^4He^{++}{}_{Bloch}$* dd fusion reaction
2) $D^+{}_{Bloch} + {}^6Li^+ \rightarrow {}^8Be^{++}{}_{Bloch}$* Oriani heavy water reaction
3) $H^+{}_{Bloch} + {}^7Li^+ \rightarrow {}^8Be^{++}{}_{Bloch}$* Oriani light water reaction
4) $^8Be^{++}{}_{Bloch}$* $\rightarrow {}^8Be^{++*}$ degradation of lattice symmetry creates a preferred mass center
5) $^8Be^{++*} \rightarrow {}^4He^{++} + {}^4He^{++}$ fission creates 2 alphas in CR39
6) $^4He^{++}{}_{Bloch} + {}^4He^{++}{}_{Bloch} \rightarrow {}^8Be^{++}{}_{Bloch}$* second step in Iwamura reactions
7) $^8Be^{++}{}_{Bloch} + {}^{133}Cs^+ \rightarrow {}^{141}Pr$ Iwamura alpha addition transmutation step

The synthesis reactions are promoted by scanned Li-Feshbach resonances. Reactions 1 and 6 occur in co-deposition experiments. Premature separation of $^8Be^{++}{}_{Bloch}$* from its hosting interface leads to a flakelike neutral atom $^8Be_{Bloch}$*, which can diffuse through liquids and solids. Reaction 7 requires a cascade of energy transfers to a hosting lattice. Some of the available excited nuclear states of ^8Be* are shown in an energy level chart provided by Heyde.[8]

References

1. T.A. Chubb and S.R. Chubb, *Fusion Technol.*, **20**, 93 (1991), ibid. *Proc. ICCF5*, 315(1995).
2. *ICCF14 Abstracts*: R.A. Oriani, Abstr. 23; S. Szpak, P. Mossier-Boss, F. Gordom, and L. Forsley, Abstr, 20*;* L. Forsley, and P. Mossier-Boss, Abstr. 61; L Kowalski,, Abstr. 66.
3. Y. Iwamura , M. Sakano, and T. Itoh, *Jpn. J. Appl. Phys.* **41**, 4642 (2002).
4. D. Jaksch, C. Bruder, J.I. Cirac, C.W. Gardiner, and P. Zoller, *Phys. Rev. Lett.* **81**, 3108 (1998); M. Greiner, O. Mandel, T. Esslinger, T.W. Hansch, and I. Bloch, *Nature* **415**, 39 (2002).
5. T.A. Chubb, *Infinite Energy*, Vol.13, Issue 74 (2007).
6. S. Yamaura, K. Sasamori, H. Kimura. A. Inoue, Y. C. Zhang, Y. Arata, *J. Mater. Res.* **17**, 1329-1334, (2002); Y. Arata and Y-C Zhang, *Proc. Japan Acad..*, **78B**, 57-64, (2002).
7. G. Barcaro, A. Fortunelli, G. Rossi, F. Nita, and R. Ferrando, *Phys. Rev. Lett.* **98**, 156101 (2007).
8. K. Heyde, "Basic Ideas and Concepts in Nuclear Physics", (IOP Publishing Ltd, Bristol, 1994) p. 54.

Toward an Explanation of Transmutation Products on Palladium Cathodes

Norman D. Cook
Department of Informatics
Kansai University
Osaka, Japan

Abstract

A lattice model of nuclear structure that is isomorphic with the conventional independent-particle model (IPM) has previously been shown to predict the asymmetrical fragments produced by the thermal fission of the actinides. The same model can be used to predict the transmutation products found on palladium cathodes following electrolysis, as reported by Mizuno [1]. It is concluded that the substructure provided by the lattice may be a crucial addition to conventional nuclear structure theory in order to explain the nuclear transmutations in both thermal fission and "cold fusion".

Introduction

Several decades ago, various nucleon lattice structures were examined theoretically in the search for stable, condensed configurations of nucleons, possibly present in "neutron stars" [2]. Amidst such research, several lattice models of nuclei at normal nuclear densities [e.g., 3, 4] were developed and shown to exhibit the properties that are normally described using the conventional (shell, liquid-drop, cluster, etc.) models of nuclear structure theory. The lattice models have proved most useful in predicting the multifragmentation products of heavy-ion experiments [3, 5, 6] – an area where conventional models are inapplicable. Notable among such theoretical work was the quantitative explanation of the high-energy fragmentation of Xe and Kr nuclei using an FCC lattice [5] and the parameter-free explanation [7, 8] of the ***asymmetrical*** fragments produced in the thermal fission of uranium and plutonium: "the perennial puzzle of nuclear physics" [9].

The present study was undertaken to examine the use of the FCC lattice model for explaining the transmutation products that have been reported in low-energy "cold fusion" experiments. Mizuno [1] found not only deviations from the natural abundance of Pd isotopes on Pd cathodes, but also deposits of various light elements on the cathode surface. Those results are undisputed as empirical studies, but questions remain concerning the physical mechanisms. Here I apply the same lattice-fission technique that explains the asymmetrical fission of uranium [7, 8] to the break-up of the Pd isotopes, again ***without*** the use of model parameters to produce the results.

The Lattice Model

Central to an understanding of the lattice model itself is a mathematical identity between the quantum mechanical description of nuclear quantum states (summarized by the quantum numbers, ***n, j, m, s*** and ***i,*** that are used in the Schrodinger wave-equation) and a specific lattice structure [4, 8]. Specifically, in the conventional description of nuclear states, each nucleon is presumed to be in an energetic state specified by its unique set of quantum numbers. The description of nucleon states is analogous to (although, in detail, somewhat different from) the quantum mechanical states of the electrons in electron orbitals and described by similar quantum numbers. The motivation underlying the lattice model is the fact that a specific lattice structure that reproduces all of the nucleon energy states of the so-called independent-particle (~shell) model. That same lattice (an antiferromagnetic face-centered-cubic [FCC] lattice with isospin layering) has been independently shown to be the lowest-energy condensed state of nuclear matter (N=Z) [11]. The significance of the isomorphism between the lattice and quantum mechanics lies in the fact that, if the conventional IPM structure of a nucleus is known, then the 3D lattice positions of all its nucleons can be deduced directly from Eqs. 1-5 (and vice versa, starting with occupied lattice sites and deducing its IPM state, Eqs. 6-8).

$\boldsymbol{n} = (\lvert x\rvert + \lvert y\rvert + \lvert z\rvert - 3) / 2$	Eq. 1	$\boldsymbol{i} = ((-1)^{(z-1)}) / 2$	Eq. 5
$\boldsymbol{j} = (\lvert x\rvert + \lvert y\rvert - 1) / 2$	Eq. 2	$x = \lvert 2\boldsymbol{m}\rvert(-1)^{(\boldsymbol{m}+1/2)}$	Eq. 6
$\boldsymbol{m} = \lvert x\rvert / 2$	Eq. 3	$y = (2\boldsymbol{j}+1-\lvert x\rvert)^{(\boldsymbol{i}+\boldsymbol{j}+\boldsymbol{m}+1/2)}$	Eq. 7
$\boldsymbol{s} = ((-1)^{(x-1)}) / 2$	Eq. 4	$z = (2\boldsymbol{n}+3-\lvert x\rvert-\lvert y\rvert)^{(\boldsymbol{i}+\boldsymbol{n}-\boldsymbol{j}-1)}$	Eq. 8

where x, y and z are all odd-integers defining FCC lattice coordinates. Full details of the lattice structure and its application to the unresolved problems in nuclear theory are available elsewhere [8]. Suffice it to say that the ***n***-shells of the harmonic oscillator are literally shells in the lattice (Fig. 1), and all of the ***j***-, ***m***-, ***s***- and ***i***-subshells of the IPM model are defined in terms of lattice symmetries. It bears emphasis that the occupancies of ***all*** of the shells and subshells in the lattice model are identical to those in the IPM model – from which the shell model is derived. In other words, the FCC lattice is a geometrical analog of the quantal regularities of the Schrodinger equation. It therefore provides a natural inroad to questions concerning nuclear substructure ***without*** the need for ad hoc postulates concerning nucleon-clustering or dynamics (i.e., "model" parameters that are not derived from quantum mechanics).

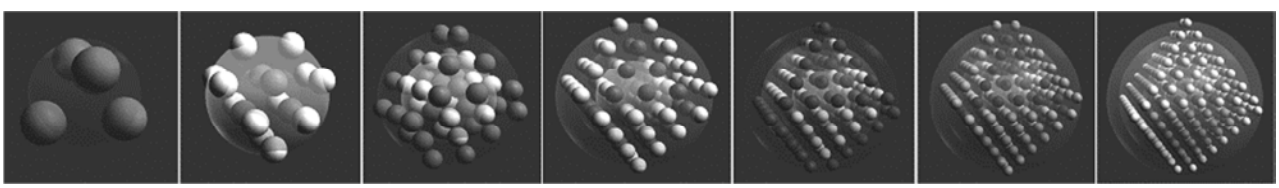

Figure 1. The n-shells in the lattice built from a central tetrahedron show the same occupancy as the harmonic oscillator [4, 9]: $_{2}He^{4}$, $_{8}O^{16}$, $_{20}Ca^{40}$, $_{40}Zr^{80}$, $_{70}Yt^{140}$, $_{112}Xx^{224}$, $_{168}Xx^{336}$.

Given the well-established validity of the IPM (~shell model) description of nucleon states, a unique lattice structure for any combination of N and Z is implied (Eqs. 1~8) – so that the lattice structure itself can be examined in terms of its fragmentation dynamics.

Fission of the Actinides

The break-up of a mini-lattice (A~240) is favored along those lattice planes where the number of interfragment 2-body interactions is low and simultaneously the interfragment Coulomb effect is high [7]. These are competing tendencies: ***asymmetrical*** fission is favored by the small number of nucleon-nucleon interactions binding small fragments to the larger parent nucleus, whereas the ***symmetrical*** (~1:1) split of the parent nucleus is favored when equal numbers of proton charges are in both daughter fragments. Note that the prediction of ***symmetrical*** fission fragments is the classic deficiency of the liquid-drop model (LDM) explanation of thermal fission. Without an "asymmetry parameter" – introduced explicitly to enhance asymmetrical fragmentation, the presumed liquid-like interior of large nuclei in the LDM inevitably predicts ***symmetrical*** fission – contrary to all findings on low-energy fission of the actinides. Shell model theorists have sought to introduce nuclear substructure (i.e., asymmetry) via the stability of "magic" numbers of protons and neutrons – and that view is the qualitative explanation of asymmetrical fission in most textbooks today. To the contrary, however, Strutinsky et al., who worked explicitly on this problem, have noted that the manipulations of the nuclear potential well needed to produce asymmetric fission have "little to do with the magicity of spherical fragments" [11] and the magic numbers 28 and 50 among the final fragments do not explain – qualitatively or quantitatively – the known fragment asymmetries. In contrast, the lattice model contains substructure inherent to the lattice itself. Using the default FCC structures for the uranium and plutonium isotopes, calculation of the interfragment binding along lattice planes, together with interfragment Coulomb effects, already shows the predominance of ***asymmetrical*** fission fragments (~3:2) (Fig. 2).

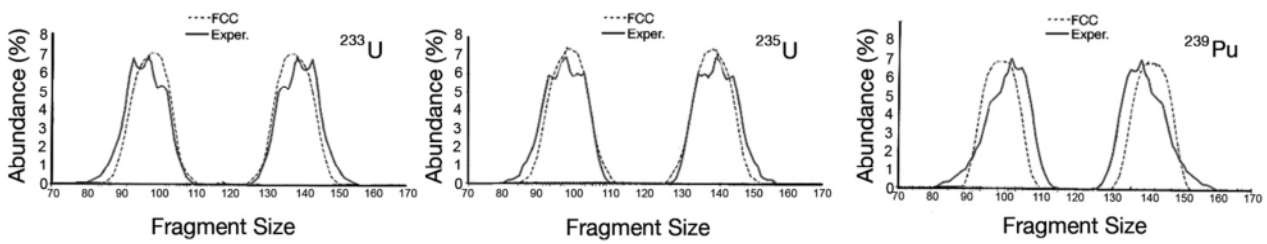

Figure 2. The parameter-less prediction of asymmetrical fragments in the thermal fission of the actinides using the lattice model [7, 8]. The experimental data are shown by the solid lines (experimental error lies within the width of the lines). Not only is the asymmetry of the fragments unexplained in conventional theory (known since 1938), but there is real substructure in the fragments that survives the fission process and cannot be explained by the LDM or shell model.

Transmutation of Palladium

Among the most dramatic results on the transmutation of deuterium-loaded palladium are those reported by Mizuno [1]. As experimentalists, they have been concerned chiefly with the measurement of heat and reaction products, and have reported not only changes in the abundance of various Pd isotopes, but also the deposition of various light- and medium-size elements on the surface of the Pd cathodes. They found that: (i) Prior to the experiment, the measured abundances of Pd isotopes were virtually identical to the known natural abundances (Table 1, Column B). (ii) Subsequent to electrolysis, there were significant changes in the relative abundances (Column C), suggestive of nuclear transmutation at the surface of the electrode, with (iii) gradually smaller changes in the natural abundances as measurements proceeded from the surface to 30,000 Angstroms into the depth of the cathode. Issues of heat production aside, these are profoundly interesting experimental findings.

Table 1: Experimental and Theoretical Changes in Palladium Isotopes Following Electrolysis

	EXPERIMENT			SIMULATION				
Isotope	% Abundance	Mizuno Data	% Change	Initial No.	Loss	Final No.	% Loss	% Abundance
Pd^{102}	1.0%	4%	+3.0%	1,000	600	400	60%	3.8%
Pd^{104}	11.0%	17%	+6.0%	11,000	9,190	1,810	84%	17.1%
Pd^{105}	22.2%	20%	-2.2%	22,200	20,080	2,120	90%	20.0%
Pd^{106}	27.3%	21%	-6.3%	27,300	25,070	2,230	92%	21.0%
Pd^{108}	26.7%	21%	-5.7%	26,700	24,470	2,230	92%	21.0%
Pd^{110}	11.8%	17%	+5.2%	11,800	9,990	1,810	85%	17.1%
Total	100.0%	100%	0.0%	100,000	89,400	10,600	89%	100.0%
A	B	C	D	E	F	G	H	I

The percentage changes in the abundance of Pd isotopes (Column D) do not suggest any obvious regularity in the transmutation process, but a simple simulation indicates that essentially all of the Pd isotopes were equally involved in the transmutation process. That is, assuming that measurements of the cathode surface were made on, say, 100,000 Pd nuclei (Column E), the "loss" of 600, 9190, 20080, 25070, 24470 and 9990 of, respectively, the Pd^{102}, Pd^{104}, Pd^{105}, Pd^{106}, Pd^{108} and Pd^{110} isotopes results in percentages (Column I) virtually identical to those reported by Mizuno (Column C). What is of interest about these values is that they indicate that (with the exception of Pd^{102}, that accounts for only 1% of the natural abundance) ***all*** of the Pd isotopes were involved in nuclear reactions at approximately equal rates (84~92%, Column H). In other words, if transmutation of Pd is the source of heat energy in cold fusion experiments, then it is ***not*** the case that one or a few unusual isotopes are responsible for the effects, in so far as similar percentage decreases of all isotopes were involved. Clearly, this simulation does not indicate how deuterium is able to overcome the Coulomb barrier and enter the Pd nucleus [12], but it does show that, if some such mechanism is at work, the seemingly irregular changes in Pd isotopic abundances (Column D) are a consequence of similar percentage depletions in all isotopes (Column H).

The next question is, therefore, if a constant percentage of surface Pd isotopes were transmuted, what were they transmuted to?

Palladium Fission Fragments

Simulation of the fission of palladium was carried out on each of the six stable Pd isotopes using the lattice model [4, 7, 8,]. The nucleon build-up process in the model is given by Eqs. 1~4, with the assignment of equivalent "valence" nucleon positions determined solely by the maximization of nearest-neighbor interactions. In other words, 46 protons and 56~64 neutrons were placed at lattice sites, such that the final nucleus had (i) maximal nearest-neighbor binding, (ii) minimal Coulomb repulsion, and (iii) a total ***J***-value (calculated from the sum of nucleon ***j***-values) as experimentally known. A deuteron was then added at random to surface lattice sites of each nucleus. Finally, scission of the Z=47, N=57~65 system was simulated along 17 lattice planes cutting through or parallel to the origin of the coordinate system, and statistics collected. For each fissioning nucleus, the total number of "bonds" crossing the fission-plane was counted and the total Coulomb repulsion between the fragments calculated. Assuming an average nearest-neighbor binding energy of ~2.77 MeV (giving a total binding energy of the Pd isotopes within 1% of experimental values) and subtracting the Coulomb effect between the fragments, the four lowest-energy fission events per nucleus were calculated. The final steps in the simulation were (i) adjustment of the percentages of fragments using the natural abundances of Pd isotopes and then (ii) collation of the fission fragments per Pd isotope. The entire fission simulation is similar to that already reported concerning the actinides [7, 8], and can be easily reproduced using the NVS freeware (Windows and Mac versions) available at: www.res.kutc.kansai-u.ac.jp/~cook.

Results

The binding energy of the Pd isotopes was calculated from the total number of nearest-neighbor "bonds" in the lattice structure for a given number of Z and N, assuming a binding energy of 2.77 MeV/bond (ignoring spin and isospin effects) minus the Coulomb effect. By then calculating the total binding energy across each scission plane minus the Coulomb repulsion between the protons in each fragment, the energy required to induce fission was found to be 3.12~8.66 MeV, depending on the isotope. The fragments produced by splitting the Pd isotope along the low-energy planes contained 46~60 nucleons and 22~26 protons. In other words, fission of the Z=47, N=57~65 system was essentially ***symmetrical*** with two daughter fragments of approximately the same mass. Generally, only a few scission planes per isotope had fission energies below 10 MeV, but if fission events requiring up to 15 MeV are also included, then fragments with atomic number 14~33 and mass number 34~73 were found. Typical fission lattice-planes through a Pd isotope are illustrated in Figure 3. Qualitatively, the approximate spectrum of deposits on the Pd cathode reported by Mizuno [1] was reproduced by the lattice model. A quantitative study is in progress.

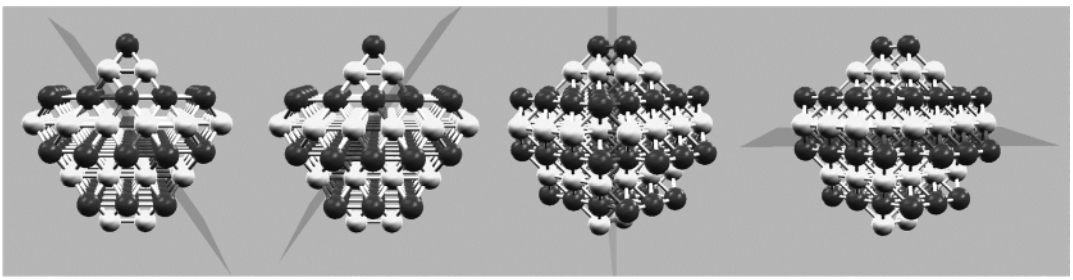

Figure 3. Examples of high (left) and low (right) probability lattice scission planes in Pd110. Note that the FCC lattice structures represent individual nuclei (protons are light spheres, neutrons are dark spheres), totally unrelated to the FCC (atomic) structure of the palladium cathode itself.

Conclusion

Conventional nuclear structure theorists are understandably reluctant to postulate new physical mechanisms to account for the transmutation results reported by Mizuno and others. Nevertheless, the excess heat found in many experimental "cold fusion" set-ups is strongly suggestive of a nuclear origin – and that suggestion alone implies that there are yet imperfectly understood nuclear phenomena at work. In fact, the ***asymmetrical*** fragmentation of U^{235} and all of the other actinides that undergo thermal fission is one of the oldest "mysteries" in nuclear physics. I suggest that both the mystery of asymmetric fission of uranium and the mystery of deuterium-induced transmutation of Pd can be solved by regarding the nucleus itself as a mini-lattice. Assuming a yet-uncertain mechanism for inducing the fission of Pd nuclei [12], the substructure implicit to the FCC lattice representation of nuclear quantal symmetries may explain transmutation results essentially without any modification to the conventional independent-particle (~shell) model of nuclear structure.

References

1. Mizuno, T. (1998) ***Nuclear Transmutation***, Infinite Energy Press, Concord.
2. Canuto, V. (1975) ***Annual Review of Astronomy and Astrophysics*** 12, 167.
3. Bauer, W., et al. (1985) ***Physics Letters B***150, 53.
4. Cook, N.D., & Dallacasa, V. (1987) ***Physical Review C***36, 1883-1891
5. Chao, N.C., & Chung, K.C. (1991) ***Journal of Physics*** G17, 1851.
6. DasGupta, S., & Pan, J., (1996) ***Physical Review*** C53, 1319-1324.
7. Cook, N.D. (1999) ***Proceedings of the St. Andrews Conference on Fission***, pp. 217-226.
8. Cook, N.D. (2006) ***Models of the Atomic Nucleus***, Springer, Berlin.
9. Fraser, J.S., & Milton, J.C.D. (1966) ***Annual Review of Nuclear Science*** 16, 1207.
10. Canuto, V., & Chitre, S.M. (1974) ***Inter. Astr. Astroph. Union Symp.*** 53, 133.
11. Brack, M., et al. (1972) ***Reviews of Modern Physics*** 44, 320.
12. Takahashi, A., et al. (1999) ***Physics Letters A*** 255, 89.

An Experimental Device to Test the YPCP ("Yukawa Pico Chemistry And Physics") Model: Implications for the CF-LENR Field

Jacques Dufour, Xavier Dufour, Denis Murat and Jacques Foos
CNAM - Laboratoire des sciences nucléaires - CC304A - 75141 Paris Cedex 03

Abstract

In the CF-LENR field (Cold Fusion and Low Energy Nuclear reactions) many experimental results are available: unexplained energy production, presence of unusual patterns of classical fusion reaction products, isotopic composition variations, sporadic emission of nuclear radiations (α, β and γ)… These effects are not always observed, for similar experimental conditions. Should a fundamental reason exist for these effects to occur, funding would be justified, to make them repeatable and more intense. In this article, a possible fundamental explanation of the phenomenon is described, together with the experimental plan to assess it.

Introduction

One of the main conceptual problems to be addressed (and solved) in the field of CF-LENR is: "how can huge potential barriers be overcome" (some 0.3 MeV in the case of d/d fusion and 30 MeV in the case of d/Pd nuclear reactions). Part of the answer is probably to be found in specificities of deuterons behavior in a lattice (deuteron/phonon interaction, resonant electromagnetic-dynamics…), that could increase the otherwise very low probability of reaction. should an attractive (and yet undiscovered) potential exist, with a pico-meter range and a coupling constant in the order of magnitude of the EM coupling constant, these probabilities could be considerably increased and result in macroscopic effects, potentially useful for technical applications. The experimental approach described below, aims at unveiling and characterizing such a potential. When positive, the path would be opened to pico chemistry and physics (YPCP).

Theoretical

Basis to assess the effects of the new potential:

A first attempt to describe the expected effects of such a potential had been presented [1]. Recently [2], arguments have been reported, (in the frame of Standard Model Extension – Lorentz symmetry violation) for the possible existence of a Yukawa type of potential, with a range extending farther than fm and up to pm distances. The YPCP model has been built on this possibility. It aims at proposing and designing unambiguous experiments, to assess the effects and hence the reality of this potential.

From [2], the following Yukawa type of potential, acting between nucleons, was extracted (and is called along this article: weak long range Yukawa potential):

$$V_{WLY} = -Cg^2 \frac{e^{-\nu r}}{r} \quad (1)$$

(C being a constant, g^2 the coupling constant of the strong nuclear force and ν (≥ 0) the reverse of the range ρ'.)

A candidate for the required boson carrying the interaction could be creation and exchange of electron-positron pairs (neutral). In the context of Feynman's equation for the Yukawa potential, the effect extends into the picometer range. This would have to be examined in detail when experiments are positive [3].

This yet unknown weak long range Yukawa potential should have an influence on neutron capture cross sections. Indeed, the variations of the neutron residence time, (depending upon its energy), in the range of this potential, is a straightforward explanation of the observed variations of the neutrons capture cross sections (apart from the resonance zones).

The model used to test the YPCP hypothesis and its main experimental predictions:

A description of the YPCP model is given in [4]. The model have been run with a range ρ' of 1,3 pm and a coupling constant Cg^2 of $5.048*10^{-28}$ that is 2 times the electro-magnetic coupling constant. Possible bound states of the proton (deuteron) at pm distances from the target atoms can thus be visualized. The amplitude of the potential barrier to be overcome to reach these bounds states, can also be evaluated. Only in the case of deuterium, were bound states visualized.

Two cases were thus considered, representative of the experimental situations to be examined:

The deuterium/palladium case (gas loading experiments YPC: Yukawa Pico Chemistry).

The deuterium/deuterium case (proton beam experiments YPP: Yukawa Pico Physics).

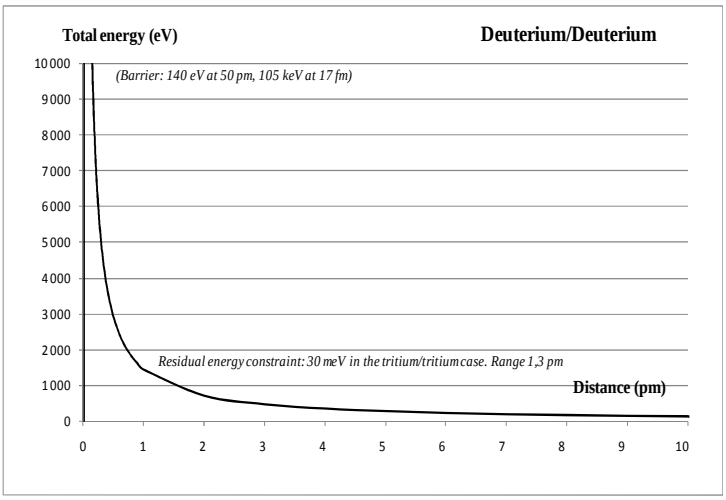

Figure 1. Palladium/deuterium total energy with Lennard-Jones potential.

It can be seen that the total energy remains positive and increases, from 0 at the periphery of the palladium (179 pm) up to 10000 eV at some 6 pm from the nucleus. The total energy then decreases to negative values and the deuteron could reach the nucleus, resulting in a nuclear reaction. It is thought that this is prevented by the Pauli exclusion principle, the K electrons having few energy levels available. To take this into account, a Lennard-Jones type of potential has been added to the other potentials. Stable bound states, such as $\left[{}^{106}_{46}Pd, {}^{2}_{1}H \right]$, a deuteron at some pm from a *Pd* nucleus, reaction enthalpy of some 9000eV), could be justified.

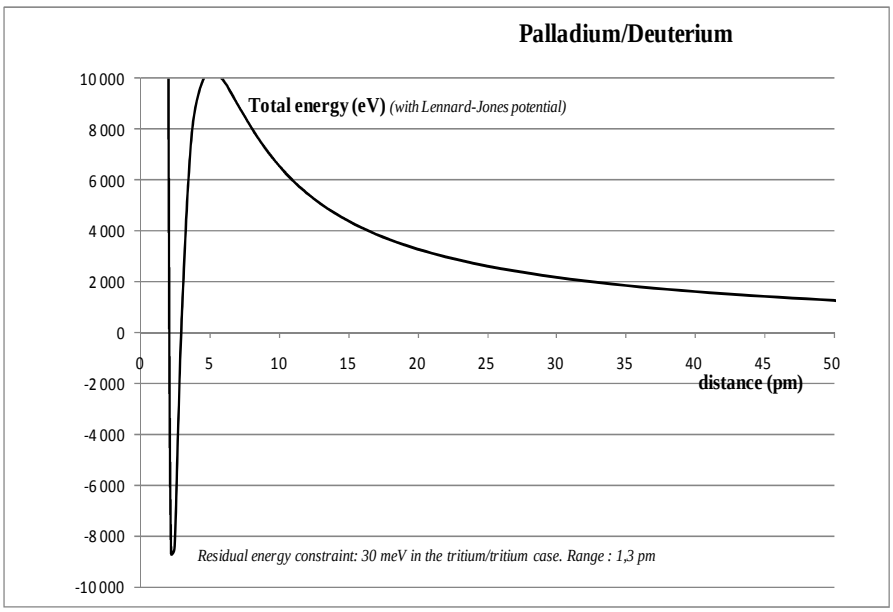

Figure 2. Deuterium/Deuterium total energy.

It can be seen that the total energy remains positive and increases from 0 at the periphery of the deuterium (73 pm) up to 140 eV at some 10 pm from the nucleus and 113 keV at some 15 fm from it. The total energy then decreases sharply and a d/d fusion reaction can take place. The potential barrier to be overcome is rather low and thin. This could be an explanation of the increase of the fusion reaction cross section at low energy of the deuteron, observed with deuteron beam experiments [5]

The YPCP conjecture and the CF-LENR field

Palladium gas loading:

The 30 MeV Coulomb barrier to be overcome, for a Pd/d reaction to occur, could be reduced to a few keV (see *Figure 1*). Collective or resonant effects in the lattice [6] could then trigger pico-chemical reactions, at the macroscopic level. X-Rays emitted in the keV level of energy could sustain the reaction once initiated ("heat after death" [7,8]) and expel helium4 present in the virgin palladium.

Products from these hypothetical pico-chemical reactions are probably rather stable (Pauli exclusion principle). The probability of reacting is nevertheless not zero. The nuclear reaction would be:

$$\left[{}^{106}_{46}Pd + {}^{2}_{1}H \right] \rightarrow {}^{108}_{47}Ag* \text{ (excess energy* 10.8 MeV)} \qquad (3)$$

${}^{108}_{47}Ag*$ then decaying through α emission (energy 10.8 MeV/α), ultimately yielding ${}^{104}_{46}Pd$ through β^- decay (1.4 MeV, and X-Ray emission) of intermediate ${}^{104}_{45}Rh$. (4) This type of reaction would cause a shift in palladium isotopes.

This could explain observations made in SPAWAR experiments, where entities such as $\left[{}^{106}_{46}Pd, {}^{2}_{1}H \right]$ (pseudo silver [12]), formed during electrolysis on the cathode, could pass into the electrolyte and then react according to (3) and (4), in unexpected places in the experiment [9].

Electrolysis and gas discharges should yield the same products patterns.

Proton (deuteron) beam experiments:

Typical experiments with deuterons beams, are run with energies of the deuterons of hundreds of keV. Recent experiments [5], run with deuterons energy round 5 keV have shown a surprising high level for the reaction cross section. This has been attributed to a screening potential of the electrons, in the order of hundreds of eV. The weak long range Yukawa potential could add to this screening effect: its action being energy dependant, lowering the energy of the impacting deuteron could be favorable. The full Coulomb barrier (some 300 keV) would also be reduced down to some 110 keV. It is then thought that the use of deuterons of energies in the range 15 to 150 eV, could increase the d/d fusion cross section observed in [5].

Experimental

Reaction enthalpies of pico-chemical reactions:

The enthalpy of formation of pico-chemical products formed by reactions such as (3) during deuterium loading of palladium, will be determined. The heat released will be measured using an ice calorimeter built and characterized for that purpose. A detailed description of this device is given in [10]. Pure palladium black (activated at 230°C, under 10^{-1} mb pressure) will be used, thus eliminating the pollution that might be caused by a support [7].

After the experiment, the processed samples will be recovered for analysis.

Charged particle emission:

The possibility of the emission of charged particles caused by the impact of low/medium energy protons or deuterons (between 15 and 150 eV) on a metallic target will be assessed. Use will be made of a device that has been built to generate protons with energies in that range.

Description of the proton (deuteron) generator:

A concept similar to the Penning ion source has been used: a cloud of protons or deuterons (and not a beam) is generated. The protons or deuterons then impact, with a controlled energy, a target made from the metal to be studied. See Figure 3 and Ref. [4].

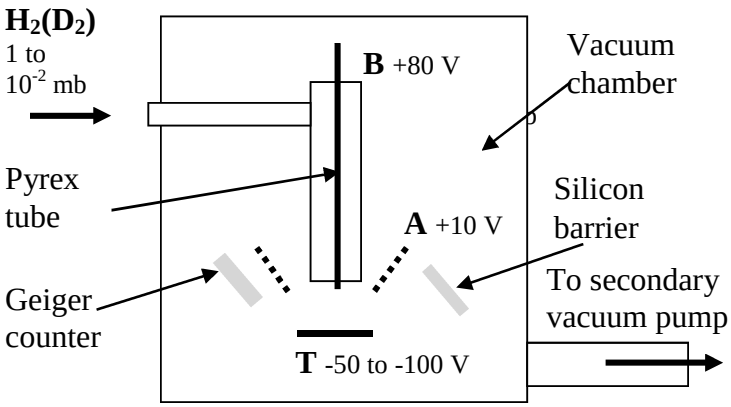

Figure 3. Proton (deuterium) generator.

Hydrogen (deuterium) leaking at a pressure between 1 and 10^{-2} mb, enters a vertical pyrex tube (12 mm diameter). At the outlet of the tube, the hydrogen expands into a vacuum chamber, maintained at a pressure between 10^{-1} and 10^{-2} mb by a primary vacuum pump. The use of a secondary vacuum pump allows the pressure in the vacuum chamber to be lowered to values in the range 10^{-2} and 10^{-3} mb.

Currents of 15 eV protons, up to 500 μA have been obtained.

Description of the analysis to be performed:

From the conclusions of the YPCP model, it is anticipated that, depending upon the experimental situation, 2 kinds of reactions will occur, pico-chemical and d/d fusion reactions:

- the enthalpy of the pico-chemical reactions (YPC), resulting from the binding of a proton (deuteron) close to the nucleus of the treated atom (in the order of some pm) will be determined from the heat released during gas loading experiments and from the amount of products formed (ICP-MS and XRF see [4,11]). This non nuclear reaction would have an enthalpy of reaction of a few keV. X-Rays of that energy could be emitted. Only deuterium is expected to react.
- true nuclear d/d fusion reactions, resulting from pico physics (YPP), will be characterized by their usual reaction products (protons, helium3 and neutrons) with associated energies. These reactions are expected to occur in the proton (deuteron) generator.

Conclusion

If positive, the proposed experiments would prove the reality of the YPCP working hypothesis and the existence of the weak long range Yukawa potential. Once this necessary scientific confirmation is obtained, funding could be obtained for developments that can be envisaged along 2 paths:

- nuclear wastes remediation [13] and small heat generators (if metals other than palladium can be used). These developments could be achieved through gas loading, electrolysis, electrical discharges …
- true cold fusion d/d reactions (deuterons beam experiments) ultimately leading to a d/d fusion reactor based on well mastered technologies, using usual temperature and pressure conditions.

References

1. J. Dufour “Very sizeable increase of gravitation at pico-meter distance: A novel working hypothesis to explain anomalous heat effects and apparent transmutations in certain metal/hydrogen systems” *J.Condensed Matter Nucl. Sci.* **1** (2007) p.47-61
2. B. Altschul “Lorentz violation and the Yukawa potential” *Physics Letter B* **639** (2006) p.679-683
3. Discussions A. Meulenburg/J. Dufour at ICCF14
4. http://arxiv.org/ftp/arxiv/papers/0810/0810.0955.pdf
5. A. Huke et alt. “Enhancement of deuteron fusion reactions in metals and experimental implications” *Physical review* C **78** 015803 (2008)
6. S. R Chubb “Resonant electromagnetic-dynamics explain the Pons-Fleischmann effect” *ICCF 14 proceedings Washington, 10/15 August 2008*
7. Y. Arata and M. J. A Yue-Chang Zhang “Solid fusion reactor with zero input energy” *ICCF 14 proceedings Washington, 10/15 August 2008*
8. S. Pons and M. Fleischmann “Heat after death” *ICCF 4 proceedings EPRI vol 2 p.91*
9. L. Forsley and P. Mosier-Boss “Quantitative spatial analysis of Pd/D co-deposition induced nuclear particles tracks” *ICCF 14 proceedings Washington, 10/15 August 2008*

10. J. Dufour, X. Dufour, D. Murat and J. Foos “A simple calorimetric method to avoid artifact in a controversial field: the ice calorimeter” *ICCF 14 proceedings Washington, 10/15 August 2008*
11. Y. Iwamura *et al.* “ Observation of surface distribution of products by X-Ray fluorescence” *ICCF 12 proceedings 2005 Yokohama Japon*
12. W. T. Williams and J. Dash “Auger and mass spectroscopy of anomalous Ag concentrations on electrolysed Pd” *ICCF 14 proceedings Washington, 10/15 August 2008*
13. I. Savvatimova and J. Dash “Transmutation of elements during conditions of low energy glow discharge exposure and the associated processes” *ICCF 14 proceedings Washington, 10/15 August 2008*

Investigation of Deuteron-Deuteron Cold Fusion in a Cavity

Cheng-ming Fou
Department of Physics and Astronomy, University of Delaware
Sharp Laboratory, Newark, DE 19716

Abstract

A cavity in a solid, first of all, serves as a place of confinement for a Deuterium molecule. Two deuterons in the molecule are trapped together in close proximity. Thus, they may engage in 'Low Energy Nuclear Reaction' which requires longer time, unlike collision type of nuclear reaction. Secondly, the electric field in the cavity (to be shown below) superimposed on this deuteron-pair would lower the Coulomb barrier between them facilitating a 'Low Energy Fusion' reaction. Furthermore, neutron exchange reaction between two deuterons (in an analogous manner like the electron exchange that forms a Deuterium molecule) is like a 'Long Range' force (as compared to the range of nuclear force) that can pull two deuterons together. This range is longer than that of the pi-plus exchange nuclear force between a proton and a neutron, because neutrons are charge neutral. [1] Longer reaction time; [2] Lowered Coulomb Barrier; [3] Longer range are the necessary conditions for (d-d) 'Cold Fusion'.

Earlier, in reference (1), the neutron exchange potential was modeled as a slow-varying function of the (d-d) separation.

$$V_{ex} = -A - B \exp (- K r_{dd}) \qquad (1)$$

A = 4.4 MeV corresponds to twice the neutron binding energy in deuteron when the two deuterons are far apart, and A+B = 28.4 MeV corresponds to the sum of the binding energies of the two neutrons in ^{4}He nucleus, when the two deuterons are combined.

This potential is not for a 'new' force between two deuterons. It is simply a manifestation of proton-neutron nuclear force. Just like the electron exchange interaction that binds two hydrogen atoms to form a molecule is a manifestation of Coulomb force between electron and proton. This exchange interaction between two neutral hydrogen atoms is mediated through the exchange of electrons when the two Hydrogen- wavefunctions overlap. One does not need to solve a four-body [two protons with two electrons] quantum mechanical problem using Coulomb forces. Because, the two protons in the pair of hydrogen atom are sufficiently far apart even after the molecule is formed. Only the Coulomb potential energy between them needs to be considered. Likewise here, the interaction mediated through neutron exchange when the two Deuteron-wavefunctions overlap has a range larger than that of nuclear force. One does not need to solve a four body (ppnn) quantum mechanical problem using nuclear force because the two protons of the deuteron pair trapped inside a cavity are also far [comparing to nuclear force range] apart.

Together with the Coulomb-repulsion potential

$$V_c = k / r_{dd} \quad (2)$$

the total potential

$$V_T = V_{ex} + V_c \quad (3)$$

as a function of r_{dd} depending on the values of K and *k* could have no maximum or minimum [monotonously drops from positive infinity to -4.4 MeV], one plateau, or one minimum and one maximum [V_T drops from positive infinity to a minimum then rises up to a maximum, finally asymptotically approaches -4.4 MeV].

In a space free of external field like inside a Deuterium molecule in vacuum, $k = e^2 / (4\pi\varepsilon_o) = 14.4$ eV/ (10^{-10} m) is a constant, not an unknown parameter. Since 'Cold fusion' of the two deuterons in a Deuterium molecule has never been observed, a lower limit for K = 9 (1/ fermi) [1 fermi = 10^{-15} m] can be determined (see reference 3). In other words, K for the neutron exchange potential must be larger than this lower limit. Which means, in vacuum space the Coulomb barrier dominates over the attraction (due to neutron exchange) at all ranges of deuteron separation. In reference (3) K = 12 (1/f) [larger than the lower limit mentioned above] was chosen to investigate cases of 'weakened' Coulomb repulsions. It was found, if the Coulomb field is weakened by 50% or more, a shallow minimum (around $Kr_{dd} = 1$) plus a broad low maximum (around $Kr_{dd} = 10$) of V_T [the total potential] exists. A pair of deuteron under this condition can in time via tunneling through this broad and low barrier ends up in this potential minimum region. Then, through de-excitation (via radiation emission) this pair may energetically drop into a stable bound state and finally fused together forming a He^4 nucleus (see reference 3).

In reference (2), it was argued that the electric field inside a cavity (or void) of a solid is not zero. Instead, this field should be very much like that inside a virtual 'anti-atom'. Here, a cavity is the void created by taking away one atom from a perfect solid. One can visualize this argument by placing or superimposing an 'anti-atom' into a perfect solid. This anti-atom would charge-wise neutralize one of the atoms and thus generating a charge void or cavity. Consequently, the electrostatic field inside a cavity can be considered to be the superposition of two fields, one due to the charge distribution of an anti-atom the other due to all atoms in a perfect solid at this site. In a first order approximation, one assumes the average field inside a perfect solid is everywhere zero because all atoms are neutral. In that case, since the field inside an anti-atom is negative or attractive to positive charges both deuterons in a trapped Deuterium molecule are pulled toward the center of the cavity. Effectively, this field inside a cavity does 'weaken' the Coulomb repulsion between the two deuterons and thus facilitating a scenario of 'Cold Fusion' described above.[1 *]

[1] The assumption that the average field inside a solid is zero everywhere is hard to justify. Furthermore, to assume the charge distribution at the location of the cavity is exactly like that of a ‘free’ atom such that the charge distribution of a ‘free’ anti-atom will charge-neutralize this location creating a charge-void like the cavity is equally hard to justify. The author is grateful to a reader of the draft for pointing out the weakness of arguments. (C.M.F.)

Direct measurement of this field is difficult. One can probably do it indirectly by measuring the energy shifts of inner-shell transition of the atoms trapped inside such cavities. It is also not easy to determine such a field analytically. Large scale simulation or numerical calculation should yield useful results to strengthen the argument for the feasibility of dd-cold fusion inside a cavity.

References

1. C.M. Fou "Deuteron-Deuteron (dd) Binding via Neutron Exchange," Infinite Energy, Vol. 11, issue 66, 26-28 (2006)
2. C.M. Fou "Coulomb Field for LENR in Solid," Infinite Energy, Vol. 12, issue 71, 25-27 (2007)
3. C.M. Fou "Calculation for dd-fusion in a weakened Coulomb Field," Infinite Energy, Vol. 14, issue 83, 57-60 (2009)

[*] *Editor's note:* A reviewer has argued that the author's ingenious construction (here and in ref. (2)) appears to contradict Gauss's law, to the extent that it entails a charge-free region with an electrical flux directed inward everywhere on the surface. The reviewer concurs that further work is desirable to clarify the character of the field.

"The Coulomb Barrier not Static in QED" A correction to the Theory by Preparata on the Phenomenon of Cold Fusion and Theoretical Hypothesis

Fulvio Frisone
Department of Physics of the University of Catania
Catania, Italy, 95125, Via Santa Sofia 64

Abstract

In the last two decades, irrefutable experimental evidence has shown that Low Energy Nuclear Reactions (LENR) occur in specialized heavy hydrogen systems [1-4]. Nevertheless, we are still confronted with a problem: the theoretical basis of LENR are not known and, as a matter of fact, little research has been carried out on this subject. In this work we seek to analyse the deuteron-deuteron reactions within palladium lattice by means of Preparata's model of the palladium lattice [5,15]. We will also show the occurrence probability of fusion phenomena according to more accurate experiments [6]. We are not going to use any of the research models which have been previously followed in this field. Our aim is to demonstrate the theoretical possibility of cold fusion. Moreover, we will focus on tunneling the existent Coulomb barrier between two deuterons. Analysing the possible contributions of the lattice to the improvement of the tunneling probability, we find that there is a real mechanism through which this probability could be increased: this mechanism is the screening effect due to d-shell electrons of palladium lattice. The accordance between theoretical and experimental results will prove the reality of cold fusion phenomena and show the reliability of our model.

1. Introduction

Our research has shown that cold fusion phenomena were verified by the Coherence Theory of Condensed Matter. In this theory [5] it is assumed that the electromagnetic (e.m.) field plays a very important role on dynamic system, due to elementary constituents of matter (i.e. ions and electrons). Due to charged matter, considering the coupling between e.m. equations and the Schrödinger equation of field matter operator, it is possible to demonstrate that the matter system shows a dynamic coherence in proximity of e.m. frequency ω_0. Hence, it is possible to define the coherence domains, whose length is about $\lambda_{CD} = 2\pi/\omega_0$.

The simplest model of matter with coherence domain is obviously the plasma system. In classical plasma theory we have to consider the plasma frequency ω_p and the Debey length that measures the Coulomb force extension, i.e. the coherence domain length. In order to address the crucial issue of the nuclear fusion reaction involving the deuterons that pack the Pd-lattice, we must have a rather detailed understanding of the environment in which such nuclear process will eventually take place.

For a system with *N* charge *Q* of *m* mass within a *V* volume the plasma frequency can be written as:

$$\omega_{\vec{k}} = \omega_p = \frac{Qe}{\sqrt{m}}\sqrt{\frac{N}{V}} \tag{1}$$

Introducing the dimensional variable $\tau = \omega_p t$ we can rewrite the above equations as follows:

$$\dot{\phi}_{\vec{n}}(\tau) = \frac{1}{2}\sum_{|\vec{k}|=\omega_p}\sum_{\vec{n}'r}\left\langle \vec{n}\left|\alpha_{kr}\vec{\varepsilon}_{kr}\vec{a}^{+} - \alpha^{*}_{kr}\vec{\varepsilon}_{kr}\vec{a}\right|\vec{n}'\right\rangle\phi_{\vec{n}'}(\tau) \tag{2}$$

$$\frac{1}{2}\ddot{\alpha}_{kr} - i\dot{\alpha}_{kr} + m\lambda\alpha_{kr} = \frac{i}{2}\vec{\varepsilon}^{*}_{kr}\sum_{\vec{n}\vec{n}'}\left\langle \vec{n}\left|\vec{a}\right|\vec{n}'\right\rangle\phi^{*}_{\vec{n}}(t)\phi_{\vec{n}'}(\tau) \tag{3}$$

Defining the state as:

$$\left|\phi\right\rangle = \sum_{\vec{n}'}\phi_{\vec{n}}(\tau)\left|\vec{n}\right\rangle \tag{4}$$

and the e.m. field amplitude as:

$$\vec{A} = \sqrt{\frac{3}{8\pi}}\sum_{r}\int d\Omega_k \alpha_{kr}\vec{\varepsilon}_{kr} \tag{5}$$

we can rewrite as follows:

$$\frac{\partial}{\partial t}\left|\phi\right\rangle = \sqrt{\frac{2\pi}{3}}\left(\vec{A}\vec{a}^{+} - \vec{A}^{+}\vec{a}\right)\left|\phi\right\rangle \tag{6}$$

$$\dot{\vec{A}} + \frac{i}{2}\ddot{\vec{A}} + im\lambda\vec{A} = -\sqrt{\frac{2\pi}{3}}\left\langle\phi\left|\vec{a}\right|\phi\right\rangle \tag{7}$$

If we only concentrate on a short time dynamics, we can write:

$$\left|\phi(0)\right\rangle = \left|0\right\rangle \tag{8}$$

then, creating a difference in the (6) and using the (7) with $\left|\phi\right\rangle = \left|0\right\rangle$, we can easily obtain:

$$\ddot{A}_j + \frac{i}{2}\ddot{\vec{A}}_j = -\left(\frac{2\pi}{3}\right)\left\langle 0\left|\left[a_j, a_l^{+}\right]0\right\rangle\right. \tag{9}$$

$$A_l = -\left(\frac{2\pi}{3}\right)A_j \tag{10}$$

This has the same form of the equations of the coherence domains as the case in which:

$\mu = 0$

$\lambda = 0$

$g^2 = \left(\frac{2\pi}{3}\right)$

$$g_c^2 = \frac{16}{27} < \frac{2\pi}{3}$$

So, a solution for the ideal plasma exists. More in detail, we can define:

$$\alpha_k = \langle \phi | a_k | \phi \rangle \tag{11}$$

$$g_0 = \left(\frac{2\pi}{3} \right)^{1/2}$$

In this case the coupling critical constant is:

$$\dot{\alpha}_k = g_0 A_k \tag{12}$$

$$\dot{A}_k + \frac{i}{2} \ddot{A}_k = -g_0 \alpha_k \tag{13}$$

so to admit the following holding quantity:

$$Q = \sum \left\{ A_k^* A_k + \frac{i}{2} \left(A_k^* \dot{A}_k - \dot{A}_k^* A_k \right) + \alpha_k^* \alpha_k \right\} \tag{14}$$

while for the Hamiltonian's it is easy to compute:

$$\frac{E}{N\omega_p} = H = Q + \sum \left[\frac{1}{2} \dot{A}_k^* \dot{A}_k - ig \left(A_k^* \alpha_k - A_k \alpha_k^* \right) \right] \tag{15}$$

With the aim of seeing if there are any externals solutions, we write

$$\alpha_k = \alpha u_k e^{i\psi} \tag{16}$$

$$A_k = A u_k e^{i\phi} \tag{17}$$

where α and A are positive constants and u_k is a complex vector.

Changing these ones in (12) and (13) we have:

$$\phi - \psi = \frac{\pi}{2} \tag{18}$$

$$\alpha = g_0 \frac{A}{\dot{\phi}} \tag{19}$$

$$\frac{1}{2} \dot{\phi}^3 - \dot{\phi}^2 + g_0^2 = 0 \tag{20}$$

and by the condition *Q=0* (we cannot have a net charge flow in a plasma), we have:

$$1 - \dot{\phi} + \frac{g_0^2}{\dot{\phi}^2} = 0 \tag{21}$$

In this case it is easy to observe that for $g_0 = \left(\frac{2\pi}{3} \right)^{1/2}$ it is unlikely that both the equations (18) and (19) are satisfied.

This result means that the energy of an ideal quantum plasma does not have a minimum; in other words, an ideal quantum plasma does not exist.

That must not be surprising, because the Hamiltonian' describes this plasma as a system whose amplitude oscillations are arbitrary, whereas the limit over a certain amplitude does not exist in a real plasma.

But by:

$$\vec{\xi} = \frac{1}{\sqrt{2m\omega_p}}(\vec{a} + \vec{a}^{+})$$

it is easy to obtain:

$$\left\langle \vec{\xi}^{2} \right\rangle = \frac{1}{m\omega_p}\alpha^2 \tag{22}$$

Also, in the plasma approximation as an homogeneous fluid, we suppose that our Hamiltonian's stops have to be valid for the oscillations bigger than the following:

$$\left\langle \vec{\xi}^{2} \right\rangle_{\max}^{1/2} \approx a = \left(\frac{V}{N}\right)^{1/2} \tag{23}$$

that is when plasma oscillations are of the same order as the inter-particle distance *a*. In order to create some more realistic models of plasma, we want to compute the breaking amplitude α_{max} obtained by the combination of the equations (22) and (23) for a gas of electrons.

Using the definition of ω_p, we have:

$$\alpha_{\max} = \sqrt{m\omega_p} \cdot \left(\frac{1}{3}\right)^{1/3} = (ma)^{1/4} e^{1/2} \tag{24}$$

taking

$$a \approx 2.5\text{Å}$$

the result is

$\alpha_{max} \cong 2.7$ Å

This simple calculation shows how it is possible to change our quantum ideal plasma in a real plasma. As the oscillations remain very low in a plasma, a two level model can be a good approximation (the dynamics only includes the first excited state). A consequence of this approximation consisting in the reduction of the plasma in a homogeneous fluid is the changing of the plasma frequency ω_p as follows:

$$\omega_p = \frac{Q}{\sqrt{m}}\sqrt{\frac{N}{V}} \tag{25}$$

Moreover, we study the "nuclear environment" that is supposed existent within the palladium lattice D_2-loaded and at room temperature as predicted by the Coherence Theory. As a matter of fact, some physicists declared that it is possible to observe traces of nuclear reactions [1,2,3] when the palladium lattice is loaded with deuterium gas. For this reason many of these physicists define that as a Low Energy Nuclear Reaction (LENR).

One of the most interesting experiments shows that in the D_2-loaded palladium case the most frequent nuclear reactions are:

1) $D + D \rightarrow {}^3H + p + 4.03MeV$
2) $D + D \rightarrow {}^4H + p + 23.85MeV$

The aim of our work is to propose a "coherence" model, by means of which we can explain the occurrence of reactions 1) and 2) and their probability according to more reliable experiments. First of all, we will start from the analysis of the environment, i.e. of plasmas present within palladium (*d*-electron, *s*-electron, *Pd*-ions and *D*-ions); we will do so using the coherence theory of matter. Then, we will use the effective potential reported in ref. [7,8] and add the role of lattice perturbations, by means of which we will compute the *D-D* tunneling probability.

2. The plasmas within non loaded palladium

According to the Coherence Theory of Condensed Matter, in a palladium crystal at room temperature the electron shells are in a coherent regime within a coherent domain. In point of fact, they oscillate in tune with a coherent e.m. field trapped in coherent domains.

So, in order to describe the lattice environment we must study the plasma of *s*-electron and *d*-electron.

a) The plasma of d-electrons

Similar arguments were proposed by Preparata, but starting from a new formulation of condensed matter theory known as Coherence Theory.

In this theory we can visualize the plasma formed by d-shell electrons as consisting of shells charged $n_d e$ (for palladium n_d =10) radius r_d =*1 Å* and thickness a fraction of one Angstrom. The classical plasma

$$\omega_d = \frac{e}{\sqrt{m}}\sqrt{\frac{n_d N}{V}} \tag{26}$$

is d-electrons plasma frequency. But according to the coherence theory of matter we must adjust this plasma frequency of a factor *1.38*.

We can understand this correction by observing that the formula (26) is obtained assuming a uniform *d*-electron charge distribution. But of course the *d*-electron plasma is localized in a shell of radius *R* (that is about 1Å), so the geometrical contribution is:

$$\sqrt{\frac{6}{\pi}} = 1.38 \tag{27}$$

If we rewrite the renormalized d-electron plasma frequency with ω_d, we have

$$\omega_d = 41.5eV/\hbar \tag{28}$$

and the maximum oscillation amplitude ξ_d is about 0.5 Å.

b) The plasma of delocalized s-electrons

The *s*-electrons are those neutralizing the absorbed deuterons ions in the lattice. They are delocalised and their plasma frequency depends on the loading ratio (*D/Pd* percentage). The formula (28) can also be written as:

$$\omega_{se} = \frac{e}{\sqrt{m}}\sqrt{\frac{N}{V}}\cdot\sqrt{\frac{x}{\lambda_a}} \tag{29}$$

where

$$\lambda_a = \left[1-\frac{N}{V}V_{pd}\right] \tag{30}$$

and V_{pd} is the volume effectively occupied by the Pd-atom. As reported in reference [5], we obtain:

$$\omega_{se} \approx x^{1/2}15.2eV/\hbar \tag{31}$$

As an example, for *x=0.5*, we have $\omega_{se} \sim 10.7\ eV/\hbar$.

c)The plasma of Pd-ions

Furthermore, we can consider the plasma according to the palladium ions forming the lattice structure; in this case it is possible to demonstrate that the frequency is (28):

$$\omega_{pd} = 0.1eV \tag{32}$$

3. The plasmas within D_2-loaded palladium

In this section we seek to show what happens when the absorbed deuterium is placed near the palladium surface. This loading can be enhanced using electrolytic cells or vacuum chambers working at opportune pressure [9, 10]. By means of Preparata's theory of Condensed Matter, it is assumed that there are three phases concerning the D_2-Pd system, according to the ratio *x=D/Pd*:

1) phase α for $x<0.1$
2) phase β for $0.1<x<0.7$
3) phase γ for $x > 0.7$

In the α – phase, the D_2 is in a disordered and not coherent state (D_2 is not charged).

As far as the other two phases are concerned, we can conclude that the following reaction takes place on the surface because of the lattice e.m.:

$$D_{lattice} \rightarrow D^+ + e^- \tag{33}$$

Then, according to the loading quantity *x=D/Pd*, the ions of deuterium can occur on the octahedrical sites (Fig. 1) or on the tetrahedral (Fig. 2) in the (1,0,0)-plane. In the coherent theory of the so called β-plasma of Preparata's the deuterons plasma are in the octahedral site and the γ-plasma are in the tetrahedral.

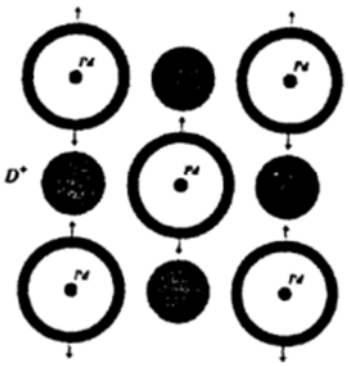

Figure 1. The octahedral sites of the Pd lattice where the deuterons are located

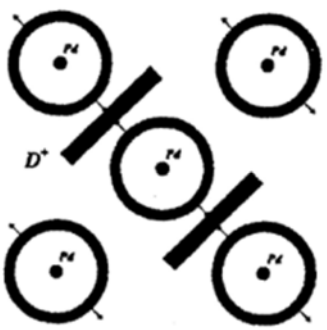

Figure 2. The thin disks of the tetrahedral sites of the Pd lattice where the deuterons are located

Regarding the β-plasma, it is possible to affirm that the plasma frequency is given by (28):

$$\omega_\beta = \omega_{\beta 0}(x+0.05)^{1/2} \tag{34}$$

where

$$\omega_{\beta 0} = \frac{e}{\sqrt{m_D}}\left(\frac{N}{V}\right)^{1/2}\frac{1}{\lambda_a^{1/2}} = \frac{0.15}{\lambda_a^{1/2}} eV/\hbar \tag{35}$$

For example, if we use $\lambda_a=0.4$ and $x=0.5$ we obtain $\omega_\beta=0.168\ eV/\hbar$.

In the tetrahedral sites the D^+ can occupy the thin disk that encompasses two sites (Fig. 3), representing a barrier to the D^+ ions. We must underline that the electrons of the *d*-shell start oscillating near the equilibrium distance y_0 (about 1.4 Å), so that the static ions have a cloud of negative charge (see reference [5]).

What follows is:

$$\omega_\gamma = \sqrt{\frac{4Z_{eff}\alpha}{m_D y_0^2}} \approx 0.65eV/\hbar \tag{36}$$

Of course, this frequency also depends on the chemical condition of the palladium (impurities, temperature etc…)

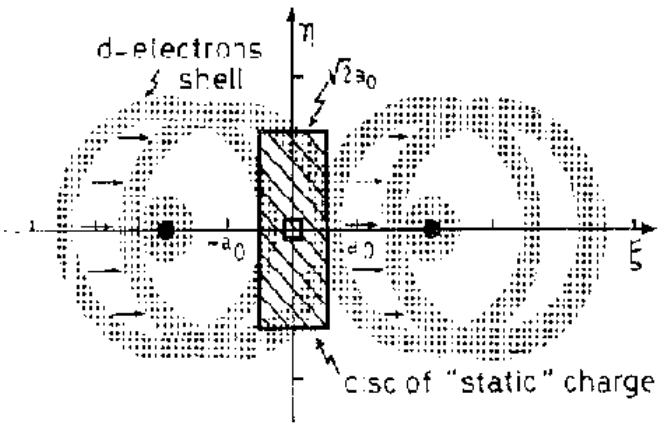

Figure 3. Possible d-electron plasma oscillation in a Pd lattice

Due to a large plasma oscillation of *d*-electrons, a high density negative charge condenses in the disk-like tetrahedral region, where the γ-phase D^+'s are located. This gives rise to a screening potential *W(t)*, whose profile is reported in Fig. 4.

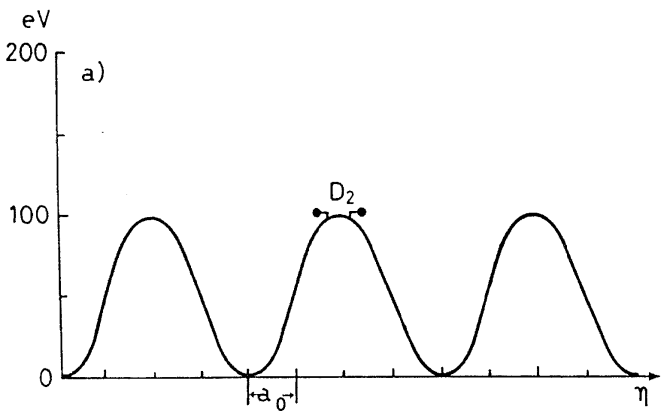

Figure 4. The profile of the electrostatic potential in the η-direction

Having mapped that the γ-phase depends on *x* value, we can experimentally observe the new phase in reference [11], which is very important in the LENR investigation. This is demonstrated by the fact that many of the "cold fusion physicists" declare that the main point of cold fusion protocol is the loading *D/Pd* ratio higher than *0.7*, i.e. the deuterium takes place in the tetrahedral sites.

4. The D-D potential

In reference [7], it was shown that the phenomenon of fusion between nuclei of deuterium in the lattice of a metal is conditioned by the structural characteristics, by the dynamic conditions of the system and also by the concentration of impurities that are present in the metal under examination.

In fact, the height of the Coulomb barrier decreases according to the varying of the total energy and of the concentration of impurities that are present in the metal itself. This can be observed studying the curves of the potential of interaction between deuterons (including the deuteron-plasmon contribution) in the case of three typical metals (*Pd*, *Pt* and *Ti*), as shown in a three-dimensional model.

The initial potential that connects the like-Morse attraction and the like-Coulomb repulsion can be written as seen in reference [7, 8]:

$$V(r) = \mathrm{k}_0 \frac{q^2}{r} \cdot \left(V(r)_M - \frac{\Sigma}{r} \right) \tag{37}$$

where $V(r)_M$ is the Morse potential, $k_0 = (1/4\pi\varepsilon_0)$, q is the charge of the deuteron, M_d is the reduced mass of the deuterium nuclei, T is the absolute temperature at which the metal is experimentally placed, J is the concentration of impurities in the crystalline lattice and R is the nuclear radius.

In (37), $V(r)_M$ is a like-Morse potential, and is given by:

$$V(r)_M = B\{\exp(-2\varphi(r-r_0)) - 2\exp(-\varphi(r-r_0))\} \tag{38}$$

Here the parameters *B*, φ *ed* r_0 depend on the lattice.

In fact, the potential (37) is an effective one whose reliability is demonstrated by its ability to fit the Coulomb potential for $r \rightarrow 0$ and the Morse potential in the attractive zone. So, Siclen and Jones [12] define ρ the point where the Coulomb potential is associated to the Morse trend, r'_0 the equilibrium distance and *D'* the well.

Of course in the free space for a D_2 molecular, ρ is about *0.3 Å* , r'_0 is about *0.7 Å* and *D'* is *-4.6 eV*.

But screening effects are present within the lattice, and the deuteron-deuteron interaction modify these parameter values by means of phonon exchange.

Since the screening effect [1] can be modulated by the giver atoms, in reference [7,8] we have considered the role of impurities and we came to the following: $J = J_0 \exp\left[\frac{\beta}{bkT}\right]$.

Furthermore, some particular reactions could occur, incorporating the impurities in the nucleus of the dislocations. This may happen as a result of a different arrangement of the atoms, with respect to that of the unperturbed lattice.

This type of process has been extensively studied in the literature concerning metals and the case of crystalline semiconductors at high temperature.

As an example, in the case of crystalline semiconductors it has been found that the concentration of interstitial impurities around a linear dislocation with a point component depends on the temperature, as shown by the law written above where J_0 is the concentration of impurities in the zone with zero internal pressure, ($b^3 \simeq$ v_i) is the volume of the ions constituting the lattice, while β is proportional to the difference (v_d - v_i) between the volume of the impurity atoms and that of the lattice ions.

Our conjecture is that in a metal, such as palladium, a similar phenomenon could occur between the atoms of deuterium penetrating the lattice. This would be a result of the deuterium loading and of the microcracks produced by variations in temperature. In this case, the parameter β of the previous expression would be negative, determining an increase in the concentration of deuterons in the vicinity of the micro-crack, which would then catalyse the phenomenon of fusion as:

$$\Sigma = JKTR \tag{39}$$

and

$$B = J/\zeta \tag{40}$$

So we can write the effective *d-d* potential as follows:

$$V(r) = k_0 \frac{q^2}{r} \cdot \left(V(r)_M - \frac{JKTR}{r} \right) \tag{41}$$

where $V(r)_M$ is the Morse potential, $k_0 = (1/4\pi\varepsilon_0)$, q is the charge of the deuteron, M_d is the reduced mass of the deuterium nuclei, T is the absolute temperature at which the metal is experimentally placed, J is the concentration of impurities in the crystalline lattice and R is the nuclear radius.

Considering the attractive force, due to the exchange of plasmons, the main contribution are as follows:

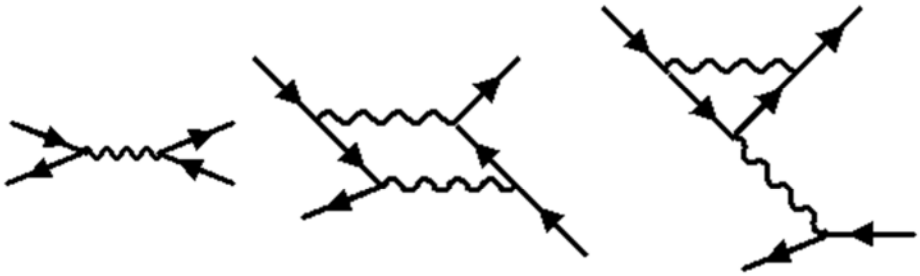

Figure 5. Plasmon exchanges. Solid lines indicate deuterons and wiggly lines indicate plasmons

Taking into account the role of coupling between deuteron and plasmons, in reference [13] a *D-D* potential was numerically evaluated, having the features of the potential (14) with *D'= -50 eV* , with r'_0*=0.5 Å* and with ρ *=0.2 Å* (it has to be also taken into account that only two plasmon excitations at *7.5 eV* and at *26.5 eV* are considered in ref. 13).

The features of the potential (37) is shown in Fig. 6.

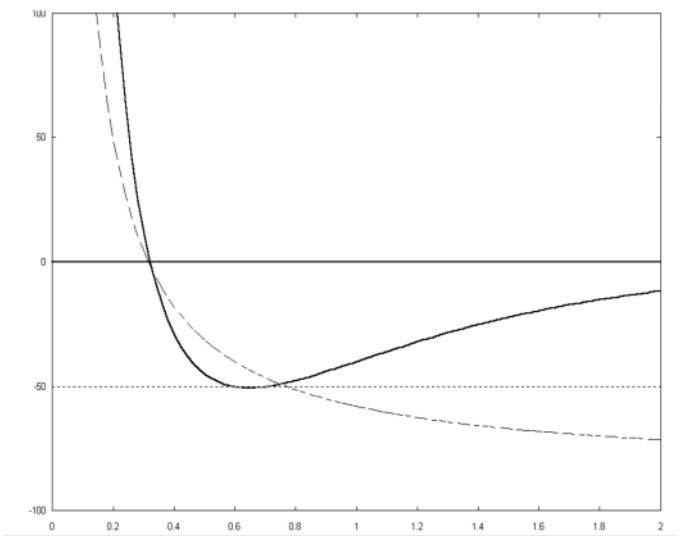

Figure 6. The solid line shows the features of potential (37) computed in order to obtain D'=-50 eV and ρ=0.165 Å. The coulomb potential in dashed line is computed using a screening constant of 85 eV. The distance in Bohr radius unit is reported on the x-axes, and the energy in eV is shown on the y-axes.

We are now going to study the role of potential (41) in the three different phases α, β and γ according to the coherence theory of condensed matter.

A couple of points require preliminary explanations before we proceed, namely:

1) what KT is;
2) what the role of plasma ions and of electrons is;

Let us start with point 1. According to the different deuteron-lattice configurations, *KT* can be:

i. the loaded lattice temperature if we consider the deuterons in the α-phase;
ii. ω_β if we consider the deuterons in β-phase;
iii. ω_γ if we consider the deuterons in the γ-phase;

The second point requires a much more complicated explanation. In fact, the lattice environment is a combination of coherent plasmas (ion Pd, electron and deuterons plasma) at different temperature, due to different masses, which makes the description of the emerging potential very difficult.

The method we propose to follow in this work is to consider the total screening contribution of lattice environment at *D-D* interaction (i.e. V_{tot}) as random potential *Q(t)*. According to this model, we have

$$V_{tot}(t) = V(r) + Q(t) \tag{42}$$

Of course, we assume that:

$$\langle Q(t) \rangle_t \neq 0 \tag{43}$$

that is to say that *Q(t)* (a second order potential contribution) is a periodic potential that oscillates between the maximum value Q_{max} and 0. The frequency will be called by ω_Q.

More exactly, the oscillation charges of *d-shell* produce a screening potential having an harmonic feature:

$$eV(r) = -Z_d \frac{ke^2}{2a_0} r^2 \tag{44}$$

Considering $Z_d=10/3$ and $a_0= 0.7$ Å in reference [5], a screening potential V_0 is evaluated of about *85 eV*. In this way we can compute $\rho = V_0/26.9$ and at last ρ = 0.*165 Å*. Resuming, in a palladium lattice we can have the following cases according to the loading ratio:

i) α-phase

In the phase α the deuterons are in a molecular state and the thermal motion is about:

$0.02 \text{ eV} < \hbar\omega_\alpha < 0.1 \text{ eV}$

This phase takes places when *x* is lower than 0.1, and since *W(t)* is zero, the D-D potential is:

$$V(r) = k\frac{q^2}{r} \cdot \left(V_M(r) - \frac{J\hbar\omega_\alpha R}{r} \right) \tag{45}$$

The expression (45) was partially evaluated in a previous paper [7]; in fact, we were only interested in the dependence of the tunneling probability on impurities present within the lattice. Through the present work, we seek to examine the correlation between potential features and loading ratio. Some numerical results are showed in the paragraph 5.

ii) β-phase

Phase β happens when *x* is higher than *0.1* but lower than *0.7*. The interaction takes place among deuteron ions that oscillate between the following energy values:

$0.1\ \text{eV} < \hbar\omega_\beta < 0.2\ \text{eV}$

In this case *W(t)* is zero, we can express the potential as follows:

$$V(r) = k\frac{q^2}{r}\cdot\left(V_M(r) - \frac{J\hbar\omega_\beta R}{r}\right) \tag{46}$$

Comparing the expressions 45 and 46, it seems clear that the weight of impurities is more important in the β-phase. Of course this conclusion relates to previous papers [7,8] in which we have studied the role of temperature on tunneling effect.

iii) γ-phase

Lastly, the deuteron-palladium system is in the phase γ when the loading ratio is higher than *0.7*.

This is the most interesting case. The deuterons cross the screening through the *d*-electrons shell. In this respect, we did a numeric simulation where we supposed that the *D-D* potential must be computed on the assumption that the potential (37) well disappears because of the Morse contribution. In fact, if we use a classical plasma model where the D^+ ions are the positive charge and the *d*-electrons the negative one, it is very "realistic" to obtain the following potential:

$$V(r,t) = k\frac{q^2}{r}\cdot\left(V_M(r) - \frac{J\hbar\omega_\gamma R}{r}\right) + Q(t) \tag{47}$$

where *Q(t)* is an unknown perturbative potential. On this topic, we can also add that:

$$\left\langle Q(t)\right\rangle_t \approx \frac{W_{\max}}{\sqrt{2}} \tag{48}$$

In the next evaluation it is given as:

$$\left\langle Q(t)\right\rangle_t \approx 85eV \tag{49}$$

5. Conclusions

The aim of this section is to present the *D-D* fusion probability normalized to number of events per second regarding the *D-D* interaction in all different phases. More exactly, we seek to compare fusion probability in phases α, β and γ according to the variation of energy between

–50 to *50 eV*. We also consider the role of *d*-electrons screening as a perturbative lattice potential.

This process only involves the case where *Q(t)* is different from zero. It involves a change of the value on the *x*-axes point where the Coulomb barrier takes place; in this case, what we obtain as a final result is that the screening enhances the fusion probability. In order to evaluate the fusion rate (Λ) we applied the following formula:

$$\Lambda = A\Gamma \tag{50}$$

Where Γ is the Gamow factor and *A* is the nuclear reaction constant obtained from cross sections measured (value used was 10^{22} sec^{-1}).

From an experimental point of view, it is possible to affirm that there are three typologies of experiments in the cold fusion phenomenology [14]:

1) Experiments giving negative results
2) Experiments giving some results (little detection signs with respect to background, fusion probability about 10^{-23} using a very high loading ratio)
3) Experiments giving clear positive results, such as the Fleischmann and Pons experiments.

In our opinion, the experiments of the third type lack accuracy from the experimental point of view. In this sense, we prefer a theoretical model of the controversial phenomenon of cold fusion to explain only experiments of type 1 and 2. In this case it is important to consider the role of the loading ratio in the experimental results. Now, let us begin from the α-phase.

Results for the α-phase are shown in Table 1. As shown there, the theoretical fusion probability is lower than 10^{-74}, that is to say, extremely low. Consequently, we can affirm that no fusion is possible through the loading of a percentage of $x < 0.2$ in the deuterium. The same absence of nuclear phenomenon is compatible for a loading ratio of about *0.7* (Table 2), since in this case the predicted fusion probability is lower than 10^{-42}. These predictions, of course, agree with the experimental results (for $x>0.7$, look at reference [6]). The result of our model is confirmed in the γ-phase, where we can observe some background fluctuations. Due to a high loading ratio, we predict a fusion probability at about 10^{-22} in these background fluctuations. This is a previously unattained result. This is also a very important one for references [7,8], since in those cases the fusion probability was independent of the loading ratio.

To conclude, our aim is also to show that the model proposed in this paper can explain some irregular nuclear traces in solids, unifying nuclear physics with condensed matter. On the other hand, regarding the experiments of type 3, we want to consider other contributions as micro-deformation occurrence, in order to explain the very high fusion rate. The role of micro-crack and impurities linked to the loading ratio will be explored in other speculative works. “The nuclear physics within condensed matter” may be a new device through which an understanding of new productive scientific issues could be possible.

Table 1. Using the α–phase potential (potential 45), the fusion probability has been computed for Pd "Impure" (J ≈ 0.75%), normalized to the number of event/sec for different values of energy (*- 50 eV<E<50 eV*). Palladium *J ≈ 0.75%* ρ ≈ 0. 34 Å *r'$_0$=0.7 Å D'= -50 eV*

	$\omega_\alpha \approx 0.0025$ eV	$\omega_\alpha \approx 0.05$ eV	$\omega_\alpha \approx 0.075$ eV	$\omega_\alpha \approx 0.1$ eV
$E \approx -50$	$P \approx 10^{-100}$	$P \approx 10^{-103}$	$P \approx 10^{-100}$	$P \approx 10^{-99}$
$E \approx -40$	$P \approx 10^{-99}$	$P \approx 10^{-101}$	$P \approx 10^{-98}$	$P \approx 10^{-97}$
$E \approx -30$	$P \approx 10^{-97}$	$P \approx 10^{-100}$	$P \approx 10^{-96}$	$P \approx 10^{-96}$
$E \approx -20$	$P \approx 10^{-95}$	$P \approx 10^{-99}$	$P \approx 10^{-94}$	$P \approx 10^{-93}$
$E \approx -10$	$P \approx 10^{-94}$	$P \approx 10^{-97}$	$P \approx 10^{-91}$	$P \approx 10^{-90}$
$E \approx -0$	$P \approx 10^{-92}$	$P \approx 10^{-96}$	$P \approx 10^{-90}$	$P \approx 10^{-86}$
$E \approx 10$	$P \approx 10^{-91}$	$P \approx 10^{-94}$	$P \approx 10^{-87}$	$P \approx 10^{-83}$
$E \approx 20$	$P \approx 10^{-90}$	$P \approx 10^{-92}$	$P \approx 10^{-85}$	$P \approx 10^{-80}$
$E \approx 30$	$P \approx 10^{-89}$	$P \approx 10^{-90}$	$P \approx 10^{-82}$	$P \approx 10^{-78}$
$E \approx 40$	$P \approx 10^{-86}$	$P \approx 10^{-89}$	$P \approx 10^{-80}$	$P \approx 10^{-74}$
$E \approx 50$	$P \approx 10^{-84}$	$P \approx 10^{-87}$	$P \approx 10^{-79}$	$P \approx 10^{-71}$

Table 2. Using the β-potential (potential 46), the fusion probability P has been computed for Pd "Impure" (J ≈ 0.75%), normalized to the number of event/sec for different values energy (*- 50 eV<E<50 eV*). Palladium *J ≈ 0 .75% α ≈ 0. 34 Å r'$_0$=0.7 Å D'= -50 eV*

	$\omega_\beta \approx 0.125$ eV	$\omega_\beta \approx 0.150$ eV	$\omega_\beta \approx 0.175$ eV	$\omega_\beta \approx 0.2$ eV
$E \approx -50$	$P\ 10^{-83}$	$P \approx 10^{-88}$	$P \approx 10^{-86}$	$P \approx 10^{-81}$
$E \approx -40$	$P \approx 10^{-81}$	$P \approx 10^{-87}$	$P \approx 10^{-85}$	$P \approx 10^{-75}$
$E \approx -30$	$P \approx 10^{-80}$	$P \approx 10^{-86}$	$P \approx 10^{-83}$	$P \approx 10^{-73}$
$E \approx -20$	$P \approx 10^{-79}$	$P \approx 10^{-85}$	$P \approx 10^{-80}$	$P \approx 10^{-70}$
$E \approx -10$	$P \approx 10^{-78}$	$P \approx 10^{-84}$	$P \approx 10^{-74}$	$P \approx 10^{-68}$
$E \approx -0$	$P \approx 10^{-76}$	$P \approx 10^{-82}$	$P \approx 10^{-73}$	$P \approx 10^{-62}$
$E \approx 10$	$P \approx 10^{-75}$	$P \approx 10^{-81}$	$P \approx 10^{-72}$	$P \approx 10^{-60}$
$E \approx 20$	$P \approx 10^{-74}$	$P \approx 10^{-79}$	$P \approx 10^{-71}$	$P \approx 10^{-54}$
$E \approx 30$	$P \approx 10^{-73}$	$P \approx 10^{-76}$	$P \approx 10^{-70}$	$P \approx 10^{-50}$
$E \approx 40$	$P \approx 10^{-72}$	$P \approx 10^{-75}$	$P \approx 10^{-69}$	$P \approx 10^{-45}$
$E \approx 50$	$P \approx 10^{-71}$	$P \approx 10^{-70}$	$P \approx 10^{-65}$	$P \approx 10^{-42}$

Table 3. Using the γ-potential (potential 47), the fusion probability has been computed for Pd "Impure" (J ≈ 0.75%), normalized to the number of event/sec for different values of energy (- 50 eV<E<50 eV). Palladium J≈ 0 .75% ρ ≈ 0. 165 Å r'0=0.35 Å D'= -50 eV

	$\omega_\gamma \approx 0.6$ eV	$\omega_\gamma \approx 0.65$ eV	$\omega_\gamma \approx 0.7$ eV	$\omega_\gamma \approx 0.75$ eV
$E \approx -50$	$P \approx 10^{-71}$	$P \approx 10^{-51}$	$P \approx 10^{-57}$	$P \approx 10^{-50}$
$E \approx -40$	$P \approx 10^{-68}$	$P \approx 10^{-49}$	$P \approx 10^{-54}$	$P \approx 10^{-47}$
$E \approx -30$	$P \approx 10^{-66}$	$P \approx 10^{-47}$	$P \approx 10^{-51}$	$P \approx 10^{-44}$
$E \approx -20$	$P \approx 10^{-62}$	$P \approx 10^{-44}$	$P \approx 10^{-49}$	$P \approx 10^{-41}$
$E \approx -10$	$P \approx 10^{-60}$	$P \approx 10^{-41}$	$P \approx 10^{-46}$	$P \approx 10^{-39}$
$E \approx 0$	$P \approx 10^{-57}$	$P \approx 10^{-39}$	$P \approx 10^{-43}$	$P \approx 10^{-36}$
$E \approx 10$	$P \approx 10^{-54}$	$P \approx 10^{-38}$	$P \approx 10^{-42}$	$P \approx 10^{-33}$
$E \approx 20$	$P \approx 10^{-51}$	$P \approx 10^{-35}$	$P \approx 10^{-40}$	$P \approx 10^{-32}$
$E \approx 30$	$P \approx 10^{-49}$	$P \approx 10^{-32}$	$P \approx 10^{-36}$	$P \approx 10^{-29}$
$E \approx 40$	$P \approx 10^{-47}$	$P \approx 10^{-30}$	$P \approx 10^{-33}$	$P \approx 10^{-25}$
$E \approx 50$	$P \approx 10^{-45}$	$P \approx 10^{-27}$	$P \approx 10^{-30}$	$P \approx 10^{-21}$

Our aim is to propose a theoretical model explaining the experiments implying a high production of energy, so as to be repeatable, reproducible, and shared by the scientific community. Our starting point is the following: the phenomenon of the low-energy fusion critically depends on the interaction between the d-d nuclear system and the D_2 gas system on one side, and the lattice of the palladium on the other side.

In fact, the typical deuterium-plasma interaction of the γ phase grows at the variation of the loading percentage. So, the electrostatic repulsion is weakened. But while the deuterium loading in the gas phase grows, the palladium lattice is deformed.

Other theoretical and experimental studies about the electric field are in progress. To be clearer, here is a brief explanation of the main passages of the lattice reaction: firstly, we have the deformation; secondly, the dislocation; and lastly, the micro-crack.

If the lattice is deformed, the creation of a microscopic electric field occurs within the micro-crack, in which the D^+ and the plasmons collide. Moreover, the deuterium nuclei are accelerated in that field, as it happens in a classic accelerator of nuclear physics. This acceleration can also generate the phenomenon of low-energy fusion.

References

1. Iwamura et al., "Japanese Journal of Applied Physics A, vol. 41, (1994) p.4642
2. O. Reifenschweiler, Physics Letters A, vol 184, (1994),p.149
3. O. Reifenschweiler, Fusion Technology, vol 30, (1996),p.261
4. Melvin H. Miles et al., Fusion Technology, vol. 25, (1994), p. 478
5. G. Preparata, QED Coherence in Matter, World Scientific Publishing 1995
6. S. Aiello et al. Fusion Technology vol.18 (1990), p.125
7. F. Frisone, Fusion Technology, vol. 39, (2001),p.260
8. F. Frisone, Fusion Technology, vol. 40, (2001),p.139
9. Fleishmann and Pons, J. Electroanal. Chem. 261 (1989),p. 301-308

10. A.De Ninno et al. Europhysics Letters, vol.9 (1989), p. 221-224
11. G. Mengoli et al., J. Electroanal. Chem. Vol.350, (1989), p.57
12. C. DeW Van Siclen and S. E. Jones, J. Phys. G. Nucl. Phys. Vol. 12 (1986)
13. M.Baldo and R. Pucci, Fusion Technology, 18, p. 47, 1990
14. D. Morrison, Physics World, 1990
15. F.Frisone, Condensed Matter Nuclear Science Editor of the MIT "Tunneling Effect Enhanced by Lattice Screening as Main Cold Fusion Mechanism: An Brief Theoretical Overview" 2004

Quantum Fusion Hypothesis

Robert E. Godes
Profusion Energy

Abstract

The field of cold fusion is not “fusion” as the current establishment defines it.

A basic tenet of research is that correlation does not equal causation. The current assumption of Deuterium Deuterium (DD) fusion based on the excellent work of Dr. Michael McKubre showing a near perfect match of excess heat to helium produced is only a correlation. The assumption of DD fusion may be fallacious and leading to a dead end. In many cases the Pons Fleischmann reaction starts with deuterium and ends with helium. This would seem to indicate DD fusion, but this is assuming that correlation equals causation.

Related Fields

The Quantum Fusion (QF) Hypothesis explains the Fleischmann-Pons Effect and a large cross section of experiments researchers in this field have observed. It is an explanation of how cold to ultra cold neutron(s) form. QF draws on work in the fields of mechanics, chemistry including molecular, quantum and computational, material science, physics, including quantum and astro, and electronics. Depending on your background, recognition of different aspects of what is presented in this paper will vary. This paper is written for people with a scientific background to understand what underlies the phenomena and how to drive it. Understanding the phenomena requires integration of many concepts across the fields mentioned above. There are some systems that may operate on different principals and have not yet been analyzed relative to the Quantum Fusion hypothesis. Edmund Storms’ plasma discharge work may fall into this category. I believe that the Quantum Fusion hypothesis is correct for many of the systems this community has been investigating. Details may be found on-line in Ref [1].

Testing the hypothesis

Profusion Energy built and ran several prototype reactors in open beakers in a partially controlled environment. Tests used both electric heaters and copper reactor cores for comparison. Systems with nickel or palladium cores can always outperform both electric heaters and copper core devices regardless of the position in the testing environment.

Typical results

Figure 1 shows a 0.05 mm Pd core system outperforming an electric heater. All power into the Quantum Fusion reactor is considered strictly as power into the beaker. The loss caused in the generation of oxygen and hydrogen gas was ignored. The power drawn off of the Q or Quantum compression supply (Q power discussed later) was calculated as power into the beaker even though the circuitry generated significant heat outside the beaker. The Quantum

Fusion system still outperformed the electric heater, which turns every watt second of power into 1 joule of heat energy.

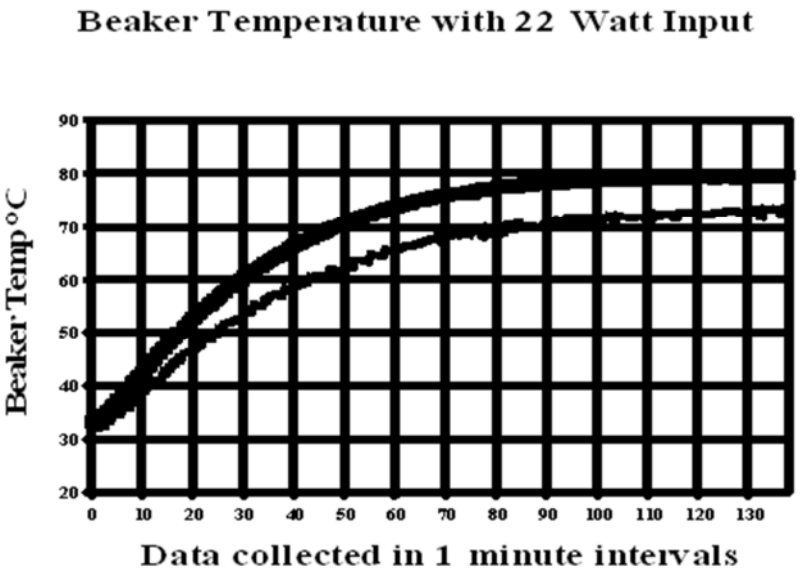

Figure 1. A 0.05 mm Pd core producing more heat than an electric heater.

Molecular Hamiltonian

In atomic, molecular, Quantum, and optical physics as well as in quantum chemistry, molecular Hamiltonian is the name of the operator representing the energy of the electrons and nuclei in a molecule (to be taken as the trapped nuclei and lattice elements in a unit cell of the matrix running the reaction). This equation plays a central role in computing properties of molecules and aggregates of molecules such as conductivity, optical, and magnetic properties, and reactivity. By quantizing the classical energy in Hamilton form, one obtains a molecular Hamilton operator. This Hamiltonian is a sum of 5 terms[1]. This was a handy starting point but is used to describe systems in equilibrium. When the molecular system is moved away from equilibrium, nonlinear effects begin to dominate.

In general, evaluation of a Hamiltonian results in another function. The function of the QF Hypothesis includes terms not previously included in a Hamiltonian because QF addresses a system far from equilibrium. In the solution space of this expanded Hamiltonian there are absolute values greater than 782KeV and up to 9.3 MeV. You may recognize 782KeV as the mass difference between the sum of a proton and an electron and the mass of a neutron. At first glance 9.3 MeV may seem preposterous, however it is no more preposterous than 80+GeV for the well-accepted W bosons. The energy is concentrated by virtue of being a compression function. Deuterons may require up to 3 MeV and Tritons up to 9.3 MeV.

[1] The sum of all kinetic energy operators for each nucleus, electron, electrons and nuclei interaction, electron- electron interaction, and nuclei-nuclei interaction in the system

Material science

The elements and materials that support the Fleischmann-Pons Effect have the following shell similarities in common. They have a full or nearly full D_n shell and an empty or at least room in the $S_{(n+1)}$ shell. Palladium is the only element in the periodic table with a full D_n shell D_4 and an empty $S_{(n+1)}$ or S_5 shell in the ground state. I believe that this $S_{(n+1)}$ orbital energy well represents the trapping points that hydrogen occupies in the materials that support the Fleischmann-Pons Effect. Hydrogen will pass through palladium but helium will not. As atoms go, helium is about ½ the size of hydrogen, yet it will not pass through palladium and hydrogen will. It has been shown that hydrogen actually enters with a fractional charge or less than one electron per hydrogen nuclei entering the lattice. One way to visualize the transport of hydrogen through palladium is as an external gear pump mechanism.

The tear dropped shaped P orbitals act like the teeth of an external gear pump and the D orbitals in combination with the lattice nuclei act as the casing. There is only room for a single hydrogen nuclei in-between each set of P orbital teeth. The walls of that "space" are a combination of electrostatic repulsion of the lattice nuclei and the $P_{(n)}$ $D_{(n)}$ electron wave functions. Hydrogen nuclei can easily tunnel to an adjacent lattice element site in palladium providing extraordinary mobility within the palladium lattice. Given this extraordinary mobility, it is inconceivable that two hydrogen nuclei would occupy the same octahedral point and fuse at a loading ratio of less than 3. What trapping in the octahedral points **does do** is limit the uncertainty or standard deviation of the position of the hydrogen nuclei. All the hydrogen loving lattice structures that support the transmutation of elements have this trapping capability.

Heisenberg uncertainty formula

As it turns out, the greater than symbol used in the Heisenberg uncertainty formula is correct. If one variable is forced to an extremely or a "super" low value, the uncontrolled variable becomes large. In a Bose-Einstein condensate, super cooling a cloud of evaporated atoms achieves a very small Δp or uncertainty of momentum or energy. To satisfy $\Delta p\ \Delta q$ or uncertainty of momentum times uncertainty of position $\geq h / 4\pi$ (Heisenberg Uncertainty Principle), a very large Δq or uncertainty of position occurs and if the atoms follow Bose statistics, a Bose-Einstein condensate is formed. The atoms assume the same quantum state and can overlap or be in the same place at the same time. When this happens, the atoms become indistinguishable from each other and behave as a single super atom. It is possible to see a collection of only a few thousand atoms with an unaided eye because the standard deviation of position is very large. To reliably control the PF reaction, one must supply what the patent application describes as Heisenberg Confinement Energy or super confinement of the nuclei, forcing a very small Δq or uncertainty in position, affecting a large Δp (energy). This is the first new additional term to the Hamiltonian describing how QF works.

Non bonding energy

The term non-bonded energy is the second term added to the Hamilton describing QF. This term refers specifically to atoms that are not bonded to each other in a molecule. The non-bonded energy accounts for repulsion, van der Waals attraction, and electrostatic interactions.

Van der Waals attraction occurs at short range, and rapidly dies off as the interacting atoms move apart by a few Angstroms. Repulsion occurs when the distance between interacting atoms becomes even slightly less than the sum of their contact radii. The hydrogen in the lattice is not bonded and actually causes some deformation of the lattice on entry, indicating that it has forced entry into the portion of the equation controlled by a factor of $1/r^{12}$. It is the $1/r^{12}$ effects driven by phonons. Phonons are bosons and can be in the same place at the same time, driving electron capture events. This second new term to the Hamiltonian drives the Fleischmann-Pons Effect.

Q Energy

In Profusion Energy's work to date, both the non-bonded energy and Heisenberg Confinement energy are driven by what Profusion Energy calls Q or quantum compression energy. This is used to stimulate super confinement waves in the lattice.

The primary Q pulse delivers the bulk of its power in ~100ns achieving a peak current density of over 7 thousand amps per square mm. The polarity of the Q pulses alternate to limit the degrading effects of electromigration on both the core material lattice elements and the hydrogen in the core. The portion of Q power reported as going to the beaker is calculated as $½*C*V^2$ *repetition rate. $½*C*V^2$ is the energy or joules contained in the capacitor being discharged across the wire and repetition rate is times time or the joules per second which equals Watts. A Quantum Fusion reactor uses Q waveforms to force the value of the Molecular Hamiltonian. Once the value is high enough to supply the mass energy difference between a hydrogen ion plus an electron and the mass of a neutron or neutron cluster, that energy converts to mass in an electron capture event. A large number of hypotheses have been put forward to correlate the production of tritium and helium with heat. Accusations that it could not be fusion due to the lack of Gamma rays and fast neutrons were almost instantaneous. I propose that the QF Hypothesis can account for all the Fleischmann-Pons Effect experiments and some of the other excess heat experiments such as Bubble Driven sono fusion style devices, laser activation of metal hydride systems and gas load plus heat systems. This reaction is not fusion as the current establishment defines it. The perceived reaction is not DD.

What is Quantum Fusion (QF)?

When the system energy or molecular Hamiltonian achieves or exceeds the energy necessary to make up the mass difference between a hydrogen ion plus an electron and the mass of a neutron or neutron cluster, the hydrogen nucleus undergoes an electron capture event as a natural energy reduction mechanism. This highly endothermic reaction, in combination with the dispersion of the phonons that caused the increased confinement, results in a cold to ultra-cold neutron and/or neutron cluster. Neutrons are attracted to each other but the attraction is not strong enough to be "bound". At energy levels of a few meV (38 meV is roughly 70°F or 21°C), the Brownian motion will shake the multi neutron systems apart. However, a deuteron that has just converted up to 3 MeV of energy or a triton that has just converted up to 9.3 MeV of energy to mass has an extremely low energy level. The energy level is low enough that the neutrons remain together long enough to interact with another hydrogen nucleus moving through or into the lattice location occupied by the newly formed neutron or neutron cluster.

With the removal of the proton's charge, it is possible for a new hydrogen nucleus to enter the same trapping point and bond with the neutron or neutron cluster. This is similar to concepts used in astrophysics and referred to as the S and R process that build the heavier elements inside of stars through accumulation of neutrons and β^- decay. In QF cold to ultra-cold neutron(s) interact with another hydrogen nucleus moving through the lattice, resulting in ^{4}H.

Part of the problem for established physics is that their information is based on big science accelerator experiments. This led to a policy at the National Nuclear Data Center (NNDC) that defines the "ground state" of a nucleus as the "lowest energy at which it has been observed". The first three links you are likely to run across at the NNDC in relation to ^{4}H indicate that it undergoes a 100% neutron ejection decay path, even at what they have arbitrarily defined as the "ground state". Another document, mass.mas03.txt states the mass of ^{4}H as being greater than the mass of tritium + a neutron. This was referred to as an un-bound nucleus. (Meaning what?)

Researchers extrapolated the path of a neutron and a triton back to the same point. For ^{4}H that time of existence is so short it is given as a width of 4 MeV. That calculates out to roughly 10^{-24} seconds, more precisely 82.28 yocto-seconds after an 8 MeV neutron collides with a ^{7}Li nuclei. I have discussed this with J. H. Kelly of the National Nuclear Data Center (NNDC). He assured me that this was the absolute lowest energy level at which you could possibly create ^{4}H. (Does this sound like the ground state?) When ^{4}H is formed as an early intermediate decay product from a high-energy collision, there is sufficient momentum to make it energetically favorable for a neutron to carry the excess energy away before β^- decay occurs. In a metallic lattice where low energy neutrons accumulate, β^- is the decay path. Papers compiled in NNDC do indicate this. (The data is somewhat difficult to access. To retrieve it, go to http://www.nndc.bnl.gov/ensdf/, enter ^{4}H in the Quick search: box, and click "Search". Click the check the box next to the ^{4}H and click "HTML". See the first sentence in the data sheet.)

According to Kelly, if there were some way to make ^{4}H at a low enough energy ($\leq$3.53 MeV), then it would undergo β^- decay. That can't be done in an accelerator. When solid-state systems produce ^{4}He, each helium nucleus formed liberates between 23.2 MeV and 27.5 MeV depending on the exact path taken.

Gross loading

Existing attempts to harness the Fleischmann-Pons Effect depend on what I call Gross loading. By achieving a loading ratio greater than 0.85, the movement of hydrogen ions is limited by the number of open octahedral points. It also moves the lattice away from equilibrium and raises the base level result of the Hamiltonian operator. Why don't all palladium samples work once the loading ratio exceeds 0.85? Researchers have talked about the grain structure and cracking. Wave phenomenon or phonons are reflected and refracted by grain boundaries and cracks or discontinuities. The Nuclear Active Environment is one where enough phonon peaks intersect to obtain the $1/r^{12}$ + Heisenberg confinement energy necessary to affect electron capture events. Typical gross loading problems are driven in part by the quantity of hydrogen present in the lattice when the reaction starts. The bonding energy released in the formation of helium or transmutation causes a local chain reaction release of energy that eventually destroys the mechanical structure that was supporting the reaction.

Quantum Fusion (QF)

Quantum Fusion avoids these problems by explicitly driving the required phonons or displacement of the lattice elements. By performing this in an explicit manner, it is possible to run the reaction at a very low level and low loading ratio. At this point Profusion Energy has not yet ascertained the minimum (loading*phonon level) necessary to run the reaction but the systems appear to begin producing excess heat as soon as they are activated. Another aspect that leads me to believe that the Fleischmann-Pons Effect is driven by rogue or super waves causing electron capture events is the system response to Q repetition rate. As the Q repetition rate is adjusted up, the reaction has peaks and then rolls off before picking back up to a higher peak as the repetition rate continues to increase. The current hardware has a maximum Q repetition rate of 100KHz but the best results obtained are below that frequency. The patent applications show a number of different ways to build a practical reactor but systems to date have been built using wire cores and fast current pulses for the Quantum Compression.

Most of the scientific community agrees, it is not possible to overcome the coulumbic repulsion of hydrogen within a metallic lattice. However as I have just outlined, it is not necessary to overcome columbic repulsion. This is not fusion as currently defined.

The Quantum Fusion Hypothesis not only explains the reaction but points to multiple ways of making industrially useful devices by controlling the underlying physics.

References

1. R. E. Godes, *The Quantum Fusion Hypothesis*, Profusion Energy Inc., September 2008 www.profusionenergy.com/PhaseIVerificationData/ProfusionEnergyHypothesis.pdf

Excitation Transfer and Energy Exchange Processes for Modeling The Fleischmann-Pons Excess Heat Effect

Peter L Hagelstein[1] and Irfan U Chaudhary[2]
[1]*Research Laboratory of Electronics,*
Massachusetts Institute of Technology, Cambridge, MA
[2]*Department of Computer Science and Engineering,*
University of Engineering and Technology, Lahore, Pakistan

Abstract

The absence of energetic particles commensurate with the energy produced is the single most notable feature of the Fleischmann-Pons experiment for theory, assuming that a new nuclear process is involved. We discuss briefly energy exchange between two-level systems and a low energy oscillator, concluding that spin-boson models augmented with loss are able to describe coherent energy exchange involving a large number of oscillator quanta. Since the coupling between deuterons and the lattice is weak, the excitation must be transferred to a different system with stronger coupling, in order to develop a simple model relevant for heat production. The resulting toy model can be used for simulation, and we describe briefly ongoing efforts to develop a computational model.

Introduction

The Fleischmann-Pons effect consists of excess heat production in experiments where palladium cathodes are electrolyzed in heavy water; the amount of energy measured in such experiments is much too large to be of chemical origin; and energetic particles commensurate with the energy produced are absent. When first described in 1989, the response of the scientific community was one of skepticism and disbelief. Early efforts to confirm the effect were largely unsuccessful, due to a lack of understanding as to what are the critical issues. Subsequent experimental work in the following years has provided enough confirmations that the effect is at present held to be real among researchers who work in the area.

There is at present no accepted theoretical explanation for the effect. Since the inception of nuclear physics in the early 20th century, nuclear reactions have been understood in part through the concept of local energy and momentum conservation. In an exothermic nuclear reaction, the net energy produced is expressed in terms of energetic particles. No nuclear reactions are known in which most of the energy produced goes into other channels.

However, this foundation of nuclear physics is precisely what is challenged in the Fleischmann-Pons experiment. Hence, the primary theoretical focus, if one accepts that the energy is of nuclear origin and that commensurate energetic particles are not present, must be on physical mechanisms that lead to a violation of local energy and momentum conservation (while conserving overall momentum and energy).

Energy exchange

There is some experimental support for a reaction Q-value of 24 MeV per ^{4}He atom observed in the gas phase, in experiments where an effort was made to scrub the helium out of the cathode [1,2]. This directs our attention to mechanisms in which two deuterons (as fuel) combine to make ^{4}He (as ash), where the mass difference (24 MeV) is to be converted to a very large number of lower energy quanta. Experiments have been reported recently in which cathodes have been observed to respond to laser beat frequencies at 8 THz and 15 THz (and also 20 THz), which correspond to the optical phonon band edges of PdD (and also PdH) [3]; these are modes with zero group velocity. This motivates us to consider optical phonon modes as oscillator modes involved in the energy exchange process.

The theoretical problem to be addressed, then, is how a large energy (24 MeV) quantum can be split up efficiently into a very large number of small energy (33 or 62 meV) quanta. We have studied models in which two-level systems with a large transition energy (representing local molecular D_2 and ^{4}He states at vacancy sites in the PdD lattice) couple to a low energy harmonic oscillator (representing optical phonon modes with low group velocity). Such models at first glance appear to be closely related to spin-boson models that appear in the literature in connection with NMR, cavity QED, and other applications. When a two-level system is coupled to an oscillator with much lower characteristic energy, then the models predict that energy can be exchanged between the two systems. For this to occur, the resonance must be very precise, and the resulting energy exchange rate is very slow. In the end, one would not expect to see more than about 100 oscillator quanta exchanged for a two-level system quanta, due to the weakness of the energy exchange effect in the multi-quanta limit.

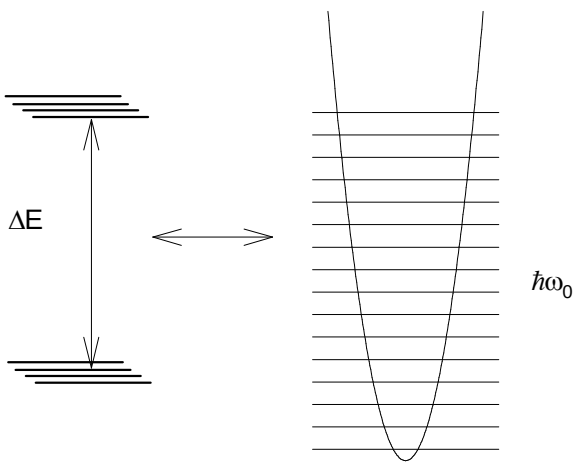

Figure 1. Two-level systems coupled to a harmonic oscillator, in a many-spin spin-boson model.

However, if we examine the many-spin version of the spin-boson problem, we find that energy exchange is hindered by destructive interference effects between the different individual pathways involved. If this destructive interference is spoiled, then the rate of energy exchange is greatly enhanced, and the number of oscillator quanta that can be exchanged with a two-level system is increased dramatically. Spin-boson models augmented with loss exhibit greatly increased energy exchange rates. An example of this is discussed in the Appendix. Such models

allow energy exchange between low energy oscillators and energetic two-level systems that is sufficiently rapid to account for the kind of energy exchange required in Fleischmann-Pons experiments, at least in principle.

Excitation transfer

The use of spin-boson models requires an estimate for the coupling matrix elements between the two-level system and the oscillator. To apply this kind of model to describe nuclear transitions involving phonon exchange, we require an estimate for the associated matrix element. There is no difficulty in principle with a direct computation of the matrix element between molecular D_2 and nuclear ^4He states in the lattice, including phonon exchange [4]. However, we know that this matrix element is small due to the presence of a Gamow factor associated with tunneling through the Coulomb barrier. Many-spin spin-boson models augmented with loss require the coupling to be strong in order for the energy exchange process described above to function. As a result, the simplest possible models for energy exchange cannot work in the case of direct transitions between D_2 and ^4He.

Consequently, we seek a modification of this basic model. In recent years we have focused on models involving two different sets of two-level systems, both coupled to a common oscillator. One of these sets of two-level systems is strongly coupled to the oscillator, and the other is assumed to be weakly coupled to the oscillator. The basic idea in this kind of model is that the excitation associated with the weakly-coupled two-level systems is transferred over to the strongly-coupled two-level systems, where many-quantum energy exchange can occur [5]. This is indicated schematically in Figure 2.

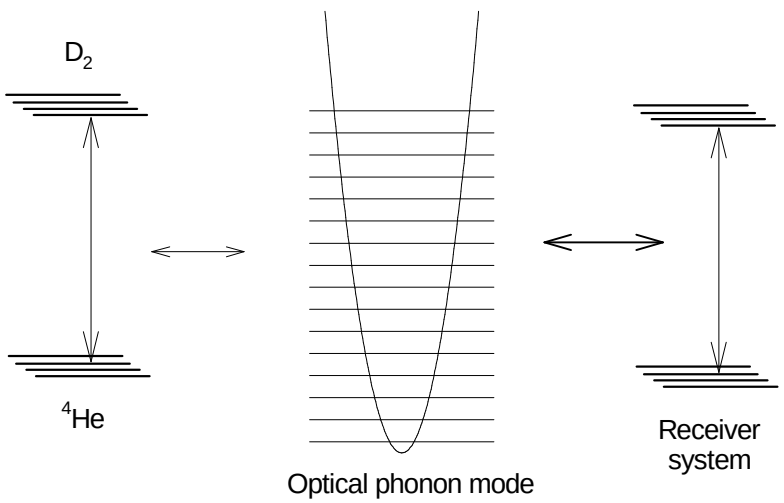

Figure 2. The D_2/^4He system (modeled as a set of equivalent two-level systems) is weakly coupled to a low energy oscillator. A second set of two-level systems (indicated as the receiver system) is strongly coupled to the oscillator.

Computations done to date indicates that the basic scheme seems up to the task of modeling the Fleischmann-Pons excess heat effect, as long as the associated many-spin model is augmented with loss (which greatly accelerates the excitation transfer process as well as the energy exchange process). The enhanced excitation transfer rate is sufficiently fast in the case

of the weak coupling matrix element associated with the D_2-^{4}He transition to be consistent with experiment (as long as substantial screening effects comparable to those estimated by Cserki and coworkers [6] for PdD are included).

However, input from experiment does not tell us what the relevant physical states are that correspond to the strongly-coupled two-level system on the receiver side. There are at least two plausible candidates which seem to have theoretical support and are not inconsistent with experiment:

One possibility is that nuclear states of the host lattice participate. In this case, the ground state of the two-level system would correspond to the ground state of neutron rich isotopes of the host (such as ^{110}Pd). The upper state would correspond to an exotic nuclear state in which a neutral cluster (such as ^{4}n) separated from the daughter nucleus (^{106}Pd) by about 10 fm, perhaps with some angular momentum. Such a state would be favored by the selection rules associated with coupling to the lattice (phonon exchange in association with nuclear excitation in general seems to be a weak effect, that becomes much stronger in the event that the lattice "sees" a mass change of the nucleus). Whether this kind of state can be sufficiently stable to do what is required within the context of the model has not been demonstrated.

Another possibility is that nuclear states similar to those of the D_2-^{4}He two-level systems participate. In this case, the ^{4}He ground state would match the ground state of the receiver-side two-level systems. The excited state in this scenario would be a compact molecular D_2 state, formed by a competition between production (where the source involves creation at fermi-level separation) and destruction (where transitions back down to the ground state occur sufficiently rapidly to prevent D_2 separation out to 0.74 Angstroms). As long as the reduced D_2 separation was sufficiently large so that the difference in the electronic wavefunctions is significant (ultimately leading to phonon exchange), and conventional fusion pathways occurred sufficiently slowly so as not to drain off the excitation, then such a state would be able to fulfill the functional requirements of the model.

Simulation model

The development of an idealized microscopic model for excitation transfer and energy exchange allows us to consider using it in the context of a simulation model. A picture has been in the process of emerging over a great many years which seems to be consistent with many experiments, and which seems to be consistent with the requirements of the microscopic model.

In this picture, deuterium is loaded into Pd so that the associated chemical potential becomes high enough to support vacancy stabilization (which occurs near a D/Pd ratio of 0.94). At this loading, Pd that is codeposited will have a large number of single-atom vacancies. There is the possibility that vacancies can diffuse from the outer surface, but the associated kinetics are expected to be slow unless there exists an enhancement under conditions where a deuterium flux is present. In the basic Fleischmann-Pons experiment, the formation of the vacancies is thought to require about a month (and a much shorter time in the Szpak experiment). The loading and vacancy stabilization can be simulated from information available in the literature; to model the surface vacancy distribution requires knowledge of the rate of codeposition, or enhanced vacancy diffusion rates.

We conjecture that σ-bonded dideuterium [7] (essentially molecular D_2) forms in the vacancies at more modest loadings. These are the active sites, which occur in the outer (micron-scale) region of the cathode. Dideuterium formation can be modeled using simple statistical mechanics given an estimate of the binding energy. Excitation transfer is then stimulated by phonon exchange with compressional phonon modes (the matrix element between D_2 and ^{4}He couples predominantly to compressional phonon modes) that are highly excited. Phonon excitation in this picture is produced by the deuterium flux through the near-surface of the cathode. Energy exchange occurs in the presence of high compressional optical phonon excitation in the case of assumed ^{4}He-compact D_2 states (which at present seems to match experiment best). The simplified model described above consisting of two-sets of two-level systems to account for the nuclear states, and a harmonic oscillator (augmented with loss) to model optical phonon modes, can be used to develop equations describing the associated coherent dynamics for the simulation model.

As energy is produced, ^{4}He accumulates in the active sites. At first, this would be helpful as there would be more capacity for anomalous energy exchange, since in general there is little helium present initially. However, as more energy is produced, we expect helium to block active sites, since the diffusion of helium away from the active sites is very slow near room temperature. In the event that helium diffusion limits excess heat production, we would expect to see a strong temperature dependence associated with excess heat production (as has been reported in a number of experiments [8]). With an appropriate simulation model, we can model this effect, and compute the fraction of helium released into the gas.

We have begun the development of the simulation model outlined above. The results obtained so far seem to be interesting, and we hope to compare our results with experiment in the coming months.

Appendix

Consider the enhancement of multi-quantum coherent energy exchange in a many-spin spin-boson model augmented with loss. We take the Hamiltonian to be of the form

$$\hat{H} = \Delta E \frac{\hat{S}_z}{\hbar} + \hbar\omega_0 \hat{a}\hat{a}^\dagger + V \frac{2S_x}{\hbar}\left(\hat{a} + \hat{a}^\dagger\right) - i\frac{\hbar}{2}\Gamma\left(E\right)$$

Where the first term in the Hamiltonian describes the energy of the two-level systems, the second term describes the oscillator, the third term implements linear coupling, and the final term accounts for the loss added to the model. The model is discussed further in [9].

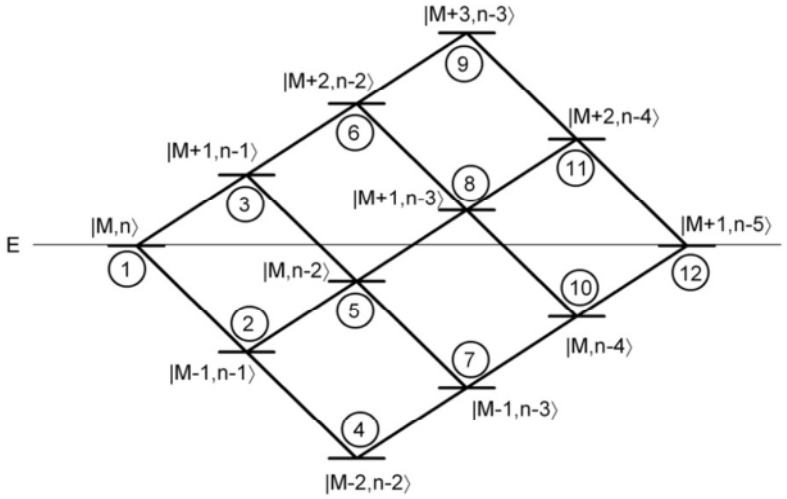

Figure 3. Energy levels that contribute to indirect coupling between |M,n⟩ and |M+1,n-5⟩ in the case of multi-quantum exchange involving 5 quanta.

The impact of loss on energy exchange can be illustrated through a concrete example. We consider a finite basis solution constructed from a combination of 12 basis states composed individually of products of Dicke states and oscillator states

$$\Psi = \sum_j c_j \left| S, M_j \right\rangle \left| n_j \right\rangle$$

We consider indirect coupling from an initial state |M,n⟩ to a final state |M+1,n-5⟩, in which a single two-level system excitation is matched to a loss of 5 oscillator quanta. The states are illustrated in Figure 3.

If no loss is present, the indirect matrix element between the initial state and the final state can be found to lowest-order in perturbation theory to be

$$V_{1,12} = \frac{625}{64}\frac{V^5}{\Delta E^4}\sqrt{n(n-1)\cdots(n-4)}\sqrt{(S-M)(S+M+1)} \qquad \Gamma \to 0$$

If loss is present and large for all intermediate states with a basis energy less than E, such that the associated paths do not contribute, then the indirect coupling matrix element is

$$V_{1,12} = \frac{1}{18}\left[5S^4+10S^3-S^2\left(10M^2-8M-22\right)+\cdots\right]\left[V_{1,12}\right]_{\Gamma=0} \qquad \Gamma \to \infty$$

For modest S the enhancement in indirect coupling is orders of magnitude. Loss breaks the destructive interference between the contributions from different pathways, and results in a dramatic increase in the indirect coupling responsible for coherent multi-quantum energy exchange.

References

1. M. C. H. McKubre et al, as discussed in the report prepared for the 2004 DoE review; *Proc. ICCF11*, page 23 (2004).
2. M. Apicella et al, *Proc. ICCF12* page 117 (2005).
3. D. Letts and P. L. Hagelstein, *Proc. ICCF14* (2008).
4. P. L. Hagelstein, I. U. Chaudhary et al, *Proc. ICCF14* (2008).
5. P. L. Hagelstein and I. U. Chaudhary, *J. Phys. B*, **41** 135501 (2008).
6. K. Czerski, A. Huke, P. Heide, and G. Ruprecht, *Europhys. Lett.* **68** 363 (2004).
7. G. Kubas, *Metal dihydrogen and σ-bond complexes*, Kluwer Academic/Plenum Publishers, New York (2001).
8. E. Storms, *Proc. ICCF4*, vol 2, page 4-1 (1993).
9. P. L. Hagelstein and I. U. Chaudhary, submitted (2008).

Input to Theory from Experiment in the Fleischmann-Pons Effect

Peter L. Hagelstein[1], Michael Melich[2] and Rodney Johnson[2]
[1] *Research Laboratory of Electronics, MIT, Cambridge, MA*
[2] *Naval Postgraduate School, Monterey, CA*

Excess heat in the Flesichmann-Pons effect constitutes a new physical effect unlike other physical processes with which we are familiar. Many groups have proposed theoretical mechanisms to account for the effect, but at present none has been generally accepted. This motivates us to review what experiment tells us about theory. There exists a relatively large body of experimental results, and it is possible to connect many of these individual results to theoretical statements, which might then be used as the basis for the development of new theoretical models.

1. Introduction

Nuclear physicists have studied deuteron-deuteron fusion over the years using energetic deuteron beams incident on different targets that contain deuterium. Local conservation of energy and momentum dictates that in an exothermic reaction, the reaction energy is expressed in the kinetic energy of the reaction products. As a result, we know what the primary reaction channels (p+t and n+^{3}He) are, since the reaction products can be observed directly. The particle energies and angular distributions are also available directly from experiment. A theoretical model for the deuteron-deuteron reaction follows directly from solving the Schrodinger equation (approximately) for the relevant four-body problem, with two deuterons in the input channel, and with p+t and n+^{3}He in the exit channels. The results from such models are in good agreement with experiment.

Because the associated theoretical problem is so simple, at least conceptually, one would not imagine that there could be anything that could compete with the primary reaction mechanism, or change fundamentally what happens when two deuterons interact. The excess heat effect in the Fleischmann-Pons experiment seems not to follow this clear and simple picture. As such, if the experiments are right, then they suggest that something else can happen. In the decades following the announcement of the excess heat effect, there have been a great many positive experiments which seem to confirm the existence of the effect. Hence, we are faced with the theoretical problem of figuring out how the effect works.

We might turn to nuclear physics and solid-state physics, both mature disciplines, in order to develop a theoretical model. Unfortunately, over the years no one has had much luck convincing their colleagues that a suitable explanation can be obtained from such a starting place. Moreover, such a model if developed would not be accepted without very strong experimental support. In the end, one must understand theory through an experimental foundation. We only know what happens because we can observe it in an experiment.

This presents a serious issue when we address the Fleischmann-Pons experiment. The basic effect is nuclear, yet due to the absence of commensurate energetic nuclear particles, we are not able to study the primary reaction mechanism directly as we can in the case of deuteron-deuteron fusion. This provides us with the motivation to re-examine the experiments in order to understand better what we can learn about theory.

2. Excess heat effect

The excess heat effect is observed as a temperature increase in heavy water electrochemical experiments where palladium cathodes are loaded with deuterium. The increase in temperature appears to be due to power generation in the palladium cathode. Perhaps the most important question regarding the excess heat effect itself is whether or not it is real.

The first report of excess power in association with PdD electrochemical experiments was by Fleischmann, Pons and Hawkins [1]. Unfortunately, this work was not well written, and the discussion provided was insufficient to allow for replication in general; this resulted in a large number of subsequent negative results early on (see [2] as an example). Confirming experiments were reported subsequently by Fleischmann and Pons [3]; by the SRI effort [4]; by Storms [5]; and by many other groups around the world. By now, there have been reported more than 100 observations of excess heat in Fleischmann-Pons experiments.

2.1. Energy

Much discussion has been devoted to the issue of excess energy in the experiments. In the basic Fleischmann-Pons experiment the Pd cathode must be charged for a month or so prior to the observation of excess power events. As a result, it has been argued that the energy produced in the bursts is small compared to the input energy, so that there may be no net energy production, but only the release of stored power not accounted for during charging.

We note that in the experiment reported in [3] the excess power integrated over a roughly 100 hour burst event was comparable to the total input energy, so that the total output energy was roughly twice the input energy. A hypothetical storage mechanism for this experiment would need to accommodate 4 MJ in 0.157 cc of cathode; which can be compared to the 1.2 kJ energy release which would be produced by the detonation of an equivalent volume of the explosive TNT. This argues strongly against any conventional storage mechanism.

Other experiments have been reported with higher energy gains. Swartz has claimed reproducible energy gains over 250% using the method described in [6]. The Energetics team reported in 2003 an observed energy gain of 6.7 in a glow discharge experiment [7], and in 2004 an observed energy gain of 25 in an electrochemical PdD experiment [8]. The conclusion from these experiments and others is that net energy is produced, and that the energy storage argument is inconsistent with experiment.

2.2. Power density

To determine the associated power density, we require information about what part of the cathode is active. One relevant observation (to be discussed below) concerns the emission of ^{4}He (as ash) into the gas stream, which could only occur if the helium were created within about a micron from the surface. In the Szpak experiment, Pd is co-deposited on a copper

substrate, and excess heat is observed [9]. The observed power per unit area is on the order of 80 mW/cm^2, and the corresponding power per unit Pd volume is in the range of 160-800 W/cm^3 for an active Pd thickness estimated to be in the range of 5 μm to 1 μm. In some experiments significantly higher numbers can be estimated. For the experiment described in [8], the power per unit area reaches about 4 W/cm^2, which corresponds to about 8 kW/cm^3 if we assume a 5 micron active thickness. There is evidence for hot spots [10] and localized surface melting in some experiments [11].

2.2. Loading, current density and flux

There appear to be two different requirements on deuterium loading. In the SRI experiments, the cathodes need to achieve a loading of about 0.95 (deuterium atoms per palladium atom) for excess heat to be observed at all [12]. A cathode which has achieved this during the roughly month-long charging period then later on needs to be loaded above a threshold near 0.85 to produce an excess heat burst. In many experiments [13-15] there has been observed a linear dependence of the excess power on current density above a threshold as first described by Fleischmann and Pons [16].

Excess power in Fleischmann-Pons experiments is dependent on the deuterium flux in the cathode. Although this is implicit in the ideas presented by Fleischmann on the Coehn effect in ICCF4 [17], it was first noticed in connection with a Fleischmann-Pons experiment at SRI, where the excess heat seemed to increase when a cathode spontaneously went into a breathing mode. This led to an empirical relation [18] for the excess power P_{xs}

$$P_{xs} \prec (I - I_0)(x - x_0)^2 \left|\frac{dx}{dt}\right|$$

where I is the current and x is the loading. Subsequently, experiments reported by Li and coworkers have taken advantage of deuterium flux [19], and also by Arata and Zhang [20].

2.3. Temperature

Fleischmann and Pons noticed that the excess heat increased following the application of a resistive calibration pulse to their cell, which suggested that they could take advantage of the effect to achieve higher power operation [21]. Somewhat later, Storms observed a dependence of excess power on temperature of the form

$$P_{xs} = P_0 \, e^{-\Delta E / k_B T}$$

where ΔE was reported as 15 Kcal/mole, or 670 meV [22].

This dependence is not seen in all experiments. It has been suggested that since the observed ΔE is close to that for helium diffusion in Pd, that this temperature dependence may be associated with helium accumulation in active sites in experiments with high local excess power per unit volume.

3. Helium

In association with the press conference in March 1989, Fleischmann and Pons apparently claimed that helium had been observed in association with the excess heat effect. Subsequent

measurements did not provide a confirmation, and the issue of helium production subsequently has been contentious.

3.1. Detection in the gas phase

A significant step forward was made with the observation of ^{4}He in the gas phase by Miles and Bush [23]. Prior to this, a great deal of effort had been focused on searches for elemental and isotopic anomalies in the Pd cathodes, as well as for trapped helium, with few positive results. Since the excess heat effect has no accompanying energetic particles, one could not learn much about reaction mechanisms or possible products, and all elements and isotopes were potential suspects. Helium as a reaction product had been considered previously, but was expected to be trapped in the metal if it was produced. That it might be observed in the gas was unexpected.

Subsequent work has largely confirmed the presence of ^{4}He in the gas outside of the cathode in Fleischmann-Pons experiments [24]. At ICCF6, Gozzi presented some striking results that appeared to show that heat bursts were time-correlated with ^{4}He bursts in the gas phase [25].

3.1. Mass difference, helium in the gas, and retention

Helium as a product has been of interest since the Fleischmann-Pons experiment requires deuterium, and two deuterons contain two protons and neutrons which is the same as ^{4}He. The mass difference is

$$E[dd] - E[^4He] = 23.86 \text{ MeV}$$

If the excess energy was produced through a physical process in which deuterons interacted somehow to make ^{4}He, then one should be able to tell from a comparison of the energy produced per ^{4}He atom detected. In Gozzi's experiments, the ratio of ^{4}He atom detected seemed to vary from burst to burst in the range of 10% to 100% of that expected from the mass difference. A possible explanation for the results observed was that the helium was produced initially near the cathode surface, so that it could get out; but different amounts would be released during particular events. The missing helium was assumed to remain inside the outer surface of the cathode.

3.2. Energy per ^{4}He

In an experiment carried out at SRI, excess heat was observed in a calorimeter that was helium leak tight, and ^{4}He was measured. The amount of helium measured was 62% of that expected based on the 23.86 MeV mass difference. Subsequently an effort was made to recover the helium remaining in the cathode; this was done through cycling deuterium in and out of the cathode. More helium was captured, and in the end the ratio of energy to ^{4}He was observed to be 104% of the 23.86 MeV mass difference with 10% error [12]. This result is supported by the measurements reported in [26]. In two of the experiments reported, the amount of ^{4}He detected was low (about 51% and 69%, taking into account the background) of the amount expected based on the mass difference. However, in another experiment (Laser-3) an attempt was made to recover the helium remaining in the cathode [27], and the result was that the amount of helium observed was slightly over 100% of the expected amount. Hence, the two experiments reported to date in which helium recovery was attempted both give results in agreement with the mass difference within experimental error.

4. Laser stimulation

Letts and Cravens [28] found that an excess heat could be triggered in a Pd cathode near threshold with a laser beam at low intensity. In these experiments, an incident diode laser beam of 30 mW was shown to lead to excess power levels in the range of 200-800 mW. Polarization dependence was observed, which was later studied by the ENEA group [26]. It was found that p-polarized light (with electric field partly normal to the surface) could stimulate excess heat, but s-polarization (with electric field aligned with the surface) was ineffective. This is consistent with coupling to compressional plasmon modes. In the Letts and Cravens experiment, a thin gold coating is deposited on the surface, with a surface plasmon resonance expected near the frequency of the incident light.

At this conference, Letts presented results for dual laser stimulation where the excess heat was found to respond to the beat frequency [29]. Strong responses were found at three difference frequencies (8.3 THz, 15.3 THz, and 20.4 THz), the first two of which can be associated with the **k**=0, or zero group velocity, optical phonon frequencies of PdD (the 20.4 THz frequency matches the upper **k**=0 frequency in PdH, but as yet there is no experimental evidence to support this). Once again, the dual laser beating effect is sensitive to laser polarization, and requires both laser beams to be oriented with p-polarization.

5. Connection with low-level nuclear emission

There has been much discussion over the years as to whether the low-level nuclear emissions which have been reported are related to the excess heat effect. Attempts to detect nuclear signatures at the time of an excess heat event have yielded no commensurate signals, and generally no low-level signals [30].

In Fleischmann-Pons experiments, excess heat is reported at relatively high current density (200-1000 mA/cm^2), while neutron emission tends to be seen at much lower current density (10-30 mA/cm^2). In [31] results from experiments that were run using Takahashi's high-low current protocol showed that cathodes which produced excess heat (and no neutron emission) at high current density, also showed low-level neutron emission (and no excess heat) at low current density. Such observations indicate a connection, in this case an anticorrelation.

5.1. Low-level deuteron-deuteron fusion

Evidence for low-level neutron and proton emission consistent with deuteron-deuteron fusion has been put forth over the years. Jones first reported the effect in TiD in 1989, and subsequent measurements after 1989 have provided confirmation (some of this work is reviewed in [12]), and evidence that deuteron-deuteron fusion reaction products are seen in Fleischmann-Pons experiments in PdD at low current density.

5.2. Other energetic emissions

Cecil and coworkers have claimed the observation of low-level energetic particles from TiD up to and beyond 10 MeV [33,34], as well as protons consistent with deuteron-deuteron fusion. Lipson and coworkers have reported repeated observations of low-level nuclear emissions from PdD included protons near 3 MeV (consistent with deuteron-deuteron fusion), as well as alpha particles between 10 and 20 MeV [35,36].

5.3. Karabut's x-rays

Karabut has reported the collimated emission of x-rays between 1-1.5 keV from Ti and Pd cathodes in glow discharge experiments run in deuterium, as well as in other gases [37,38]. The x-ray energy from energy-integrated absorption appears to be correlated with the cathode metal, and discharge voltage. Ti and Pd do not have fluorescence lines in the range. These observations raise the possibility that the emission is of nuclear origin, and that the collimation arises from local phase coherence among the emitters (the collimation is observed to be normal from the cathode surface). It seems implausible that phase coherence could be established in the case of electronic transitions.

6. Relevant beam experiments

There are at least two different kinds of beam experiments that have been done with metal deuterides that are of note in this discussion. One of these addresses the question of screening, and the other concerns localization.

6.1. Screening

There was much discussion about the impact of screening between deuterons in metal deuterides back in 1989, with the general consensus that significant screening effects would not be expected in PdD. However, low-energy deuterium beam experiments over the past decade has shown strong screening effects for deuteron-deuteron fusion reactions in metals in general, and particularly strong screening in PdD in particular [39,40].

6.2. Kasagi effect

In the mid-1990s, Kasagi and coworkers described beam experiments (in TiD and in PdD) where broad energetic proton and alpha signals were observed. Normally, deuteron-deuteron fusion produces two-body products, such as p+t and n+^{3}He. In this case, the reaction energy is sharp, with the reaction energy apportioned inversely to the mass. In a secondary reaction such as t(d,α)n, there is a spread in the alpha energy due to the initial 800 keV energy of the triton. However, in the experiments described in [41], a much broader alpha and proton signal was seen. Such a broad signal could only come about from a three-body exit channel, which in this case was attributed to n+p+α. The particles and end-point energies in this case are consistent with a three-body reaction d+d+d $\rightarrow$ n+p+α, which would require two of the deuterons initially within the same to be localized on the 10 fm scale.

7. Discussion

Based on the discussion above, which is incomplete both in scope and in citations to the relevant literature (by necessity given the limitations of a proceedings paper), we can begin to discuss what experiment provides as input to theory. Perhaps the most significant feature is that experiment seems to support the notion of a new kind of nuclear reaction in which the reaction energy is not expressed through the kinetic energy of the products. This statement is very significant, in that as commented on above, local conservation of energy and momentum require that energetic particles result from an exothermic reaction. No such process has been observed previously in nuclear physics. We note that among those working on excess heat in the Fleischmann-Pons experiment, that many are convinced even now that commensurate

energetic particles are produced, only to have escaped detection so far. Future experiments that address upper limits on the energy of possible reaction products would be helpful in this discussion.

As to what it is that reacts, there is no general consensus at this time. However, deuterium seems implicated (since for the most part no excess heat is reported with Fleischmann-Pons experiments using Pd cathodes and light water), and the correlation of ^{4}He with the energy produced implicates it as the ash. The two experiments in which an effort was made to account for retained ^{4}He give results consistent with 24 MeV per ^{4}He, consistent with the mass difference between two deuterons and ^{4}He. However, there is agreement among a subset of workers that the mechanism involved converted deuterons to ^{4}He, while others contest this. Badly needed are new experiments which address the correlation of ^{4}He with energy, taking care to collect all helium produced. Also needed are experiments which address how close to the surface the retained helium is, which should help shed light on where the reactions occur.

If the reaction energy is not expressed kinetically, then it is a reasonable question as to where it does go. In the end, the energy produced shows up as heat. There are no direct measurements of the energy produced in condensed matter modes prior to thermalization. The dual laser experiment may be relevant to this question, since the excess heat responds to the beat frequency, suggesting a nonlinear response, under conditions where the laser intensity is orders of magnitude too weak for any nonlinear response to be expected by conventional means. If the reaction energy were deposited into plasmon modes [keeping in mind that one would expect hybridization of low energy (2 eV) plasmon modes with optical phonon modes], then these internal modes may have sufficient excitation to provide a nonlinear response. Hence, there is an indirect argument for where the energy goes at least in one kind of experiment. The very high local power per unit volume production may be connected with the dual laser nonlinearity. What is really needed is some new experiment which can detect enhanced excitation in longitudinal plasmon modes and in optical phonon modes in association with excess heat production.

Attention should be drawn to the three-body Kasagi experiment, which suggests the possibility of deuteron-deuteron localization on the fermi scale. If correct, this experiment is of great significance, and may provide a glimpse into part of the internal reaction dynamics. Deuteron-deuteron fusion anticorrelated with excess heat production is supportive of mechanisms involving deuterium, but this is not universally agreed on at present. The strong screening effects observed in beam experiments are thought by many to be related to the low-level fusion effect; however, neutron production seems to come in (hour long) bursts events, similar to excess heat bursts. Most likely, there is more involved in low-level deuteron-deuteron fusion than simple screening effects.

Attention should also be drawn to the energetic alpha signal. The key question here should be: where does the energy come from? There are no energetic particles with even greater energy present in the amounts needed for the disintegration of nuclei with alpha particles in the 10-20 MeV range. So, the energy must come from somewhere else. But from where? The significance of the observation is in the implication that a large quantum may be communicated somehow by the local condensed matter environment leading to the disintegration of a nucleus.

This would be unprecedented in nuclear physics, but seems to be a direct consequence of the Cecil and Lipson experiments. If such a large quantum can be so communicated, then the possibility of it somehow being chopped up into a large number of small quanta seems perhaps more plausible.

The requirements on loading probably tell us something about the local environment needed for the reactions to occur. Arguments put forth over the years include: increased density results in increased conventional reaction probability; a connection with the D to Pd loading at which PdD becomes thermodynamically unstable; the development of a new phase; and a connection with the D to Pd loading at which host Pd vacancies are stabilized. Calculations indicate that D_2 cannot form inside bulk PdD due to occupation of antibonding orbitals, but perhaps the situation is different near vacancies where the electron density is lower. NMR experiments may be able to clarify this in the case of thin film samples of PdD with high vacancy concentration. There is no agreement on these issues at this time, and experiments have not yet clarified the role of loading.

References

1. M. Fleischmann, S. Pons, and M. Hawkins, *Journal of Electroanalytical Chemistry* **261** 301-308 (1989).
2. N. S. Lewis, C. A. Barnes, M. J. Heben, A. Kumar, S. R. Lunt, G. E. McManis, G. M. Miskelly, R. M. Penner, M. J. Sailor, P. G. Santangelo, G. A. Shreve, B. J. Tufts, M. J. Youngquist, R. W. Kavanagh, S. E. Kellogg, R. B. Vogelaar, T. R. Wang, R. Kondrat, and R. New, *Nature* **340** 525 (1989).
3. M. Fleischmann, S. Pons, M.W. Anderson, L.J. Li and M. Hawkins, *J. Electroanal. Chem.* **287** 293 (1990).
4. M. C. H. McKubre, S. Crouch-Baker, R. C. Rocha-Filho, S. I. Smedley, F. L. Tanzella, T. Passell, and J. Santucci, *J. Electroanal. Chem.* **368** 55 (1994).
5. E. Storms, *Fusion Technology* **23** 230 (1993).
6. M. R. Swartz and G. M. Verner, *Proc. ICCF10* 29 (2003).
7. I. Dardik, H. Branover, A. El-Boher, D. Gazit, E. Golbreich, E. Greenspan, A. Kapusta, B. Khatchatorov, V. Krakov, S. Lesin, B. Michailovitch, G. Shani, and T. Zilov *Proc. ICCF10* p. 61 (2003).
8. I. Dardik, T. Zilov, H. Branover, A. El-Boher, E. Greenspan, B. Khatchaturov, V. Krakov, S. Lesin and M. Tsirlin, *Proc. ICCF11* p. 84 (2004).
9. S. Szpak, P. A. Mosier-Boss, M. H. Miles, and M. Fleischmann, *Thermochimica Acta* **410** 101 (2004).
10. S. Szpak, P. A. Mosier-Boss, J. Dea, and F. Gordon, *Proc. ICCF10* p. 13 (2003).
11. J. Dash, G. Noble, and D. Diman, *Proc. ICCF4*, p. 25-1 (1994).
12. P. L. Hagelstein, M. C. H. McKubre, D. J. Nagel, T. A. Chubb, R. J. Hekman, *Proc. ICCF11* p. 23 (2004).
13. M. C. H. McKubre, S. Crouch-Baker, A. M. Riley, S. I. Smedley, and F. L. Tanzella, *Proc. ICCF3* p. 5 (1992).
14. E. Storms, *Proc. ICCF6* p. 105 (1996).

15. K. Kunimatsu, N. Hasegawa, A. Kubota, N. Imai, M. Ishakawa, H. Akita, and Y. Tsuchida, *Proc. ICCF3* p. 31 (1992).
16. M. Fleischmann and S. Pons, *Proc. ICCF1* p. 1 (1990).
17. C. Bartolomeo, M. Fleischmann, G. Larramona, S. Pons, J. Roulette, H. Sugiura, and G. Preparata, *Proc. ICCF4* p. 19-1 (1994).
18. M. C. H. McKubre, S. Crouch-Baker, A. K. Hauser, S. I. Smedley, F. L. Tanzella, M. S. Williams, and S. S. Wing, *Proc. ICCF5* p. 17 (1995).
19. X. Z. Li, B. Liu, J. Tian, Q. M. Wei, R. Zhou, Z. W. Yu, *J. Phys. D* **36** 3095 (2003).
20. Y. Arata and Y.-C. Zhang, *Proc. ICCF12* p. 44 (2005).
21. S. Pons and M. Fleischmann, Proc. ICCF2 p. 349 (1991).
22. E. Storms, Proc. ICCF4 vol. 2 p. 4-1 (1993).
23. M. H. Miles and B. Bush, *Proc. ICCF3* p. 189 (1992).
24. M. H. Miles, *Proc. ICCF10* p. 123 (2003)
25. F. Cellucci, P. L. Cignini, G. Gigli, D. Gozzi, M. Tomellini, E. Cisbani, S. Frullani, F. Garibaldi, M. Jodice, and G. M. Urciuoli, *Proc. ICCF6* p. 3 (1996).
26. M. Appicella, E. Castagna, L. Capobianco, L. D'Aulerio, G. Mazzitelli, F. Sarto, A. Rosada, E. Santoro, V. Violante, M. McKubre, F. Tanzella, and C. Sibilia, *Proc. ICCF12* p. 117 (2005).
27. V. Violante, private communication.
28. D. Letts and D. Cravens, *Proc. ICCF10* p. 159 (2003).
29. D. Letts and P. L. Hagelstein, *Proc. ICCF14* (2008).
30. S. Isagawa, Y. Kanda, and T. Suzuki, *Proc. ICCF5* p. 124 (1995).
31. H. Ogawa, S. Yoshida, Y. Yoshinaga, M. Aida, and M. Okamoto, Proc. ICCF5, p. 116 (1995).
32. P. Mosier-Boss, S. Szpak, F. E. Gordon, and L. P. G. Forsley, submitted for publication.
33. F. E. Cecil, H. Liu, D. Beddingfield, and C. S. Galovich, *Anomalous Effects in Deuterium/Solid Systems*, *AIP Conference Proceedings* **228** p. 375 (1990).
34. H. Liu, *Studies of nuclear reactions D-D, D-^{6}Li, and D-^{10}B at low energies and charged particle emission from deuterium-metal systems*, PhD Thesis, Colorado School of Mines, 1992.
35. A. G. Lipson, A.S. Roussetski, G.H. Miley, and E.I. Saunin, *Proc. ICCF8* p. 231(2000); A. G. Lipson, A.S. Roussetski, G.H. Miley, and C. H. Castano, Proc. ICCF9 p. 218 (2002).
36. A. G. Lipson, A.S. Roussetski, G.H. Miley, and E.I. Saunin, Proc. ICCF10 p. 539 (2003).
37. A. B. Karabut and S. A. Kolomeychenko, *Proc. ICCF10* p. 585 (2003).
38. A. G. Lipson, A. S. Rusetskii, A. B. Karabut, and G. Miley, *Journal of Experimental and Theoretical Physics* **100** 1175 (2005)
39. F. Raiola, L. Gang, C. Bonomo, G. Gyurky, M. Aliotta, H. W. Becker, R. Bonetti, C. Broggini, P. Corvisiero, A. D'Onofrio, Z. Fulop, G. Gervino, L. Gianella, M. Junker, P. Prati, V. Roca, C. Rolfs, M. Romano, E. Somorjai, F. Streider, F. Terrasi, G. Fiorentini, K. Langanke, and J. Winter, *Eur. Phys. J. A* **19** 283 (2004).
40. F. Raiola, B. Buchard, Z. Fulop, G. Gyurky, S. Zeng, J. Cruz, A. Di Leva, B. Limata, M. Fonseca, H. Luis, M. Aliotta, H. W. Becker, C. Broggini, A. D'Onofrio, L. Gianlanella, G. Imbriani, A. P. Jesus, M. Junker, J. P. Ribereiro, V. Roca, C. Rolfs, M. Romano, E. Somorjai, F. Streider, and F. Terrasi, *J. Phys. G: Nucl. Phys.* **31** 1141 (2005).

41. J. Kasagi, T. Ohtsuki, K. Ishu and M. Hiraga, *Phys. Soc. Japan* **64**, 777 (1995).

A Theoretical Formulation for Problems in Condensed Matter Nuclear Science

Peter Hagelstein[1], Irfan Chaudhary[2], Michael Melich[3] and Rodney Johnson[3]
[1]*Research Laboratory of Electronics,*
Massachusetts Institute of Technology, Cambridge, MA
[2] *University of Engineering and Technology, Lahore, Pakistan*
[3] *Naval Postgraduate School, Monterey, CA*

Abstract

Over the years theorists have adopted a wide variety of approaches to theoretical problems in condensed matter nuclear science. If one starts with a formulation adapted to condensed matter, then the resulting model may be well adapted to describing electrons and phonons, but perhaps less well adapted to describing nuclear states. If one starts with a formulation adapted to nuclear calculations, then the resulting model may be well adapted to structure and reaction calculations, but perhaps less well adapted to phonon or plasmon modes. We discuss here the use of a more general formulation based on nucleons and electrons which can be used for problems in condensed matter physics, nuclear physics, or for problems that involve interactions between nuclear and condensed matter systems.

1. Introduction

Excess heat in the Fleischmann-Pons experiment appears to be the result of a new kind of nuclear process [1]. The experimental arguments supporting this include: (a) the amount of energy measured greatly exceeds that which could be stored conventionally, or which could be of chemical origin; (b) ^{4}He is observed as an ash in amounts commensurate with the energy produced, where the amount of energy observed per ^{4}He is near 24 MeV (which is the mass difference between two deuterons and ^{4}He); and (c) low-level nuclear emissions have been observed in samples at low current density which produce excess heat at high current density. However, the excess heat is produced without commensurate energetic particle production, which is unprecedented. In a conventional exothermic nuclear reaction, the reaction energy is expressed as kinetic energy in the reaction products. In the Fleischmann-Pons experiment the excess heat is thought to be due to an exothermic nuclear process, but experiment shows an absence of corresponding energetic emissions.

If the energy does not appear as kinetic energy, then it must be expressed through other channels, since ultimately it is seen in thermal measurements. The only available non-kinetic channels into which the energy might go are those of the host metal deuterides structure, which are condensed matter modes. From the results of single and dual laser experiments, there is indirect evidence that some of the energy may be going into plasmon or optical phonon modes prior to thermalization. As such, it seems reasonable to consider the theoretical question as to

what kind of coupling occurs between these modes and the local nuclear systems which have been put forth in proposed reaction mechanisms.

More generally, there are by now numerous experiments which show anomalies of one sort or another (beyond excess heat), in which nuclear and condensed matter effects are probably connected. To address such issues, theorists over the years have been using a variety of tools to develop models, and to make predictions. However, if a condensed matter approach is adopted, then there are issues associated with including nuclear effects. If the starting point is some kind of nuclear physics calculation, then there are issues as to how one includes condensed matter effects. Within the literature one finds a variety of approaches which have been employed, so far with no systematic formulation. For each problem and each author, one must often put in effort to understand both the underlying formulation as well as the result.

Because of this, it seems worthwhile to see whether a formulation might be constructed which has a foundation sufficiently general to encompass aspects of condensed matter and nuclear physics on a uniform footing. If so, then we might be able to use it to advantage in modeling problems in areas where both are equally important in accounting for physical effects that are observed. In what follows, we describe one approach to such a formulation. In essence, if we do nothing more than start from a set of fundamental building blocks, such as electrons and nucleons, then the resulting formulation has the potential to speak to problems in the two disciplines on equal footing starting from a common foundation. Armed with such a foundation, we would be able to bring in results from the relevant literature in both disciplines within a unified framework to address problems of interest. Workers with backgrounds in either discipline could then have a common language that could be used to address such problems.

2. Electrons and nucleons

As a foundation, we consider models at the outset composed of a set of electrons and a set of nucleons. Within the isospin formalism, neutrons and protons are considered to be simply nucleons; identical particles differing only by whether they are isospin up (proton) or isospin down (neutron). This is similar to a set of electrons, which are identical particles, and which may have spin up or spin down.

Computations of nuclear structure or dynamics can in many cases be described adequately from such a starting place, and over the years good models have been developed that describe the interaction between nucleons. Restricting ourselves to a description based on nucleons bars us from addressing more sophisticated problems in which quarks become important. However, given the difficulty of working with QCD at present in association with bound state problems, this limitation seems a good trade off against a much improved ability to perform calculations much more easily.

Condensed matter computations in general assume electrons and nuclei, so that breaking down nuclei into their component nucleons greatly increases the complexity of what is already a pretty complicated theoretical problem. If one needs to account for the nuclear structure of every nucleus in a solid at the outset, then one would expect that subsequent calculations will quickly become a mess. Since the expanded formulation includes condensed matter physics as a subset, we are sure that it will be capable of address relevant problems in principle. However,

at some point we will require tools to reduce our description in order to allow us to focus on important parts of a problem. Hence, using a starting point of a set of electrons and nucleons at the outset will have to be viewed as formal for condensed matter calculations, and we will need a way to collect the nucleons back into their constituent nuclei for those that are not directly involved in a reaction under consideration.

Consequently, we require of our formulation a basic definition for the electron-nucleon Hamiltonian, and then we will need a systematic way to reduce problems so that we can focus on those parts which are particularly important for a specific calculation.

2.1. The electronic part

Focusing first on the electronic part, it seems clear that the place to start in general is with QED, which describes electrons and photons (the focus on electrons above is simplistic, since the interaction with electromagnetic fields is ubiquitous in condensed matter systems). In the literature over the years, one can find problems worked in configuration space (relativistic and nonrelativistic), in **k**-space, in second quantization, and using a wide range of approaches. We have no plans here to restrict in any way which part or formulation of QED to be used, and we would consider configuration space models that include only Coulomb interactions to be a good low-end example of a useful subset of QED.

2.2. The nucleon part

One can find much literature on structure and dynamics calculations of nuclei presented in configuration space, with empirical nucleon-nucleon potentials and Coulomb interactions. This would constitute a useful low-end example of the nucleon part of the problem. At the other end of the spectrum, there have been published nucleon-based field theories which are empirical generalizations of QED, including relativistic effects and coupling with the electromagnetic field (see for example [2] which discusses QHD). Such models would equivalently be suitable for the general formulation under discussion in this paper. In order to model beta decay, we assume that such models are augmented as needed with neutrinos and their associated weak interactions.

2.3. A simple example of a configuration space Hamiltonian

As an example of a minimal low-end model, we might adopt a Hamiltonian of the form

$$\hat{H} \;=\; -\sum_i \frac{\hbar^2}{2m}\nabla_i^2 - \sum_\alpha \frac{\hbar^2}{2M}\nabla_\alpha^2 + \sum_{i<j}\frac{e^2}{\left|\mathbf{r}_i-\mathbf{r}_j\right|} + \sum_{\alpha<\beta} V_n\left(\left|\mathbf{r}_\alpha-\mathbf{r}_\beta\right|\right) + \sum_{\substack{i,\alpha \\ protons}}\frac{e^2}{\left|\mathbf{r}_i-\mathbf{r}_\alpha\right|}$$

In this model, the first two terms account for the (nonrelativistic) kinetic energies of the electrons (with mass m) and nucleons (with mass M); the third term describes Coulomb interactions between electrons; the fourth term describes strong force and Coulomb interactions between nucleons; and the final term describes the attractive Coulomb interaction between electrons and protons.

2.3. The nucleon-nucleon interaction

The nucleon-nucleon potential is far more complicated than the simple Coulomb interaction (which could be used as a first approximation for the electron-electron potential). This is because nucleons are composite particles made up of quarks. In the past decades, nuclear physicists have developed empirical nucleon-nucleon potentials that are accurate for "low energy" (below a few hundred MeV) applications by fitting scattering data and bound state energies to appropriate functional forms [3]. One such potential that was proposed early on was the Hamada-Johnston potential [4]. A more modern example is the Argonne potential, which is now widely used [5]. More complicated nonlocal potential models have been developed in recent years [6,7].

2.4 Antisymmetrization

Electrons are identical fermionic particles, so that the overall wavefunction must be antisymmetric under the exchange of any two electrons, which leads to constraints on the spin and spatial pieces. Nucleons in this kind of model are also identical fermionic particles, so that once again the overall wavefunction must be antisymmetric under the exchange of any two nucleons, which in this case leads to constraints on the spin, isospin, and spatial parts of the problem. The extra degree of freedom in the nucleon part of the problem makes the construction of properly antisymmetrized nuclear wavefunctions a more complicated exercise than in the electronic case.

In the case of two electrons, there are two ways to construct an antisymmetric wavefunction:

$$\Psi = \begin{cases} (\text{antisymmetric in spin})(\text{symmetric in space}) \\ (\text{symmetric in spin})(\text{antisymmetric in space}) \end{cases}$$

In the case of two nucleons, there are three ways to construct an antisymmetric wavefunction:

$$\Psi = \begin{cases} (\text{antisymmetric in spin})(\text{symmetric in isospin})(\text{symmetric in space}) \\ (\text{symmetric in spin})(\text{antisymmetric in isospin})(\text{symmetric in space}) \\ (\text{symmetric in spin})(\text{symmetric in isospin})(\text{antisymmetric in space}) \end{cases}$$

For three-nucleon or four-nucleon wavefunctions, there are many more combinations, and one needs to make use of group theory for classification and construction [8]. This issue is much more important for the nucleon part of the problem than for the electron part of the problem, since the Coulomb interaction is scalar, and since an independent particle approximation can provide a useful starting place. The independent particle approximation is a much poorer starting place in the case of few-nucleon problems due to the absence of a fixed attractive core.

3. Matrix element example

The approach under discussion is very powerful, and to illustrate this we consider a formal example in the case of a phonon exchange matrix element. The discussion that follows is a brief summary of one given previously in Ref. [9]. We consider phonon exchange associated with a nuclear transition mediated by the nucleon-nucleon interaction. We assume that the initial and final nucleon states are nearly stationary in the lattice, which means that the associated physical process is not energy conserving, so that the matrix element would describe a piece of a more complicated physical process that does conserve energy.

3.1. Formal initial and final state wavefunctions

We take as a formal starting place initial and final state wavefunctions that are much more general than will be needed, but which are consistent with the formulation under discussion

$$\Psi_i = \Psi_i\left(\{\mathbf{r}_j\},\{\sigma_j\},\{\mathbf{r}_\alpha\},\{\sigma_\alpha\},\{\tau_\alpha\}\right)$$
$$\Psi_f = \Psi_f\left(\{\mathbf{r}_j\},\{\sigma_j\},\{\mathbf{r}_\alpha\},\{\sigma_\alpha\},\{\tau_\alpha\}\right)$$

Where the subscript j is used for electron position and spin variables, and α is used for nucleon position and spin variables. The matrix element under discussion can be written formally as

$$M_{fi} = \left\langle \Psi_f \middle| V_n \middle| \Psi_i \right\rangle$$

where V_n is the nucleon-nucleon interaction. At this point, since the wavefunctions are assumed to be properly antisymmetrized functions of the nucleon spin, isospin, and position variables, the matrix element is expressed appropriately for a calculation of the nucleon-nucleon interaction. Unfortunately, there is no hope of describing phonon exchange or condensed matter effects at this level with such a description. Starting from this formulation as a formal starting place, we need to reduce the problem systematically so that it might be amenable to computation.

3.2. Spectator nuclei

One thing that complicates matters is that most of the nuclei in the lattice do not participate in the reaction of interest, and contribute only through their center of mass coordinates. For example, consider a nuclear rearrangement of a local four nucleon system involving two deuterons; in this case, none of the host metal nuclei participate, and we should not need to carry around a description of the internal structure at the nucleon level. Hence, our first task is to eliminate individual nucleon coordinates of the spectator nuclei, and replacing them by a smaller number of nuclear center of mass coordinates. This can be done rigorously by expressing the parts of the spectator wavefunctions in terms of center of mass coordinates and relative coordinates, and then integrating over relative coordinates. In the end, we can denote this through

$$\Psi_i\left(\{\mathbf{r}_j\},\{\sigma_j\},\{\mathbf{r}_\alpha\},\{\sigma_\alpha\},\{\tau_\alpha\}\right) \rightarrow \Psi_i\left(\{\mathbf{r}_j\},\{\sigma_j\},\{\mathbf{r}_\alpha\},\{\sigma_\alpha\},\{\tau_\alpha\},\{\mathbf{R}_k\}\right)$$

The electron variables remain the same, but now the set of nucleon coordinates under consideration is reduced, and we have explicit center of mass coordinates for the spectator nuclei. In this form, we are now much closer to a problem formulation suitable for the condensed matter part of the problem.

3.3. Born-Oppenheimer approximation

As long as we are interested in processes assumed to be adiabatic relative to electron dynamics, we can make use of a Born-Oppenheimer approximation in order to reduce the problem further. The associated product wavefunction can be written as

$$\Psi_i\left(\{\mathbf{r}_j\},\{\sigma_j\},\{\mathbf{r}_\alpha\},\{\sigma_\alpha\},\{\tau_\alpha\},\{\mathbf{R}_k\}\right) = \Phi_i\left(\{\mathbf{r}_j\},\{\sigma_j\};\{\mathbf{r}_\alpha\},\{\sigma_\alpha\},\{\tau_\alpha\},\{\mathbf{R}_k\}\right)\Psi_i\left(\{\mathbf{r}_\alpha\},\{\sigma_\alpha\},\{\tau_\alpha\},\{\mathbf{R}_k\}\right)$$

Where the first term is the electronic wavefunction given fixed nucleon and nuclei positions, and the second is the adiabatic nucleon and nuclei wavefunctions. If our focus is on phonon exchange, then we are interested in the second term, and it may be possible to integrate out the electronic part of the problem if we have some reason to believe that the electronic wavefunctions in the initial and final states are sufficiently alike. If not, then the overlap integral coupling to the relevant electronic states in the final state will have to be estimated. For simplicity, we will assume in the matrix element under consideration that there are no important electronic or plasmon excitations. This approximation has the effect of reducing the wavefunction according to

$$\Psi_i\left(\{\mathbf{r}_j\},\{\sigma_j\},\{\mathbf{r}_\alpha\},\{\sigma_\alpha\},\{\tau_\alpha\},\{\mathbf{R}_k\}\right) \rightarrow \Psi_i\left(\{\mathbf{r}_\alpha\},\{\sigma_\alpha\},\{\tau_\alpha\},\{\mathbf{R}_k\}\right)$$

3.4. Phonons

Our goal was to develop a description for phonon exchange, and we require yet one more modification of the problem in order to bring phonons into our description. One way to do this is to recast the local nucleon problem in terms of relevant center of mass and relative coordinates. For example, if there are two deuterons present, then two different center of mass coordinates would be appropriate. If a helium nucleus is present, then only a single center of mass coordinate would be appropriate. We can denote this through

$$\{\mathbf{r}_\alpha\} \rightarrow \{\mathbf{R}\},\{\boldsymbol{\xi}_i\}$$

This change in coordinates then leads to wavefunctions that we may denote through

$$\Psi_i\left(\{\mathbf{r}_\alpha\},\{\sigma_\alpha\},\{\tau_\alpha\},\{\mathbf{R}_k\}\right) \rightarrow \Psi_i\left(\{\boldsymbol{\xi}_i\},\{\sigma_\alpha\},\{\tau_\alpha\},\{\mathbf{R}_k\}\right)$$

Now the wavefunction on the RHS has a full set of center of mass coordinates, and from the Born-Oppenheimer approximation (or from experiment) we can in principle develop equilibrium positions and force constants, so that we can recast the center of mass position operators in terms of phonon mode amplitudes. This we can denote according to

$$\Psi_i\left(\{\boldsymbol{\xi}_i\},\{\sigma_\alpha\},\{\tau_\alpha\},\{\mathbf{R}_k\}\right) \rightarrow \Psi_i\left(\{\boldsymbol{\xi}_i\},\{\sigma_\alpha\},\{\tau_\alpha\},\mathbf{q}_i\right)$$

where $\mathbf{q}_i$ is a vector that contains all of the initial state phonon mode amplitudes. The nucleon center of mass coordinates in this case can be expressed as phonon operators.

3.5. Matrix element integrations

We now have wavefunctions in a form suitable for describing phonon exchange matrix elements, at least formally. The matrix element can be written as [9]

$$M_{fi} = \iint\!\!\iint \Psi_f^*\left(\{\boldsymbol{\xi}_f\},\{\sigma_\beta\},\{\tau_\beta\},\mathbf{q}_f\right) V_n \Psi_i\left(\{\boldsymbol{\xi}_i\},\{\sigma_\alpha\},\{\tau_\alpha\},\mathbf{q}_i\right) \times \Delta\left(\mathbf{q}_i,\mathbf{q}_f\right)\Delta\left(\boldsymbol{\xi}_i,\boldsymbol{\xi}_f\right) d\mathbf{q}_i d\mathbf{q}_f d\boldsymbol{\xi}_i d\boldsymbol{\xi}_f$$

where the center of mass coordinates of the initial state lattice must agree with the center of mass coordinates in the final state lattice

$$\Delta\left(\mathbf{q}_i,\mathbf{q}_f\right) = \delta\left(\mathbf{q}_i - \mathbf{A}\cdot\mathbf{q}_f - \mathbf{b}\right)$$

This is consistent with the linear relation between vibrational coordinates that is sometimes used in the case of Franck-Condon factors in polyatomic molecules [10,11]

$$\mathbf{q}_f = \mathbf{A}\cdot\mathbf{q}_i + \mathbf{b}$$

In addition, the individual nucleon coordinates in the initial state must agree with those for the same nucleons in the final state, which is imposed through

$$\Delta\left(\boldsymbol{\xi}_i,\boldsymbol{\xi}_f\right) = \prod_\alpha \delta\left(\mathbf{r}_\alpha^f - \mathbf{r}_\alpha^i\right)$$

3.6. Coupling between phonons and internal nuclear coordinates

In the expression for the matrix element M_{fi} above, the initial state and final state wavefunctions are expressed in terms of phonon coordinates and internal relative nuclear coordinates. To within an excellent approximation, these two degrees of freedom are independent, so that we could reasonably use product wavefunctions for both. If so, then the issue of the origin of coupling between them becomes of interest. The coupling between these degrees of freedom comes about implicitly in this formulation through the nucleon-nucleon interaction, which depends on the relative position of two nucleons. The nucleon coordinates themselves depend on the local nuclear center of mass coordinate (which itself is a function of the phonon mode coordinates), and the relative coordinates. As a result, under certain

conditions (for example, if the intial state contains two deuterons, and the final state contains a ^{4}He nucleus), V_n can cause a mixing between the phonons and internal relative coordinates.

4. Discussion

We can use this approach to address problems systematically in condensed matter nuclear science which involve both nuclear and condensed matter pieces. In order to handle nuclear models, we begin with a description at the outset in terms of nucleons and electrons. This allows us to specify the problem in a way that is consistent with the requirements for the nuclear part of the calculation. However, the wavefunctions and matrix elements that result initially are far too complicated to work with for the condensed matter part of the problem. The idea is to subsequently reduce the problem into a form suitable for condensed matter calculations by using successive transformations.

We illustrated this in a formal example involving a phonon exchange matrix element. From this example, we see that the nucleon-electron starting place does indeed provide for a suitable starting point for a nuclear calculation. If the strong force is involved, then we need fully antisymmetric nucleon wavefunctions expressed in terms of nucleon variables, and the formalism outlined here provides for this. The utility of the approach for the condensed matter part of the problem is that it allows for a well-defined foundation that can be used as a starting point for approximations and transformations commonly used in condensed matter calculations. In the end, the formalism allows us to see explicitly how mixing between phonon modes and internal nuclear coordinates come about.

Limitations imposed on the conference proceedings restrict us from any detailed consideration of other problems, but it should be clear that we can apply the method generally to problems that have arisen within the field. Should we wish to describe condensed matter screening effects in the same computation with deuteron-deuteron fusion reactions, the formulation outlined here can handle the problem systematically. If we are interested in coupling nuclear reactions with plasmon mode excitation, then we can start from the same place, but make different approximations and transformations to obtain a formula for a matrix element in a form suitable for computation.

References

1. P. L. Hagelstein, M. Melich, and R. Johnson, this proceedings.
2. B. D. Serot, J. D. Walecka, *Int. J. Modern Physics*, **6** 515 (1997).
3. R. Machleidt, *Advances in Nuclear Physics* **19** 189 (1989).
4. T. Hamada and I. D. Johnston, *Nucl. Phys.* **34** 382 (1962).
5. R. B. Wiringa, R. A. Smith, and T. L. Ainsworth, *Phys. Rev. C* **29** 1207 (1984).
6. R. Machleidt, F. Sammarruca, and Y. Song, *Phys. Rev. C* **53** R1483 (1996).
7. R. Machleidt, *Phys. Rev. C* **63** 024001 (2001).
8. G. Derrick and J. M. Blatt, *Nuclear Physics* **8** 310 (1958).
9. P. L. Hagelstein and I. U. Chaudhary, LANL ArXiV:cond-mat/0606585v2.
10. F. Duschinsky, *Acta Physicochimica* **7** 551 (1937).
11. T. E. Sharp and H. M. Rosenstock, *J. Chem. Phys.* **41** 3453 (1964).

Theory of Low-Energy Deuterium Fusion in Micro/Nano-Scale Metal Grains and Particles

Yeong E. Kim
Purdue Nuclear and Many-Body Theory Group (PNMBTG)
Department of Physics, Purdue University
West Lafayette, IN 47907, USA

Abstract

A consistent conventional theoretical description is presented for anomalous low-energy deuterium nuclear fusion in micro/nano-scale metal grains and particles. The theory is based on the Bose-Einstein condensate (BEC) state occupied by deuterons trapped in a micro/nano-scale metal grain or particle. The theory is capable of explaining most of the experimentally observed results and also provides theoretical predictions. Experimental tests of theoretical predictions are proposed. Scalabilities of the observed effects are discussed based on theoretical predictions.

1. Introduction

The conventional deuterium fusion in free space proceeds via the following nuclear reactions:

{1} D+D→p(3.02 MeV) + T (1.01 MeV);
{2} D+D→n(2.45 MeV)+^{3}He(0.82 MeV); and
{3} D+D→^{4}He+γ(23.8 MeV).

The cross-sections (or reaction rates) for reactions {1} – {3} have been measured by beam experiments at intermediate energies (≥10 keV), and are expected to be extremely small at low energies (≤ 10 eV) due to the Gamow factor arising from Coulomb barrier between two deuterons. The measured cross-sections have branching ratios: (σ{1}, σ{2}, σ{3}) ≈ (1, 1, 10^{-6}).

From many experimental measurements by Fleischmann and Pons in 1989, and many others over 19 years since then [1], including the recent work by Szpak, Mosier-Boss, and Gordon [2] and the most recent work by Arata and Zhang [3], the following fact has been established. At ambient temperatures or low energies (≤ 10 eV), deuterium fusion in metal proceeds via the following reactions:

{4}D(m) + D(m)→p(m) + T(m) + 4.03 MeV (m);
{5} D(m) + D(m)→n(m) + ^{3}He(m) + 3.27 MeV (m); and
{6} D(m) + D(m)→^{4}He(m) + 23.8 MeV (m),

where m represents a host metal lattice or metal particle. Reaction rate R for {6} is dominant over reaction rates for {4} and {5}, i.e., R{6} >> R{4} and R{6} >> R{5}. Additional

experimental observations include requirements of both higher deuteron loading (D/Pd ≥1) and deuterium purity (H/D << 1), the phenomenon of "heat after death", and enhancement of the effect by electromagnetic fields and laser stimulation. In this paper, a consistent conventional theoretical description is presented for explaining the above observations of deuterium nuclear fusion in micro/nano-scale metal grains and particles. The theory presented in this paper is capable of explaining the above observations, and provides theoretical predictions which can be tested experimentally for the confirmation of the theory.

In the following, a detailed description of the theoretical explanation, based on the theory of Bose-Einstein condensation nuclear fusion (BECNF) [4-7] and on selection rules recently derived for a mixed system of two species [8], will be presented along with suggested experimental tests of predictions of the theory and a discussion of the scalability of the fusion rates based on the theory.

2. Theory of Bose-Einstein Condensation Nuclear Fusion (BECNF)

Bose-Einstein condensation (BEC) mechanism: The concept of the Bose-Einstein condensation (BEC) [9] has been known for 84 years (since 1924), and has been used to describe all physical scales, including liquid ^{4}He, excitons in semiconductors, pions and kaons in dense nuclear matter (neutron stars, supernovae), and elementary particles [10]. It is only 13 years ago in 1995 that the BEC phenomenon was observed directly in dilute vapors of alkali atoms, such as rubidium [11], lithium [12], and sodium [13] confined in magnetic traps and cooled down to nano Kelvin temperatures.

In the atomic BEC case [11], the BEC state was created by cooling dilute Rb atoms loaded into a magnetic confinement potential at 300 K. It was cooled by laser cooling (Doppler cooling) to ~ 90 μK (4 x 10^6 atoms) with a density of 2 x 10^{10} atoms/cm^3. Further cooling was accomplished by evaporation cooling removing energetic atoms to 170 nK. At 170nK, it consists of 2000 atoms at a number density of 2.6 x 10^{12}/cm^3 in BEC state (near zero velocity) while other 2 x 10^4 atoms in the trap had a Maxwell-Boltzmann (MB) velocity distribution with a exponential tail characteristic of T ≈ 170nK. The requirement for BEC, $\lambda_{db} > d$, is satisfied, where λ_{db} is the de Broglie wavelength and d is interatomic spacing distance.

In our nuclear BEC phenomenon, we have deuteron number density of ~ 6.8 x 10^{22}cm^{-3} in metal, corresponding to an average separation distance of d ≈ 2.45 Å between deuterons. In order to achieve the nuclear BEC state of deuterons in metal, we need to have the average deuteron kinetic energy T_d smaller than $T_d^c = 0.0063$ eV, i.e. $T_d < T_d^c$, in order to satisfy the requirement $\lambda_{db} > d$.

The MB distribution is originally derived for weakly interacting dilute gas (ideal gas). For strongly interacting and dense systems such as mobile deuterons in metal, the MB distribution is not applicable and hence average deuteron kinetic energy of kT = 0.026 eV at T = 300 K is not applicable for deuterons in metal.

Mobility of deuterons in a metal is a complex phenomenon and may involve a number of different processes [14]: coherent tunneling, incoherent hopping, phonon-assisted processes, thermally activated tunneling, and over-barrier jump/fluid like motion at higher temperatures.

If mobile deuterons in a metal are confined by a confining potential provided by metal atoms and electrons, it may be possible that deuteron momentum or velocity distribution in a metal may have the average deuteron kinetic energy smaller than $T_d^c = 0.0063$ eV, thus satisfying $\lambda_{db} > d$. We note that $T_d^c = 0.0063$ eV corresponds to the average deuteron velocity of $v_c = 0.78 \times 10^5$ cm/sec while the average deuteron kinetic energy of kT = 0.026 eV with T = 300 K corresponds to the average deuteron velocity of $v_k = 1.6 \times 10^5$ cm/sec. Boundaries for micro/nano-scale metal grains and particles can act as barriers and may slow down mobile deuterons resulting in lower average velocity $v < v_c$ and smaller average kinetic energy $T_d < T_d^c$ near boundaries. Therefore, it may be possible that the conditions, $T_d < T_d^c$ and $\lambda_{db} > d$, are achieved for mobile deuterons in localized regions of the metal without cooling as done in the atomic BEC case, and hence, it may be possible to observe experimentally the effects of the nuclear BEC.

Mobility of proton and deuteron in metals: It is well know that the hydrogen ions are highly mobile within metal hydrides [14,15]. Hydrogen mobility takes various temperature dependent forms. The mobility extends to "fluid like" motion at temperatures comparable to the interstitial site or self-trapping, binding energy ~ 0.15 eV. At higher temperatures below the melting point, hydrogen ions no longer remain within the potential wells of interstitial sites but undergo free motion similar to the motion of atoms in gases [14]. It is expected that the mobility of hydrogen ions (or deuterium ions) will increase, as the loading ratio H/metal (or D/metal) of hydrogen atoms (or deuterium atoms) increases and becomes larger than one, H/metal ≥ 1 (or D/metal ≥ 1).

Theoretical formulation for single species case: For applying the concept of the BEC mechanism to deuterium fusion in a nano-scale metal particle, we consider *N* identical charged Bose nuclei (deuterons) confined in an ion trap (or a metal grain or particle). Some fraction of trapped deuterons are assumed to be mobile as discussed above. For simplicity, we assume an isotropic harmonic potential for the ion trap to obtain order of magnitude estimates of fusion reaction rates. N-body Schroedinger equation for the system is given by

$$H\Psi = E\Psi \tag{1}$$

with the Hamiltonian H for the system given by

$$H = \frac{\hbar^2}{2m}\sum_{i=1}^{N}\Delta_i + \frac{1}{2}m\omega^2\sum_{i=1}^{N}r_i^2 + \sum_{i<j}\frac{e^2}{|\boldsymbol{r}_i - \boldsymbol{r}_j|} \tag{2}$$

where *m* is the rest mass of the nucleus. The detailed derivations are given elsewhere [5,6,7,16] for obtaining the approximate the ground state solution for Eq. (1) and the approximate theoretical formula for the deuteron-deuteron fusion rate in an ion trap (nano-scale metal particle). The use of an alternative method based on the mean-field theory for bosons (see Appendix in [6]) yields the same result.

Our final theoretical formula for the nuclear fusion rate R_{trap} for a single trap containing N deuterons is given by

$$R_{trap} = \Omega B N \omega^2 \tag{3}$$

$$\text{with } \omega^2 = \sqrt{\frac{3}{4\pi}}\alpha\left(\frac{\hbar c}{m}\right)\frac{N}{\langle r\rangle^3} \tag{4}$$

where $\langle r\rangle$ is the radius of trap/atomic cluster, $\langle r\rangle = \langle \Psi | r | \Psi \rangle$, N is the average number of Bose nuclei in a trap/cluster, and B is given by B=3 Am/(8παħc), with A= $2Sr_B/(\pi\hbar)$, $r_B=\hbar^2/(2\mu e^2)$, and μ=m/2. S is the S-factor for the nuclear fusion reaction between two deuterons. For D(d,p)T and D(d,n)^{3}He reactions, we have S ≈ 55 keV-barn. We expect also S ≈ 55 keV-barn for reaction {6}. Only one unknown parameter is the probability of the BEC ground state occupation, Ω. It may be proportional to $N^{-1/3}$, $\Omega \propto N^{-1/3}$, or to N^{-2}, $\Omega \propto N^{-2}$.

We can rewrite Eq. (3) as

$$R_{trap} = 4\left(3/4\pi\right)^{3/2}\Omega A\frac{N^2}{D_{trap}^3} \propto \Omega\frac{N^2}{D_{trap}^3} \tag{5}$$

where D_{trap} is the average diameter of the trap, $D_{trap} = 2\langle r\rangle$.

The total fusion rate R_t is given by

$$R_t = N_{trap}R_{trap} = \frac{N_D}{N}R_{trap} \propto \Omega\frac{N}{D_{trap}^3} \tag{6}$$

where N_D is the total number of deuterons and $N_{trap} = N_D/N$ is the total number of traps.

Two species case and selection rule: We consider a mixture of two different species of positively charged nuclear particles, labeled 1 and 2, with N_1 and N_2 particles, respectively, both trapped in a micro/nano-scale metal grain or particle. We denote charges and masses as $Z_1 \geq 0$, $Z_2 \geq 0$, and m_1, m_2, respectively. We use the mean-field theory [7,17] for a system of interacting bosons confined in a harmonic potential to derive the following selection rule:

$$\frac{Z_1}{m_1} = \frac{Z_2}{m_2} \tag{7}$$

The detailed derivations are given in reference [8]. We now apply the selection rule, Eq. (7). If we use m as mass number approximately given in units of the nucleon mass, we have [Z_1 (D)/m_1 (D)] = ½, [Z_2 (p)/m_2 (p)] = 1, [Z_2(T)/m_2 (T)] = 1/3, [Z_2 (n)/m_2 (n)] = 0, and [Z_2(^{3}He)/m_2 (^{3}He)] = 2/3.

Since $[Z_1/m_1] \neq [Z_2/m_2]$ for reactions {4} and {5} they are forbidden or suppressed, and fusion reaction rates for reactions {4 and {5} are expected to be small, while reaction {6} is

allowed since $[Z_1/m_1] = [Z_2/m_2]$, and fusion reaction rate is expected to be large for reaction {6}. In summary, we obtain R{6} >> R{4} and R{6} >> R{5}.

3. Theoretical Implications and Predictions

Eqs. (3) and (6) provide an important result that nuclear fusion rates R_{trap} and R_t do not depend on the Gamow factor in contrast to the conventional theory for nuclear fusion in free space. This could provide explanations for overcoming the Coulomb barrier and for the claimed anomalous effects for low-energy nuclear reactions in metals.

This is consistent with the conjecture noted by Dirac [18] and used by Bogolubov [19] that boson creation and annihilation operators can be treated simply as numbers when the ground state occupation number is large. This implies that for large N each charged boson behaves as an independent particle in a common average background potential and the Coulomb interaction between two charged bosons is suppressed.

For a single trap (or metal particle) containing N deuterons, the deuteron-deuteron fusion can proceed with the following three reaction channels.

$$\begin{aligned}\psi_{BEC}\{(N-2)D's+(D+D)\} &\rightarrow \psi^*\{^4He+(N-2)D's\} \quad (Q=23.84\,MeV)\\ &\psi^*\{T+p+(N-2)D's\} \quad (Q=4.03\,MeV)\\ &\psi^*\{^3He+n+(N-2)D's\} \quad (Q=3.27\,MeV)\end{aligned}$$

where ψ_{BEC} is the Bose-Einstein condensate ground state (a coherent quantum state) with N deuterons and ψ^* are final excited continuum states. Excess energy (Q value) is absorbed by the BEC state and shared by (N-2) deuterons and reaction products in the final state.

We now consider the total momentum conservation. The initial total momentum of the initial BEC state with N deuterons (denoted as D^N) is given by $\vec{P}_{D^N} \approx 0$. Because of the total momentum conservation, the final total momenta for reactions {4}, {5}, and {6} are given by

$$\begin{aligned}&\{4\} \quad \vec{P}_{D^{N-2}pT} \approx 0,\ \langle T_D\rangle \approx \langle T_p\rangle \approx \langle T_T\rangle \approx Q\{4\}/N\\ &\{5\} \quad \vec{P}_{D^{N-2}n^3He} \approx 0,\ \langle T_D\rangle \approx \langle T_n\rangle \approx \langle T_{^3He}\rangle \approx Q\{5\}/N\\ &\{6\} \quad \vec{P}_{D^{N-2}\,^4He} \approx 0,\ \langle T_D\rangle \approx \langle T_{^4He}\rangle \approx Q\{6\}/N\end{aligned}$$

where T represents the kinetic energy.

For a micro-scale metal grain confined by grain boundaries of ~ 1μm diameter, we expect to have $N \approx 10^{10}$ and $Q\{6\}/N \approx 10^{-3} \sim 10^{-4}$ eV, and hence we expect the excess heat and ^{4}He production due to reaction {6} but no nuclear ashes from some of the reactions described below in section 4.

For nano-scale metal particles, the above consideration shows that excess energies (Q) lead to a micro/nano-scale fire-work type explosion, creating a crater/cavity and a hot spot with fire-work like star tracks. The size of a crater/cavity will depend on number of neighboring Pd nanoparticles participating in BEC fusion almost simultaneously. Since sizes of deuteron and Pd nucleus are of the order of $\sim 10^{-4}$ Å (~ 10 fm) while the average distance between two

neighboring Pd atoms is ~ 2.5 Å , ~ 10 keV deuteron from the BEC deuterium fusion encounters mostly electrons and transfers its kinetic energy to electrons. Occasionally, ~ 10 keV deuteron may interact with Pd nucleus to initiate nuclear reactions, Pd(d,p)Rh, etc. When the BEC deuterium fusion takes place in a Pd nanoparticle, exploding deuterons are expected to damage and leave the host Pd nanoparticle, but some of the Pd nanoparticles may remain intact and may participate again in the BEC deuterium fusion after absorbing again a sufficient number of deuterons, D/Pd ≥ 1.

4. Further Consequences of BEC Mechanism and of Selection Rule

Effects due to deuterons: Deuterons with Q{6}/N ≈ ~10 keV energy from reaction {6} can undergo reactions {1} and {2} producing p(3.02 MeV), T(1.01 MeV), n(2.45 MeV), and ^{3}He(0.82 MeV), which in turn will proceed with further reactions.

Tritons produced by reaction {1} (1.01 MeV triton) and by reaction {4} (average kinetic energy of Q{4}/N ≈ ~keV) will interact with surrounding deuterons via the following reaction

{7} T + D → ^{4}He(3.52 MeV) + n (14.07 MeV).

Because of triton kinetic energies of 1.01 MeV or ~ keV, the reaction rate for {7} could be large enough to produce 14.07 MeV neutrons, which may have been recently observed by Forsley and Mosier-Boss [20]. We note that ^{4}He produced by reaction {7} has much higher kinetic energy (3.52 MeV) compared with deuterons from reaction {6} (Q{6}/N ≈ ~10 keV).

Effects due to neutrons: Neutrons with 2.45 MeV kinetic energy from reaction {2}, neutrons with Q{5}/N ≈ ~ keV kinetic energy from reaction {5}, or neutrons with 14.07 MeV kinetic energy from reaction {7} can undergo further reactions, {8} and/or {9} below:

{8} n + D →T + γ + 6.26 MeV

{9} Neutron induced transmutation with other nuclei.

In addition, 14.07 MeV neutrons from reaction {7} may initiate reactions, ^{12}C(n,n')3 ^{4}He and ^{12}C(n,n'α)^{8}Be(^{8}Be→2^{4}He), which may have been recently observed by Mosier-Boss et al. [21].

Since reaction {8} produces more tritiums than neutrons, we expect R(T) > R(n), and also R (T) > R(^{3}He).

High deuterium loading requirement: D/Pd ≥ 1 is required for sustaining deuteron mobility in Pd metal. The mobility of deuterons is required for the BEC mechanism.

Deuterium purity requirement: Because of violation of the selection rule, $[Z_1(D)/m_1(D)] \neq [Z_2(p)/m_2(p)]$, presence of hydrogens in deuteriums will surpress the formation of the BEC states, thus diminishing the fusion rate due to the BEC mechanism. The required H/D ratio is expected to be $H/D < N^{-1}$. For a 5 nm Pd nanoparticle with $N \approx 10^4$, $H/D < 10^{-4}$, and hence 99.99 % deuterium purity is required.

Heat after death: There have been observations of continued heat generation after the input for experiment is switched off. This effect is known as “heat after death”. Because of mobility of deuterons in Pd particle traps, a system of ~ 10^{22} deuterons contained in ~ 10^{18} Pd particle

traps (in 3g of Pd particles with average particle diameter of ~ 50 Å) is a dynamical system. BEC states are continuously attained in a small fraction of the ~ 10^{18} Pd particle traps and undergo BEC fusion processes, until the formation of the BEC state ceases or becomes negligible.

Enhancement by electromagnetic fields and laser stimulation: Application of electromagnetic fields [2] and laser stimulation [22] have been shown to enhance the excess heat production and other anomalous effects. These effects may be due to a decrease of the average kinetic energy of mobile deuterons and/or to an increase of mobile deuterons participating in the BEC fusion processes.

Increase of resistance: When the BECNF occurs, more mobile deuterons will be created. This in turn will increase the resistance of metal. This effect may have been recently observed by Celani et al. in deuterium gas loading experiments with Pd nanoparticles coated on a Pd wire [23].

5. Experimental Tests of Theoretical Predictions

The first experimental test of the BEC mechanism for deuterium fusion with nano-scale Pd particles was carried out with Pd blacks loaded by high-pressure deuterium gas [16]. The result of this experiment shows no excess heat production. This may be due to the fact that Pd nanoparticles (Pd Blacks) used had too large sizes (80 nm – 180 nm) and were clumped together (not isolated). Furthermore, deuterium purity requirement was not satisfied. The recent report of deuteron gas-loading experiment by Arata and Zhang [3] show positive results of observing excess heat and ^{4}He production using ~ 5 nm Pd particles imbedded in ZrO_2 and purified deuterium. For experimental tests of the predictions of the theory, it would be advantageous scientifically to use samples of Pd nanoparticles deposited on thin films such as Al_2O_3/NiAl(111) [24-26], even though bulk materials such as Pd nanoparticles imbedded in SiO_2 aerogels [27] are more suitable for practical applications. Other possibilities are to use other metals such as Zr or Ti nanoparticles. In all cases, the theory requires that metal nanoparticles and micrograins are to be separated from each other by boundaries.

Tests based on the average size of metal particles: From Eq. (6) with $N=N_D(\pi/6)\,D_{trap}^3$, we obtain $R_t(D_{trap}) \propto D_{trap}^{-1}$ or D_{trap}^{-6}, where D_{trap} is the average trap diameter, assuming $\Omega \propto N^{-1/3}$ or N^{-2}, respectively. This can be tested experimentally. This result provides a theoretical justification for using 50 Å Pd nanoparticles to maximize the total fusion rates.

Tests based on the temperature dependence: Since the probability Ω of the BEC ground state occupation increases at lower temperatures ($\Omega \approx 1$ near $T \approx 0$), the total fusion rate R_t will increase at lower temperatures, $R_t(T_{low}) > R_t(T_{high})$. However, R_t is proportional to N_D where N_D is the total number of mobile deuterons. Since $N_D(T_{low}) < N_D(T_{high})$, we expect $R_t[N_D(T_{low})] < R_t[N_D(T_{high})]$. The above opposite temperature dependences for R_t will complicate analysis of the temperature dependence of R_t.

Tests for reaction products and heat after death: Some examples of this type of tests are (1) to look for micro/nano-scale craters/cavities and hot spots with micro/nano-scale fire-work like

star tracks at Pd nanoparticle sites, before and after death, and (2) to measure neutron energies to check the reaction products carries kinetic energies of 2.45 MeV from the secondary reaction {2}, and $Q\{5\}/N \approx \sim \text{keV}$ from reaction {5}.

Tests for increase of resistance: Resistance of the metal should be measured to test predicted increase of resistance during the BECNF process.

Tests for scalability: One example is a scalability test based on the total number of $N_{traps.}$ Since we have $R_t \propto N_{trap}$ $R_{trap} \propto N_{trap}$ for the same R_{trap}, we have theoretical prediction, $R_t(\text{30g Pd particles}) / R_t(\text{3g Pd particles}) \approx 10$, etc., which can be tested experimentally.

6. Conclusion and Summary

Theory of the BEC mechanism described in this paper provides a consistent conventional theoretical description of the results of many experimental works started by Fleischmann and Pons in 1989 and by many others since then [1], including the recent work of Szpak, Mosier-Boss, and Gordon [2] and the most recent work of Arata and Zhang [3]. Theory is based on the concept of nuclear Bose-Einstein condensate state for mobile deuterons trapped in a micro/nano-scale metal grain or particle, which acts as a confinement or trapping potential, similar to a magnetic trap used to observe the atomic BEC phenomenon with atoms in 1995 [11-13]. To validate this new concept of the nuclear BEC phenomenon, experimental tests for a set of key theoretical predictions are proposed. Scalabilities of the observed effects are also discussed.

References

1. P.L. Hagelstein et al., "New Physical Effects in Metal Deuterides", Proceedings of ICCF-11 (Marseille, France, 2004), Condensed Matter Nuclear Science, pp. 23-59, World Scientific Publishing Co., Singapore (2006) and references therein.
2. S. Szpak, P.A. Mosier-Boss, and F.E. Gordon, Proceedings of ICCF-11, Condensed Matter Nuclear Science, pp. 359-373 World Scientific Publishing Co., Singapore (2006); S. Szpak, et al., Proceedings of ICCF-14 (2008); S. Szpak, P.A. Mosier-Boss, and J.J. Smith, Physics Letters A **210,** 382-390 (1996); S. Szpak, P.A. Mosier-Boss, and R.D. Boss, Fusion Technology **33,** 38-51 (1998); P.A. Mosier-Boss and S. Szpak, Nuovo Cimento Soc. Ital. Fis. A **112,** 577 (1999); S. Szpak, P.A. Mosier-Boss, C. Young and F.E. Gordon, Naturwissenschaften **92**, 394-397 (2005)
3. Y. Arata and Y.C. Zhang, J. High Temp. Soc **34** (2), 85 (2008)
4. Y. E. Kim and A.L. Zubarev, Proceedings of ICCF-7, 186 (1998)
5. Y.E. Kim and A.L. Zubarev, "Nuclear Fusion for Bose Nuclei Confined in Ion Traps", Fusion Technology **37**, 151 (2000)
6. Y.E. Kim and A.L. Zubarev, "Ultra Low-Energy Nuclear Fusion of Bose Nuclei in Nano-Scale Ion Traps", Italian Physical Society Proceedings (ICCF-8) **70**, 375 (2000)
7. Y.E. Kim and A.L. Zubarev, Physical Review A**64**, 013603 (2001); A**66**, 053602 (2002)
8. Y.E. Kim and A.L. Zubarev, Proceedings of ICCF-11, Condensed Matter Nuclear Science, pp. 711-717, World Scientific Publishing Co., Singapore (2006)

9. S.N. Bose, Z. Phys. **26**, 178 (1924); A. Einstein, Sitz. Preuss Akad. Wiss. **1924**, 3 (1924)
10. A. Griffin, et al., *Bose-Einstein Condensation*, Cambridge, New York, NY (1995)
11. M.H. Anderson, et al., Science **269**, 198 (1995)
12. C.C. Bradley, et al., Phys. Rev. Lett. **75**, 1687 (1995)
13. K.B. Davis, et al., Phys. Rev. Lett. **75**, 3969 (1995)
14. Y. Fukai, *The Metal-Hydrogen System*, Second Edition, Springer Berlin Heidelberg New York (2005)
15. Q.M. Barer, *Diffusion in and through Solids*, Cambridge University Press, New York, NY (1941)
16. Y.E. Kim, D.S. Koltick, R. Pringer, J. Myers, and R. Koltick, Proceedings of ICCF-10 (Massachusetts, USA, 2003), Condensed Matter Nuclear Science, pp. 789-799, World Scientific Publishing Co., Singapore (2006)
17. B.D. Esry, Phys. Rev. A **55**, 1147 (1997)
18. P.A.M. Dirac, *The Principles of Quantum Mechanics*, second edition, Clarendon Press, Oxford 1935, Chapter XI, Section 62.
19. N. Bogolubov, "On the Theory of Superfluidity", Journal of Physics **11**, 23 (1966)
20. P.A.Mosier-Boss,et al., Naturwissenschaften, DOI 10.1007/s 00114-008-0449-x, Supplemental Material
21. P.A. Mosier-Boss, et al., Naturwissenschaften, DOI 10.1007/s 00114-008-0449-x
22. D. Letts and D. Craven, Proceedings of ICCF-11, pp. 159-170 (2006)
23. F. Celani, et al., Proceedings of ICCF-14 (2008)
24. K.H. Hansen et al., Phys. Rev. Lett. **83**, 4120 (1999)
25. Sh. Shaikhutdinov, et al., Surf. Sci. **501**, 270 (2002)
26. M. Morkel, G. Rupprechter, and H.-J. Freund, Surf. Sci. **588**, L209 (2005)
27. Y.E. Kim, et al., Proceedings of ICCF-11, Condensed Matter Nuclear Science, pp. 703-710, World Science Publishing Co., Singapore (2006)

Complexity in the Cold Fusion Phenomenon

Hideo Kozima
Cold Fusion Research Laboratory
597-16 Yatsu, Aoi, Shizuoka, 421-1202 Japan

Abstract

Based on the similarity between cold fusion (CF) materials and such systems as cellular automata and a set of recursion relations that occur in phenomena characterized by complexity, we show that typical experimental data sets obtained in the cold fusion phenomenon (CFP) are qualitatively explained using concepts of complexity. Using the adjustable parameter n_n introduced in the Trapped-Neutron Catalyzed Fusion model for the CFP, as a parameter specifying a set of recursion relations, classic experimental data sets such as those by Fleischmann et al. (1989), De Ninno et al. (1989), and McKubre et al. (1993) have been reexamined as typical examples showing some phases of the CFP related with complexity. Thus, we have to expect only qualitative or statistical reproducibility in the CFP and the controversial questions such as quantitative reproducibility and controllability of events in the CFP should be considered meaningless.

1. Introduction

It is well known now that complex dynamical systems consisting of many interacting components (sub-units or agents) exhibit behavior called complexity [1, 2] that is interesting but at the same time is not an obvious consequence of the known interaction among the agents. The complexity includes such phenomena as (1) emergence, which refers to the appearance of laws, patterns or order through the cooperative effects of the agents, (2) fractals, complex geometric shapes with fine structure at arbitrarily small scales [3] and (3) power-laws, the average frequency of a given size of event is inversely proportional to some power (close to 1) of its size [4] in out-of-equilibrium states, and (4) chaos, which appears in a property of some non-linear dynamical systems showing extreme sensitivity to initial conditions and long-term aperiodic behavior that seems unpredictable [5].

The cold fusion phenomenon (CFP) in CMNS (condensed matter nuclear science) or SSNP (solid-state nuclear physics) including various events occurs automatically or induced by external effects in various complex systems consisting of many interacting components (agents) in various manners [6, 7]. The external effects include thermal neutrons, electric field, temperature change, irradiation of laser or charged particle beam, etc.

The relation between the complexity and the CFP has been explored in our works [6, 8]. There are several features of the CFP corresponding to characteristics of the complexity such as the inverse-power relation, the bifurcation and chaos; thus, we can understand that the CFP is a phenomenon characterized by nonlinear interactions between multi-component agents in the

system composed of host nuclei and hydrogen isotopes both in periodic arrays and in ambient thermal neutrons.

In this paper, we investigate qualitatively further relations between mathematical models of complexity and the CFP. It is shown that the cellular automaton and a set of recursion equations have common characteristics with CF materials where the CFP occurs. The mathematical tools used in these mathematical models could be used in investigation of events in corresponding events of the CFP.

2. Complexity in Systems with Nonlinear Interactions between Components

2.1 The Cellular Automata and the CFP

A very interesting situation arises in systems consisting of a lattice of identical boolean components interacting locally in space. Such dynamic systems are referred to as cellular automata [1, §3.12]. A factor in the CFP closely related to the cellular automata is the occupation number of hydrogen isotopes in a host lattice if we assume the latter is perfect. The occupation number $X(\boldsymbol{r}_{i\,;}\, t)$ of D or H (D/H) at a site $\boldsymbol{r}_i \equiv (x_{i,} y_i, z_i)$ and a time t satisfies the following relation:

$$X(\boldsymbol{r}_{i\,;}\, t+1) \equiv X(x_{i,} y_i, z_{i\,;}\, t+1) = F_i\,(\{X(\boldsymbol{r}_{j\,;}\, t)\}) \tag{2.1.1}$$

where $\{X(\boldsymbol{r}_j\,;\, t)\}$ is a set of values $X(\boldsymbol{r}_{j\,;}\, t)$ for $\boldsymbol{r}_j$ adjacent to $\boldsymbol{r}_i$ and $F_i(\{X(\boldsymbol{r}_{j\,;}\, t)\}) \equiv F_i$ is a function characterizing the change of the occupation number of D/H at $\boldsymbol{r}_i$ by processes in the system such as (1) diffusion of D/H and (2) consumption of D/H by nuclear reactions $n + d = t + \phi$, $n + p = d + \phi$ and so forth (ϕ means phonons in these equations).

The function F_i is therefore a function of the parameter n_n (number density of thermal neutrons in the CF material) of the Trapped-Neutron Catalyzed Fusion model if we use the model to describe the CFP.

2.2 Recursion relations and the CFP

Recursion equations $x_{n+1} = \lambda\, f(x_n)$ have been investigated in nonlinear dynamics for its usefulness to describe a variety of problems [9]. From our point of view, it is interesting to notice that a few experimental data obtained in the CFP seems to have characteristics of the type seen in recursion equations, which suggests complexity in the CFP.

2.2.1 Recursion Relations

The recursion relations

$$x_{n+1} = \lambda\, f(x_n), \tag{2.2.1}$$

which have been well investigated in nonlinear dynamics, have interesting characteristics, as shown by Feigenbaum [9]. A large class of recursion relations (2.2.1) exhibiting infinite bifurcation possesses a rich quantitative structure – essentially independent of the recursion functions $f(x)$ – when they have a unique differentiable maximum $\underline{x}$. With $f(\underline{x}) - f(x) \sim |x - \underline{x}|^z$ (for $|x - \underline{x}|$ sufficiently small) and $z > 1$, the universal details depend only upon z. In particular,

the local structure of high-order stability sets is shown to approach universality rescaling in successive bifurcations, asymptotically by the ratio α (α = 2.5029078750957… for z = 2) [9].

We can investigate the CFP from the point of view described by the recursion relations (2.2.1). The cold fusion phenomenon (CFP) contains events related to nuclear reactions accompanying excess energy production. In these events, we have experimentally determined parameters governing the occurrence of the CFP such as the loading ratio η (=D/Pd, H/Ni, etc.), temperature T, current density i to the cathode in electrolytic and discharge systems, etc. The events also show a characteristic of the recursion relations (2.2.1).

2.2.2 Structure of the Population (Density) Equation

The recursion equations (2.2.1) provide a description for a variety of problems. For example, a discrete population (density) satisfies the formula

$$p_{n+1} = f(p_n), \tag{2.2.2}$$

which determines the population (density) at one time in terms of its previous value [9].

The events we observe in the CFP seem to belong to this type of quantities obeying the relations (2.2.1) as we have partly shown in recent works [8].

If the population (or density) referred to is such that of a dilute group of organisms (or agents e.g. the density of trapped neutrons n_n in the CFP), then the population (density) equations,

$$p_{n+1} = b\, p_n, \tag{2.2.3}$$

accurately describe the population (density) growth with a growth rate b so long as it remains dilute, with the solution of the equation

$$p_n = p_0\, b^n. \tag{2.2.4}$$

For a given species of organism (agent) in a fixed milieu, b is a constant – the static birth rate for the configuration.

As the population grows, the dilute approximation will ultimately fail: sufficient organisms (agents) are present and mutually interfere. At this point, the next value of the population (density) will be determined by a dynamic or effective birth rate b_{eff}:

$$p_{n+1} = b_{\text{eff}}\, p_n \tag{2.2.5}$$

with $b_{\text{eff}} < b$. Clearly, b_{eff} is a function of p, with

$$\lim_{p\to 0} b_{\text{eff}}\,(p) = b, \tag{2.2.6}$$

the only model-independent quantitative feature of b_{eff}. It is also clear that

$$\lim_{p\to \infty} b_{\text{eff}}\,(p) = 0. \tag{2.2.7}$$

Accordingly, the simplest form of b_{eff} to reproduce the qualitative dynamics of such a population (density) should resemble Fig. 1, where $b_{\text{eff}}\,(0) = b$ is an adjustable parameter.

A simple specific form of $b_{\text{eff}}(p)$ is written with a constant a;

$$b_{\text{eff}}(p) = b - a\,p, \tag{2.2.8}$$

so that

$$p_{n+1} = b_{\text{eff}}\,p_n - a\,p_n^2.$$

By defining $p_n \equiv (b/a)x_n$, we obtain the standard form of logistic difference equations (l.d.e.)

$$x_{n+1} = b\,x_n\,(1 - x_n). \tag{2.2.9}$$

In (2.2.9), the adjustable parameter b is purely multiplicative. With a different choice of b_{eff}, x_{n+1} would not in general depend upon b in so simple a fashion [9]. Nevertheless, the internal b dependence may be (and often is) sufficiently mild in comparison to the multiplicative dependence that at least for qualitative purposes the internal dependence can be ignored. Thus, with $f(p) = p\,b_{\text{eff}}(p)$, any function like Fig. 1,

$$p_{n+1} = bf(p_n) \tag{2.2.10}$$

is compatible and representative of the population (density) equation discussed in [9].

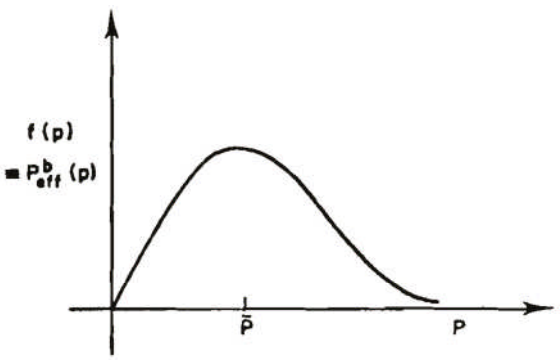

Fig. 1

Figure 1. Dependence of $f(p) = p\,b\text{eff}(p)$ on p after Feigenbaum [9].

To investigate the structure of the population (density) equation (2.2.9), we can use such a study of the l.d.e. as given by J. Gleick [5].

3. Discussion – The Cold Fusion Phenomenon in Composite Systems with Hydrogen Isotopes

As discussed in the preceding two subsections, the CF systems where the CFP occurs have characteristics common with cellular automata and the set of recursion equations which are well investigated mathematically. We discuss further here only the relation of the CFP with cellular automata.

Cellular automata, explained in Section 2.1, have a corresponding structure to the CF systems. In the present situation of analysis of the CFP, it is difficult to determine the exact form of the function F_i in Eq. (2.1.1) for an event in the CFP. A possible investigation of a cellular automaton in the CFP is facilitated on the quantal approach given by us [6 §3.7]. The number of neutrons $n_i(\tau)$ is a function of values of $n_i(\tau')$ and $n_{i'}(\tau')$ where $\tau = \tau' + d\tau'$;

$$n_i(\tau) = f(\nu_{np}(ii'j; \tau')). \tag{3.1.1}$$

Unfortunately, this approach is not complete, and we are far from a position of being able to determine the functional form F_i in Eq. (2.1.1) or f in Eq. (3.1.1) which will be objects of future works.

Acknowledgement

This work is supported by a grant from the New York Community Trust.

References

1. G. Nicolis and I. Prigogine, *Exploring Complexity – An Introduction*, Freeman and Co., New York, 1989. ISBN 0-7167-1859-6.
2. R. Parwani, *Complexity – A Lecture Note*, Posted at National University of Singapore website; http://staff.science.nus.edu.sg/~parwani/c1/node2.html
3. S. H. Strogatz, *Nonlinear Dynamics and Chaos*, Westview, 1994. ISBN-10 0-7382-0453-6, p. 398
4. M. M. Waldrop, *Chaos*, Touchstone, 1992. ISBN 0-671-76789-5. p. 305
5. J. Gleick, *Chaos*, Penguin books, ISBN 0-14-00.9250-1
6. H. Kozima, *The Science of the Cold Fusion Phenomenon*, Elsevier Science, 2006. ISBN-10: 0-08-045110-1.
7. E. Storms, *The Science of Low Energy Nuclear Reaction – A Comprehensive Compilation of Evidence and Explanations about Cold Fusion*, World Scientific, Singapore, 2007. ISBN-10 981-270-620-8
8. H. Kozima, "The Cold Fusion Phenomenon as a Complexity (3) – Characteristics of the Complexity in the CFP" *Proc. JCF8*, pp. 85 – 91 (2008) and also Reports of CFRL (Cold Fusion Research Laboratory), 7-3, pp. 1 – 7 (2007); http://www.geocities.jp/hjrfq930/Papers/paperr/paperr13.pdf
9. M. J. Feigenbaum, "Quantitative Universality for a Class of Nonlinear Transformations" *J. Statistical Physics*, 19, 25 – 52 (1978).

Nuclear Transmutations in Polyethylene (XLPE) Films and Water Tree Generation in Them

Hideo Kozima and Hiroshi Date*
Cold Fusion Research Laboratory (hjrfq930@ybb.ne.jp)
597-16 Yatsu, Aoi, Shizuoka, 421-1202, Japan
**Recruit R&D Staffing Co., Ltd.*

Abstract

An explanation of the nuclear transmutation (NT) observed in XLPE (cross-linked polyethylene) films is presented based on the neutron-drop model used in the theoretical investigation of the cold fusion phenomenon in other cold fusion materials (CF materials); transition-metal hydrides/deuterides. The NT's, K → Ca, Mg → Al, $^{56}_{26}$Fe → $^{57}_{26}$Fe and Fe → Ni, are explained by a single-neutron absorption with or without a succeeding beta-decay to get final nuclides. On the other hand, the NT's, $^{56}_{26}$Fe → $^{64}_{30}$Zn and $^{56}_{26}$Fe → $^{60}_{28}$Ni, are explained by an absorption of a neutron drop $^{8}_{4}\Delta$ and $^{4}_{2}\Delta$, respectively, in the cf-matter formed in CF materials. Production of extraordinary elements Li, Pb and Bi is discussed from our point of view. Thus, we concluded that the generation of water trees in XLPE samples is caused by nuclear reactions induced by cold fusion phenomenon at around spherulites. The NT found in XLPE may have a relation with the NT's found in biological bodies (biotransmutation).

1. Introduction

We have tried to explain the wide-spread experimental facts in the cold fusion phenomenon (CFP) from a unified point of view using a phenomenological models, the trapped neutron catalyzed fusion model (TNCF model) at first [1] and then the neutron-drop model (ND model), a generalized version of the former [2]. It should be remembered here that the development of the model demands an explanation for NT's with large changes of the nucleon and proton numbers observed in the CFP.

In the process of verification of the basic premises of these successful models, we have developed a quantal investigation of the CF materials such as transition metal hydrides/deuterides composed of a host lattice of transition metals and interlaced lattice of interstitial protons/deuterons [3]. It was shown that it is possible for cf-matter to exist when it is composed of neutron drops $^{A}_{Z}\Delta$ with Z protons, Z electrons and $(A - Z)$ neutrons in a dense neutron liquid at boundary /surface regions of the crystals.

Recently, Kumazawa *et al.* [4, 5] observed the nuclear transmutation (NT) in XLPE (closslinked polyethylene) including water trees, and then detected weak mission of gamma or X-rays from similar samples [6]. Their results show, generally speaking, that water trees are formed macroscopically at boundaries of XLPE samples and microscopically at amorphous

portions of the sample among spherulites composed of crystalline lamellae. Use of heavy water instead of light water did not show any positive effect on the occurrence of NT [5]

The NT observed in the XLPE films by Kumazawa *et al.* [4–6] has characteristics in common with CF materials as a part of the CFP. Therefore, it is natural to apply the same model (TNCF model) [1, 2] to explain the NT in XLPE that successfully explained the NT in the CF materials [3].

2. Experimental Facts about Water Tree in Cross-linked Polyethylene (XLPE)

We give an explanation of characteristics of the experimental data sets obtained by Kumazawa *et al.* [4 – 6] in this section.

2.1 Summary of Experimental Data Sets obtained by Kumazawa *et al.*

We can summarize the experimental results obtained by Kumazawa *et al.* [4–6] as follows:

In the experiments, a XLPE (cross-linked polyethylene) sheet 0.5 mm thick was used. Au was deposited as a ground electrode onto the bottom surface of the sample. Then, the sample was dipped in aqueous solutions of electrolytes (a) KCl, (b) NaCl and (c) $AgNO_3$ to make the Blank samples. The Blank samples were placed in the aqueous solutions, and electric fields with high -frequency (2.4–3.0 kHz) and high-voltage (3.0 – 4.0 kV/mm) were applied between the voltage application wire above the sample and the ground electrode for 140 – 320 hours to obtain “the samples after voltage application” (let us call them the Experimental samples, for simplicity). Quantitative analysis of elements were performed for (I) the **Original**, (II) the **Blank** and (III) the **Experimental** samples for three electrolytes (a) **KCl**, (b) **NaCl** and (c) **$AgNO_3$.** In the case (c), there are no data on the blank samples but data on the two distinct regions selected visually (i) **with water trees** and (ii) **without water trees**.

Characteristics in the changes of elements from (I) the Original to (II) the Blank and (III) the Experimental samples were summarized as follows:

In case (a) (KCl),

(1) K decreased and Ca increased,

(2) ^{56}Fe decreased and ^{57}Fe increased,

(3) ^{64}Zn increased while other isotopes of Zn decreased.

In case (b) (NaCl),

(4) Mg decreased and Al increased in which the gross weight of the two elements was hardly different compared to the Blank or the Original samples.

In case (c) ($AgNO_3$),

(5) Fe decreased and Ni increased,

(6) New elements Li, Na, Pb and Bi were detected, and

(7) There are changes of elements in both regions with and without water trees.

Furthermore, there are interesting features of the blank samples (II) in case (a);

(8) In Blank samples, Mg and Ca are increased from those in the Original one while Fe is decreased.

In their second paper, [5] Kumazawa *et al.* reported detection of weak and burst-like radiation, which they assumed was low energy gamma or X-rays. In the CFP, there are a few observations of gamma and X-rays but they are peripheral (cf. Section 6.3 of [1] for the data of gamma ray observation). We concentrate our investigation in this paper to the data reported in the first paper [4].

3. Explanation of Nuclear Transmutation in XLPE by the TNCF Model

3.1 Microscopic Structure of Polyethylene (PE), Lamella and Spherulites in XLPE

The lengths of the C-C and C-H bonds of PE are estimated as 1.54 and 1.09Å, respectively. The carbon chain is composed of tetrahedrally connected carbons with an angle between two C-C bonds of 109.5 degree. A lamella has a lattice structure with ordered carbon nuclei (lattice nuclei) interlaced with ordered protons even when the structure is not so simple, as in the case of transition-metal hydrides/deuterides. The size of spherulites, crystal components of solid polyethylene, also depends on conditions in which the sample is produced and ranges from ≃ 1 μm to ≃ 1 mm, in general. The ratio of portions occupied by crystalline component and amorphous component of a solid PE sample depends also on the conditions.

3.2 Cold Fusion (CF) Matter in XLPE

It is natural to investigate nuclear transmutations observed in XLPE with the same phenomenological approach as that used to analyze the CFP observed in transition-metal hydrides/deuterides as a first step.

We have to notice common factors in transition-metal hydrides/deuterides and XLPE if we take the point of view explained above. First of all, (1) there are crystalline structures of host and hydrogen isotopes in both cases. Second, (2) the reaction products of nuclear transmutations were found localized in boundary or surface regions of crystalline structure in both cases. Third, (3) the neutron affinity we have defined to specify responsibility of nuclides for the CFP [1, 2] is positive (favorable for the CFP) for C (2.22 MeV for $^{6}_{12}$C) in XLPE and Ti (0.602 for $^{22}_{48}$Ti, for instance), Ni (4.80 for $^{28}_{58}$Ni), Pd (2097 for $^{46}_{105}$Pd) in transition-metal hydrides/deuterides. Lattice constants of CF materials are tabulated in Table 1.

Table 1. Lattice constants of host nuclides lattices

Host nuclides	**Lattice constants** (Å)
Ti (*hcp*)	$a = 2.95$, $c = 4.792$
Ni (*fcc*)	$a = 3.52$
Pd (*fcc*)	$a = 3.89$
XLPE (*orthorhombic*)	$a = 7.40$, $b = 4.93$, $c = 2.53$

From our point of view, the super-nuclear interaction between neutrons mediated by protons/deuterons in lattice nuclei (carbon in the case of XLPE), cross-linking in XLPE is decisive; cross-linking protons (covalent bonded to two carbon atoms) mediate the interaction of neutrons in carbon nuclei $^{12}_{6}C$ on adjacent PE chains.

3.3 Explanation of Nuclear Transmutation in XLPE where observed Water Trees

We give explanations of the seven characteristics of the nuclear transmutations (NT) in XLPE giving counterparts in the CFP for reference.

(1) Decrease of K and increase of Ca in the case (a) are explained by such a reaction in the solids by absorption of a neutron followed by beta decay with a liberated energy ΔE = 1.31 MeV;

$$n + {}^{39}_{19}K \rightarrow {}^{40}_{20}K^{*} \rightarrow {}^{40}_{20}Ca + e^{-} + \underline{\nu}_{e,} \ (\sigma_{nK39} = 2.10 \text{ b}) \qquad (3\text{-}1)$$

where $\underline{\nu}_e$ is an electron neutrino. As a measure of the reaction cross-section in solids we cited the value in free space in the parenthesis behind the equation.

(2) Decrease of $^{56}_{26}Fe$ and increase of $^{57}_{26}Fe$ in the case (a) are similarly explained but without beta decay due to the stability of $^{57}_{26}Fe$ with an energy Q = 1.15 keV transferred to the lattice system instead of gamma ray emission in free space;

$$n + {}^{56}_{26}Fe \rightarrow {}^{57}_{26}Fe + Q. \ (\sigma_{nFe56} = 2.81 \text{ b}) \qquad (3\text{-}2)$$

(3) Increase of $^{64}_{30}Zn$ and decrease of $^{66}_{30}Zn$, $^{67}_{30}Zn$ and $^{68}_{30}Zn$ in the case (a) are explained by using the neutron drop $^{A}_{Z}\Delta$, for example;

$$^{56}_{26}Fe + {}^{8}_{4}\Delta \rightarrow {}^{64}_{30}Zn. \qquad (3\text{-}3)$$

The decrease in other isotopes may be explained by nuclear reactions to transform them into other elements but its details are left for another work.

(4) Increase of Al and decrease of Mg in the case (b) are explained by reactions similar to (3-2) with Q = 7.08 MeV and Q' = 12.11 MeV and a reaction similar to (3-1) with ΔE = 2.61 MeV.

$$n + {}^{24}_{12}Mg \rightarrow {}^{25}_{12}Mg + Q. \ (\sigma_{nMg24} = 0.05 \text{ b})$$
$$n + {}^{25}_{12}Mg \rightarrow {}^{26}_{12}Mg + Q'. \ (\sigma_{nMg25} = 0.19 \text{ b})$$
$$n + {}^{26}_{12}Mg \rightarrow {}^{27}_{12}Mg^{*} \rightarrow {}^{27}_{13}Al + e^{-} + \underline{\nu}_{e}. \ (\sigma_{nMg26} = 0.04 \text{ b})$$

(5) Decrease of Fe and increase of Ni in the case (c) are explained similarly with use of the neutron drop, for example;

$$^{56}_{26}Fe + {}^{4}_{2}\Delta \rightarrow {}^{60}_{28}Ni.$$

Thus, we may imagine the following scenario of growth of a water tree: (i) a NT of impurity nuclides occurs at a boundary region heating there by a liberated energy, (ii) a seed of a water tree is induced by the liberated energy, and (iii) the applied high-frequency electric field makes the water tree grow.

The NT's in phenanthrene [7] may have close relation with that in XLPE discussed in this paper.

Acknowledgement

The authors would like to express their thanks to Hiroshi Yamada of Iwate University and Takao Kumazawa of Chubu Electric Power Co. for their valuable discussions on the work by Kumazawa *et al.*

This work is supported by a grant from the New York Community Trust.

References

1. H. Kozima, *Discovery of the Cold Fusion Phenomenon – Evolution of the Solid State-Nuclear Physics and the Energy Crisis in 21st Century*, Ohtake Shuppan KK., Tokyo, Japan, 1998. ISBN 4-87186-044-2 (§10.1 Bio- transmutation)
2. H. Kozima, *The Science of the Cold Fusion Phenomenon*, Elsevier Science, 2006. ISBN-10: 0-08-045110-1.
3. H. Kozima, "Physics of the Cold Fusion Phenomenon" *Proc. ICCF13* (2007, to be published).
4. T. Kumazawa, W. Nakagawa and H. Tsurumaru, "A Study on Behavior of Inorganic Impurities in Water Tree" *Electrical Engineering in Japan* **153**, 1 – 13 (2005). (Experiment with Light Water)
5. T. Kumazawa, W. Nakagawa and H. Tsurumaru, "Experimental Study on Behavior of Bow-tie Tree Generation by Using Heavy Water" (in Japanese) *IEEJ Trans. FM,* **126**, 863 – 868 (2006). (Experiment with Heavy Water)
6. T. Kumazawa and R. Taniguchi, "Detection of Weak Radiation Involving Generation and Progress of Water Tree" (in Japanese) *IEEJ Trans. FM,* **127**, 89 – 96 (2007). (Experiment with Light Soft and Hard Waters)
7. T. Mizuno, K. Kurokawa, K. Azumi, S. Sawada and H. Kozima, "Heat Generation during Hydrogenation of Carbon (Phenanthrene)", *Proc. ICCF14* (to be published).

Exploring a Self-Sustaining Heater without Strong Nuclear Radiation

Xing Z. Li[1], Bin Liu[1], Qing M. Wei[1], Shu X. Zheng[2] and Dong X. Cao[2]
[1] *Dept. of Physics, and* [2]*Dept. of Engineering Physics, Tsinghua University, Beijing, CHINA*

Abstract

The comparison between the new 3-parameter formula and the old 5-paramter formula for five major fusion cross-sections strongly confirms the selective resonant tunneling model which forms the physical basis of a self-sustaining heater without strong nuclear radiation. The development of condensed matter nuclear science is not contrary to all understanding gained of nuclear reactions in the last half century, but instead it improves our knowledge of the nuclear physics of resonant tunneling of the Coulomb barrier. The detection of neutrino emission from metal deuterides is proposed as a decisive step to further develop this model.

1. Introduction

Building a self-sustaining heater without strong nuclear radiation is the fundamental goal of the world-wide research into cold fusion, or condensed matter nuclear science (CMNS). After 19 year we have reached the stage of demonstration (Arata and Zhang's experiment[1]), correlation between the excess heat and the surface features (Violante et al. [2]). We still need an explanation of why there is no strong neutron emission or gamma radiation from CMNS experiments. The study on the nuclear fusion cross-section of the light nuclei just provided such an explanation.

Early in 1972, Duane[3] did a survey on the theory of the nuclear fusion of the light nuclei. He found that there was not enough experimental data to do a detailed study. However, based on the Breit-Wigner formula, he developed a 5-parameter formula to describe the available experimental data. He tried to reduce the number of the parameters, but he found that at least 5 parameters were necessary to fit the cross-sections for major fusion reactions. This 5-parameter formula was adopted in a Handbook of Plasma Formulary edited by Naval Research Laboratory (NRL) in 1978[4]. As a result, this 5-parameter formula has been widely cited in the plasma fusion community. In 1992, Bosch and Hale[5] developed a better 9-parameter formula based on the newly available experimental data and the R-matrix theory for nuclear reactions. Bosch and Hale pointed out that the 5-parameter formula was not correct at the low energy region, because it did not give the right dependence on energy. Nevertheless, this 5-parameter formula is still cited in the Plasma Formulary even in the new edition in 2007[6].

In 1999, an identity was derived for the nuclear fusion cross-section[7]. This new identity clearly showed the resonant effect using a complex quantity: W defined as the cotangent of the phase shift. When the real part of W equals 0, there will be a resonance. When the imaginary part of W equals (-1), the resonant effect will reach its maximum possible. This new identity

explains why there is no neutron emission or gamma radiation accompanied with the "excess heat" in CMNS. We call it selective resonant tunneling theory. In 2008, it was found that the real part of W depended on the incident energy linearly, and the imaginary part of W was almost a constant. This immediately led to a 3-parameter formula for the fusion cross-section of the light nuclei. This new 3-parameter formula gives an even better fit with newly available experimental data than the 5-parameter formula does, because the astrophysical S-function in the 3-parameter formula includes a new term which is directly related to the selectivity of the resonant tunneling[8]. Therefore, the comparison with experimental data has confirmed the existence of the cold fusion phenomenon.

2. 3-parameter formula

The nuclear fusion cross-section may be written as [7]:

$$\sigma(E) = \frac{\pi}{k^2} \frac{(-4W_i)}{W_r^2 + (W_i - 1)^2} \tag{1}$$

if the S-partial wave is dominant. Here, W is related to the phase shift, δ , of the S-partial wave as $W \equiv Cot\delta$. When Coulomb field is applied to describe the repulsion between two charged reactant nuclei, W is the coefficient in the linear combination of the regular and irregular Coulomb wave functions. We have shown that the main dependence of W on energy is in the form of Gamow factor[7,8]:

$$W = \theta^2 w. \tag{2}$$

$$\theta \equiv \sqrt{\frac{Exp[\frac{2\pi}{ka_c}] - 1}{2\pi}}. \tag{3}$$

Here, *k* is the wave number of the interacting particle in the system of mass center; a_c is length of the Coulomb unit. w is defined as the reduced coefficient. $a_c \equiv \frac{4\pi\varepsilon_o\hbar^2}{Z_1 Z_2 e^2 \mu}$. $Z_1 e$ and $Z_2 e$ are the electrical charges of the colliding nuclei, respectively. $\hbar$ is the Planck constant divided by 2 π , μ is the reduce mass, ε_o is the dielectric constant of the vacuum. We found that the real part of this reduced coefficient, *w*, may be written as

$$w_r = C_1 + C_2 E, \tag{4}$$

The imaginary part of *w* may be approximated by a constant. Here, *E* is the kinetic energy of the incident particle in the laboratory system. Consequently, the fusion cross-section may be expressed as a function of 3 parameters (C_1,C_2,and w_i) only,

$$\sigma(E) = \frac{\pi}{k^2} \frac{1}{\theta^2} \frac{(-4w_i)}{w_r^2 + (w_i - \frac{1}{\theta^2})^2} = \frac{\pi}{k^2} \frac{1}{\theta^2} \frac{(-4w_i)}{(C_1 + C_2 E)^2 + (w_i - \frac{1}{\theta^2})^2} \tag{5}$$

The upper row of Fig. 1 shows the results of fitting this 3-parameter formula (5) to the experimental data for D+T, D+^{3}He, and D+D fusion reactions, respectively.

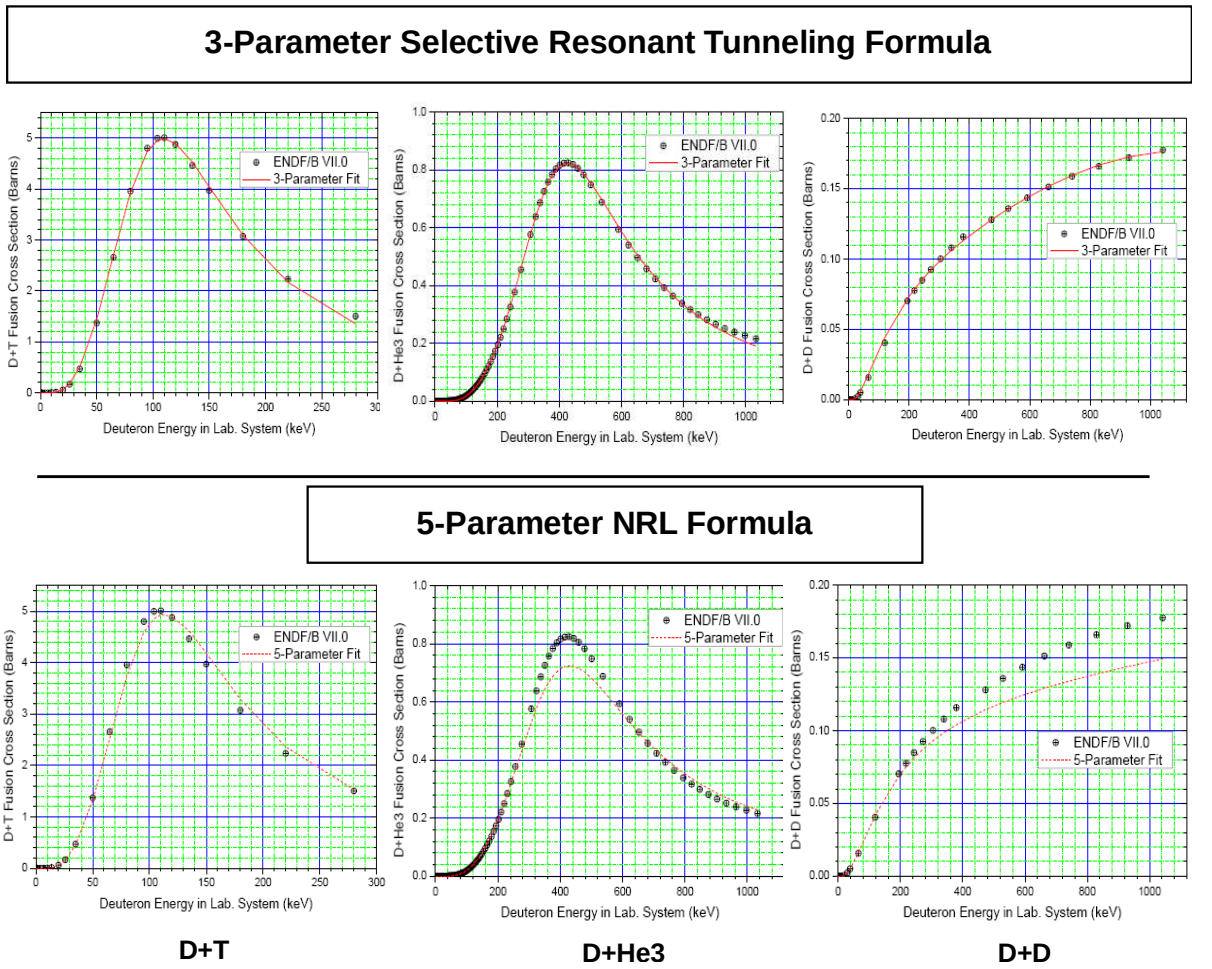

Figure 1. Selective resonant tunneling formula for D+T, D+^{3}He, and D+D

The upper row of Fig. 2 shows the results of fitting this 3-parameter formula (5) to the experimental data for T+T and T+^{3}He fusion. Table I gives the values of three parameters (C_1, C_2, and w_i) for each case. In these figures, the black points are the experimental data from The National Nuclear Data Center (ENDF/B VII.0 [9]). The solid lines are the results of calculation using 3-parameter formula (5). The dotted lines in the lower row of figure 1 and 2 are the results of calculation using the following 5-parameter NRL formula (6) with the parameters (A_1, A_2, A_3, A_4 and A_5) listed in that NRL Plasma Formulary[4,6].

$$\sigma(\boldsymbol{E}) = \frac{1}{\boldsymbol{E}}\left(\frac{1}{\exp[\frac{A_1}{\sqrt{\boldsymbol{E}}}]-1}\right)\left(A_5 + \frac{A_2}{(A_4 - A_3\boldsymbol{E})^2+1}\right) \tag{6}$$

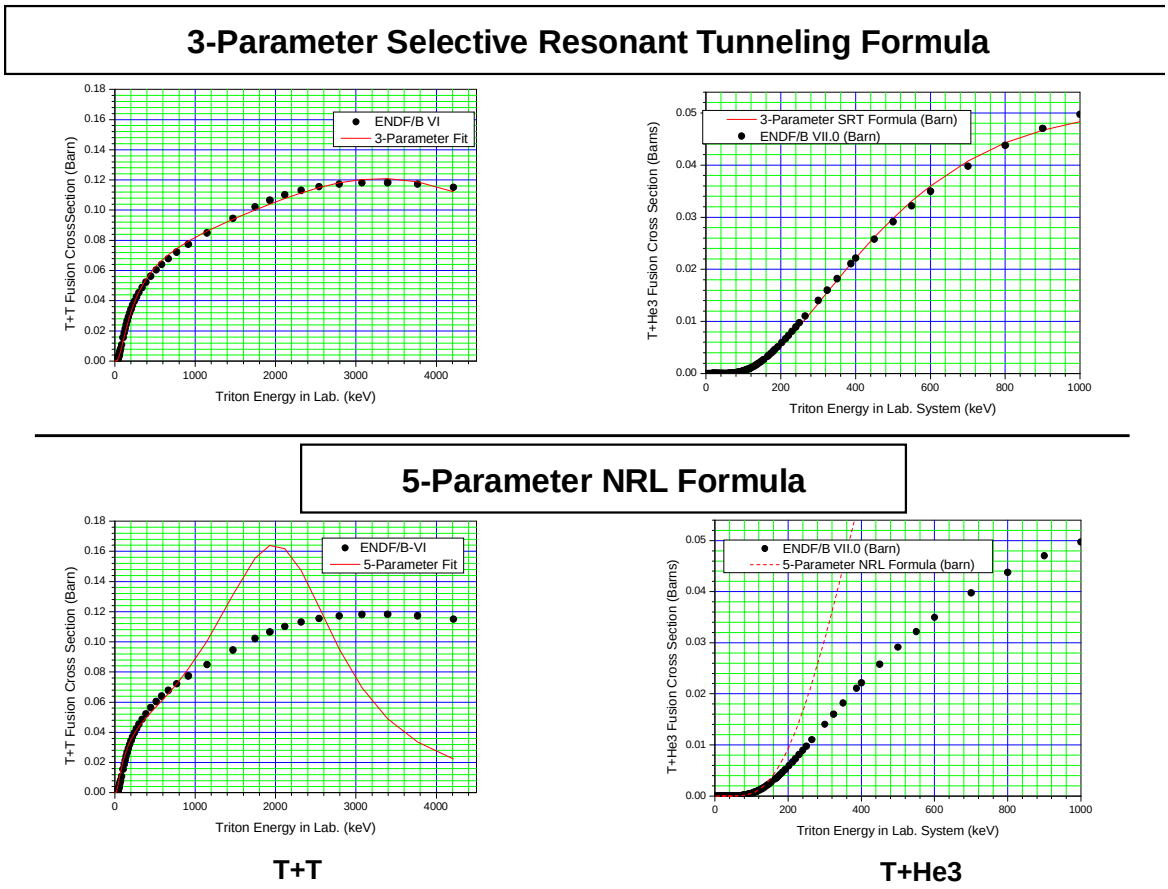

Figure 2. Selective resonant tunneling formula for T+T and T+^{3}He fusion.

Table I. PARAMETER LIST FOR 3-PARAMETER FORMULA

	D+T	D+^{3}He	D+D (p+T&n+^{3}He)	T+T	T+^{3}He
C_1	-0.54168	-1.13575	-60.2913	-36.7805	2.78836
C_2*	0.0055601	0.0030453	0.05068	0.00927803	0.000959464
w_i	-0.39189	-0.67162	-55.0122	-24.5337	-1.04059

*C_2 is in unit of (1/keV) when E in the Eq. (5) is the incident energy in the laboratory system in units of keV.

It is clear that the 5-parameter formula gives a comparable result only in the case of the D+T fusion. In all the other cases, NRL 5-parameter formula is not able to give the right position of the peak and the height of peak of the cross-section. On the other hand, this new 3-parameter formula is able to give the right position and the height of the peak of the cross sections,

because this new 3-parameter formula includes a new term in its denominator with a strong energy dependence: i.e. $(w_i - \frac{1}{\theta^2})^2 = (w_i - \frac{2\pi}{Exp[\frac{2\pi}{ka_c}]-1})^2$.

3. A New Term in the Astrophysical S-function

The astrophysical S-function was introduced in astrophysics and nuclear physics in order to extract the geometric factor, $\frac{\pi}{k^2}$, and the Gamow factor, $\frac{1}{\theta^2}$ from the cross-section. It was thought that the remaining astrophysical S-function is supposed to be a **slowly** varying function to express the **INTRINSIC** nature of the nuclear state. In Duane's 5-parameter formula, only the $(A_4 - A_3\boldsymbol{E})^2$ term shows the resonant nature of the nuclear state. Bosch and Hale attempted to improve the energy-dependence of the astrophysical S-function using 2 polynomials with 9 parameters. In this 3-parameter formula, a new term has been introduced into the denominator of the astrophysical S-function. This new term depends on the energy as **rapidly** as the Gamow factor does. The comparison with the experimental data strongly confirmed that it is important to include this new energy-dependence in the denominator of the astrophysical S-function, and it is not simply an expression of the **INTRINSIC** nature of the nuclear state only(it includes a factor related to Coulomb field outside the nuclear potential well).

4. The Matching of the Channel Width of Energy

In order to see the physical meaning of this new term, we rewrite the cross-section in the form of Breit-Wigner formula.

$$\sigma(E) = \frac{\pi}{k^2}\frac{(\Gamma_a\Gamma_{in})}{(E-E_0)^2 + (\frac{\Gamma_a + \Gamma_{in}}{2})^2}; \quad \text{with} \quad \Gamma_{in} = \frac{2}{\theta^2 C_2}; \quad \Gamma_a = -\frac{2w_i}{C_2}; \quad E_0 = -\frac{C_1}{C_2}. \tag{7}$$

This new term is related to the incident channel width, $\Gamma_{in} = \frac{2}{\theta^2 C_2}$, and the parameter w_i is related to the absorption channel width, $\Gamma_a = -\frac{2w_i}{C_2}$. It is well known that the matching between the incident channel width and the absorption channel width is very important for the resonant tunneling process. When the incident energy, E, approaches the resonant energy, $E_0 = -\frac{C_1}{C_2}$, the cross-section has a peak. The height of the peak depends on the matching strongly. Only if the incident channel width matches the absorption channel width, $\Gamma_a \approx \Gamma_{in}$; then, cross-section of resonance reaches its maximum possible. Otherwise, even if there is a resonance, it might not be observable because of the mismatching between the incident channel width and the absorption channel width($\Gamma_a << \Gamma_{in}$ or $\Gamma_a >> \Gamma_{in}$). In the case of condensed matter nuclear

science, the incident energy is so low that the incident channel width, Γ_{in}, is very narrow. This means that the absorption channel width, Γ_a, must be very narrow in order to observe the resonant tunneling process. Therefore, only the long lifetime resonant state might appear as a result of resonant tunneling at low energy. The neutron emission or gamma radiation could not be the products of the resonant tunneling at low energy because their lifetimes of resonant state are too short to match the incident channel width (i.e. $\Gamma_a >> \Gamma_{in}$). Only the weak interaction process might be involved in low energy resonant tunneling of Coulomb barrier. This explains the cold fusion phenomenon — "excess heat" without commensurable neutron emission or gamma radiation. This is just the physical basis we have sought for 19 year in pursuit of a self-sustaining heater without strong nuclear radiation**.**

5. Hot Fusion Data Imply Existence of Cold Fusion Phenomena

If we use a spherical square-potential well to describe the nuclear interaction inside the nuclear potential well, the real part and the imaginary part of the potential depth and the radius of the potential well (U_{1r}, U_{1i}, and a) are just the 3 parameters related to these 3 parameters in our formula (C_1, C_2, and w_i). Hence, it is possible to use the hot fusion data to figure out the nuclear potential well. Once we have the nuclear potential well, it is possible to predict if there is a resonance when the incident energy is approaching zero (i.e. in the case of CMNS).

In mathematics, the resonance simply means the wave function reaches almost its maximum at the interface between the nuclear potential well and the Coulomb barrier, because this boundary condition of the wave function will make the amplitude of the wave function enhanced inside the nuclear potential well. Figure 3 shows the hot fusion data for the p+D → ^{3}He+γ fusion process.

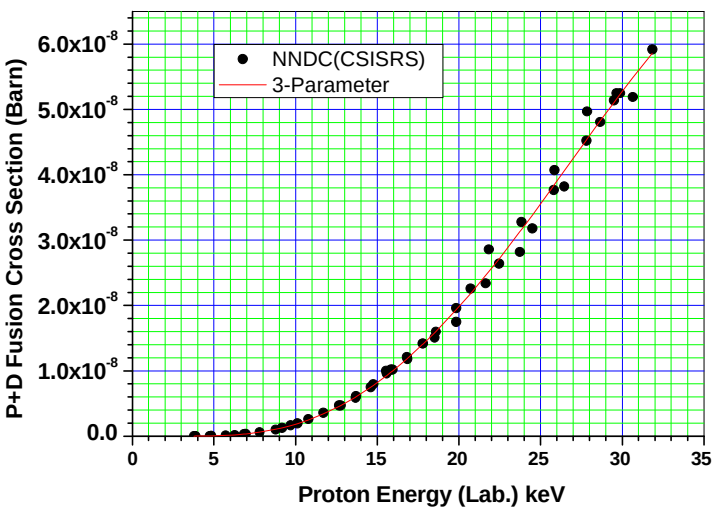

Figure 3. $p + D \rightarrow {}^3He + \gamma$

We may fit these hot fusion data using U_{1r}=-43.90 MeV, U_{1i}=-0.0233 eV, and a=3.9458×10^{-15} m, as shown in Fig. 4.

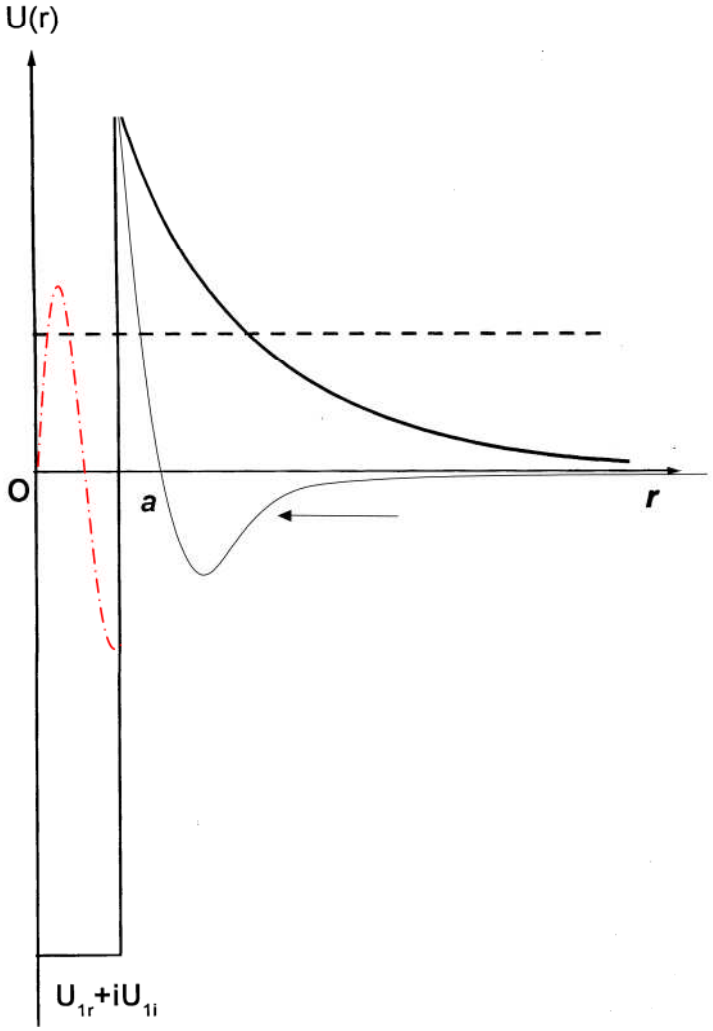

Figure 4. When Coulomb field is replaced by molecular well in a crystal, the nuclear potential is assumed unchanged

When the deuteron and proton are trapped in palladium crystal, the nuclear potential is supposed to be the same as that in the beam-target situation. Then we are able to calculate the phase of the wave function at the boundary between nuclear potential well and the molecular well in crystal (Fig. 4):

$$\mathrm{Re}[k_1 a] \equiv \mathrm{Re}[\sqrt{\frac{2\mu}{\hbar^2}(E - U_{1r} - iU_{1i})}\ a] \xrightarrow[E\to 0]{} 2.98\times(\frac{\pi}{2}) \tag{8}$$

When the incident energy approaches zero, the phase of wave function just approaches $3\pi/2$. This means that the wave function reaches almost the maximum at the interface between the nuclear potential well and the molecular well in crystal. (See the dot-dash-dot line for the wave function in Fig. 4). Hence, it predicts that the resonant tunneling may appear when deuteron and hydrogen are trapped inside the palladium crystal lattice.

The match between the incident channel width and the absorption channel width implied that the product of resonant tunneling in CMNS should be the product of a weak nuclear interaction. The calculation shows that K-capture of electrons by deuteron followed by a decay of triton is the possible candidate for this weak interaction[10]:

$$\begin{array}{l} p + d + e^- \rightarrow T + \nu \quad (5.474 MeV) \\ \qquad\qquad T \rightarrow {}^3He + e^- + \tilde{\nu} \quad (18\ keV) \\ \hline p + d \rightarrow {}^3He + \nu + \tilde{\nu}\,(5.492 MeV) \end{array} \tag{9}$$

The anomalous helium-3 and the triton in condensed matter nuclear processes are the experimental evidence [11] for this assumption. The recent successful repetition of 3 deuteron fusion reaction experiments at NRL provided an additional strong evidence of this long lifetime 2 deuteron resonant state in the titanium crystal as well[12].

6. Conclusions

(1) Nineteen years ago, some nuclear physicists alleged that the cold fusion phenomenon is contrary to all understanding gained of nuclear reactions in the last half century [13]. Indeed, after careful study of the nuclear physics accumulated in the last half century it is found that the hot fusion data themselves imply the existence of the cold fusion phenomenon.

(2) A 3-parameter formula is proposed to replace that 36 years old 5-parameter formula with better fit to experimental data:

$$\sigma(\boldsymbol{E}) = \frac{1}{\boldsymbol{E}} \left(\frac{1}{\exp[\frac{Z_a Z_b e^2}{2\varepsilon_0 \hbar}\sqrt{\frac{M_a}{2\boldsymbol{E}}}] - 1} \right) \left(\frac{-4 w_i (\frac{\pi\hbar}{\mu})^2 M_a}{(C_1 + C_2\boldsymbol{E})^2 + (w_i - \frac{2\pi}{\exp[\frac{Z_a Z_b e^2}{2\varepsilon_0 \hbar}\sqrt{\frac{M_a}{2\boldsymbol{E}}}] - 1})^2} \right) \tag{10}$$

Here $\boldsymbol{E}$ is the incident energy in the laboratory system, (M_a, $Z_a e$) and (M_b, $Z_b e$) are the mass and electrical charge of the projectile and target, respectively. For convenience, we substitute all the constants in the formula, and leave only (m_a, Z_a) and (m_b, Z_b) in this unified formula as:

$$\sigma(E_{lab}) = \frac{-16389 w_i (m_a + m_b)^2}{m_a m_b^2 E_{lab} \left[Exp\left(\frac{31.4 Z_a Z_b}{\sqrt{\frac{E_{lab}}{m_a}}} \right) - 1 \right] [(C_1 + C_2 E_{lab})^2 + (w_i - \frac{2\pi}{\left[Exp\left(\frac{31.4 Z_a Z_b}{\sqrt{\frac{E_{lab}}{m_a}}} \right) - 1 \right]})^2]} \quad (11)$$

Here, E_{lab} is the incident energy in the laboratory system in unit of keV. For deuteron incident, (m_a, Z_a)=(2,1), etc. (C_1, C_2, w_i) is from Table I and II.

(3) Detection of neutrino emission from the metal deuterides would be a critical step for the research of the condensed matter nuclear science because the selective resonant tunneling of Coulomb barrier at very low energy must be accompanied neutrino emission which is the necessary products of any weak interactions.

There are four possible sites for neutrino detection: DUSEL (South Dakota, USA), KamLand (Japan), Gran Sasso(Italy), and Da-Ya Bay (Canton, China). The positive results of neutrino detection from the metal deuterides would finally turn over the world view on CMNS research

Acknowledgments

This research is supported by the Natural Science Foundation of China(#10475045), the China Association of the Science and Technology, The Ministry of Science and Technology (Fundamental Research Division), Tsinghua University (Basic Research Fund (985-II)).

References

1. Arata, Y., and Zhang, Y-C., Proceedings of ICCF-14, Washington D.C., Aug. 10-15, 2008.
2. Violante,V. et al., Proceedings of ICCF-14, Washington D.C., Aug.10-15, 2008.
3. Duane, B. H., “Fusion cross section theory”, in annual Report on CTR Technology 1972(WOKENHAUER, W.C. Ed.), Rep.BNWL-1685, Battelle Pacific Northwest Laboratory, Richland, WA (1972).
4. Book, D. L., NRL Plasma Formulary, Naval Research Laboratory, Washington D.C. (Revised 1980) p.44.
5. Bosch, H. S., Hale, G. M., Nuclear Fusion **12** (1992) 611.
6. Huba, J. D., NRL Plasma Formulary, Naval Research Laboratory, Washington D.C. (Revised 2007) p.44.(Indeed there was another mistake in the citation of NRL Plasma Formulary. The reference [28] there “Rept.BNWL-1685 (Brookhaven National Laboratory, 1972) ” should be corrected as “Rept.BNWL-1685(Battelle Pacific Northwest Laboratory, 1972), p.76”. This mistake was pointed out early in 2002[14].)
7. Li, X. Z., Tian, J., Mei, M. Y., and Li, C. X., Phys. Rev. C **61** (2000) 024610.
8. Li, X. Z., Liu, B., Chen, S., Wei, Q. M., and Hora, H., Laser and Particle Beams **22** (2004) 469.

9. Chadwick, M. B., Oblozinsky, P., Herman, M., at al.,"ENDF/B-VII.0: Next Generation Evaluated Nuclear Data Library for Nuclear Science and Technology", Nuclear Data Sheets, vol. **107**, pp. 2931-3060, 2006.
10. Chen, S., Li, X. Z., “Tritium Production and Selective Resonant Tunneling Model”, Proceedings of ICCF-9, May 19-24, 2002, Beijing China, Ed. X. Z. Li, (Tsinghua Univ. Press), p.42
11. Mamyrin, B. A., Khbarin, L. V., and Yuderich, V. S., “Anomalously High Isotope Ratio $^{3}He/^{4}He$ in Technical-grade Metals and Semiconductors,” Sov. Phys. Dokl. **23**(8). Aug. 1978, p. 581.
12. Hubler, G. K., et al., private communication. August, 2008.
13. ERAB, *Report of the Cold Fusion Panel to the Energy Research Advisory Board*. November, 1989, Washington, DC. DOE/S-0073 DE90 005611
14. Li, X. Z., Fusion Sci. and Tech. **41** (2002) 63.

A Model for Enhanced Fusion Reaction in a Solid Matrix of Metal Deuterides

K. P. Sinha[a] and A. Meulenberg[b]
[a] *Department of Physics, IISc, Bangalore 560012, India (kpsinha@gmail.com)*
[b] *HiPi Consulting, Frederick, MD, USA (mules333@gmail.com)*

Abstract

Our study shows that the cross-section for fusion improves considerably if d-d pairs are located in linear (one-dimensional) chainlets or line defects. Such non-equilibrium defects can exist only in a solid matrix. Further, solids harbor lattice vibrational modes (quanta, phonons) whose longitudinal-optical modes interact strongly with electrons and ions. One such interaction, resulting in potential inversion, causes localization of electron pairs on deuterons. Thus, we have attraction of $D^+ - D^-$ pairs and strong screening of the nuclear repulsion due to these local electron pairs (local charged bosons: acronym, lochons). This attraction and strong coupling permits low-energy deuterons to approach close enough to alter the standard equations used to define nuclear-interaction cross-sections. These altered equations not only predict that low-energy-nuclear reactions (LENR) of $D^+ - D^-$ (and $H^+ - H^-$) pairs are possible, they predict that they are probable.

Introduction

The central idea of this paper is that the solid matrix in which LENR takes place provides conditions such as: (1) confinement of deuterons (or deuterium atoms) in linear chains or in line defects, (2) dynamical solid-state modes (phonons), which can store and exchange energy, and (3) the strong interaction between appropriate phonon modes (particularly longitudinal-optical modes) with electrons and ions. The resultant resonant D^+-D^- pairs in this environment permit attractive forces and/or strongly-screened repulsive forces, rather than the normally-expected strong-repulsive Coulomb forces between positively-charged nuclei. These options are not available in a gaseous plasma, or in materials that lack (at least) short-range order.

It is a goal of this paper to provide an understandable, standard-physics basis (under special conditions) for the extensive body of results presently available from LENR.[1]

Model

Let us consider a linear chain of deuterons surrounded by an equal number of electrons. The Hamiltonian for such a system is [2]

$$H = H_e + H_L + H_{eL} + A, \tag{1}$$

where the electron contribution is

$$H_e = \sum_\sigma E_m C^+_{m\sigma} C_{m\sigma} + \sum t_{mn} \ (C^+_{m\sigma} C_{m\sigma} + h.c). \quad (2)$$

Here the $C^+_{m\sigma}$ ($C_{m\sigma}$) denote the electron creation (annihilation) operators in the Wanneir state $|m\sigma>$, at site "m" with spin σ. E_m is the onsite single-particle energy of the electron and $t_{mn} = -|t|$ is the nearest-neighbor hopping integral. The lattice Hamiltonian is

$$H_L = \hbar\omega_D \sum_m (d^+_m d_m + ½), \quad (3)$$

where ω_D is the vibration frequency of the deuterium atom D (taken as an Einstein oscillator) and with d^+_m (d_m) denoting the phonon creation (annihilation) operators.

The interaction of electrons with the above phonon modes is described by

$$H_{eL} = g\hbar\omega_D \sum_\sigma C^+_{m\sigma} C_{m\sigma} (d^+_m + d_m), \quad (4)$$

where g is a dimensionless coupling constant. The last term in Equation 1, A, is a constant negative energy due to negative space charge in the channel. Note that in a low-dimension (one or two) structure, the potential energy between two deuterium atoms is much deeper and negative, relative to that of atoms in a 3-D lattice.[3] A suitable unitary transformation[4,5] leads to a displaced harmonic oscillator [$d'_m \rightarrow (d_m + \delta)$] and, in the transformed total Hamiltonian, the on-site single-electron energy $E^*_m = E_m - E_d$, with $E_d = g^2 \hbar\omega_D$; the hopping integral (in Equation 2)

$$t^*_{mn} = t_{mn} \exp(-g)^2; \quad (5)$$

and the electron effective mass[2]

$$m^* = m_e \exp[E_d/\hbar\omega_D] = m_e \exp[g^2]. \quad (6)$$

Even for a very conservative value of $g^2 = 1.6$, this will give $m^* = 5m_e$ (see below Equation 9).

Let us now consider the situation of two deuterons and two electrons in a chain. This introduces Coulomb repulsion (U_e) between two electrons about an atom at site "m" in the same orbital state $|m>$, but having opposite spin. The displacement transformation

$$(C^+_m)^* = C^+_m \exp [-g (d_m - d^+_m)], \quad (7)$$

gives the effective Hamiltonian and the various parameters are obtained as

$$E^*_m = E_m - E_d; \qquad U_e^* = U_e - 2 E_d; \qquad \text{and } t^* = |t| \exp [- g^2] \quad (8)$$

For $U < 2E_d$, U^* becomes negative. Thus, there is potential inversion for the 2 electrons in the singlet state and they will form a small on-site localized pair, a sort of composite boson (lochon)[2,6]. Under this condition, the D^- state will be more stable (has lower energy) than the neutral atom D (though not necessarily more stable than the $D^+ = d$ state). This would lead to the existence of D^+-D^- pairs. They would exist in the resonating state, D^--$D^+ \leftrightarrows D^+$-D^-, further reducing their energy and inter-nuclear distance.

Strong Screening

Bound electrons reduce the effective charge of nuclei. An occasional transfer of one such electron between two deuterium atoms forms a transient electron pair within a D^+-D^- pair. At

separations larger than the orbital radius of the electrons, this transfer changes a neutral relationship to an attractive one. At separations smaller than a fraction of the orbital radius of the electrons, it still gives a significant reduction in "effective" Coulomb repulsion between the nuclei. This effective potential will be represented by

$$U_d^* = ((e^*)^2/r) = (e^2/r)\,(1- \exp\,[-a_s/\lambda\!\!\!^{-}_L]) \qquad , \tag{9}$$

where a_s is the strong-electron-screening length, $\lambda\!\!\!^{-}_L = (\hbar/m_L^*\,\upsilon_L)$ is the rationalized deBroglie wavelength[1] of the lochon, m_L^* being the effective mass of the lochon, and υ_L its speed (as determined from its energy in the atomic and molecular potential wells of the two deuterons) . This screening by lochons is a short-range effect and reduces the repulsive potential between reacting nuclei (deuterons here). Screening by itinerant electrons is weak in this range (relative to that of the bound electrons) and hence not considered here.[7]

The coupling into an optical-phonon mode, along with the attractive potential of the D^+-D^- pair, briefly produces a nearly 1-D encounter that greatly increases the potential-well depth of this short-lived "molecule."

Penetration Factor and Cross Section

Next, we discuss the fusion reaction of a screened d-d reaction in 1-D. For an incident particle of effective charge e^*, the penetration factor $P(l, E_a)$ decreases rapidly with its decreasing total energy, E_a, where l is its orbital angular-momentum state. In this low-energy situation, particles in an $l = 0$ state contribute most.[8] We have:

$$\begin{aligned} P(0, E_a) &= (V_o(R)/E_a)^{1/2}\, \exp\,[-2\int_R^{r_0}(|\,k^2 - (2M_d/\hbar^2)(e^*)^2/r)\,|)^{1/2}\,dr] \\ &= (V_o(R)/E_a)^{1/2}\, \exp\,[-2\,k\int_R^{r_0}(|\,1 - (r_o/r)\,|)^{1/2}\,dr]\ , \end{aligned} \tag{10}$$

where k is the wave vector of particle a, M_d is the reduced mass of two deuterons, and with $V_o(R) = (e^{*2})/R$:

$$r_o = (e^*)^2\, 2M_d/\hbar^2\, k^2, \qquad R << r_o\,. \tag{11}$$

The integral requires careful treatment since, as $r \rightarrow 0$, it has a singular term. Hence, resorting to an asymptotic expansion (a better approximation for expression of the integral as $r \rightarrow 0$), we get,

$$P(0,E_a) = (V_o(R)/E_a)^{1/2}\, \exp\,[-\,(e^*)^2/\hbar\,\upsilon_r]\,, \tag{12}$$

where υ_r is the relative velocity. The cross-section $\sigma(a,b)$ of this reaction is

$$\begin{aligned} \sigma(a,b) &= (\text{constant} / E_a)\, \exp[-(e^*)^2/\hbar\,\upsilon_r] \\ &= (\pi/k^2)\, \exp[-(e^2/\hbar\,\upsilon_r)\,(1 - \exp\,(-a_s/\lambda\!\!\!^{-}_L))] \qquad , \end{aligned} \tag{13}$$

---

[1] Several of the references herein use $\lambda\!\!\!^{-}$, rather than λ (the deBroglie wavelength), in their equations. We follow suit.

where $k^2 = (2 M_d E_a / \hbar^2) = M_d^2 \upsilon_r^2 / \hbar^2$ and M_d, E_a, a_s, and $\lambda\!\!\!^{-}_L$ are as above. The critical difference between this development[9] and the prior work (standard model) is a factor of 2π in the exponent that exists in the regular solution and is gone here (valid at least for r => R).

The key values in the present model are those calculated for the deBroglie wavelengths for the lochon and the deuterons, as a function of d-d gap, and the value taken for a_s. This value is the screening provided by the bound electrons/lochon and is given in Ichimaru[7] (page 9) based on the ion-sphere model. Normally this is ½ the sum of the atomic-orbital radii for the charge state of the two atoms [$a_{ij} = (a_i + a_j)/2$]. In our model, a_{ij} = 0.53A for the D-D case and, since we can ignore the radius of the bare deuteron, a_{ij} = ~ 0.3A for the D^+ - D^- case. So, we assume a range of values between the initial value $a_s = a_{ij} /2\pi$ (the Bohr radius divided by 2π, since we are using $\lambda\!\!\!^{-}_L$ in the equation) and that of the 1-D case (as described above and under the appropriate circumstances), which will reduce a_s by up to an order of magnitude.

The value of $\lambda\!\!\!^{-}_L$ varies from ~10^{-9} down to ~10^{-10} cm, while the lochons accelerate between the deuterons and the Coulomb field grows as the gap shrinks. This large lochon size, relative to the nuclear-interaction distances, is a major limitation for strong screening. However, being bound, the electron/lochon screening of the deuterons increases with kinetic energy (i.e., as orbits shrink), rather than decreasing as is the case for free electrons. The 1-D nature of the problem affects the electron s-orbital orientation, in that the electron/lochon direction of motion is along the d-d axis, and therefore this localization and the velocity-induced shrinkage of $\lambda\!\!\!^{-}_L$ (along the d-d axis) aids in the screening.

Reaction Rate

The reaction rate (per cm^3 per second) for d-d- fusion with lochon screening is given by

$$R_{dd} = r^*_{dd} K_B T \lambda\!\!\!^{-}_L{}^2 N_d^2/\hbar \left[(e^2/\hbar \upsilon_r)(1 - \exp(-a_s/\lambda\!\!\!^{-}_L)\right] \times \exp\left[-(e^2/\hbar \upsilon_r)(1 - \exp(-a_s/\lambda\!\!\!^{-}_L))\right] \quad ; \qquad (14)$$

where $r^*_{dd} = \hbar^2/2 M_N e^2$ is the nuclear Bohr radius for a pair of deuterons; M_N is the average mass per nucleon ≈ 1.66 x 10^{-24} gm; K_B is the Boltzmann constant; T is the temperature (with $K_B T \lambda\!\!\!^{-}_L{}^2$ having dimensions of energy x area); and N_d is the concentration of deuterons per unit volume.

The model presented in the foregoing section is more appropriate for reaction on the surface or defect-plane in the lattice. The reaction rate is the number of effective collisions of deuterons per unit area per sec. To convert to this picture, set $K_B T \lambda\!\!\!^{-}_L{}^2$ => $K_B T \lambda_L$ = energy x length and set N_d => N_S = number of deuterons per unit area (rather than per unit volume).

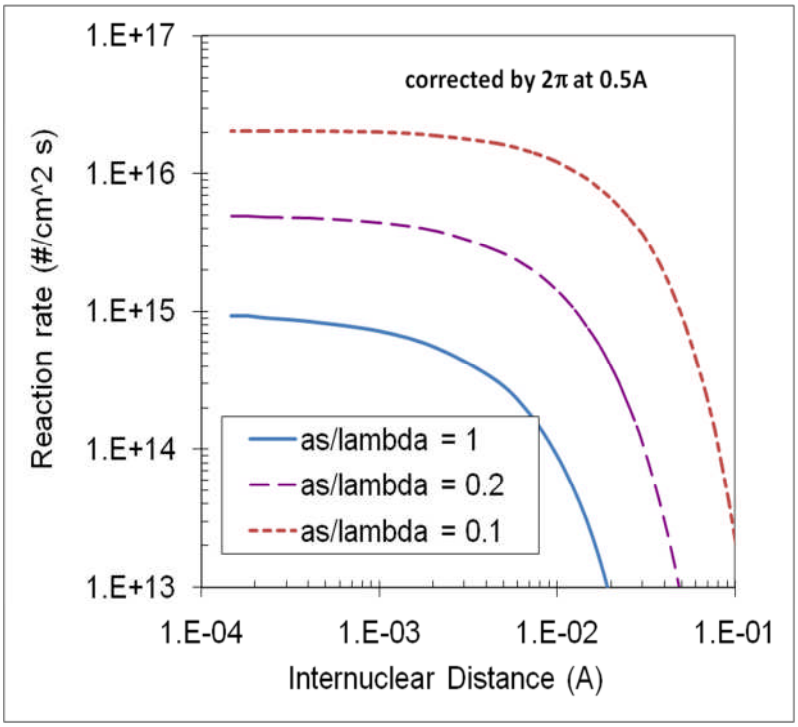

The results of Equation 14, modified for surfaces, are plotted in Figure 1, taking some acceptable values of the parameters involved. However, the figure plots the reaction rate assuming that 100% of the available lattice sites are actively involved. It is likely that only a percentage of the sites can be made to contribute to LENR. Three values of $a_s/\lambda\!\!\!^{-}_L$ (1, 0.2, and 0.1) have been selected for the lochon case.

Figure 1 The D^+ - D^- *reaction rate (for a surface), as a function of* D^+ - D^- *separation distance, for three ratios of* $a_s/\lambda\!\!\!^{-}_L$ (1, 0.2, & 0.1).

Conclusion

In the foregoing sections, we have presented a model incorporating conditions in the condensed matter state that can facilitate fusion of deuterons aided by interaction of electrons with phonon modes of the system. The cross-section of the reaction improves considerably owing to the presence of d-d pairs in line defects and with strong screening provided by bound electron pairs (lochons). However, only a mechanism, such as D^+ and D^- pairing can bring the deuterons close enough to permit a modified standard nuclear model to predict LENR.

Recent experiments by several workers, in which the material (e.g., powder or particles), is taken to be in the nanometer range, suggest that the creation of large surface area plays an important role.[10] These surfaces may provide the required active sites, in the 2-D geometry that can harbor lochons and $D^+ + D^-$ ion pairs. Our computed reaction rate is found to be $> 10^{14}$ per cm^2 per second (Figure 1) for two-dimensional surfaces, in agreement with the estimate of some workers.

The role of optical-phonon modes is important for their bringing the $D^+ + D^-$ pairs together, for coupling of ions to electrons, and as a source of resonant coupling to provide the required surface-mode excitation (surface plasmon or phonon) that can lead to enhanced-optical potentials. Recent work, on excitation of surface plasmon/polaritons with "tuned" lasers,[11,12] indicates the importance of this mechanism, where the induced-optical potential aids the fusion reaction by several orders of magnitude. The known presence of resonant $D^+ + D^-$ ion pairs in the solid state (coupled via optical phonons) greatly increases the d-d interaction cross-section

by altering the shape of the Coulomb barrier to the extent of requiring a change in the equations normally used in nuclear physics.

Acknowledgements

This work is supported in part by HiPi Consulting, New Market, MD, USA, by the Science for Humanity Trust, Bangalore, 560094, India, by the Science for Humanity Trust, Inc, Tucker, GA, USA, and by the Indian National Science Academy.

References

1. P. L Hagelstein, M. McKubre, D. J. Nagel, T. A. Chubb and R. J. Jekman, Report to DOE, USA (2004).
2. K. P. Sinha, Infinite Energy 29, 54 (2000).
3. S.H. Patil, J. Chem. Phys. 118, 2197 (2003).
4. A. P. B. Sinha and K.P. Sinha, Ind. J. Pure and Appl. Phys. 1, 286 (1963).
5. I. G. Lang and Yu. A. Firsov, Sov. Phys. JETP, 16, 1301 (1963).
6. P.W. Anderson, Phys. Rev. Lett. 34, 953 (1975).
7. S. Ichimaru, Statistical Plasma Physics, Vol II, Condensed Plasmas (Addison – Wesley Pub. Comp. 1994).
8. J. M. Blatt and V. F. Weisskopf, Theoretical Nuclear Physics, (Wiley & Sons, N.Y., '52).
9. K. P. Sinha and A. Meulenberg, "Lochon Catalyzed D-D Fusion in Deuterated Pd in the Solid State," Nat. Acad. of Sc. (India) Letters, Vol.30, No. 7&8, 2007, (arXiv:0705.0595v1)
10. D. J. Nagel, "Proc. of the 13th International Conf. on Cold Fusion, Sochi, Russia (2007).
11. K.P. Sinha and A. Meulenberg, Current Science, 91, 907 (2006), (arXiv:cond-mat/0603213).
12. D. Letts and P. L. Hagelstein, "Stimulation of Optical Phonons in Deuterated Palladium," this proceedings.

Optimal Operating Point Manifolds in Active, Loaded Palladium Linked to Three Distinct Physical Regions

Mitchell Swartz
JET Energy, Inc. Wellesley, MA (USA)

Dr. Mitchell Swartz does not wish to have his papers uploaded to LENR-CANR.org. A copy of this paper can be found here:

http://www.iscmns.org/iccf14/ProcICCF14b.pdf

This page intentionally left blank

This page intentionally left blank

This page intentionally left blank

This page intentionally left blank

This page intentionally left blank

This page intentionally left blank

This page intentionally left blank

This page intentionally left blank

This page intentionally left blank

This page intentionally left blank

This page intentionally left blank

This page intentionally left blank

This page intentionally left blank

Analysis and Confirmation of the "Superwave-as-Transitory–OOP-Peak" Hypothesis

Mitchell R. Swartz[1] and Lawrence P.G. Forsley[2]
[1] *JET Energy, Inc. Wellesley, MA 02481 (USA)*
[2] *JWK Technologies Corporation, Annandale, Virginia*

Dr. Mitchell Swartz does not wish to have his papers uploaded to LENR-CANR.org. A copy of this paper can be found here:

http://www.iscmns.org/iccf14/ProcICCF14b.pdf

This page intentionally left blank

This page intentionally left blank

This page intentionally left blank

This page intentionally left blank

This page intentionally left blank

This page intentionally left blank

This page intentionally left blank

This page intentionally left blank

This page intentionally left blank

Dynamic Mechanism of TSC Condensation Motion

Akito Takahashi
Technova Inc.
The Imperial Hotel Tower, 13th Fl., 1-1, Uchisaiwai-cho 1-chome, Chiyoda-ku, Tokyo 100-0011 Japan

Abstract

This paper gives further discussions and explanations on the time-dependent quantum-mechanical behaviors of electron-clouds in 4D/TSC condensation motion by Langevin equation, in comparison with steady ground state electron orbits and their de Broglie wave lengths for D-atom and D_2 molecule.

1. Introduction

The formation of 4D/TSC (tetrahedral symmetric condensate) at T-sites of a regular PdD lattice under D-phonon excitation, or on topological (fractal) nano-scale surface of PdDx and/or along interface of metal-oxide-metal nano-composite was proposed as seeds of deuteron-cluster fusion to produce heat with helium-4 as 4D fusion ash[1]. Dynamic motion of TSC condensation was quantitatively studied by the quantum-mechanical stochastic differential equation (Langevin equation) for many-body cluster systems of deuterons and electrons under Platonic symmetry[2-6].

This paper gives further discussions and explanations on the time-dependent quantum-mechanical behaviors of electron-clouds in 4D/TSC condensation motion, in comparison with steady ground state electron orbits and their de Broglie wave lengths for D-atom and D_2 molecule.

2. Condensation Motion of 4D/TSC by Langevin Equation

The basics of methods with Langevin equations for D-cluster dynamics, especially for D-atom, D_2 molecule, D_2^+ ion, D_3^+ ion, 4D/TSC (tetrahedral symmetric condensate) and $6D^{2-}$/OSC (octahedral symmetric condensate) are described in our latest paper[4] and book[6].

First one-dimensional Langevin equations for D-clusters with the R_{dd} (d-d distance) are formulated under the Platonic symmtery[2,6] of multi-particle D-cluster systems with deuterons and quantum-mechanical electron centers. Under the orthogonally coupled Platonic symmetry for a Platonic deuteron-system and a Platonic electron system, dynamic equations for so-many-body system of deuterons and electrons with metal atoms a simple one-dimensional Langevin equation for the inter-nuclear d-d distance R_{dd} can be formulated, as we showed in our previous papers[4,6]. The Langevin equation of electron-cloud-averaged expectation value of d-d distance R_{dd} for D-cluster is given by,

$$N_e m_d \frac{d^2 R}{dt^2} = -\frac{k}{R^2} - N_f \frac{\partial V_s}{\partial R} + f(t) \qquad (1)$$

This is the basic Langevin equation for a Platonic symmetric D-cluster having N_e d-d edges and N_f faces of "d-d-e" (D_2^+) or "d-e-d-e" (D_2) type. Here, R is the d-d distance and m_d is the deuteron mass, V_s is the d-d pair trapping potential of either "d-e-d-e"-type (i=2) or "d-d-e"-type (i=1) molecule. The first term on the right side in Eq. (1) is the total Coulomb force converted to a one-dimensional variable R, of D-cluster system, and f(t) is the fluctuation of force for which we introduce quantum mechanical fluctuation of deuteron positions under condensation motion. The quantum mechanical effect of electron clouds is incorporated with the second term of right hand side as "friction" in Langevin equation. Parameters for different D-clusters are given in Table 1.

Table 1: parameters of D-cluster Langevin equation

Cluster	N_e: Number of d-d edges	K: Total Coulomb Force parameter (keVpm)	Type of electron trapping potential on a surface	N_f: number of faces
D_2	1	0	i = 2	1
D_2^+	1	0	i = 1	1
D_3^+	3	6.13	i = 1	6
4D/TSC	6	11.85	i = 2	6
$6D^{2-}$/OSC	12	29.3	i = 1	24

By taking QM ensemble average with d-d pair wave function, assumed as Gaussian distribution, we derived Langevin equation for 4D/TSC. By taking QM ensemble average we obtained Eq. (2) for expectation value $<R_{dd}>$ we obtained the time-dependent TSC-cluster trapping potential[3] shown in Eq. (3).

$$6 m_d \frac{d^2 \langle R_{dd} \rangle}{dt^2} = -\frac{11.85}{\langle R_{dd} \rangle^2} - 6 \frac{\partial V_s(\langle R_{dd} \rangle; m, Z)}{\partial \langle R_{dd} \rangle} + 6.6 \left\langle \frac{(R' - R_{dd})^2}{R_{dd}^4} \right\rangle \qquad (2)$$

$$V_{tsc}(R' : R_{dd}(t)) = -\frac{11.85}{R_{dd}(t)} + 6 V_s(R_{dd}(t); m, Z) + 2.2 \frac{|R' - R_{dd}(t)|^3}{[R_{dd}(t)]^4} \qquad (3)$$

Similar Langevin equation and trapping potential were derived for $6D^{2-}$ ion molecule also[4,6]. We compared central potential curve (at $R'=R_{dd}$) in Fig. 1. The balancing to the Platonic symmetry after distortion (deviation from symmetry) works by the 3rd term of Eq. (3). We found that 4D(or H)/TSC can condensate ultimately to very small charge neutral entity and has no stable or ground state. This may be the reason that we do not observe D_4 molecule in nature. On the contrary, the $3D^+$ molecule and $6D^{2-}$ molecule have stable and ground states[4,6]. Equation (2) was numerically solved by the Verlet method[3,6], and the result is shown in Fig. 2.

Time dependent barrier penetration probabilities (as a function of R_{dd}, since we have one-to-one relation between elapsed time and $R_{dd}(t)$) were calculated by the Heavy-Mass Electronic Quasi-Particle Expansion Theory (Heavy Mass EQPET, HMEQPET) method[3,6] .

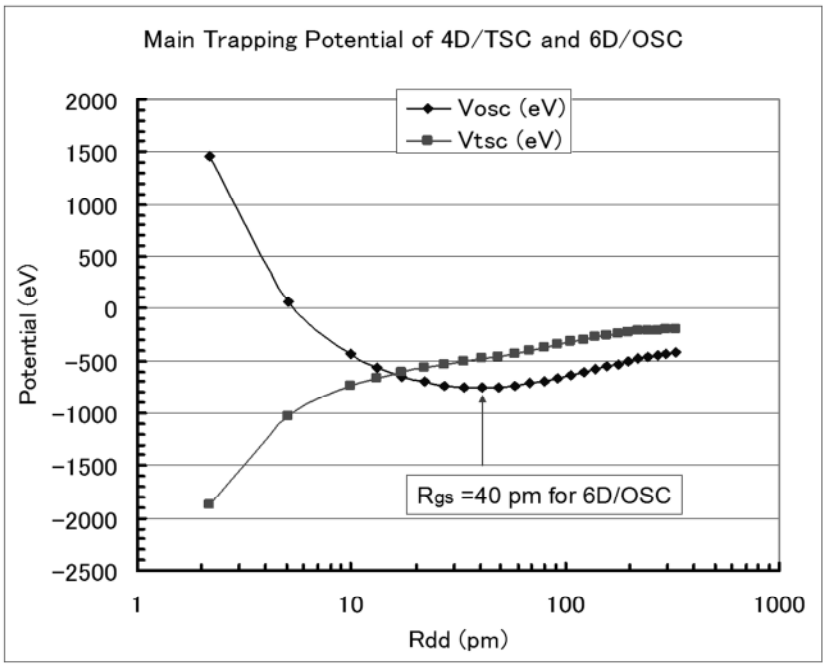

Figure 1. Comparison of cluster trapping potential between 4D/TSC and $6D^{2-}$/OSC. TSC condenses ultimately to very small R_{dd} value (ends at R_{dd}-min=about 20 fm), while OSC converges at R_{dd}=about 40 pm (corresponding to the ground state).

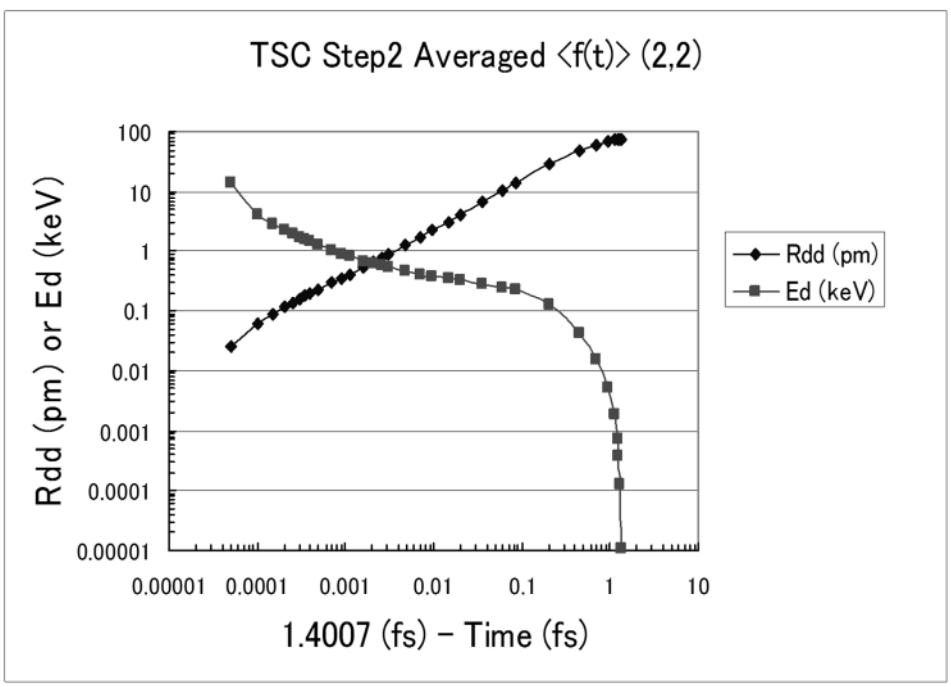

Figure 2. Numerical solution of Eq. (2) by the Verlet method[3]. Time is reversed starting from the condensation time 1.4007 fs.

The fusion rate is calculated by the following Fermi's golden rule[3,4,6],

$$\lambda_{nd} = \frac{2}{\hbar}\langle W \rangle P_{nd}(r_0) = 3.04 \times 10^{21} P_{nd}(r_0)\langle W \rangle \quad (4)$$

Here P_{nd} is barrier factor for nD-cluster and <W> is the averaged value of imaginary part of nuclear optical potential[3,4]. The extrapolation of <W> value to 4d fusion was made[3] by using the scaling law $\langle W \rangle \propto (PEF)^5$ with PEF-value which is given in unit of derivative of one pion exchange potential (OPEP) (a simple case of Hamada-Johnston potential[4] for the pion exchange model). We estimated the next value of 4D fusion yield per TSC generation,

$$\eta_{4d} = 1 - \exp(-\int_0^{t_c} \lambda_{4d}(t)dt) \quad (5)$$

Using time-dependent barrier factors, we obtained[3] $\eta_{4d} \cong 1.0$. This result means that we have obtained a simple result that 4D fusion may take place with almost 100% yield per TSC generation, so that macroscopic 4d fusion yield is given simply with TSC generation rate Q_{tsc} in the experimental conditions of CMNS.

The ultimate condensation is possible only when the double Platonic symmetry of 4D/TSC is kept in its dynamic motion. **The sufficient increase (super screening) of barrier factor is also only possible as long as the Platonic symmetric 4D/TSC system is kept. Therefore, there should be always 4 deuterons in barrier penetration and fusion process, so that 4d simultaneous fusion should take place predominantly. The portion of 2D (usual) fusion rate is considered to be negligible[3].** The order (or constraint) of condensed matter incubates this[6]. Typical nuclear products of 4D fusion are predicted to be two 23.8 MeV α-particles, although the final state interaction of ^{8}Be* is complex, and yet to be studied[5,6].

3. Time Dependent QM Behavior of Electron Clouds

We consider now the principle of dynamic condensation motion of TSC in the view of Heisenberg uncertainty principle (HUP).

At the starting condition of 4D/TSC (t=0), d-d distance R_{dd} was estimated to be the same value (74.1 pm) as that of a D_2 molecule. At this starting point, the mean electron kinetic energy of one "d-e-d-e" face EQPET molecule out of TSC 6 faces was 17.6 eV (19 eV by semi-classical model[6]). During the non-linear condensation of TSC, the size of "d-e-d-e" EQPET molecule as a face of 4D/TSC decreases from R_{dd}=74.1 pm at t=0 to R_{dd}=20.6 fm at t=1.4007 fs. In the view of HUP, electron wave length should decrease accordingly to the decrement of R_{dd}. At around t=1.4007 fs, the mean kinetic energy of electron for "d-e-d-e" EQPET molecule was estimated[3] to be 57.6 keV. The original Langevin equation for D_2 molecule, before the quantum-mechanical ensemble averaging is done, as given by,

$$m_d \frac{d^2 R_{dd}}{dt^2} = -(4\sqrt{2} - 2)\frac{e^2}{R_{dd}^2} + \frac{2m_e v_e^2}{(R_{ee}/2)} - \frac{\partial V_{s2}(R_{dd};1,1)}{\partial R_{dd}} + f(t) \quad (6)$$

We consider the averaged force-balance between the first term and the second term of right side of Eq. (6), with ensemble averaging by weight of "adiabatic electron wave function" of

modified 1S wave function with decreased de Broglie wave length during every small time step interval. R_{ee} is the distance between two quantum mechanical electron centers.

We understand that the effective quantum mechanical wave length of trapped electron in TSC has decreased dramatically in the 1.4007 fs condensation time. The estimated trapping potential depth of TSC at t=1.4007 fs was -130.4 keV. This state is understood as an adiabatic state in very short time interval (about 10^{-20} s) to trap such high kinetic energy (57.6 keV) electrons in very deep (-130.4 keV) trapping potential, to fulfill the HUP condition. By the way, mean kinetic energy of relative d-d motion was estimated[3)] to be 13.68 keV at this adiabatic state, which also diminished relative deuteron wave length trapped in the adiabatic TSC potential. In this way, very short R_{dd} (in other words, super screening of mutual Coulomb repulsion) was realized in the dynamic TSC condensation in very fast condensation time (t_c=1.4007 fs) to give however a very large 4D simultaneous fusion rate[3,4)].

We know that the ground state electron orbit (sphere) of D (or H) atom is the Bohr radius (R_B=52.9 pm). The mean kinetic energy of 1S electron is 13.6 eV, the de Broglie wave length of which is 332 pm. And we know $2\pi R_B$=332 pm to satisfy the continuation of 1S electron wave function (same with the Bohr's condition) by one turn around the central deuteron. No other states with shorter or longer wave length can satisfy the condition of smooth continuation of wave function, as ground state, for which we must in addition keep the condition that mean centrifugal force equals mean centripetal force.

On the other hand, electron orbit in a "d-e-d-e" quasi-molecular system of a face of 4D/TSC under time-dependent condensation makes a spiral track, finally getting to the center-of-mass point of TSC, with tail of time-varying "relatively long" effective wave length.

Similarly to the case of a D-atom, the ground state electron wave function of D_2 molecule has a steady ground state torus (ring) orbit of two centers of electron clouds[4,6)]. The mean kinetic energy of a centrifugal electron motion around the center-of-mass point (middle point of d-d distance) was calculated to be 17.6 eV, de Broglie wave length of which is 234 pm and equals to $2\pi R_B/1.4142$ to satisfy the smooth continuation of electron wave function along the torus orbit around the center-of-mass point. Dynamic motion of "d-e-d-e" 4 body system by Langevin equation (Eq. (6)) is illustrated in Fig. 3-a. When starting with an arbitrary electron wave length (or momentum), the center of electron cloud draws spiral orbit to converge finally to the steady torus (ring or circle) orbit with 234pm one turn length which equals to the ground state effective electron wave length of D_2 molecule. When we have the strong constraint of TSC trapping potential, center of electron cloud draws spiral orbit time-dependently as shown in Fig. 3-b **without converging ground state.** Calculated mean (eigen) energy-values of D_2 molecule are E_{gs} (ground state system energy) = -35.1 eV, E_c (mean Coulomb energy) = -70.3 eV, $E_{d\text{-}d}$ (mean relative deuteron energy) = 2.7 eV and E_{ke} (mean electron kinetic energy) = 35.2 eV for two electrons (17.6 eV per electron)[3,6,7)].

As a result, centrifugal electron motion in a "d-e-d-e" face draws a spiral curve conversing to the central focal point as illustrated in Fig. 3-b. If we do not have the strong centripetal Coulombic condensation force by the first term of Eq. (1) right side, for 4D/TSC, "d-e-d-e"

EQPET molecule must go back and converge to the ground state orbit of D_2 molecule, as drawn in Fig. 3-a.

4D/TSC has no steady ground state and effective electron wave length of a "d-e-d-e" face varies from time to time as illustrated in Fig. 3-b.

The spiral motion of an electron center under 4D/TSC condensation is illustrated with an expanded scale (right figure), compared with the estimation of mean rotation number of electron in each discrete change of R_{dd} steps, as given in Fig. 7 of our detailed paper to JCMNS[7].

The electron center rotates about 6 times in each step of R_{dd} changes, as shown in Fig. 7 of Ref. 7. This means the time-dependent electron wave function distributes with "long" tail along the spiral orbit. This situation does not contradict the Heisenberg uncertainty principle, as steady ground state does not exist and particles are non-linearly moving from time to time.

4. Conclusions

A further explanation on 4D/TSC condensation motion by quantum-mechanical stochastic differential equations (Langevin equations) has been given in this paper.

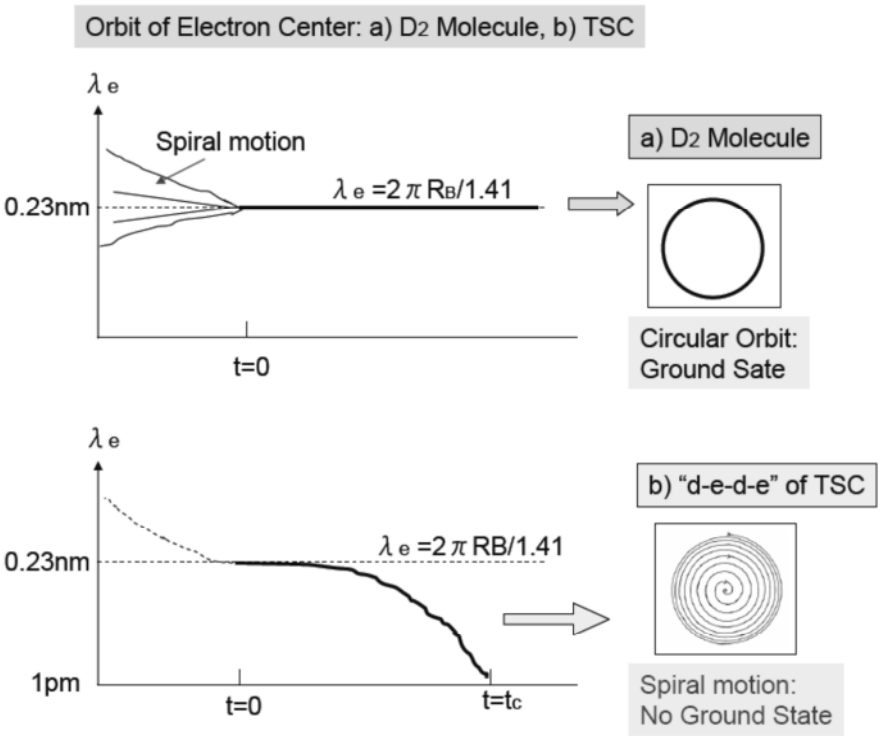

Figure 3. Time dependent behavior of effective electron wave length, a) D_2 molecule, b) "d-e-d-e" EQPET molecule of 4D/TSC

The electron orbit in a "d-e-d-e" quasi-molecular system of a face of 4D/TSC under time-dependent condensation makes a spiral track, finally getting to the center-of-mass point of

TSC, with a tail of time-varying effective wave length. This does not contradict the Heisenberg uncertainty principle. A more detailed paper on this work will appear in JCMNS[7].

References

1) A. Takahashi: A theoretical summary of condensed matter nuclear effects, *J. Condensed Matter Nuclear Science*, 1(2007)129-141
2) A. Takahashi, N. Yabuuchi: Condensed matter nuclear effects under Platonic symmetry, Proc. ICCF13, Sochi, Russia, 2007 (to be published)
3) A. Takahashi, N. Yabuuchi: Study on 4D/TSC condensation motion by non-liniear Langevin equation, *LENR Source Book, American Chemical Society*, 2007, to be published from Oxford Univ. Press, August 2008
4) A. Takahashi, N. Yabuuchi: D-cluster dynamics and fusion rate by Langevin equation, Proc. 8th Int. Workshop on Anomalies in D/H Loaded Metals, Catania, Italy, 2007, to be published in 2008
5) A. Takahashi: A chronicle of condensed cluster fusion models, Proc. JCF8, Kyoto, 2007, pp.51-62, Japan CF Research Society, 2008
6) Akito Takahashi: "Cold Fusion 2008 – mechanism of condensed cluster fusion" (in Japanese), Kogakusha, Tokyo, 2008
7) Akito Takahashi: Dynamic Motion of TSC Condensation Motion, submitted to JCMNS, September 2008

Introduction to Challenges and Summary

The field of LENR has all the challenges of any accepted part of science, plus the burden of gaining acceptance and recognition as a legitimate field of scientific inquiry. The normal challenges include the design and performance of sound experiments, and the development and application of theories to explain past observations or make predictions. They also include communications of results through discussions, presentations and journal articles. Now, all of these things do apply to LENR, although it is difficult or impossible to get many of the appropriate journals to even consider papers from scientists in the field.

The problem of LENR becoming a recognized field of scientific research is very challenging. Acceptance as a part of science would have far reaching consequences. Now, in the US, responsible people in both the Congress and the Administration correctly assert that they are not scientists. They are waiting for the scientific community to examine LENR and pronounce judgment, not on its details, but only whether or not it should be considered as a science. Administrators in the US Patent and Trademark Office, who are not scientists, have the same refrain. They await scientists with relevant competencies to examine information on LENR and render an opinion on its being, or not being, part of science. Those responsible for documentation and communication of scientific results, the editors of scientific journals and magazines, also correctly assert note that they are not scientists (even though many of them were scientists earlier in their careers). They want others, who are now practicing (publishing) scientists, to examine results on LENR and say what they think about the field as a science.

So, why is are key scientists individually and the scientific community, broadly considered, unwilling to (a) examine the evidence, (b) draw conclusions about the nature of work on LENR and (c) communicate them to other scientists and the public? Part of the reason is that most scientists are busy with their own research, and not willing to spend time on examining LENR information. There is, after all, little likelihood of either support or fame in such an activity. Some scientists are fear-filled as a result of the residual poor reputation of the field. They are afraid that their reputations would be tainted and, maybe, their careers destroyed. Then, there are a few very prominent and vocal ex-scientists who speak out against the field even though they seem not to be aware of key results from LENR research. They may have had strong scientific careers at one time, but they no longer contribute to the advancement of knowledge by actually doing research and publishing the results. Whatever motivates these people, money or ego or anything else, they do themselves and the field a real disservice. This is especially true in the case of LENR.

It is uncertain if and when the current research phase of LENR will be the basis for practical energy sources. However, the prospects of small distributed nuclear power sources, without dangerous prompt radiation nor significant radioactive waste, deserves consideration. Those possibilities are in addition to the wonderful scientific challenge of understanding how it is possible to stimulate MeV nuclear reactions by using eV chemical energies.

Whether or not LENR energy sources prove to be important, there are some basic requirements for the operation of LENR experiments. One of the most fundamental is replication. Hence, this conference included an invited paper by McKubre on replication. He

defines it as the ability to demonstrate an effect of interest on demand. In that paper, McKubre provides an important summary of the temperature dependence of the ability to produce excess heat, as summarized in this table:

Temperature Range	Energy Gain in a LENR experiment
Below 70°C	0 to 5 %
70 to 99°C	About 10 %
At boiling	Up to 150 %

McKubre ends with the assertion that replication, however significant, is not as important as proving that the energy produced in LENR experiments is nuclear and not chemical.

Swartz confronted the critical challenge of getting enough electrical power out of a LANR cell to do useful electrical work, and to feed back power to drive the cell in a steady-state condition, which he calls “renewable electricity”. Such as system is termed a “Self Sustaining Electrical Generator”. Swartz is particularly concerned with the poor energy conversion in going from heat to electricity, which he found to be in the range 13-19%. He also measured the ability to use energy from LANR to operate fuel cells. But, that was found to have high loses in both gas generation (13-20%) and water (energy) generation (54-69%). While high efficiencies were not achieved, this is an important start on the serious electrical generation from the heat generated by LANR electrochemical cells.

The paper by David and Giles is in a class by itself. It seeks to directly convert the results of LENR into a voltage, rather than into heat that might then be transformed into electricity. Their gas phase device contains a mixture of powders of Pd and semiconductors. Voltages of 0.5 V have been measured. These authors note that the power to weight ratio in their device is similar to that of the first atomic pile made by Fermi and his team in Chicago in 1942.

The question of the Fleischman-Pons effect being real and nuclear is the focus of two other papers in this section. In the first, Johnson and Melich provide a Bayesian probabilistic analysis for the criteria offered by Cravens and Letts as being necessary for the operation of the FPE. That set of criteria is in the first paper in the section on Heat Measurements in these Proceedings. They show that, on the basis of only eight papers, the likelihood ratio (the FPE Effect is real/the FPE Effect is not real) is over 10. This analysis could be usefully extended to include more papers. However, with only those few papers, the conclusion of the reality of the FPE effect (and its subsequent conclusion of necessarily being nuclear) is already quite robust.

Kowalski also confronts the question of nuclear or not? He summarizes results for an affirmative conclusion in what he calls the “protoscience” of LENR. Excess heat, its correlation with Helium production, changes in isotope distributions, production of new elements, chemically-induced changes in radioactive decay rates and the emissions of high-energy photons and particles are cited.

Grimshaw provided a study of modern approaches to Condensed Matter Nuclear Science. He advocates what is called “Open Source Science” or OSSc. This idea is modeled on the widespread use of open source software, for which there are many successful examples. He

notes that the common usage of the internet by LENR researchers for posting papers and for discussions already makes the field part of Open Source Science. He asserts: “The prospects of cold fusion success may be significantly enhanced by extending the current informal and implicit use of OSSc-type methods to more organized and explicit deployment under the sponsorship of a recognized professional organization such as the International Society for Condensed Matter Nuclear Science.”

A summary of ICCF-14 was written by Passel, and is the final paper in this section. In that paper, he provided both a sociological context and a review of a sampling of the results presented at the conference. Passel notes correctly that the field, although 20 years old, has done only a very small fraction of possible experiments. Many of us, who have been in the field since the outset, look forward to the day when LENR is a part of recognized scientific research with funding to attract new scientists with useful skills and equipments. Then, many more of the needed experiments will be done and reported.

The Importance of Replication

Michael C. H. McKubre
Director, Energy Research Center
Principal Scientist in the Materials Research Laboratory
SRI International, Menlo Park, California

Abstract

Much discussion in the Condensed Matter Nuclear Science or "Cold Fusion" fields centers on the subject of replication. It is a topic that comes up in essentially every conversation about the Fleischmann Pons Effect (FPE). Assembled here is a set of essentially personal views on this subject of replication.

Why is replication important?

We might begin with the dictionary definition of replication as the action of copying or reproducing something [1]. More specifically in science we mean the repetition of a scientific experiment or trial to obtain a consistent result. Note that replication is defined in terms of reproduction and that the key test in science is consistency, not identicality.

Reproducibility is the "Touchstone" of Scientific Method. Scientific method does not work if you cannot perform trials with different input parameters, learning something certain from the observed change in output. Critics argue that for something to be "not reproducible" means that it is "not science", implying that it is "not real". This last inference is a false argument. Reality and reproducibility are different concepts.

If the effect one is attempting to study is rarely seen, then it is hard to study. It would be a great advantage for experimenters to have a more reproducible effect. But its lack does not make the effect unreal. Without quantitative reproducibility it is harder (but not impossible) to perform parametric studies which are the basis of the empirical method that we use to gauge the effect of input variables that should – or should not – influence the effect under study.

What does it mean to "replicate"?

Replicability conveys the ability to demonstrate the effect that you are observing and studying on demand. We can extend the definition and difficulty of replication to include the ability to transport and transplant a successful experiment from one laboratory to another. This is something that the group at SRI has been very much involved with. In the extreme case we would like the ability to interchange experiments between laboratories on the basis of a written instruction set alone. This is more or less the basis of US Patent Law that applies the test of a fictional "person having normal skill in the art" following written instructions (the Patent). Although we would consider ourselves to meet the standard of "normal skill" our experience in replication at SRI, in essentially every instance, written instructions alone have been

insufficient to allow us to reproduce the experiments of others. It is not clear that this inability is limited to the FPE; other classes of replications have not been attempted.

Another extreme and desirable condition particularly on the pathway to application is the ability to reproduce (in every case) the magnitude and timing of the effect. If one has an effect completely under control then the input variables lead immutably to the output variables. In this extreme case it is not necessary to perform the experiment, the result is predetermined. To have complete empirical understanding requires a comprehensive, quantitative, fundamental understanding of the effect under study. This can be based on physical theory, although it should be noted that many physical laws that represent apparently entirely reproducible and predictable phenomena are not so based.

Have we succeeded?

More particularly, to what extent have we succeeded? The answer depends on what one is looking at; what effect, what evidence? We have succeeded in a number of regards and I will go through some of the examples and review some evidence. It is appropriate to note that a number of effects claimed in the CMNS field have not been replicated with sufficient rigor or diversity to have achieved widespread support of success.

We have certainly successfully transported and replicated the Fleischmann Pons Effect, by which is meant the production of nuclear level heat from the electrochemical stimulation of the heavy water – palladium system. This effect has been observed by hundreds of people in dozens of laboratories around the world, and published in hundreds of papers as recently reviewed [2, 3]. In fact the very breadth of diversity in experiment and calorimeter choice has contributed to the illusion of irreproducibility (although, as will be argued later, the primary cause of apparent irreproducibility is the lack of measurement and control of variables critical to the effect).

The observation of ^{4}He also appears to meet the criterion of transportability. Miles and Bush were the first to demonstrate semi-quantitative correlation between the rates of creation of ^{4}He and excess heat [4]. That effect has now been observed in a number of laboratories around the world [5-7] including SRI [2, 8] with considerable assistance from Dr. Benjamin Bush. The Case experiment was successfully replicated at SRI [2, 8]. However, we were not able to replicate this experiment simply based on written instructions alone, and required the intervention of Dr. Leslie Case. The Arata experiment in its original form involving electrolysis of a double structured cathode [7] was successfully replicated at SRI [2, 8] after soliciting help from Professors Arata and Zhang. Again, however, we were also not successful in replicating this experiment simply based on published materials.

Experiments involving laser triggering of excess heat by laser triggering of deuterium loaded palladium cathodes with specially modified surfaces were initially discussed by Letts and Cravens [9]. This class of experiments has been successfully transported from laboratory to laboratory although again requiring hands-on tuition and involving long periods of unexplained failure [10-12].

At SRI we have been unsuccessful in a number of attempts at experiment replication. We were not able at any time to reproduce the claims of heat from nickel – light water electrolysis experiments. We were able uncover one source of systematic error in the experimental procedures involving large area nickel – carbonate electrolyte experiments that blunted our interest. This inability should not be taken to mean that the claims are wrong or an effect not real, particularly in light of previous failures to replicate before personal, hands-on guidance was sought. We were not able to replicate the Patterson-CETI experiments [13]. Despite the very able hands on support of Dr. Dennis Cravens we were never able to observe an excess heat effect for this experiment in our mass flow calorimeters, although it is now understood that an important experimental element may have been lacking. A similar situation exists in respect of the Stringham [14] ultrasonically induced Pd-D_2O excess heat effect using SRI mass-flow calorimeters, although this condition of uncertainty was exacerbated by the complexities of input energy measurement and coupling between the ultrasonic power source and the transducer and experiment.

These last two cases (Patterson and Stringham) highlight a feature and two rules to be observed in any attempt to replicate calorimetrically an already difficult experiment and study a fragile effect.

i. The calorimeter is part of the experiment. This is true whether the "effect" is a systematic error or an unexplained heat source. Changing the calorimeter may change the triggering or amplitude of the phenomenon under test. One simple example of this phenomenon is the extent to which the unaccounted excess heat changes the temperature of the experiment; other feedback systems are possible.
ii. The experiment cannot be compromised and become subordinate to the calorimetric needs. If the experiment needs to be changed <u>in any significant way</u> to accommodate the requirements of the calorimetric method that is preferred (by some criterion or that happens to be on hand), then the test of replication is compromised. This condition can be relaxed only after all variables critical to the effect are known and measured.

To the extent that it occurs, the lack of reproducibility is reflected in the magnitude, timing, gain, and termination of the effect. We perform intentionally identical experiments repeatedly and obtain clear evidence of the effect, but with variable (and inconstant) magnitude, variable initiation time, or the power and energy ratios output:input are not in every case the same. Even the termination of the experiment is not fully under experimental control. One may turn the stimulus off, discontinuing laser, ultrasonic, electrochemical current or other stimulus, and still continue to observe the effect, sometimes requiring minutes, hours or even days to decline to the thermal baseline. The effect may persist after discontinuation of all externally generated stimuli, the so-called "heat-after-death" or more logically "heat-after-life" effect. Thus we cannot even stop our experiments always on demand and we do not yet have quantitative reproducibility in any case of which I am aware.

Every one of the CMNS subtopics still needs further research. To get from where we are to where we need to go requires a substantial level of physical materials support. Much as it was

in the early days of semiconductors, today it is our materials that are letting us down. In current FPE studies it is the metallurgy of palladium that is the principle barrier to complete quantitative replicability. On the other hand we do have a limited empirical model. We are able to explain experiment failures and the failure to produce excess heat in terms of our inability to meet certain input conditions: loading, deuterium flux, input stimulus. This ability to explain failures, and thus learn from them, is very valuable.

Why are there failures?

At this point a reasonable question might be: if you know what you need to do, why can't you always do it? Why is there any degree of irreproducibility? What are you waiting for? The answer is straightforward: the material conditions of our experiments are not completely under our control. Solids are more complex than liquids; liquids more complex than gases or plasmas. The solid:liquid interface may be the most complex structure of all material science. This is a structure that we are only just beginning to understand in any level of detail and are still struggling to control.

Electrochemistry takes place at an electrified interface between two "difficult" materials, neither of which are fully under our control. In the early days of studying the FPE at SRI experiments were designed to probe the parameters of reproducibility. Sets of 12 cells were prepared, intentionally identically, and operated simultaneously to monitor the time evolution of electrochemical and physico-chemical parameters believed to be or potentially pertinent to the FPE.

A single length of palladium wire was used from a known source and sectioned into 13 identical lengths (12 active electrodes plus a reserved blank). These wire sections (typically 3 or 5 cm in length and 1 or 3 mm in diameter) were machined to remove surface damage and inclusions, spot welded with 5 contacts (one cathode current and 4 wires for axial resistance measurement), annealed, surface etched (to remove surface contaminants) and mounted in 12 identical cells of the type shown in Figure 1. These processes all were performed in the same batch and by the same person. The twelve cells were filled with the electrolyte from a single source and then operated electrically in series, in a 3 x 4 matrix in the same constant temperature chamber.

The variables measured continuously were current (one measurement), cell voltage, pseudo-reference cathode potential, temperature and electrical resistance (D/Pd loading) all being monitored in a multiplexed manner with the same instruments. Intermittent measurements were made of the cathode interfacial impedance. With 12 intentionally identical experiments, every one behaved differently. Not only in terms of their heat production, significant and marked differences were observed in: the current-voltage-time profile for both the cell voltage and reference potential; the ability and willingness of each electrode to absorb deuterium measured by the resistance ratio-time curve; the maximum loading achievable; the interfacial kinetic and mass transport processes reflected in the interfacial impedance. Every one of these parameters was importantly different for each of the 12 electrodes.

This set of experiments was repeated several times in an attempt to understand the origins of the irreproducibility, and therefore control it. Trace impurity differences were observed to be

contributory and these divided into two sets: deleterious impurities (poisons) that we learned to avoid; impurities that were beneficial to high loading in controlled amounts. This was a highly useful (and somewhat surprising) exercise. Although we were able to make progress and reduce the dispersion, we were not able to control the irreproducibility simply by electrochemical (and trace chemical) means. We continued to operate sets of cells in what we called “farms”, selecting the most promising for promotion into calorimeters of the sort shown in Figure 2.

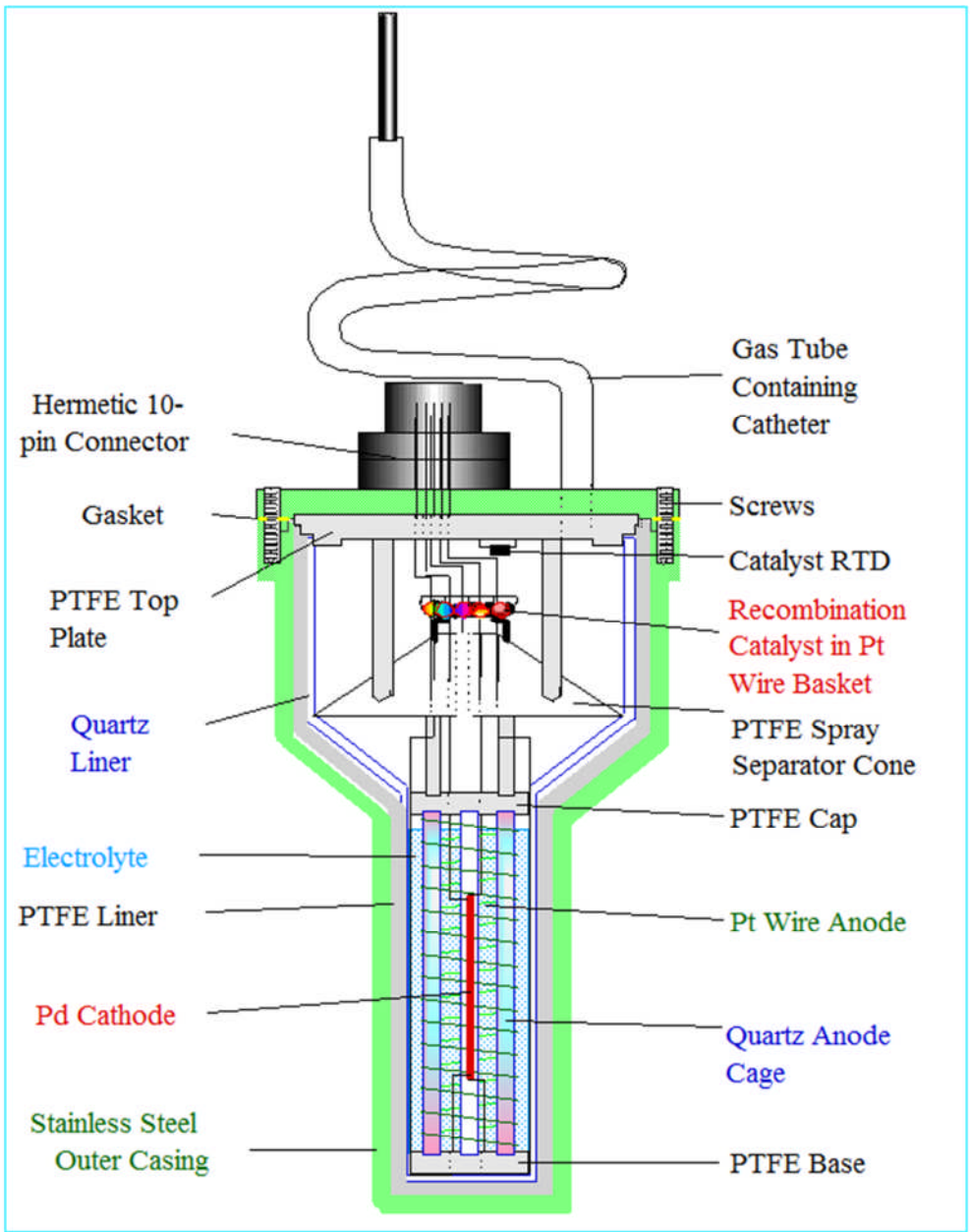

Figure 1. Electrochemical cell for loading and calorimetric studies.

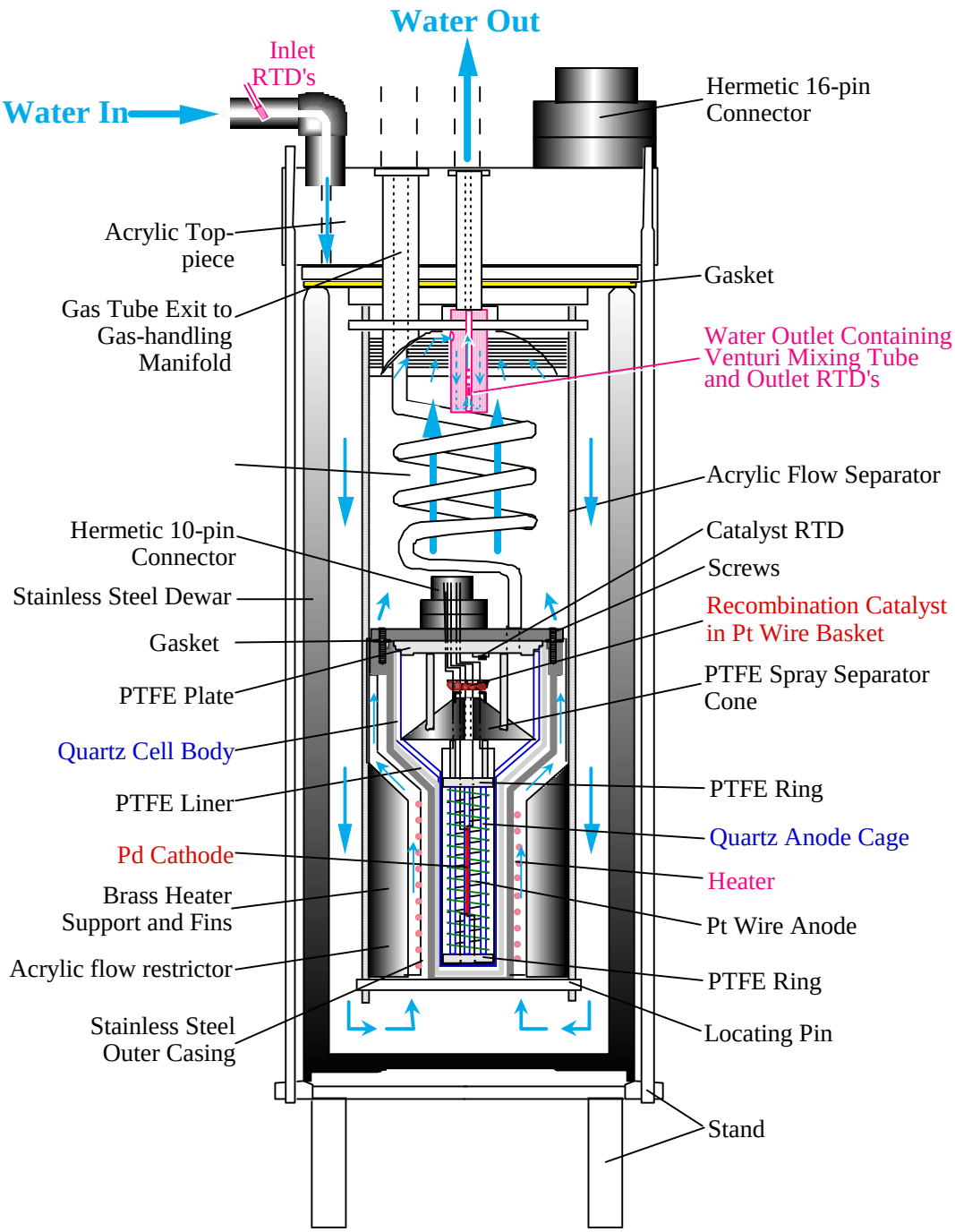

Figure 2. Labyrinth Mass Flow Calorimeter incorporating Degree-of-Loading Cells

Four important understandings developed from these intensive studies at SRI of deuterium loading and calorimetry:

i. Irreproducibility in FPE experiments can be fully or at least sufficiently explained in terms of the electrochemistry of loading D into Pd.
ii. In the absence of a measure or knowledge of the D/Pd loading the experimenter has no basis to judge whether an experiment could or should have produced excess heat.
iii. After basic precautions are taken the irreproducibility of loading and interfacial kinetics is not largely or even primarily controlled by the electrolyte or the electrochemistry, it is controlled by the bulk palladium metallurgy.
iv. An empirical and near quantitative understanding of the measured magnitude of excess heat effects, and more particularly of the failure to achieve the FPE, can be obtained from measurements made of the controlling variables, and the failure to achieve critical threshold values.

If the metallurgy varies so greatly between adjacent sections of the same wire, annealed and surface treated in the same way and at the same time, how great might the difference (irreproducibility) be between metal samples from different sources? Until recently we have not had sufficient resource of time, money or talent to begin a serious campaign to understand the issues of materials irreproducibility as these pertain to the defect and impurity structure of polycrystalline palladium. Many people recognized this as one of or the most important problems to be faced right from the beginning in 1989 or before, Fleischmann, Bockris, and Huggins amongst others.

Several people have taken up the challenge of palladium metallurgy with limited resources, amongst others Imam at NRL, Letts in his own lab and Violante at ENEA. These efforts have resulted in significant progress and even patents. Most recently the efforts of Vittorio Violante's group to control the metallurgy and surface morphology of palladium foils has contributed significantly to the formal laboratory-to-laboratory replication of Energetics FPE results at ENEA and SRI [15]. Recent experiments at ENEA and NRL [16] have demonstrated that identical annealing and rolling treatments of different starting batches of palladium results in markedly different foil characteristics. To make rapid progress into the light of reproducibility, significant resource must be directed as was done previously for electrochemistry, to identify those characteristics of bulk palladium that are crucial and those that are detrimental.

There has been some discussion of "hidden" variables; a controlling or contributing parameter that so far remains unidentified. In a difficult experiment or situation it can be comforting but also debilitating to attribute failure to a hidden agent. Without further empirical knowledge or theory to guide us, the only rational position is the middle ground. We must to proceed along the path of increasing control of the electrochemical and metallurgical variables that we understand and can measure, in the attempt to exert full control over the FPE. Along this path we need to remain alert to the possibility of a critical undiscovered parameter.

Much of this uncertainty would be resolved and a great deal of tedious and repetitious matrix study avoided with a theory to guide us on the path and point towards the answer. While the FPE is the first and most concrete demonstration of a condensed matter nuclear effect it is highly unlikely that this is the only or best manifestation of a new physical effect. Either by means of theory or ingenious engineering it is likely to be far more practical to avoid the challenges and limitations present in the electrochemical loading of bulk palladium rather than climb the mountain of ever increasing materials control of difficult systems.

What have we accomplished so far?

This is not intended as a review but simply is a set of examples taken from the works at SRI and our immediate collaborators. By 1992 we had demonstrated a nuclear scale heat output, and had determined that the effect was real if you controlled the loading variable. There was also an initiation effect that we (and others) had discovered at that point. Figures 3 and 4 show two of the controlling variables, the effect of current density and D/Pd loading on the excess heat effect [2, 3].

By 1995 we had uncovered the importance of flux, the movement of deuterium through the interface and that this was not an equilibrium effect, and we had formed these various terms into an empirical heat equation [2, 17]. Between 1996 and 1998 we measured associated nuclear products, specifically ^{4}He [2] following Miles in 1992 [4]. By 2000 we had measured ash uncorrelated with heat (^{3}He). Figures 5 and 6 show our results replicating the Arata double-structured (DS) cathode electrolysis experiment [8]: Figure 5 plots the excess power measured in heavy and light water electrolyte, and the percentage excess in heavy water; Figure 6 shows the profile of ^{3}He measured through the wall of the DS cathode produced by the disintegration of tritium diffusing from the inner void where it was created, to the outer electrolytic surface.

In 2003 we published [10] a replication of the Letts-Cravens laser triggering result [9] and a significant new result came in 2007 working in collaboration with ENEA and Energetics. As discussed above the knowledge gained at ENEA helped achieve an improved control (if not mastery) of the palladium metallurgy. The knowledge developed at Energetics using the Dardik SuperWave concept enabled us to achieve much greater reproducibility in the control of loading and interfacial deuterium flux. With this improved understanding we gained a higher degree of command over two parameters crucial to the production of excess heat.

As a consequence we were able to achieve high levels of reproducibility in excess heat production. Table 1 shows the complete set of experiments performed at SRI [15, 18] following Energetics protocols and SuperWave current excitation profiles [19], in all except one case using Pd foil cathodes fabricated at ENEA [16]. The rows labeled “E” were performed at SRI with Energetics electronics and data acquisition; those labeled “S” were performed at SRI with SRI electronics and data acquisition. Of the 15 experiments performed in the latter mode, 11 (*73%*) demonstrated power excess at or above the 5% level that was determined to be the calorimeter 3σ accuracy.

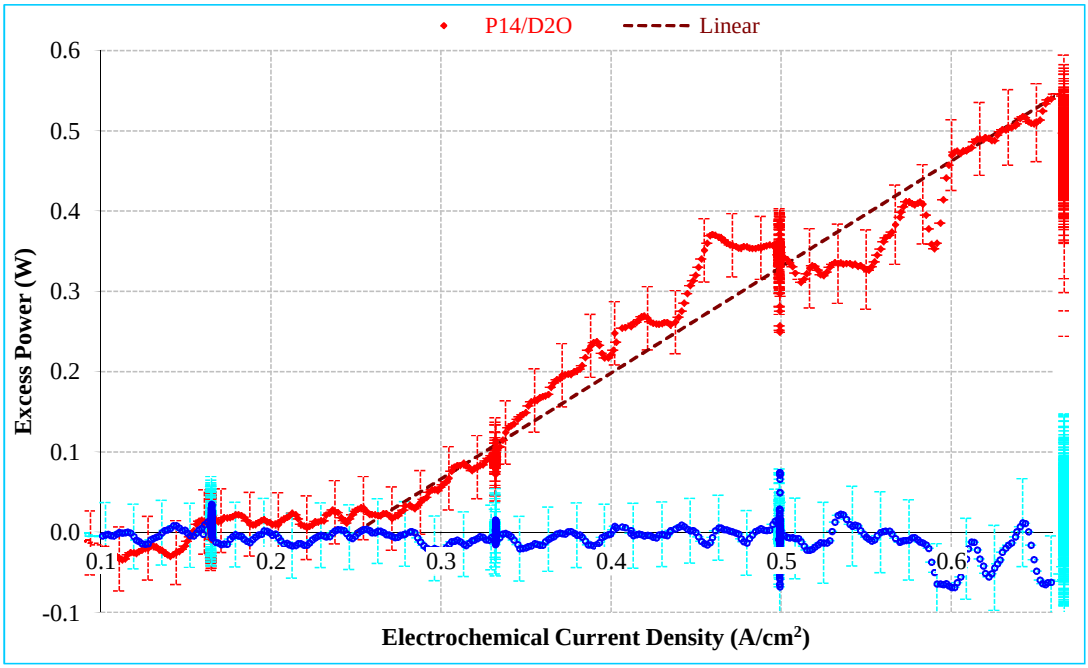

Figure 3. The effect of Electrochemical current density on excess heat production in FPE electrolysis experiments.

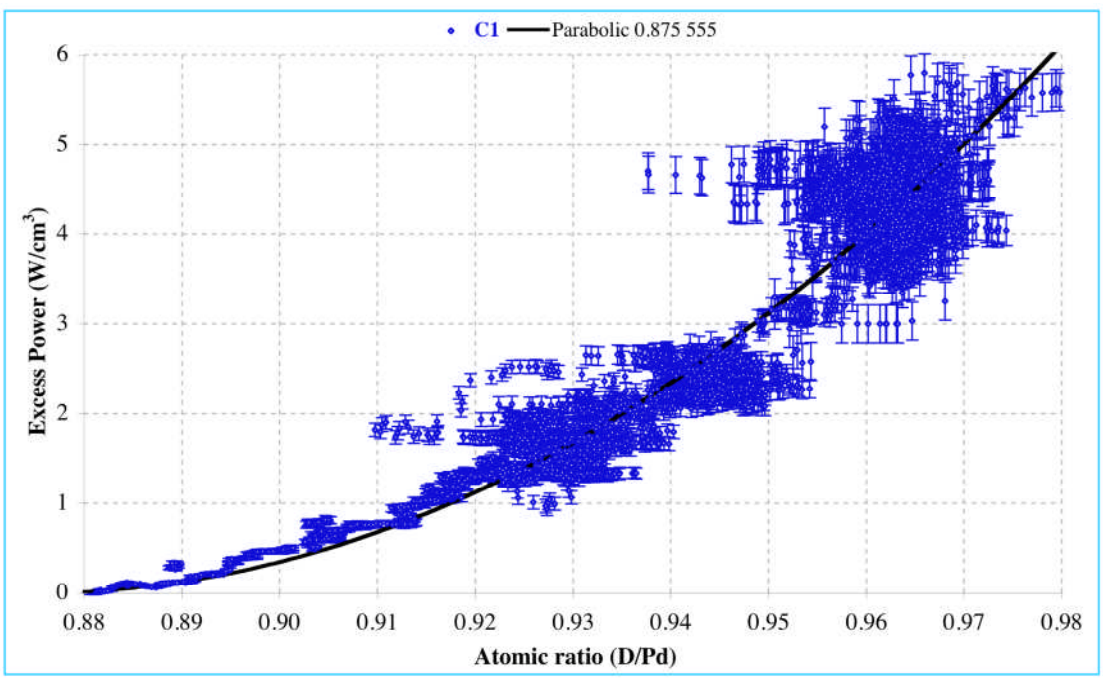

Figure 4. The effect of deuterium loading on excess heat production in FPE electrolysis experiments.

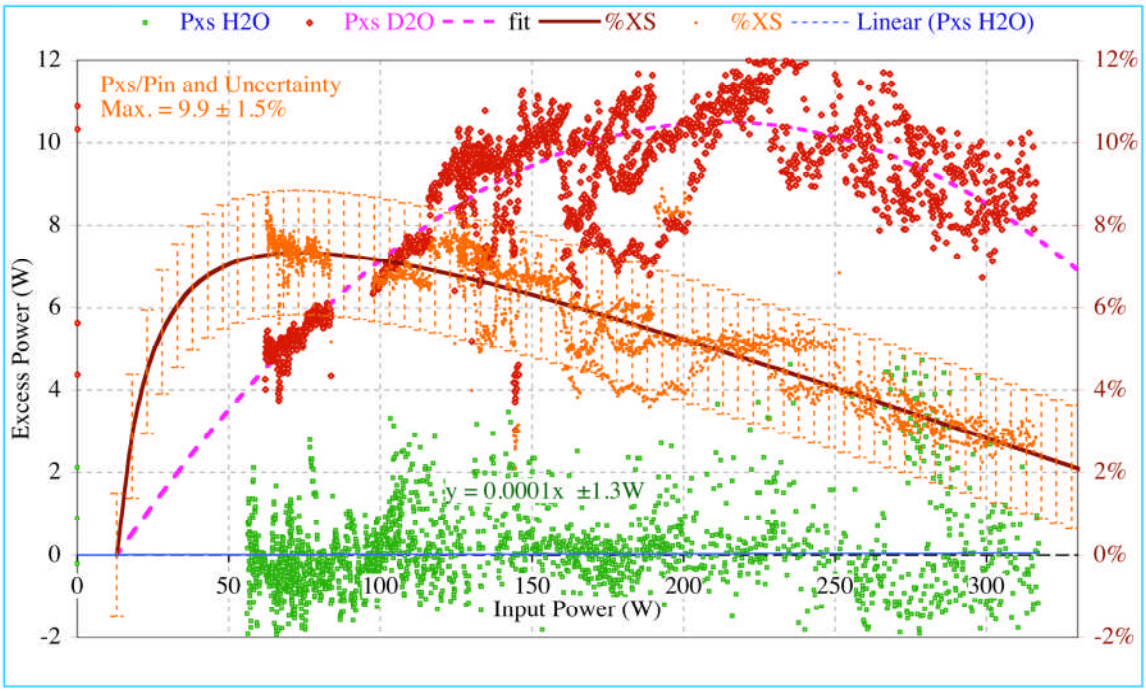

Figure 5. The effect of input power (and time) on excess heat production in Arata DS cathode experiments.

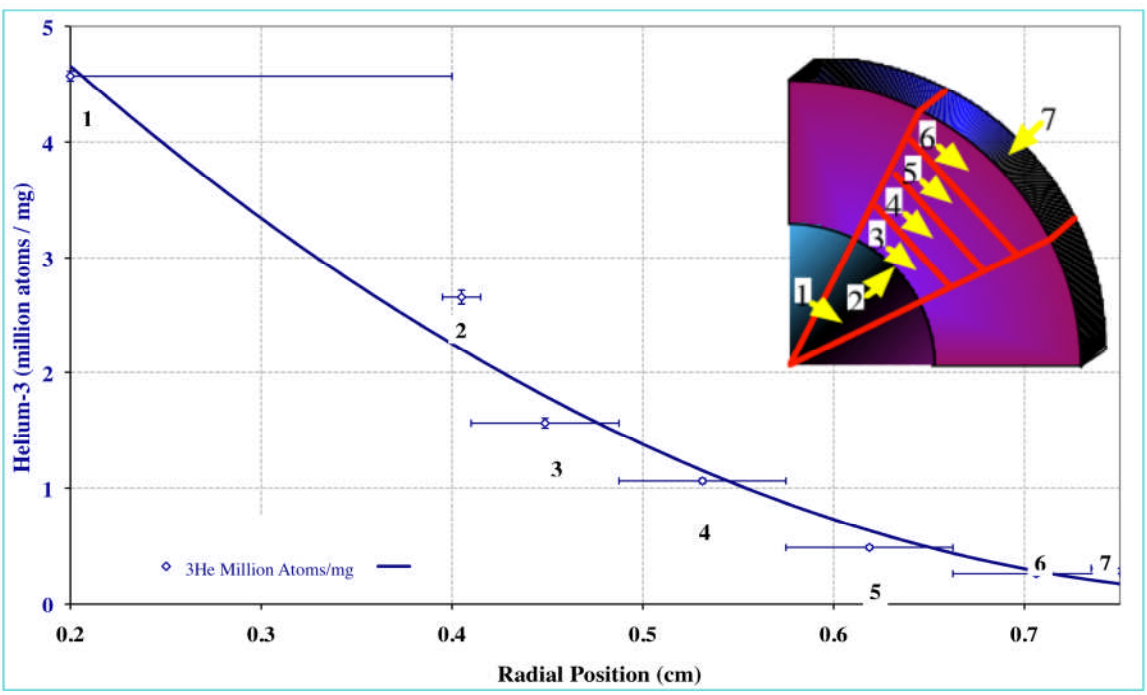

Figure 6. Logarithmic diffusion profile of ^{3}He following on excess heat production in Arata DS cathode experiments.

Table 1. Energetics Replication Results

	Cell - Calorimeter	Cathode	Min. R/R°	Max. D/Pd	Excess % of P_{In}	Power (mW)	Energy (kJ)
1	9-7 E	Lot A	1.77	0.895	<5%		
2	11-8 E	L5(2)	1.67	**0.915**	**60%**	**340**	**514**
3	12-9 E	Lot A	1.84	0.877	<5%		
4	15-7 E	L5(1)	1.77	0.895	<5%		
5	16-8 E	L5(4)	1.86	0.871	<5%		
6	17-9 E	L1(1)	1.55	**0.939**	**20%**	**460**	**407**
7	21-7 E	# 830	1.92	0.836	<5%		
8	22-8 E	L5(3)	1.8	**0.888**	**30%**	**200**	**188**
9	35-7 S	L17(1)	1.32	**0.985**	**12%**	**1800**	**553**
10	35-8 S	L17(2)	0.95	**1.059**	**13%**	**2066**	**313**
11	35-9 S	L17	1.39	0.971	1%		
12	43-7 S	L14-2	1.73	**0.903**	**80%**	**1250**	**245**
13	43-8 S	ETI	1.63	0.923	**5%**	**525**	**65**
14	43-9 S	L14-3	1.61	0.927	1%		
15	51-7 S	L25B-1	1.55	**0.939**	**12%**	**266**	**176**
16	51-8 S	L25A-2	1.52	**0.945**	**5%**	**133**	**14**
17	51-9 S	L19	1.54	**0.941**	**43%**	**79**	**28**
18	56-7 S	L24F	1.55	**0.939**	**15%**	**2095**	**536**
19	56-8 S	L24D	1.84	0.877	4%		
20	56-9 S	L25B-2	1.56	0.937	3%		
21	57-8 S	Pd-C	N.A.	N.A.	**300%**	**93**	**115**
22	58-9 S	L25A	1.69	**0.911**	**200%**	**540**	**485**
23	61-7 S	L25B-1	1.63	**0.923**	**50%**	**105**	**146**

E = Energetics and S = SRI Data Acquisition.

In addition to the high levels of loading and reproducibility of excess heat production this set of experiments had several other desirable characteristics. Experiment failures (null results) were understandable in terms of our inability to meet and exceed known threshold criteria: loading, maximum loading, loading duration and interfacial deuterium flux.

One striking feature is the power of the SuperWave in moving deuterium through the interface. Figure 7 shows the measured resistance ratio and deuterium loading calculated for three points in the 20 minute SuperWave current exercise cycle: the minimum, mean and

maximum values. From these values we can calculate the net interfacial flux of deuterium absorption and desorption. For an electrode with an active surface these values were measured to be as high as 20 mA cm^{-2}. This value is higher by far than any previously measured at SRI using dc or any other waveforms except under strong transient conditions.

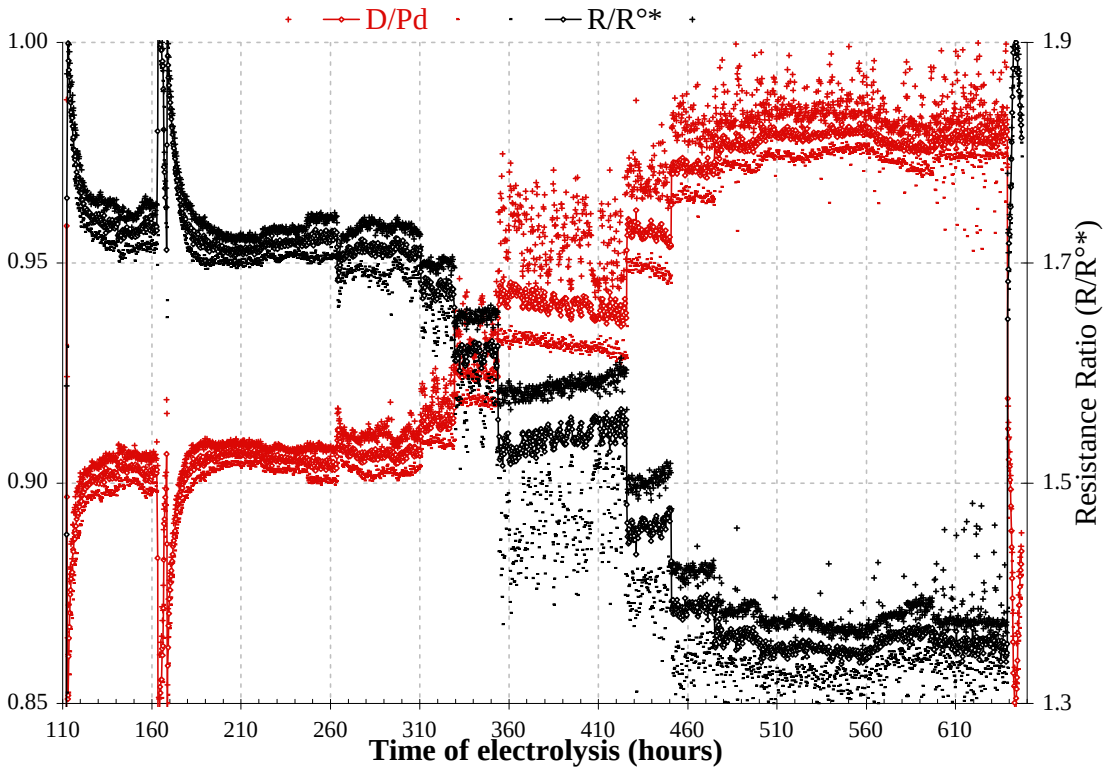

Figure 7. Resistance ratio and deuterium loading during SuperWave electrolysis of an 80 × 7 mm 50 mm thick ENEA Pd foil in 0.1 M LiOD.

The existence of data sets demonstrating high power gain and, even more particularly, high energy gain offers several specific benefits to FPE researchers:

i. High power gain and large values of excess power compared to calorimeter accuracy makes it easy to rule out systematic mismeasurement of input power or temperature as being the source of the FPE, even in discussions with individuals unfamiliar with calorimetric principles and practice.
ii. High energy gains and large values of integrated excess energy (often expressed in terms of eV per Pd atom) makes it easy to rule out energy storage or anomalous unseen chemical effect as being the source of the FPE, even in discussions with scientists and engineers not having specialized knowledge of materials science and chemistry.
iii. One spectacular experiment performed at Energetics designated as experiment 64 exhibited energy gains exceeding 25 and accumulated several keV/Pd atom of energy at temperatures at or above the boiling point of water [19]. Results such as

these suggest the potential for practical application and the possibility that FPE studies may move from experiment and research into engineering and development.

Conclusions

At least in this field the "reproducibility" standard is generally far harder to meet than most experimenters or the US Patent and Trademarks Office anticipate. The reasons for this are several:

1. Particularly in the early stages of invention the experimenter himself or herself may not be aware of all critical details of his or her experiment, and succeeds because of a knack or skill or habit that is not recognized and not easily transported or identified except by direct, careful observation.
2. All communication is imperfect. The advantage of written communication is that it creates a record capable of being improved. However writing suffers two great weaknesses. It is slow and painful and therefore shortcuts are taken and tedious and seemingly superfluous detail truncated or eliminated. It is therefore incomplete. Because of its permanent nature and the possibility (usually viewed as certainty) that posterity will be watching, scientists tend to make written reports appear far more rigorous than their actual procedures. The written record may therefore be over-complete and over-complex while possibly being a false or misleading report of what in fact was done.
3. In my experience scientists cannot resist the compulsion to improve. When first they hear of an experiment they begin immediately to think of a new and better way to get a bigger and more interesting effect. Don't! If the effect is artifactual it is important to reproduce the artifact that may precisely lie in the means of temperature measurement or the experiment geometry, *etc*. If the effect is real it may depend critically a peculiarity of the pump or power source, or on an interaction between variables that is unseen, unanticipated or misunderstood.

From nearly twenty years of work at SRI two important conclusions have emerged. Scientists can sometimes be wrong, and often oversimplify, but they are not incompetent or dishonest. Even after significant effort (and none of the experiments we worked on in this field required less than 3 months sustained effort to form even a provisional opinion), don't assume you were lied to or that "the other guy" is "an incompetent boob". If it doesn't work it is your fault.

Reproduce exactly first. Work with the originator directly, in person, understand their procedures at every step until the original effect is recreated. In 1996 Lonchampt *et al* [20] set themselves the task of reproducing the original FPE work, in their words *"simply to reproduce the exact experiments of Fleischmann and Pons - to ascertain the various phenomena involved in order to master the experiments"*. The phrase underlined is critical. Only from the point of mastery can systematic effects be studied, whether these are errors, artifacts or new physical processes.

As far as I am aware Lonchampt and his team were and remain the only group ever to attempt an exact engineering replication of the original Fleischmann Pons experiment. It helps

considerably that they were engineers, not scientists. Lonchampt *et al* may also have been the only group ever to publish a paper with the goal of FPE replication in its title [20]. They also were successful and closely specified the conditions under which replication was possible:

i. The Fleischmann Pons calorimeter with precautionary measures taken is simple and precise.
ii. Their calorimeter is very accurate and well adapted to study cold fusion.
iii. The maximum error might be in the higher temperature range, and under any condition should not exceed 1% of the input power.
iv. The effect measured [now called the FPE] *is:*
- below 70°C, between 0 and 5%
- between 70°C and 99°C, about 10%
- at boiling, up to 150%

At this point I hope I am permitted to conclude with a personal remark or two. If the claim is made that replication is crucial to the development of our field to determine the parameters for advancement, to prove reality to critics, or to uncover systematic error, then it is astonishing that attempts to replicate the FPE have been so few, and methodologically so limited. I do understand the reasons, and am as guilty as any FPE researcher. But it must be completely understood that this lack of attention to detail and the failure to assimilate what Lonchampt taught us, is precisely the reason that the question of replicability remains on the table, and is the motivation for this paper.

One important reason for this lack of focused attention on the question of reproducibility is that this is not the most important question now, and was not in 1989 although it may become so in the near future. The question of reproducibility, while undeniably important, is almost trivial compared with the question of whether or not there is evidence of a new physical effect. Confining attention to the FPE, the pressing and fundamental question is: is there evidence for heat production consistent with nuclear but not chemical effects in the deuterium-palladium system? Clearly the answer is yes. This fact has been established at a level far above working hypothesis as a "working reality" to a by a large numbers of experimenters in many and diverse experiments.

References

1. New Oxford American Dictionary.
2. Hagelstein, P. L., McKubre, M. C. H., Nagel, D. J., Chubb, T. A., and Hekman, R. J., "*New Effects in Metal Deuterides*", in *11th International Conference on Cold Fusion*, Biberian, J-P., Marseilles, France, 2004, pp. 23.
3. Storms, E., The science of low energy nuclear reactions, World Scientific, 2007.
4. Miles, M. H., and Bush, B., "*Search for Anomalous Effects Involving Excess Power and Helium during D_2O Electrolysis Using Palladium Cathodes*", in *3rd International Conference on Cold Fusion*, Ikegami, H., Nagoya, Japan, 1992, p. 189.
5. Gozzi, D., Caputo, R., Cignini, P. L., Tomellini, M., Gigli, G. Balducci, G. Cisban, E., Frullani, S., Garibaldi, F. , Jodice, M., and Urciuoli, G. M., "*Excess heat and nuclear*

product measurements in cold fusion electrochemical cells", in *4th International Conference on Cold Fusion*, Passell, T. O., Lahaina, USA, Vol. 1, 1993, p. 2-1.
6. Botta, E., Bracco, R., Bressani, T., Calvo, D., Cela, V., Fanara, C., Ferracin, U., and Iazzi, F., "*Search for* 4*He production from Pd/D systems in gas phase* in *5th International Conference on Cold Fusion*, Pons, S. IMRA Europe, Sophia Antipolis Cedex, France, Monte-Carlo, Monaco, 1995, p. 233.
7. Arata, Y., and Zhang, Y-C., "*Helium (^{4}He, ^{3}He) within deuterated Pd-black*", Proc. Japan Acad. 73B (1997). p. 1.
8. McKubre, M. C. H., Tanzella, F. L., Tripodi, T., and Hagelstein, P. L., "*The Emergence of a Coherent Explanation for Anomalies Observed in D/Pd and H/Pd Systems; Evidence for ^{4}He and ^{3}H Production*", in *8th International Conference on Cold Fusion*, Scaramuzzi, F., Lerici, Italy, 2000, p. 3.
9. Letts, D., and Cravens, D., "*Laser Stimulation of Deuterated Palladium: Past and Present*", in *10th International Conference on Cold Fusion*, Hagelstein, P. L., Cambridge, USA, 2003, p. 159.
10. McKubre, M. C. H., Tanzella, F. L., Hagelstein, P. L., Mullican, K., and Trevithick, M., *"The need for Triggering in Cold Fusion Reactions"*, in *10th International Conference on Cold Fusion*, Hagelstein, P. L., Cambridge, USA, 2003, p. 199.
11. Storms, E., *"Use of a very sensitive Seebeck Calorimeter to study the Pons-Fleischmann and Letts Effects"*, in *10th International Conference on Cold Fusion*, Hagelstein, P. L., Cambridge, USA, 2003, p. 183.
12. Swartz, M. R., *"Photo-induced Excess Heat from Laser-irradiated Electricallt Polarized Palladium Cathodes in D_2O"*, in *10th International Conference on Cold Fusion*, Hagelstein, P. L., Cambridge, USA, 2003, p. 213.
13. Patterson, J. A., "System for Electrolysis", U.S. Patent #5,494,559, 1996.
14. Stringham, R., Chandler, J., George, R., Passell, T. O., and Raymond, R., *"Predictable and reproducible heat"*, in *7th International Conference on Cold Fusion*, Jaeger, F., Vancouver, Canada, 1998, p. 172.
15. McKubre, M. C. H., Tanzella, F. L., Dardik, I., El Boher, A., Zilov, T., Greenspan, E., Sibilia, C., and Violante, V., Replication of Condensed Matter Heat Production, in *Low-Energy Nuclear Reactions Sourcebook*, Marwan, J., ACS Symposium Series 998, Oxford University Press, 2008, p. 219.
16. Castagna, E., Sansovini, M., Lecci, S., Rufoloni, A., Sarto F., Violante V., Knies, D.L., Grabowski, K.S., Hubler, G.K., McKubre, M.C.H., and Tanzella, F. L., in *14th International Conference on Cold Fusion*, Washington, USA, 2008 (submitted).
17. McKubre, M. C. H., Crouch-Baker, S., Hauser, A. K., Smedley, S. I., Tanzella, F. L., Williams, M. S., and Wing, S. S., Concerning reproducibility of excess power production, in *5th International Conference on Cold Fusion*, Pons, S. IMRA Europe, Sophia Antipolis Cedex, France, Monte-Carlo, Monaco, 1995, p. 17.
18. McKubre, M. C. H., and Tanzella, "*New Effects in Metal Deuterides"*, final Phase I report submitted by SRI to DARPA, 2007.
19. Dardik, I., Zilov, T., Branover, H., El-Boher, A., Greenspan, E., Kachatorov, B., Krakov, V., Lesin, S., and Tsirlin, M., "*Excess heat in electrolysis experiments at Energetics*

Technogies”, in *11th International Conference on Cold Fusion*, Biberian, J-P., Marseilles, France, 2004, pp. 84.
20. Lonchampt, G., Bonnetain, L., and Hictor, P., “*Reproduction of Fleischmann and Pons Experiments*”, in *6th International Conference on Cold Fusion*, Okamoto, M., Toya, Japan, 1996, p. 113.

Electrical Breakeven from LANR Phusor Device Systems: Relative Limitations of Thermal Loss in Feedback Loop

Mitchell Swartz
JET Energy, Inc. Wellesley, MA 02481 (USA)

Dr. Mitchell Swartz does not wish to have his papers uploaded to LENR-CANR.org. A copy of this paper can be found here:

http://www.iscmns.org/iccf14/ProcICCF14b.pdf

This page intentionally left blank

This page intentionally left blank

This page intentionally left blank

This page intentionally left blank

This page intentionally left blank

This page intentionally left blank

Self-Polarisation of Fusion Diodes: From Excess Energy to Energy

Fabrice David and John Giles
Deuo Dynamics
Moss Side House, East Blairdaff, Aberdeenshire, AB51 5LT. (UK)
http://www.deuodynamics.com

Abstract

Conventionally, the cold fusion reaction produces heat. (1),(2) The authors have sought a different approach, wherein the device has no input energy, relying on the energy produced by cold fusion in the device. The device consists of diodes fabricated as powder, with a large surface junction made up of a semiconductor in contact with palladium charged with deuterium.

The apparent fusion reactions take place in the junction between the semiconductor and the Palladium powder, which produces an excitation which is transmitted to the electrons. This excitation increases their energy and allows them to cross the bandgap of the semiconductor and pass into the conduction band, as in a photovoltaic cell. This energy very quickly appears as a spontaneous potential difference which can reach over 0.5 volt per junction.

The potential drop concentrates on the junction region, and at a nano scale the electric field reaches considerable values, higher than the megavolt per meter, which constrains the deuterium nuclei and increases the probability of deuterium fusion. (3),(4)

Experimental Device

Diodes comprising of a stack of junctions were made, making it possible to obtain over 1 volt at the poles of a very compact device of a few centimetres long. The power generated by the device remains very low for the moment, but it should be noted that it is in the form of directly usable electrical energy, and not thermal energy. The authors compare the density of energy obtained in their device, with the density of energy released by the first atomic pile produced by Fermi in Chicago. The levels of energy are very comparable to the fusion diode. The authors describe the various devices experimented with and used during this work over the last two years.

As part of this work, an extremely sensitive calorimetry device was built. The authors present the principle of this device, as well as a project for detecting of neutrons from very weak sources. This neutron counter records the particles emitted in all the directions of space, and can be scaled to the size of the neutron source.

Our concept considers that before transforming itself into heat, the energy released by fusions of the deuterium initially will produce an excitation of the atoms. It is the same thing when a

photon of visible light hits a solid, initially electrons of the atoms of the solid are excited, and after this first step, the energy is decayed into heat.

It is possible to take this energy away before its transformation into heat: in a photovoltaic cell. A solar cell is a diode with a large surface. When photons fall on the junction zone, certain atoms are excited, and electrons pass from a low energy level to a higher energy level.

The photons are absorbed by the silicon atoms, it is why this material is dark. In a crystal of silicon, or in a black paint, the energy is converted into heat. In a silicon solar cell, or in a dyed organic solar cell, part of this energy is transformed into electric current. It appears a voltage between the poles of the cell.

In our experiment, we tried to replace the light with fusion energy.

Materials and Methods

The following materials are used to make these devices:

Palladium powder (Sigma)
Gas Deuterium (Sigma)
Silicon powder (Sigma)
Other semiconductors (Sigma)

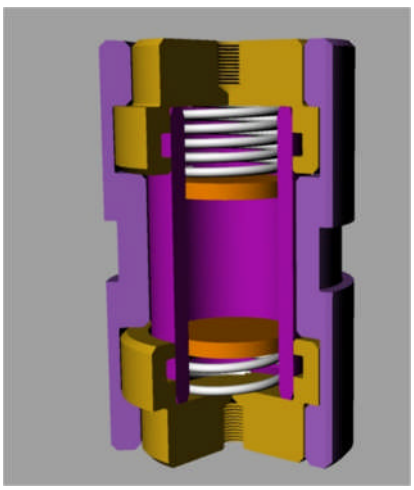

Figure 1. Fusion cell

We built our Fusion Diode by mixing palladium powder and semiconductor powder, in order to obtain a decreasing silicon gradient, and a increasing palladium gradient throughout the tube. This forms a zone of contact (junction) between the semiconductor and palladium. This zone of contact generates a very a large contact surface. Importantly it will be noticed that not only a voltage appears, but that this voltage is concentrated in a thin zone, the junction zone. If the junction thickness is 0.5 micrometer, and the voltage 0.5 volt, the field equals one million volts per meter.

We propose that in this field of one million volts per meter, the deuterium fusion reaction occurs.

Our first diodes were made in glass tubes. At the base of these tubes (0.7 cm in diameter) is welded a platinum wire. Palladium powder is packed around this wire. The powder is then packed using a glass push rod. Finally a glass fibre stopper is put in place to retain the powder but allow the gas to flow. A copper connection passes through this stopper. The glass tube is then placed in a pressure vessel with an electrical connection. See Figure 2.

The terminals of the diode are connected to a datalogger.

This vessel is evacuated, and then filled with deuterium gas.

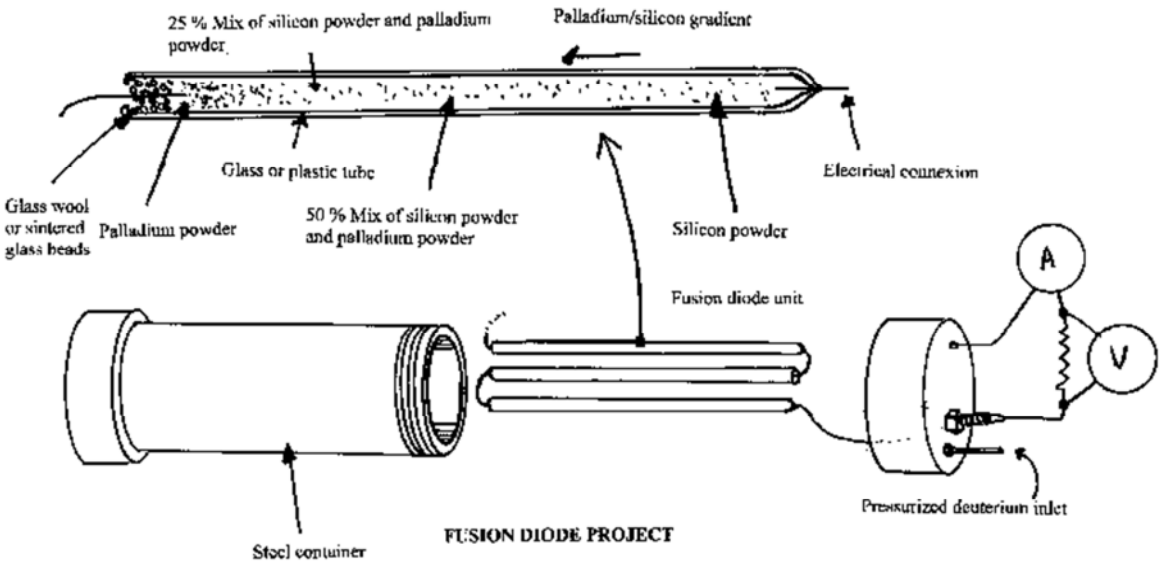

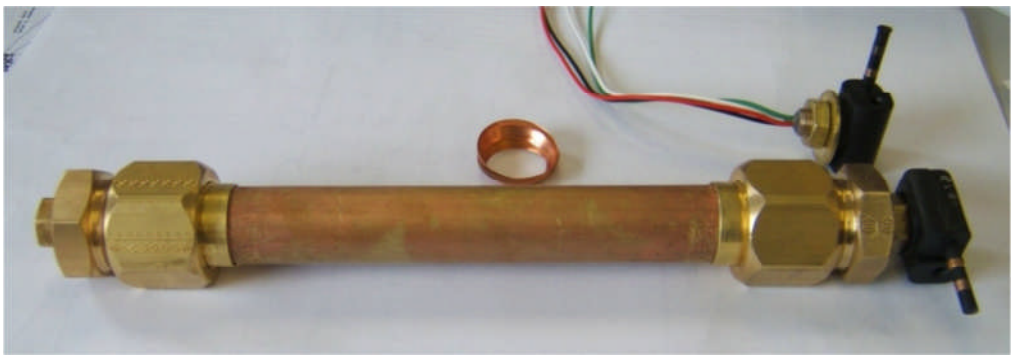

Figure 2. First generation diode and pressure vessel

Figure 3. Diode being prepared.

We developed another procedure using a nylon plastic tube with brass end fittings. Each metal cap contains a strong spring, which compress the powder. The whole device is protected by another polypropylene tube (Fig. 1).

We used Swagelok ™ valves at each end.

Figure 4. Second generation devices.

Results

A. Self-sustained voltage

Once the D_2 is introduced to our device, voltage quickly rises from zero to 0.5V.

To exclude environmental noise, we first use argon as the cell gas and log the cell for a week, following the argon the cell is evacuated, then filled with H_2, and left for a second week. The H_2 is then removed from the cell, which is evacuated and then filled with D_2, and run for a week. The results are shown in Fig. 5.

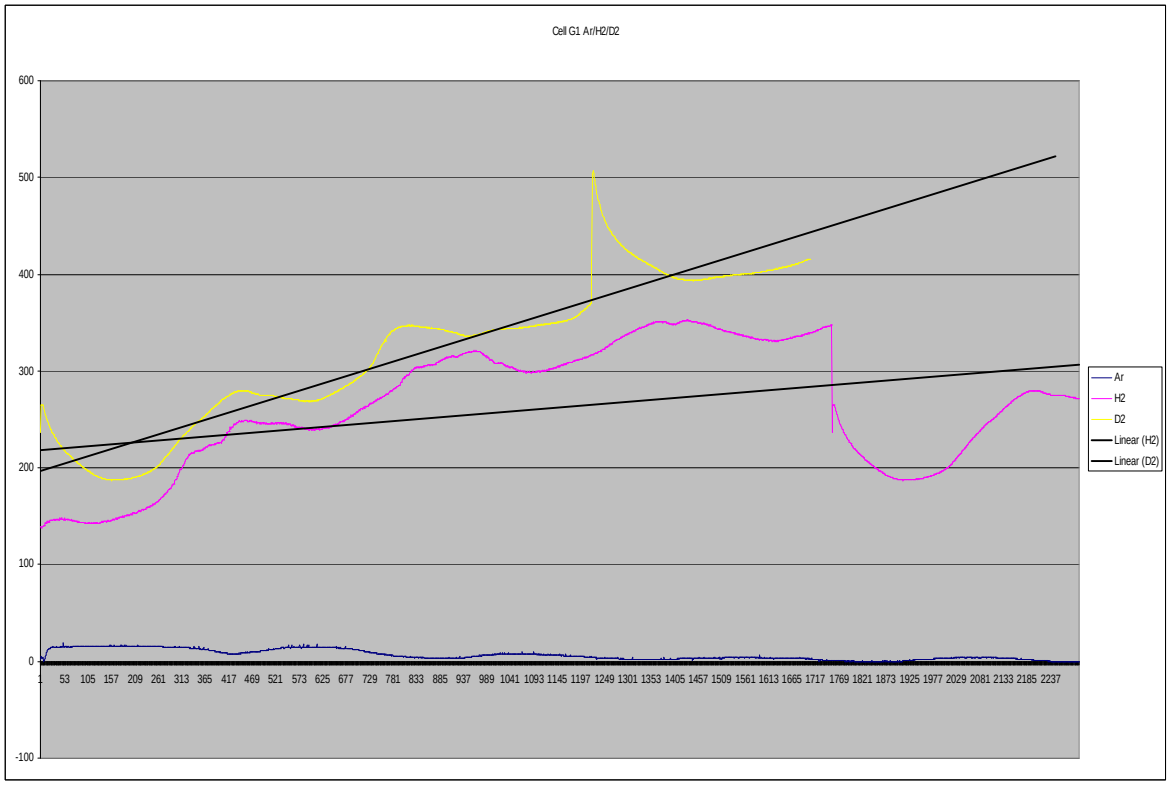

Figure 5. Voltage rise with D_2 and H_2

We conducted a triple-blind test with each diode. The triple-blind results on the chart followed a three week test period. A week on Argon, during which no voltage was observed, a week on H_2, which showed a level of voltage, and a week of D_2 which showed a higher level of voltage.

The argon experiment demonstrated that factors such an external electrical energy, or some galvanic action between the powders of the cell are not the reason for the voltage. However obviously, as a voltage was seen with the H_2 some hydrogen oxidation can not be ruled out.

We know that the H_2 is impure, and there is always 0.03% deuterium present in the gas (mainly in the form of HD molecules). In the palladium, HD dissociate, and we think that the

voltage observed with H_2 is the sign of the fusion of the deuterium nuclei. At the end of several weeks, the deuterium stock would disappear and the voltage should decrease.

We get 0.5 volt with D2. Connected to a resistor of the same range than the internal resistance of the diode (some hundred of kilo ohms) we have recorded a power in the microwatt range. After several weeks, the power began to reduce, because there were leaks of deuterium through the “Swagelok” valves.

Summary measurement of radioactivity

Gamma ray measurements. We tested our device with two types of Geiger counters and semiconductor radiation meter. We did not detect any significant radioactivity.

Quick look for neutrons. To look for neutrons, we included some Cadmium into the cell mixture. We placed the cell against a Geiger counter but we did not detect any gamma rays. We were looking for the reaction: $^{113}Cd + n \rightarrow {}^{114}Cd$ + gamma ray

Experiments in progress

We are not sure that what we are seeing is Cold Fusion. We have some indications, but we do not wish to jump to hasty conclusions.

We built a new differential calorimeter, and we hope that this apparatus will be sensitive enough to correlate measurements of current and electric tension (electrical power) with measurement of calorific release.

Here is the principle of our differential calorimeter: Two similar Dewar flasks contain distilled water. Two similar resistance heaters heat the water to 100°C. The water is raised to boiling in both Dewars. The two resistance heaters are placed in series. The fusion device is placed in one of the Dewar flasks, a weight of the same mass in the other one.

Both Dewar flasks are placed on electronic weight scales (Fig. 6). We record the difference of the mass during the experiment. If the atmospheric pressure drops, or if the temperature of the laboratory varies, or if the electric current of heating varies, the variation will be the same in the both Dewar flasks. The device is self-correcting.

Of course, the resistances and the two Dewar flasks are never completely identical, which is why a variable resistance is placed in parallel with one of the flasks. This makes it possible to zero the system before the diode is introduced into the device. The diode is sealed in a glass tube.

Figure 6. Differential calorimeter

Conclusion

For nearly two decades, cold fusion researchers have tried to prove the existence of cold fusion on the basis of empirically produced excess heat. Many mainstream scientists have rejected this, claiming that heat alone is inconclusive. The authors have developed a different approach, in which the device has no input energy, producing energy spontaneously. The diodes are fabricated as powder diodes, with a large surface area of a semiconductor in contact with palladium and charged with deuterium.

The apparent fusion reaction takes place in the junction between the semiconductor and the palladium powder. This produces an excitation which is transmitted to the electrons. This excitation increases their energy and allows them to cross the bandgap of the semiconductor and pass into the conduction band, as with a photovoltaic cell. The energy very quickly appears as a spontaneous potential difference, which can reach over 0.5 volt per junction.

The potential drop concentrated in the junction region (at nano scale) reaches considerable values, higher than a megavolt per meter. This constrains the deuterium nuclei and increases the probability of deuterium fusion. Our observations are compatible with the theories which were presented by the majority of the eminent theorists who have worked on the subject for years. We can quote some: Resonant Tunnelling, Condensates of Bose-Einstein, Diafluidity, Erzions, Polyneutrons, Monopoles, etc...(5),(6)

A diode, comprising of a stack of junctions was made, producing over a volt. While it may be possible to obtain many volts with a very compact device, of a few centimetres length, we have never tried this. The released power remains very low for the moment, but it should be noted that it is directly usable electrical energy, not low temperature thermal energy.

The energy density produced by this devices is comparable to that of the first atomic pile at the University of Chicago in 1942 (Chicago-Pile 1): the Fusion Diode has 1 g of palladium, and had an electrical power in the range of the microwatt, giving a mass/power ratio of 10^{-6} W/g. Chicago-Pile 1 weighed 864,000 pounds (nearly 431 tons) and produced 100 W of thermal energy. This was probably peak power, because the reactor was not shielded, and most of the scientists of the Fermi team managed to live to a ripe old age. The Chicago-Pile 1 had a power to weight ratio of 0.25×10^{-6} W/g.

It is important to note that palladium is not the only effective material to obtain fusion reactions. There are other possibilities we have yet to explore. We expect to find in the future other materials which may be even more favourable to the establishment of fusion reactions. We think that we are at the dawn of a new era, such as when Kamerlingh Onnes discovered superconductivity. At that time, the only super conductor was mercury, which loses resistivity at 4 K. With mercury it would be impossible to build the magnets of ITER and of the LHC.

Acknowledgement

The authors thank the Municipality of the town of Franconville (Val d'Oise, France) and the Honorary Deputy and Mayor, Mr F. Delattre, for funding of this work.

References

1. M. Fleischman and S. Pons. *J. Electroanal. Chem.*, (261):301, 1989
2. S.E. Jones, E.P. Palmer, J.B. Czirr, D.L. Decker, G.L. Jensen, J.M. Thorne, and S.F. Taylor & J. Rafelski, Nature 338: 737-740 (1989).
3. French patent n° **FR 2662537 (25/05/1990)**
4. **French patent n°** FR2729249 (11/01/1995)
5. Fabrice David. *FUSION* n° 49 jan.-fev. 1994 (french edition of *XXIth Century Science et Technology*)
6. Fabrice David , *FUSION* n°92 sept-oct 2002 pp 23-29

Weight of Evidence for the Fleischmann-Pons Effect

Rodney Johnson and Michael Melich
W. E. Meyer Institute of Systems Engineering,
Naval Postgraduate School, Monterey, CA[1]

Abstract

D. Cravens and D. Letts [1] have analyzed a portion (167 papers) of the published literature reporting on D_2O electrolysis experiments such as Fleischmann and Pons's (FP). They identify four criteria for what constitutes a "proper" FP experiment and state that experiments that satisfy all four criteria are likely to succeed in producing excess heat, while those that do not are likely to fail. This paper presents results of using a Bayesian network for probabilistic analysis of this claim. Consideration of a small subset of the papers (eight) is sufficient to give a likelihood ratio of about 10 to 1 in favor, and this number appears to grow generally rapidly, though not monotonically, as more papers are added to the set.

1. Introduction

Some of us, when asked why we tend to accept the reality of the Fleischmann-Pons effect, reply with the statement:

> *"It's not any one experiment; it's the number and variety of confirmations by independent researchers around the world."*

More generally, independent replication is considered an important step in acceptance of new experimental results. This paper reports an attempt to model the situation using a Bayesian network: a proposition ("The effect is real") with a number of pertinent reports, each open to doubt, but collectively sufficient to convert initial doubt (a low prior probability) into acceptance (a high posterior probability, conditional on the evidence).

1.1. Cravens-Letts database

D. Cravens and D. Letts [1] report a study of 167 selected papers concerning heat generation in electrochemical systems of the "classical" Fleischmann-Pons type: electrolytic cells with Pd cathodes in D_2O-based electrolyte. The list spans the years 1989–2007 and is non-exhaustive mainly because papers were included only if available in digital form. The authors rated the papers, when possible, according to four *yes/no* "enabling criteria," related to (1) cathode loading, (2) good chemical procedures, (3) operating current densities, and (4) non-equilibrium operation. (See the paper [1] for detailed statements of how the criteria were assigned.) In addition they assigned a *yes/no* value according to whether excess power was reported or not.

[1] The views expressed herein are those of the authors and not necessarily those of the U.S. Government, Department of Defense, Department of the Navy, or the Naval Postgraduate School.

They succeeded in rating 122 of the 167 papers and, after statistical analysis, concluded that production of excess power was highly correlated with the number of criteria satisfied—very likely if all four were met and less likely if fewer were met. We here report on a probabilistic test of that claim by use of a Bayesian network.

1.2. What is the problem?

We are interested in questions such as:

> "*Given* that in paper #1, where all 4 criteria were met, heat was observed, *and* in paper #2, where only 2 criteria were met, no heat was observed, *and* . . . in paper #167, . . . heat was observed, *then* what can we say about the probability that the FP effect is "real"? And what is the probability that a new experiment satisfying all 4 criteria will produce excess heat?"

In condensed-matter nuclear science in general we face multiple observations and experimental results, and multiple conjectures and hypotheses that might explain them.

To illustrate, consider the propositions:

A: Nuclear reactions occur at low temperature in solids.

B: Excess heat is observed.

C: Helium production is observed.

D: Emission of energetic particles is observed.

Then *B, C,* and *D* are observations that can serve as evidence in support for *A*, considered as a hypothesis. Likewise, consider propositions:

E: Known nuclear reactions & quantum many-body effects.

F: "New physics".[1]

G: Error / deception.

H: Excess heat is reported.

Then *E, F,* and *G* are alternative hypotheses that might explain observation *H.* The relations between the propositions are shown schematically in Figs. 1 and 2. These are simple examples of *Bayesian networks,* which are discussed in Section 2.2 below.

[1] . . . whatever we might choose to mean by the phrase. The propositions listed here are informal, abbreviated, and intended primarily as illustration.

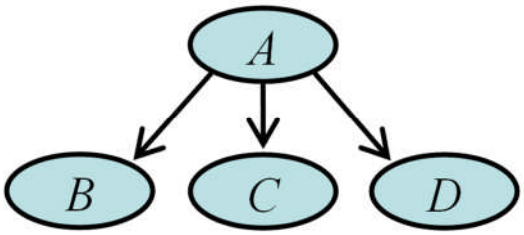

Figure 1. Multiple support for a hypothesis

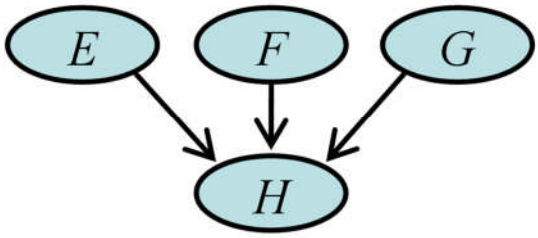

Figure 2. Alternative explanations

2. Bayesian methods

In general there may be more complicated interrelations (as in Fig. 3 further down). We need help in thinking quantitatively about such problems, and probability theory provides tools for doing so. *Bayes's rule* (or *Bayes's theorem*) is a fundamental rule of probability, used in updating the probability of a proposition in the light of new information. There are various methods based on it (called "Bayesian"), including *Bayesian networks,* which allow representing complex relations between propositions and making inferences concerning their probabilities.

2.1. Rules for probability

The degree of credence we accord to a proposition is (or should be) subject to change when we learn new relevant information. In quantitative terms, if A is a proposition to which we have initially assigned a probability $P(A)$, and we then obtain new information in the form of a proposition B, we update the probability of A to a quantity $P(A \mid B)$, the *conditional probability of A, given B.* One also uses the terms *prior* and *posterior* probabilities for $P(A)$ and $P(A \mid B)$, respectively. The process could continue, of course. Obtaining further new information, say C, leads to $P(A \mid BC)$, and so on. In this section we collect some basic rules, prominent among them Bayes's theorem, for dealing with conditional probabilities. We recommend the textbook by Jaynes [2] for (along with much else) a thorough discussion of what we here touch on lightly.

2.1.1. Bayes example problem

It is common in textbooks to introduce Bayes's theorem with an example: medical screening. Say you are a doctor screening for an uncommon but serious disease, where "uncommon" means

> 1% of people in the general population have the disease.

Also suppose there is a quite reliable test for the disease:

> 98% of people with the disease will test positive;
> 95% of those without the disease will test negative.

You give one of your patients the test as part of a routine physical, and the results come back positive. Do you tell the patient: "There is a 98% chance that you have a serious disease"?

We will see that the probability is actually closer to 16.526%, or about one chance in six, not 98%. Your patient is probably healthy. (Expensive or risky treatment is unjustified. But more testing is mandatory; ignoring a 1 in 6 chance amounts to Russian roulette.)

We express the given information symbolically:[1]

D: disease T: test positive
D': no disease T': test negative

$P(D) = 0.01$: probability of having the disease in the absence of test results
$P(D \mid T)$: the conditional probability of having the disease, given positive test results.

We want $P(D \mid T)$. We have $P(D)$ and two other conditional probabilities:

$P(T \mid D) = 0.98$: probability of a positive test, given that the disease is present;
$P(T' \mid D') = 0.95$: probability of a negative test, given that the disease is absent.

2.1.2 Rules

Product rule: probability that A and B are both true

$$P(AB) = P(A)\, P(B \mid A) = P(B)\, P(A \mid B)$$

Bayes's rule:

$$P(A \mid B) = P(B \mid A)\, P(A) / P(B)$$

Sum rule:

$$P(B) = P(B \mid A)\, P(A) + P(B \mid A')\, P(A') + P(B \mid A'')\, P(A'') + \ldots$$

where $A, A', A'', \ldots$ are an exhaustive set of mutually exclusive propositions—that is, one must be true, but no two can be true at once.

Bayes's theorem follows directly from the product rule: divide by $P(B)$. The sum rule is useful for evaluating the denominator $P(B)$ on the right-hand side of Bayes's rule. Some variants of these rules can be useful; we may use

$$P(A \mid B) = P(AB) / P(B) \tag{1}$$

in place of Bayes's rule as just given, and we may use the sum rule in the form

$$P(B) = P(AB) + P(A'B) + P(A''B) + \ldots \tag{2}$$

2.1.3 Solution of example problem

Applying Bayes's rule to the previously given probabilities gives

[1] In general (as in the "sum rule" of Section 2.1.2) we use a notation such as $A, A', A'', \ldots$ to denote a set of propositions exactly one of which is true. Here we assume that D and D' are such a set (one either has the disease or one doesn't) and likewise for T and T' (only two test results are possible: positive and negative). In this special case of just two alternatives, one can read the prime symbol as logical negation: *not-D* for D' and *not-T* for T'.

$$P(D \mid T) = P(T \mid D)\, P(D) / P(T)$$
$$= 0.98 \times 0.01 / P(T)$$

and the sum rule gives

$$P(T) = P(T \mid D)\, P(D) + P(T \mid D')\, P(D')$$
$$= 0.98 \times 0.01 + 0.05 \times 0.99$$
$$= 0.0098 + 0.0495 = 0.0593$$

where we have used the fact that $P(T \mid D') = 1 - P(T' \mid D') = 1 - 0.95 = 0.05$. Finally,

$$P(D \mid T) = 0.98 \times 0.01 / 0.0593 = 0.16526$$

which is the stated result of 16.526%, or about one chance in six.

2.2. Bayesian networks

A Bayesian network is a graphical representation of complex relations between propositions; it allows inferences concerning their probabilities. Figure 3 shows an example slightly more general than the ones shown in Figs. 1 and 2.

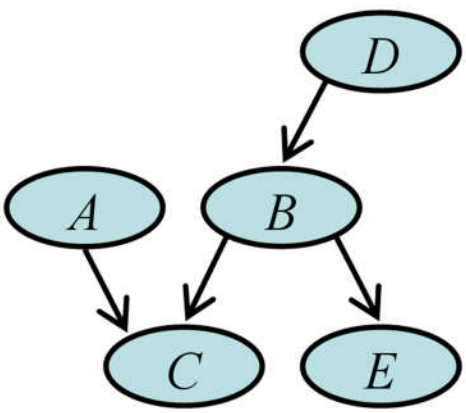

Figure 3. Bayesian network.

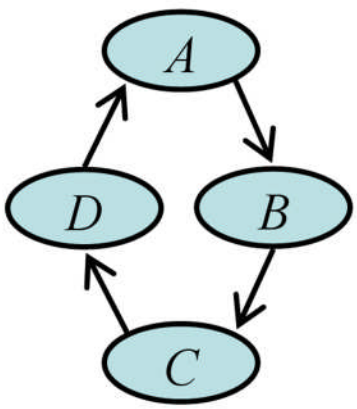

Figure 4. Loop (not allowed)

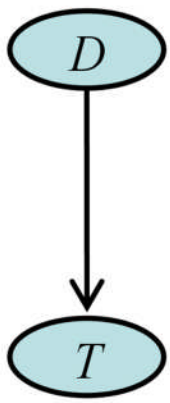

Figure 5. Medical screening example

A Bayesian network consists of nodes connected by arrows. Loops, as in Fig. 4, can lead to contradictions and are not allowed. (This means that the network is a *directed acyclic graph*.) With each node is associated a "random variable" (such as *A*, *B*, *C*, … in Fig. 3). By calling a variable such as *A* "random" we mean simply that:

(1) There is a set of possible values $\{a_1, a_2, \ldots, a_n\}$, so that the propositions $A = a_1$, $A = a_2$, …, $A = a_n$ form an exhaustive set of mutually exclusive propositions; and

(2) We can talk about probabilities (perhaps conditional) of these propositions, e.g. $P(A = a_i)$, $P(B = b_j \mid A = a_i)$.

True-false proposition, such as *D* and *T* of the medical screening example, are included (see Fig. 5); the set of values is just {*true*, *false*}.

Arrows indicate conditional dependence. If there is an arrow from a node *X* to a node *Y*, we call *X* a *parent* of *Y*. Thus the parents of *C* in Fig. 3 are *A* and *B*. A variable has a probability distribution conditional on its parents. In the case of *A*, *B*, and *C*, this means that conditional probabilities $P(C = c \mid A = a, B = b)$ are given for all values *a*, *b*, and *c* in the value sets of *A*, *B*, and *C*, respectively. This generalizes in a straightforward way to any number of parents. For a node without parents, such as *A*, we require the unconditional probabilities $P(A = a)$ for each *a*.

Bayesian networks can be used for updating our probabilities for values of some variables when we obtain new information in the form of values for other variables. This generalizes what we did in the medical screening example. There, we learned the value $T = true$ for the test result, making it no longer uncertain (or "random"). Consequently we were able to update our probability for *D*, disease, from the prior value $P(D)$ to the posterior value $P(D \mid T = true)$. Analogously, we could suppose we learn values for some of the variables, say *C* and *E*, in the more elaborate network of Fig. 3, and we could ask how the new information affects the probabilities for the values of some other variable or variables, such as *B*.

To begin, in terms of the conditional and unconditional probabilities associated with the nodes, we can write an expression for the *joint* probability distribution for the entire set of variables; for the illustrative network of Fig. 3, this is the set of probabilities $P(A = a, B = b, C = c, D = d, E = e)$ that $A = a$ *and* $B = b$ *and* $C = c$ *and* $D = d$ *and* $E = e$, where *a*, *b*, *c*, *d*, and *e* range over their respective value sets. We show this in a shorthand notation, writing *A* for $A = a$, *B* for $B = b$, etc., so that the desired set of probabilities is denoted by $P(ABCDE)$; they are then given by:

$$P(ABCDE) = P(A)\, P(B \mid D)\, P(C \mid AB)\, P(D)\, P(E \mid B) \tag{3}$$

In general there is one factor for each node, consisting of the associated probability expression (conditional or unconditional). From this we can calculate other conditional probabilities such as $P(B \mid CE)$, for example: the updated probabilities for *B*, given that we have learned values for *C* and *E*.

By equation (1), the alternative form of Bayes's rule from §2.1.2, we can write:

$$P(B \mid CE) = P(BCE) / P(CE) \tag{4}$$

We can get the numerator, $P(BCE)$, by using essentially the alternative form of the sum rule, equation (2) from §2.1.2: sum (3) over the variables that do not occur in $P(BCE)$:

$$P(BCE) = \sum_{a,d} P(A = a, B, C, D = d, E)$$

Likewise we get the denominator by summing over *B* as well:

$$P(CE) = \sum_{a,b,d} P(A = a, B = b, C, D = d, E) = \sum_{b} P(B = b, C, E)$$

And the last two equations allow us to compute the desired quotient in (4).

For more information about Bayesian networks, see the textbook by Jensen [3], for example. There are also useful on-line tutorials by Breese and Koller [4] and by Murphy [5].

Software support is necessary for work with networks of any substantial size. For the work reported here we took advantage of a Java applet written by Yap, Santos, et al. [6] at the University of British Columbia and made available for download.

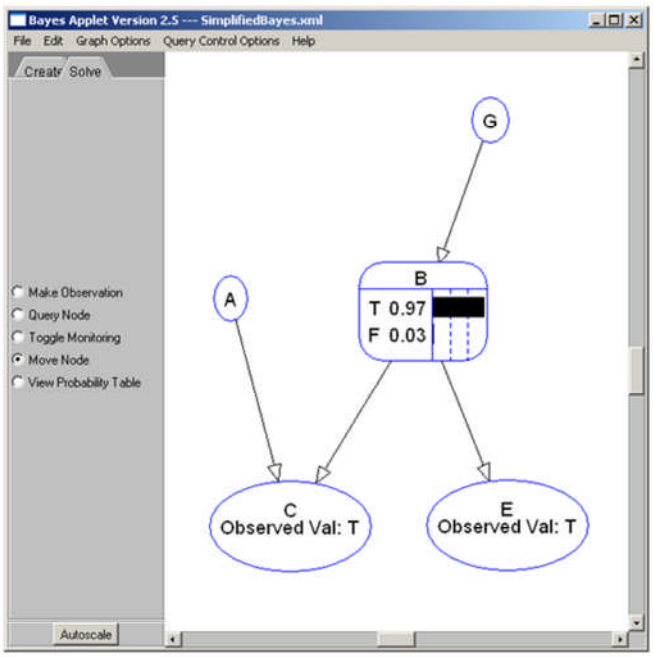

Figure 6. Bayesian network applet

This allows one to draw a network by means of a graphical interface, enter conditional probabilities in tabular form, set observed values for selected nodes, and display the resulting probabilities for other nodes. Figure 6 shows the display for a network similar to the one in Fig. 3.

2.3. Weight of evidence

For inference about a *yes/no* proposition, a formulation of Bayes's theorem in terms of *odds* and *likelihoods ratios* can be useful. First, a bit of terminology: The quantities $P(B \mid A)$, $P(B \mid A')$, $P(B \mid A'')$, … that occur in the sum rule (§2.1.2) are called the *likelihoods* of $A, A', A'', \ldots$.[1] For a pair of alternatives, A and A', the quotient $P(B \mid A) / P(B \mid A')$ is called the likelihood ratio. When these are the only alternatives, we have $P(A) / P(A') = P(A) / (1 - P(A))$; this quantity is the (prior) odds for A and denoted by $O(A)$. Similarly, the posterior odds for A are $O(A \mid B) = P(A \mid B) / P(A' \mid B)$.

Now write Bayes's rule for A and for A':

[1] Recall that $A, A', A'', \ldots$ form an exhaustive set of mutually exclusive propositions. "Likelihood" is used in a technical sense. The terminology is unfortunate because it may give the impression that the likelihoods are conditional probabilities of $A, A', A'', \ldots$, which they are not; in particular they need not sum to 1.

$$P(A \mid B) = P(A)\, P(B \mid A) / P(B)$$
$$P(A' \mid B) = P(A')\, P(B \mid A') / P(B)$$

and divide the first equation by the second. The factors of $P(B)$ cancel, and we get:

$$P(A \mid B) / P(A' \mid B) \;=\; [P(A) / P(A')]\, [P(B \mid A) / P(B \mid A')]$$

The left-hand side is the posterior odds for A, the first factor on the right is the prior odds, and the second factor is the likelihood ratio. Thus:

$$O(A \mid B) \;=\; O(A)\, [P(B \mid A) / P(B \mid A')]$$

which we can state as:

"posterior odds = prior odds × likelihood ratio"

If the "evidence" B consists of several observations B_1, B_2, … that are *independent* in the sense that $P(B_1B_2, \ldots \mid A) = P(B_1 \mid A)\, P(B_2 \mid A) \ldots$ and $P(B_1B_2, \ldots \mid A') = P(B_1 \mid A')\, P(B_2 \mid A') \ldots$, then the equation generalizes to

$$O(A \mid B_1B_2, \ldots) \;=\; O(A)\, [P(B_1 \mid A) / P(B_1 \mid A')]\, [P(B_2 \mid A) / P(B_2 \mid A')] \ldots$$

Taking logs of all the factors gives an additive version. Thus taking a new piece of independent evidence B_i into account just increments the log of our odds for A by

$$\log [P(B_i \mid A) / P(B_i \mid A')]$$

which is called the *weight of evidence* for A provided by B_i. (See Good [7] and Jaynes [2, pp. 91 ff.].)

If one starts with noncommittal prior odds of 1:1, evenly balanced between acceptance and rejection of a proposition, then the likelihood ratio of the evidence gives ones posterior odds. On the other hand, one can view the reciprocal of the likelihood ratio as a "critical prior": the prior odds such that the evidence would bring us to posterior odds of 1:1. In this latter role, the likelihood ratio can help us in assigning a numerical value to our prior odds for a preposition; imagine a successions of independent repetitions B_1, B_2, … of an experiment with a given likelihood ratio and ask how many successful outcomes would bring us to a state of uncertainty, poised between acceptance and rejection. (See Good [7] and Jaynes [2, Ch. 5].)

Our task will be to evaluate the likelihood ratio (equivalently, the weight of evidence) for the proposition that "the FP effect is real" provided by Cravens and Letts's ratings of a subset of the papers in their database.

2.4. Estimating probabilities

In the medical example we were *given* the values $P(T \mid D) = 0.98$, $P(T' \mid D') = 0.95$, $P(D) = 0.01$. In practice such numbers are commonly gotten from a study, e.g. give the test to some people known to have the disease, and observe that about 98% test positive. The numbers are known only with some uncertainty, e.g. "The fraction of people with the disease who test

positive is in the range 0.980 ± 0.002 with probability 68%. This seems to be saying that $P(T \mid D)$ is in a certain range with a certain probability. What do we mean by the probability of a statement about other probabilities?[1]

Our treatment of Cravens and Letts's evidence will involve probabilities that are not known in advance but are estimated from the data. To illustrate the considerations involved, we present a simple problem.

The "biased coin" problem concerns a coin for which the probability p of heads is some arbitrary number between 0 and 1, not known to us and not necessarily 0.5. It is not at all clear how one could construct such an object in practice,[2] so it may be better to think of a game spinner with two sectors, marked *H* and *T*, with *H* containing a fraction p of the full circle (Fig. 7).

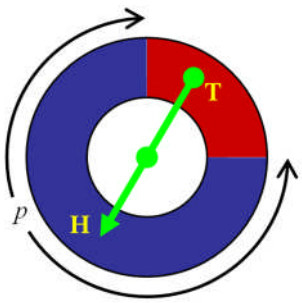

Figure 7. "Biased coin" spinner

If we spin so that the probable location of the pointer is uniformly distributed over the circle, the probability of its showing heads is p. Now write H_p for the proposition that the size of the *H* sector is p, and suppose that this unknown size was chosen at random (uniformly) between 0 and 1 (Fig. 8). We are now dealing with continuous probability distributions; $P(H_p)$ is a probability *density*, not a discrete value, and satisfies $\int P(H_p)\,dp = 1$ rather than $\sum_p P(H_p) = 1$. Suppose we spin once and observe a head. What is our revised probability for H_p, given E_{11}: one head in one trial? Bayes's rule for continuous probability distributions gives:

$$P(H_p \mid E_{11}) = P(E_{11} \mid H_p)\, P(H_p) / P(E_{11})$$
$$= p / P(E_{11})$$

[1] The need to take systematic account of uncertainties in our information is ubiquitous and has a long history. It played a central role in Laplace's comparison of imperfect astronomical observations with Newtonian gravitational theory; see Jaynes [8; 2, Ch. 5].

[2] We might try loading a coin by making it of two layers with lead on one side and aluminum on the other. This turns out not to be effective; see Jaynes [2, §10.3], "How to cheat at coin and die tossing." Jaynes shows in fact that the probability of heads is not just an intrinsic physical property of the coin and may have little to do with quantities such as the displacement of the center of gravity of the coin from its geometrical center.

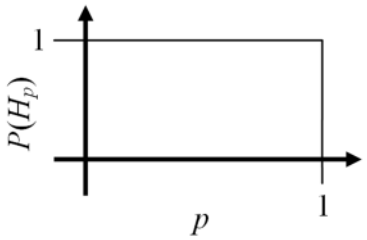

Figure 8. Uniform prior $P(H_p)$

Here $P(E_{11} \mid H_p)$ is p, because that's what H_p says: the probability of getting a head is p. And $P(H_p)$ is 1 by assumption.

The continuous version of the sum rule (§2.1.2) gives

$$\begin{aligned} P(E_{11}) &= \int_0^1 P(E_{11} \mid H_p) P(H_p)\, dp \\ &= \int_0^1 p\, dp = 1/2 \\ P(H_p \mid E_{11}) &= 2p \end{aligned} \tag{5}$$

as in Fig. 9.

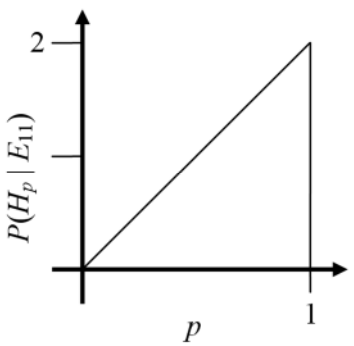

Figure 9. One head in one trial observed

Now the probability of heads on the next trial is:

$$P(\text{“one more head”} \mid E_{11}) = \int_0^1 P(\text{“one more head”} \mid E_{11}H_p)\, P(H_p \mid E_{11})\, dp$$

The first factor in the integrand is p by definition of H_p, and equation (5) gives the second. So

$$P(\text{“one more head”} \mid E_{11}) = \int_0^1 2p^2\, dp = 2/3$$

We can continue making trials and updating our probability distribution for H_p. Possible results are shown in Figs. 10–12.

With the notation E_{mn} = "m heads observed in n trials," these represent:

$$P(H_p \mid E_{22}) = 3p^2 \qquad P(H_p \mid E_{12}) = 6p(1-p) \qquad P(H_p \mid E_{24}) = 30\, p^2(1-p)^2$$

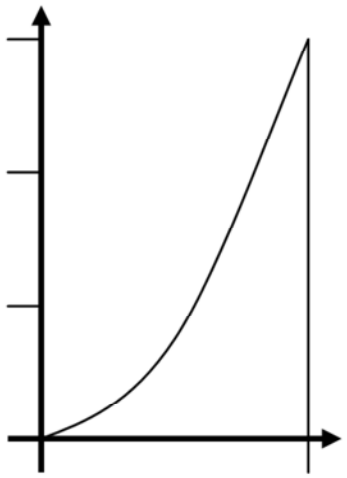

Figure 10. 2 heads in 2 trials

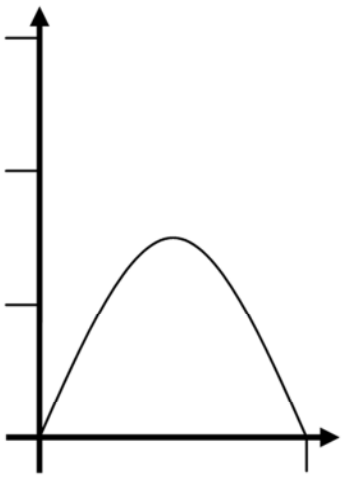

Figure 11. 1 heads in 2 trials

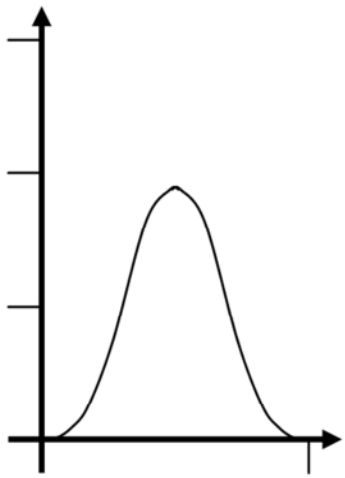

Figure 12. 2 heads in 4 trials

The general formula for m heads out of n trials is:

$$P(H_p \mid E_{mn}) \;=\; [(n+1)!\,/\,m!(n-m)!]\; p^m(1-p)^{n-m}$$

and the formula for the probability of heads on the next trial is:

$$P(\text{"one more head"} \mid E_{mn}) \;=\; (m+1)\,/\,(n+2).$$

This is Laplace's *rule of succession*: assuming a uniform prior for H_p and m "successes" out of n independent trials, the probability μ of success on the next trial is given by

$$\mu \;=\; (m+1)\,/\,(n+2)$$

The successive posterior distributions peak up more and more sharply as the number of trials increases (Fig. 13). The width of the peak is 2σ, where the standard deviation σ is given by

$$\sigma = \sqrt{\mu(1-\mu)/(n+3)}$$

and the mean μ is as just given. For a derivation of σ, see equation (6.35) in Jaynes [2, ch. 6].

The assumption of a uniform prior may or may not be justified, depending on available information. But if the prior is continuous and non-zero near μ, the shape of the posterior will often be found to resemble Fig. 13.

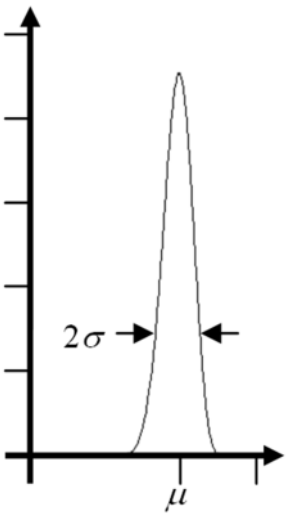

Figure 13. Peak shape

3. Problem setup

The network we developed is shown in Fig. 14. Node *R* is the proposition of interest—roughly speaking, "is the FP effect 'real'?" The nodes E_2, E_8, … , E_{28} refer to the results published in the set of papers selected for initial consideration; the subscripts are index numbers of the papers in the Cravens–Letts [1] database. The other "*E*" nodes are auxiliary nodes associated with the papers, and the "*P*" nodes are various probabilities to be estimated from the data by means illustrated in §2.4.

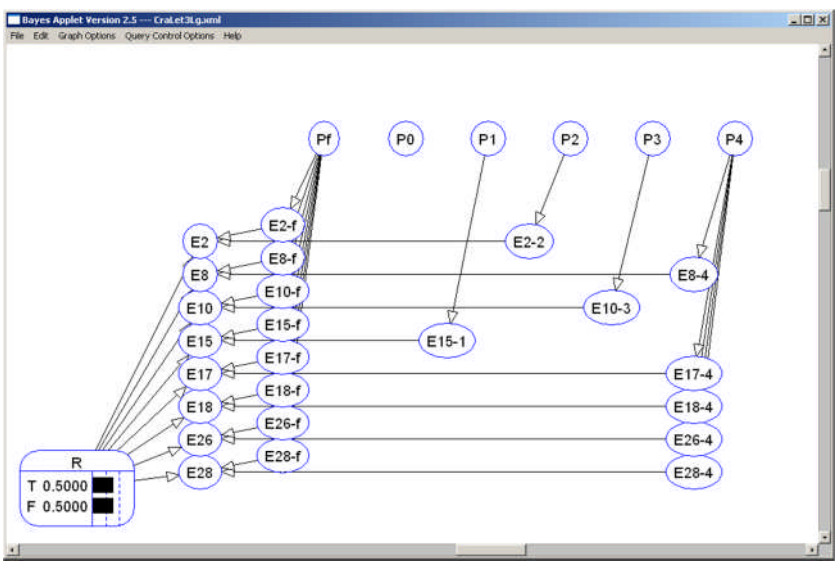

Figure 14. Network for eight selected papers (initial configuration)

3.1. Selected papers

Cravens and Letts [9] suggested the following eight papers for initial consideration:

#	Cri	Heat	Citation
2	2	No	R. D. Armstrong et al., *Electrochimica Acta* **34** (9) 1319–1322 (Sep. 1989).
8	4	Yes	R. C. Kainthla et al., *Electrochimica Acta* **34** (9) 1315–1318 (Sep. 1989).
10	3	No	N. S. Lewis et al., *Nature* **340** (6234) 525–530 (Aug. 17, 1989).
15	1	No	D. E. Williams et al., *Nature* **342** (6248) 375–384 (Nov. 23, 1989).
17	4	Yes	A. J. Appleby et al., *Proc. First Ann. Conf. Cold Fusion*, 32–43 (Mar. 1990).
18	4	Yes	Y. Arata & Y.-C. Zhang Proc. *Japan Acad. B* **66** (1) 1–6 (1990).
26	4	Yes	S. Guruswamy & M. E. Wadsworth, *Proc. First Ann. Conf. Cold Fusion*, 314–327, (Mar. 1990).
28	4	Yes	T. Lautzenheiser & D. Phelps, Amoco Production Company Research Report T-90-E-02, 90081ART0082 (Mar. 1990).

The numbers under "#" are the index numbers of the papers in Cravens and Letts's database. The numbers under "Cri" give the number of enabling criteria satisfied by the paper. A Yes or No under "Heat" indicates whether excess heat was reported.

3.2 Network propositions

Proposition *R* can also be phrased as "the experimental treatment makes a difference". We consider two alternatives:

- *R* = *false*:[1] the probability of observing excess heat is the same (P_f) regardless of whether all, some, or none of Cravens and Letts's enabling criteria are satisfied. This would imply that reported observations of excess heat are the result of error, deception, or extraneous factors.
- *R* = *true*: the probability of observing excess heat has one of several values (P_0, … , P_4), depending on the number of enabling criteria that are satisfied.

E_i states that excess heat was reported in paper number *i* of the data base.

E_{if} states that excess heat was reported in paper number *i* in case *R* = *false*. Its truth value is irrelevant in case *R* = *true*. Its conditional probability is simply the value of P_f.

E_{in} states that excess heat was reported in paper number *i* in case *R* = *true*, where *n* is the number of enabling criteria met by the paper. Its truth value is irrelevant in case *R* = *false*. Its conditional probability is simply the value of P_n.

Nodes E_{if} and E_{in} exist to simplify the expression of the conditional probabilities of E_i, rather than for any intrinsic interest of their own. E_i is *true* if either (1) *R* and E_{in} are both *true* or (2) *R* is *false* and E_{if} is *true*; E_i is *false* otherwise. The E_{if} and E_{in} nodes could be eliminated and E_i made directly dependent on *R*, P_f, and P_n at the expense of expanding Table 2 below to a table with 50 rows.

[1] A statistician of the orthodox persuasion might call this alternative a "null hypothesis."

3.3 Network variables

P_f is the probability of excess heat being reported in case R = *false*.

P_n is the probability of excess heat being reported in an experiment satisfying n of the enabling criteria (n = 0, … ,4) in case R = *true*.

P_f and P_0, … , P_4 are probabilities to be estimated from the data by means illustrated in §2.4. Ideally they would each be described by a continuous probability density on the interval from 0 to 1. Because of practical limitations of the software, we used fairly coarse discrete approximations.

3.4. Probability tables

The prior and conditional probabilities for the nodes of the network are specified in tabular form.

We set the prior probability of R equal to 0.5, as shown in Table 1, giving prior odds of 1. Consequently the posterior odds are equal to the likelihood ratio. (See §2.3.) This makes it easy to determine the weight of evidence from the program outputs.

Table 1. *P*(*R*)

R	
true	false
0.5	0.5

The conditional probability of E_i is specified as in Table 2. This simply makes E_i agree with E_{if} when R is false and with E_{in} when R is true. The actual probability values are those of E_{if} in the first case and E_{in} in the second.

Table 2. *P*(E_i | R E_{if} E_{in})

			E_i	
R	E_{if}	E_{in}	true	false
true	true	true	1	0
true	true	false	0	1
true	false	true	1	0
true	false	false	0	1
false	true	true	1	0
false	true	false	1	0
false	false	true	0	1
false	false	false	0	1

The conditional probabilities of E_{if} and E_{in} are given in Tables 3 and 4. The probability of E_{if}, given P_f, is by definition simply the value of P_f ; and the probability of E_{in}, given P_n, is the value of P_n.

Table 3. $P(E_{if} \mid P_f)$

P_f	E_{if} true	E_{if} false
0.1	0.1	0.9
0.3	0.3	0.7
0.5	0.5	0.5
0.7	0.7	0.3
0.9	0.9	0.1

Table 4. $P(E_{in} \mid P_n)$

P_n	E_{in} true	E_{in} false
0.1	0.1	0.9
0.3	0.3	0.7
0.5	0.5	0.5
0.7	0.7	0.3
0.9	0.9	0.1

The prior probabilities of P_f and P_n (n = 0, … ,4) are shown in Tables 5 and 6. They are all the same: a coarse discrete approximation to a uniform distribution on the unit interval.

Table 5. $P(P_f)$

P_f				
0.1	0.3	0.5	0.7	0.9
0.2	0.2	0.2	0.2	0.2

Table 6. $P(P_n)$

P_n				
0.1	0.3	0.5	0.7	0.9
0.2	0.2	0.2	0.2	0.2

4. Results

After entering the probability tables in the nodes of the network of Fig. 14, we successively declared "observed" values for the nodes E_i, starting with *false* for E_2 and finishing with *true* for E_{28}. The final state of the network is shown in Fig. 15, in which display of the probability distributions of the nodes P_f, P_0, … , P_4, has been enabled.

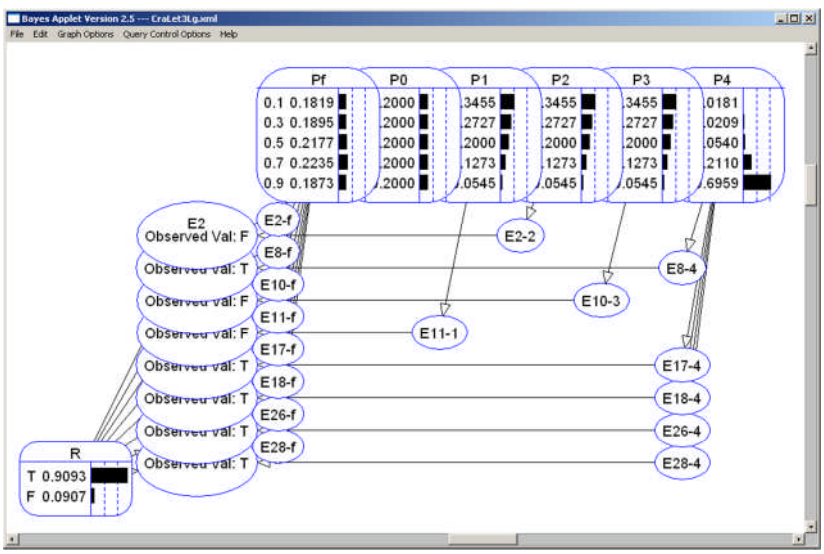

Figure 15. Final configuration of network for eight selected papers

The posterior probabilities for R = *true* and R = *false* are 0.9093 and 0.0907, giving posterior odds of 10.025. This is also the final value of the likelihood ratio, since we started with prior

odds of 1.0. The value of the likelihood ratio is plotted in Fig. 16 as a function of the number of papers taken into account, from 1 paper (#2 only), 2 papers (#2 and #8), through 8 papers.

The likelihood ratio for *R*, give 1 paper, is 1.0, exactly equal to the prior value of 1.0 with no papers at all (not plotted). With one paper, the distributions of P_f and P_2 were identical—a bit biased toward the low values, as the first paper (#2) reported no heat. There was not yet a basis for choosing between the two. Adding a second paper (#8, reporting heat) increased the ratio to about 1.47, and adding a third (#10, reporting no heat) made no difference. The next four, consistently showing heat with four criteria satisfied, brought a steep increase in the likelihood ratio to 10.025.

At that point the posterior distribution for P_4 was strongly biased toward high values, as shown in Fig. 15, and as one would expect. P_1, P_2, and P_3 showed weaker and identical biases toward low values, since in each case (1, 2, or 3 criteria met) one instance was observed, reporting no heat. P_0 was flat, unchanged from its prior, as no evidence was included bearing on the case of 0 criteria met. The distribution of P_f was relatively flat, close to its prior, as the probability for *R = false* was at that point estimated as being rather small. Note that if *R* were definitely known to be *true*, the value of P_f would be irrelevant, and we would expect it to be no different from its prior. As an experiment, we changed the prior value for *R = false* to 0.99, sufficiently skeptical that the posterior value came to about 0.91; in that case, the posterior distribution for P_f showed an apparent peak between 0.5 and 0.6, about where the rule of succession would predict for 5 successes (heat observed) out of 8 trials.

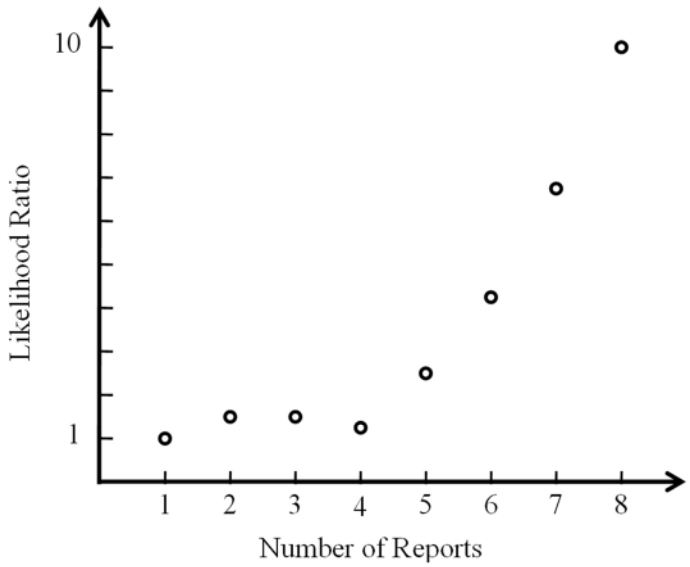

Figure 16. Change in likelihood ratio as more and more papers are taken into account

Eight papers is a small enough sample that no particular significance should be attached to the particular final numerical value of 10.025 for the likelihood ratio for *R*, though the qualitative behavior of Fig. 16 is suggestive. Moreover, the set of eight is not a representative sample of the data base; some were selected for historical significance. In particular, papers #10 and #15 are accounted by Cravens and Letts [1] as “the most important papers in the field of

Condensed Matter Nuclear Science" for their early and lasting negative impact. On the other hand the announcement by Fleischmann and Pons (#1 in the database) was omitted.

In addition, the model presented here does not address the important question of publication bias. We have looked at toy models for experimenter bias, but incorporating such factors in the present model is a matter for future work. The problem is less severe for the period immediately following the Fleischmann–Pons announcement, when a number of researchers were quite willing to report negative results. However, the more recent papers in the Cravens–Letts database are preponderantly positive, and incorporating them all in the computation would risk producing inflated values for the likelihood ratio for *R* unless the tendency not to report failures were taken into account.

It was nevertheless felt desirable to include a larger number of papers. Attempts to increase the number of papers from 8 to 12, while successful (Johnson and Melich [10]), made it clear that we were approaching the computational limits of the Java applet. Moreover the scheme we have described lumps together all papers that meet the same number of criteria; those meeting the first two enabling criteria are counted together with those meeting the last two. It was thought to be also desirable to consider particular subsets of the four criteria, rather than simply the count, expanding the number of cases from 5 to 16.

We have subsequently obtained an exact analytical expression for the likelihood ratio. This not only circumvents the computational limits, but it uses exact uniform priors for the *P*'s (P_f, P_0, P_1, P_2, P_3, P_4) rather than the coarse discrete approximations of Tables 5 and 6. And it generalizes easily from 5 classes of papers (0, 1, … , 4 criteria satisfied) to 16 classes (all distinct subsets of the 4 criteria). Here is a sketch of the results.

To begin, remove the intermediate nodes E_{if}, E_{ik} in Fig. 14 so that, e.g., E_2 depends directly on P_f and P_2. The joint probability for the network becomes:

$$P(R)\, P(P_f)\, P(P_1) \ldots P(P_4)\, P(E_2 \mid R\, P_f P_2)\, P(E_8 \mid R\ P_f P_4) \ldots P(E_{28} \mid R\, P_f P_4)$$

and dividing by $P(R)$ gives the probability conditional on *R*:

$$P(\cdots \mid R) \;=\; P(P_f)\, P(P_1) \ldots P(P_4)\, P(E_2 \mid R\, P_f P_2)\, P(E_8 \mid R\ P_f P_4) \ldots P(E_{28} \mid R\, P_f P_4)$$

where $\cdots$ stands for all the variables other than *R*. The priors for the *P*'s are uniform, i.e. 1. The conditional probabilities are given by, e.g.

Table 7. $P(E_2 \mid R\, P_f P_2)$

	E_2	
R	True	false
true	P_2	$1 - P_2$
false	P_f	$1 - P_f$

for $P(E_2 \mid R\, P_f P_2)$. Thus the joint probability is

$$P(\cdots \mid R = \textit{false}) \;=\; (1 - P_f)\, P_f\, (1 - P_f)\, (1 - P_f)\, P_f\, P_f\, P_f\, P_f$$
$$P(\cdots \mid R = \textit{true}) \;=\; (1 - P_2)\, P_4\, (1 - P_3)\, (1 - P_1)\, P_4\, P_4\, P_4\, P_4$$

for the case E_2 = *false*, E_8 = *true*, E_{10} = *false*, E_{11} = *false*, E_{17} = *true*, E_{18} = *true*, E_{26} = *true*, E_{28} = *true*. (For the subscripts in the second expression, recall that the values of *k*, number of criteria satisfied, are 2, 4, 3, 1, 4, 4, 4, 4 for the respective papers numbered 2, 8, …, 28.)

For a general collection of papers, not necessarily those of Fig. 14, the expressions are

$$P(\cdots | R = \ false) = P_f^M \, (1 - P_f \,)^{N-M}$$
$$P(\cdots | R = true) = \prod_{k=0}^{4} P_k^{m_k} \, (1 - P_k \,)^{n_k - m_k}$$

where N is the total number of papers, M is the number reporting excess heat, n_k is the number of papers in class k (i.e. k enabling criteria satisfied) and m_k is the number of those reporting excess heat. Integrating out the P's gives the probability of the observed quantities (criteria satisfied, heat reported) conditional on R:

$$P(\text{observed} \mid R = \ false) = M!(N - M)!/(N + 1)!$$
$$P(\text{observed} \mid R = true) = \prod_{k=0}^{4} m_k!(n_k - m_k)!/(n_k + 1)!$$

and the likelihood ratio is the second of these quantities divided by the first.

For the 8 selected papers,

$n_0 = 0, \quad n_1 = 1, \quad n_2 = 1, \quad n_3 = 1, \quad n_4 = 5 \quad N = 8$
$m_0 = 0, \quad m_1 = 0, \quad m_3 = 0, \quad m_4 = 0, \quad m_5 = 5 \quad M = 5$
$P(\text{observed} \mid R = false) \ = \ 1/504$
$P(\text{observed} \mid R = true) \ = \ (1/1)(1/2)(1/2)(1/2)(1/6) \ = \ 1/48$

The likelihood ratio is therefore 504/48, or 10.5 (exactly). This is to be compared with the value of 10.025 obtained numerically with the applet, using a 5-point discrete approximation to a uniform prior for the P's. It appears that the use of such a discrete approximation has not resulted in serious error in the computed likelihood ratio.

There is no problem in generalizing from 5 classes of papers (0, 1, … , 4 criteria satisfied) to 16 classes (all distinct subsets of the 4 criteria): just let k above index the 16 classes and adjust the limits of k in the products accordingly.

Acknowledgements

The authors gratefully acknowledge the support of the Defense Threat Reduction Agency for this work.

References

1. D. Cravens and D. Letts, "The enabling criteria of electrochemical heat: beyond a reasonable doubt," *Proc. 14th International Conference on Condensed Matter Nuclear Science (ICCF-14)*, Washington, D.C., August 10–15, 2008
2. E. T. Jaynes, *Probability Theory: the Logic of Science*, Cambridge University Press, Cambridge, UK, 2003
3. F. V. Jensen, *Bayesian Networks and Decision Graphs*, Springer-Verlag, New York, 2001.

4. J. Breese and D. Koller, “Tutorial on Bayesian networks,” <http://ai.stanford.edu/~koller/BNtut/BNtut.ppt>, 1997
5. K. Murphy, “A brief introduction to graphical models and Bayesian networks,” <http://www.cs.ubc.ca/~murphyk/Bayes/bnintro.html>, 1998
6. A. Yap, J.R. Santos et al. (CIspace Group, Laboratory for Computational Intelligence, University of British Columbia), available for download under “Belief and Decision Networks” at <http://www.aispace.org/downloads.shtml>; see also “Terms of Use” at <http://www.aispace.org/about.shtml>
7. I. J. Good, *Probability and the Weighing of Evidence*, C. Griffin, London, 1950
8. E. T. Jaynes, “Confidence intervals vs. Bayesian intervals,” in W. L. Harper and C. A. Hooker (eds.), *Foundations of Probability Theory, Statistical Inference, and Statistical Theories of Science*, vol. II, 175–257, D. Reidel Publishing Company, Dordrecht, Netherlands, 1976
9. D. Cravens and D. Letts, personal communication
10. R. Johnson and M. Melich, “Weight of Evidence for the Fleischmann-Pons Effect,” in J. Marwan (ed.), *Low-Energy Nuclear Reactions Sourcebook*, American Institute of Physics, in press

Nuclear or Not Nuclear: How to Decide?

Ludwik Kowalski
Montclair State University
http://csam.montclair.edu/~kowalski/cf
Kowalskil@mail.montclair.edu

Abstract

A recent claim demonstrating a nuclear process triggered by electrolysis is challenged. An analysis, based on relative diameters, is used to demonstrate that predominant pits could not possibly be attributed to alpha particles, or to less massive nuclear projectiles. This conclusion is supported not only by positive results from a replication experiment, but also by results from the experiment on which the original claim was based. While the numerous SPAWAR-type pits seem to be highly reproducible, their interpretation is not yet clear. The SPAWAR discovery can be called scientific (rather than protoscientific) because it is reproducible.

Introduction

The first version of this paper was devoted to my participation in The Galileo Project. More specifically I wanted to explain why, in my opinion, alpha particles, or less massive nuclear projectiles, could not be responsible for copious pits discovered by the SPAWAR team. I wanted to justify this conclusion not only on the basis of my own experimental data but also on the basis of SPAWAR results published in (1). It occurred to me, after writing the first version, that my manuscript could be published in a mainstream journal.

Not counting on success, I decided to submit the paper as soon as possible. Surprisingly, my paper (2) was accepted; it will probably be published in September or November of 2008. This presentation briefly summarizes my investigations of SPAWAR results and addresses some topics of general interest.

Investigations of SPAWAR results

In 2007 I was one of several researchers who used SPAWAR protocol, distributed by Steve Krivit, and reported the results (3) at the APS Winter Meeting (Denver, 2007). These results, and results reported by other researchers, demonstrated that dominant pits discovered by SPAWAR researchers are reproducible. No one disputed this fact. As far as I know, everyone who used the protocol observed copious pits on the face of the CR-39 detector that was in contact with the silver cathode during electrolysis.

But disagreements emerged about how to explain these pits. Are they due to nuclear projectiles created during electrolysis or are they due to something else? If copious pits are due to nuclear projectiles then what kind of projectiles are emitted? Can they be alpha particles and protons, as suggested by SPAWAR researchers (4)?

Taking the nuclear origin of copious pits for granted, I convinced myself that SPAWAR-type pits could not possibly be due to alpha particles, or to less massive projectiles, such as protons. That conclusion, based on my own experimental data, was reported in (3). In the paper to be published (2) I show that SPAWAR's experimental data, reported in (1), lead to the same conclusion. Additional observations can be seen in (9).

The paper (2) also refers to experimental results reported by several CMNS researchers. In an experiment conducted by Tanzella et al. (5), the CR-39 detector was surrounded by a six-micron mylar film. This was done to eliminate direct contact between the CR-39 detector and the cathode (or the electrolyte). The film was sufficiently thin to allow alpha particles (with energies higher than 1.5 MeV) to be transmitted. No copious pits were observed in this experiment. I consider this to be a direct proof that SPAWAR-type pits are not due to alpha particles with energies higher than about 1.5 MeV.

The most interesting result of (5), however, was the presence of another kind of pits, on both sides of the CR-39 detector surrounded by the thin mylar film. These pits were not as abundant as SPAWAR-type pits (only about 100 per square centimeter versus millions per square centimeter) and they were considerably smaller than copious pits in SPAWAR-type experiments. A subsequent investigation (by Lipson et al.) showed that sizes of pits, on the mylar-protected CR-39 chip, are about the same as sizes of pits due to protons with energies between 2 MeV and 3 MeV. In my opinion, proton-like pits offer a more convincing evidence of a nuclear process due to electrolysis than much more abundant SPAWAR-type pits, near the cathode.

General observations and suggestions

1) Problem of reproducibility: science versus protoscience

Use of scientific methodology of validation, in a given field, is not sufficient to make a field scientific. At least some demonstrations of new phenomena must be reproducible on demand. Without this a field should be characterized as protoscientific. The expected evolution of a protoscience into science is schematically represented in Flowchart 1, below.

2) Struggle for recognition

A field in which scientific methodology of validation is used, and in which some new phenomena are reproducible on demand, is scientific. The expected evolution of a new scientific field, toward general acceptance, is schematically represented in Flowchart 2.

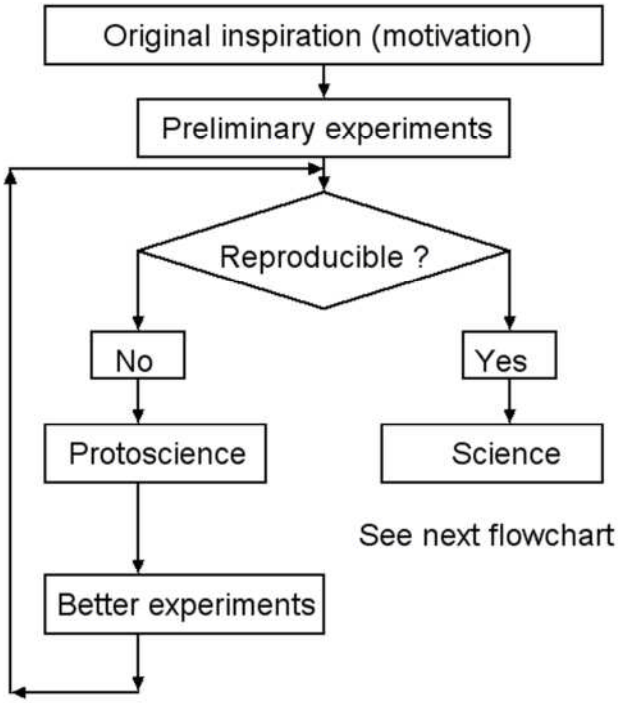

Flowchart 1

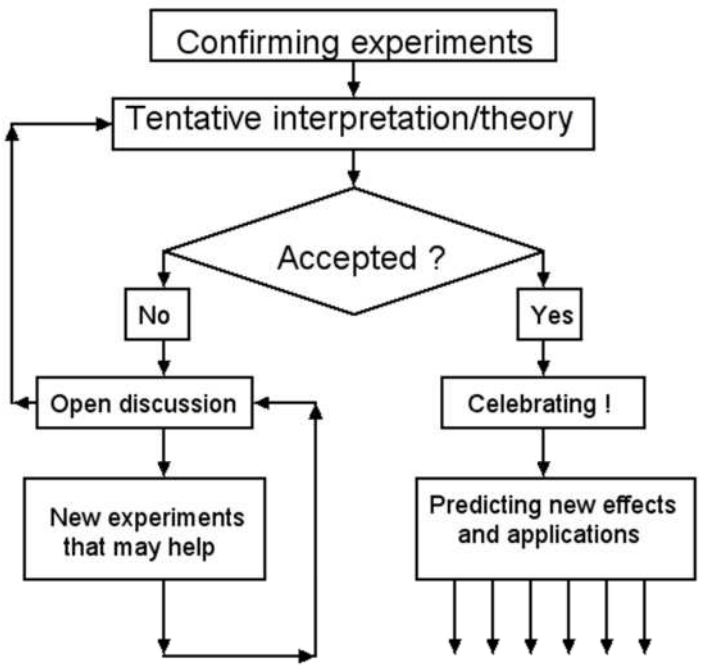

Flowchart 2

The evolution of protoscience into science (Flowchart 1) can be very slow because experiments are not reproducible and because researchers are not guided by a reliable theory. Theories based on ad hoc assumptions are not reliable. Success depends on sheer luck in accidentally identifying necessary preconditions for reproducibility, and on available resources.

But the path from reproducibility of a new effect to general acceptance (the second flowchart above) is likely to be much faster. Starting with a reproducible experiment one can quickly learn how different parameters influence the effect. Some parameters will have only negligible effect on the outcome while others will have dramatic influence. Success will no longer depend on chance; it will become a matter of skill in systematic investigations.

3) Coordinated research versus working in isolation

It is unfortunate that, except for The Galileo Project, initiated by Steve Krivit (7), CMNS researchers work in isolation from each other. This is understandable; each researcher does what matches his/her expertise and limited resources. This kind of work has been going on for 19 years. It produced remarkable protoscience, in the subfields listed below:

---

1) Excess heat, sometimes orders of magnitude larger than what can be attributed to known chemical reactions.

2) Excess heat correlated with production of 4He (generated at a rate close to 23 MeV per atom of produced helium).

3) Chemically-induced changes in isotopic composition of elements. Note that the term "chemically" is very broad; it covers all atomic and molecular processes, including diffusion of gasses through solids.

4) Production of new elements, either stable or radioactive, in amounts high above what can be attributed to omnipresent impurities.

5) Chemically-induced changes in the rate of radioactive decay.

6) Production of high energy photons, for example, gamma rays, during chemical processes.

7) Emission of energetic nuclear particles

But the task of turning protoscience into accepted science is still waiting for us. How to approach this difficult task and how to proceed more effectively? In my opinion, well-focused cooperative investigations, as in The Galileo Project, are likely to be more productive, in the next two or three years, than uncoordinated efforts of many individuals. Who should select the one or two most promising effects on which to focus? Who should coordinate these investigations? And who should cover the costs (probably not more than three to five million dollars)?

I think that the task of selecting one or two effects, on which to focus, belongs to us; our CMNS discussion list, run so well by Haiko, seems to be an ideal platform to debate various proposals. A decision is likely to emerge after about three months of intensive debating. But the

two other tasks, coordination and providing financial support, belong to our governments. Acting as a group, we should approach government organizations, such as NSF, National Academy of Science, or DOE, and ask for coordination and support. That is the declared mission of such organizations. National laboratories best equipped for the selected projects should be selected, to minimize additional costs. That is the only way to get a clear yes-or-no answer about the new kind of nuclear activity.

How to convince governments that a relatively modest amount of additional money is worth investing to solve the puzzle? By being organized and acting as a group rather than as independent individuals. This kind of action was already tried, about five years ago, and it produced a result; the second DOE investigation of CMNS would not have taken place without such initiative. Unfortunately, that investigation turned out to be a failure. The reason is obvious; the DOE decisions were based on voting, rather than on experimental data. Scientific decisions should be based on available data, obtained by the most qualified scientists in the most suitable laboratories. Voting is not part of scientific methodology.

4) Which experiments would I recommend?

If only one experiment were to be selected, my choice would be from the second subfield (see the above table), preferably the protocol of Mike McKubre et al. Several independent, highly qualified, investigators reported production of helium during electrolysis. Each of them reported that results were reasonably reproducible in consecutive experiments. If two experiments were to be selected then the second experiment would be from the last field, preferably the protocol described in (5). But at least one more replication of the Tanzella-type experiment would be needed; a single experiment is not enough to make the decision. Production of helium and production of protons are undeniable nuclear signatures. No matter which experiments will be selected, for coordinated investigations, the purpose should be the same, to demonstrate a nuclear activity resulting from a chemical process.

Will we be able to act in unison and accomplish the first task quickly? Will at least one team of scientists emerge, ready to cooperate with mainstream scientists in a national lab? Will they obtain the necessary support from in at least one country? All this remains to be seen. In the final analysis, the outcome will depend on our willingness to fight for a clear yes-or-no answer.

5) On positive and negative contributions

It is difficult to present a negative CMNS report at a formal gathering of CMNS researchers. Most attendees want and expect positive results and convincing interpretations. Reporting something negative is likely to produce discomfort and personal friction. What fraction of CMNS researchers prefer to report nothing rather than reporting negative results? Reporting negative results is just as important as reporting positive results. We all know this. But how does this influence what we actually say, and not say, in public? Friendship and other considerations (“that is bad for CMNS reputation”) might play a role, in practice. That would introduce bias.

References

1. Mosier-Boss, P.A., et al. “Use of CR-39 in Pd/D copdeposition experiments,” Eur. Phys. J. Appl. Phys., 40, 293 (2007)
2. Ludwik Kowalski, “Interpreting SPAWAR-type Pits: Comments,” accepted for publication (on July 24, 2008) in European Physical Journal Applied Physics.
3. Ludwik Kowalski et al., “Our Galileo Project March 2007 Report,” Winter Meeting of American Physical Society. (2007). Content of the presentation can be seen at <http://pages.csam.montclair.edu/~kowalski/cf/319galileo.html>
4. Mosier-Boss, P.A., et al. “Production of High Energy Particles Using the Pd/D Co-deposition Process,” Winter Meeting of American Physical Society. (2007).
5. A.G. Lipson et al., “Analysis of the CR-39 detectors from SRI's SPAWAR/Galileo type electrolysis experiment #7 and #5. Signature of positive neutron emission.” To be published in [6]. (F. Tanzella was one of several coauthors.)
6. Proceedings of 8th International Workshop on Anomalies in Hydrogen / Deuterium Loaded Metals; 13-18 October 2007, Sheraton Catania, Sicily, Italy
7. Editors: Jed Rothwell and Peter Mobberley; Copyright © 2008; The International Society for Condensed Matter Nuclear Science. Printed by Instant Publisher
8. S. Krivit “2007 Galileo Project Report” at http://www.newenergytimes.com/tgp/2007TGP/2007TGP-Report.htm
9. Ludwik Kowalski, http://csam.montclair.edu/kowalski/357.html This webpage offers a link to a SPAWAR paper that was published after the conference. The paper is a rebuttal of arguments presented in (2).

Open Source Science Applied to CMNS Research: A Paradigm for Enhancing Cold Fusion Prospects and the Public Interest

Thomas W. Grimshaw
Lyndon B. Johnson School of Public Affairs, The University of Texas at Austin

Abstract

Open Source Science (OSSc) is a collaborative, voluntary (uncompensated) and highly distributed method of research that emphasizes the use of new digital technologies, particularly the Internet. The OSSc paradigm grew out of the open source software movement, which has resulted in wide availability of free software (such as the Linux operating system) as an alternative to proprietary software products.

The public interest in the success of cold fusion has long been recognized because of the potential social welfare benefits related to its possibilities for very low cost energy. Cold fusion researchers, because of rejection of their field by mainstream science and continued highly marginalized research conditions, employ many of the methods and tools of OSSc. For example, they use websites for posting research papers and Internet discussion groups for introducing ideas and dialoguing online about the relative merits of those ideas.

The prospects of cold fusion success may be significantly enhanced by extending the current informal and implicit use of OSSc-type methods to more organized and explicit deployment under the sponsorship of a recognized professional organization such as ISCMNS. A formal, sponsored use of OSSc for support of cold fusion could bring powerful OSSc methods into play that are not currently used. The prospects for cold fusion success, and the associated public interest in that success, may be significantly enhanced by expanded and more disciplined application of OSSc methods by the research community.

1. Introduction

Open Source Science (OSSc) is a recent development in the methodologies of scientific investigation that departs significantly from scientific practice as it has evolved in recent decades. OSSc is enabled by technologies of the digital revolution, particularly the Internet, and embraces a collaborative investigative approach. OSSc grew out of Internet-supported collaborative development of software under a paradigm known as Open Source Software (OSS). One particularly successful example of the OSS paradigm is the Linux operating system software.

Cold fusion (CF) is a potentially revolutionary scientific discovery in which nuclear fusion is achieved at non-explosive rates and at ambient (near-earth-surface) temperatures. CF[1] was announced by two research chemists[2] in 1989 as a scientific breakthrough with promise of meeting most of the energy needs of society. However, for a variety of reasons (both technical and sociological), CF was rejected by the mainstream scientific community within a year of its announcement.

Despite this rejection, research into CF has continued under highly marginalized conditions by a relatively small group of capable and reputable scientists. This research appears to show evidence of the validity of CF phenomena. With its current state of rejection and marginalization, CF appears to be an ideal candidate for research under the OSSc paradigm, not only because of the appeal of voluntary research contributions in the absence of funding from conventional resources, but also because of theoretical challenges whose resolution may benefit from the insights and perspectives of other fields besides nuclear physics.

2. The Open Source Science Paradigm

Open Source Science is a paradigm for conducting research that differs substantially from conventional science as it has evolved in the last few decades. In the OSSc perspective, research (and the resulting knowledge) is viewed as a public good – as belonging to the commons – and as freely accessible rather than protected by property rights. This perspective was initially brought forth in the context of collaborative development of computer software (OSS) and has extended into other areas, including publication of technical literature (Open Access, OA) and scientific investigation (OSSc).

OSSc not only reemphasizes a traditional viewpoint toward science and knowledge as part of the commons, but it also makes use of powerful tools, such as communication and electronic file management functions of the Internet, to further or enhance collaboration in scientific investigation. It also encourages, and provides the means for, the synergy of many people with different backgrounds and perspectives to attack a problem. Such collaborative effects provide the basis for cross-fertilization among different fields and disciplines, one of the most powerful methods of achieving new insights into a problem area[3].

Although OSSc represents a constructive return to the traditional values and practices of science, and adds significantly to scientific practice through the power of the Internet, it is not without issues. For OSSc specifically, Schweik (2007) identifies four areas needing urgent

---

[1] Some CF researchers have sought to replace “cold fusion” with other more accurate terms, including “low energy nuclear reactions” (LENR), “chemically assisted nuclear reactions” (CANR), and “condensed matter nuclear science” (CMNS). Although the new terms are legitimate and helpful, “cold fusion” continues to be readily recognized and widely used.

[2] Martin Fleischmann and Stanley Pons

[3] Several websites have been set up specifically to offer rewards and provide a venue for creative people of different disciplines to seek solutions to problems that have proven to be intractable within the field in which they originated. See, for example, the *Innocentive* website at http://www.innocentive.com.

attention: 1) how to license digital material besides software; 2) how to achieve success in the context of current incentive structures for researchers; modify incentives and develop a "next-generation" e-journal; 3) how to govern collaboration under the OSSc paradigm; and 4) how to finance projects under the OSSc paradigm.

The central question for successful application of the OSS paradigm to science (OSSc) is the provision of adequate incentives for the broad spectrum of potential participants.

3. Cold Fusion Research and Reporting Today

If it proves to be real, CF will be good news for the welfare of humanity because it holds the promise of providing abundant supplies of energy from nuclear sources at temperatures close to the surface of the earth and with little or no associated harmful radiation. Despite the initial rejection of CF, a number of capable and reputable researchers continued their investigations – and continued to achieve positive results. For example, a recent CF publication (Storms 7007) tabulated some 184 confirmations of excess heat (indicating cold fusion reactions) from 1989 to 2004. The situation with CF – continued affirmative results without general acceptance initially by the scientific community – is typical for radical new discoveries and has been well characterized by Kuhn (1986).

Cold fusion researchers, in spite of (or perhaps because of) the rejection and marginalization of the field, have formed a relatively close-knit (although often fractious) community that has its own methods of conduct, communication, critique and reporting of research results,. The Internet has played a key role in the success achieved in that research. Continued and expanded use of the Internet will be a major ingredient of support of CF research in the future. The salient communication and reporting methods currently used are described below.

Professional Organization. The International Society for Condensed Matter Nuclear Science (ISCMNS) is the accepted CF-dedicated professional organization. According to its website[1], the ISCMNS mission is "to promote the understanding, development and application of Condensed Matter Nuclear Science for the benefit of the public". The organization is governed by a constitution and executive committee, and it maintains a code of conduct for its members.

Conferences. The CF research community presents papers on theory and experimental results in mainstream science conferences where such opportunities can be found. Because of its marginalization, CF has also been the topic of dedicated conferences (International Conferences on Cold Fusion, ICCF) since 1991, with meetings held in various countries about every 18 months. The ICCF conferences are held under the auspices of the ISCMNS. ICCF-14 took place in August 2008 in Washington, D.C.[2] with over 180 attendees.

Peer-Reviewed Journal. As in the case of conferences, CF researchers publish peer-reviewed papers in mainstream scientific journals – where their papers are not rejected outright because of the topic. In response to a strong need for additional publication outlet,

[1] http://www.iscmns.org/
[2] http://www.iscmns.org/iccf14/index.htm

ISCMNS has initiated a CF-dedicated open-access and peer-reviewed journal, the Journal of Condensed Matter Nuclear Science[1] (JCMNS).

Publications Repository. A website entitled LENR-CANR[2] provides an online library with a bibliography of more than 3500 journal papers, books and news articles related to CF. Included in the library are more than 500 scientific papers in PDF (Acrobat) format. Three e-books are also available on LENR-CANR for free downloading. Jed Rothwell's "Cold Fusion and the Future" (2007) is intended to "show that with cold fusion we can accomplish marvelous things" (p. 1). Edmund Storms' "A Student's Guide to Cold Fusion" (2003) is somewhat more technically oriented. Beaudette's "Excess Heat – Why Cold Fusion Prevailed (2002)" is one of the most important CF reference works published to date.

Newsletters. The best-known and most complete CF newsletter is "New Energy Times" (Krivit 2007), which is produced bimonthly by the New Energy Institute, with Steven Krivit as editor and publisher. It is available online for downloading[3].

E-mail Thread in CMNS Google Group. An e-mail thread for about 100 CF researchers is maintained in Google Groups by Haiko Leitz[4]. Participation is by invitation – new members must be recommended by a current member before being added to the list by Leitz. The CMNS list is quite active, typically with 12 to 20 postings daily.

Thus, cold fusion research as it is conducted today already has many of the characteristics of research under the OSS paradigm, such as performance of low-budget research by many investigators and at many locations.

4. Enhanced Application of Open Source Science to Cold Fusion Research

Although the methods currently used by the CF research community have many open access features, additional measures are available under the OSSc paradigm to enhance development, communication and reporting of research results. One of the primary contributions that OSSc can make to the CF research effort is to provide the means for increased collaboration, particularly by those having expertise in other fields. Examples of Internet tools that are available to enhance communication and reporting are shown in Table 1.

[1] http://www.iscmns.org/CMNS/publications.htm
[2] http://www.lenr-canr.org/
[3] http://www.newenergytimes.com
[4] cmns@googlegroups.com

Table 1. Internet Tools for Communication and Reporting[1]

Information Type	Online Tools	Method of Distribution
News	Blogs Podcasts Moblogging	RSS Automated e-mail newsletter User checking Web site
Events	Calendars	Open standard event formats (.ics, iCal, vCal, etc.) RSS E-mail alerts User checking Web site
Participatory Dialog/Interactivity	Forums Blog entry comments Polls Real-time text chat Video chat Webinars	RSS E-mail subscriptions to comments or forums Online polls/surveys User interacting with Web site Chat programs Webinar services
Documents/Images	File manager Searchable image gallery	FTP, RSS E-mail notification Dashboard
Contacts/Members/ Groups	Membership database	Searchable database, links in forums/blogs
Shared applications/ documents	Google Docs Zimbra.com Basecamp.com	Online access to shared application
Summary, quick glance, monitoring change	Digital dashboard	Web page Desktop application (*e.g.*, Visio) Mobile phone application

Under an upgraded scenario (referred to as the CF/OSSc paradigm), emphasis would be placed on developing a clear statement of the "CF case" in a mildly promotional tone and making it easily accessible. The various sources of CF information – books, websites, papers, repositories, etc. – would be identified and categorized to facilitate the task of newcomers to the field in "coming up the learning curve." The needs of both the general public – for general information for making an informed decision about CF – and potentially interested sophisticated researchers, who need a more in-depth introduction to the field, will be addressed. Table 2 provides a summary of the inferred CF research and communication requirements along with a listing of current and proposed CF/OSSc methods of meeting the requirements.

[1] Adapted from "Models of Collaboration Tools," Prof. Gary Chapman, LBJ School of Public Affairs, The University of Texas at Austin. Online. http://www.21stcenturyproject.org/collaboration_tools.htm.

Table 2. Current Methods and Proposed OSSc Approaches for CF Research and Communication

Function/Requirement	Current Method or Tool	OSSc Approach[1]
Real-Time Professional Exchanges	-E-mail list on GoogleGroups, managed by Heiko Leitz	-As currently; periodically post e-mail threads on ISCMNS website -ISCMNS assume responsibility for GoogleGroups if/when necessary -RSS feed feature on ISCMNS website; webinar services; blogs & podcasts
Collaborative Publication	-E-mail list on GoogleGroups, managed by Heiko Leitz	-Post draft papers for download and addition through collaborative research
Cross-Fertilization Promotion	-None?	-Formulate unresolved theoretical and experimental problems and post on ISCMNS website -Provide management for responses from researchers from other fields
Shared Software & Other Tools (e.g., Experimental Design)	-Informal exchanges among individual researchers	-OSSc enhancement: Identify and post most important software and tools (e.g., experimental software) on ISCMNS website for online access
News	-"New Energy Times" newsletter (primarily) by Steven Krivit	-Mirror "New Energy Times" newsletter on ISCMNS website (or at least provide hyperlink) -Provide Internet functions , such as blogs, podcasts, RSS feeds
Scheduled Events	-"Events" on ISCMNS and New Energy Times websites	-As currently. Implement online calendar on ISCMNS website to supplement Events on existing sites
Professional Meetings & Proceedings	-ICCF Conferences sponsored by ISCMNS -Mainstream science conferences (e.g., APS March meeting) -Conference proceedings posted on LENR-CANR	-As currently. Post proceedings on ISCMNS website as mirror to LENR-CANR - OSSc enhancement: Provide webinar services?
Publication of Peer-Reviewed Papers	-Submit and publish papers in mainstream scientific journals (where available) -Publish in newly-established CMNS Journal	-As currently. Maintain posting of CMNS Journal on ISCMNS
Publications Repository	- LENR-CANR, operated by Jed Rothwell	-Mirror LENR-CANR repository on ISCMNS website -ISCMNS assume responsibility for repository if or when necessary
Public Awareness & Cold Fusion Promotion	-"New Energy Times" website (primarily), with newsletter - LENR-CANR website, with three downloadable books by Beaudette, Rothwell and Storms	-As currently. Add links from ISCMNS website -Webinar services, FAQs, wiki, RSS feed service for ISCMNS website

[1] Most OSSc enhancements are taken from "Models of Online Collaboration" by Professor Gary Chapman, LBJ School of Public Affairs, The University of Texas at Austin. See: http://www.21stcenturyproject.org/collaboration_tools.htm

5. Website Support of Enhanced Open Source Science

Implementation of CF/OSSc will make full use of the functions of the Internet. The website of ISCMNS, the accepted CF professional organization, may serve as a suitable platform for supporting the CF/OSSc implementation.

The ISCMNS website, as modified to support CF/OSSc research, would be set up to meet the requirements as set forth in Table 2. The homepage would be designed for the general public but would also fully support the sophisticated needs of the CF research community. Hyperlinks to the topical webpages and other CF websites will be used extensively to avoid "information overload" on the homepage.

Individual webpages on the revised ISCMNS website would be developed by CF topical area as described in Table 2. They would range from descriptive and promotional pages for the general public and researchers new to the field to highly technical forums and download facilities to help researchers to collaborate on such topics as theoretical underpinnings of CF and experimental designs and results. The following webpages are expected to be needed for the revised website:

Basic Non-Technical CF Descriptions
News and Scheduled Events
Professional Contacts and Group Members
Professional Real-Time Exchanges
Collaborative Publication
Intellectual Property Information
Shared Software and Other Tools
Publication of Peer-Reviewed Papers
Publications Repository
Monitoring Changes and Quick Glance
Financial Contributions

6. Financial Support

The issues around financial support of OSSc initiatives were well articulated by Schweik (2007), apparently based in part on experience with the ORS project described above. The main points of this review are summarized as follows:

Financial support must be carefully addressed for OSSc projects to be successful.

Support must be considered in two areas – the time and effort involved in contributing to the OSSc project, and the required administrative and collaborative infrastructure.

Project financing in the past has come from seven types of revenue – government subsidies, philanthropy, corporate consortia, corporate investment, venture capital and investment banking, user or participant donations, and a hybrid or mix of the first six sources.

The costs for the time and effort for contributions may be covered by sources that are implicit in the OSSc paradigm and Mertonian science in general – donations from contributors who gain their livelihood by other means.

Administrative and infrastructure costs may be recovered in a similar manner to that used for OA publication costs, including compensation for ancillary support services, subscription models, and author-pays-to-publish models.

For the CF/OSSc project, the ISCMNS organization could establish a subsidiary foundation to control risk to the organization and to receive and manage funds. Decisions on the overall content and structure of the website will be subject to the approval of the ISCMNS Executive Committee.

7. References

Beaudette, Charles G. Excess Heat: *Why Cold Fusion Research Prevailed*. 2nd ed. South Bristol, Maine: Oak Grove Press, 2002.

Krivit, Steven B., Editor and Publisher. *New Energy Times – The Leader in News and Information on Low Energy Nuclear Reactions*. San Rafael, CA: New Energy Institute, Inc. Online. Available: http://www.newenergytimes.com. Accessed: November 2007.

Kuhn, Thomas. *The Structure of Scientific Revolutions*. Chicago: Univ. of Chicago Press, 1986.

Rothwell, Jed. *Cold Fusion and the Future*. LENR-CANR.org. 4th Edition, April 2007. Online. Available: http://lenr-canr.org/acrobat/RothwellJcoldfusiona.pdf. Accessed: November 2007.

Schweik, Charles M. "Free/Open-Source Software as a Framework for Establishing Commons in Science." In *Understanding Knowledge as a Commons – from Theory to Practice*, ed. Charlotte Hess and Elinor Ostrom. Cambridge, Massachusetts: The MIT Press, 2007.

Storms, Edmund. *A Student's Guide to Cold Fusion*. LENR-CANR.org, 2003. Online. Available: http://www.lenr-canr.org/acrobat/StormsEastudentsg.pdf . Accessed: November 2007.

Storms, Edmund. Science of Low Energy Nuclear Reaction: A Comprehensive Compilation of Evidence and Explanations about Cold Fusion. Singapore: World Scientific Publishing, 2007.

ICCF-14 Summary

Thomas O. Passell
TOP Consulting, P.O. Box 336, Palo Alto, CA 94302-0336

Introduction

Some 180 people attended the 14th International Conference on Cold Fusion held in Washington D.C., USA from August 10 through 15, 2008. This summary is intended to highlight the key results that I found persuasive, as well as some wider scope sociological context in which the meeting took place. This is no substitute for a careful reading of each paper in these proceedings by each interested person trying to advance the field toward the prime objective of obtaining a reliable energy source to replace our existing ones. No more significant objective can be imagined since our entire modern civilization is dependent upon enormous quantities of energy of high quality. Quality is roughly synonymous with energy density of the fuel and the higher temperatures at which it can be more readily utilized. The idea of unlocking the potential energy of the lightest elements in a fusion process is remarkable, considering the vast amount of the fuel available on the earth. The night sky shows that the universe is powered by fusion of hydrogen to helium at the high temperatures in the stars. The notion that we might release the energy of fusion in a solid at lower temperatures is a concept beyond all our expectations as recently as 20 years ago.

We have yet to demonstrate this process in a sufficiently convincing manner to attract the required effort and funding to take these observed phenomena from imperfectly predictable episodes to a demonstration of a controllable energy source of high quality. Progress over the past 19 plus years has nonetheless been steady enough to inspire a number of our scientifically-trained colleagues to soldier on in spite of the meager funding and extensive controversy.

Sociological Context

One way to illustrate the context in which the meeting took place is to relate the background leading to the appearance of a videotaping crew from CBS's "60 Minutes" throughout the first day's proceedings. An informal inquiry led to the following picture explaining why ICCF-14 should suddenly be the subject of interest to the national media: The primary investor in the Israeli company, Energetics, Inc., apparently requested CBS's help in getting a wider audience for their reports of unprecedented net energy production by deuterium in palladium cathodes. The "60 minutes" operatives were active that first day of the meeting, interviewing several of the attendees. They asked interviewees for their evaluation of the reliability of the evidence for cold fusion production of energy. Among the list of interviewees was a representative of the mainstream physics community who was asked to advise them on when and/or if CBS should schedule this subject on the air. In my discussion with my friend Paul Grant who served in the

role of skeptical mainstream physicist, I discovered his intended recommendation was to postpone the airing for a year or more on the assumption that more reliable data would be forthcoming by then. Grant also mentioned that Richard Garwin had written a letter supporting this delay. My response to this was to quote to the CBS representative one of C. Northcote Parkinson's Laws, his Law of Delay. This law states that Delay equals Denial, in most practical bureaucratic organizational situations. At this writing it is not clear what "60 Minutes" will decide. Stay tuned!

Why bring up this tempest in a teapot? Because it illustrates the remnant of the intense controversy surrounding this field in the first few years following the announcement by Pons and Fleischmann on March 23, 1989. After 19 plus years the protagonists in that controversy, who included many mainstream physicists beyond Garwin and Grant, still feel compelled to suppress publicity about the subject. My initial reaction is that their response is reminiscent of defenders of the faith in religious wars. In today's climate in which "war" is waged for government funding of research, their response may be just another battle in that "war".

Another question to consider is "Why make a special issue over this field of research?" If the claims of cold fusion were really as unfounded as the many wild claims of truly pathological science, why not simply ignore such claims rather than actively suppress publicity about the evidence? Again, it appears that the field of energy is currently so filled with competing claims of uncertain validity that cold fusion claims are in a separate class more threatening than all the others to existing energy research interests.

To sum up this situation, cold fusion researchers are faced with a community that resists taking a hard look at the evidence we are generating; a community that appears more interested in defending turf in the battle for research funds. If the mainstream community truly believed we have no reliable evidence, why would they not just ignore us? One possible answer is the precarious situation in the traditional field of plasma fusion (or "hot" fusion). That field has persisted for over 50 years working heroically against the steep odds of finding a reliable container for hot plasma with temperatures in the 100 million degree temperature range. Having seen the situation up close in its early years (1958-1961) at Lawrence Livermore National Laboratory, it was apparent to me even then that fundamental materials and magnetic field instability problems might eventually defeat the effort. At this time, I personally prefer the odds in favor of cold fusion versus "hot" fusion! Of course, both of these approaches may ultimately prove impractical. We may be stuck with nuclear fission of uranium and thorium for the next 40,000 years, the approximate time at which even uranium and thorium supplies are depleted!

Review of a Small Sample of Results Presented at ICCF-14

As Thomas Edison said, even failures are valuable results because they steer you past blind alleys in your search for something that works. Therefore I honor all the presenters at the conference because they all are making useful contributions. Of course there is sometimes a carryover to a meeting of scientists from the game-playing that occurs in the political arena. In that arena they are known as dirty tricks or distractions from the agendas of most people. The scientific method we hope is in the minds of attendees can usually detect such behavior,

especially when the presenter makes claims that omit the evidence for such claims on the basis of proprietary issues. Another is the assertion that the only acceptable evidence for cold fusion would be an auto driving down the street powered by it, as was expressed at ICCF-1. Finally the assertion that only extraordinary evidence would support extraordinary claims is made by the same people that speak against spending enough research money to collect that extraordinary evidence!

Finally, on to a few selected papers! For me, the most impressive results were given in four papers:

1) S. Lesin, et al., "Ultrasonically Excited Electrolysis Experiments at Energetics Technologies" (ET)
2) Y.Arata and Y. Zhang, "Solid Fusion" Reactor with Zero Input Energy" (AZ)
3) F. Celani et al., "Deuteron Electromigration in Thin Pd Wires Coated With Nano-Particles:Evidence for Ultra-Fast Deuterium Loading and Anomalous, Large Thermal Effects" (IT)
4) M. Swartz, "Excess Power Gain and Tardive Thermal Power Generation using High Impedance and Codepositional Phusor ™ Type LANR Devices" (MS)

Paper (1) ET:

Using ultrasonic (US) cleaning and modification of cathode surfaces along with varying the current to the cathode by use of their 3-frequency super waves by magnitudes of around 10%, some ratios of output heat to input electrical energy of 30 to 1 were observed for times up to 40 days at net output powers up to 32 watts. While this is still far from a commercially interesting heat source, it represents a large step forward toward such an objective. If the Arata-Zhang experience in finding the He-4 ashes of the heat generation process almost entirely sequestered within the metal phase, then these cathodes represent possible He-4 contents that would be easily measurable. Also noteworthy is the extensive collaboration between the McKubre-SRI, Violante-ENEA, and the Hubler-NRL groups in achieving these impressive results. Many challenges remain, since the US process sometimes destroys the integrity of the fairly fragile cathodes.

Paper (2) AZ:

Applying high gas pressures of D_2 and H_2 to nanometer sized Pd and Pd alloys mixed with nanometer diameter ZrO_2 apparently gives a larger heat effect with D_2 versus H_2. Both give the expected exothermic heat of hydrogen absorption widely observed as a chemical heat effect. After several hundred hours the D_2 case remains above ambient temperature by 1.6°C as opposed to essentially null temperature difference with H_2. This experimental evidence is not so convincing until we consider the data on He-4 content. The metal samples are evaporated in the source chamber of a mass spectrometer in which the D_2 sample shows 1E17 atoms of He-4 whereas no appreciable He-4 is observed in the H_2 sample. The only input energy to the system is that of the energy density of the compressed gases. If this work is confirmed, it says that permeation of D_2 gas through a metal matrix is the active process producing the cold fusion reaction. The role of the ZrO_2 particles is apparently to prevent agglomeration of the nanometer

sized Pd and Pd alloy particles. Apparently the surface of the particles is essential to success, even though the He-4 appears to remain with the metal particle and not escape to the gas phase.

Paper (3) IT:

Celani and coworkers from throughout Italy showed the most innovative departure from previous studies. Pd wires in the 50-100 micron diameter range were bundled with two Pt wires in a set of individual fiberglass insulating tubes and exposed to 5 to 6 bar D_2 or H_2. The Pd wires were coated with a chemical mixture that resulted in nanometer sized Pd particles coating the Pd wire. Calibration with He-4 gas gave a system not subject to significant variation in heat transfer conditions. The two Pt wires served as a calibration joule heater and distributed thermometry, respectively. The D_2 case showed an extra 5 watts with 52 watts input whereas the H_2 case gave less than 1/3 as much. These wire systems are fragile and many experiments failed early. One set of wires lasted for 50 days, however. A major fraction of the excess power was obtained when 10 watts of input power was added by current applied down the axial length of the Pd wire. Even though extremely rapid loading was observed with the coated Pd wire, the electromigration was carried out with Pd in the lightly loaded alpha phase. This was done because the diffusion rate of H_2 or D_2 is 100 times faster in the alpha phase than in the highly loaded beta phase! The advantage of this and other gas-metal systems is their ability to operate in the several hundred degrees Celsius range at which the energy produced will be more commercially useful. It will be interesting if He-4 is found in the active Pd wire in amounts commensurate with the excess heat observed.

Paper (4) MS:

Swartz has produced a long series of papers on calorimetry of Pd and Ni using nearly pure electrolytes of very high impedance, hence requiring much higher voltages than is widely used by other electrochemists. His results show excess power and energies well above any reasonable uncertainties, and in a few cases observing excess heat with Ni in light water. His evidence for socalled heat after death (HAD) after all input power is turned off is particularly convincing. If He-4 has been produced within all these cathodes, they should be tested for He-4 content to compare with the total excess energy produced during the life of each cathode.

Other interesting papers include those by Dufour et al., Nohmi et al., Parchamazad-Miles, and Kasagi et al.:

Dufour used an ice calorimeter of high accuracy to observe the known heat of absorption of Pd by H_2 and D_2. In the D_2 case, evidence for a delayed heat effect was obtained not present in the H_2 case in one of two attempts. Again as with the AZ experiment, simple loading to normal levels (0.6 D or H per Pd atom) appears to trigger an unusual excess heat effect with D_2 and not H2. The total HAD was about 10 joules/gram of Pd or about 1.0 Kilojoules/mole of Pd. It is not clear why HAD showed up in the first try but not in the second try. It is remarkable that all these experiments were for D and H loading in the conventional range of about 0.6 D or H/Pd. Also this was all with just a single ingestion of D_2 or H_2 at 0°C and 2 bars pressure.

Nohmi et al. made a serious and potentially effective effort to replicate the claims of AZ with fine particles of Pd. No mention was made of adding ZrO_2 particles. Their results using a flow calorimeter appears to be positioned to provide a credible measurement of excess energy. Their

plan is to also measure any He-4 generated, presumably within the metal particles as originally claimed by Arata and Zhang.

Parchamazad et al. explored the possibility of producing Pd particles in the well-characterized pores in the zeolites. These pores have useful characteristics for chemical catalysis. The authors believe some interesting phenomena similar to gas-metal reactions reported by others might be observed in this unique environment.

Kasagi et al. described a uniquely-designed detection system for high energy charged particles (alphas?) hypothesized to be emitted from the permeation of D2 gas through the complex Pd/CaO films used by Iwamura, et al. in which transmutations Cs→Pr and Sr→Mo have been claimed. The authors have done a heroic job of particle detection and claim that even 3 counts per day are significantly above the cosmic ray background.

Discussion

Considering the size of the material and temperature conditions matrix among the solids and gases energized by Pons and Fleischmann's initial 1989 announcement, it is small wonder that we have only scratched the surface of possible experiments. Still lacking is a definitive measurement of both excess energy and the hypothesized He-4 ashes from that excess energy. Professor Arata and Dr. Zhang have come the closest to this objective but clearly such a clear cut connection would be the holy grail of this scientific research.

Many of the papers at ICCF-14 were light on hard evidence and heavy on hopes for more detailed experimental evidence. The lack of robust funding is the greatest impediment to resolving the scientific issues associated with this subject.

Thanks to everyone who participated in this meeting. I invite all my readers of this all too brief and inadequate summary to scan all the published papers. There are nuggets of helpful information in many of them that may eventually lead to one of the most significant research results in the past 200 years.

Acknowledgements

I ask forgiveness from authors of many worthy papers not covered in this summary. My only hope is that this inadequate sampling will induce the reader to thoroughly mine the treasures to be found in many more of the ICCF-14 papers. The encouragement and assistance in this endeavor by Co-chairmen David Nagel and Michael Melich is gratefully appreciated.

Honoring Pioneers

For most fields of science, there are one or two people who are essentially the originators of the field. In many very important areas, they are the people recognized by receiving a Nobel Prize or some other major prize. Fleischmann and Pons are those people in this field. Then, there are other intellectual pioneers, who have two characteristics. They were active in the early days of the field and they made major contributions. In the case of LENR, there are very roughly a dozen such people, most of them still alive. However, the scientists who pioneered the study of nuclear reactions induced by chemical effects are relatively old. Many of them were at or near retirement, when the field originated two decades ago. Some of them were recognized after their death, as is the case with Professor Guiliano Preparata, who later had a medal named after him.

The organizers of ICCF-14 were moved by the notion that it is appropriate to honor key members of the LENR community while they are still alive and contributing. But, there were and are are too many such scientists to honor within the time constraints of one conference. Hence, two particularly important leaders were singled out for recognition. They were Yoshiaki Arata from Japan and Stanislaw Szpak from the US. The form of the honor was a pair of sessions, each devoted to the work of those individuals. Commemorative plaques were presented to the two pioneers. Broad reviews of the work and results of Arata and Szpak were presented. This appendix contains the papers that resulted from the two sessions.

Talbot Chubb graciously agreed to introduce the work of Professor Arata. That introduction is summarized in the following paper. It set the stage for a presentation by Professor Arata on his recent and remarkable findings. He described the development of a “solid fusion” reactor that he invented and still studies with his long-time collaborator, Dr. Yue-Chang Zhang. Their data shows that the reactor, loaded with Pd nanoparticles coated with zirconia and pressurized with deuterium gas, produced nuclear heat for “hundreds of hours”. When operated with hydrogen gas, no heat was produced. The remarkable demonstration was accomplished with no electrical power input to the reactor during the heat-producing runs.

Frank Gordon organized the session honoring Dr. Szpak, who was unable to travel to participate in the session. His colleagues presented both what was done and what was found, while using the “co-deposition” technique, which was invented by Szpak. In that method, there is no need to acquire and characterize Pd metal for use as the cathode in electrolytic LENR experiments. Rather, the Pd is deposited from a heavy water electrolyte. Such an experiment takes less time than those in which a sheet or rod of Pd is loaded with hydrogen isotopes. The team found a wide variety of effects during the last two decades, which were systematically reviewed at ICCF-14. A paper summarizing those findings follows. The last paper in this section is a set of references to 21 papers published by Szpak’s group in refereed journals. Brief comments on each of the papers are provided in the set of references.

In Honor of Yoshiaki Arata

Talbot A. Chubb
Physicist Consultant, 5023 N. 38th St., Arlington VA 22207, USA, tchubb@aol.com

Abstract

This paper seeks to make readers aware that Arata and Zhang (A&Z) in 2007/8 demonstrated operation of an autonomous fusion "heater". The heater generated a steady outflow flow of heat at slightly above room temperature throughout a run lasting hundreds of hours. The steady nuclear heat occurred after a brief burst of chemical heat during D_2 absorption. No other energy input was present.

The paper also seeks to make readers aware that in 2005 A&Z demonstrated continuous fusion heat at 191°C in a gas loaded reactor which was initially maintained at 141°C by an electrical heater. It is estimated that 25% of the heat delivered to the room was fusion energy and 75% was electrical heater energy. The catalyst temperature was high enough for practical generation of electrical power.

Introduction

The paper introduced a session on catalytic fusion in honor of Professor Arata and the pioneering work which he has carried out in conjunction with Yue-Chang Zhang (A&Z). The A&Z team has pioneered and defined what is meant by nano-Pd fusion. They proved that nuclear reactions can be made to take place in nanometer solid material. Their work opens the road to development of commercial fusion heaters.

Dr. Arata is Professor Emeritus at Osaka University. Born in 1923, he graduated from Osaka U. with a Bachelors in Engineering in 1949, received a Doctorate in 1957, and became Professor. in 1964 . He started Japan's plasma fusion program. Since there was no D_2 gas available for his arc plasma studies, he made his own deuterium gas by plating D_2O electrolyte onto a Pd cylinder, collecting the gas that permeated the cylindrical tube. In 1958 he achieved the world's record for arc discharge current density. He was a pioneer in electron beam and laser beam welding and became Director General of the Osaka U. Welding Institute in 1977. Arata was elected Member of the Japan Academy in 1988, received the Arthur Schawlow Prize in 1992 from the American Society of Metals, and was honored by the Emperor of Japan in both 1995 and 2006. He has received many other awards.

Arata and Zhang began their cold fusion studies in 1989. Arata applied his engineering science background to the goal of proving or disproving cold fusion reality. He was initially a skeptic.

A&Z published their first nano-Pd work excess heat studies using a "DS-Cathode" in 1994, presenting strong evidence that fusion heat release had occurred.

A&Z introduced new terms to describe the new hardware and concepts that were unique to their investigations. One of these is “DS-cathode”, which means “double structure” cathode, i.e., an outer Pd metal cylinder with stainless steel (ss) welded end pieces and an inner reactive filling of nano-Pd powder. D^+ ions are deposited onto the Pd cylinder, and the cylinder is filled with contacting nano-Pd grains. The A&Z cathode contrasts with the pieces of wire, sheet, or metal rod used by other experimenters in 1989. Another A&Z term is “spillover effect”, taken from catalyst chemistry, where it means that effective catalytic area exceeds area measured by a standardized N_2 adsorption protocol. As used here it means that the evacuated nano-Pd catalyst bed absorbs and redistributes by grain-grain contact the deuterium permeating a DS cathode’s Pd wall, creating an almost uniform D/Pd ratio throughout the catalyst bed. The high surface mobility largely avoids the deuterium density gradients existing in electrolysis-loaded bulk Pd cathodes. The chemical pumpimg caused by high surface mobility and high absorbtivity at low pressure can be called “spillover effect” pumping.

Figure 1. The experimental setup used in 1996.

Figure 1 shows the experimental setup used in 1996. The cabinet on the left maintains a reservoir of constant temperature water that serves as the water supply for 2 constant displacement pumps sitting on the desk. The pumps feed water to 2 independent test cells inside dewars in the styrafoam box on the right. The styrafoam box is covered by a lid during normal operation. Electronics in the cabinet to the far right digitizes input voltage and current which are used to calculate input electrolysis power. Inflow and outflow temperature for the 2 cells is measured by thermocouples. The stability of the water flow calorimetry is verified by the equality of input and output powers during an incubation period within which no fusion power is liberated, as shown in the first part of Figure 3.[1]

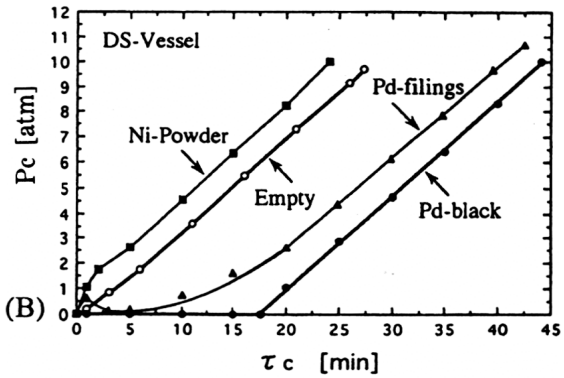

Figure 2. Illustration demonstrating spillover effect pumping

Figure 2 shows how A&Z quantify the hydrogen absorption behavior of Pd-black by measuring its ability to absorb inflowing H_2 at low pressure. In a standard test a constant cc-atm/min of H_2 gas flows into a vessel of known volume. The pressure-rise time history of powder samples is compared with the pressure rise of the empty test vessel. When the test sample is Ni powder, the pressure rise is faster than for the empty vessel, partially due to inertly occupied volume. When the sample is Pd-filings, there is a small lag in the pressure rise due to the Pd absorption of H_2. When the test sample is Pd-black, there is initially no measured rise in pressure, presumably due to immediate transfer of adsorbed H throughout the catalyst bed, accompanied by its rapid absorption within the individual nanometal grains. The duration of the spillover effect period has been used by A&Z to identify good catalyst for fusion promotion.

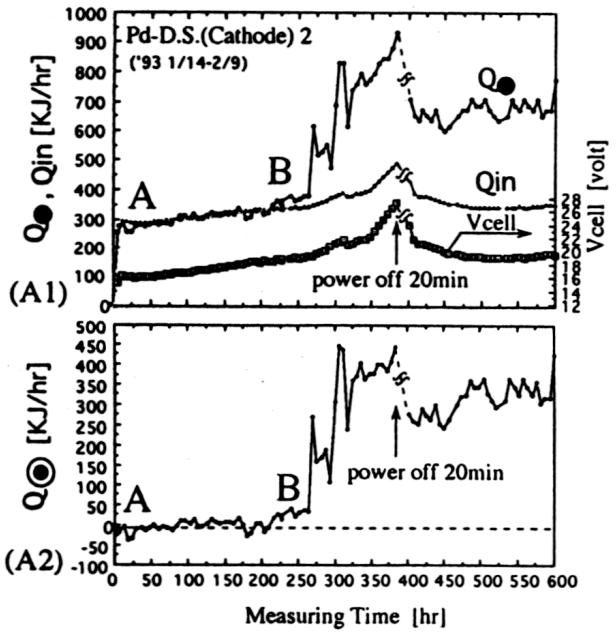

Figure 3. A&Z excess heat run published in 1994

The top portion of Fig. 3 shows plots of output power, input power, and cell voltage vs. run time. Fig. 2 bottom shows excess power = output minus input power vs. run time. The period of zero excess power between times A and B is called the incubation period.

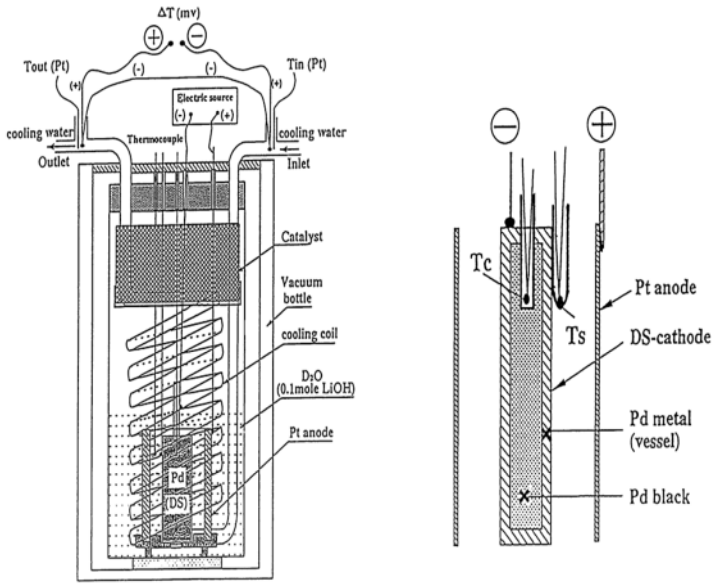

Figure 4. Electrolysis cell and DS-cathode used in 1995. DS-cathode shown on right.

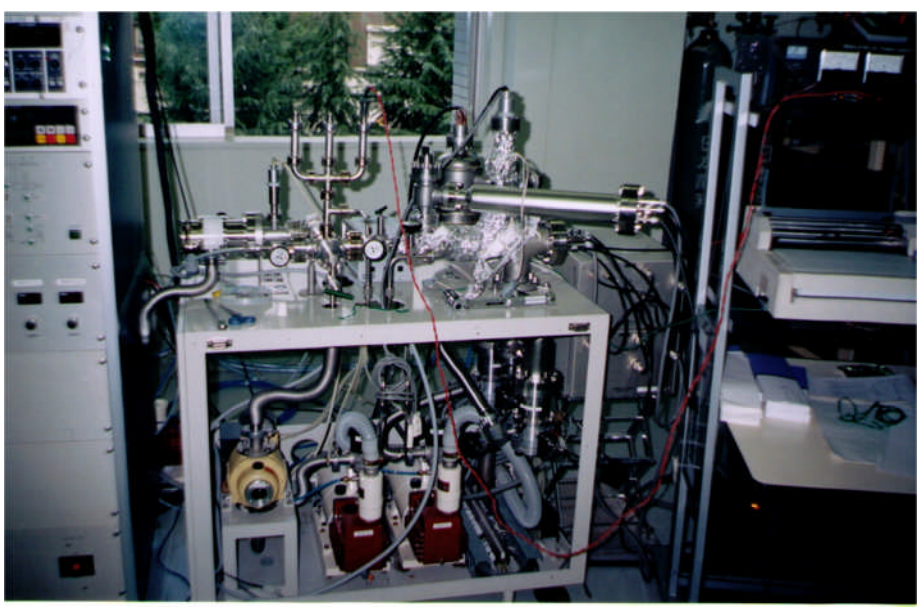

Figure 5. Stainless steel (ss) manifold system used in analysis of desorbed gases

By 1996 A&Z had designed a mass spectrometer system to look for ^{4}He and ^{3}He in their post-run powder. They constructed a turbo-pumped welded ss manifold with separate quadrupole spectrometers which were programmed to repeatedly scan the mass-4 and the mass 3 peaks. They included a small oven to outgas strongly absorbed D_2, HD, and He molecules in post-run catalyst powder, and later added a titanium sputter pump to selectively absorb D_2 and DH in isolated samples of desorbed gas, as shown below, further verifying the identity of the ^{4}He peak. As-received Pd-black shows no ^{4}He.

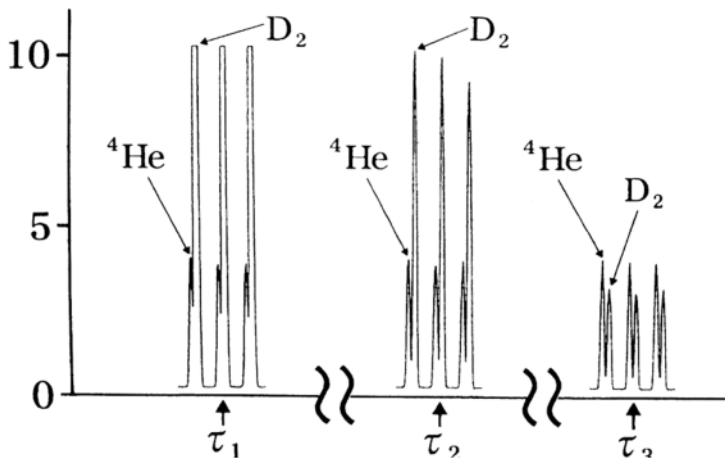

Figure 6. Spectra of sample of desorbed gas

The clearly resolved ^{4}He and D_2 peaks shown in Fig. 6 demonstrate what can be accomplished by a skilled experimenter using a high quality quadrupole mass spectrometer. In one run A&Z actually resolved the ^{3}He peak from the DH peak, which is much more difficult.

During the period 1992-2001 A&Z convinced themselves that cold fusion was real. They published 10 excess heat runs, showed excess heat when D_2O electrolysis was used and not when H_2O was used, and when Pd-black was used and not when Pd filings were used. They observed ^{4}He and sometimes ^{3}He in post-run powder, and not in as-received powder, and they successfully exported their DS-cathode experiment to the McKubre's SRI lab. In 2002 they made a major advance, producing fusion in ZrO2+nano Pd catalyst.[1]

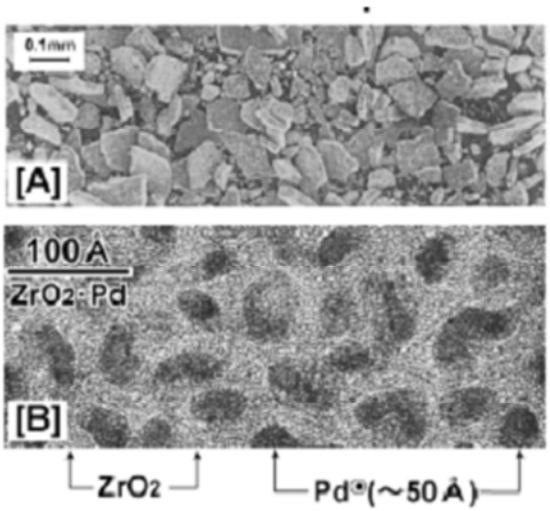

Figure 7. New catalyst shows nano-Pd embedded in ZrO_2

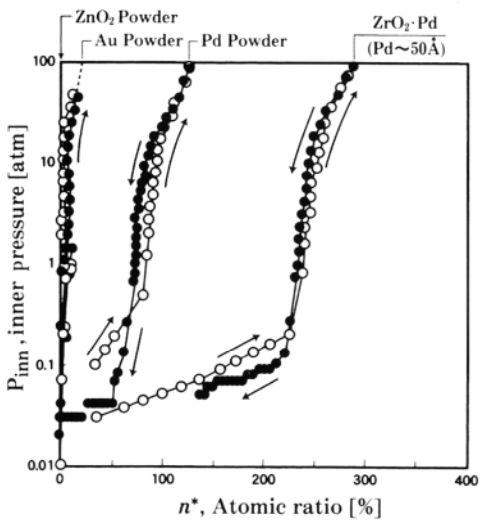

Figure 8. H/Pd = 2.9 at 100 atm

The invention of ZrO_2,nano-Pd catalyst by the Institute of Materials Research at Tohoku U. permitted gas loading to replace electrolysis. Their catalyst is produced by a well defined protocol.[2] In 2005 A&Z demonstrated fusion heat at 141°C starting temperature. D_2 pressurization of new catalyst raised catalyst temperature to 191°C. Catalytic fusion power = ~0.33 × the heater power that had maintained reactor wall at 141°C.[1]

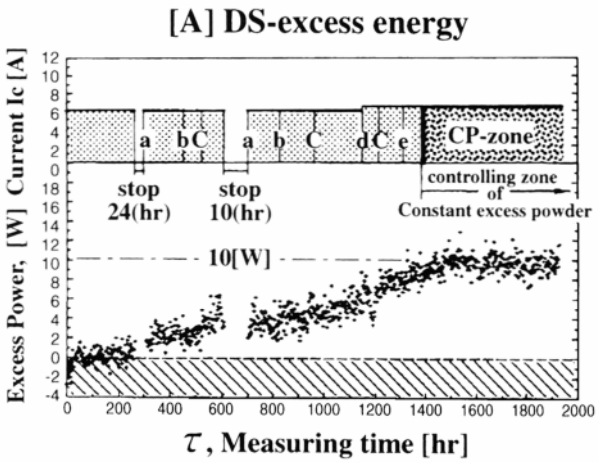

Figure 9. Deuterium deposited by D_2O electrolysis onto DS-cathode containing ZrO_2, nano-Pd catalyst produced 3 weeks of stable excess heat at 10 W. Integrated heat ≈ best hot fusion result.

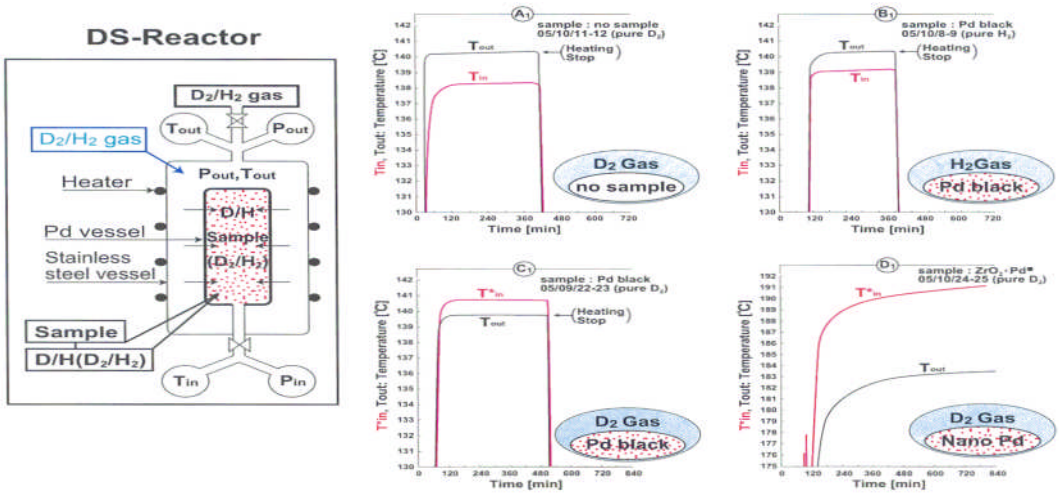

Figure 10. Gas loading tests at elevated temperature

The DS-Cathode is called the inner–vessel of a double cylinder reactor. Four tests were carried out using a reactor pre-heated to 141°C:

(1) D_2 flows into volume between outer and inner vessels, no catalyst
(2) H_2 flows into volume between outer and inner vessels, uses Pd–black: $T_{out} > T_{in}$
(3) D_2 flows into volume between outer and inner vessels, uses Pd–black: $T_{in} > T_{out}$
(4) D_2 flows into volume between outer and inner vessels, uses ZrO2,nano-Pd catalyst: $T_{in} > T_{out}$ and T_{in} rose from 141°C to 191°C

Test 2 shows that no heat is generated when the catalyst is Pd-black and the pressurizing gas is H_2. Test 3 on lower left shows reversed heat flow from Pd-black catalyst. Heat is flowing from the inner vessel that holds the catalyst towards the outer vessel wall where the electrical heater is located. Test 4 shows that when ZrO_2,nano-Pd catalyst is used the heat flow from

catalyst to outer vessel wall is 7 times greater than when Pd-black is used. The study indicates that a larger system of the same design would generate enough catalytic fusion heat to permit the heater to be turned off. This means that ZrO_2,nano-Pd catalytic heaters can be used to provide fusion heat at 191°C.

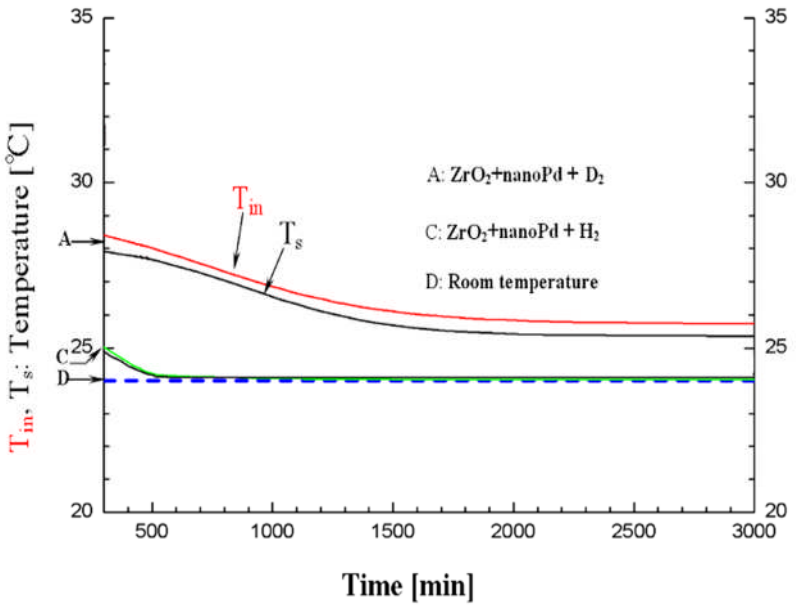

Figure 11. Autonomous heat with D_2; no nuclear heat with H_2

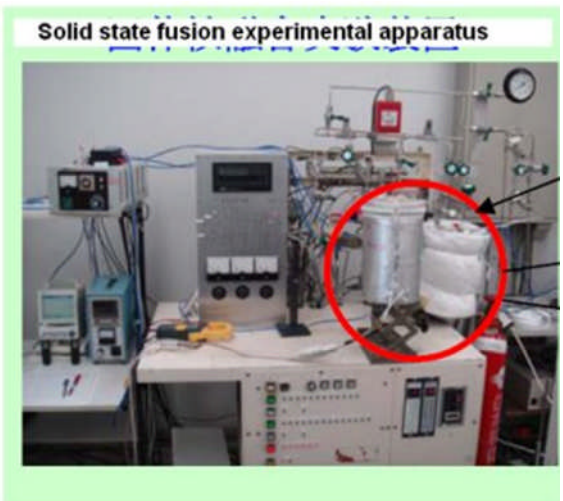

Figure 12. Test reactors

In their 2007/8 study A&Z replaced the double cylinder reactor used in 2005 with a simple single stainless steel cylinder sealed off at both ends and containing 7 grams of ZrO_2,nano-Pd catalyst. No internal Pd cylinder was used. The reactor was well insulated and operated at room

temperature. Zero electrolysis and zero heater power were used in the experiment. The catalyst bed was first evacuated. Then a Pd-filtered inflow of D_2 gas was applied so as to gradually raise the reactor vessel pressure towards 100 atm.[1] Fig. 12 shows 2 thermally insulated test reactors.

During the D_2 gas inflow period there was initial heat production due to the exothermic formation of palladium deuteride PdD_x. Reactor wall temperature rose from room temperature to about 34°C. The chemical heat flowed out of the system, so that by about 33 hours of run time all chemical heat had been lost to the room temperature environment. The assembly surface temperature returned gradually to 1.8°C above room temperature, and remained at 1.8°C above room temperature for hundreds of hours. A control run with H_2 gas inflow showed a comparable initial-transient wall temperature with a subsequent fall to room temperature by run time = 9 hr. The only plausible energy source for the sustained higher temperature produced by D_2 pressurization is the catalytic release of nuclear energy.

References

1. Yoshiaki. Arata and YueChang Zhang, Proc. Japan Acad. **70B**, 106 (1994); ibid. *Proc. Japan Acad*. **78B**, 57 (2002); ibid. Proc. ICCF12, 44 (2006); *ibid. J. High Temp. Soc., Jpn* **34**. 1 (2008).
2. S. Yamaura, K. Sasamori, H. Kimura. A. Inoue, Y. C. Zhang, Y. Arata, J. Mater. Res. 17, 1329 (2002).

Establishment of the "Solid Fusion" Reactor

Yoshiaki Arata and Y-C Zhang

Abstract

A gas-loaded fusion reactor operating at room temperature using ZrO_2 + nanoPd catalyst produced nuclear heat for hundreds of hours when pressurized with D_2 gas, but no measurable nuclear heat when pressurized with H_2. ^4He was produced during the D_2 run, and not during the H_2 run. No electrical power was supplied to the reactor during the runs, thereby demonstrating operation of an autonomous fusion "heater".

Introduction

About 50 Years ago (1955-1958), one of the authors (Y. Arata) investigated "solid-state plasma fusion" (simply "Hot Fusion") together with "thermonuclear fusion", he was the first researcher in the world to discover "Solid Fusion", as well as the first researcher in Japan to discover "Hot Fusion". Moreover, on Feb 6, 1958, he carried out large "open experiments" for the general public, which strongly impacted not only Japan but also the world, although he was at a young age (33 years old) at that time.

In addition, the authors continued to demonstrate experimentally the existence of "Solid Fusion" for the first time in the world, by publishing research reports in over 70 papers[(1-53)] presented in the Proc. Japan Acad., and other societies during about 20 years (1989~2007). In these experiments, many kinds of alloys, which include Pd and Pd-black etc. were developed and used as specimens. Recently, the authors started to develop the usefully practical reactor of "Solid Fusion" (Solid Reactor), and it was achieved some month ago at last. This reactor is a remarkable improvement over the many known models developed so far.

[Among many things that Arata learned during his hot fusion studies was that high temperatures occur when bulk Pd metal containing a large D/Pd ratio is exposed to air. When Fleischmann and Pons (F-P) reported high temperatures and the melting of a Pd electrode, he recognized that air likely had made contact with the test electrode and oxidized the dissolved deuterium. Since these F-P studies had not been carried out in an argon atmosphere, he resolved to convince himself whether or not "cold fusion" was real. As a result, considerable independence has characterized the Arata and Zhang (A-Z) program.]

"Solid Fusion Reactor" Experiment*

Figure A shows the principle of the "Solid Fusion Reactor" which is constructed with the following system. Firstly, microscopic solid fine powders are set inside the high vacuum, stainless steel vessel, and then pure D_2 gas is injected as "Streaming D_2 gas" into the stainless steel vessel. This "Streaming D_2 gas" penetrates instantly into the many solid fine samples as the "Streaming Deuterons"(=D^+-Jet stream") without storing inside the stainless vessel.

This was an amazing event. Moreover at this time, nuclear fusion reaction was generated inside the solid with synchronous creation of both much Helium (^{4}He) and large thermal energy under the equation:

^{2}D + ^{2}D = ^{4}He + thermal energy (a)

(4 ^{2}D = 2 ^{4}He + thermal energy) (b)

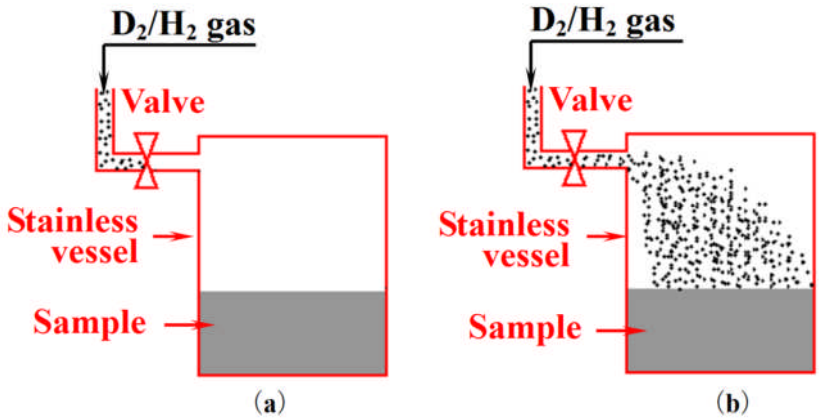

Figure A. Principle of "Solid Fusion" Reactor Vessel. (a): Reactor before introduction of D_2 or H_2 gas (only stainless steel vessel and sample (b): Introducing of D_2 or H_2 as the D_2 or H_2 -"jet-stream" into reactor vessel; and then D^+ or H^+ -"jet stream" penetrate into the sample)

(Note) : If D_2 or H_2 was introduced, D_2 or H_2 -"jet stream" immediately penetrates into the sample as D^+ or H^+- "Jet-stream: and Fusion Reaction", (^{4}He and thermal energy) immediately generated in the case of the "D^+-jet stream"; but in the H^+-jet stream" only chemical reaction heat is generated, (It will be explained in detail in Fig. 2, Fig. 3, Fig. 6 for D_2 and Fig. 4 for H_2).

Experiment and discussion

These experiments show the characteristics of "solid nuclear fusion reactor suitable for practical use".

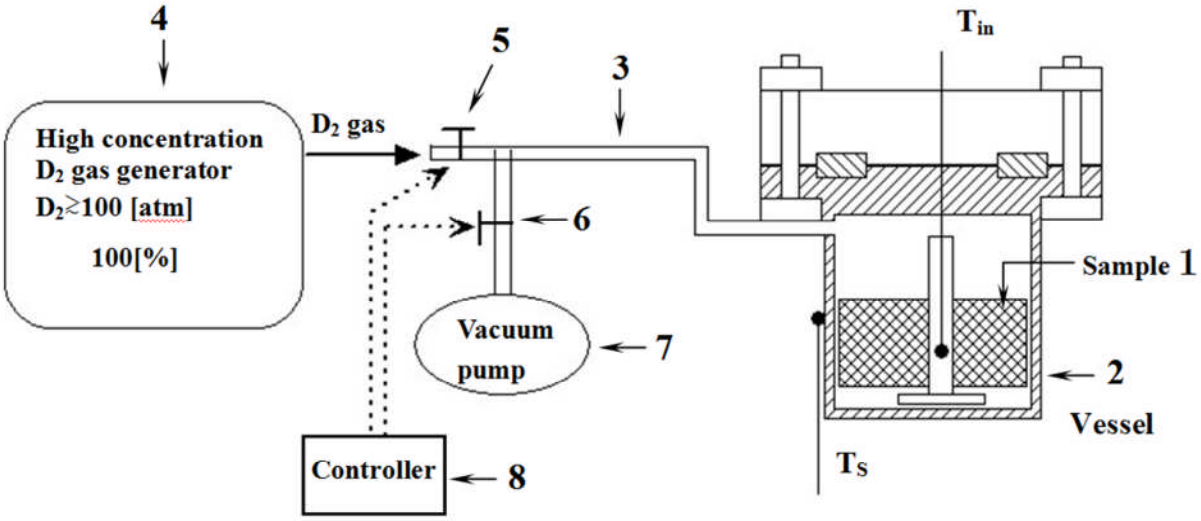

Figure 1. Experimental Device

Figure 1 is a diagram showing the principle of the "Solid Fusion Reactor" suitable for practical use. The fuel for the reactor is D_2 gas **4** having a high isotopic purity (almost 100%). The vessel **2** is made of stainless steel. A sample is provided within the high vacuum vessel **2**. The inner temperature T_{in} is measured by a thermocouple placed on the central axis of the sample. The temperature T_s of the stainless steel vessel **2** is measured by a thermocouple placed on the outer wall of the vessel **2**. The D_2 gas generator **4**, the vessel **2** and the vacuum pump **7** are coupled to each other via the stainless steel pipe **3**. The valves **5** and **6** are connected to the stainless steel pipe **3.** Opening and closing of the valves **5** and **6** is controlled by the controller **8**. The feature of the reactor is that once the D_2 gas is supplied to the vessel **2**, the supplied gas directly enters into the sample as the "D^+-jet stream" without staying within the vessel **2**. The reaction occurs between these streaming deuterons within clouds of electrons within the sample. In other words, where the supplied D_2 gas is converted into ^{4}He and thermal energy only in accordance with the following formula:

$$^2D + {}^2D = {}^4He + \text{thermal energy} \quad \text{(a)}$$

$$(4\ {}^2D = 2\ {}^4He + \text{thermal energy}) \quad \text{(b)}$$

Here, the thermal energy includes additionally the chemical energy generated between "streaming deuterons" (= D^+-jet stream") and "sample solid atoms". In other words, during the reaction period, the reactor serves as "^{4}He generation reactor" as well as a "thermal energy generation reactor". It can be understood that this reactor is an ideal reactor suitable for practical use.

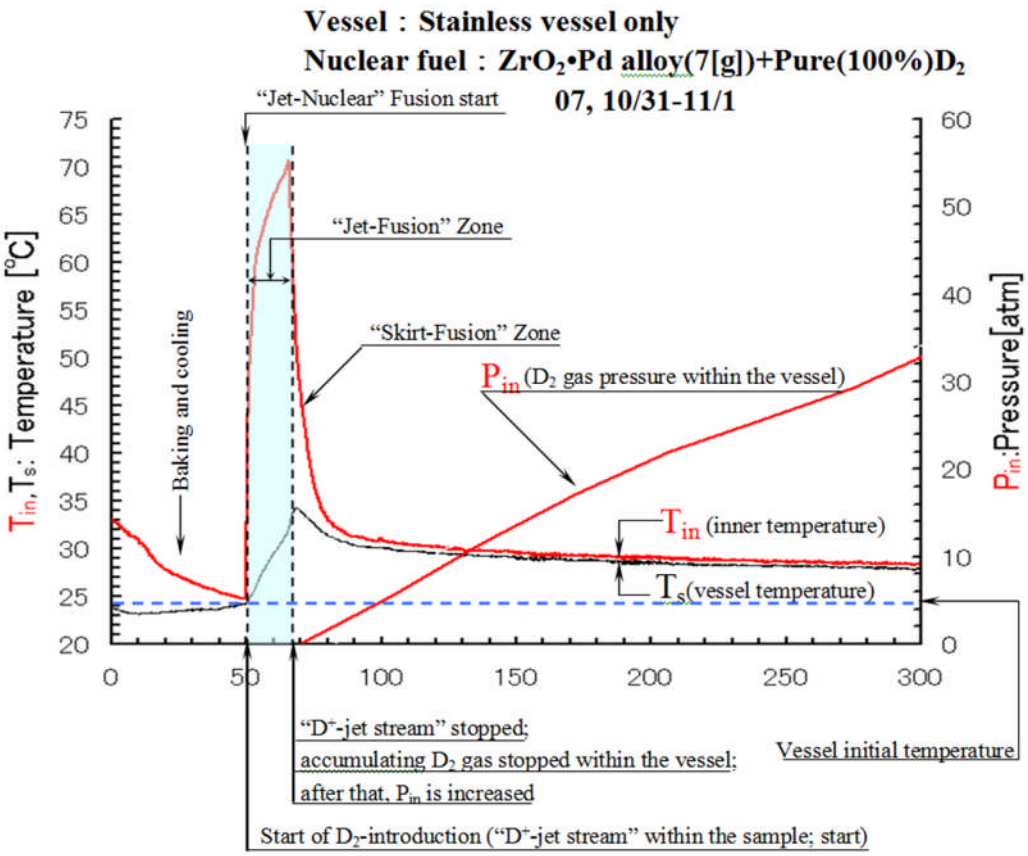

Figure 2. Simultaneous generation of thermal energy and ^{4}He

In the case where the sample is ZrO_2-Pd (nano Pd) alloy, as shown in Figure **2**, the nuclear fusion reaction rapidly occurs inside the sample simultaneously with the supply of D_2 gas, and the thermal energy is generated (in which, chemical reaction energy generated between "D^+-jet stream and sample atoms" is included). Then, "D^+-jet stream" was stopped, in other words the generation of thermal energy is stopped simultaneously with the completion of the nuclear fusion reaction, which is called as the "Jet-Fusion". During the "Jet-Fusion" reaction period, the gas pressure within the reactor is zero, and all the supplied D_2 gas enters as the "D^+-jet stream" into the sample without staying in the reactor, and chemical reaction energy occurs inside the sample. For instance, each 2~4 D-atoms in the "D^+-jet stream" are coagulated as the "lumpy solid-state deuterons" (simply "Solid-deuteron")[52] inside the innumerable each crystal lattice "space" ("electron box")[52] within the sample solid, and these "Solid deuteron" fulfill its function to create the "Solid nuclear fusion reaction". In other words, "Solid-deuteron" corresponds to the "Nuclear fuel"[52]. And then, the generation of the thermal energy is stopped simultaneously with the completion of the "Jet-Fusion" reaction. Thereafter, the D_2 gas is accumulated within the reactor and the gas pressure P_{in} within the reactor is increased over time, unlike the reaction period during which P_{in} is equal to zero.

[The protocol for producing the ZrO_2-nanoPd catalyst is given in Ref. (54). The protocol for preparing the catalyst before use is different from that used with Pd-black. Prior to exposure to D_2 gas, the ZrO_2-nanoPd catalyst is first reduced by a controlled inflow of D_2 at about 20 cc-atm/min, next is outgased at 150°C until a vacuum of about 6 x 10^{-7} Torr is achieved, and then is cooled to room temperature. Ref. (58). Figure 2 shows the end of the cooling interval during run time interval 0 - 50 min, and the start of the Jet-Fusion period at time = 50 min.]

This experimental result is a very epoch-making one which is beyond any expectation. This is an unexpected new phenomenon. This new phenomenon can occur in the same manner in the case where another sample is used, as shown in Figure **3**. This should be called “historical phenomena”

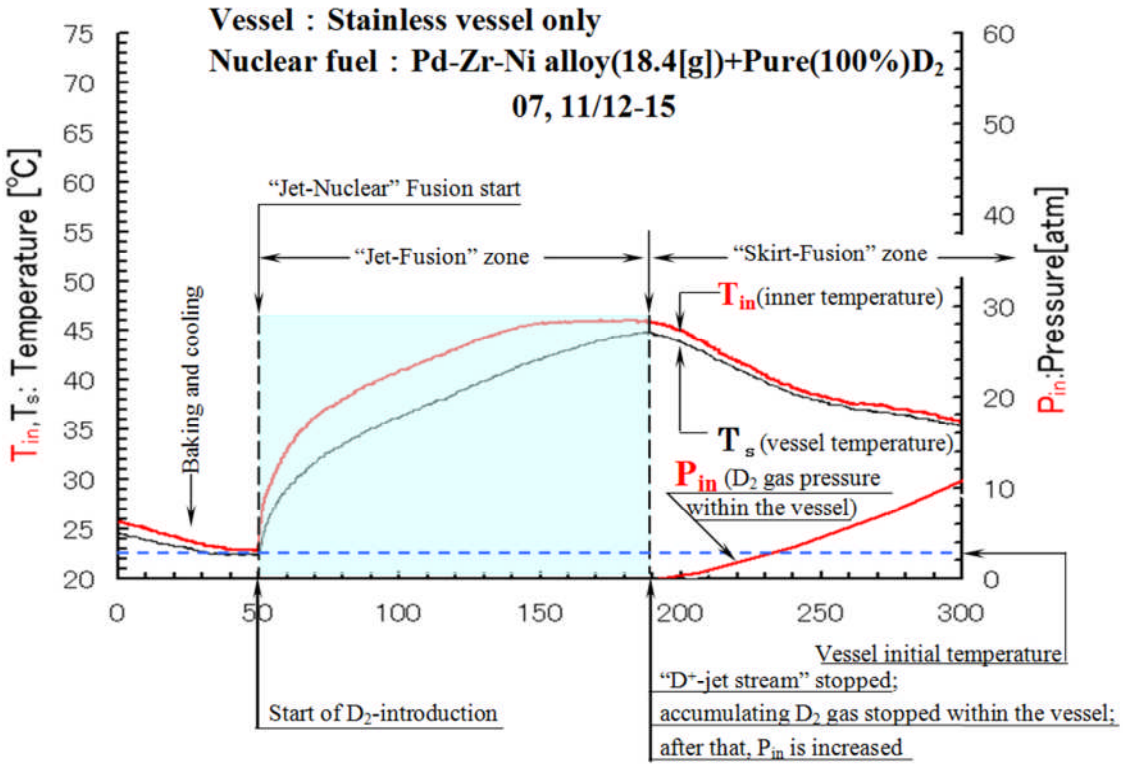

Figure 3. Simultaneous generation of thermal energy and 4He

In order to understand this new phenomena more deeply, another definitive experimental result will be presented based on the above conclusion. It is the comparison between D and H from the viewpoint of the nuclear fuel. In the past 20 years, it has been well known that the authors were far ahead of others and achieved brilliant success on “verification of solid fusion”.[(1-53)] The authors named this device a “verification reactor”. The authors continuously developed several kinds of verification reactors, not only one kind of verification reactor, confirmed the “verification of solid fusion”, and published the results in reports. Fifty-five are listed at the end of this paper. One example of the “verification reactor” is a world-famous electrolysis-type reactor using D_2O or H_2O: “DS-cathode”(=“Double Structure Cathode”). With

the DS-Cathode, D/H is generated within the electrolytic solution of D_2O/H_2O, i.e., within the Cathode. The generation of D/H corresponds to the presence/absence of the solid fusion reaction. In the former case where D is used, anything other than a small amount of chemical reaction heat cannot be recognized.

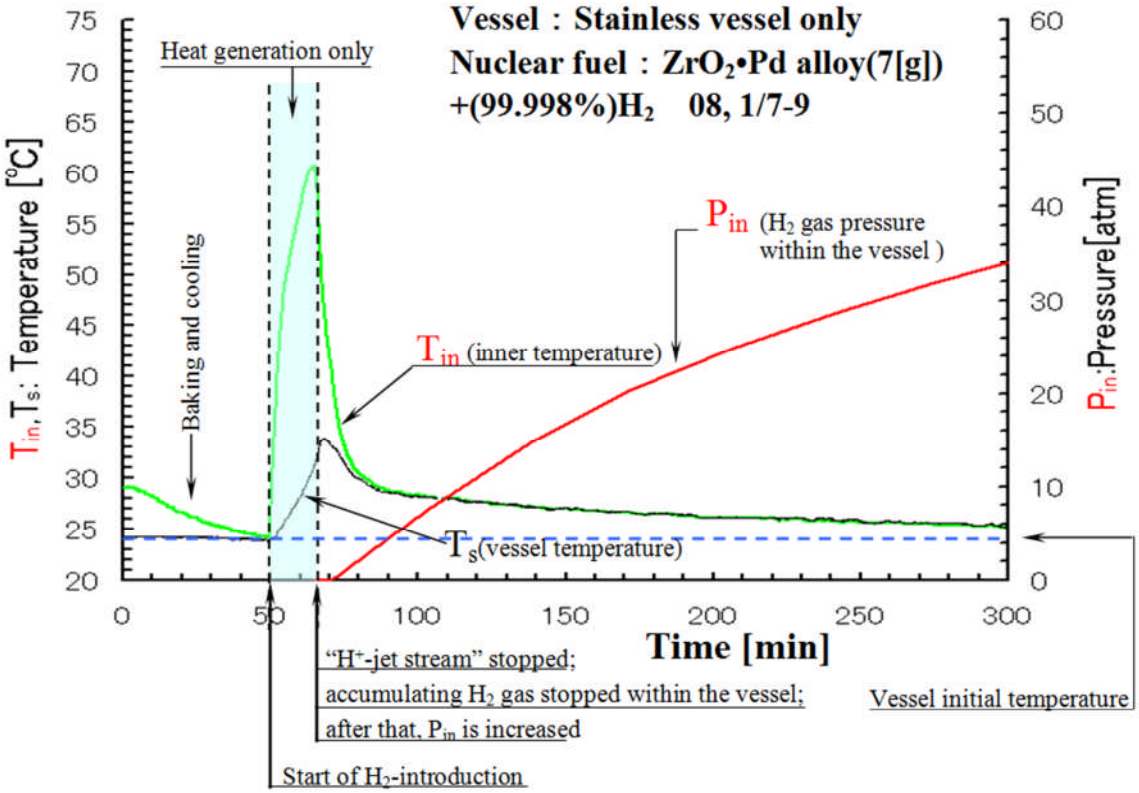

Figure 4. Heat Generation for H_2 Introduction

The comparison between D and H is made from the viewpoint of the nuclear fuel, using a newly developed "practical use reactor"("Solid Reactor"). In the case where D is used, an intensive reaction (^{4}He and thermal energy) due to the solid fusion occurs for both the "verification reactor" and the "Solid Reactor". On the other hand, in the case where H is used as shown in Figure 4 and Figure 7[A], [B], chemical reaction heat is generated, but ^{4}He is not generated at all.

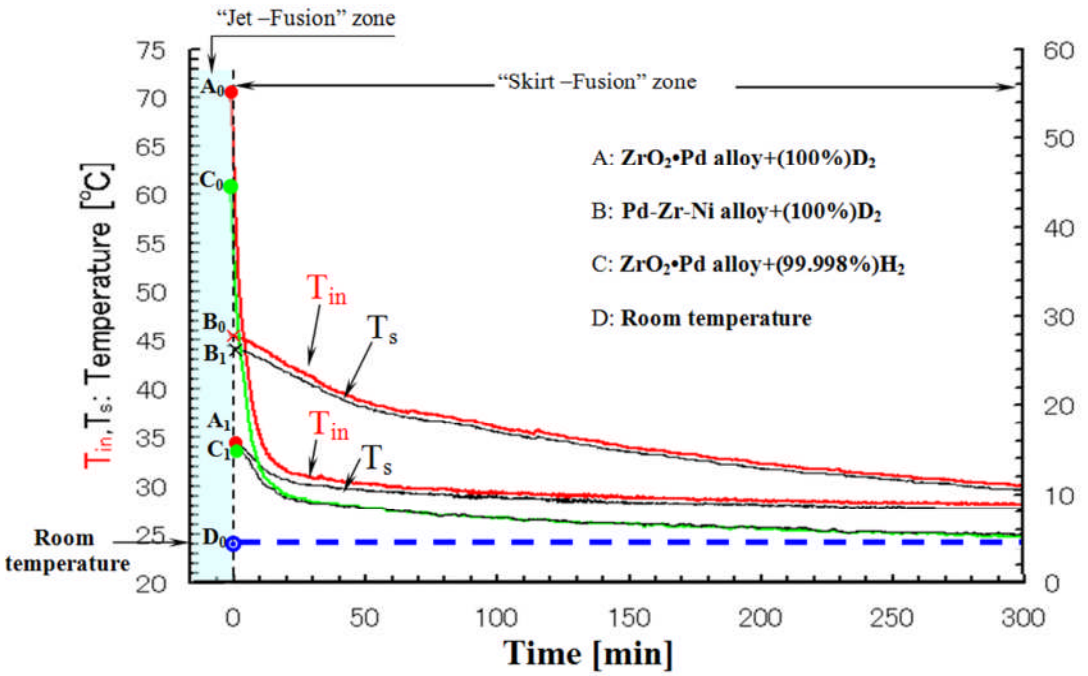

Figure 5A. Comparison of generation characteristics of Nuclear fusion during "Skirt-Fusion" zone for each fuel (0~300min)

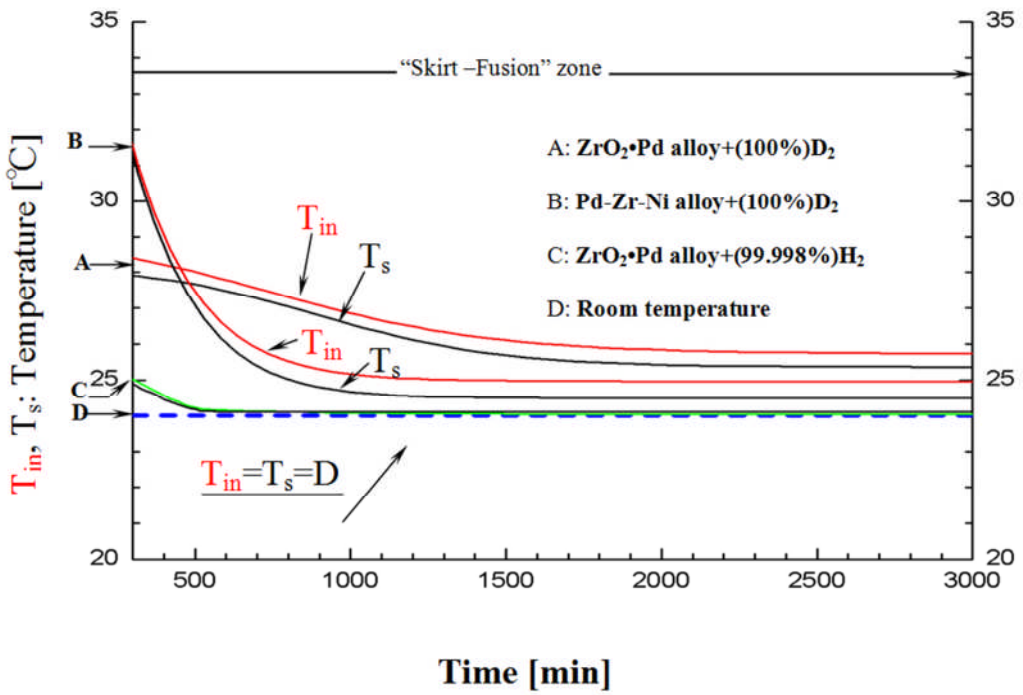

Figure 5B. Comparison of generation characteristics of Nuclear fusion during "Skirt-Fusion" zone for each fuel (after 300min)

The difference between the “Solid Reactor” and the “verification reactor” is that the structure of the “Solid Reactor” is much simpler than that of the “verification reactor”, and the reaction period of time of the “Solid Reactor” is in comparably shorter (10^{-2}~10^{-3} times) than that of the “verification reactor”, although the principle of these reactors is the same. In the “Solid Reactor”, the stream of D^+ (“D^+-jet stream”) directly and entirely enters into the sample for a very short period of time. On the other hand, in the “verification reactor”, this phenomena occurs indirectly, and therefore, a very long period of time is required for the reaction. For instance, D-atoms should be passing through the wall of Pd vessel in the “DS-Cathode” with a long period of time.

Based on this experimental fact and the comparison result between Figure **2** and Figure **3**, it can be clearly understood that this is a historical experimental fact.

Moreover, the relation of each gas temperature (red line/T_{in}) and vessel; temperature (black line/T_s) as shown in Fig. 5A and Fig. 5B; which indicated through long period with expanded scale in temperature compared with Fig. 5A. It is clear that both gaseous and vessel temperature (C) in the H_2 gas drop into the room temperature (D-line) is very short period. However, both A and B samples continue in long and long period at the separated state between red T_{in} and black T_s lines($\Delta T=T_{in}-T_s$: this is very important “ΔT-characteristics”). These results depend on the continued nuclear reaction of the “Skirt-Fusion”. This is the extreme very important result. These phenomenon continue about several hundred hours.

Finally, the D_2 pressure characteristic in the case where there is no sample within the vessel is shown in Figure **6**. In this case, once the D_2 gas is supplied to the vessel, the increase in the pressure P_{in} is started immediately as shown in the red line and then the pressure P_{in} is increased over time. On the other hand T_{in} (inner temperature) and T_s (vessel temperature) are not influenced by the supply of D_2 gas at the room temperature (i.e. T_{in} and T_s are not changed). Even though P_{in} is changed, T_{in} and T_s (always, $\Delta T=T_{in}-T_s=0$) are not changed as shown in Figure **6**. This is common sense in the conventional art, and conforms to the experimental result.

Consequently, “Skirt-Fusion” start immediately at the end of “Jet-Fusion”, and continue in long period (over 100 hours) as shown in Fig. 5B. Generated heat energy were about 4.4 kJ in “Jet-Fusion” ≅18 kJ/hour) and about 200 kJ in “Skirt-Fusion(≅250 kJ in “Skirt-Fusion”(≅4 kJ/hour). About 5 x 10^{15} ^{4}He were produced in “Jet-Fusion” and about 3 x 10^{17} ^{4}He in “Skirt-Fusion” zone. Sample is ZrO_2-Pd alloy (6.5 gram) in this case.

[Line Plots A are for ZrO_2-Pd alloy (6.5 gram sample) and Line Plots B are for ZrO_2-Ni,Pd alloy (18.4 gram)]

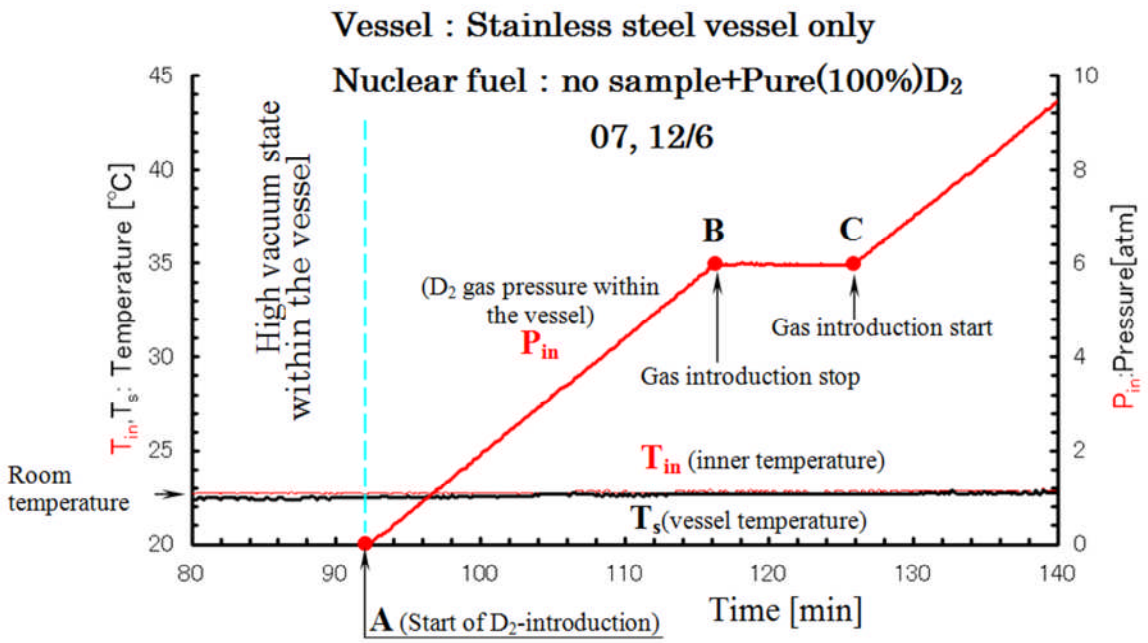

Figure 6. Gas pressure characteristics within vessel (no sample)

In order to further clarify this conclusion, Figure **7[C]**(within fuel gas) and Figure **7[D]** (within sample solid) are shown using Mass-spectrometer. In particular, it can be understood that a large amount of ^{4}He is generated within the sample solid as shown in Figure **7[D]**. It is well known as the characteristics of ^{4}He cannot enter into any solid and ^{4}He cannot egress from any solid under the temperature level from the room temperature to several-100°C. Figure **7[C], [D]** shows a situation in which a large amount of ^{4}He fully fills into the sample during a very short time. And then, it should be named as the Jet-nuclear Fusion Reaction (simply "Jet-Fusion"), because of these "Solid nuclear fusion reactions" generated like a jet cleaning extremely short periods as shown in Figures 2, 3 and 7. This clearly shows that this amazing phenomena results from the reaction within the sample.

Accordingly, this reactor is a thermal energy generation device as well as a ^{4}He production device. It is obviously clear to us which one of the following is more important to human beings: (a) the thermonuclear fusion device of the "era"; or the solid nuclear fusion described above.

It is considered that the solid nuclear fusion described above is useful for an energy source for homes, cars, ships airplanes and the like. Quickly implementing measures is desired in view of the current air pollution problem. It is possible that a further science and new industry are to be developed.

In the last word, in very important for "Actual Nuclear Reactor" that the solid nuclear fusion reaction does not generate any pollution, whereas a hot nuclear fusion reaction is commonly known to generate a considerable amount of harmful pollution.

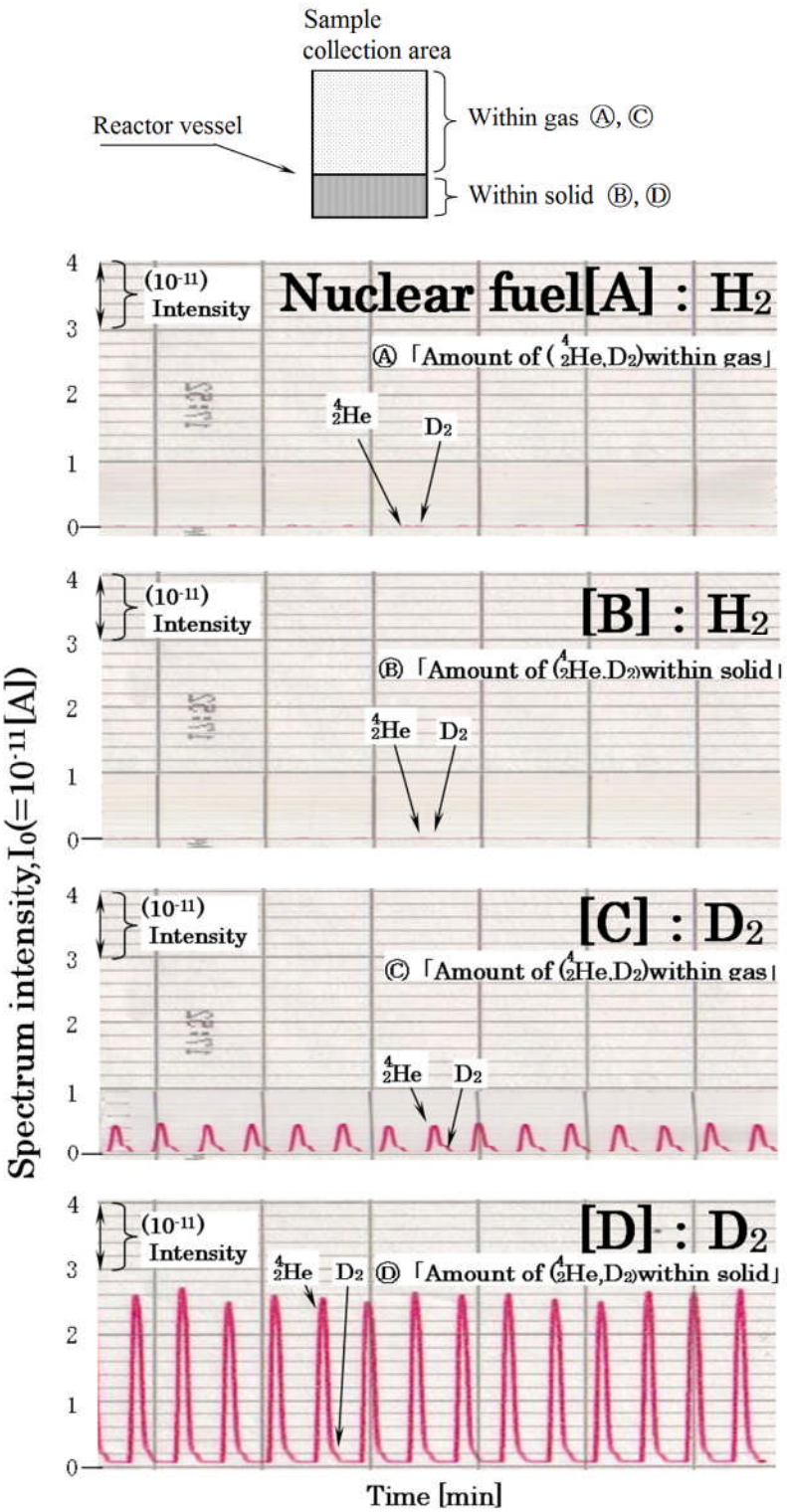

Figure 7. Mass analysis result for fuel (H_2 or D_2) and reaction product (^4He)

Note on Sources

The Abstract is a rewritten version of a statement on the Cover of his Arata Award lecture at ICCF14[54]. Explanations by editor (Talbot Chubb) based on References (52-55) are enclosed in square brackets. Text used in the Abstract is based on a presentation made by Arata and Zhang on May 22, 2008 in Osaka, Japan[53].

References

1. Arata Y, Zhang Y-C; Kaku Yugo Kenkyu 62 (1989) 398. Cited in Chem. Abstr. 112: 224669 [1990]. (in Japanese). "Achievement of intense 'cold fusion' reaction".
2. Arata Y, Zhang YC; proc. Jpn. Acad. 66, Ser. B (1990) 1. "Achievement of intense 'cold' fusion reaction".
3. Arata Y, Zhang Y-C; proc. Japan Acad. 66, Ser. B (1990) 33. "Cold' fusion caused by a week'on-off effect'".
4. Arata Y, Zhang Y-C; proc. Japan Acad. 66, Ser. B (1990) 110."Corroborating evidence for 'cold' fusion reaction".
5. Arata Y, Zhang Y-C; Fusion Technol. 18 (1990) 95. "Achievement of an intense cold fusion reaction". But see; "Corrigendum",FT 19 [1991] 196.
6. Arata Y, Zhang Y-C; Fusion Technol. 22 (1992) 287. "Reproducible 'cold' fusion reaction using a complex cathode".
7. Arata Y, Zhang Y-C; Kaku Yugo Kenkyu 67 (5) (1992) 432 (in Japanese). "'Cold' fusion in deuterated complex cathode".
8. Arata Y, Zhang Y-C; Koon Gakkaishi(J.High Temp.Soc.). 20(4) (1994) 148(in Japanese, Engl.abstr.). "A new energy generated in DS-cathode with 'Pd-black' ".
9. Arata Y, Zhang Y-C; proc. Japan Acad. 70 Ser. B (1994) 106. "A new energy caused by 'Spillover-deuterium' ".
10. Arata Y, Zhang Y-C; Proc. Japan Acad. 71 Ser. B (1995) 304. vol. 71, No. 8, 304-309, (1995). "Achievement of Solid-State Plasma Fusion ("Cold Fusion")".
11. Arata Y, Zhang Y-C; proc. Japan Acad. 61, Ser. B (1995) 98. "Cold fusion reactions driven by 'Latticequake'".
12. Arata Y, Zhang Y-C; Koon Gakkaish (J. High Temp. Soc.). 21 (6) (1995) 303 (in Japanese, Engl. abstr. & Fig. captions). "Achievement of solid-state plasma fusion ("cold fusion")".
13. Arata Y, Zhang Y-C; Koon Gakkaishi (J. High Temp. Soc.). 21 (1995) 130 (in Japanese, Eng. abstr.); "Peculiar relation between hot plasma fusion and solid-state plasma fusion ("cold fusion")".
14. Arata Y, Zhang Y-C; Koon Gakkaishi (J. High Temp. Soc.). 21 (1995) 43 (in Japanese, Engl. abstr.). "Cold fusion caused by 'lattice quake'".
15. Arata Y, Zhang Y-C; Koon Gakkaishi (J. High Temp. Soc.). 22 (1) (1996) 29 (Japanese, Engl. abstr.) "Generation and mechanism of solid-state plasma fusion ("cold fusion")".
16. Arata Y, Zhang Y-C; proc. Japan Acad. 72 Ser. B (1996) 179. "Deuterium nuclear reaction process within solid".
17. Arata Y, Zhang Y-C; proc. Japan Acad. 73, Ser. B (1997) 62. "Presence of helium (4/2He, 3/2He) confirmed in deuterated Pd-black by the "vi-effect" in a "closed QMS" environment".

18. Arata Y, Zhang Y-C; J. High Temp. Soc. 23 (1997): (special volume pp 1-56). "Solid-state plasma fusion ('cold fusion')".
19. Arata Y, Zhang Y-C; J. High Temp. Soc. 23 (1997) 110 (in Japanese, Engl.abstr.). "Presence of helium (4/2He, 3/2He) confirmed in highly deuterated Pd-black by the new detecting methodology".
20. Arata Y, Zhang Y-C; proc. Japan. Acad. 73, Ser. B (1997) 1-6. "Helium(4/2He, 3/2He) within deuterated pd-black".
21. Arata Y, Zhang Y-C; Jpn. J. Appl. Phys. 237 (1998) L1274. "Anomalous difference between reaction energies generated within D2O-cell and H2O-cell".
22. Arata Y, Zhang Y-C;Kaku Yugo Kenkyu 69 (1998) 963 (in Japanese). "Excess heat in a double structure deuterated cathode".
23. Arata Y, Zhang Y-C; proc. Japan. Acad. 74, Ser B (1998) 110. "Anomalous 'deuterium-reaction energies' within solid".
24. Arata Y, Zhang Y-C; Proc. Japan Acad. 74 Ser. B (1998) 201. "The importance of sono-implantation".
25. Arata Y, Zhang Y-C; proc. Japan Acad. 75 Ser. B (1999) 71. "Definitive difference between [DS-D2O] and [Bulk-D2O] cells in 'deuterium-reaction'".
26. Arata Y, Zhang Y-C; proc. Japan Acad. 75 Ser. B (1999) 76. "Critical condition to induce 'excess energy' within [DS-H2O] cell".
27. Arata Y, Zhang Y-C; proc. Japan. Acad. Ser. B 75 (1999) 281. "Anomalous production of gaseous 4He at the inside of 'DS cathode' during D2O-electrolysis".
28. Arata Y, Zhang Y-C; Jpn. J. Appl. Phys. 38 (1999) L774. "Observation of Anomalous Heat Release and Helium-4 Production from Highly Deuterated Palladium Fine Particles".
29. Arata Y, Zhang Y-C; Genshikaku Kenkyu (Anomalous Nuclear Fusion Reaction). 45(2)(2000). vol.45, No.2, July 2000; and ICCF8 (Lerici, Italy, May 2000). "Definitive Defference among [DS-D2O],[DS-H2O] and [Bulk-D2O] cell in the Deuterization and Deuterium-reaction".
30. Arata Y; Kotai Butsuri 35 (1) (2000) 67 [in Japanese]. Cited in Chem. Abstr. 132: 128508 (2000) "Developmental challenge in new energy source; 'Solid state plasma fusion'".
31. Arata Y, Zhang Y-C; Appl. Phys. Lett. 76 (2000) 2472. vol.76, No.17, 2472, (2000). "Sono Implantation of hydrogen and deuterium from water into metallic fine powders".
32. Arata Y, Zhang Y-C; Jpn. J. Appl. Phys. 39 (2000) L4198. "Deuterization and Deuterium Reactions in the Electrolyses of D2O with the Double Structure Cathode and the Bulk Cathode".
33. Arata Y, Zhang Y-C; Proc. ICCF 8, Italy (2000) 11 and 293. "Definitive Difference among [DS-D2O], [DS-H2O], [Balk-D2O] cells in the Deuterization and Deuterium-reaction" (pp. 11-16), and "Sonoimplantation of hydrogen and deuterium from the water into metallic fine powders", (pp. 293-298).
34. Arata Y, Zhang Y-C; Proc. Japan Acad. 77 Ser. B (2001) 43. "Intense sono implantation of gases into metals".
35. Arata Y, Zhang Y-C; proc. Japan. Acad. 78 ser. B (2002) 57. "Formation of condensed metallic deuterium lattice and nuclear fusion".
36. Arata Y, Zhang Y-C; Proc. Japan Acad. 78 Ser. B (2002) 63. "Nuclear fusion reacted inside metals by intense sonoimplantion effect".

37. Arata Y, Zhang Y-C; Proc. Japan Acad. 78 Ser. B (2002) 201. "Intense deuterium nuclear fusion of pycnodeuterium-lumps coagulated locally within highly deuterated atom clusters".
38. Arata Y, Zhang Y-C; Appl. Phys. Lett. 80 (2002) 2416. "Intense sonoimplantation of atoms from gases into metals".
39. Arata Y, Zhang Y-C; Proc. ICCF 9, China (2002) 5-16. "Pycnonuclear Fusion Generated in "Lattice-Reacter" of Metallic Deuterium Lattice within Metal Atom-clusters".
40. Yamamura T, Shiokawa Y, Inoue A, Zhang Y-C, Arata Y; J.High Temp. Jpn 28 (2002) 144. "Neutron Activation Analysis of Pd Atom Clusters Caused Pycnonuclear Fusion".
41. Arata Y, Zhang Y-C; ICCF10 (Boston (2003); "Development of Compact Nuclear Fusion Reactor Using Solid Pycnodeuterium as Nuclear Fuel".
42. Arata Y; Kotai Butsuri 38 (1) (2003) 83 [in Japanese]. "Discovery of Pycnodeuterium-lumps and Intense Solid-state Nuclear Fusion in Highly Deuterated (Nano-particles)".
43. Arata Y, Zhang Y-C, Fujita H, Inoue A; Koon Gakkaishi 29 (2) (2003) 68. "Discovery of solid deuterium nuclear fusion of pycnodeuterium-lumps solidified locally within nano-pd particles": English translation (Il Nuovo Saggiatore, 20 (2004) 66 in Italy phys. soc.).
44. Arata Y, Zhang Y-C; J. High Temp. Soc. Jpn 29 (2003) 171. "Deuterium Absorption Characteristics of Peculiar Composite Powder (Zr3NiO・NiO)".
45. Arata Y, Zhang Y-C; J. High Temp. Soc. Jpn 29 (2003)(special vol: pp 1-44). "The Basics of Practical Nuclear Fusion Reactor Using Solid Pycnodeuterium as Nuclear Fuel".
46. Arata Y; Il Nuovo Saggiatore 20 (5-6) (2004) 66. "The formation of 'solid deuterium' solidified inside crystal lattice and intense solid-state nuclear fusion ('cold fusion')".
47. Arata Y, Zhang Y-C; Progress of Theoretical Phys. (Supplement), No. 154 (2004) 241: Fusion 03. "The Basics of Nuclear Fusion Reactor using Solid Pycnodeuterium as Nuclear Fuel".
48. Arata Y; Special Volume, IIW (Osaka), July 11st (2004). "Relation between Welding Science and Nuclear Fusion".
49. Arachi Y, Emura S, Omura A, Nunogaki M, Asai T, Yamamura S, Inoue A, Arata Y; Solid State Ionics (2006). "Structural Analysis on High Density H (D) Absorbed Nano-sized-Pd/ZrO2 Composite for Hydrogen Storage Materials".
50. Arata Y, Zhang Y-C; ICCF12 (Yokohama, Jpn; (2006)). "Development of "DS-Reactor" as the Practical Reactor of "Cold Fusion" based on the "DS-Cell" with "DS-Cathode".
51. Arata Y;IL NUOVO SAGGIATORE, (2004)6, "The formation of 《solid deuterium》 solidified inside crystal lattice and intense solid-state nuclear fusion (《cold fusion》) ".
52. Yamaura, S., Sasamori, K., Kimura, H., Inoue, A. Zhang, Y-C, and Arata Y. (2002) J. Mater, Res. 17,.1329. “Hydrogen absorption of nanoscale Pd particles embedded in ZrO2 matrix prepared from Zr-Pd amorphous alloys”.
53. Arata, Y and Zhang, Y-C. (2008), J. High Temp. Soc. 34, 85. “Establishment of Solid Fusion Reactor”, English version.
54. Yoshiaki Arata, “Toward the Establishment of Solid Fusion as a Perpetual Energy for Humankind, Book distributed at ICCF14 (2008).
55. Yoshiaki Arata, ICCF14 Award Lecture (2008). “History of 'Solid Fusion'“.

Glossary

Cold fusion as used in this paper means dd fusion in bulk Pd as studied by F-P and followers, also referred to as F-P effect

D+-Jet Stream means Jet-Fusion deuterons adsorbed onto nanoPd catalyst where metal electrons provide charge neutralization

DS-Cathode means same as Double Structure Cathode: hermetically sealed vessel with Pd cylinder and ss welded end pieces, filled with nanoPd catalyst

Electron box is envisioned cubic volume containing 4 electrons + 4 deuterons in octahedral site of fcc lattice[51,57]

Hot fusion is the same as plasma fusion

Jet-Fusion reaction means nuclear fusion occurring during Jet-Fusion zone

Jet-Fusion zone means run-time interval during which D_2 or H_2 gas is flowing onto sample and back pressure in reactor is too low to record on mechanical gage.

Sample means catalyst bed material

Skirt-Fusion zone means run-time interval starting at end of Jet-Fusion zone and continuing thereafter. The verb “skirt” means “to form edge of” (Oxford Dictionary)

Solid-state fusion is same as solid fusion

Solid fusion means nuclear fusion in a solid containing nanometal Pd: sometimes called “metal catalyzed fusion”, also referred to as A-Z effect

Solid Reactor means same as Solid Fusion Reactor: gas-loaded reactor producing heat and 4He without using any applied electrical power

Streaming D2 gas is same as Streaming Deuterons: long mean free path D_2 molecules enter reactor against negligible back pressure before impacting nanoPd

Thermonuclear fusion is same as plasma fusion, as sought in ITER program

Verification reactor means electrolysis-loaded DS-Cathode containing nanoPd catalyst and producing excess heat

LENR Research using Co-Deposition

S. Szpak[1], P. A. Mosier-Boss[1], F. Gordon[1], J. Dea[1], M. Miles[2], J. Khim[3] and L. Forsley[3]
[1] *SPAWAR Systems Center-Pacific, San Diego, CA 92152*
[2] *Dixie State College, St George, UT 84770*
[3] *J W K International, Annandale, VA.*

ABSTRACT

The Pd/D co-deposition process was developed by Stan Szpak at the Naval Laboratory in San Diego as an alternative means of initiating LENR. Besides heat, other nuclear products that have been measured using Pd/D co-deposition include tritium and the emission of γ- and X-rays, neutrons, and energetic particles. This communication summarizes 19 years of LENR research that has focused on the Pd/D co-deposition process.

In March 1989, two chemists in Utah, Fleischmann and Pons, announced that they had performed electrochemical experiments that produced more excess energy than could be accounted for by chemical reactions. Therefore they speculated that the source must involve nuclear reactions and the effect became known as "Cold Fusion." The claims of Fleischman and Pons caused a global sensation. Much of the uproar was due to the fact that their observations disagreed with the accepted theory of nuclear reactions. Within days scientists around the world had started work on duplications of the experiments. Many of these efforts failed. Reasons for the failures varied. Many researchers used palladium cathodes whose past histories were unknown. Others used improper cell configurations that precluded achieving the high D/Pd loadings necessary to initiate the effect. Still others did not realize that, with bulk electrodes, long incubation times were necessary to produce the effect. However, despite the large number of failures, there were other scientists who did observe anomalous behaviors that could not be explained. These other scientists continued to investigate the effect, which is now called Low Energy Nuclear Reactions (LENR).

Stan Szpak, an electrochemist at the Naval laboratory in San Diego, developed the Pd/D co-deposition process as a means of initiating LENR that greatly reduces the incubation time and gives reproducible results. In this process, working and counter electrodes are immersed in a solution of palladium chloride and lithium chloride in deuterated water. Working electrode substrates that have been used include Cu and Au foils and Ni mesh. Palladium is then electrochemically reduced onto the surface of the working electrode in the presence of evolving deuterium gas. SEM analysis of electrodes prepared by Pd/D co-deposition exhibit highly expanded surfaces consisting of small spherical nodules.[1,2] Cyclic voltammetry[2,3] and galvanostatic pulsing[4] experiments indicate that, by using the co-deposition technique, a high degree of deuterium loading (with an atomic ratio D/Pd>1) is obtained within seconds. These experiments also indicate the existence of a D_2^+ species within the Pd lattice. Because an ever expanding electrode surface is created, non-steady state conditions are assured, the cell geometry is simplified because there is no longer a need for a uniform current distribution on the cathode, and long charging times are eliminated.[5] Using a Dewar-type electrochemical

cell/calorimeter, it was shown that the rates of excess enthalpy generation using electrodes prepared by the Pd/D co-deposition technique were higher than that obtained when Pd bulk electrodes were used.[6] Positive feedback and heat-after-death effects were also observed with the Pd/D co-deposited electrodes. In one experiment that was done in the open air, boil off of the electrolyte occurred as well as melting of the Pd deposit, Figure 1a (Note Pd melts at 1554.9°C).[1] Infrared imaging of electrodes prepared by Pd/D co-deposition, Figures 1b and 1c, show that the working electrode is hotter than the solution indicating that the heat source is the Pd/D co-deposited electrode and not Joule heating. As shown in Figure 1b, the heat generation is not continuous, but occurs in discrete spots on the electrode. The steep temperature gradients of the hot spots, Figure 1c, indicate that the heat sources are of high intensity and located very close to the contact surface.

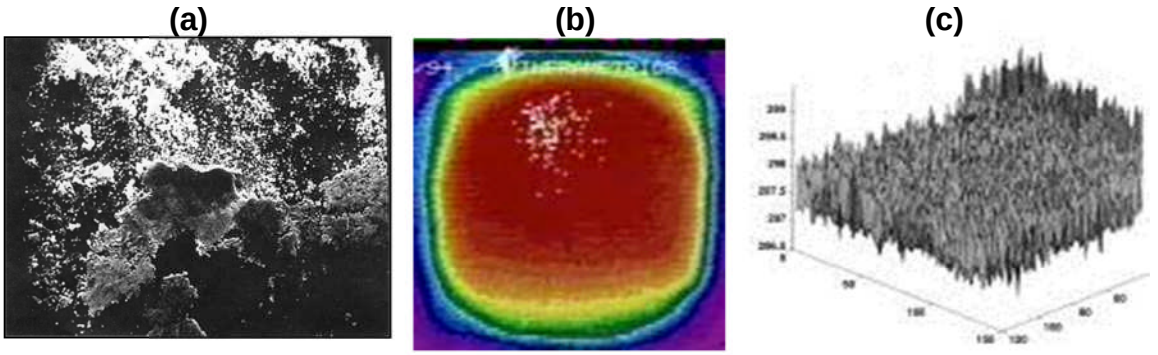

Figure 1. (a) SEM of the Pd film showing features consistent with Pd melting under water. Infrared images of the electrode surface prepared by Pd/D co-deposition. (b) View of the obverse side of the cathode showing the distribution of hot spots ranging from <29°C (purple) to >49°C (white). (c) Temperature gradients on the back side of the cathode.

The 'hot spots' observed in the infrared imaging experiments are suggestive of 'mini-explosions' (Figure 1b[7]). To verify this, the Ag electrode on a piezoelectric transducer was used as the substrate for the Pd/D co-deposition. If a mini-explosion occurred, the resulting shock wave would compress the crystal. The shock wave would be followed by a heat pulse that would cause the crystal to expand. In these experiments, sharp downward spikes followed by broader upward spikes were observed in the piezoelectric crystal response. The downward spikes were indicative of crystal compression while the broader upward spikes are attributed to the heat pulse and the consequent crystal expansion following the explosion.

After confirming the Pd/D co-deposition process produces heat, experiments were conducted to detect the resulting nuclear ash. Measurements of X-ray emission,[8] tritium production,[9] transmutation,[10] and particle emission[11,12] were explored. In early experiments, exposure of photographic film was observed that was indicative of the emission of soft X-rays.[5] Using Si(Li) X-ray and HPGe detectors, it was shown that the cathodically polarized Pd/D system emits X-rays with a broad energy distribution with the occasional emergence of recognizable peaks due to Pd K_α and Pt L peaks.[8] Furthermore, the emission of X-rays was sporadic and of limited duration. The evidence of tritium production was based on the difference between the computed and observed concentration of tritium in the liquid and gaseous phases. It was shown

that the tritium production was sporadic and burst-like. During bursts, the average rate of tritium production ranged between 3000-7000 atoms sec^{-1} over a 24 hr period.[9]

Both the radiation emission and tritium production indicated that the reactions were nuclear in origin and occurred in the subsurface. To enhance these surface effects, experiments were conducted in the presence of either an external electric or magnetic field. SEM analysis showed that when a polarized Pd/D electrode was exposed to an external field, significant morphological changes were observed.[13] These changes ranged from minor, e.g. re-orientation and/or separation of weakly connected globules, through forms exhibiting fractal and molten-like features, Figures 2a and 2b respectively. It has been reported that the micro-volcano like features shown in Figure 2b are consistent with damage that has been observed in materials such as Californium which undergo spontaneous nuclear fission. EDX analysis of a blister-like such feature, Figure 2c, showed the presence of additional elements (Al, Mg, Ca, Si, and Zn) that could not be extracted from cell components and deposited on discrete sites. [10]

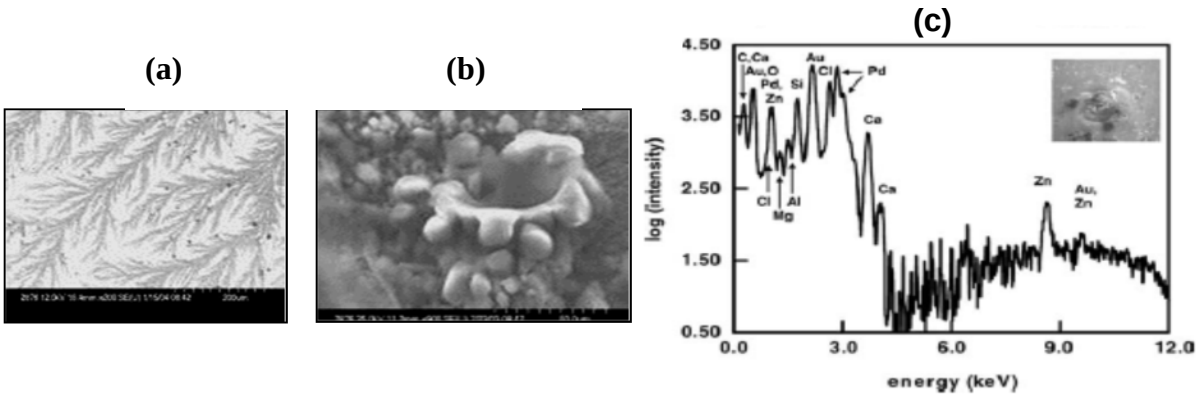

Figure 2. SEM of (a) fractal and (b) micro-volcano-like features formed when Pd/D co-deposition has been conducted in an external electric field. (c) EDX of blister-like (insert) structure formed after exposure of the Pd/D film to an electric field.

More recently, Pd/D co-deposition experiments have been conducted using "CR-39" polyallydiglycol carbonate polymers that have widely been used as a solid state nuclear track detectors.[14] These detectors have been used to detect energetic particles such as alphas, protons, deuterons, tritons and neutrons. CR-39 is the detector of choice in Inertial Confinement Fusion (ICF) as it is not affected by the electromagnetic pulse that disables electronic detectors. When traversing a plastic material such as CR-39, charged particles create along their ionization track a region that is more sensitive to chemical etching than the rest of the bulk. After treatment with an etching agent, tracks remain as holes or pits and their size and shape can be measured.

Pd/D co-deposition experiments were conducted using an Au wire, that was in direct contact with a CR-39 chip, as the substrate.[12] After the Pd was completely plated out, the cell was exposed to an external magnetic field. The experiment was terminated after two days and the CR-39 chip was etched using standard protocols. After etching, the chip was examined under a microscope. Figure 3a shows an image of the CR-39 detector, at 20X magnification. Damage to the detector is observed where the cathode was in contact with the surface of the detector. This

indicates that the source of the damage is the palladium that had been plated on the Au wire. Figure 3b shows a higher magnification image taken near the edge of the cathode where there was less damage to the CR-39 detector. The image shows both small and large, dark pits as well as what look like double and triple pits. Figure 3c is an image of the CR-39 surface while Figure 3d is an overlay of two images taken at two different focal lengths (one focal length is at the surface of the CR-39 detector and the other focal length is at the bottom of the pit). On the surface image, the pits are either circular or elliptical in shape and dark in color, Figure 3c. When focusing deeper into the CR-39 detector, bright points of light are observed in the center of the pits, Figure 3d. These bright points are due to the bottom tip of the conical track. The pits also exhibit a high optical contrast. The optical contrast, shape, and bright spot in the center of the pit are used to differentiate between real particle tracks (which tend to be dark) from false events (which are often lighter in appearance and irregular in shape).

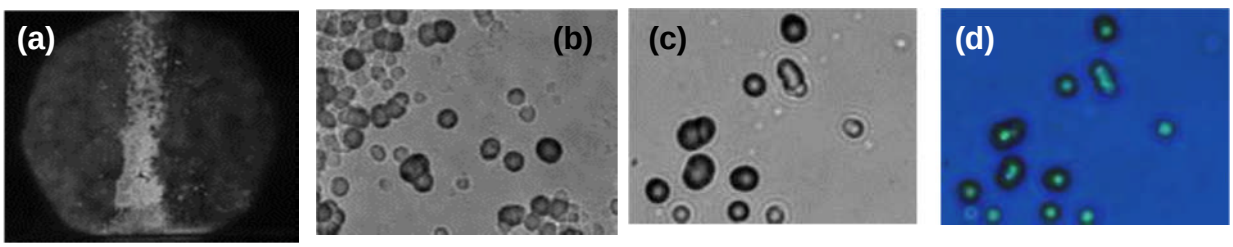

Figure 3. (a) 20X magnification of a cloudy area observed where the Au/Pd cathode was in contact with the CR-39 detector during an external magnetic field experiment. (b) 500X magnification taken near the edge of the Au/Pd cathode where less damage to the CR-39 detector is observed. 1000 X image of pits in CR-39 created during Pd/D co-deposition: (c) the focus is on the surface of the CR-39. (b) Overlay of two images taken at two different focal lengths (surface and the bottom of the pits).

The CR-39 detectors used in the Pd/D co-deposition experiments also show evidence of neutrons. A neutron generated during the Pd/D co-deposition has a probability of 10^{-5} of encountering a proton, carbon, or oxygen atom inside the plastic. Depending upon the energy of the neutron, it can elastically knock an atom out of place. Further etching of a CR-39 detector exposed to neutrons reveals "knock-on" tracks inside the CR-39. Figure 4a shows an image obtained for a CR-39 detector that had been used in a Pd/D co-deposition experiment after additional etchings. The large pit was first observed on the surface and was 10 μm in diameter. After longer etching, the pit on the surface gets larger in size (50 μm in diameter) and is shallower. However, on the left hand side of the large pit, a new elliptical track attributed to a knock-on is observed. Microscopic examination of the CR-39 detectors after a Pd/D co-deposition experiment also shows the presence of what appear to be triple tracks, Figures 4b and 4c. Microscopic examination of the bottom of the triple track pit shows that the three lobes of the track are splitting apart from a center point. The presence of three α-particle tracks outgoing from a single point is diagnostic of the $^{12}C(n,n')3\alpha$ carbon break up reaction and is easily differentiated from other neutron interactions occurring within the CR-39 detector.[15] In order to shatter a carbon atom into three α-particles, the energy of the neutron needs to be ≥9.6 MeV.

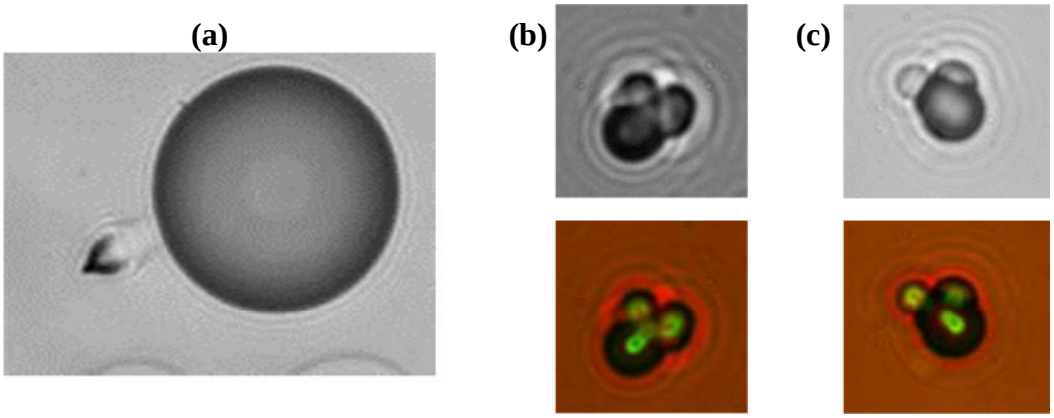

Figure 4. Images obtained at 1000X magnification. (a) Image of CR-39 detectors taken after longer etching times showing a track due to a knock-on. (b) and (c) Images of triple tracks. In the top images, the focus is on the surface of the CR-39 detector. Bottom images are an overlay of two images taken at two different focal lengths (top and bottom of pit).

In conclusion, the Pd/D co-deposition process, that was developed by Stan Szpak, has proven to be a versatile tool to explore LENR activities. Research efforts using Pd/D co-deposition are ongoing. Collaborations have been established with Energetics to explore coupling the Super-wave charging protocol to Pd/D co-deposition and with Dr. Mitchell Swartz of Jet Energy, Inc. to apply his optimum operational points (OOPs) analysis to the co-deposition process.

References

1. S. Szpak and P.A. Mosier-Boss, 'On the Behavior of the Cathodically Polarized Pd/D System: a Response to Vigier's Comments', *Phys. Letts. A*, Vol. **221**, pp. 141-143 (1996).
2. S. Szpak, P.A. Mosier-Boss, S.R. Scharber, and J.J. Smith, 'Charging of the Pd/^{n}H System: Role of the Interphase', *J. Electroanal. Chem.*, Vol**. 337**, pp. 147-163 (1992).
3. S. Szpak, P.A. Mosier-Boss, S.R. Scharber, and J.J. Smith, 'Cyclic Voltammetry of Pd+D Codeposition', *J. Electroanal. Chem*., Vol. **380**, pp. 1-6 (1995).
4. S. Szpak, P.A. Mosier-Boss, and J.J. Smith, 'Deuterium Uptake During Pd-D Codeposition', *J. Electroanal. Chem.*, Vol. **379**, pp. 121-127 (1994).
5. S. Szpak, P.A. Mosier-Boss, and J.J. Smith, 'On the Behavior of Pd Deposited in the Presence of Evolving Deuterium', *J. Electroanal. Chem*., Vol. **302**, pp. 255-260 (1991).
6. S. Szpak, P.A. Mosier-Boss, M.H. Miles, and M. Fleischmann, 'Thermal Behavior of Polarized Pd/D Electrodes Prepared by Co-Deposition', *Thermochim. Acta*, Vol. **410**, pp. 101-107 (2004).
7. P.A. Mosier-Boss and S. Szpak, 'The Pd/^{n}H System: Transport Processes and Development of Thermal Instabilities', *Il Nuovo Cimento*, Vol. **112A**, pp. 577-585 (1999).
8. S. Szpak, P.A. Mosier-Boss, and J.J. Smith, 'On the Behavior of the Cathodically Polarized Pd/D System: Search for Emanating Radiation', *Phys. Letts. A*, Vol. **210**, pp. 382-390 (1996).

9. S. Szpak, P.A. Mosier-Boss, R.D. Boss, and J.J. Smith, 'On the Behavior of the Pd/D System: Evidence for Tritium Production', *Fusion Technology*, Vol. **33**, pp. 38-51 (1998).
10. S. Szpak, P.A. Mosier-Boss, C. Young, and F.E. Gordon, 'Evidence of Nuclear Reactions in the Pd Lattice', *Naturwissenschaften*, Vol**. 92**, pp. 394-397 (2005).
11. S. Szpak, P.A. Mosier-Boss, and F.E. Gordon, 'Further Evidence of Nuclear Reactions in the Pd/D Lattice: Emission of Charged Particles', *Naturwissenschaften*, Vol. **94**, pp. 511-514 (2007).
12. P.A. Mosier-Boss, S. Szpak, F.E. Gordon, and L.P.G. Forsley, 'Use of CR-39 in Pd/D Co-Deposition Experiments', *European Physics Journal-Applied Physics*, Vol. **40**, pp. 293-303 (2007).
13. S. Szpak, P.A. Mosier-Boss, C. Young, and F.E. Gordon, 'The Effect of an External Field on Surface Morphology of Co-Deposited Pd/D Films', *J. Electroanal. Chem*., Vol. **580**, pp. 284-290 (2005).
14. F.H. Séguin, J.A. Frenje, C.K. Li, D.G. Hicks, S. Kurebayashi, J.R. Rygg, B.-E. Schwartz, R.D. Petrasso, S. Roberts, J.M. Soures, D.D. Meyerhofer, T.C. Sangster, J.P. Knauer, C. Sorce, V.Y. Glebov, C. Stoeckl, T.W. Phillips, R.J. Leeper, K. Fletcher, and S. Padalino, 'Spectrometry of Charged Particles from Inertial-Confinement-Fusion Plasmas', ***Rev. Sci. Instrum***., Vol. 74, pp. 975-995 (2003).
15. A.M. Abdel-Moneim and A. Abdel-Naby, 'A Study of Fast Neutron Beam Geometry and Energy Distribution Using Triple-α Reactions,' *Radiat. Meas*., Vol. **37,** pp. 15-19 (2003).

SPAWAR Systems Center-Pacific Pd:D Co-Deposition Research: Overview of Refereed LENR Publications

S. Szpak[1], P. A. Mosier-Boss[1], F. Gordon[1], J. Dea[1], J. Khim[2] and L. Forsley[2]
[1] *SPAWAR Systems Center-Pacific, San Diego, CA 92152*
[2] *J W K International, Annandale, VA.*

Abstract

Scientists at the US Navy SPAWAR Systems Center-Pacific (SSC-Pacific), and its predecessors, have had extraordinary success in publishing LENR papers in peer-reviewed journals. This success hasn't come easily and is due to several factors. One key reason for this success was the courage of the SSC-Pacific upper management in allowing scientists to conduct research and publish results in a controversial field. The few journal editors, who had the fortitude to consider our work, also contributed to this success. This contrasts with the majority of their peers who, taking the path of least resistance, ignored our work out of hand and returned manuscripts with, 'the subject matter is not in the purview of the journal'. The reviewers also played a role in the successful publication of LENR-related papers. A multitude of reviewers, many outside the LENR field, had to put aside their biases and look objectively at our data. In turn, the reviewers' relentless concerns forced us to tenaciously address their issues. Ultimately, the SSC-Pacific team published 21 refereed papers in seven journals and a book chapter, spanning 19 years beginning in 1989. This paper is a brief synopsis of those publications.

1. S. Szpak, P.A. Mosier-Boss, and J.J. Smith, "On the Behavior of Pd Deposited in the Presence of Evolving Deuterium," *J. Electroanal. Chem.*, **302** (1991) 255-260

This was a preliminary note introducing the Pd/D co-deposition protocol as an alternative experimental approach to initiate LENR. Temperature measurements using thermocouples placed in the cathode and solution show that the cathode was hotter than the solution. This indicates that the observed heat is not due to Joule heating. A ten fold increase in tritium content in the solution was observed. Experiments were conducted with photographic film in close proximity of the cathode. After development, the film showed a grid pattern due to the Ni screen cathode and was attributable to the emission of soft X-rays.

2. S. Szpak, C.J. Gabriel, and R. J. Nowak, "Electrochemical Charging of Pd Rods," *J. Electroanal. Chem.*, **309** (1991) 273-292

A model was developed to describe the electrochemical charging of palladium rods. This model coupled the interfacial processes with the transport of interstitials in the electrode interior. It was shown that boundary conditions arise from the solution of equations governing the elementary adsorption-desorption and adsorption-absorption steps as well as the symmetry of the electrode.

3. S. Szpak, P.A. Mosier-Boss, S.R. Scharber, and J.J. Smith, "Charging of the Pd/^{n}H System: Role of the Interphase," *J. Electroanal. Chem.*, **337** (1992) 147-163.

Slow scan cyclic voltammetric studies of Au/Pd/^{n}H were conducted to examine the dynamics of transport of electrochemically deuterium/hydrogen across the electrode/electrolyte interphase. It was found that a coupled, two-layer model of the interphase describes the observed behavior as a function of scan rate and electrolyte composition. The effect of chemisorbing species, thiourea, and pH on the transport across the interphase was also investigated.

4. S. Szpak, P.A. Mosier-Boss, C.J. Gabriel, and J.J. Smith, "Absorption of Deuterium in Palladium Rods: Model vs. Experiment," *J. Electroanal. Chem.*, **365** (1992) 275-286.

A model that incorporates variables such as electrochemical rate constants, bulk diffusion coefficient, and charging current has been developed. Such a model can be used to predict the overpotential, surface coverage, and bulk loading of the electrode during charging. The computed time dependence of the bulk loading has been compared with published experimental charging curves. Microscopic examination of a charging Pd cathode using Nomarski optics has shown that, even within a single grain, there are preferred sites of absorption. *In-situ* XRD measurements of the charging Pd cathode shows that deuterium preferentially enters the Pd lattice through the 111 sites. With additional charging, a broadening and a shift to lower 2θ angles was observed which suggested the presence of a supercharged layer.

5. S. Szpak, P.A. Mosier-Boss, R.D. Boss, and J.J. Smith, "Comments on the Analysis of Tritium Content in Electrochemical Cells," *J. Electroanal. Chem.*, **373** (1994) 1-9.

The time dependence of tritium content of an open cell operating galvanostatically with intermittent sampling has been derived and is given by the following expression:

$$f(t) = f(0)\left(\frac{m(0) - r(i)t}{m(0)}\right)^{S-1} + \frac{q}{(S-1)r(i)} \bullet \left\{1 - \left[\frac{m(0) - r(i)t}{m(0)}\right]^{S-1}\right\}$$

where f is the tritium mass fraction, m is the mass of the electrolyte phase, r(i) denoted the rate of change associated with the cell current, q is the rate at which tritium is added/removed, and s is the isotopic separation factor. It was concluded that a complete mass balance between the liquid and gas phases was necessary in order to determine that tritium was produced in the Pd/D system.

6. S. Szpak, P.A. Mosier-Boss, and J.J. Smith, "Deuterium Uptake During Pd-D Codeposition," *J. Electroanal. Chem.*, **379** (1994) 121-127.

Deuterium uptake during Pd-D co-deposition was examined using galvanostatic perturbation techniques. The resultant potential relaxation curves exhibit four distinct potential-time intervals where the relaxation process is controlled by the interaction between the transport of deuterium from inside the lattice to the surface to form adsorbed deuterium and the reduction of palladium from solution.

7. S. Szpak, P.A. Mosier-Boss, S.R. Scharber, and J.J. Smith, "Cyclic Voltammetry of Pd + D Codeposition," *J. Electroanal. Chem*., **380** (1995) 1-6.

Processes associated with the Pd + D alloy codeposition were examined by cyclic voltammetry. The dynamics of the interphase region are discussed.

8. S. Szpak, P.A. Mosier-Boss, and J.J. Smith, "On the Behavior of the Cathodically Polarized Pd/D System: Search for Emanating Radiation," *Phys. Lett. A*. **210** (1996) 382-390.

Pd/D co-deposition experiments were conducted inside lead caves while measuring gamma and X-rays, as a function of time, using a HPGe detector with an Al window and a Si(Li) detector with a Be window. The cathodically polarized Pd/D system was observed to emit X-rays with a broad energy distribution and with an occasional emergence of recognizable peaks attributable to the Pd K_α and Pt L lines. The emission of X-rays is sporadic and of limited duration.

9. S. Szpak and P.A. Mosier-Boss, "On the Behavior of the Cathodically Polarized Pd/D System: A Response to Vigier's Comments," *Phys. Lett. A*. **221** (1996) 141-143.

Preliminary results of thermal imaging of the Pd/D cathode prepared using the co-deposition technique are presented. Hot spots are observed that appear/disappear chaotically. With time these hot spots merge into larger islands that exhibit oscillatory behavior. SEM images of a Pd/D cathode that had melted during electrolysis are shown.

10. S. Szpak, P.A. Mosier-Boss, R.D. Boss, and J.J. Smith, "On the Behavior of the Pd/D System: Evidence for Tritium Production," *Fus. Technol*., **33** (1998) 38-51.

In these experiments, the D_2 and O_2 gases were recombined in a separate chamber. The tritium content in the liquid and gas phases were measured daily using a liquid scintillation. The measured data were analyzed using the mass balance expression that was derived earlier. It was observed that tritium production occurred in bursts and sporadically. During a burst, the rate of tritium production was estimated to be 10^3 to 10^4 atoms s^{-1}. Tritium produced during prolonged electrolysis was transported out of the electrode interior by two distinct paths. One path results in enrichment of tritium in both the electrolyte and gas phases. The second results in enhancement only in the gas phase.

11. S. Szpak and P.A. Mosier-Boss, "On the Release of from cathodically polarized Palladium Electrodes," *Fus. Technol*. **34** (1998) 273-278. $^{n}_{1}H$

The release paths for tritium produced during electrochemical compression of deuterium in a Pd lattice were examined. The results indicate that tritium production requires high D/Pd atomic ratios. This requirement is met if there are no channels reaching the contact surface. The electrogenerated tritium is distributed among the voids and bulk material. Gas evolution promotes a continuous exchange between the $^{n}_{1}H$ atoms residing in the subsurface layer and with those in the adsorbed state. Atoms in the adsorbed state exchange with the molecules of the contacting electrolyte phase or gaseous phase, leading to two distinct transfer paths.

12. P.A. Mosier-Boss and S. Szpak, "The Pd/^{n}H System: Transport Processes and Development of Thermal Instabilities," *Nuovo Cimento Soc. Ital. Fis. A*, **112** (1999) 577-587.

The surface temperature distribution of the cathode prepared by Pd/D co-deposition on a Ni screen was measured using an infrared camera. It was observed that, unlike joule heating, excess enthalpy generation occurs in the form of localized events in close proximity to the contact surface. It was also observed that, the higher the electrolyte temperature, the more frequent the events. In the limit, these events overlap to produce oscillating islands.

13. S. Szpak, P.A. Mosier-Boss, and M. H. Miles, "Calorimetry of the Pd + D Codeposition," *Fus. Technol.*, **36** (1999) 234-241.

Calorimetric measurements indicate that the excess enthalpy generated in cells using cathodes prepared by the co-deposition process is, on average, higher than that produced in cells using solid Pd rods. Infrared imaging of the cathodes prepared by Pd/D co-deposition shows that the heat sources are highly localized. The steepness of the temperature gradients indicate that the heat sources are located in close proximity to the electrode-solution contact surface.

14. S. Szpak, P.A. Mosier-Boss, M. H. Miles, and M. Fleischmann, "Thermal Behavior of Polarized Pd/D Electrodes Prepared by Co-deposition," *Thermochimica Acta*, **410** (2004) 101-107.

The thermal behavior of Pd/D electrodes, prepared by the co-deposition technique, was examined using a Dewar-type electrochemical cell calorimeter. Results indicated that excess enthalpy is generated during and after the completion of the co-deposition process. The rates of excess enthalpy generated using the co-deposition technique were higher than those obtained using Pd wires or other forms of Pd electrodes. Positive feedback and heat-after-death effects were observed. The rates of excess power generation were found to increase with an increase in both cell current and cell temperature.

15. S. Szpak, P.A. Mosier-Boss, C. Young, and F.E. Gordon, "The Effect of an External Electric Field on Surface Morphology of Co-deposited Pd/D Films," *J. Electroanal. Chem*., **580** (2005) 284-290.

After plating out the Pd on a Au foil, the cell current was increased and an external electric field was applied across the cell. The experiment was terminated after 48 h. The cell was disassembled and the cathode was subjected to analysis using an SEM. In the absence of an external electric field, the Pd deposit exhibits a cauliflower structure. After exposure to an external electric field, significant changes in the morphology of the Pd/D deposit were observed. Fractal features were observed as well as dendritic growths, rods, wires, and craters. Considerable work is needed to account for the variety of shapes. The process of shape change is driven by energy transferred from the electrostatic field and directed by the field.

16. S. Szpak, P.A. Mosier-Boss, C. Young, and F.E. Gordon, "Evidence of Nuclear Reactions in the Pd Lattice," *Naturwissenschaften*, **92** (2005) 394-397.

When a cathode prepared by Pd/D co-deposition is subjected to an external electrostatic field, SEM analysis of the deposit shows discrete sites exhibiting molten-like features. Such features require substantial energy expenditure in order to form. EDX analysis of these features shows the presence of new elements (Al, Mg, Ca, Si, Zn,…) that could not be extracted from cell components.

17. S. Szpak, P.A. Mosier-Boss, and F.E. Gordon, "Further Evidence of Nuclear Reactions in the Pd/D Lattice: Emission of Charged Particles," *Naturwissenschaften*, **94** (2007) 511-514.

CR-39 is a solid state nuclear track detector that is used to detect energetic particles such as alphas, protons, tritons, and helium-3. Pd/D co-deposition was done, in the presence of an external electric or magnetic field, with the cathode in direct contact with a CR-39 detector. Tracks on the CR-39 detector were observed where the cathode was in contact with the plastic indicating that the source of the tracks is the cathode. The features of these tracks (optical contrast, shape, and bright spot in the center of the pit) are consistent with those observed for pits in CR-39 that are of a nuclear origin. The emission of the energetic particles is sporadic and occurs in bursts.

18. P.A. Mosier-Boss, S. Szpak, F.E. Gordon, and L.P.G. Forsley, "Use of CR-39 in Pd/D Co-deposition Experiments," *Eur. Phys. J. Appl. Phys.*, **40** (2007) 293-303.

A series of control experiments were conducted. It was shown that the tracks observed in CR-39 detectors subjected to Pd/D co-deposition were not due to radioactive contamination of the cell components. No tracks were observed when Cu was electrochemically plated on the surface of the CR-39 detectors. This indicates that the pits cannot be attributed to chemical attack of the surface of the CR-39 by either D_2, O_2, or Cl_2 present in the electrolyte. Nor can the pits be attributed to the metal dendrites piercing into the surface of the detectors. Additional experiments showed that LiCl is not essential for the production of pits and that the density of pits significantly decreases when light water is substituted for D_2O. Quantitative analysis using an automated scanner shows that there are three populations of tracks (0.1-0.5 μm, 0.9-4.0 μm, and 4.1-12 μm) and that the pits can be either perfectly circular or elliptical in shape.

19. P.A. Mosier-Boss, S. Szpak, F.E. Gordon, and L.P.G. Forsley, **"**Detection of Energetic Particles and Neutrons Emitted during Pd:D Co-deposition," *Low Energy Nuclear Reactions Source Book*, American Chemical Society , Chapter 14, pp 311-334. (2008).

Co-deposition procedures and control experiments specifically identified the conditions under which nuclear particles were observed, and ruled out chemical means of mimicking nuclear tracks. The nuclear tracks are quantitatively examined and are consistent with neutron knock-ons. Triple tracks are presented as evidence of $^{12}C(n,n')3\alpha$ indicative of DT fusion.

20. P.A. Mosier-Boss, S. Szpak, F.E. Gordon, and L.P.G. Forsley, **"**Triple Tracks in CR-39 as the Result of Pd/D Co-deposition: Evidence of Energetic Neutrons," *Naturwissenschaften*, in press. (2008).

Triple tracks have been observed in CR-39 detectors used in Pd/D co-deposition experiments. Microscopic examination of the bottom of the triple track pit shows that the three lobes of the track are splitting apart from a center point. The presence of three α-particle tracks outgoing from a single point is diagnostic of the $^{12}C(n,n')3\alpha$ carbon break up reaction and is easily differentiated from other neutron interactions occurring within the CR-39 detector. The presence of triple tracks suggests that DT reactions that produce ≥9.6 MeV neutrons are occurring inside the Pd lattice.

21. P.A. Mosier-Boss, S. Szpak, F.E. Gordon, and L.P.G. Forsley, **"**"Use of CR-39 in Pd/D Co-deposition Experiments: A Response to Kowalski," *Eur. Phys. J. Appl. Phys.*, **41** (2008) in press.

Earlier we reported that the pits generated in CR-39 detectors during Pd/D co-deposition experiments are consistent with those observed for pits that are of a nuclear origin. Recently, that interpretation has been challenged. In this communication, additional experimental data and further analysis of our earlier results are provided that support our original conclusions.

Preparata Prize Acceptance Speech

I. Dardik
Energetics Technologies
P.O.Box 3026
Omer Industrial Park
Omer, Israel

During ICCF-14, Irving Dardik was awarded the Preparata Medal for 2008. The honor, named after the late Italian physicist Giuliano Preparata, is awarded at ICCF conferences for contributions to progress in Condensed Matter Nuclear Science.

Thank you Bill and Mike. I am honored to be this year's recipient of the Preparata Prize and thank the Committee for this recognition. Back in 1991 I applied for a low energy nuclear reaction patent based on SuperWaves. The United States patent office shelved it along with all the other applications that our community has submitted over the years. In 2001, one brave man, Professor Herman Branover, stepped forward and listened to my predictions that SuperWaves would make a difference in LENR results. Next in, was Ehud Greenspan who stated that even if there was a 1% chance that I was right, he would listen. After hearing me out, he upped that percentage to 50% and joined Dr. Branover, Alison Godfrey and me in a meeting with the visionary Sidney Kimmel. In a bold and daring move, Sidney Kimmel committed his personal resources towards funding a SuperWaves laboratory in Israel whose mission was to use SuperWaves to produce usable energy.

I am grateful to Alison Godfrey for her extraordinary leadership in building Energetics Technologies into what it is today…. to Shaul Lesin for taking the lead in establishing Energetics in Israel and hiring a team of brilliant scientists in 2001 — 10 long years after my first patent application in this field. Their work is impeccable and has justified Dr. Greenspan's participation. They have surpassed all expectations of what could be accomplished in a few short years using SuperWaves.

By 2003, we presented some of our early results at ICCF 10 and had the honor of drawing the attention of Mike McKubre. Mike's scientific sophistication and leadership in the DARPA replication projects with SRI, has been invaluable. I also want to thank Vittorio Violante of ENEA and the extraordinary team at NRL.

I would like to acknowledge Dave Nagel and Mike Melich for organizing an extraordinary conference, bringing in new faces and presenting the field in a cohesive and well developed way.

As Llewellyn King pointed out in his Keynote Address, we are coming off of a summer of skyrocketing energy costs. It is only August, and many in this country and around the world are already in fear; wondering how they will afford to heat their homes this coming winter.

With all the talk of possible alternatives to the finite fossil fuel reserves, our community is not even part of the public dialogue. That… ladies and gentlemen… troubles me, because history teaches us that the driving forces behind the great ages of advancement, were not only people's needs and hopes and dreams — but also our innate hunger for knowledge. Yet in the midst of this traumatic awakening to our disastrous energy crisis, our research is missing from the radar of public debate. Yet… even though our community operates virtually in the shadows of science…. we are under attack and have been so for nearly two decades. But as we expend positive and negative energy to protect ourselves… struggle financially for the survival of our research….we remain at the core…. strong and resolute… because this is a community of courageous people, committed against all odds.

The stakes are easily articulated. The survival of civilization is dependant upon finding a safe, sustainable, and readily accesible solution to the energy crisis. It is our job to remain focused on our goals and not take on a victim's mentality, nor get caught up in the tempting web of infighting. This quiet revolution is yielding results that are more and more reproducible. We are on the verge of developing a technology that promises to rescue our future. And it is the people in this room that are going to save the world.

But the revolution is now too quiet for our times. While they say we stand on the shoulders of giants, history is ripe with pivotal moments when the greatest minds of an age, doubted alternative thought, based on an assertion that all there was to be known… was known. Make no mistake about it. We live in such a time.

The greatest advances in all of science have always come from ideas that were vilified. From Galileo, to Columbus, to Semmelweis whose career was destroyed for having the audacity to suggest that physicians should wash their hands before delivering a baby. We can proudly add to that list Martin Fleischmann, Stanley Pons, and many of the people in this very room today.

It is nearly impossible to fathom… that despite living in the modern age where advances in science, medicine and technology arrive at seemingly lightning speed, that there are those who would argue that LENR is not even worth the effort of exploring. They would keep our work in the shadows, and insist that the public must not know about our research… for fear that they… the public… might join us in our commitment for a better tomorrow.

For those of us here tonight… I say… stay the course, because our time is now.

Cold Fusion Country History Project

Xing Z. Li[1], Jean-Paul Biberian[2], Jacques Dufour[3], M. Srinivasan[4], F. Scaramuzzi[5], J. Kasagi[6], Y. Iwamura[7], Andrei Lipson[8], Ivan Chernov[9] and Yu. N. Bazhutov[10]

[1] *Dept. of Physics, Tsinghua University, Beijing, CHINA*

[2] *Université d'Aix-Marseille, 163 Avenue de Luminy, 13288 Marseille cedex 9, France*

[3] *CNAM - Laboratoire des sciences nucléaires - CC304A - 75141 Paris Cedex 03*

[4] *Formerly of Bhaba Atomic Research Centre, Trombay, Mumbai*

[5] *LNF/INFN, Frascati – Italy*

[6] *Laboratory for Nuclear Science, Tohoku University, Japan*

[7] *Advanced Technology Research Center, Mitsubishi Heavy Industries*

[8] *A.N. Frumkin Institute of Physical Chemistry and Electrochemistry, Russian Academy of Sciences, 119991 Moscow, Russia*

[9] *Tomsk Polytechnic University, 634050 Tomsk, Russia*

[10] *Institute of Terrestrial Magnetism, Ionosphere and Radiowave Propagation (RAS), 142092, Troitsk, Moscow region, Russia*

The 20th Anniversary of the Fleischmann-Pons announcement was approaching as we prepared for ICCF-14. An adjunct project was initiated to write histories of the research activities on a country-by-country basis, preferably one in the language of the country and then a translation into English. It had become clear that the normal historical record of the field's scientific development was in danger of being lost due to deaths, slow development of the field, and general absence of institutional records. Thus was born the "cold fusion" Country History Project. Our objective was to give each of the countries that have contributed significantly an opportunity to record their research efforts and results in a form both accessible to native speakers and to English speakers. Teams were assembled in China, France, India, Italy, Japan, Russia, United Kingdom and the United States. At ICCF-14, six status reports were presented, covering the history in China, France, India, Italy, Japan, and Russia. Selected text from these presentations is shown below. There was no presentation at ICCF-14 Wednesday morning session devoted to the Country Histories of the USA and UK history work.

It is our intention that these reports, when finished, will be brought together as a set and made widely available in English. An editorial board of scientists not involved in the field has been assembled to review the final manuscripts. The United Kingdom "book" will likely be an expansion of the history of the UK's Atomic Energy Research Establishment, Harwell. The USA history is directed at extracting and making available research work that has hitherto not been available, particularly in an organized form, from US government laboratories.

The science of nuclear physics and nuclear fission developed in the politically charged 1930s and moved to national importance with Roosevelt's receipt of Einstein's 2 August 1939 warning letter of the potential of nuclear energy. The Manhattan Project pushed into existence the atomic bomb and the foundations of nuclear power generation leaving behind the development of a basic scientific understanding of what is a very difficult many-body problem. The physical models we have used for about 70 years still retain much of the flavor of the

needs of an engineering project. Their scientific limitations are discussed by Norman Cook in his book, Models of Nuclear Physics, Springer 2006. Cook's book and presentation at ICCF-14 provide a useful context for gaining a deeper understanding the history of development of the Fleischmann-Pons Effect and why it was controversial. We hope that, when finished, this Country History project will offer a better appreciation of what will be required to deal with some of the most fundamental problems of the physical sciences.

1. "Condensed Matter Nuclear Science" Research in China

Presentation Title: Normal Temperature Nuclear Fusion
Xing Z. Li, Department of Physics, Tsinghua University, Beijing
Presentation at ICCF-14, Washington D.C., Aug.13 2008,

Abstract. Five features of "Condensed Matter Nuclear Science" research in China are addressed. Five important meetings are described from the beginning to April of 2008. Twenty institutions are listed with their principle investigators, research staffs, and main research subjects. Twenty-nine articles are cited for reference.

Nomenclature. Cold fusion is referred to as "normal temperature nuclear fusion" in China. It was given this name by Academician, Qian Xue Sen. In 2002, during ICCF-9, International Advisory Committee decided on a new name, Condensed Matter Nuclear Science (CMNS), in order to show the progress of the normal temperature nuclear fusion which had initiated this research field. This article mainly discusses the history; hence, it still adopts the name of normal temperature nuclear fusion (or in some cases "cold fusion").

Introduction. Normal temperature nuclear fusion has been conducted for 19 years in China. When reviewing it, five aspects of the research stand out:

1. National policy has always kept an expectation established at the beginning.
2. A group of top scientists have continued to support this research, even though it appears to violate common-sense.
3. International collaboration has been an important aspect from beginning until the present day.
4. Chinese researchers have attempted to develop the basic research independently with our own approaches.
5. Hot fusion institutions have kept abreast of development in normal temperature nuclear fusion, and have even given a hand occasionally.

Over 20 institutions have continued research into these phenomena since the 1989 FPE announcement. The map below provides an indication of the work as of August 2008.

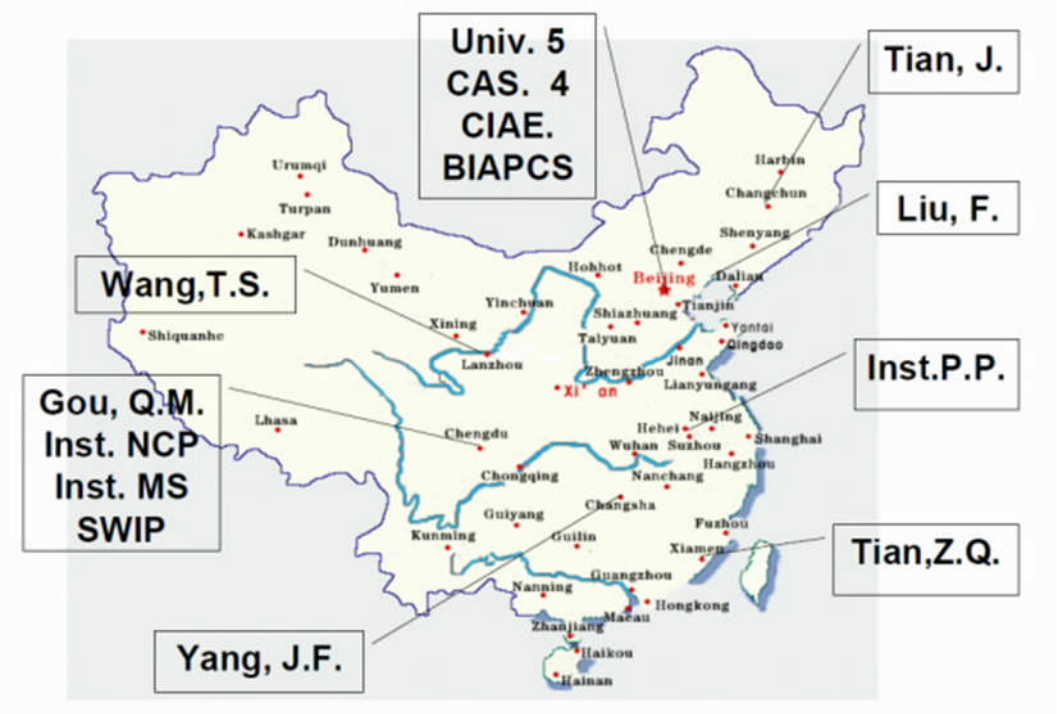

2. “Condensed Matter Nuclear Science” Research in France

History of Cold Fusion France

Jean-Paul Biberian, Faculté des Sciences de Luminy, Marseille
Jacques Dufour, CNAM, Paris

The players. These scientists and engineers have entered the field at one time or another :

The CEA Grenoble (Georges Lonchampt).
CNAM (Jacques Dufour).
CNAM (Pierre Clauzon).
The EDF (Electricité de France).
Université Aix-Marseille (Jean-Paul Biberian).
IMRA Sophia Antipolis (Stan Pons and Martin Fleischman).
Independent researcher (Jean-Louis Naudin).
Independent researcher (Fabrice David).
Fondation Louis de Broglie (Georges Lochak and Henri Lehn).

The future. Unless something striking happens soon, the field will disappear in France. Today’s active researchers”

CNAM (Pierre Clauzon, already retired).
Université Aix-Marseille (Jean-Paul Biberian, will retire in three years).
Fondation Louis de Broglie(George Lochak and Henri Lehn, already retired).
Fabrice David.

Research interest among younger scientist can be found at CNAM where Jacques Dufour has a team of two young scientists actively testing a novel working hypothesis (picochemistry) that based on a current center of interest in main stream physics (long range weak Yukawa potential in the Standard Model Extension).

3. "Condensed Matter Nuclear Science" Research in India

History of Cold Fusion Research in India
M. Srinivasan, Formerly of Bhaba Atomic Research Centre, Trombay, Mumbai

Phases of CF Research in India

Phase i : 1989 to 1991 (ICCF 1) - Most productive era!
Phase ii : 1992 to 1995 (ICCF 3,4,5) - Post Iyengar period
Phase iii : 1996 to 2007 (12 years) India totally blanked out!
Phase iv : 2008 Revival - Following NIAS meeting of 9th January 2008

Overview of BARC (1989-90)

- BARC has > 50 Divisions & 3000 Scientists!
- 12 teams (~ 50 scientists) took up challenge
- To verify "nuclear origin" of phenomenon
- Looked for neutrons & Tritium
- First neutrons detected on 21st April 1989!
- Within a year all teams reported both n & T
- Among first groups to find branching ratio anomaly namely (n/T) = ~ 1E (-7)
- ICENES Karlsruhe 4th to 7th July 1989
- Report BARC 1500 (Aug '89) (Historical role!)
- ICCF 1 & Fusion Technology paper of Aug '90 with 50 authors summarize work of 89-90!

4. "Condensed Matter Nuclear Science" Research in Italy

Cold Fusion in Italy
Francesco Scaramuzzi , LNF/INFN, Frascati – Italy

Introduction. I will discuss a book produced by ENEA: "The history of Cold Fusion in Italy". I will touch the following issues:

- The book
- The beginning of the Italian History of CF
- The years of maximum effort
- The decay
- Comments

Comments.

- cold fusion is a reality
- it is prominently a scientific problem, very much interesting at that

need for a coordinated effort in material science
- it is important to convince the scientific world of the validity of the issue, through neat, reproducible experiments
- it is still too early to put the accent on the possible applicative fall-outs, even though everyone hopes in them, in particular in the field of energy production.

5. "Condensed Matter Nuclear Science" Research in Japan

Country History of Japanese Work on Cold Fusion - Toward further development of Condensed Matter Nuclear Science

J. Kasagi
Laboratory of Nuclear Science, Tohoku University
Y. Iwamura
Advanced Technology Research Center, MHI

Abstract. We briefly summarize the history of Japanese work on cold fusion after 1989. Since the excellent work performed by Prof. Arata are introduced and discussed in the special session, we try to summarize other works in Japan. The history can be divided into three periods: the 1st period is from the announcement by Fleischmann and Pons to the ICCF3 Nagoya Conference (1989 - 1993); the 2nd period is during the New Hydrogen Energy (NHE) Project (1994 – 1998); and the 3rd after the NHE project (1999 – present). Characteristics of each period and the present situation are presented.

Introduction. In the 19 years following the announcement of Professors Martin Fleischmann and Stanley Pons, much work on the cold fusion has been carried out in Japan as well as in other countries. The organizers of this conference have asked us to edit a document on "cold fusion" research in Japan. Many official reports for various projects, proceedings of domestic meetings on cold fusion and research papers describe the progress of this research in Japan. Thus, we thought that it is worthwhile to collect and summarize such records as an interim report in the cold fusion research. Since the excellent works performed by Prof. Arata were introduced and fully discussed in the special session of ICCF14, we have tried to summarize other work based on many official reports in Japan.
The history of cold fusion research in Japan can be divided into three periods: the 1st period is from the announcement of F-P to the ICCF3 Nagoya Conference (1989 - 1993), the 2nd period is during the New Hydrogen Energy (NHE) Project (1994 – 1998), and the 3rd after the NHE project (1999 – present), as schematically shown in Fig. 1. We will show background and characteristics of each period, as well as notable research.

6. "Condensed Matter Nuclear Science" Research in Russia (Former Soviet Union)

Status of Russian Research on Low Energy Nuclear Reactions in Non-Equilibrium Condensed Matter, Based on Publications in Peer-Reviewed Journals

Andrei G. Lipson, A.N. Frumkin Institute of Physical Chemistry and Electrochemistry, Russian Academy of Sciences, Moscow 199915, Russia
Ivan P. Chernov Tomsk Polytechnic University, Tomsk, 634050 Russia

Why peer-reviewed journals only in this history? LENR (CMNS) is a new science and still shows poor reproducibility. In some sense it is a "Proto-science" (the definition of L. Kowalski). In some cases poor experimental equipment, reflecting a lack of support, and overselling of results, while seeking support, leads to a lack of credibility. Lacking independent confirmations one may not believe in each result! It is hard to distinguish the grains of truth from the stream of informational noise. Because peer reviewed journals take on the responsibility for the integrity of their publications they use respected scientists in the field of journal, although also this introduces biases. Thus, we have chosen only per-reviewed papers that have been filtered by editors and published.

Wide Survey of FSU/Russian CMNS Related Activities. CMNS Russian activity, based on local conference and seminar proceedings has been prepared by Yuri Bazhutov and will be described in the so-labeled section below.

What we are studying. Under LENR or CMNS we study specific nuclear processes at very low kinetic energy of projectile nuclei (say, $kT < E_{lab} < 1$ KeV) that originate and are enhanced by strictly non-equilibrium condensed matter/crystalline lattice environment. These peculiarities make LENR (and nuclear cross-sections) drastically distinctive from the nuclear reactions taking place in vacuum/plasma collision. Broadly, the LENR/CMNS effects include nuclear, calorimetric, electrochemical, condensed matter physics, material science and other accompanying aspects. This field is inherently an interdisciplinary research area.

Some dates and statistics. After the discovery of deuterium's role in Pd cathodes during electrolysis (by Fleischmann and Ponce in 1989) many groups in the former USSR started their works on LENR. In April 1989 to support this research at the national government level a special Council on Cold Fusion was been created in the USSR Academy of Sciences, headed by a vice-president of Academy Academician V. Nefedov.
The First All-Union Conference on Cold Fusion at JINR-Dubna was in March 1991. Fourteen local Russian conferences and a monthly Cold Fusion seminar at PF University, Moscow (N. Samsonenko) were organized. More than 250 Russian papers have appeared in peer-reviewed journals since1989. Since 1993 there has been no central government funding of research in this area. FSU scientist suffer from the Bill Collis Vicious Cycle: "insufficient funding leads to poor research, poor research leads to poor papers, poor papers lead to insufficient funding".

Critical Russian Contributions in LENR/CMNS Research - Prior to 1989 F-P announcement.
First experimental study and development of the microscopic acceleration model: *Fractofusion on fracture of deuterated dielectrics: LiD and heavy ice crystals (Klyuev VA, Lipson AG et al., Sov. Tech. Phys. Lett 12, 551 (1986), Deryaguin BV, Klyuev VA, Lipson AG, Toporov YuP,*

Colloid J. USSR 48, 8(1986)). In 1989 TiDx fracture neutrons: [B.V. Deryaguin et al, Nature, 341, 492, (1989)].
Theoretical considerations re the effects on the Coulomb barrier that is reduced in deuterated crystals, depending on crystallographic direction, resulting in excess energy production using deuteron beam and crystalline target: *V.V. Vysotsky and R.N. Kuzmin, Sov.Tech. Phys. Lett., 7, 981 (1983)*

1986 Neutron emission experiment on LiD fracture (Klyuev VA, Lipson AG, Deryaguin BV et al., Sov. Tech. Phys. Lett **12**, 551 (1986))-**Confirmed**: Kaushik TC, Kulkarni LV, Shyam A, Srinivasan M, Physics Lett. A **232** (1997) 384; *Shyam A* et al, Indian J. Pure and Appl. Phys., vol: 36(2), 56 (2008).

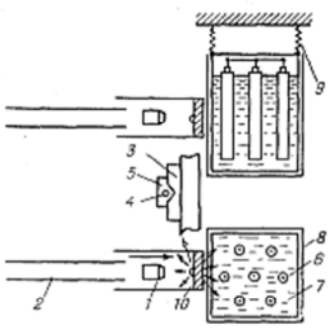

Рис. 16. Схема экспериментальной установки [9]

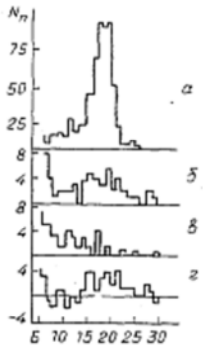

Рис. 17. Гистограмма распределения импульсов по каналам анализатора от источника нейтронов (*а*), при разрушении мишеней из дейтерида лития (*б*), при стрельбе по мишеням, не содержащим кристаллов LiD, «импульсный фон» (*в*) и результат вычитания «импульсного» и космического фонов из амплитудного спектра снятого при разрушении мишеней из LiD (*г*)

ICCF-14, Washington DC, 10-15
August, 2008

Summary of FSU/Russian Contributions. Russian research in LENR has made a critical, important contribution. The significant areas include, but are not limited by fracto-fusion, nuclear emissions during acoustic cavitation, glow discharge effects (isotopic shifts and soft X-ray emission first observed by Karabut et al), energetic alpha particle emissions, and the first application of CR-39 and so on. These contributions are pioneering results and have affected international development of CMNS. Despite the clear evidence and high value of Russian achievements, much of Russian researcher work has been ignored and have not been cited (in time) in international publications on LENR and other related fields. Particular examples – fractofusion, cavitation fusion, neutrons emitted from ferroelectrics and so on. It is worth noting that main stream Soviet/Russian physics journals (JETP, JETP Lett., Tech. Phys. Tech.

Phys, Lett.) have been translated to English (almost simultaneously with the Russian version) by American Institute of Physics. So the failure to make reference to this literature cannot be attributed being only available in Russian.

Conclusion. The research product of Russian groups answer affirmatively that the question existence of LENR. Numerous peer reviewed and published Russian papers on CMNS in non-equilibrium condensed matter repeatedly show the occurrence of LENR in the form of excess heat and/or nuclear emissions. The main problems of Russian LENR studies is a total lack of institutional funding resulting in fragmentation of the research conducted and the low circulation and readership of the results in international community. Much has been done so it is clear that concentration of Russian efforts and international cooperation are highly productive. The result of concentrated efforts and international collaboration finally put in place a complete CMNS experiments where simultaneous detection of excess heat, atomic ^{4}He, ^{3}T, charged particles (DD-products +energetic alphas), neutron emission is accomplished.

7. Role of Russian Scientists in Cold Nuclear Transmutation – Condensed Matter Nuclear Science (According to Conferences Proceedings, 1991-2007)

Yu.N. Bazhutov
Institute of Terrestrial Magnetism, Ionosphere and Radiowave Propagation (RAS),
142092, Troitsk, Moscow region, Russia, bazhutov@izmiran.ru

Abstract. The following presents a statistical analysis of Russian scientists' personal research (together with Ukrainian scientists) according to their publications in different Cold Fusion Conferences Proceedings. Among these conferences are following: 11 International Conferences on Cold Fusion (3-13 ICCF, 1992-2007); Soviet Union Conference on Cold Nuclear Fusion (JINR-MSU, 1991); Soviet Union Seminar on Chemistry & Technology of Hydrogen (Zarechnyi, 1991); 2-d International Symposium on Cold Fusion (Minsk, 1994); all 14 Russian Conferences on Cold Nuclear Transmutation (Abrau-Dyurso, Sochi, Dagomys, 1993-2006). An analysis is presented of the total number of Russian scientists publications in International Conferences on Cold Fusion compared to publications from other countries. This analysis has demonstrated the considerable contribution of Russian Scientific Community to the World Cold Fusion researches.

Introduction. Immediately after M. Fleishmann and S. Pons's press conference on 23 March 1989 and in the scientific press [1,2] about discovery of the new phenomenon named by them as Cold Nuclear Fusion the Russian scientists have actively joined in its research. Moreover, some researches have been lead even earlier [3,4,5], but they were not considered by authors, as essentially new direction in a science (mechanoemission by Deryagin B.V. – see references in the first part of this Russian/FSU history above), or simply were not published in scientific journals since they were seen as contradicting orthodox theoretical representations (Yaroslavskiy M.A). Therefore already at the First (and last) Soviet Union Conference on Cold Fusion (SUC CF) there were presented almost a hundred reports from nearby fifty various scientific groups. It was the first large congress of Russian (and also Ukrainian and Belarus)

scientists on the problem of Cold Fusion which took place in the 2nd anniversary of announcement of this phenomenon (22-23 March, 1991) in the Joint Institute of Nuclear Researches in Dubna and also has come to the end in the Moscow State University. Unfortunately, all papers of this meeting have not been published, only Abstracts SUC CF [6] has been published.

Synopsis of Some Aspects of Russian Meetings. The very first RCCNT (more exact then it still referred to RCCNF) took place in September 1993 in Abrau-Dyurso near Novorossiysk on the basis of sport camp of the Rostov State University. It became long-awaited heiress to All-Union Conference on Cold Nuclear Fusion (1991). On it outstanding representatives CNT from abroad have been presented more than 30 Russian and Ukrainian scientists. At the second RCCNT (RCCFNT-2) that took place on September, 19-23rd at the rest house of the Moscow State University in Sochi, 39 scientists from Russia, Ukraine and Belarus and also from the far abroad. All the subsequent RCCNT (3-14, 1995-2006) were held at the resort "Olympic-Dagomys" (Sochi). At each were present about 30 Russian (and also Ukrainian, Kazakh and Belarus) scientists with their reports and some from a few scientists of the far abroad.

Views of the status of Russian Research and Organiation. The main "Gold" stock of high scientific physical and chemical potential in researches of Cold Fusion in Russia is its highly professional researchers managing in the hardest conditions of full disorder of a science in the country to spend solid theoretical and experimental researches, recognized by all international community as priority. From our statistics it is apparent, that many Russian scientists, not having a financial opportunity to attend ICCF, actively enough work and are published in RCCNT Proceedings. Such professional activity of the Russian scientists allows hoping, eventually, will find recognition and support and will allow the Russian science to bring still the defining contribution to World scientific and technical progress.

Activity of the Russian scientific community on a problem Cold Nuclear Transmutation is coordinated by its Interdepartmental Coordination Committee (ICC), created at vice-president of the Russian Academy of Sciences, academician Nefyodov O.M. in 1995. Its chairmen in different years were academicians Kolotyrkin Ya.M., Baraboshkin A.N. and Kazarinov V.E. In 2004 in connection with reorganization of Presidium of the Russian Academy of Science, ICC also has been reorganized in the structure and has been registered at the Russian Physical Society by its president, Professor Mikhailin V.V. The academician of the Russian Academy of Nature Sciences Rukhadze A.A. is now the new ICC CNT Chairman.

Acknowledgements

Many people and organizations contributed to the planning and execution of ICCF-14. We are grateful to all those who helped us in myriad ways.

The offer to hold the conference in Washington DC in 2008 was accepted by the International Advisory Committee at ICCF-12 in Yokahama Japan in 2005 and reaffirmed at ICCF-13 in Sochi in June 2007. The members of the International Advisory Committee (IAC) committee at the time of ICCF-13 were:

Yuri Bazhutov, IZMIRAN RAS, Russia (ICCF-13 chairman); Jean Paul Biberian, University of Marseilles Luminy, France (ICCF-11 chairman); Tullio Bressani, Dept. di Fisica Sperimentale, Universita di Torino, Italy; Francesco Celani, INFN, Frascati, Italy; William Collis, ISCMNS Secretary; Igor Goryachev, Russian Research Center "Kurchatov Institute", Russia; Antonella De Ninno, ENEA, Frascati, Italy; Peter Hagelstein, MIT, USA (ICCF-10 chairman); Yasuhiro Iwamura, Mitsubishi Heavy Industries, Japan; Jirohta Kasagi, Laboratory for Nuclear Science, Tohoku University, Japan; Xing Zhong Li, Tsinghua University, China (ICCF-9 chairman); Andrei Lipson, Institute of Physical Chemistry, RAS, Moscow, Russia; Michael McKubre, SRI International, USA (ICCF-4 chairman); George Miley, Fusion Studies Laboratory, University of Illinois, USA; Ken-ichiro Ota, Dept of Energy and Safety Engineering, Yokohama, Nation. Univ., Japan; Nikolai Samsonenko, People Friendship University, Russia; Francesco Scaramuzzi, ENEA, Frascati (retired), Italy, (ICCF-8 chairman); Mahadeva Srinivasan, BARC (retired), India; Edmund Storms, Lattice Energy, LLC, USA; Akito Takahashi, Osaka University, Japan, (ISCMNS President and ICCF-12 chairman).

The members of the Technical Program Committee for ICCF-14 were: Michael E. Melich, Chairman, (Naval Postgraduate School, USA), Ashraf Imam, Secretary (Naval Research Laboratory, USA), Jean-Paul Biberian (University of Marseilles Luminy , France), Ivan Chernov (Tomsk Polytechnical University , Russia), Talbot Chubb (Naval Research Laboratory (Retired), USA), Peter L. Hagelstein, (MIT, USA), Yasuhiro Iwamura (Mitsubishi Heavy Industries, Japan), Jirohta Kasagi (Tohoku University, Japan), Xing Zhong Li (Tsinghua University, China), Michael C. H. McKubre (SRI International, USA), Franco Scaramuzzi (ENEA Frascati, Italy), Mahadeva Srinivasan (BARC, Retired, India), and Tanya Zilov (Energetics Technologies, Israel).

Several major contributors to the field were commissioned to provide reviews for the conference. They include:

D. Cravens, D. Letts	Experiments Reporting Heat
J. Dufour	Ice Calorimetry
T.V. Lautzenhiser, D.W. Phelps, M. Eisner	Constant Heat Flow Calorimetry
M.C.H. McKubre, F. Tanzella	Mass Flow Calorimetry
M.H. Miles, M. Fleischmann	Isoperibolic Calorimetry
E. Storms	Seebeck Calorimetry
J.-P. Biberian	Gas Loading

Financial support for the conference came from both government and private sources. Dr. G. Peter Nanos and Dr. William H. Wilson of the Defense Threat Reduction Agency provided major support. The New York Community Trust has long been a major benefactor of research and outreach activities, including ICCF-14, driven by the interest of its retired businessman founder. Brian and Cynthia Chang Scanlon were particularly helpful in funding the ICCF-14 scholarship program for college. Energetics Technologies and its president Alison Godfrey provided both funding and access to major US media coverage. Christy Frazier of the New Energy Foundation helped with administration of some of this support as well as manning the book desk and providing technical materials for the attendees. Steven Krivit of the New Energy Institute administered some of this support. Robert Smith of Oakton International assisted with letters of invitation and funding administration.

Capitol Meeting Planning, Inc. provided invaluable, highly professional assistance in the planning and conduct of the conference. Marjorie Burdetsky lead that effort and performed many functions. Matthew Burdetsky provided timely assistance with proper handling of the government funding. Mindy Stewart served as registrar for the conference. On-site support was provided by Stephanie Hines and Trinh Lieu of Capitol Meeting Planning and Carol Ann Nagel.

Two past ICCF chairmen, Michael McKubre and Peter Hagelstein, gave us many suggestions and comments. Marianne Macy and Faqir Khanna also provided much useful advice during the planning of the conference.

The Hyatt Regency Hotel on Capitol Hill ably and responsively helped plan the conference. Kelly MacIntyre was the initial management contact. Isabella Jabart served as the conference point of contact immediately before and during the conference. Vidia Nigam helped with meal planning and supervised the preparation and serving of the meals.

Meetings were held in Moscow in February 2008 with Mark Tervakoski of the US Consulate in Moscow for the purpose of establishing the process for Russians to obtain visas. N.V. Samsenenko brought together in Moscow many of the Russian’s so that they could appreciate the complex process required to obtain a US visa. As the process for granting visas was in constant flux Jerome Conley Research, Director, Operational Concepts, LLC and Larry Forsley of JWK Corporation brought to bear their extensive experience in expediting the granting of clearances and visas.

Llewellyn King provided an appropriate and stimulating keynote address. Professor George Miley of the University of Illinois organized and conducted a post-conference workshop on the topic of transmutations. It was attended by approximately 50 scientists.

Talbot Chubb undertook the organization of the session honoring Prof Arata and wrote interpretive materials to assist in understanding his work. Frank Gordon similarly organized and conducted the session honoring Stanislaw Szpak.

A few colleagues gave much time and talent to preparation of these proceedings. Scott Chubb of the Naval Research Laboratory and Rodney Johnson of the Naval Postgraduate School provided reviews of the theoretical papers, which constitute almost one-third of the papers in these proceedings.

Jed Rothwell provided inspired and invaluable editorial, formatting and other services without which these proceedings would be much less useful. He also posted many of the papers from this conference on the web site lenr-canr.org in order to make them widely available.

The Marriott Library of the University of Utah is the repository for the archives of materials on cold fusion. Dr. Joyce Ogburn, head of that library, and Dr. Gregory Thompson, responsively agreed to both print and mail these proceedings to conference attendees. The proceedings will also be available on DVD after the initial distribution of paper copies. Orders for these proceedings can be placed at http://www.infinite-energy.com. Further, the entire proceedings, less copyrighted papers, can be downloaded from LENR-CANR.org.

Author Index

Pages are in Volume 1 unless otherwise indicated. Volume 2 begins on page 409.